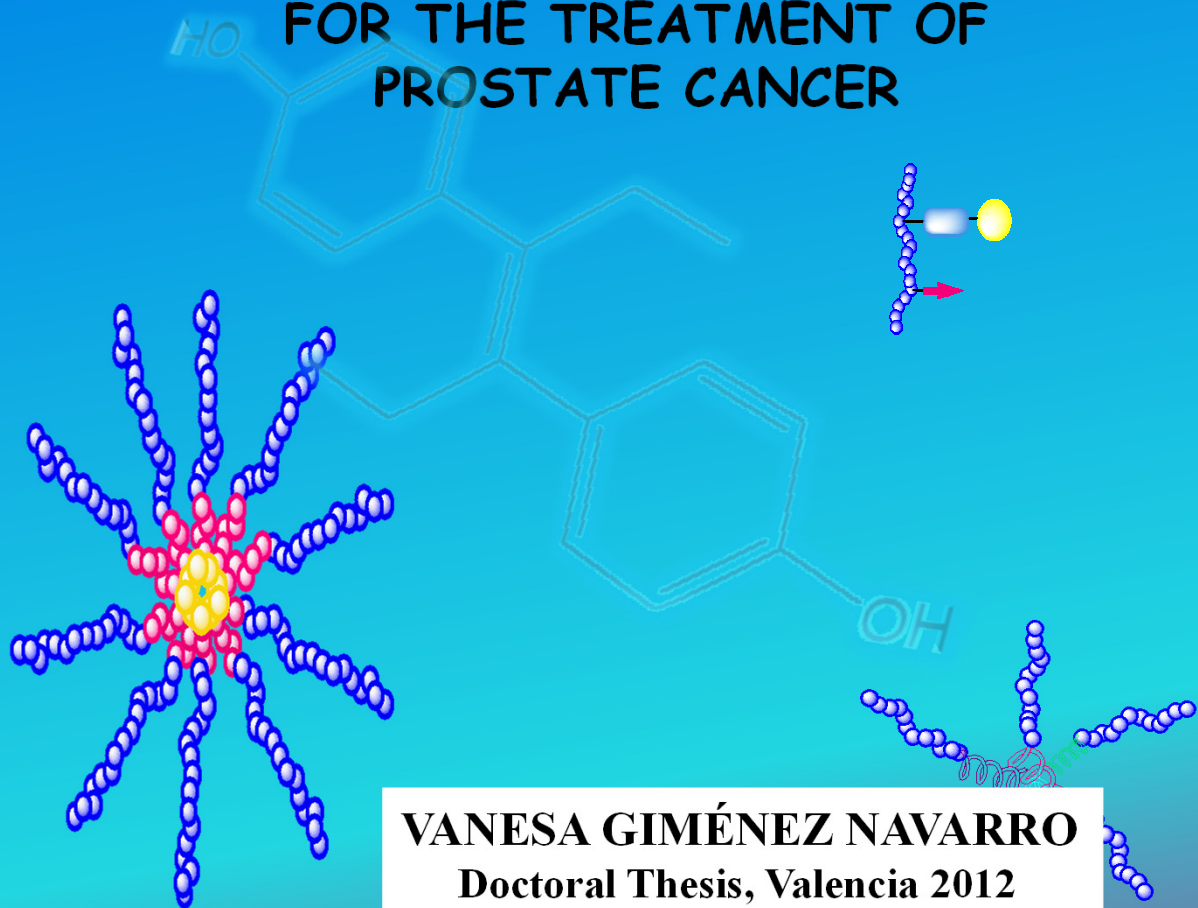


# DES-POLYACETALS AS POLYMER THERAPEUTICS FOR THE TREATMENT OF PROSTATE CANCER



**VANESA GIMÉNEZ NAVARRO**  
Doctoral Thesis, Valencia 2012



VNIVERSITAT  
ID VALÈNCIA



PRINCIPE FELIPE  
CENTRO DE INVESTIGACION

# **DES-POLYACETALS AS POLYMER THERAPEUTICS FOR THE TREATMENT OF PROSTATE CANCER**

Thesis Project presented by

**Vanesa Giménez Navarro**

in order to obtain the  
International Doctorate in Biochemistry

Thesis supervisor

**Dr. María J. Vicent Docón**



**PRINCIPE FELIPE**  
CENTRO DE INVESTIGACION



VNIVERSITAT  
ID VALÈNCIA



Departament de Bioquímica i  
Biologia Molecular



Dr. María Jesús Vicent Docón, Ph.D. in Chemistry and Head of the Therapeutic Polymers Laboratory in Centro de Investigación Príncipe Felipe, Valencia, Spain.

CERTIFY, that the work “DES-POLYACETALS AS POLYMER THERAPEUTICS FOR THE TREATMENT OF PROSTATE CANCER” has been developed by Vanessa Giménez Navarro under her supervision in Prince Felipe Research Centre in Valencia, as a thesis project in order to obtain a Ph.D. degree in Biochemistry at University of Valencia, Biochemistry and Molecular Biology Department.

Dr. María J. Vicent Docón

**A mis padres y  
a mis abuelos**

# INDEX

## Abbreviations

<b>CHAPTER 1- GENERAL INTRODUCTION.....</b>	<b>1</b>
<b>1.1 PROSTATE CANCER .....</b>	<b>2</b>
1.1.1 Introduction .....	2
1.1.2 Prostate cells .....	7
1.1.3 Origin of Prostate Cancer .....	8
1.1.3.1 Biosynthesis of the testosterone.....	10
1.1.3.2 Metabolism of the testosterone.....	11
1.1.3.3 Androgen receptor (AR) and pathways involved in apoptosis and Proliferation.....	12
1.1.3.4 Examples of therapeutic targets in the AR pathway and the site of action of different drugs to treat prostate cancer.....	16
1.1.4 Diagnosis of prostate cancer and stage determination .....	18
1.1.5 Current Prostate Cancer Treatments.....	19
1.1.5.1 Active surveillance.....	20
1.1.5.2 Surgery.....	21
1.1.5.3 Radiation therapy for advanced or recurrent Prostate Cancer	21
1.1.5.4 Cryotherapy.....	21
1.1.5.5 High-intensity focused ultrasound (HIFU) .....	21
1.1.5.6 Hormonal Therapy .....	22
1.1.5.6.1 Orchiectomy <sup>57</sup> .....	22
1.1.5.6.2 Anti-androgens.....	23
1.1.5.6.3 Luteinizing hormone-releasing hormone (LHRH) agonists or LHRH analogs .....	25
1.1.5.6.4 Luteinizing hormone-releasing hormone (LHRH) antagonists .....	29
1.1.5.6.5 Combination Therapy Strategies.....	29
1.1.5.6.6 Other androgen-suppressing drugs .....	32
1.1.5.7 Chemotherapy.....	34
1.1.5.8 Other therapeutic strategies.....	38
1.1.5.8.1 Prostate cancer vaccines.....	38
1.1.5.8.2 Angiogenesis inhibitors .....	39
1.1.5.8.3 Treating bone pain.....	39
1.1.6 Prostate cancer cells models .....	40

<b>1.2 POLYMER THERAPEUTICS AS NANOSIZED MEDICINES FOR TREATING CANCER.....</b>	<b>42</b>
1.2.1 Introduction .....	42
1.2.2 Polymer Therapeutics: from origins to current development .....	43
1.2.3 The Rational behind the design of Polymer Therapeutics.....	48
1.2.3.1 Enhanced Permeability and Retention (EPR effect).....	48
1.2.3.2 Intracellular Trafficking Lysosomotropic Drug Delivery Concept for Polymer-Drug Conjugates.....	50
1.2.4 Current status of Polymer Therapeutics .....	53
1.2.4.1 Polymeric drugs .....	53
1.2.4.2 Polymeric micelles.....	54
1.2.4.3 Polymer-based non-viral vectors for gene delivery (polyplexes).....	56
1.2.4.4 Polymer conjugates .....	57
1.2.4.4.1 Polymer-drug conjugates.....	61
1.2.5 Challenges and future trends for Polymer-Drug Conjugates.....	62
1.2.6 Polyacetals as biodegradable drug carriers.....	64
1.2.7 Physico-chemical characterization .....	68
References .....	73
<b>CHAPTER 2 - OBJECTIVES.....</b>	<b>89</b>
<b>CHAPTER 3 - MATERIALS AND METHODS.....</b>	<b>93</b>
3.1 Instruments .....	94
3.2 Materials .....	95
3.3 Synthesis and Characterisation of PEG-based DES-polyacetalic systems.....	97
3.3.1 Synthesis of Terpolymer (or Tert-DES) (1). .....	97
3.3.2 Synthesis of Block-copolymer (or Block-DES) (2). .....	98
3.3.3 Synthes of N-Fmoc protection of serinol (Fmoc-Serinol) (3). .....	100
3.3.4 Synthesis of DES-Serinol-polyacetal, Tert-DES-Serinol (or Tert-DES -Ser) (4).....	100
3.3.5 Synthesis of Block-DES-Serinol (or Block-DES-Ser)(5).....	102
3.3.6 N-Fmoc deprotection of the polyacetals, Tert-DES-Ser <sub>NH2</sub> (6) and Block-DES-Ser <sub>NH2</sub> (7).....	103
3.3.7 Synthesis of Fluorescently-labeled conjugates.....	104
3.3.8 Synthesis of Paclitaxel-DES conjugates, novel conjugates used for Combination Therapy. ....	108
3.3.9 Synthesis of Fluorescence-labeled PTX-conjugates. ....	110

3.4 NMR Spectroscopy.....	112
3.5 Determination of the Molecular Weight (Mw) and Polydispersity(Pdi) of the polyacetals using Gel Permeation Chromatography (GPC), also known as Size Exclusion Chromatography (SEC). ....	113
3.6 Determination of total and free DES content in DES-polyacetal conjugates .....	114
3.6.1 Total drug loading .....	114
3.6.2 Free drug content .....	116
3.7 Free amino group quantification by Ninhydrin assay. ....	116
3.8 Determination of Critical Micelle Concentration (CMC) of the polyacetals synthesised.....	117
3.9 Dynamic Light Scattering (DLS) studies .....	117
3.10 Transmission and Scanning electron microscopy (TEM) and (SEM) techniques.....	118
3.11 Small Angle Neutron Scattering (SANS) studies .....	118
3.12 pH-dependent degradation in buffer solution .....	119
3.13 Plasma Stability .....	119
3.14 Techniques and methods in cell culture .....	120
3.14.1 Thawing and recovering cells .....	120
3.14.2 Cell maintenance and passaging .....	121
3.14.3 Freezing cells .....	122
3.14.4 MTT or MTS assays to assess cell viability: Growth curve.....	123
3.14.5 Evaluation of polymer cytotoxicity using the MTT assay .....	124
3.14.6 Haemolytic Activity of Free DES and DES-polyacetals .....	125
3.14.7 Confocal fluorescence microscopy: live cell imaging .....	126
3.14.8 Flow cytometry analysis .....	126
3.14.9 Flow cytometry: Annexin-PI.....	127
3.14.10 Western Blot .....	127
3.14.11 Cell cycle assay.....	128
3.14.12 Statistical Analysis .....	128
3.15 Biodistribution and tumor accumulation of the conjugates with Cy5.5 in a Xenograft Rat model.....	129
References.....	130

<b>CHAPTER 4- TERT-DES VS. BLOCK-DES. POLYACETALIC CONJUGATES.....</b>	<b>131</b>
<b>4.1 SYNTHESIS, CHARACTERIZATION AND <i>IN VITRO</i> STUDIES.....</b>	<b>132</b>

4.1.1 Introduction .....	132
4.1.2 Synthesis and Characterization of DES-polyacetals .....	133
4.1.3 Kinetics of Drug Release .....	139
4.1.4 Plasma Stability of DES-polyacetals.....	142
4.1.5 Preliminary biological evaluation in cell models.....	143
4.1.5.1 Amino-pendant polyacetals (APEG). .....	144
4.1.5.1.1 Synthesis of Fmoc-protected serinol 3.....	144
4.1.5.1.2 Synthesis of APEG-DES-polyacetals derivatives.....	145
4.1.5.1.3 Determination of amine groups .....	149
4.1.5.1.4 Conjugation of APEG-DES polyacetals with different fluorochromes.....	150
4.1.5.2 In vitro studies in prostate cancer cell lines.....	152
4.1.5.2.1 Cell model characterization: Cell Growth Curve .....	153
4.1.5.2.2 Cell Viability Studies.....	157
4.1.5.2.3 Haemocompatibility studies .....	159
4.1.5.2.4 Confocal fluorescence microscopy: live-cell imaging.....	160

## **4.2 INVESTIGATING CONFORMATION IN SOLUTION OF DES-POLYACETALS.....165**

4.2.1 Introduction .....	165
4.2.2 Determination of Critical micelle concentration (cmc) of the conjugates.....	165
4.2.3 Transmission and Scanning Electron Microscopy,TEM and SEM.	169
4.2.4 Dynamic Light Scattering, DLS technique. ....	171
4.2.5 Pulsed-Gradient Spin-Echo NMR (PGSE-NMR) experiments to determine solution behavior of DES-polyacetals 1b and 2b.....	173
4.2.5.1 Introduction.....	173
4.2.5.1.1 Pulsed Spin Echo- NMR.....	174
4.2.5.1.2 Pulsed Gradient Spin Echo- NMR .....	174
4.2.5.1.3 Results of PGSE-NMR obtained for DES- Polyacetals....	177
4.2.6 Determination of solution behavior of DES-polyacetals by SANS.	178
4.2.6.1 Introduction to neutron radiation .....	178
4.2.6.2 Results from SANS obtained for DES-Polyacetals .....	183

## **4.3 MECHANISM OF ACTION AND IN VIVO STUDIES WITH DES-POLYACETALS.....193**

4.3.1 Introduction .....	193
Growth factor receptors .....	194
(i) Insulin growth factor.....	194



(ii) The protooncogenic protein, wnt.....	196
(iii) Epidermal growth factor receptor .....	198
(iv) Her-2/neu (erbb2) .....	200
(v) Phosphoinositide-3/akt .....	201
Mechanism of action of diethylstilbestrol .....	203
4.3.2 Useful in vitro techniques to determine the mechanism of action of DES -polyacetals.....	204
Apoptosis or programmed cell death .....	204
Cell cycle analysis .....	207
Control on the cell cycle .....	208
Key protein expression analyzed by western blot .....	209
4.3.3 Results .....	209
4.3.3.1 Cell death studies by Flow Cytometry: Annexin V-PI.....	209
4.3.3.2 Cell cycle analysis .....	214
4.3.3.3 Determination of Akt, Autophagy and Apoptosis- Related Proteins by Protein Immunoblotting.....	216
4.3.4 In vivo studies in xenograft mice models. ....	220
4.3.4.1 Body weight studies .....	220
4.3.4.2 In vivo biodistribution and tumor accumulation in a xenograft mouse model.....	221
4.3.4.3 Antitumoral effect on subcutaneous PC-3 tumors in Athymic nu/nu mice. ....	224
References.....	230

## **CHAPTER 5 POLYACETAL-BASED COMBINATION THERAPY FOR THE TREATMENT OF HORMONO-DEPENDENT DISEASES**

.....	241
5.1 Introduction .....	242
5.1.1 Combination Therapy.....	242
5.1.2 Rationale to develop Polymer-based combination Therapies .....	246
1. Type I: Polymer drug conjugate + low molecular weight drugs. ....	248
2. Type II: Polymer drug conjugates + polymer-drug conjugate. ....	251
3. Type III: Single polymeric carrier carrying a combination of drugs. ....	252
4. Type IV: Polymer-directed enzyme prodrug therapy (PDEPT) and polymer enzyme liposome therapy (PELT).....	255
5.1.3 Challenges to develop the most efficient conjugated systems for combination therapy. ....	256
5.1.4 Combination Index.....	258
5.1.5 Paclitaxel as second chemotherapeutic drug in the polyacetalic	

system. ....	259
5.2 Synthesis and Characterization of novel Paclitaxel-DES conjugates used for Combination Therapy. ....	261
5.2.1 Strategy 1: Synthesis of Tert-DES-Ser-PTX (18) and Block-DES-Ser-PTX (19). ....	262
5.2.2 Strategy 2: Synthesis of Tert-DES-Ser-PTX <sub>COOH</sub> (21) and Block-DES-Ser-PTX <sub>COOH</sub> (22). ....	264
5.2.3 Synthesis and Characterization of Fluorescence-labeled paclitaxel conjugates, Tert-DES-Ser-PTX-OG and Block-DES-Ser-PTX-OG and Tert-DES-Ser-PTX-Cy and Block-DES-Ser-PTX-Cy. ....	267
5.2.3.1 Strategy 1. Synthesis of fluorescence-labeled-PTX conjugates I. ....	267
5.2.3.2 Strategy 2. Synthesis of fluorescently-labeled-PTX conjugates II. ....	270
5.3 Physicochemical characterization: SANS and PGSE-NMR studies. ....	273
a) Influence of Serinol in polyacetal conformation. ....	273
b) Solution conformation of polyacetal-based combination conjugates. Influence of the presence of paclitaxel in DES-polyacetals. ....	276
PGSE-NMR studies with DES-Serinol Polyacetals. ....	278
5.4 Biological evaluation of Polyacetal-DES-Ser-PTX combination conjugates. ....	279
5.4.1 Evaluation of DES-PTX derivatives in Breast and prostate human cell models. ....	279
5.4.1. 1 In vitro Efficacy of DES-Polyacetals conjugates in breast cancer cell models. ....	279
5.4.1. 2 In vitro Efficacy of DES-Polyacetals conjugates in prostate cancer cell models. ....	280
5.4.2 Evaluation of DES-polyacetals in vivo breast model. ....	290
5.4.2. 1 In vivo & ex vivo biodistribution of Tert- and Block-Ser-DES-PTX polymer-Cy5.5 in mice MDA-MB-435S xenografts. ....	290
In vivo studies. Tert- and Block-Ser-DES-PTX-polymer Cy5.5 tumor-accumulation. ....	290
Ex vivo studies: Tert- and Block-Ser-DES-PTX-Cy5.5 polymer tumor-accumulation and excretion. ....	292
References. ....	294

**CHAPTER 6- GENERAL DISCUSSION .....303**

**CHAPTER 7- CONCLUSIONS.....317**

## **Appendices**

Appendix 1: Definition and Classification of TNM staging.....	323
Appendix 2: Thesis project index, objectives, methodology and conclusions in Spanish .....	327

## **Acknowledgements**

## FIGURE INDEX

### CHAPTER 1

<i>Figure 1.1. 1 Age-Standardized Prostate Cancer Incidence and Mortality Rates by World Area.</i>	4
<i>Figure 1.1. 2 Illustration showing the prostate and the nearby organs.</i>	7
<i>Figure 1.1. 3 Molecular structure of testosterone.</i>	8
<i>Figure 1.1. 4 Illustration showing the different organs where usually prostate cancer cells can metastasize.</i>	9
<i>Figure 1.1. 5 Biological process of steroids synthesized from cholesterol.</i>	10
<i>Figure 1.1. 6 Scheme of the feedback loop involving the testicles, the hypothalamus, and the pituitary glands.</i>	12
<i>Figure 1.1. 7 Molecular pathways of androgen action.</i>	14
<i>Figure 1.1. 8 Non-genomic androgen actions via changes in intracellular ion concentrations and membrane fluidity.</i>	15
<i>Figure 1.1. 9 Molecular pathways of androgen action.</i>	17
<i>Figure 1.1. 10 An updated version of Dr. Gleason's simplified drawing of the five Gleason grades of prostate cancer.</i>	19
<i>Figure 1.1. 11 Treatments usually administered in the progression of prostate disease.</i>	20
<i>Figure 1.1. 12 Different mechanisms showing how hormonal therapy works in order to destroy prostate cancer cells.</i>	23
<i>Figure 1.1. 13 Anti-androgens molecules used for the treatment of Prostate Cancer (PCa). The anti-androgen sits in the AR and prevents the interaction of testosterone (T) and DHT with the AR (target).</i>	24
<i>Figure 1.1. 14 Anti-androgens molecules used for the treatment of PCa inhibiting the enzyme 5-<math>\alpha</math>-reductase.</i>	25
<i>Figure 1.1. 15 Luteinizing hormone molecule (Glp-His-Trp-Ser-Tyr-Gly-Leu-Arg-Pro-Gly-NH<sub>2</sub>).</i>	25
<i>Figure 1.1. 16 LHRH analogs administered to treat PCa.</i>	27
<i>Figure 1.1. 17 A. Dimensions of the rod polymer depot formulation of Zoladex® and B. schematically representation of drug delivery once is diffused into the cell.</i>	27
<i>Figure 1.1. 18 Molecule of Abiraterone, a LHRH analog used for the treatment of PCa by blocking the enzyme CYP17 which secretes testosterone.</i>	28
<i>Figure 1.1. 19 LHRH antagonists administrated to treat PCa.</i>	29
<i>Figure 1.1. 20 Mechanism of action of different drugs in order to reduce the production of testosterone as First (A) and as Second (B) Line of Hormone therapy.</i>	30
<i>Figure 1.1. 21 A. Molecule of Dehydroepiandrosterone (DHEA). B. Production of DHEA from Cholesterol.</i>	31

<i>Figure 1.1. 22 Molecule of ketoconazole, an estrogen used for the treatment of PCa by blocking the enzyme 17, 20-lyase which secretes testosterone.</i>	31
<i>Figure 1.1. 23 Molecule of the Diethylstilbestrol, the most well known synthetic estrogen used to treat PCa.</i>	32
<i>Figure 1.1. 24 Molecule of cisplatin.</i>	35
<i>Figure 1.1. 25 Molecule of Paclitaxel.</i>	35
<i>Figure 1.1. 26 Schematic representation of paclitaxel-induced effects upon signal transduction pathways. Figure adapted from Okano et al in 200167.</i>	37
<i>Figure 1.1. 27 LNCaP cell line.</i>	40
<i>Figure 1.1. 28 PC-3 cell line.</i>	41
<i>Figure 1.1. 29 DU-145 cell line.</i>	41
<i>Figure 1.1. 30 Prostate cancer cell lines, PC-3 (a), LNCaP (b), and DU-145 (c) immunostained for <math>\alpha</math>-tubulin (green). DNA was stained with Hoechst dye (blue).</i>	42
<i>Figure 1.2. 1 Schematic representation of polymer therapeutics.</i>	44
<i>Figure 1.2. 2 Time-scale tracking the developments of polymers and their uses in nanomedicines</i>	46
<i>Figure 1.2. 3 The EPR effect</i>	48
<i>Figure 1.2. 4 Ringsdorf's model of polymer-drug conjugates.</i>	50
<i>Figure 1.2. 5 Possible endocytosis pathways for cellular uptake of nanostructures.</i>	51
<i>Figure 1.2. 6 Lysosomotropic drug delivery of polymer conjugates.</i>	52
<i>Figure 1.2. 7 Polymeric drug structures.</i>	53
<i>Figure 1.2. 8 Polymeric Micelles structure.</i>	55
<i>Figure 1.2. 9 Polyplexes structures.</i>	56
<i>Figure 1.2. 10 Polymer conjugates structure.</i>	57
<i>Figure 1.2. 11 Common polymers and dendrimers used as potential macromolecular carriers in the field of polymer therapeutics.</i>	59
<i>Figure 1.2. 12.....Acid labile linkers used to conjugate drugs to the polymer backbone</i>	61
<i>Figure 1.2. 13 Structures of (A) PK1 and (B) PK2.</i>	62
<i>Figure 1.2. 14 New polymer architecture for the development of better polymeric carrier</i>	64
<i>Figure 1.2. 15 pH-dependent degradation profile of polyacetal 1.</i>	66
<i>Figure 1.2. 16 DES molecule.</i>	66
<i>Figure 1.2. 17 DES-Polyacetal polymer structure.</i>	67
<i>Figure 1.2. 18 Schematic representation of the HPLC with a gradient elution mode.</i>	69
<i>Figure 1.2. 19 Schematic representation of the GPC system.</i>	70

### CHAPTER 3

- Figure 3. 1 (A) Reactor at ILL, Grenoble (France) (image taken from [www.ill.eu](http://www.ill.eu)) and (B) Scheme of a synchrotron such as it could be found at ISIS, Oxford (UK) ..... 118
- Figure 3. 2 Haemocytometer thick glass slide used for counting cells. The addition of trypan blue helps to distinguish viable, unstained cells (white circles) from non-viable, blue-stained cells (blue circles). ..... 122
- Figure 3. 3 Sterile 96-well microtitre plate for carry on a cellular Growth study by MTT or MTS assay. From left to right it was increasing the concentration of cells. Column 2 was the control data. All the surrounding wells were filled with PBS for the best maintenance conditions of the cells. .... 124
- Figure 3. 4 Sterile 96-well microtitre plate for carry on a cell viability study by MTT or MTS assay. The effect of the compounds in causing death or changing the metabolism of the cells can be deduced comparing cells treated with drug compounds (which produce purple formazan) with the formazan produced by untreated control cells. .... 125

### CHAPTER 4

- Figure 4.1. 1 <sup>1</sup>H-NMR of Tert-DES synthesized in different solvents; (A) THF, Toluene, Dichloromethane (DCM), Dimethylformamide (DMF); (B) Dioxane. .... 135
- Figure 4.1. 2 <sup>1</sup>H-NMR spectra of DES-polyacetal 1 (Tert-DES). ..... 137
- Figure 4.1. 3 Example of <sup>1</sup>H-NMR spectrum of Block-DES 2 with assigned signals. .... 138
- Figure 4.1. 4 pH-Dependent DES release: (A) tert-DES 1b at pH 7.4, 6.5 and 5.5; (B) block-DES 2b at pH 7.4, 6.5 and 5.5. The results show the percentage of DES release from total at each time point. Mean values  $\pm$  SD (n = 3). .... 140
- Figure 4.1. 5 pH-Dependent DES release as cis- and trans-DES forms from tert-DES 1b and block-DES 2b at pH 5.5. The results show the percentage of DES release from total at each time point. Mean values  $\pm$  SD (n = 3). .... 141
- Figure 4.1. 6 pH-Dependent DES release DES from: (A) tert-DES 1a-c at pH 5.5, (B) block-DES 2a-c at pH 5.5. The results show the percentage of DES release from total at each time point. Mean values  $\pm$  SD (n = 3). 142
- Figure 4.1. 7 Stability in plasma of DES-polyacetal derivatives (mean  $\pm$  SD, n=3). .... 142
- Figure 4.1. 8 <sup>1</sup>H-NMR spectrum of Serinol-Fmoc monomer 3. .... 145
- Figure 4.1. 9 <sup>1</sup>H NMR spectra of Tert-DES-Ser 4. .... 147
- Figure 4.1. 10 <sup>1</sup>H NMR spectra of Block-DES-Ser 5. .... 147
- Figure 4.1. 11 An example <sup>1</sup>H-NMR spectra showing successful Fmoc-deprotection and preservation of DES and serinol in the APEG conjugate polymers. .... 148

Figure 4.1. 12 Calibration curve use to quantify the pendant amino groups in the polyacetals. ....	149
Figure 4.1. 13 Representative images of the elution profile of labeled conjugates used to quantify Cy5 (A, C) and OG- (B, D) polymer loading .....	152
Figure 4.1. 14 Schematic representation of the four different phases in a growth curve. ....	154
Figure 4.1. 15 A) Mitochondrial reductase reduces MTT or MTS (in the presence of phenazine methosulfate (PMS)) to purple formazan dyes..	155
Figure 4.1. 16 Growth curve for optimizing the LNCaP cell seeding density. ....	156
Figure 4.1. 17 Growth curve to optimise PC3 cell seeding density. ....	156
Figure 4.1. 18 Cytotoxicity of DES derivatives measured by MTT assay after 72 h incubation. Tert-DES vs block-DES in (A) PC3 cells and (B) LNCaP cells. Data are expressed as mean $\pm$ SD ( $n \geq 3$ ). * $p < 0.05$ . ...	158
Figure 4.1. 19 Cytotoxicity of DES derivatives measured by MTT assay after 72 h incubation. DES content influence on cytotoxicity against PC3 cells (A) tert-DES 1a-c vs (B) block-DES 2a-c. Data are expressed as mean $\pm$ SD ( $n \geq 3$ ). * $p < 0.05$ .....	159
Figure 4.1. 20 Haemolytic activity of DES, NaDES and DES-polyacetals at 24h. Data expressed as mean $\pm$ SEM ( $n=3$ ). ....	160
Figure 4.1. 21 Kinetics of cell trafficking with polyacetals 8a and 9a in prostate cancer cell lines (A) LNCaP and (B) PC3.....	162
Figure 4.1. 22 Confocal microscopy images were taken from live: (A) PC3 cells, (B) LNCaP cells after 2 h incubation with tert-DES-Ser-OG 8a and block-DES-Ser-OG 9a. Dextran-Texas Red was employed as lysosomal marker (in red) and polymers were labeled with OG (in green, left panel). Co-localization is seen in yellow (central panel). ....	163
Figure 4.2. 1 CMC determination for (A) Tert-DES and (B) Block-DES. ...	166
Figure 4.2. 2 CMC determination for Tert-DES 1b and Block-DES 2b in DPH and Pyrene solution. ....	168
Figure 4.2.3 Scanning electron microscopy images for Tert-DES 1b (A and B) and for Block-DES 2b (C and D)) at concentration above CAC.....	169
Figure 4.2. 4 Transmission electron microscopy for Tert-DES 1b (A and B) and for Block-DES 2b (C and D).....	170
Figure 4.2. 5 Hypothetical Dynamic light scattering of large particles (on the top) and small particles (on the bottom). ....	172
Figure 4.2. 6 DLS profiles for (A) Block-DES and (B) Tert-DES in PBS. ...	173
Figure 4.2. 7 Diagram showing the process occurred in a standard pulsed spin echo-NMR experiment where the free induction decay (F.I.D) signal	

is refocused using a $\pi$ rf pulse, producing a spin echo, S.E. (Figure taken from 38).	174
Figure 4.2. 8 Diagram showing the pulse sequence for a PGSE-NMR experiment.	175
Figure 4.2. 9 Diagram showing the pulse sequence for a stimulated echo PGSE-NMR experiment.	175
Figure 4.2. 10 Diagram showing the thirty-two 1D spectra on a 2D plot showing the signal attenuation.	176
Figure 4.2. 11 Normalized PGSE-NMR data from 1wt% conjugate solutions at 25°C; Tert-DES in D2O (filled circles) and methanol (open circles); Block-DES in D2O (filled squares) and methanol (open squares).	178
Figure 4.2. 12 Schematic representation of a SANS experiment. The distance between the sample to the detector is usually 1 – 20 m and the scattering angle $\theta < 10^\circ$ .	180
Figure 4.2. 13 SANS from 1wt% conjugates solutions in (A) D2O. Lines are best-fits to the data as described in the text. (B) MeOD. Solid lines are best-fits to a rod model. Tert-DES (triangles), Block-DES (squares), dilute block-DES solution (circles).	185
Figure 4.2. 14 SANS from 1wt% conjugates solutions of Tert-DES at different drug concentrations (T-DES 1a, 1b and 1c with 2,4 and 6wt%DES respectively) in (A) D2O and (B) MeOD. T-DES 1a (triangles), T-DES 1b (squares), T-DES 1c (circles).	188
Figure 4.2. 15 SANS from 1wt% conjugates solutions of Block-DES at different drug concentrations (Block-DES 2a, 2b and 2c with 2,4 and 6wt%DES respectively) in (A) D2O and (B) MeOD. Block-DES 2a (triangles), Block-DES 2b (squares), Block-DES 2c (circles).	189
Figure 4.2. 16 SANS from conjugates solutions of Block-DES 2b (A) and Tert-DES 1b (B) at different polymer concentrations (1.5 triangles), 0.8 (circles) and 0.4 (squares) wt% Polymer in D2O.	191
Figure 4.3. 1 An overview of major signal transduction pathways. The figure shows examples of pathways for proliferation (Ras/MAPK), STAT signaling (STAT's) and survival/metabolism (PI3K/Akt).	194
Figure 4.3. 2 IGF1 and IGF2 signaling pathway involved in prostate cancer.	196
Figure 4.3. 3 The Wnt signaling pathway showing some influences of other signaling pathways and factors.	197
Figure 4.3. 4 The EGFR signaling pathway encountered in the treatment of prostate cancer.	199
Figure 4.3. 5 A model of HER-2/neu activation of the Akt-AR pathway that promotes survival and proliferation of androgen-dependent prostate cancer cells upon androgen deprivation.	200
Figure 4.3. 6 PI3K/Akt signaling pathway involved in prostate cancer.	202
Figure 4.3. 7 Extrinsic and intrinsic apoptosis pathways.	205



<i>Figure 4.3. 8 Detection of surface morphology changes during apoptosis. During apoptosis, the distribution of neutral phospholipids (black symbols) and anionic phospholipids such as phosphatidylserine (red symbols) in the cell membrane changes. ....</i>	<i>206</i>
<i>Figure 4.3. 9 Cell cycle: A schematic overview. Mammalian cell cycle regulation by CDK/cyclin holoenzymes and CKIs. The cell cycle consists of four distinct phases: G1, S (DNA replication), G2, and M (mitosis). Activation of specific CDK/cyclin complexes drives progression through these cell cycle phases. CKIs of the Cip/kip and the INK4 families interact with and inactivate CDK/cyclin holoenzymes, thereby blocking cell cycle progression and cell proliferation. ....</i>	<i>207</i>
<i>Figure 4.3. 10 Example of protein immunoblotting/western blotting of apoptosis-related proteins. In this example, the protein-expression study show upregulation of Tp53, Caspase-3, and Bax but downregulation of Bcl-2. ....</i>	<i>209</i>
<i>Figure 4.3. 11 Typical flow cytometric profile of the DNA content in PC3 and LNCaP cell lines stained with AnnexinV and PI. A prominent subG1 peak (between 100 and 200) should appear in apoptotic cells but not in normal cells. ....</i>	<i>210</i>
<i>Figure 4.3. 12 Typical histogram from FACS analysis after AnnexinV-PI test. Single parameter histograms are shown at the top (Annexin) and on the right side (PI) of the diagram. Two parameter histograms are shown in quadrants E1-E4. ....</i>	<i>211</i>
<i>Figure 4.3. 13 Example of obtained histogram from FACS analysis after AnnexinV-PI test. PC3 and LNCaP Cell lines were cultivated with the drug alone and DES-polyacetals. Cells were stained with Annexin-V and PI, then incubated and analyzed. ....</i>	<i>212</i>
<i>Figure 4.3. 14 Annexin-PI test with Tert-DES and Block-DES polyacetals in PC3 (A) and LNCaP (B) cell lines. Data are expressed as mean <math>\pm</math> SD (<math>n \geq 3</math>). * <math>p &lt; 0.05</math>. Cell death (%) expressed as Annexin V-positive cells (quadrants E2+E4). ....</i>	<i>213</i>
<i>Figure 4.3. 15 Cell cycle study for Tert-DES and Block-DES polyacetals in PC3 cell line. Data are expressed as mean <math>\pm</math> SD (<math>n \geq 3</math>). * <math>p &lt; 0.05</math>. ....</i>	<i>215</i>
<i>Figure 4.3. 16 Cell cycle in LNCaP cell line for Tert-DES and Block-DES. ....</i>	<i>216</i>
<i>Figure 4.3. 17 Protein immunoblotting/western blotting of Akt pathway, autophagy and apoptosis-related proteins in PC3 prostate adenocarcinoma cell line. The treatment was done with Tert-DES (1a,1b) and Block-DES (2b,2b). ....</i>	<i>217</i>
<i>Figure 4.3. 18 Protein immunoblotting of cell cycle-related proteins in PC3 cell line upon incubation in presence of free DES, Tert-DES 1 and Block-DES 2. ....</i>	<i>218</i>

Figure 4.3. 19 Schematic representation of the relationship of the protein p21 involved in cell cycle. ....	219
Figure 4.3. 20 Western blotting of proteins related with apoptosis in LNCaP cell line. Cells were incubated in absence and presence of DES, Tert-DES and Block-DES polyacetals for 24 h. ....	219
Figure 4.3. 21 Body weight control for CD1 mice after polyacetal i.v. administration. ....	220
Figure 4.3. 22 Tumor accumulation; In vivo fluorescence imaging of subcutaneous Xenograft models after 3 days of intravenous injection of 3.5, 5 and 7 mg/kg Tert-DES-Ser-Cy5.5 polyacetal 10a. ....	222
Figure 4.3. 23 Tissue accumulation; Cyane fluorescence detected into tumor, kidneys, liver and urine by in vivo fluorescence imaging after 3 days of i.v. injection of 7 mg/kg 10a. ....	222
Figure 4.3. 24 Tert-DES-Ser-Cy5.5 tumor accumulation results. A. In vivo fluorescence imaging of subcutaneous HT-29 colon bearing mice after i.v. injection of 7 mg/kg of Cy5.5-labelled-Tert-DES 10a polyacetal. The tumor accumulation can be easily visualized at 6h-17days (D=day) postinjection. B. The fluorescence intensity was recorded and quantified as Efficiency over time. ....	223
Figure 4.3. 25 Tumor growth inhibition. Comparative analysis of the localized subcutaneous growth of PC3-Fluc prostate cancer cells treated with the DES, Tert-DES and Block-DES in athymic nude mice by external measurements of tumor volume (A), and by tumor bioluminescent signals (B). ....	225
Figure 4.3. 26 Effect of the DES-polyacetals (tert-DES 1b and block-DES 2b) on Tumor Weight (A) and Tumor Volume (B) at the end of the experiment. Scatter plots show all values with the median values represented by a bar. Statistical analysis was done using a Dunn's Multiple Comparison test. ....	226
Figure 4.3. 27 Correlation between tumor volume and bioluminescence. The correlation $r^2$ value was 0.5793 ( $p=0.0002$ ), 0.5436 ( $p=0.0007$ ), 0.6384 ( $p<0.0001$ ) and 0.5610 ( $p<0.0001$ ) for vehicle, DES, Tert-DES-Ser-Cy 10a and Block-DES-Ser-Cy 11a, respectively. ....	227
Figure 4.3. 28 Representative images of the mice at day 21 after treatment with DES 1mg/kg or Tert- or Block-DES (1b and 2b resp.) at 5mg/kg for 29days. Images were set at the same pseudocolor scale to show relative bioluminescent changes over time. ....	228
Figure 4.3. 29 Body weight profiles of treated mice. ....	228

## CHAPTER 5

Figure 5. 1 Schematic representation of the four different types of polymer-based combination therapy for targeted drug delivery by the EPR effect <sup>12</sup> . ....	248
---	-----

Figure 5. 2 Isobologram graph representing synergism and antagonism effect combining two different drugs76.....	259
Figure 5. 3 Molecule of Paclitaxel (already mentioned at chapter 1). .....	260
Figure 5. 4 <sup>1</sup> HNMR spectrum of Tert-DES-SerCOOH 12 or Block-DES-Ser-COOH 13.....	262
Figure 5. 5 <sup>1</sup> HNMR spectrum of Tert-DES-Ser-PTX 18 or Block-DES-Ser-PTX 19.....	263
Figure 5. 6 <sup>1</sup> HNMR spectrum of 2'-succinyl-paclitaxel 20. ....	265
Figure 5. 7 <sup>1</sup> HNMR spectrum with assigned signals fobtaned from Tert-DES-Ser-PTX 21 or Block-DES-Ser-PTX 22. ....	266
Figure 5. 8 SANS data from (A) Tert-polymers and (B) Block-polymers in D2O and MeOD solutions at fixed DES content (4wt%) concentrations. ....	273
Figure 5. 9 (A) SANS data from Tert-DES-Ser, 3.7wt%DES and 3.1wt%Serinol, (black squares) and block-DES-Serinol, 3.6wt%DES and 3.2wt%Serinol, (blue triangles) polymer solutions in D2O (filled figures) and MeOD (open figures). (B) SANS data from Tert-DES (black squares) and Block-DES-Serinol (blue triangles) polymer solutions in D2O (filled figures) and MeOD (open figures) both at same DES concentration 4wt%. Error bars are shown. ....	274
Figure 5. 10 SANS data from 1wt% Tert-polymer solutions in D2O. Tert-DES 1b (squares); Tert-DES-Ser-PTX 21a (inverted triangles); Tert-Ser-PTX 1a (triangles). Error bars are shown. Where shown, lines are best model fits to the data as described in the text. ....	275
Figure 5. 11 Normalized PGSE-NMR data from 1wt% conjugate solutions at 25°C; Tert-DES-Ser in D2O (filled circles) and methanol (open circles); Block-DES-Ser in D2O (filled squares) and methanol (open squares). All of them are fitted to stretch diffusion coefficients.....	277
Figure 5. 12 In vitro MTT cell viability assays after 72 h incubation of DES derivatives againstMDA-MB-4355.eGFP breast cancer cell line.....	278
Figure 5. 14 In vitro MTT cell viability assays after 72 h of the single drugs, the combination of single drugs and the combination of PTX with DES-polymers .....	280
Figure 5. 15 In vitro MTT cell viability assays of PTX, T-PTX (Tert-PTX) and T-DES-PTX (Tert-DES-Ser-PTX) compounds. PC-3 (A) and LNCaP (B) cells.....	281
Figure 5. 16 Flow cytometry internalization studies for the combined polyacetals, (A) Tert-DES-Ser-PTX and (B) Block-DES-Ser-PTX. Both conjugates done at 4°C and at 37°C in PC3 cell line. Graphical view of the geometric mean.....	285
Figure 5. 17 Flow cytometry studies for Tert-DES-Ser-PTX (blue) and Block-DES-Ser-PTX (red) at 37°C in PC3 cell line.....	286

<i>Figure 5. 18 Flow cytometry studies for the combined polyacetals, (A) tert-DES-Ser-PTX and (B) Block-DES-Ser-PTX. Both conjugates done at 4°C and at 37°C in LNCaP cell line. ....</i>	<i>287</i>
<i>Figure 5. 19 Flow cytometry studies for the combined polyacetals, tert-DES-Ser-PTX (blue) and Block-DES-Ser-PTX (red) at 37°C in LNCaP cell line. ....</i>	<i>287</i>
<i>Figure 5. 20 Whole-body biodistribution of Tert- and Block-Ser-DES-PTX-Cy5.5 polyacetals measured by the means of in vivo FLI from the dorsal (A), lateral (B) and ventral (C) views using the IVIS® Spectrum. ....</i>	<i>289</i>
<i>Figure 5. 21 In vivo MDA-MB-435S subcutaneous tumor-accumulation after a single administration of 6 mg polymer/mouse of Tert-Ser-DES-PTX-Cy5.5 25a (A, right pannel) and Block-Ser-DES-PTX-Cy5.5 26a (A, left pannel). (B) Cy5.5 tumor-accumulation quantified by Radiant Efficiency. ....</i>	<i>290</i>
<i>Figure 5. 22 Tissue accumulation of T-DES-PTX-Cy5.5 and B-DES-PTX-Cy5.5 in different organs: tumor (A), liver (B), kidneys (C), spleen (D), lungs (E) and heart (F). The compounds are measured non-invasively by FLI and the fluorescence signal is quantified in Radiant Efficiency....</i>	<i>291</i>
<i>Figure 5. 23 Tissue distribution and excretion of polyacetals with DES and PTX labeled with Cy5.5. The compounds are measured non-invasively by FLI and the fluorescence signal is quantified in Radiant Efficiency....</i>	<i>292</i>
<i>Figure 5. 24 Illustration of ex vivo BLI images of prostatic tumor and spontaneous metastasis. ....</i>	<i>293</i>

## TABLE INDEX

### CHAPTER 1

<i>Table 1.1. 1 Estimated new cancer cases and deaths worldwide in 2008.....</i>	<i>3</i>
<i>Table 1.1. 2 Hormonal agents commonly used in the treatment of PCa.....</i>	<i>33</i>
<i>Table 1.2. 1 Examples of polymer therapeutics in the market and clinical trials. ....</i>	<i>47</i>
<i>Table 1.2. 2 Examples of techniques used to characterize polymer–drug conjugates. ....</i>	<i>71</i>

### CHAPTER 3

<i>Table 3. 1 Method employed to make the calibration curve of DES in the RP-HPLC.....</i>	<i>115</i>
<i>Table 3. 2 Conditions for the cell line growth.....</i>	<i>121</i>

### CHAPTER 4

<i>Table 4.1. 1 Conditions tested during polyacetal synthesis optimization. ...</i>	<i>134</i>
<i>Table 4.1. 2 Physico-chemical characteristics of the polyacetals synthesized. ....</i>	<i>139</i>
<i>Table 4.1. 3 Physico-chemical characteristics of DES-Serinol polyacetals. ....</i>	<i>149</i>
<i>Table 4.1. 4 Physico-chemical characteristics of the polyacetals with serinol synthesized. ....</i>	<i>150</i>
<i>Table 4.1. 5 IC50 of the drug and polyacetals evaluated by MTT after 72h in PC3 and LNCaP prostate cancer cell lines. ....</i>	<i>157</i>
<i>Table 4.3. 1 Distinguishing apoptosis from necrosis using Annexin-V and propidium iodide (PI).....</i>	<i>210</i>
<i>Table 4.3. 2 Annexin V-PI studies at 24h for Tert-DES and Block-DES. Data are expressed as mean <math>\pm</math> SEM (<math>n \geq 3</math>).....</i>	<i>213</i>
<i>Table 4.3. 3 Cell cycle in PC3 cell line for Ter-DES (1a and 1b) and Block-DES (2a and 2b). Data are expressed as mean <math>\pm</math> SEM (<math>n \geq 3</math>).....</i>	<i>214</i>
<i>Table 4.3. 4 Biochemical parameters for CD1 mice after polyacetal i.v. administration. ....</i>	<i>221</i>

### CHAPTER 5

<i>Table 5. 1 Examples of the four different types of polymer-based combination therapy for targeted drug delivery. ....</i>	<i>250</i>
<i>Table 5. 2 Physico-chemical characteristics of the synthesized polyacetals for combination therapy. ....</i>	<i>271</i>
<i>Table 5. 4 IC50 values of the single drugs and the polyacetals at concentrations of DES (A, C) and at concentrations of PTX (B, D), in PC3 (A, B) and LNCaP (C, D) prostate cancer cells.....</i>	<i>280</i>

<i>Table 5. 5 IC50 values for PTX, Tert-PTX (Tert-Ser-PTX or T-PTX) and Tert-DES-PTX compounds in PC-3 (A) and LNCaP cell lines (B).</i> .....	282
<i>Table 5. 6 IC50 for Tert-DES, Block-DES and their analogues in combination with PTX (DES-PTX-poyacetalic-based) systems.</i> .....	283

## SCHEME INDEX

### CHAPTER 1

<i>Scheme 1.2. 1 Synthesis of Polyacetal 1 using the polymerization technique described by Heller and Tomlinson.</i> .....	65
--	----

### CHAPTER 4

<i>Scheme 4.1. 1 Synthesis of DES-polyacetal 1 (Tert-DES).</i> .....	136
<i>Scheme 4.1. 2 Synthetic approach followed to obtain Block-DES 2.</i> .....	138
<i>Scheme 4.1. 3 Synthesis of Serinol-Fmoc monomer 3.</i> .....	145
<i>Scheme 4.1. 4 Synthesis of Tert-DES-Ser 4.</i> .....	146
<i>Scheme 4.1. 5 Synthesis of Block-DES-Ser 5.</i> .....	146
<i>Scheme 4.1. 6 Synthesis of Tert-DES-Ser 4 or Block-DES-Ser 5 with Fmoc group deprotected, yielding 6 or 7 respectively.</i> .....	148
<i>Scheme 4.1. 7 Scheme to synthesize OG- or Cy5.5- Tert-DES-Ser.</i> .....	151
<i>Scheme 4.1. 8 Scheme to synthesize OG- or Cyane5.5-Block-DES-Ser.</i> .....	151

### CHAPTER 5

<i>Scheme 5. 1 Synthesis of Tert-DES-Ser<sub>COOH</sub> 12 or Block-DES-Ser-<sub>COOH</sub> 13.</i>	262
<i>Scheme 5. 2 Synthesis of Tert-DES-Ser-PTX 18 or Block-DES-Ser-PTX 19.</i> .....	263
<i>Scheme 5. 4 Synthesis of Tert-DES-Ser-PTX 21 or Block-DES-Ser-PTX 22.</i> .....	265
<i>Scheme 5. 5 Synthesis of Tert-DES-Ser-PTX<sub>COOH</sub>-OG<sub>NHS</sub> 23 or Block-DES-Ser-PTX<sub>COOH</sub>-OG<sub>NHS</sub> 24.</i> .....	267
<i>Scheme 5. 6 Synthesis of Tert-DES-Ser-PTX<sub>COOH</sub>-C<sub>YNHS</sub> 25 or Block-DES-Ser-PTX<sub>COOH</sub>-C<sub>YNHS</sub> 26.</i> .....	267
<i>Scheme 5. 7 Synthesis of Tert-DES-Ser-PTX-OG<sub>cad</sub> 27 or Block-DES-Ser-PTX-OG<sub>cad</sub>28.</i> .....	268
<i>Scheme 5. 8 Synthesis of Tert-DES-Ser-PTX-Cy<sub>cad</sub> 29 or Block-DES-Ser-PTX-Cy<sub>cad</sub>30.</i> .....	269
<i>Scheme 5. 9 Synthesis of Tert-DES-Ser-PTX<sub>COOH</sub>-OG<sub>NHS</sub> 31 or Block-DES-Ser-PTX<sub>COOH</sub>-OG<sub>NHS</sub> 32.</i> .....	270

*Scheme 5. 10 Synthesis of Tert-DES-Ser-PTX<sub>COOH</sub>-Cy<sub>NHS</sub> 33 or Block-DES-Ser-PTX<sub>COOH</sub>-Cy<sub>NHS</sub> 34..... 270*

## Abbreviations

AAs	Antiandrogens
Abs.	Absorbance
ACN	Acetonitrile
ACTH	Adenocorticotrophic Hormone
AIDS	Acquired Immuno Defficiency Syndrome
5 $\alpha$ R	5-Alpha Reductase Enzyme
anh.	Anhydrous
ANOVA	Analysis of variance
APC	Annual Percent Change for the regression line segments
APEG	Amino-pendant Polyacetal
approx.	Approximately
AR	Androgen receptor
Bax	Bcl-2 associated X protein
Bcl-2	<u>B-cell lymphoma 2</u>
BSA	Bovine Serum Albumin
BPH	Benign prostatic hypertrophy
cAMP	Cyclic Adenosine Monophosphate
Cat.	Catalyst
CDCl <sub>3</sub>	Deuterated Chloroform
CHCl <sub>3</sub>	Chloroform
CMC	Critical Micelle Concentration
<sup>13</sup> C-NMR	Carbon nuclear magnetic resonance
CPT	Camptothecin
CRPC	Castration resistant prostate cancer
CRT	Conformal radiotherapy
CT	Computed Tomography
Cy, Cy5.5	Cyane 5.5
d	Doublet ( <sup>1</sup> H-NMR)
DCC	Dicyclohexylcarbodiimide
DCM	Dichloromethane
ddH <sub>2</sub> O	Double distilled water
DEGDVE	Di(ethylene glycol) divinyl ether
DES	Diethylstilbestrol
DHE	Dehydroepiandrosterone
DHT	Dehydrotetosterone
DIC	<i>N,N'</i> -Diisopropylcarbodiimide
DIEA	Diisopropyl ethyl amide
DIPEA	<i>N,N</i> -Diisopropylethylamine
DLS	Dynamic Light Scattering
DMAP	4-( <i>N,N</i> -dimethylamino)pyridine
DMF	<i>N,N</i> -Dimethylformamide
DMSO	Dimethyl sulfoxide



DMSO-d <sub>6</sub> :	Deuterated dimethyl sulfoxide
DRE	Digital Rectal Exam
DU-145	Brain cancer of prostate cancer
D <sub>2</sub> O	Deuterated water
EGF	Epidermal growth factor
EGFR	Epidermal growth factor receptor
EPR	Enhanced permeability and retention
equiv	Equivalent(s)
EtOAc	Ethyl acetate
FACS	Fluorescence-activated cell sorting
FBS	Fetal bovine serum
FC	Flow-cytometry
FDA	Food and drug administration
Fig.	Figure
Fmoc-Cl	9-Fluorenylmethoxycarbonyl chloride
FSH	Follicle-Stimulating Hormone
5-FU	5-fluorouracil
Gly	Glycine
GnHR	Gonadotropin-Releasing Hormone
GP	Glucoprotein
GPC	Gel permeation chromatography
h	hour(s)
HCl	Hydrochloric acid
HIFU	High-intensity focused ultrasound
<sup>1</sup> H-NMR	Proton nuclear magnetic resonance
HOBt	1-Hydroxybenzotriazole
hPAP	Human Prostatic Acid Phosphatase
HPLC	High Performance Liquid Chromatography
HREs	Hormone response elements
IC <sub>50</sub>	Concentration of a drug required for 50% inhibition in vitro
IGFR	Insulin growth factor receptor
IMRT	High resolution intensity modulated radiotherapy
i.v.	Intravenous administration
J	Coupling constant ( <sup>1</sup> H-NMR)
leu	Leucine
LH	Luteinizing Hormone
LHRH	Luteinizing Hormone-Release Hormone
LNCaP	Lymph node cancer of the prostate)
m	Multiplet ( <sup>1</sup> H-NMR)
mAR	membrane associated androgen receptor
MAP	Mitogen-Activated protein
MAPK	Mitogen-Activated protein Kinase
MeOH	Methanol
min	minute(s)

Mn	Number-average molecular weight
mol	Moles
mPEG	methoxy poly(ethylene glycol)
MTD	maximum tolerated dose
MTT	3-(4,5-Dimethylthiazol-2-yl)-2,5-diphenyltetrazolium bromide
Mw	Molecular weight
Mw/Mn	Polydispersity Index
NADH	Nicotinamide Adenine Dinucleotide
NADPH	Nicotinamide Adenosine Dinucleotide Phosphate
NaOH	Sodium Hydroxide
NCI	National Cancer Institute
NHS	N-Hydroxysuccinimide
nm	nanometre(s)
NMR	Nuclear Magnetic Resonance
NSCLC	Non small cell lung cancer
N <sub>2</sub>	Nitrogen
OG®	Oregon Green
PBS	Phosphate buffered saline
PC	Prostate Cancer
PC-3	Bone cancer of the prostate cancer
PDI	Polydispersion index
PEG	Poly(ethylene glycol)
PEO	Poly(ethylene oxide)
PGA	Poly(glutamic acid)
PGSE-NMR	Pulsed Gradient Spin Echo-Nuclear Magnetic Resonance
PHPMA	Poly(N-hydroxypropylmethacrylamide)
PIN	Prostatic Intraepithelial Neoplasia
PKA	Protein Kinase A
PK1	HPMA-gly-phenylalanine-leu-gly-doxo copolymer
PK2	PK1 with galactosamine
PLA	Poly(lactic) acid
PLL	Poly(lysine)
ppm	Parts per million
PSA	Prostate-Specific Antigen
PTK	Protein Tyrosine Kinase
p-TSA	p-Toluenesulfonic acid
PTX	Paclitaxel
PTX <sub>COOH</sub>	2'-succinyl-paclitaxel
RES	Reticulo-endothelial system
Rg	Gyration radius
Rh	Hydrodynamic radius
RI	Refractive Index
RT, rt	Room Temperature
s	Singlet (1H-NMR)

SANS	Small Angle Neutron Scattering
SD	Standard error deviation
sec	Second(s)
SEC	Size exclusion chromatography
SEM	Scanning Electron Microscopy
Ser, S	Serinol
SEER	Surveillance, Epidemiology, and End Results
SH2	Src homology domain 2
SH3	Src homology domain 3
SHBG	Steroid Hormone Binding Globulin
SHBGR	Steroid Hormone Binding Globulin Receptor
SMANCS	Styrene-co-Maleic Anhydride-NeoCarzinoStatin
t	Triplet (1H-NMR)
T	Testosterone
TAB	Total androgen blockade
TEGDVE	Tri(ethylene glycol) Divinyl Ether
TEM	Transmission Electron Microscopy
TFA	Trifluoroacetic acid
THF	Tetrahydrofuran
TLC	Thin Layer Chromatography
UV	Ultraviolet

# 1

## General Introduction

## **1.1. PROSTATE CANCER**

### **1.1.1. Introduction**

Worldwide, cancer is the second most common cause of death exceeded only by heart diseases. Cancer death rates are higher in men than in women. The most common cancers in man are prostate, lung and bronchus, colon and rectum, pancreas, liver, leukemia, non-Hodgkin lymphoma, kidney and bladder cancers while the most common cancers in woman are breast, colon and rectum, lung and bronchus, cervix uteri, stomach and ovary cancer. About 12.7 million cancer cases and 7.6 million cancer deaths are estimated to have occurred in 2008 worldwide, with 56% of the cases and 64% of the deaths in the economically developing world<sup>1</sup>.

In economically developed countries, the incidence rates (the number of newly diagnosed cases each year) for all types of cancers are twice as high as in economically developing countries in both males and females. However mortality rates (number of cases or deaths per 100.000 persons per year) in developed countries are only 21% higher in males and 2% higher in females<sup>2</sup>. Incidence and mortality rates were estimated in GLOBOCAN<sup>\*3, 4</sup> by country, using the most recently available data collected at the IARC or available in routine reports from the registries themselves.

Breast cancer is the most frequently diagnosed cancer and the leading cause of cancer death in females worldwide, accounting for 23% (1.38 million) of the total new cancer cases and 14% (458.400) of the total cancer deaths in 2008. Half the breast cancer cases and 60% of the deaths are estimated to occur in economically developing countries. In developed countries, breast cancer death rates have been decreasing during last 25 years as a result of early detection through mammography and improved treatment. In contrast in many African and Asian countries incidence and mortality rates have been rising. Changes in reproductive patterns, physical inactivity and obesity are the main contributory factors in the increased breast cancer<sup>1</sup>.

---

\*GLOBOCAN 2008 data are updated every year. A new set of estimates for 2012 will be made available in 2013 after the publication of CI5 Vol. X.

Lung cancer was the most commonly diagnosed cancer as well as the leading cause of cancer death in males in 2008 globally. Among females, it was the fourth most commonly diagnosed cancer and the second leading cause of cancer death. Lung cancer accounts for 13% (1.6 million) of the total cases and 18% (1.4 million) of the deaths in 2008<sup>1</sup> (Table 1.1. 1). Lung cancer rates are 2 to 5 times higher in developed countries compared with developing countries. The main risk factor of this cancer is the consumption of tobacco.

**Prostate cancer** is in men the second most frequently diagnosed cancer and the sixth leading cause of cancer death in males, accounting for 14% (903.500) of the total new cancer cases and 6% (258.400) of the total cancer deaths in males in 2008<sup>1</sup> (Table 1.1. 1).

**Table 1.1. 1** Estimated new cancer cases and deaths worldwide in 2008.

Estimated New cases		Estimated Deaths	
Male	Female	Male	Female
<b>Lung &amp; bronchus</b>	<b>Breast</b>	<b>Lung &amp; bronchus</b>	<b>Breast</b>
1.095.200	1.383.500	951.000	458.400
<b>Prostate</b>	<b>Colon &amp; rectum</b>	<b>Liver</b>	<b>Lung &amp; bronchus</b>
<b>903.500</b>	570.100	478.300	427.400
<b>Colon &amp; rectum</b>	<b>Cervix Uteri</b>	<b>Stomach</b>	<b>Colon &amp; rectum</b>
663.600	529.800	464.400	288.100
<b>Stomach</b>	<b>Lung &amp; bronchus</b>	<b>Colon &amp; rectum</b>	<b>Cervix Uteri</b>
640.600	513.600	320.600	257.100
<b>Liver</b>	<b>Stomach</b>	<b>Esophagus</b>	<b>Stomach</b>
522.400	349.000	276.100	273.600
<b>Esophagus</b>	<b>Corpus uteri</b>	<b>Prostate</b>	<b>Liver</b>
326.600	287.100	<b>258.400</b>	217.600
<b>Urinary bladder</b>	<b>Liver</b>	<b>Leukemia</b>	<b>Ovary</b>
297.300	225.900	143.700	140.200
<b>Non-Hodgk lymph</b>	<b>Ovary</b>	<b>Pancreas</b>	<b>Esophagus</b>
199.600	225.500	138.100	130.700
<b>Leukemia</b>	<b>Thyroid</b>	<b>Urinary bladder</b>	<b>Pancreas</b>
195.900	163.000	112.300	127.900
<b>Oral Cavity</b>	<b>Non-Hodgk lymph</b>	<b>Non-Hodgk lymph</b>	<b>Leukemia</b>
170.900	156.300	109.500	113.800
<b>All sites but skin</b>	<b>All sites but skin</b>	<b>All sites but skin</b>	<b>All sites but skin</b>
6.629.100	6.028.400	4.225.700	3.345.800

The highest incidence rates worldwide correspond to the developed countries of Oceania, Europe, and North America (Figure 1.1 1) due to the wide utilization of prostate-specific antigen (PSA) testing that detects early stage of prostate adenocarcinoma. In contrast, males of African have the highest prostate cancer mortality rates in the world, which is thought to reflect partly difference in genetic susceptibility<sup>2</sup>. Older age, race (black), high dietary fat and family history remain the well-established risk factors and there are no established preventable risk factors for prostate cancer. Death rates<sup>5</sup> for prostate cancer have been decreasing in last decades in many developed countries, including Australia, Canada, the United Kingdom, the United States, Italy, and Norway in part because of the improved treatment with curative intent<sup>6</sup> and the use of PSA<sup>7</sup> test which help to detect an early prostate cancer stage and consequently the tumor can be treated and cured with higher possibilities than in an advanced stage. However in western countries, incidence and mortality rates are rising in several Asian and Central and Eastern European countries, such as Japan<sup>1</sup>. Also cancer death rates for metastatic diseases have been not changed during last years.

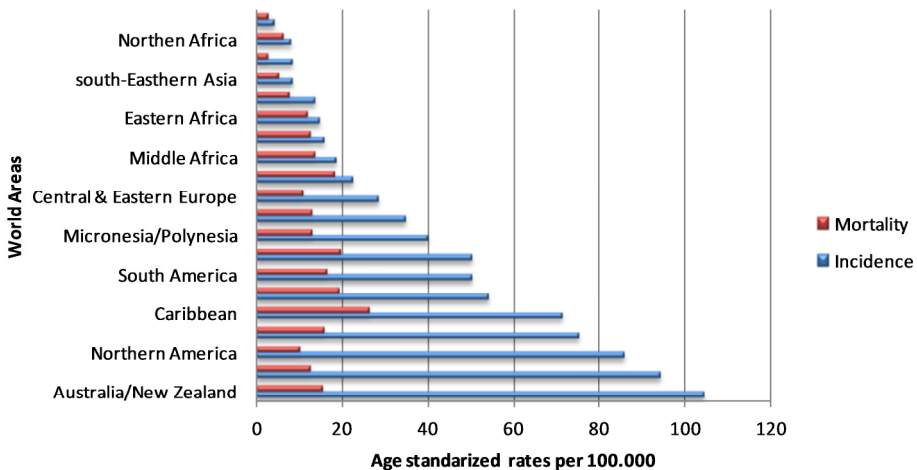


**Figure 1.1. 1** Age-Standardized Prostate Cancer Incidence and Mortality Rates by World Area (adapted from Globocan 2008<sup>1</sup>).

Prostate cancer at early stage covers multiple, very small primary tumors within the prostate where the disease is often curable with rates of more than

90% of men diagnosed, involving treatments such as surgery or radiation and could be disease-free after five years.

Unfortunately, early prostate cancer stage produces few or no symptoms difficulting an early diagnosis and consequently early treatment. Prostate cancer at an advanced stage is mostly metastasized and therefore, the cure is more difficult if not impossible. In most cases, prostate cancer represents a slow growing tumor, taking years to be large enough to be detectable, and even longer to spread beyond the prostate. However, some patients experience aggressive forms of prostate cancer. Unfortunately, up to now it is difficult to predict the aggressiveness of prostate tumors and many researchers are devoting their work in order to identify biomarkers to achieve this goal. The prostate cancer can be metastases outside the prostate such as the seminal vesicle, lymph nodes, the rectum and the bones with the possibility also to reach other organs such as the lungs and liver. Recent approaches such as sentinel node diagnosis throughout PET chemistry are helping to identify metastatic tumor nodes (<http://www.oncovision.es>).

Apart of PSA test, digital rectal exam (DRE) is the second easiest and fastest test to diagnose this disease. However, in order to confirm the presence of a prostate tumor, different tests such as biopsy, computed tomography (CT) and bone scans may be performed. Current treatment for prostate cancer includes surgery, radiation therapy, hormonal therapy, chemotherapy, cryosurgery and high intensity focused ultrasound (HIFU) used alone or in combination. Depending on the stage of the tumor and personal conditions the doctors will offer different treatments. During last decades, the most used treatments for early stage of prostate cancer have been surgery to remove the testicles (orchiectomy) or the use of anti-androgens, GnRHs antagonists or oestrogens as hormonal-therapy, which consist on the reduction of testosterone effects, the main factor to stimulate prostate cancer growth. For example one of the synthetic estrogens classically used in hormonal therapy is diethylstilbestrol (DES). Other antiandrogens such as ketoconazole and megestrol are also used.

Nowadays there is no effective treatment for advanced and/or metastatic prostate cancer. Normally chemotherapy with docetaxel (Taxotere®, made by Aventis Pharmaceuticals, Inc) ([www.taxotere.com](http://www.taxotere.com)) is the anticancer chemotherapy drug in routine 1<sup>st</sup> line clinical used<sup>8</sup> approved by FDA in 2004.



Docetaxel is also used in combination with the steroid prednisone (standard treatment) or with estramustine to treat metastatic prostate cancer. Docetaxel in combination with estramustine improve the survival 20 percent longer than similar patients receiving the standard therapy. However, most patients go off docetaxel due to the poor drug tolerability, limited efficacy and the development of drug resistance. A novel nanoparticle formulation for the delivery of docetaxel named Cellax<sup>9</sup> has been studied and exhibits increased tumor delivery, reduced toxicity and enhanced efficacy in multiple preclinical models, showing promise results<sup>9, 10</sup> for metastatic tumors such as bone metastatic cancer. Bisphosphonates appear to be helpful for many men, whose cancer has spread to the bones<sup>11</sup>, reducing pain and even slowing cancer growth.

The recurrent prostate cancer (when cancer prostate has not been cured or has come back after initial treatment) also seems not to respond to other treatment. Usually is not a good option to use the same treatment used as first therapy. If prostatectomy was the first treatment, radiation therapy may be the best option. If the initial treatment was radiation, radical prostatectomy should be the therapy chosen. Cryosurgery may be an option in both cases. However if metastasis are already present, hormone therapy alone or in combination with chemotherapy is probably the most effective treatment also studies. When cancer is no longer responding to hormone therapy is considered a hormone-refractory prostate cancer (HRPC). Several chemotherapeutics as docetaxel (used as well for metastatic prostate cancer) seems to improve survival by several months. However when tumors have become resistant to docetaxel, the antimetabolic Jevtana® (cabazitaxel) injection ([www.jevtana.com](http://www.jevtana.com)) approved by the FDA in September 2010, is a treatment of option, also used together with prednisone.

Finally it is important to mention PROVENGE® (sipuleucel-T) ([www.provenge.com](http://www.provenge.com)), a vaccine for hormone resistant prostate cancer approved by the FDA in April 2010 as an autologous cellular immunotherapy. Provenge® uses the body's own immune system to fight the disease and can extend survival by several months.

## 1.1.2. Prostate cells

### Prostate gland

The **prostate**<sup>12</sup> is a male sex gland of the male mammalian reproductive system (Figure 1.1. 2). The prostate is a muscular organ that helps produce and store the major components of the seminal fluid and it is mixed with the sperm produced by the testes. It also produces a protein called prostate-specific antigen (PSA) that turns the semen into liquid. The size of the prostate varies with age. In adult men the prostate is about three centimeters long and weighs around twenty grams, similar in size to a walnut, but it can be much larger in older men<sup>13</sup>. It is located in the pelvis and lies at the base of the urinary bladder in front of the rectum and surrounding the urethra. Often the inner part of the prostate keeps growing as men get older and can lead to a common condition called benign prostatic hyperplasia (BPH). In BPH<sup>14</sup>, the prostate tissue can press on the urethra making difficult in urinating, ejaculating and in rare cases defecation. BPH is not cancer and does not develop into cancer but can reach serious medical problem for some men. The treatment then will be the use of medicines, e.g. combination of GHRH antagonist with LHRH antagonist<sup>15</sup>, to shrink the size of the prostate or to relax the muscles within it for helping the pass of the urine and semen. Sometimes some type of surgery, such as a transurethral resection of the prostate (TURP) may be needed.

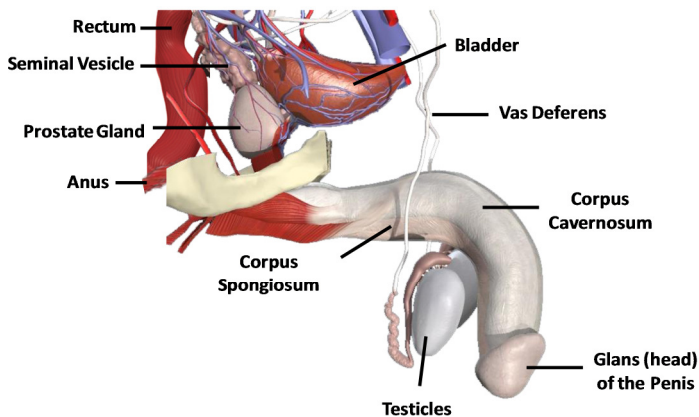


**Figure 1.1. 2** Illustration showing the prostate and the nearby organs (Images formed in [www.anatomy.tv](http://www.anatomy.tv)).

For the correct function of the prostate gland, androgens<sup>16</sup> such as testosterone (Figure 1.1. 3), are required. Testosterone is mainly secreted in the testes, but adrenal glands can also produce it in small amounts.

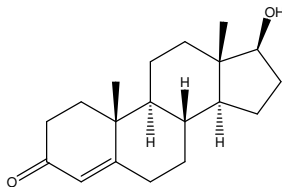


**Figure 1.1. 3** Molecular structure of testosterone.

Testosterone is essential for health and well-being<sup>17</sup> as well as the prevention of osteoporosis<sup>18</sup>. In adult human female bodies this steroid hormone is also produced but typically ten times less than in males. On the other hand, females are more sensitive to this hormone. Androgens are also responsible for hair growth<sup>19</sup>, the muscle volume and bone mass, and for controlling the development of male features. Androgens are also the original anabolic steroids and the precursor of all estrogens, the female sex hormones. However one of the major risk factors<sup>17</sup> to cause prostate cancer is the amount of testosterone which helps on prostate cancer growth. Androgen ablation is then, the more effective therapy in prostate cancer<sup>20</sup>.

### 1.1.3. Origin of Prostate Cancer

In normal prostate cells the androgen receptors, localized in the nucleus, are waiting for testosterone or dihydrotestosterone, DHT, to cause cell growth and divide itself. The production and use of testosterone is the only one of several hormones that the body manufactures that affects the prostate. In prostate cancer, cells require the presence of testosterone or DHT to promote growth and reproduction, playing an important role in all phases of prostate cancer. Laboratory and clinical studies indicates that prostate cancer is the result of a combination of mainly three factors: genetics, carcinogens and testosterone. Many men present a genetic predisposition for having prostate cancer caused by a hereditary factor or because the presence of carcinogens in the environment (heavy metals, such as lead, arsenic and mercury in the water

supply). But it is unlikely that these factors alone would be enough without the presence of testosterone.

Prostatic Intraepithelial Neoplasia (PIN)<sup>21</sup> is believed to be the first sign of prostate cancer. When PIN appears in prostate cells it is possible to distinguish differences between healthy cells and those that have PIN. However, PIN does not exhibit uncontrolled cells growth and reproduction but if the presence of genetics<sup>22</sup> or carcinogens combined with testosterone continues, they trigger a mutation process from PIN to prostate cancer. Mutation is a disturbance in the genetic material<sup>23</sup> of the cells, from chemical actions of carcinogens or hereditary defects from the parents, thus leading to an abnormal growth and uncontrolled reproduction, which ultimately results in prostate cancer. Once prostate cancer starts the mutations can continue develop to advance stages and even metastases to other parts of the body, but usually the development of prostate cancer takes many years as this disease is considered to be a slow growing tumor type. Metastasis occurs during advanced prostate cancer and it refers to prostate cancer cells that have left the prostate gland to reach other organs of the body, (Figure 1.1. 4) usually, bones and lymph nodes but also, lung and liver are the second most common organs to be associated with metastasis of prostate cancer.

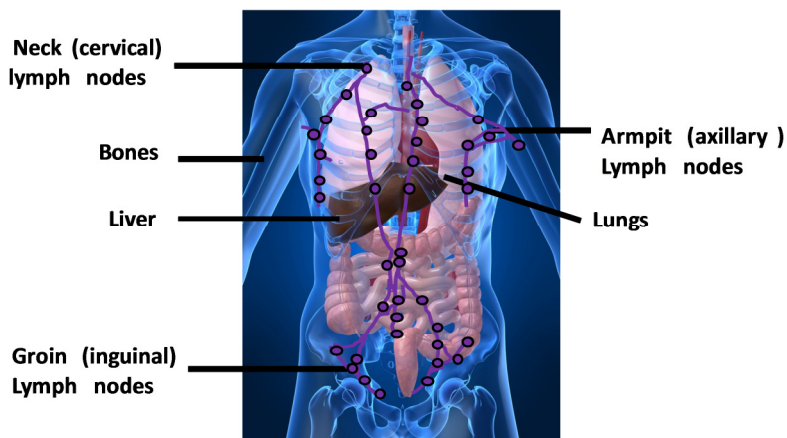


**Figure 1.1. 4** Illustration showing the different organs where usually prostate cancer cells can metastasize. Picture provided and adapted from the Office Online Clip Art and Media.

### 1.1.3.1. Biosynthesis of the testosterone

Testosterone is derived from cholesterol<sup>24</sup> (Figure 1.1. 5). In the first step in the biosynthesis of testosterone, a mitochondrial cytochrome P450 (CYP11A) oxidize cholesterol loses six atoms of carbon to produce pregnenolone. Then two more carbon atoms are eliminated by an endoplasmic reticulum enzyme (CYP17A) to yield different steroids of nineteen carbons.<sup>25</sup> The 3-hydroxyl group is then oxidized by 3-  $\beta$ -HSD to obtain androstenedione which in last step is reduced by 17- $\beta$  hydroxysteroid dehydrogenase to yield testosterone.

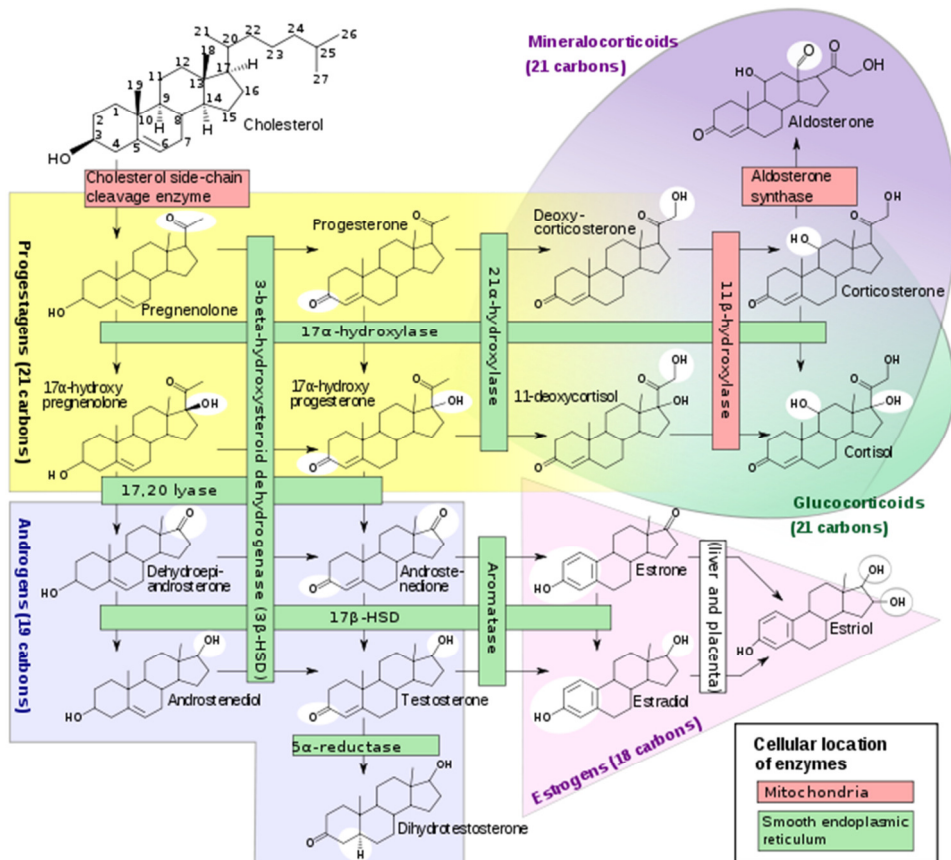


**Figure 1.1. 5** Biological process of steroids synthesized from cholesterol (Picture taken from Walter<sup>26</sup> *et al.* Medical Physiology: A Cellular and Molecular Approach, 2003).

Therefore, the products generated by human steroidogenesis include androgens (testosterone), estrogens, progesterone and corticoids (cortisol and aldosterone). Testosterone is produced in Leyding cells also called interstitial cells of Leyding in the testicles, which produce testosterone in presence of luteinizing hormone (LH). LH regulates the expression of 17- $\beta$  hydroxysteroid dehydrogenase<sup>27</sup>.

### **1.1.3.2. Metabolism of the testosterone**

Testosterone metabolism involves the reduction of approximately 7% of the testosterone to 5 $\alpha$ -dihydrotestosterone (DHT) by the cytochrome P<sub>450</sub> enzyme 5 $\alpha$ -reductase, and then 0.3% converted into estradiol by aromatase enzyme (CYP19A1)<sup>28</sup> expressed in the brain, liver, and adipose tissues<sup>19</sup>.

DHT is produced in the adrenal cortex and is a more potent metabolite than the parent testosterone due to its greater affinity for the androgen receptor.

A feedback loop involving the testicles, the hypothalamus, the pituitary, the adrenal, and the prostate glands regulates the blood levels of testosterone and DHT (Figure 1.1. 6). Low levels of DHT triggers the production of gonadotropin releasing hormone (GnRH) by the hypothalamus. GnRH then stimulates the pituitary gland to produce follicle-stimulating hormone (FSH) and luteinizing hormone (LH), which stimulate the testicles to produce testosterone. Testosterone from the testicles and dehydroepiandrosterone from the adrenal glands stimulate the prostate to produce more DHT.

High levels of testosterone suppress the release of GnRH and FSH/LH from the hypothalamus and pituitary glands thus providing a negative-feedback control of hormone levels. Hormonal therapy in prostate cancer patients can decrease the levels of DHT by disrupting this pathway at any point.

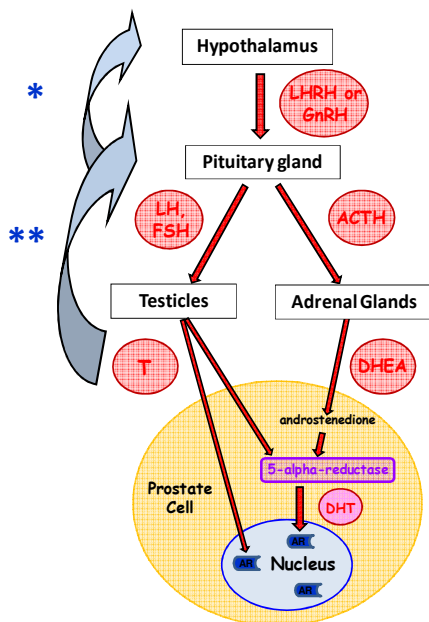


**Figure 1.1. 6** Scheme of the feedback loop involving the testicles, the hypothalamus, and the pituitary glands. Estrogen forms a negative feedback loop \*by inhibiting the production of GnRH in the hypothalamus and \*\*by inhibition of LH or FSH production in the pituitary gland.

Different factors are involved in the released levels of testosterone. Loss of dominance, advance age<sup>29</sup>, zinc deficiency, alcohol consumption, hypogonadism (deficiency of functional activity of the gonads decrease testosterone levels but rapid eye movement in sleep (REM sleep) resistance training and power motivation are some of the factors which produce an increase in testosterone levels.

### 1.1.3.3. Androgen receptor (AR) and pathways involved in proliferation and apoptosis

The AR pathway is a well-established target for treating prostate cancer. To improve its ability to treat advanced prostate cancer it is very important to perfectly understand the pathways involved in AR signaling and their capability of being activated during the androgen insensitive state.

The AR, also known as NR3C4 (nuclear receptor subfamily 3, group C, member 4), is a 110 kD nuclear receptor. AR is very important for the maintenance of male reproductive organs<sup>30</sup> as for the prostate gland. AR is activated by binding testosterone or DHT<sup>31</sup> present in the cytoplasm and translocating them into the nucleus. Once there, the T-receptor or DHT-receptor complex binds directly to specific nucleotide sequences of the chromosomal DNA. The areas of binding are called hormone response elements (HREs), and influence transcriptional activity of some genes, triggering androgen effects. The androgen receptor is very similar to the progesterone receptor; even at high doses of progestins<sup>32, 33</sup> the androgen receptor can be blocked.

AR activation occurs by three main mechanisms (Figure 1.1. 7):

- (1) By the non-genomic pathway<sup>34</sup>, androgen (testosterone or DHT) freely passes through the membrane bi-layer and binds to the cytoplasmic AR<sup>35, 36</sup>. Bound AR translocates to the nucleus, then binds to a DNA response element on a promoter of an androgen responsive gene and stimulates transcription.
- (2) Bound AR interacts with the SH3 domain of the tyrosine kinase c-Src to activate the MAPK pathway and influence AR-mediated transcription via phosphorylation<sup>37</sup> of coactivator/receptor complexes.
- (3) Androgen bound to the steroid hormone binding globulin (SHBG) can activate the SHBG receptor (SHBGR) and lead to an increase in PKA activity. PKA may influence AR-mediated transcription via alteration of phosphorylation status of AR and AR co-regulators.



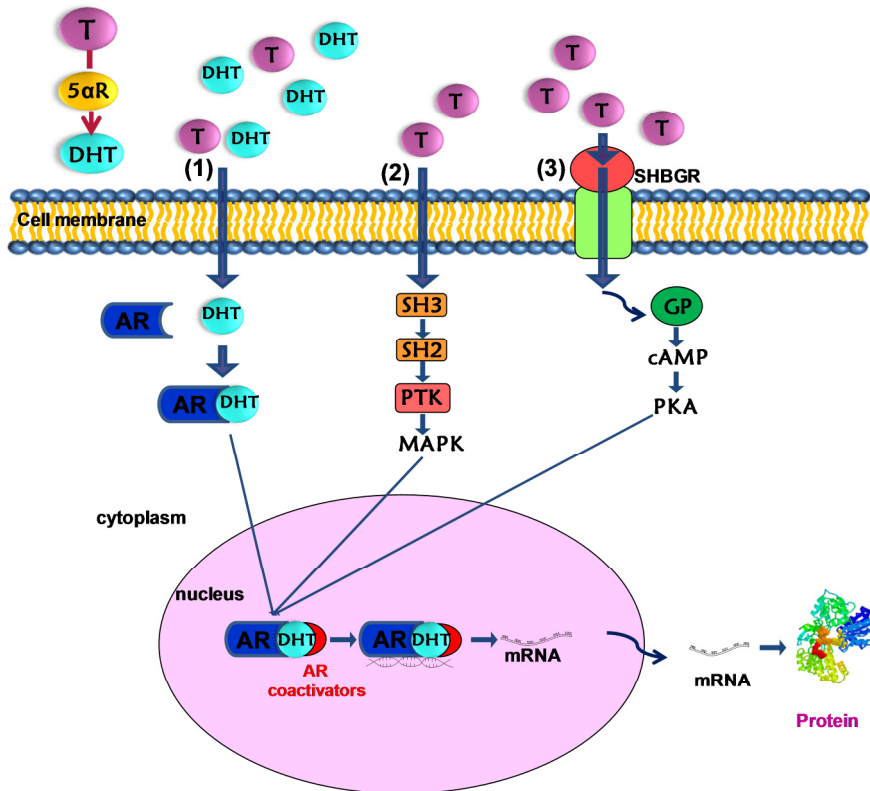


**Figure 1.1. 7** Molecular pathways of androgen action adapted from Foradoni et al <sup>38</sup>.

Androgens can also interact with intracellular calcium regulatory mechanisms, via a rapid change in  $[Ca^{2+}]_i$ . Calcium modulation is a rapid response, occurring within seconds to minutes, where the androgen binds to a receptor at the surface of the cell to achieve this (Figure 1.1. 8). Not all cell types that demonstrate a rapid androgen response express the classic nuclear AR or are blocked by AR antagonists. Therefore, it is not yet known whether the receptor located at the cell surface is the classic intracellular AR coupled to signal transduction machinery located in the membrane or, by a unique protein, capable of binding androgen and initiating signal transduction cascades.

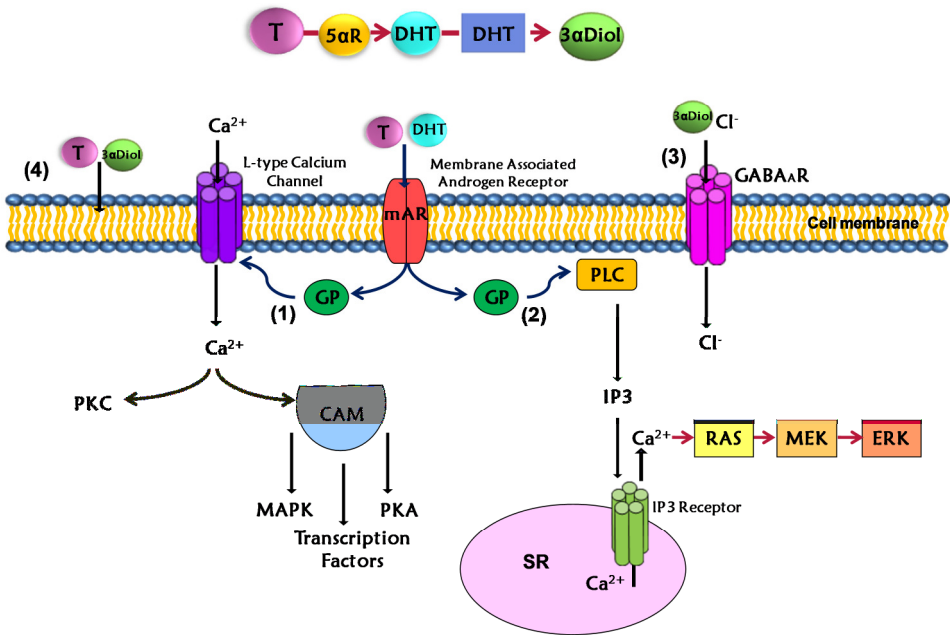


**Figure 1.1. 8** Non-genomic androgen actions via changes in intracellular ion concentrations and membrane fluidity. Figure adapted from Foradoni et al.<sup>38</sup>

From Figure 1.1. 9 it is possible to observe the actions of androgens via changes in ion concentrations in the membrane and its fluidity<sup>38</sup>. 1) Androgen interacts with a membrane associated androgen receptor (mAR) leading to the activation of L-type calcium channels through some type of inhibitory g-protein (GP). This increase in intracellular calcium can lead to activation of PKC, and via calmodulin (CAM) activates PKA and MAPK pathways, ultimately influencing gene transcription through phosphorylation<sup>38</sup>. 2) Androgen interacts with a membrane associated androgen receptor (mAR) leading to modulation of g-protein activity and subsequent activation of phospholipase C (PLC). These resulting increases in IP3 lead to the release of intracellular calcium stores from the sarcoplasmic reticulum (SR), and consequently the activation of the RAS/MEK/ERK pathway<sup>38</sup>. 3) DHT metabolite (3 $\alpha$ -Diol) may interact with the GABA<sub>A</sub> receptor and lead to increases in intracellular calcium and thus membrane potential. 4) Testosterone and its metabolites can interact with phospholipids in the

membrane bilayer to change membrane flexibility and subsequently alter the function of sodium/potassium ATPase and calcium ATPase<sup>38</sup>.

#### **1.1.3.4. Examples of therapeutic targets in the AR pathway and the site of action of different drugs to treat prostate cancer<sup>39</sup>.**

Therapeutic targets of the AR<sup>40</sup> pathway are shown in Figure 1.1. **9, 1)** AR bind chaperonin HSP90 molecule to avoid AR degradation caused by the presence of 17-AAG, HSP90 inhibitors, decreasing AR levels. **2)** Men treated with LHRH agonists may reduce testosterone levels but still some androgens can be synthesized by adrenal glands and intratumorally. Both can be inhibited by ketoconazole (synthetic estrogen) a non-specific p450 inhibitor and abiraterone (LHRH agonist), a 17-lyase inhibitor. **3)** Testosterone (by the action of the enzyme 5 $\alpha$ -reductase) is converted to DHT, which has a greater affinity for AR than testosterone. Finasteride and dutasteride (anti-androgenic drugs) can inhibit 5 $\alpha$ -reductase. **4)** DHT-AR ligands can be inhibited by antiandrogens such as bicalutamide and novel agents MDV-3100<sup>41</sup> and BMS641988. Mutation of AR as well as AR over expression can convert endogenous steroids (progestins, estrogens, corticosteroids, etc.) and some antiandrogens into agonists. MDV-3100 was designed to suppress AR function even when AR is over expressed. **5)** Activation of receptor HER2 tyrosine kinases to activate AR. Two kinases directly phosphorylate AR on tyrosine, Ack1 and SRC. Other pathways of receptor tyrosine kinases, including AKT and Mitogen-activated protein (MAP) kinase pathways are also implicated. Antibodies such as trastuzamab and pertuzumab and small molecular TKI inhibitors such as erlotinib and lapatinib target HER2. Dasatinib target SRC. **6)** The transcription of AR target genes requires the chromatin state. This transcription can be inhibited by HDAC inhibitors through the disruption of the chromatin structure and inhibition of recruitment of coactivators and RNA polymerase II.

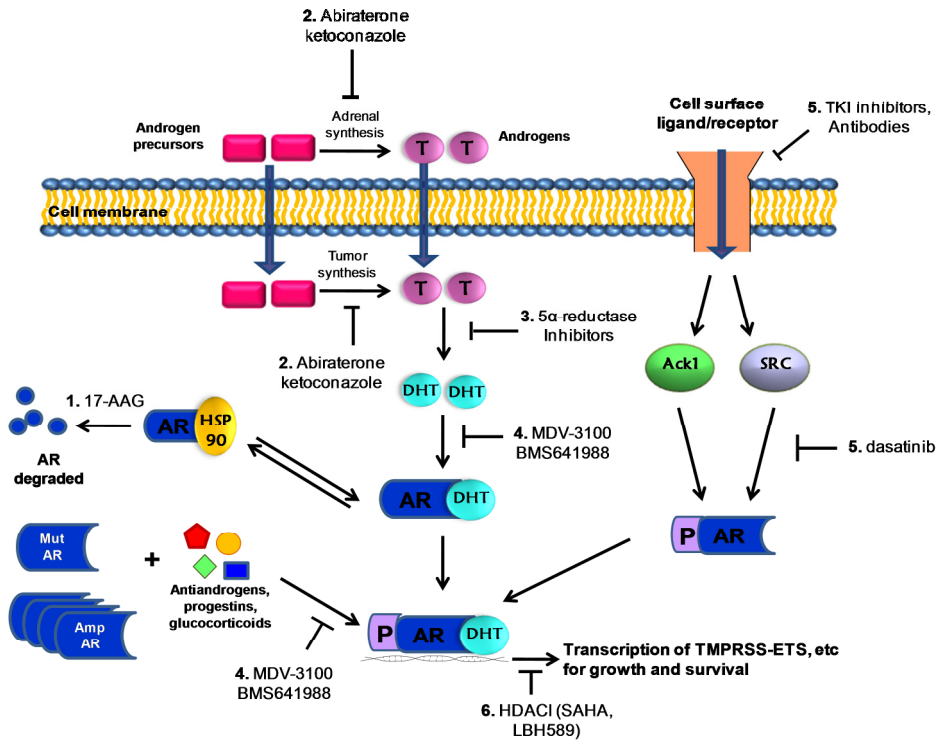


**Figure 1.1. 9** Molecular pathways of androgen action. Adapted from Ref. 40.

Around 200 compounds are currently being tested in clinical trials for treatment of advanced prostate cancer. These drugs could be used alone or in combination with cytotoxic agents<sup>42</sup>. The identification and knowledge of new pathways is essential for progress in developing efficient and suitable treatments for disease. The compounds show the efficacy of targeting prostate cancer cells. They include inhibition of pathways by kinases (phosphatidylinositol 3-kinase (PI3K), Akt, mTOR) and epidermal growth factor receptor (EGFR), platelet-derived growth factor receptor (PDGFR), insulin growth factor receptor (IGFR), Her2/Her3), immunological approaches, novel cytotoxic compounds and targeting of important cellular processes such as angiogenesis, apoptosis, vitamin D metabolism, differentiation and stem cell biology<sup>43</sup>.

### 1.1.4. Diagnosis of prostate cancer and stage determination

Due to the absence of symptoms it is very difficult to diagnose an early-stage prostate tumor. Possible symptoms to consider are burning urination, dysfunction erectile, or pain or stiffness in the lower back, hips or upper thighs or a general bone pain. However, these symptoms can also indicate the presence of other male disorders. As it was said above, DRE and PSA are considered routine biomarkers to allow early prostate cancer diagnosis and therefore are recommended an annual exam in men over 50. PSA is a specific type of protein which in the presence of prostate cancer, increases in the blood levels and makes it a valuable tool in detecting early stage prostate cancer. PSA levels provide information about the tumor size and aggressiveness depending on PSA value changes with time. However, high PSA levels does not necessarily indicate the presence of cancer because it could be caused by other diseases such as prostate inflammation, urinary retention, prostate infection, benign prostatic hypertrophy (BPH) or prostate manipulation. Therefore, in order to avoid a false positive, biopsies and x-ray analysis are also performed. Once prostate cancer is diagnosed it is crucial to determine the cancer stage. There are three main parameters to determine the extent and severity of cancer Grade (Gleason Score<sup>44</sup>), Stage and PSA (mentioned above) in order to select the best therapy for a patient. Aggressive tumors will have a higher Gleason score and consequently a worse prognosis To determine the Gleason Score, the pathologist identifies with a grade the most common tumor pattern (for example grade 2) and the next common tumor pattern with a second grade (for example 3). These two grades will indicate the Gleason score (2+3=5) also called Gleason sum<sup>45</sup>. The Gleason grade ranges from 1 to 5 (Figure 10). Bigger grades are associated with cells that have spread out, losing their glandular architecture and therefore, corresponding to the worst prognosis.

The **Gleason Score** (Figure 1.1. 10) shows the degree of abnormal microscopic appearance of the prostate cells helping in the selection of an adequate therapy depending on the grade of the tumor.

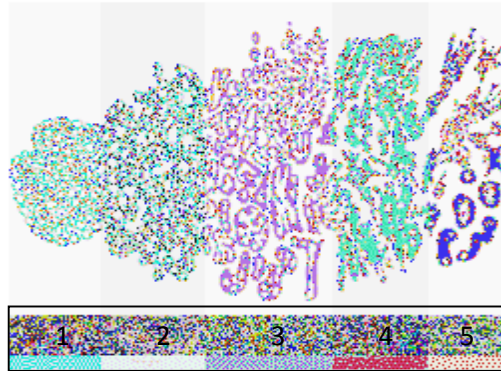


**Figure 1.1. 10** An updated version of Dr. Gleason's simplified drawing of the five Gleason grades of prostate cancer<sup>46</sup>.

Early prostate cancer with a Gleason Grade of 1 or 2 is not believed to be very dangerous. Tumors tend to grow slowly and tend to remain in or around the prostate. But in prostate cancer, cells mutate until possible invasion of other tissue in the body acquiring a Gleason Grade of 4 or 5. High-grade tumors tend to grow quickly and are more likely to spread beyond the prostate.

Other current diagnosis parameters to classify the tumor is the TNM Staging, evaluation of the tumor (T), evaluation of the regional lymph nodes (N), and evaluation of distant metastasis (M) described in detail in appendix 1.

### 1.1.5. Current Prostate Cancer Treatments

There are a wide variety of treatments of prostate cancer available depending on the stage of the disease at the time is diagnosed. Treatments include either single therapy or combinations of surgery, radiation therapy, hormone therapy and/or chemotherapy. However, the type of treatment given is influenced by different factors for example the patient's age and its general health of the patient<sup>47</sup>. There are different treatments options which are currently in the market, such as: active surveillance, surgery, radiotherapy, cryotherapy, ultrasound, hormonal therapy, chemotherapy and other treatments as treating bone pain, angiogenesis inhibitors and prostate cancer vaccines.

In Figure 1.1. 11 is shown the most accepted protocol to follow with prostate cancer patients. 1) When prostate cancer is found to be localized in the prostate gland, the first possible treatment is radical prostatectomy<sup>48, 49</sup> and/or radiation therapy (external beam, radioactive seeds or combination of both). 2) However, 20-40% of cancers relapse<sup>50</sup> and it may be coming back. Then, hormone therapy would be the best option to reduce PSA levels. 3) If PSA levels start to rise it could be that cancer is hormone refractory and does not respond to hormone treatment or gets worse while being treated with hormone therapy. In addition, if the cancer has spread outside the prostate gland, metastatic or already considered advanced tumor can reach other parts of the body, preferentially bones. If the patients have few or no prostate cancer pain-related symptoms, the therapy chosen could be immunotherapy such as PROVENGE. But patients who have significant cancer-related pain, chemotherapy should be an option. 4) If last treatments are not effective, after one type of chemotherapy, different chemotherapeutic agents or different endocrine therapy (e.g. androgen deprivation) are then the options.

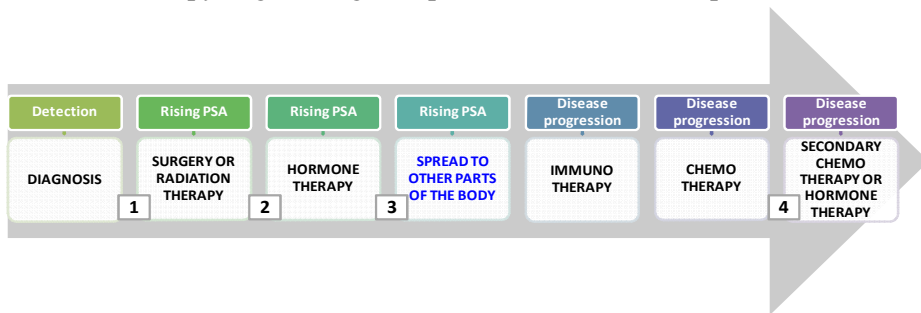


**Figure 1.1. 11** Treatments usually administered in the progression of prostate disease.

### 1.1.5.1. Active surveillance

Active surveillance<sup>51</sup> (no treatment) is the best option when the tumor presents a slow growth and the patient is of advanced age or suffer from other life-threatening conditions. This is often called active monitoring or watchful waiting, which involves monitoring the prostate cancer for signs of any variation in the tumor.

### **1.1.5.2. Surgery**

It is the most successful strategy for healthy men (usually, those under 70) with localized disease. The most common technique is a radical prostatectomy<sup>52</sup>. From the 1980s a better understanding of the periprostatic anatomy has unleashed an improvement on the surgical technique. The preservation of the cavernous nerves made possible to maintain the sexual function (40%-65% of men).

### **1.1.5.3. Radiation therapy for advanced or recurrent Prostate Cancer**

This therapy uses radiation to destroy cancer cells and can be very effective as primary treatment for localized prostate cancer. Radiation therapy<sup>52</sup> is the preferred treatment when cancer has spread to adjacent tissue and is also used in advanced cases to relieve pain from the spread of cancer to bones. Incontinence and impotence also occur with radiation and some studies have shown similar results to surgery. Recent advances allow doctors to target prostate cancer cells more precisely and with a higher dose of radiation and lower side effects while improving effectiveness.

### **1.1.5.4. Cryotherapy**

Cryotherapy involves freezing the prostate with liquid nitrogen or argon gas in order to destroy cancer cells. This treatment may be used when the prostate cancer is refractory or recurrent<sup>53</sup> but has not been widely adopted because freezing can damage the rectum or the urethra. Sexual function is also more affected than with other treatments.

### **1.1.5.5. High-intensity focused ultrasound (HIFU)**

HIFU destroys cancer cells by heating them with highly focused ultrasonic beams. This treatment<sup>54</sup> is not commonly used in the United States but is a technique frequently used in Europe. After treatment, most men experience a degree of incontinence but usually regain complete urinary control and/or impotence.



### **1.1.5.6. Hormonal Therapy**

As it has been mentioned above, in most cases prostate cancer progression depends on male hormone levels, such as testosterone. Therefore, endocrine therapy is typically the treatment employed in advanced prostate cancer, but it can also be used to shrink larger tumors thus facilitating the effect of some treatments such as radiation. The most common side effects when using hormones as treatment are nausea, diarrhea, loss of sexual interest, impotence, and fatigue. Hormone therapies are also increasingly used in combination with radiation therapy or surgery<sup>55</sup> (for more detailed information about combination therapy see introduction chapter 5).

As it was already mentioned, testosterone is the most important factor involved in prostate cancer growth. Bearing this in mind, there is a clear rationale to treat prostate cancer even before it occurs. It is possible to reduce testosterone levels by altering the diet, reducing the consumption of raw animal fat (e.g. in red meat) or by increasing the consumption of phyto-estrogens (available from vegetables as soy products), which mimic the activity of the female hormones. Different forms of hormonal therapy are currently being administered, namely: orchiectomy (surgical castration), anti-androgens, LHRH agonists<sup>56</sup> and antagonists, and the use of estrogens as androgen-suppressing drugs (Figure 1.1. 12).

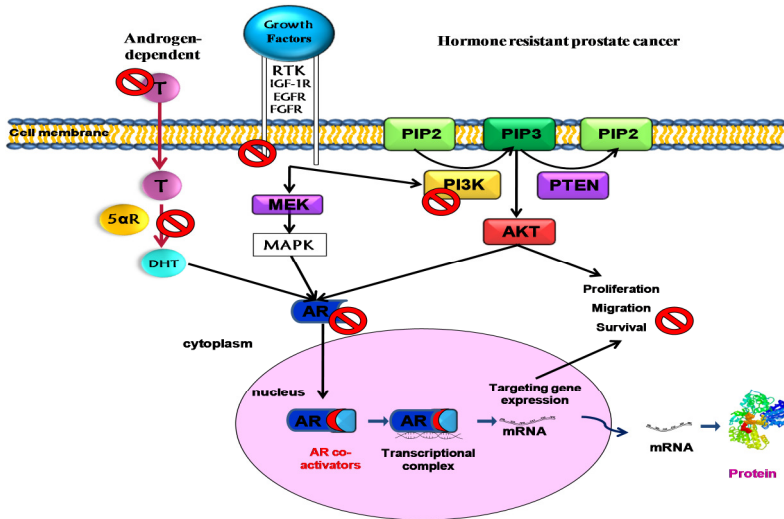


**Figure 1.1. 12** Different mechanisms showing how hormonal therapy works in order to destroy prostate cancer cells.

There are mainly two objectives in working with hormones, 1) Reducing further mutations of the cancer cells, and 2) Stopping their growth and duplication.

#### 1.1.5.6.1. Orchiectomy<sup>57</sup>

Orchiectomy<sup>57</sup> involves the pharmacological removal of the testicles used as the standard hormone therapy for prostate cancer. Because orchiectomy is an efficient, cost-effective and convenient method of reducing testosterone it is still an option for certain patients, particularly men at advanced age. Diethylstilbestrol (DES) was the first drug used as an alternative to surgical orchiectomy.

#### 1.1.5.6.2. Anti-androgens

They block the production of any androgen in the body, even from adrenal glands after orchiectomy or during treatment with LHRH analogs. Flutamide (Eulexin®), bicalutamide (Casodex®)<sup>58</sup>, and nilutamide (Nilandron®) ([www.nilutamide.com](http://www.nilutamide.com)) (Figure 1.1.13), are known as anti-androgens<sup>59</sup> and are orally taken daily for a duration of

three years. Normally they are used in combination with surgery or other hormonal therapies, typically orchiectomy or an LHRH analog. This type of therapy can also be used as radiation therapy sensitizer by giving it approximately two months before. BMS-641988 (Figure 1.1. 13) is a small anti-androgen molecule that binds to the AR, inhibiting its transcriptional activity. This drug showed an increased potency compared with the standard bicalutamide. MDV3100 (Figure 1.1. 13) is another experimental AR antagonist currently in Phase 3 clinical trials<sup>60</sup>. As opposed to bicalutamide, MDV3100 does not promote translocation of AR to the nucleus and avoids binding AR to DNA and AR to coactivator proteins<sup>61</sup>.

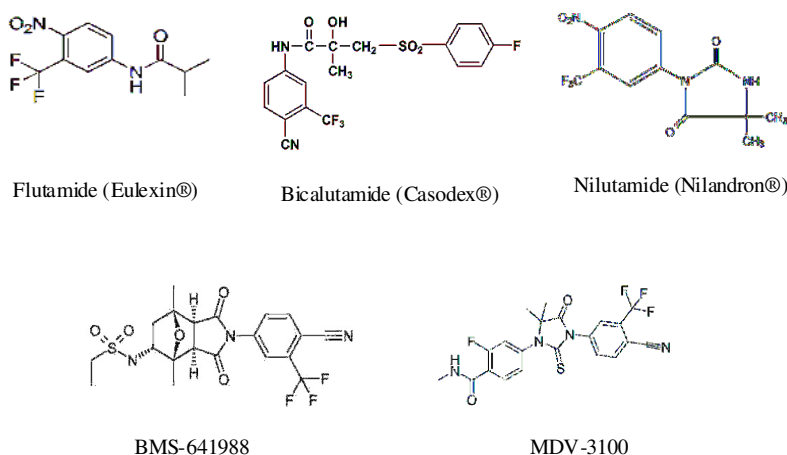
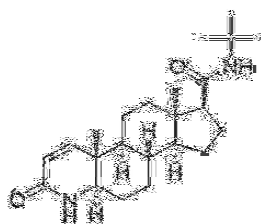
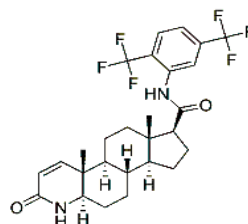


**Figure 1.1. 13** Anti-androgens molecules used for the treatment of Prostate Cancer (PCa). The anti-androgen sits in the AR and prevents the interaction of testosterone (T) and DHT with the AR (target).

Finasteride (Proscar® or Propecia®) and Dutasteride (Avodart®) (Figure 1.1. 14) are also anti-androgenic drugs but in this case they inhibit the enzyme 5- $\alpha$  reductase, blocking the conversion of testosterone to its more biologically active form, DHT. Dutasteride inhibits both isoforms of 5- $\alpha$  reductase, Type I and Type II, whereas finasteride only inhibits Type II. Both drugs decrease prostate volume similarly with greater improvements in symptom score for dutasteride but not statistically significant.



Finasteride (Proscar®)



Dutasteride (Avodart®)

**Figure 1.1. 14** Anti-androgens molecules used for the treatment of PCa inhibiting the enzyme 5- $\alpha$ -reductase.

### 1.1.5.6.3. Luteinizing hormone-releasing hormone (LHRH) agonists or LHRH analogs

This is a therapy chosen for most men as an alternative to the orchiectomy. LHRH (Figure 1.1. 15) agonists also known as gonadotropin releasing hormone (GnRH), block the release of LHRH, through the process of downregulation after an initial stimulation effect. These drugs reduce testosterone levels similar to the orchiectomy, and for this reason are considered as a chemical castration. The most common way of administering LHRH agonist is a subcutaneous implant such as polymeric depots that allow controlled release of the hormone.

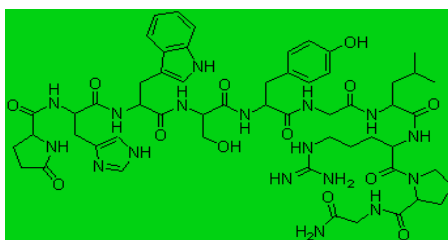
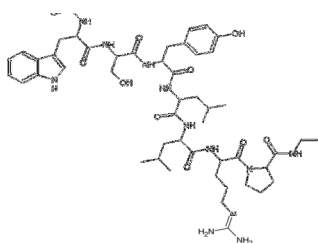


**Figure 1.1. 15** Luteinizing hormone molecule (Glp-His-Trp-Ser-Tyr-Gly-Leu-Arg-Pro-Gly-NH<sub>2</sub>).

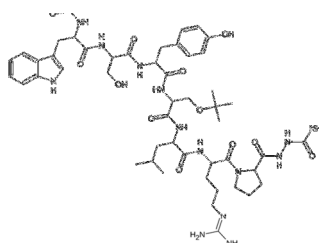
LHRH analogs (Figure 1.1. 16) include leuprolide (Lupron®, Viadur®, Eligard®), goserelin (Zoladex®, described below), triptorelin

(Trelstar®), and histrelin (Vantas®) and are administered by regular injections ranging from once a month to once a year. If these treatments are used instead of surgery, these drugs must be administered regularly for life. A disadvantage of this therapy is that it causes a testosterone spikes during several days before the suppression takes effect, this phenomenon is called flare effect (also it can be called hormone flare or tumor flare). This effect can be extremely dangerous in patients who have advanced stages of prostate cancer and bone metastasis.

Zoladex® is one of the most successful anticancer drug delivery system. It is used for the treatment of prostate cancer presenting a polymer depot formulation for GnRH (LHRH) analogues<sup>62</sup>. Currently is also being studied to treat other cancers as breast adenocarcinoma. AstraZeneca (ICI) workers in 1971 isolated the peptide hormone GnRH (discovered in 1968) and began analogue synthesis. Those GnRH analogues resulted to be more resistance to degradation and could block the action of the hormone. Originally, Zoladex® was thought to promote fertility, however it was observed that Zoladex inhibited the estrogen and androgen secretion acting as GnRH antagonist, and therefore with possibility to act as a potent antitumor agent.



Leuprolide (Lupron®, Viadur®, Eligard®)  
p-Pro-His-Trp-Ser-Tyr-D-Leu-Leu-Arg-Pro-NHEt



Goserelein (Zoladex®)  
p-Glu-His-Trp-Ser-Tyr-D-Ser(tBu)-Leu-Arg-Pro-AzaGly-NH<sub>2</sub>

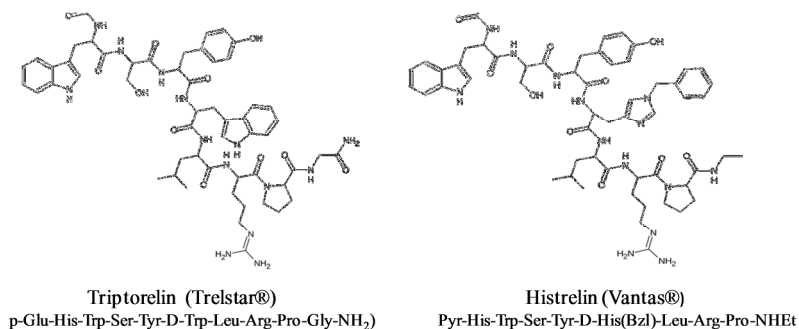


**Figure 1.1. 16** LHRH analogs administered to treat PCa.

Zoladex<sup>®</sup> was found then 100-200 more potent than the natural hormone due to the high affinity for its receptor and resulted to be more stable in vivo due to the increased residence time,  $t_{1/2}$  for Zoladex was 4.5h in contrast to GnRH which is degraded rapidly with  $t_{1/2}$  of 10 min. GnRH was released in small pulses every 90 min causing permanent receptor down regulation. For this reason a depot formulation was study and a rod system with 1cm length and 1mm of diameter (Figure 1.1. 17) was designed, which also reduced the need of repeated injection and allow local delivery. The effective dose of Zoladex<sup>®</sup> administration was 3.6mg and the depot last 28days obtaining a significant effect on PCa prostate cancer growth.

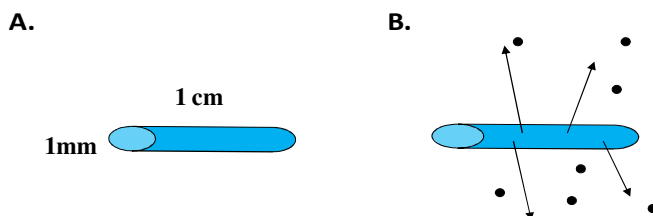


**Figure 1.1. 17** A. Dimensions of the rod polymer depot formulation of Zoladex<sup>®</sup> and B. schematically representation of drug delivery once is diffused into the cell.

The polymers used to synthesize this small rod were poly D, L lactide-co-glycolide, PLGA, (50:50), chosen as it is a FDA approved polymer, therefore clinically safe (as biodegradable sutures).

This polymer was designed to internalize and deliver the drug by controlled diffusion. This polymer depot formulation for local delivery presents some advantages, as it can be positioned after surgery and used as a controlled release (CR) depot, offering good patient compliance. However, this type of technology also presents limitations in case of metastatic disease, the drug loading is low, therefore it is necessary a non immunogenic potent drug entrapped in a biodegradable polymer.

Abiraterone (Figure 1.1. 18) is a new drug, a steroidal cytochrome P450 17 $\alpha$ -hydroxylase-17,20-lyase inhibitor (CYP17), and is currently undergoing phase II clinical trials as a potential drug for the treatment of androgen-dependent prostate cancer. CYP17<sup>63</sup> enzyme is necessary in the body to secrete many hormones such as androgens including testosterone. In preclinical studies, Abiraterone has demonstrated the ability to selectively inhibit the target enzyme (IC<sub>50</sub>=4nM for hydroxylase), resulting in inhibition of testosterone production in both the adrenals and the testes shrinking the tumors and also lowering PSA levels. Clinical studies demonstrated that CYP17 blockage by abiraterone acetate is safe and has significant antitumor activity in CRPC (castration-resistant prostate cancer).

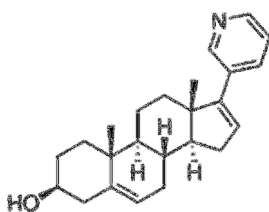


**Figure 1.1. 18** Molecule of Abiraterone, a LHRH analog used for the treatment of PCa by blocking the enzyme CYP17 which secretes testosterone.

LHRH agonists and anti-androgens are often prescribed together, as a combination therapy.

#### 1.1.5.6.4. **Luteinizing hormone-releasing hormone (LHRH) antagonists**

LHRH antagonists suppress the production of LH directly. These drugs are able to reduce testosterone levels more rapidly than LHRH agonists and do not cause the flare effect. However, those drugs are less often prescribed because they can cause a severe allergic reaction in some men.

Abarelix (Plenaxis®) (Figure 1.1. 19) was the first antagonist to be described although was removed from the market in 2005. Degarelix (Firmagon®) (Figure 1.1. 19) is another LHRH antagonist, which also reduces testosterone levels and was approved by the FDA in 2008 to treat advanced prostate cancer. It is monthly administered subcutaneously.

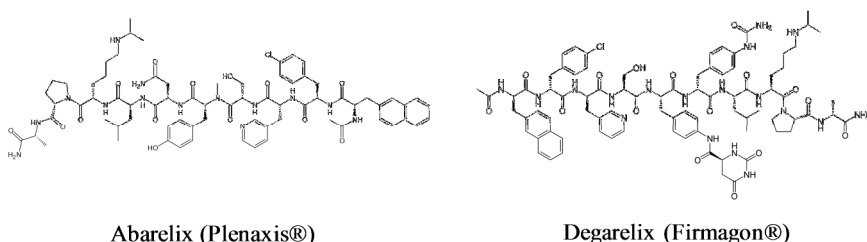


**Figure 1.1. 19** LHRH antagonists administrated to treat PCa.

#### 1.1.5.6.5. **Combination Therapy Strategies**

In the treatment of PCa, the most common method of treatment is to administer one, two or three drugs in combination, e.g. an LHRH agonist or antagonist with an anti-androgen, which may also be combined with a 5-Alpha-Reductase Inhibitor. The drug combinations reduce the levels of testosterone from the normal range of 200 ng/ml to less than 20 ng/ml. In normal prostate cells, the human body controls the production of testosterone as it was shown in Figure 1.1. 6 where is possible to observe the different and possible steps for blocking the pathway for testosterone production.

However, cancer cells can induce resistance to the first line of hormone therapy (Figure 1.1. 20A) and can survive on very low levels. Then, a



second line tactic (Figure 1.1. 20B) should be employed, using androgen blockade or estrogens.

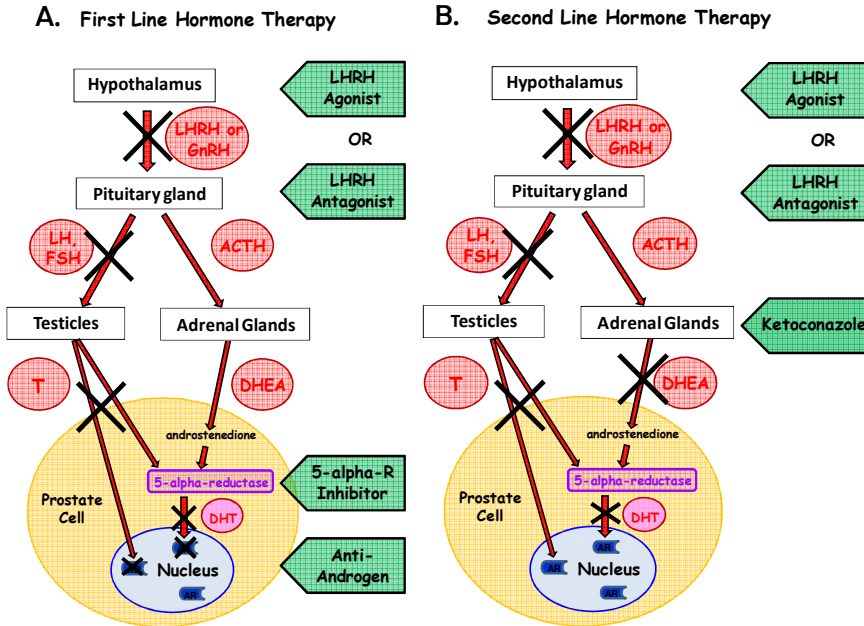


**Figure 1.1. 20** Mechanism of action of different drugs in order to reduce the production of testosterone as First (A) and as Second (B) Line of Hormone therapy. Figure adapted from Thornton<sup>21</sup>.

Total androgen blockade (TAB). In the body, 90-95% of testosterone is produced by the testes and only 5-10% by the adrenal glands. For this reason, these medications are generally used only in combination with other methods that can block 100 percent of the testosterone present in the blood stream. These combined methods are called total androgen blockade.

Examples of TAB are ketoconazole and aminoglutethimide which block the production of adrenal androgens such as 5-Dehydroepiandrosterone (DHEA), a natural steroid hormone. DHEA (Figure 1.1. 21A) is produced from cholesterol through two cytochrome P450 enzymes (Figure 1.1. 21B). Cholesterol is converted to pregnenolone by the enzyme P450 through side chain cleavage; then another enzyme,

CYP17A1, converts pregnenolone to 17  $\alpha$ -Hydroxypregnenolone and finally to DHEA.

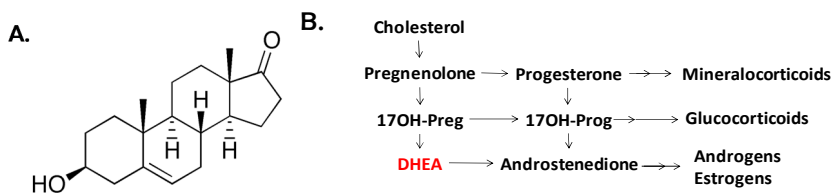


**Figure 1.1. 21** A. Molecule of Dehydroepiandrosterone (DHEA). B. Production of DHEA from Cholesterol.

Ketoconazole (Nizoral®) (Figure 1.1. 22), was originally sold as a systemic anti-fungal medication. It is taken orally (e.g. 400 mg 3x/day), and it should be accompanied by a small dose of cortisone to replace the natural cortisone no longer produced by the adrenal glands. Ketoconazole<sup>64</sup> blocks androgen production from the testes but also from the adrenal androgen biosynthesis, thus reducing testosterone levels in the body. It inhibits cytochrome P450<sup>65</sup> and 17,20-lyase, which are involved in the synthesis and degradation of steroids, including the precursors of testosterone. Ketoconazole has been used as a treatment for androgen-dependent prostate cancer due to its efficacy to reduce systemic androgen levels. This drug has also been used as androgen receptor antagonist, competing with testosterone and DHT to bind androgen receptors.

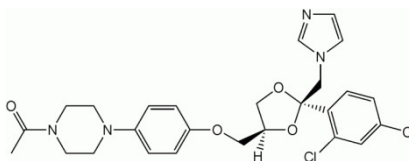


**Figure 1.1. 22** Molecule of ketoconazole, an estrogen used for the treatment of PCa by blocking the enzyme 17, 20-lyase which secretes testosterone.

Ketoconazole can be toxic to the liver, for this reason is very important to monitor the liver function during the course of medication. It can cause side effects such as anorexia and a condition called sticky skin.

#### 1.1.5.6.6. Other androgen-suppressing drugs

An example of these types of drugs is the estrogen, which is the female sex hormone. Estrogens are considered an alternative to orchiectomy in advanced prostate cancer because it cannot feed the prostatic tissue, and the hypothalamus mistakes estrogen as testosterone and stops GnRH production. Due to the side effects of administering estrogens they are now replaced by LHRH analogs and anti-androgens.

**Diethylstilbestrol (DES)** (Figure 1.1. 23) is a synthetic, non-steroidal estrogen, which has been used since the 1940s as a medication for PCa (taken orally, at 3 mg/d). DES has been found to cause certain types of cancer in women whilst taking the medication as an estrogen replacement therapy and can lead to teratogenic birth defects in pregnant women. DES has potent estrogenic abilities, capable of reaching sufficient blood levels to suppress LH release. DES suppresses serum T to levels comparable with castration. For this reason, oral DES is the most commonly used form of estrogen therapy for metastatic prostatic cancer. In many cases, after the failure of a normal hormone treatment, DES is administered.

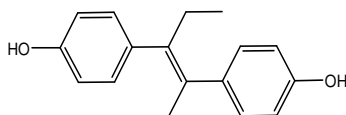


**Figure 1.1. 23** Molecule of the Diethylstilbestrol, the most well known synthetic estrogen used to treat PCa.

DES can interfere with other medications, such as bosentan, calcium salts, thyroid or growth hormone therapies, tricyclic antidepressants and cyclosporine. DES will generally be administered regularly to a patient until the tumor begins to shrink, or until a different medication is chosen.

DES was the first drug to be used as an alternative to surgical orchiectomy. Orchiectomy, DES or both together were used as a standard initial treatment for symptomatic advanced prostate cancer for over forty years. This changed when the GnRH agonist leuprolide was also found to have an efficacy similar to DES (without estrogenic effects) although it was much more expensive. General DES side effects include: changes in sexual desire and activity, mild digestion, skin rash, weight gain and fatigue. It also causes blood clots, called deep vein thrombosis, which were alleviated using anti-clotting agents as coumadin.

In addition to DES, there are other oral estrogens available. For example, at the appropriate dose, the oral estrogens premarin, provera (i.e., medroxyprogesterone acetate), and ethinyl estradiol are as effective as DES. Chlorotrianisene (TACE) (tri-*p*-anisylchloroethylene) has clinical responses but does not completely suppress LH or T levels.

The following Table 1.1. 2 describes the dosage and toxicities of the most common hormonal agents used to treat PCa..

**Table 1.1. 2** Hormonal agents commonly used in the treatment of PCa. Table taken from Swain SM et al., 1990<sup>66</sup>.

Agent	Dosage*	Toxicities
<b>LHRH agonists</b>		
Leuprolide (Lupron)	7.5 mg/mo–22.5 mg/3mo (IM)	Hot flashes, decreased libido, impotence, gynecomastia, fatigue, edema, muscle waning, osteoporosis, anemia, disease flare
Goserelin (Zoladex)	3.6 mg/mo–10.8 mg/3mo (SC)	
<b>Antiandrogens</b>		
Flutamide (Eulexin)	250 mg tid	Decreased libido, gynecomastia, hot flashes, hepatotoxicity, diarrhea,
Bicalutamide (Casodex)	50 mg daily	
Nilutamide (Nilandron)	50 mg tid	Nilandron-impaired night vision

Agent	Dosage*	Toxicities
<b>Adrenal enzyme inhibitors</b>		
Aminoglutethimide (Cytadren)	250 mg qid + HC 30 mg qday	Lethargy, dizziness, nausea, rash, weight gain, hypoaldosteronism, hypothyroidism, nausea, vomiting, requires acidic pH
Ketoconazole (Nizoral)	400 mg tid + HC 30 mg qday	
<b>Miscellaneous agents</b>		
<b>Diethylstilbesterol (DES)</b>	1 mg daily 40 mg qid	DVT, stroke, cardiac ischemia (more common at higher doses), gynecomastia, fluid retention, weight gain, DVT, impotence, gynecomastia, loss of libido, decreased HDL, side effects associated with hypercortisolism
Megesterol acetate (Megace)	40mg qid	
Cyproteron acetate (CPA)	dose varies 50–100 mg tid	
Prednisone	7.5–10 mg daily	

where IM= intramuscular; SC= subcutaneous; tid= three times daily; qid= four times daily; HC= hydrocortisone; DVT= deep venous thrombosis.

### 1.1.5.7. Chemotherapy

Chemotherapy is not particularly effective for PCa. This is considered a systemic treatment and involves the use of chemical agents capable of stopping the growth of cancer cells. More than half of all people diagnosed with cancer receive chemotherapy, particularly those with metastatic diseases. Chemotherapy can be administered orally or intravenously (i.v). Chemotherapeutics can target different cell growth patterns depending on their mechanism of action. The most common chemotherapeutics used in treating PCa are doxorubicin (brand name Adriamycin), paclitaxel<sup>67, 68</sup> (brand name Taxol), platinates (i.e. cisplatin) or carboplatin (brand name Paraplatin), 5-fluorouracil (5-FU) and different drug cocktails especially when metastasis is already present.

Some common side effects of chemotherapy are: low white blood cell count, low red blood cell count, low platelet count, nausea, vomiting, hair loss, and/or fatigue. But one of the most serious potential side effects in

this therapy is the neutropenia, a hematological disorder where the number of white blood cells (specifically neutrophils) is considerably diminished. Neutropenia can interrupt your chemotherapy schedule as it induces susceptibility to bacterial infections. This scenario results in a very serious, life-threatening disease (neutropenic sepsis).

**Cisplatin** (Figure 1.1. 24) is a platinum-based chemotherapy drug used to treat various types of cancers, including sarcomas, small cell lung cancer, ovarian cancer, lymphomas, and germ cell tumors. It was the first member of a class of anti-cancer drugs which now includes carboplatin and oxaliplatin. These platinum complexes react *in vivo*, binding to and causing crosslinking of DNA which ultimately triggers apoptosis.

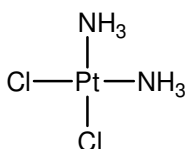


**Figure 1.1. 24** Molecule of cisplatin.

**Paclitaxel** (Figure 1.1. 25) is a chemotherapeutic drug commonly known as Taxol<sup>®</sup>. The drug comes from the bark of one particular type of yew tree. Paclitaxel works by stiffening the microtubules that make up the inner skeleton of a cell. Once the microtubules are locked into place, the cells, which require malleability to divide successfully, crumble and die during cell division, stopping cancer cell growth.

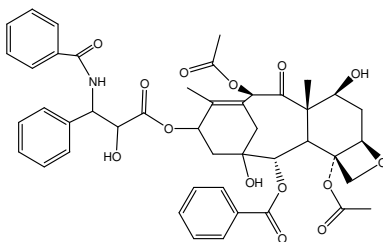


**Figure 1.1. 25** Molecule of Paclitaxel.

Paclitaxel inhibits microtubule disassembly and freezes cells during mitosis. Speicher *et al.*<sup>69</sup> evaluated the combined effect of estramustine and paclitaxel on human prostate carcinoma cell, based on the complementary mechanisms of action. It was discovered that the synergistic effect of the two had the desired cytotoxic effect. Paclitaxel was approved by the Food and Drug Administration (FDA) to treat ovarian and breast cancer and AIDS-related Kaposi sarcoma. Normally it is taken in combination with other anti-cancer drugs. It is also approved to be used together with cisplatin to treat advanced ovarian cancer, non-small cell lung cancer (NSCLC) and advanced or recurrent PCa. Nowadays it is also being studied in the treatment of other types of cancer.

The most common side effects of paclitaxel treatment include headaches, aching muscles, coughing, a sore throat, pain whilst passing urine or feeling cold and shivery (because of an increased risk of getting an infection from a drop in white blood cell count). Other common symptoms are tiredness and breathlessness, nosebleeds, and having blood spots or bruises on the arms and legs. These symptoms are related to a drop in the number of platelets in the blood and a drop in the number red blood cells (anaemia). In this case a blood transfusion is necessary. Some of these side effects can be life threatening, particularly infections. Others side effects are fatigue, vomiting, hair loss (alopecia), numbness and tingling in the hands and feet (peripheral neuropathy), diarrhoea, mouth sores and ulcers.

Paclitaxel induced cell death or apoptosis by activation of caspase-7 but not caspase-3. In addition, there is parallel, but not apparent interdependent, activation of extracellular signal-regulated kinase (ERK), p38, and Jun N-terminal Kinases (JNKs) which are members of the Mitogen-Activated Protein Kinase (MAPK) pathway<sup>68</sup>. These kinases are activated in response to growth factors, cellular and environmental stress, and cytokines<sup>70</sup>. These kinases play roles in a variety of biological processes, including cell division, survival, differentiation, and metabolism.

ERK activation is dependent upon Ras and an unknown MEK family member (Figure 1.1. 26). Ras is a protein family called small GTPase

which are involved in the cellular signal transduction. Ras took the name from the first protein family discover in a Rat sarcoma. When Ras is activated by incoming signals, it activates other proteins which finally turn on genes involved in cell growth, differentiation and survival. Ras regulates diverse cell behaviors.

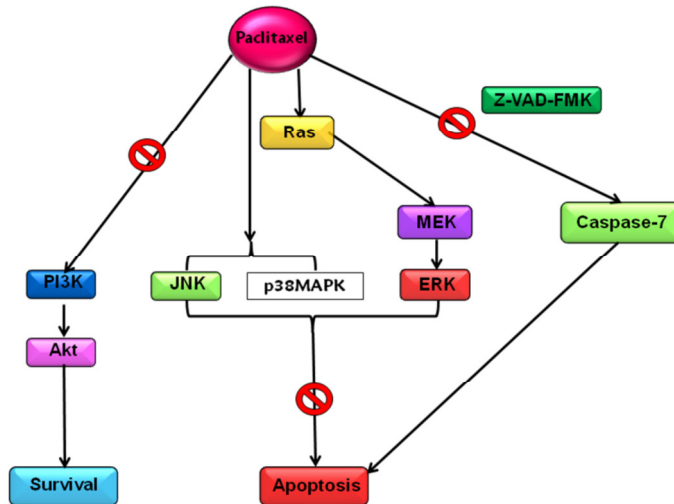


**Figure 1.1. 26** Schematic representation of paclitaxel-induced effects upon signal transduction pathways. Figure adapted from Okano *et al* in 2001<sup>68</sup>.

Docetaxel (Taxotere®) the chemotherapy taxane drug, semi-synthetic analogue of paclitaxel (Taxol®) is mainly used towards the treatment of breast, prostate and other non-small cell cancers. Docetaxel binds to tubulin, promotes the assembly of tubulin into stable microtubules and inhibits microtubule depolymerization. Microtubules formed in the presence of docetaxel are of a larger size than those formed in the presence of paclitaxel, which may result in improved cytotoxic efficacy. A greater and more slowly reversible degree of polymerization has been demonstrated for docetaxel than for paclitaxel. The cytotoxic effect of docetaxel is then mediated by disruption of the microtubular network essential for mitotic and interphase cellular functions<sup>71</sup>. In addition, docetaxel appears to have a higher affinity for tubulin than for paclitaxel and is a more potent inducer of microtubule assembly.



*Preclinical Investigations of Docetaxel*<sup>71</sup>. Several preclinical studies have demonstrated the potential activity of docetaxel in PCa. In tissue culture, docetaxel is more active than paclitaxel against established prostate cell lines. Recently, the combination of docetaxel and estramustine (Emcyt) was shown to exert significant cytotoxic effects in PC-3 prostatic cell lines. Docetaxel has been shown to have an effect on topoisomerase II enzyme, nuclear matrix proteins, and modulators of apoptosis (or programmed cell death). Several pro- and antiapoptotic pathways have been identified in androgen-independent (PC3) prostate cancer cell lines and tissues. The antiapoptotic protein bcl-2 was expressed in approximately 65% of androgen-independent human prostate cancer specimens. In vitro analyses suggest that docetaxel's mechanism of action may involve inactivation of bcl-2 by phosphorylation (which causes apoptotic cell death) demonstrating greater potency than paclitaxel<sup>72</sup>. Other different pathways for docetaxel-induced apoptosis between the androgen-responsive (LNCaP) and androgen-independent (PC-3) prostate cancer cell lines are being studied. These findings will assist researchers in choosing distinct therapies with activity against localized versus advanced prostate cancer.

### **1.1.5.8. Other therapeutic strategies**

#### **1.1.5.8.1. Prostate cancer vaccines**

Vaccines have been developed based on the hypothesis that immunotherapies can harness the immune system to fight cancer. It works by stimulating the immune response of the body to attack PCa cells. Those vaccines can target a unique cancer cell antigen, i.e. PSA which can be found in the blood, rarely present on normal cells. Research has been used healthy human prostate tissue inserted into a mutated virus to stimulate lymphocytes to attack cancer cells.

In 2010, the FDA approved the first cancer treatment vaccine, sipuleucel-T (Provenge®, manufactured by Dendreon). It is approved for use in some men with metastatic prostate cancer and designed to stimulate an immune response to prostatic acid phosphatase (PAP), an antigen that is found on most prostate cancer cells. In a clinical trial, Provenge increased the survival of men by about 4 months. PROSTVAC® is also a

therapeutic cancer vaccine in Phase 3 clinical development. This vaccine also extends significantly the lives of men with advanced prostate cancer without affecting their quality of life. This vaccine is intended to move into patients in earlier stages of the disease or whose disease has recurred after surgery or radiotherapy.

#### 1.1.5.8.2. **Angiogenesis inhibitors**

Angiogenesis is a normal and vital process in growth and development of new blood vessels from pre-existing vessels by secreting various growth factors such as vascular endothelial growth factor (VEGF). Cancers are very hard to treat when they stimulate the growth of a large number of vessels. New drugs are being studied to prevent new blood vessels from forming to stop prostate cancer growth.

One of the anti-angiogenic drugs currently tested in clinical trial is thalidomide, approved by the FDA to treat patients with multiple myeloma and in combination with chemotherapeutic agents to treat men with advanced prostate cancer. Bevacizumab (Avastin®) is another FDA-approved drug and is being tested in combination with hormone therapy and chemotherapy to treat advanced prostate cancer. It has been also studied a combination therapy which involve radiotherapy and a prostate specific antigen (PSA)- based vaccine and the National Cancer Institute (NCI) has promoted to Phase II trial to evaluate it<sup>73</sup>. The design was based on the patient's immune system stimulation, which enhances the radiotherapy effect. Indeed, based on preclinical observations, it was demonstrated that the radiation therapy can alter tumor cells and make them more susceptible to the action of the body's immune system.

#### 1.1.5.8.3. **Treating bone pain**

One of the most unpleasant side effects in metastatic advanced prostate cancer is bone pain. Apart from classical analgesia combined with the anticancer treatment, radiofrequency ablation (RFA) is also being studied. RFA consists of using computed tomography (CT) or ultrasound to guide a small metal probe into the tumor and then a high frequency pass through the probe that heats the tumor and destroys cancer cells.

RFA has been used to treat tumors in the liver and other organs but is very new for the treatment of bone pain. Still, early results are promising.

### 1.1.6. Prostate cancer cells models

The cell lines most commonly used in the study of PCa are: LNCaP (lymph node cancer of the prostate), PC-3 (bone cancer of the prostate cancer) and DU-145 (brain cancer of prostate cancer).

**LNCaP cells**<sup>74</sup> (Figure 1.1. 27) are androgen-sensitive human prostate adenocarcinoma cells derived from the left supraclavicular lymph node metastasis from a 50-year-old Caucasian male in 1977. They are adherent epithelial cells growing in aggregates and as single cells. LNCaP cells are epithelial cells with adherent qualities.

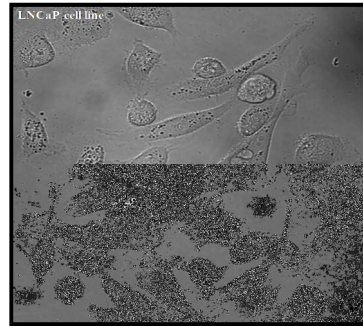


**Figure 1.1. 27** LNCaP cell line.

Highly sensitive androgen receptors are present in the cytosol of LNCaP both in culture and in tumors, making LNCaP a highly androgen-dependent cell line<sup>75</sup> (androgen receptor positive, AR+). Therefore it is sensitive to hormones (estrogen and androgen) which can be used to modulate growth. *In vitro*, LNCaP cells grow in culture as aggregates or as individual cells with the possibility to acidify the medium, but not resulting in confluence. They are resistant to human fibroblast interferon. The cells also have cytosolic estrogen receptors and 5-alpha-dihydrotestosterone that modulate cell growth and stimulates acid phosphatase production (the cells are sensitive to 5-alpha-DHT). This cell line does express PSA and Human Prostatic Acid Phosphatase (hPAP), which indicate the presence of active cytosolic androgen receptors in prostate cells. LNCaP is the only commercially available cell line that expresses hPAP, making it the only line available with which to study transcriptional regulation in the hPAP gene. The cell line is stable and the malignant qualities of the cells are well maintained, making LNCaP very useful for the study of PCa. LNCaP is a good model for studying transcriptional regulation in genes of the prostate. This is because so many

gene products in prostate cells are prostate-specific and the result of androgen-dependent processes.

**PC-3 and DU-145 human prostate cancer cell lines**<sup>76, 77</sup> are also classical cell lines of prostatic cancer. Both cell lines are epithelial cells. PC-3 (Figure 1.1. 28) and DU-145 (Figure 1.1. 29) are human prostatic adenocarcinoma and metastatic to bone and to brain, respectively. PC-3 cells have high metastatic potential compared to DU-145 cells which have a moderate metastatic potential. The proliferation of PC-3 and DU-145 cells is androgen-independent (AR -). Advanced prostate tumours present an elevation of AR expression and express PSA upon androgen treatment. But androgens also inhibit the proliferation of these androgens-independent prostate cancer cells.

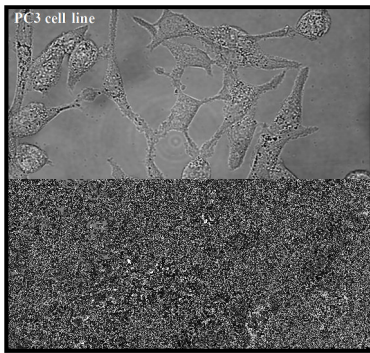


**Figure 1.1. 28** PC-3 cell line.

**PC-3 cell line**<sup>77</sup> (Figure 1.1. 28) presents a grade 4 of prostatic adenocarcinoma derived from the bone metastasis from a 62 year old caucasian male. PC-3, are unable to express hPAP but it could be due to that they are androgen sensitive, and are functionally differentiated. PC-3 cells have low testosterone-5-alpha reductase activity and low acid phosphatase.

**DU-145 cells**<sup>77</sup> (Figure 1.1. 29) are hypotriploid human prostate cancer cells derived from a brain metastasis of a 69-year-old Caucasian male. DU-145 was isolated by Stone et al This cell line is not detectably hormone sensitive, and is only weakly positive for acid phosphatase and the isolated cells form colonies in soft agar. These cells do not express PSA.

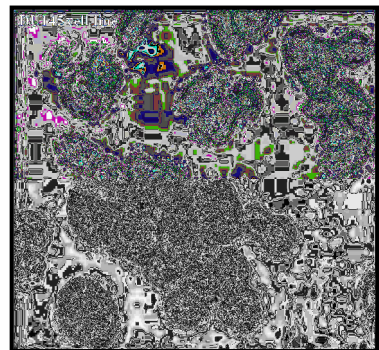


**Figure 1.1. 29** DU-145 cell line.

In Figure 1.1. 30 it is possible to observe in detail the appearance of each prostate cancer cell line (PC3, LNCaP and DU 145) when they are treated with antibodies against microtubules.

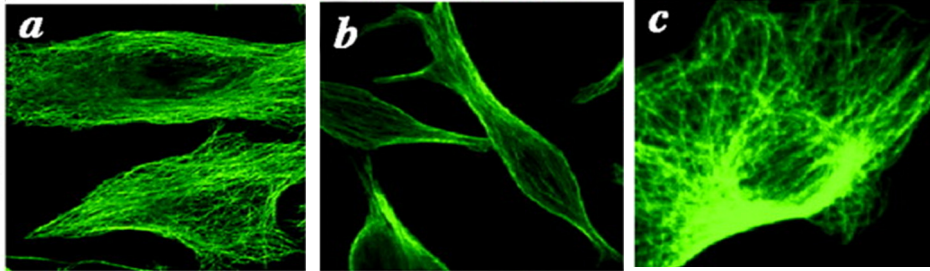


**Figure 1.1. 30** Prostate cancer cell lines, PC-3 (a), LNCaP (b), and DU-145 (c) immunostained for  $\alpha$ -tubulin (green). DNA was stained with Hoechst dye (blue). Image taken from Gloria R. et al.<sup>78</sup> in Cytoskeleton Differentially Localizes the Early Growth Response Gene-1 Protein in Cancer and Benign Cells of the Prostate.

## 1.2. POLYMER THERAPEUTICS AS NANOSIZED MEDICINES FOR TREATING CANCER

### 1.2.1. Introduction

As it was mentioned above, PCa is second most common cause of cancer death in men over fifty years old. Nowadays any effective therapeutic is available to treat PCa, survival is only achieved in approximately 35% of cases diagnosed indicating that obviously PCa therapy needs to be improved and new approaches developed<sup>79</sup>. One approach involves genomics and proteomics research used to identify new tumor-specific molecular targets. The second and complementary approach is the design of innovative drug-delivery systems (DDS), which guide the drug precisely to tumor cells, decreasing non-specific toxicity and maintaining the drug/s at a therapeutic concentration over long periods of time.

First-generation DDS include liposomes, for example DaunoXome ([www.daunoxome.com](http://www.daunoxome.com)), (daunorubicin citrate for the treatment of Kaposi's Sarcoma in people with acquired immune deficiency syndrome (AIDS)) and Doxil/Caelyx ([www.doxil.com](http://www.doxil.com))(pegylated liposomal doxorubicin to treat progressed or recurred ovarian cancer), antibody–drug conjugates, for example Mylotarg<sup>80</sup> (gemtuzumab ozogamicin to treat acute myelogenous leukemia), the first therapeutic nanoparticles (albumin-entrapped paclitaxel (Abraxane) ([www.abraxane.com](http://www.abraxane.com)) for the treatment of metastatic breast cancer and also several polymer conjugates carrying either low-molecular-weight drugs or proteins. All those examples evidence that nanotechnology applied to medicine will bring huge advances in the diagnosis and treatment of cancer. Nanomedicines are considered new nano-sized complex systems of at least two components (one should be a bioactive agent), designed for improving diagnostics, preventative medicines and efficacy disease treatments<sup>81</sup>. It is important to note that over last 20 years more than 40 nanomedicines have been approved for routine human use and many more and currently in clinical trial. Pharmaceutical nanotechnologies are designed for a specific administration route and a particular disease for this thesis Prostate Cancer is the disease of study, and **Polymer Therapeutics**<sup>81-84</sup> the type of nanopharmaceutics chosen.

### 1.2.2. Polymer Therapeutics: from origins to current development

In the 1920s Hermann Staudinger was the first to demonstrate the existence of *macromolecules* and defined them as *polymers*. For this work he was awarded the first *Nobel Prize* in polymer chemistry in 1953. At first the majority of Staudinger's colleagues refused to accept the possibility that small molecules could link together covalently to form high-molecular weight compounds. This is due in part to the fact that molecular structure and bonding theory were not fully understood in the early 20th century. However, during the second half of that century, the polymers found their place in every-day life in many diverse materials. Today they form an "indispensable contribution to the comfort, safety and expansion of our society from astronautic to medicine"<sup>85, 86</sup>. Polymers have become extensively used as biomedical materials such as sutures<sup>87</sup>, hip prostheses<sup>88, 89</sup> contact lenses<sup>90, 91</sup>, and scaffolds for tissue engineering<sup>92</sup>. In the pharmaceutical industry, they were commonly used as excipients for formulation preparation<sup>93</sup> and as controlled release systems such as matrices and gels<sup>94, 95</sup>.

A step forward in the field of polymer chemistry, biology, physics and medicine was the development of novel, water-soluble **Polymer Therapeutics** (as defined by Duncan and Connors<sup>96</sup>), synthetic polymer-based systems man-made for improved diagnostics and treatment of disease, particularly in cancer<sup>84, 97, 98</sup>. Polymer Therapeutics can be considered as the first *polymeric nanomedicines*<sup>83, 99</sup>. Polymer therapeutics are not conventional DDSs which only entrap, solubilize and control drug release. These can be considered new chemical entities (NCEs)<sup>99</sup> and are designed to improve drug, protein or gene delivery by resorting of chemical conjugation.

Polymer therapeutics reviewed by Duncan<sup>99</sup> enclose five big families (Figure 1.2. 1), active polymeric drugs<sup>100</sup>, polymer-drug conjugates<sup>101, 102</sup>, polymer-protein conjugates<sup>103</sup>, polymeric micelles<sup>104</sup> (to which drug is covalently bound)<sup>105</sup> and multi-component polyplexes developed as non-viral vectors for gene interfering ribonucleic acid (siRNA) delivery<sup>106-108</sup>. All these families are nano-sized macromolecules (conjugates 2–25 nm; block copolymer micelles/polyplexes 10–200 nm) and contain a water-soluble polymer either

as an inherently bioactive polymer per se or as a part of a covalent conjugate. All of them are described in detail in section 1.2. 4.

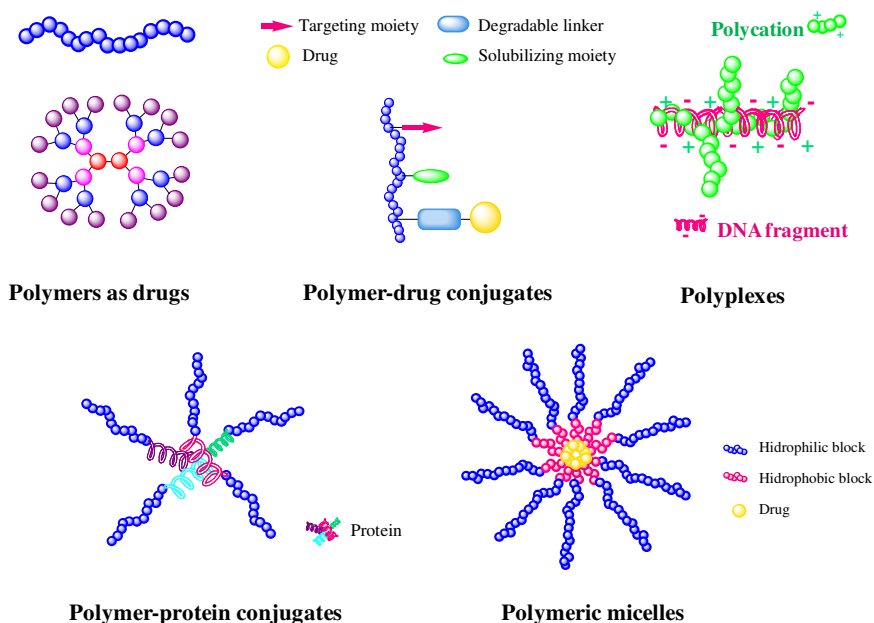


**Figure 1.2. 1** Schematic representation of polymer therapeutics (adapted from Duncan<sup>99</sup>).

The field of polymer therapeutics has exponentially grown in the last decades (Figure 1.2. 2) with several polymer-protein conjugates already launched in the market and more than 16 polymer-drug conjugates introduced into routine clinical trials (Table 1.2. 1)<sup>83</sup>. Although they were first thought to develop for parenterally administered anticancer agents<sup>81</sup> it was extended to more therapeutic goals and routes of administration. For example polymer therapeutics have been studied for treating infectious diseases (e.g. PEGIntron and PEGASYS protein-conjugates already in market), oral polymeric sequestrants (phosphate Renagel and cholesterol Welchol binders<sup>100</sup>), topical microbiocidal agents (e.g. VivaGel (polymeric-drug in clinical trial, phase II) and to promote tissue regeneration and repair (e.g. Macugen polymer-aptamer (market)). Most of the polymer-protein<sup>103</sup> and polymer-aptamer<sup>109</sup> conjugates



transferred into clinical development have used PEGs, whereas most anticancer drug conjugates have involved N-(2-hydroxypropyl) methacrylamide (HPMA) copolymers, PEG or most recently polyglutamic acid (PGA)<sup>81, 99, 103</sup> as the polymer component.

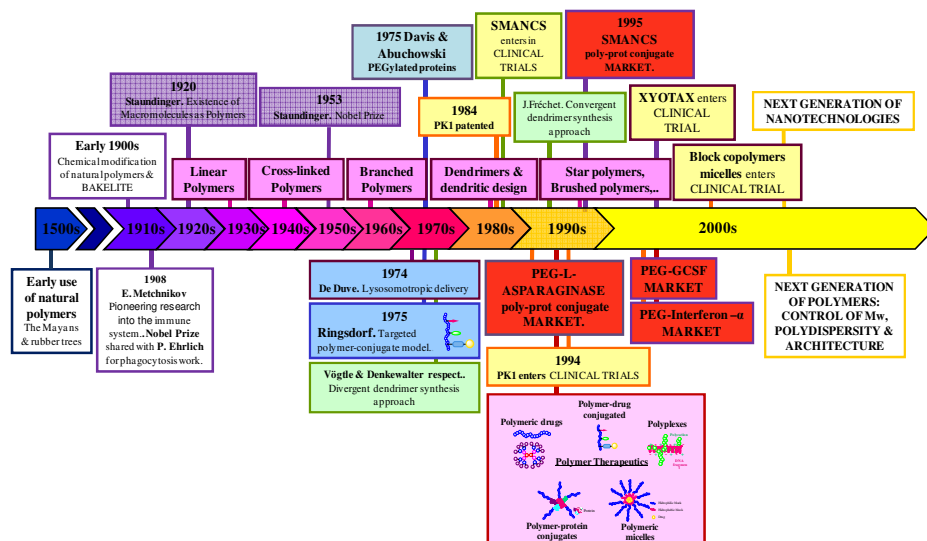


**Figure 1.2. 2** Time-scale tracking the developments of polymers and their uses in nanomedicines adapted from<sup>81</sup> Duncan, R. in Polymer conjugates as anticancer nanomedicines.

The most advanced polymer drug conjugate is Opaxio®<sup>110</sup>, poly-L-glutamic acid (PGA)-paclitaxel conjugate formerly known as Xyotax® from Cell Therapeutics Inc. currently in Phase II-III clinical trials in NSCLC, ovarian, glioblastoma and esophageal carcinoma as single agent or in combination therapy<sup>111,112</sup>. Opaxio® is the first example of personalized nanomedicine with Polymer Therapeutics as it has been shown that requires cathepsin B degradation to activate the conjugate. The levels of this enzyme seem to correlate oestradiol levels in women, and therefore this marker has been used to guide patient selection for recent clinical trials (need for plasma free oestradiol (E2) value >30 pg/mL<sup>111</sup>).

**Table 1.2. 1** Examples of polymer therapeutics in the market and clinical trials<sup>83</sup>.

Trade Name	Description/route of administration	Clinical use	Stage
<b>Polymeric Drugs</b>			
Copaxone®	Copolymer of Glu Ala,Tyr (subcutaneous injection)	Multiple Sclerosis	Market (2000)
Renagel®	Phosphate binding polymer (oral)	End Stage Renal Failure	Market (1999)
Welchol®	Cholesterol binding polymer (oral)	Reduce LDL/Type 2 diabetes	Market (2000/2008)
VivaGel®	Lysine-based dendrimer (topical)	Microbiocide	Phase II
<b>Polymer-Protein Conjugates</b>			
Zinostatin Stimaler	Styrene Maleic Anhydride-Neocarzinostatin (SMANCS) (intrahepatic artery)	Hepatocellular carcinoma	Market Japan (1990)
Adagen®	PEG-adenosine deaminase (intramuscular)	Severe Combined Immune Deficiency Syndrome	Market (1990)
Oncospar®	PEG-asparaginase (intravenous or intramuscular)	Acute Lymphocytic Leukaemia Chronic hepatitis C	Market (1990)
PEGINTRON®	PEG-interferon alfa-2b (subcutaneous)	Chronic hepatitis C	Market (2001)
PEGASYS®	PEG-interferon alfa-2 <sup>3</sup> (subcutaneous)	Hepatitis C	Market (2002)
Neulasta®	PEG-human G-CSF (subcutaneous)	Chemotherapy-induced neutropenia	Market (2002)
Somavert®	PEG-HGH antagonist (subcutaneous)	Acromegaly	Market (2003)
Mircera®	PEG-EPO (intravenous or subcutaneous)	anaemia associated with chronic kidney disease	Market (2007)
Cimzia®	PEG-antiTNF Fab (subcutaneous)	Rheumatoid arthritis/ Crohn's Disease	Market (2008/9)
Krystexxa® ( Puricase®, Pegloticase)	PEGylated uric acid- (intravenous)	Chronic Gout	Market (2010)
<b>Polymer-aptamer</b>			
Macugen®	PEG-aptamer (aptanib) (intravitrea)	AMD	Market (2004)
<b>Polymer-drug conjugate</b>			
CT-2103; XYOTAX™, OPAXIO®	Polyglutamic acid (PGA)-paclitaxel (intravenous)	Cancer-NSCLC, ovarian, various other cancers and combinations	Phase II/III
Prolindac®	HPMA-copolymer-DACH platinate (intravenous)	Cancer-melanoma, ovarian	Phase II
NKTR-102	PEG-irinotecan (intravenous)	Cancer-metastatic breast	Phase II
PEG-SN38	Multiarm PEG-camptothecin derivative (intravenous)	Cancer-various	Phase II
NKTR-118	PEG-naloxone (oral)	Opioid-induced constipation	Phase II
XMT-1001 (Fleximer® technology)	Polyacetal-camptothecin conjugate (intravenous)	Cancer-various	Phase I

## 1.2.3. The Rational behind the design of Polymer Therapeutics

### 1.2.3.1. Enhanced Permeability and Retention (EPR) effect as passive tumour targeting

The enhanced permeability and retention (EPR) effect is the unique phenomenon of solid tumors or inflammation sites related to their anatomical and pathophysiological differences from normal tissues<sup>112</sup>. It was described by Maeda and colleagues<sup>113</sup> in the late 80s. This passive targeting effect is mainly based on two facts<sup>99, 114-116</sup>: (i) The hyperpermeability and “leakiness” of the angiogenic tumor vessels that allows after intravenous administration, a selective extravasations of the macromolecule in tumor or inflamed tissue and (ii) a lack of an effective lymphatic drainage, which subsequently promote *retention* in damage tissue. The combination of these factors leads to an accumulation of the macromolecule in the tumor tissue (Figure 1.2. 3). This EPR effect served as a basis for development of macromolecular anticancer therapy.

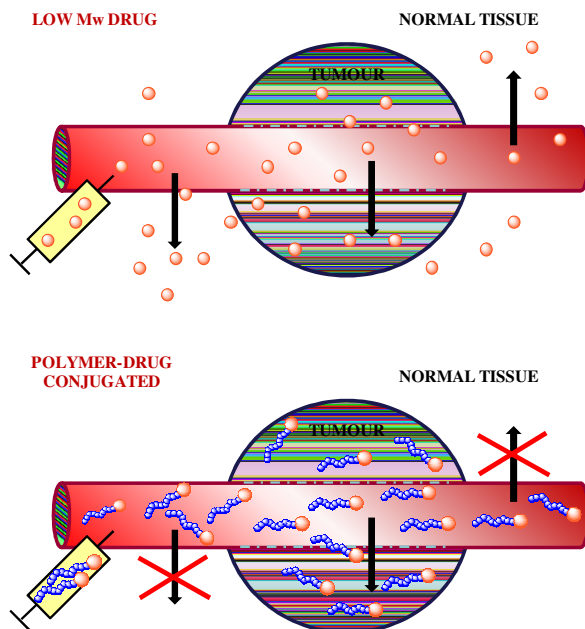


**Figure 1.2. 3** The EPR effect (adapted from Duncan(2003)<sup>99</sup>).

The EPR-effect is even more enhanced by many pathophysiological factors involved in enhancement of the extravasation of macromolecules in solid tumor tissues. Peroxynitrite, nitric oxide (NO), tumor necrosis, prostaglandins, vascular endothelial growth factor (VEGF), bradykinin and collagenase among others factors, facilitate the EPR effect.

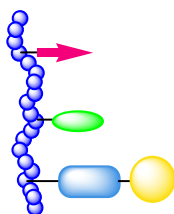
Although most polymer therapeutics rely on the enhanced vascular permeability of angiogenic tumour vessels for tumor targeting not all tumour types display EPR-mediated targeting and the process can be tumour-size dependant. Thus, Maeda was working on the enhanced of the EPR effect artificially in clinical to deeply understand and develop this effect depending of the relation tumor/conjugate. In order to enhance the EPR effect, Maeda was working on two factors, the bradykinin (which facilitates vascular leakage) and the nitric oxide (NO) (which facilitates vascular blood flow). Bradykinin is a peptide that causes blood vessels to dilate, and therefore causes blood pressure to lower and consequently enhances the EPR effect. It is known that bacterial proteases could activate the bradykinin-generating cascade called kallikrein-kinin cascade. As human plasma contains no effective inhibitors of bacterial proteases, when bradykinin (kinin family) is presented in the plasma causes very potent pain and induced vascular permeability (edema). It was found similar enhanced vascular permeability in both normal inflammatory and tumor tissue, but the faster clearance rates from normal tissue than in the tumor tissue clarify the evidence of enhanced EPR effect of macromolecules in tumor tissue<sup>117</sup>.

The other strategy was focus on the increase of the systemic blood pressure by controlling the nitric oxide (NO) levels. The NO-releasing agent used was topical nitroglycerin, which releases nitrite and then it is converted to NO<sup>117, 118</sup>. NO is more selectively in the tumor tissues and leads to a significantly increased EPR effect, improved drug delivery and consequently enhanced antitumor drug effects<sup>117</sup>. It was shown the same effect in cardiac tissues in the presence of angina pectoris<sup>119</sup>. The use of nitroglycerin, did enhanced therapeutic efficacy in a more ubiquitous manner, that is, for solid tumors in general, such as hypovascular tumors (metastatic liver cancer and pancreatic), tumors refractory to radiotherapy and most of chemotherapy<sup>119, 120</sup> and in minute tumor nodules as small of 100µm metastatic tumor foci in the liver<sup>121, 122</sup>.






The conformations in solution (size and shape) together with the architecture of the polymer therapeutic are of essential importance in time of an adequate enhanced EPR effect. These factors play an important role as they are well related with vascular permeability and cellular uptake of the macromolecules<sup>83, 123, 124</sup>. The molecular weight (Mw) of the conjugates is also important because it has been shown that by increasing Mw above the renal threshold led to significantly improved plasma circulation times, tumor accumulation and unable cleared from the circulation by the kidney. Normally the macromolecules renal threshold appears between 30.000-70.000g/mol<sup>125</sup>.

### 1.2.3.2. Intracellular Trafficking. Lysosomotropic Drug Delivery concept for Polymer-Drug Conjugates

In 1954, Jatzkewitz described the synthesis of a mescaline-N-vinylpyrrolidine conjugate attached via non-degradable or enzymatically degradable (glycyl-L-leucine) side chains<sup>126</sup>. However, was not until 1975 when the first theoretical model describing the current idea of a water-soluble-polymer conjugated to a drug was reported by Ringsdorf (Figure 1.2. 4). This novel approach to deliver therapeutics promoted cross-disciplinary discussions and collaborations in different fields such as polymer chemistry, biology, physics and medicine.



**Figure 1.2. 4** Ringsdorf's model of polymer-drug conjugates (adapted from).

Where:  is a water-soluble synthetic polymer,  is the drug,  is the degradable linker,  is a targeting moiety and  is a solubilising moiety.

In parallel, De Duve firstly observed that DNA could be used as carrier delivering drugs such as daunorubicin intracellularly uniquely by endocytosis<sup>127</sup> (Figure 1.2. 4). In contrast, low molecular weight compounds easily biodistribute via passive diffusion across cell membranes. This was the basis for the key concept of "lysosomotropic drug delivery"<sup>128</sup> that notes the

possibility to deliver the drug through lysosomes after endocytosis (Figure 1.2. 5). In the endocytic<sup>129</sup> process cells internalize molecules and macromolecules via deformation of the membrane and generation of membrane-bound carriers.

The endocytic pathways include clathrin-mediated, caveolae/lipid raft-mediated, clathrin-, and caveolae-independent endocytosis, fluid-phase endocytosis<sup>130</sup>, and phagocytosis. Phagocytosis involves the processing of large foreign particles by specialized cells such as macrophages, which form part of the reticuloendothelial system (RES). However, clathrin-dependent endocytosis represents the most studied form of endocytic internalization. The clathrin-mediated endocytosis consists first in the formation of endocytic vesicles (early endosomes) to trap the macromolecule. Depending on surface signals of membrane proteins to which nanostructures may be non-covalently linked, some may be trafficked along retrograde transport pathways for example via the Golgi apparatus and endoplasmic reticulum. Others may be carried through late endosomes to lysosomes where they may be degraded.

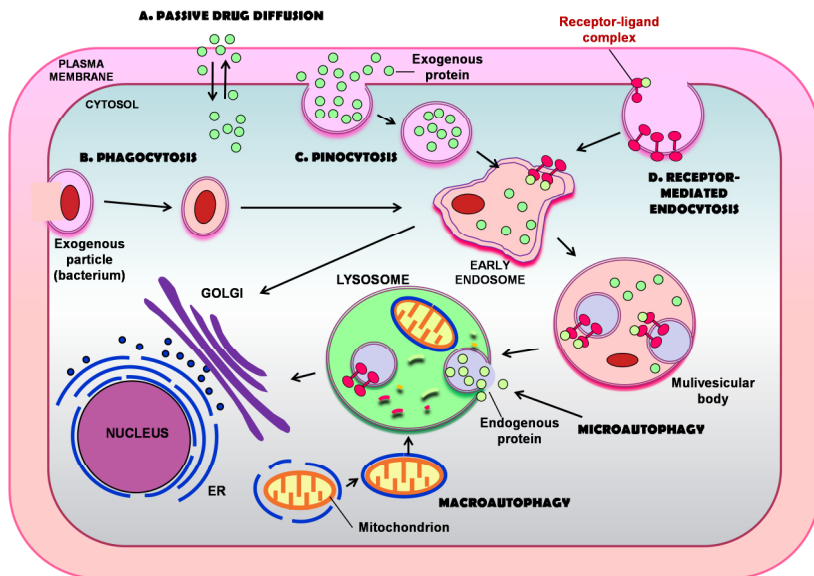


**Figure 1.2. 5** Possible endocytosis pathways for cellular uptake of nanostructures.

Then, the nanostructures, after pinching off the plasma membrane and trafficking, get fusion with endosomal/lysosomal compartments which can be extravasated for any of the different compartments depending of its nature. Once the macromolecules are internalized they are transferred via endosomes, which has a pH around 6.0 - 6.5, to lysosomal compartments which contain proteolytic enzymes and a lower pH of 5.0-5.5<sup>99</sup>.

Conjugation of therapeutic agents to macromolecules through a bioresponsive linker that only degrades when exposed to these specific lysosomal conditions would allow intracellular release of the drug, which would then passively diffuse through the lysosomal membrane to reach its pharmacological target in the cytosol.

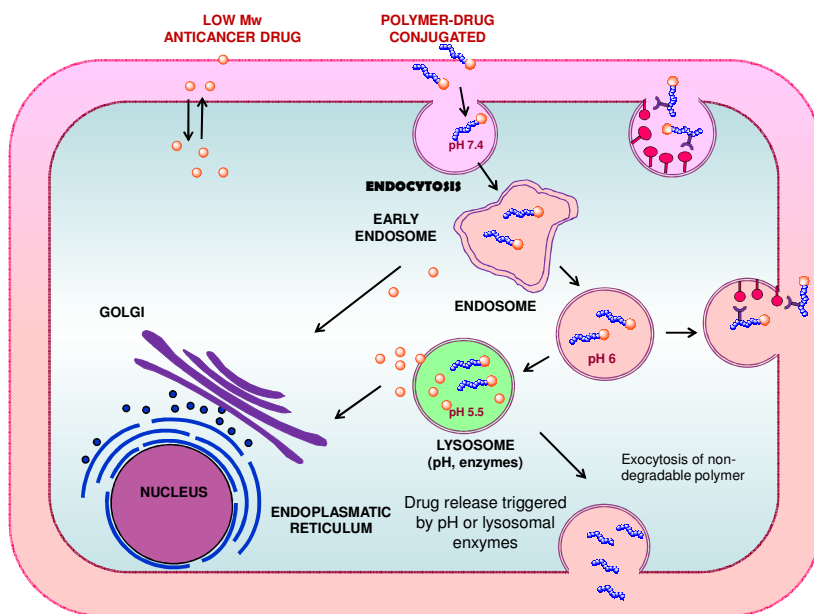


**Figure 1.2. 6** Lysosomotropic drug delivery of polymer conjugates (adapted from Duncan<sup>81</sup>).

The EPR effect together with the lysosomotropic drug delivery concept provides the fundamental basis to design polymer-drug conjugates but is perhaps an over simplification when considering the complexity of whole body distribution, cell biology and cellular trafficking. These effects are currently the most important strategy to improve the delivery of low-

molecular-weight chemotherapeutic agents to tumors by reducing toxicity and improving activity in chemotherapy-refractory patients.

All classes of polymer therapeutics are now extensively studied and have been comprehensively reviewed elsewhere<sup>125, 131</sup>.

## 1.2.4. Current status of Polymer Therapeutics

### 1.2.4.1. Polymeric drugs

Polymeric drugs<sup>100</sup> (Figure 1.2. 7) (5000-40000 g/mol) can be defined as polymers with inherent therapeutic activity.

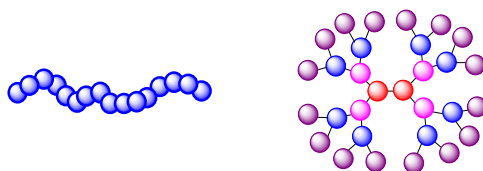


**Figure 1.2. 7** Polymeric drug structures.

The first polymeric drugs were natural polymers extracted from plants, animals and seaweed (particularly the polyanions and polysulphates) which possess antiviral and antitumour activity<sup>132</sup>. One of the first synthetic polyanionic medicine was DIVEMA (pyran copolymer), reported by Breslow in 1976<sup>133</sup>, used as a polymeric drug carrier of antitumor drugs in numerous *in vitro* and *in vivo* experiments in the form of Na salt. The preliminary results have shown DIVEMA reduce side effects and enhance the antitumor activity of the drugs being active against adenocarcinoma 755, Lewis lung carcinoma, Friend leukemia virus and Dunning ascites leukemia. But although it induced apoptosis, interferon release and activated macrophages promoting tumor cells death, DIVEMA was found to be very toxic and was dismissed in early clinical trials. Anticancer activity of other maleic anhydride copolymers with ethylene, acrylic acid, cyclohexyl-1,3-dioxane, dihydropyran, dihydrofuran, vinyladenine or styrene was studied, but those did not reach the performance of DIVEMA.

Modified polysaccharides, synthetic polypeptides and synthetic polymers have resulted in a number of successful and marketed products as polymeric drugs. For example one of the most significant compounds is the random



copolymer, Copaxone<sup>®</sup> (glatiramer acetate) (Mw 5 - 11,000 g/mol), of four amino acids (L-glutamic acid, L-alanine, L-lysine, and L-tyrosine) approved for the treatment of multiple sclerosis (MS) where it reduces both the frequency of relapse and disease progression when given subcutaneously (s.c.)<sup>134</sup> and the polysaccharide analogue, dextrin-2-sulphate (Mw=25000g/mol) intraperitoneally administered (i.p.)<sup>135</sup> daily for 28 days was well tolerated up to the maximal daily dose of 150 mg, and in Phase III clinical trials it reduced replication of HIV-1 in patients with AIDS. Although such polyanionic drugs have yet to yield a marketed product, Starpharma are developing a dendrimer, VivaGel<sup>®</sup>, as a topical, vaginal/penis virucide as a preventative to HIV-1 infection<sup>135</sup>.

Some other examples<sup>100</sup> of these marketed products include Renagel<sup>®</sup> is a phosphate binding polymer (oral administration) for the treatment of end stage of renal failure and Welchol<sup>®</sup> is a cholesterol binding polymer (oral) to reduce high low density lipoprotein (LDL) and reduce high glucose.

#### **1.2.4.2. Polymeric micelles**

Polymeric Micelles<sup>104</sup> (Figure 1.2. 8) (10-200 nm) are based on amphiphilic block copolymers with a drug covalently linked to the polymer backbone triggering in aqueous solutions at concentrations above the critical micellar concentration (CMC) nano-sized, colloidal particles which have been investigated for drug delivery in cancer therapy during the past years<sup>136</sup>.

In aqueous solution, the hydrophobic segment forms the core<sup>137</sup> which can contain the hydrophobic therapeutic drugs and the hydrophilic block forms the external micellar shell and provides the necessary interactions with the solvent to make the nanoparticles stable in the liquid. That's why micelles typically have a so-called core-shell structure. Micelle carrier's diameter plays an important role in the biodistribution and tumor accumulation of cancer drugs. The size of these polymeric micelles depends on the molecular characteristics and molecular weight of each amphiphilic block.

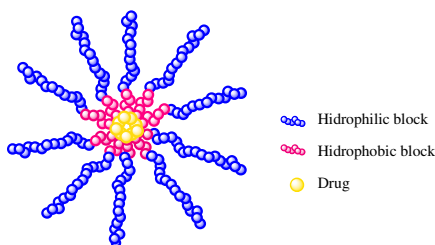


**Figure 1.2. 8** Polymeric Micelles structure.

Kataoka et al demonstrated<sup>138</sup> that different micelle sizes, between 30-100nm due to the self-assembling of their structure, readily extravasate from circulation through vascular irregularities in highly permeable tumors due to ongoing angiogenesis<sup>139</sup>, where they can then deliver encapsulated cytotoxic agents to tumor tissue, which explains their clinical success. But only the 30nm micelles could penetrate poorly permeable pancreatic tumors to achieve an antitumor effect. They also showed that the enhanced efficacy of the larger micelles by using a transforming growth factor- $\beta$  inhibitor to increase the permeability of the tumors<sup>139</sup>.

Micellar-based drugs containing doxorubicin<sup>140-143,144-146</sup> paclitaxel<sup>147</sup>, or cisplatin<sup>148</sup> are in various stages of clinical trials. While the use of micelles<sup>149</sup> in cancer therapy<sup>136</sup> seems promising, obstacles associated with drug transfer from these nanocarriers to tumor cells within the tumor site remain particularly challenging.

To cure prostate cancer, Chandran et al.<sup>150</sup> coupled a PSA (prostate specific antigen)-activated peptide prodrug to pHPMAM based copolymers. The prodrug showed antitumor activity *in vivo*, but its low solubility was dose-limiting. Then, it was coupled to pHPMAM forming stable micelles and allowing targeting to tumor tissue by the EPR effect. Once in the tumor site the active lipophilic drug was rapidly partitioned into tumor cells.

Further examples of the progress in the development of copolymer micelles include the metal complex formation of ionic block copolymers. Simply mixing cisplatin with PEG-PAsp yielded polymer-metal complexed micelles which displayed 14 times higher levels in tumours compared with free drug and reduced nephrotoxicity<sup>151</sup>.

### 1.2.4.3. Polymer-based non-viral vectors for gene delivery (polyplexes)

Polyplexes<sup>106-108</sup> (Figure 1.2. 9) (90-160 nm) are formed by polymers capable of interacting with DNA/RNA. .

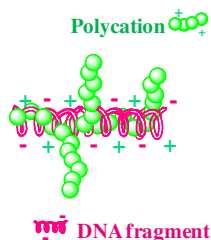


**Figure 1.2. 9** Polyplexes structures.

Many modifications can be made to the polymer to improve the gene delivery system, composition of a multi-component construct (feed ratio of DNA/polycation), molecular weight and architecture of the polymer (linear, branched, block or graft copolymers, dendrimers). This field of "non-viral vectors" for cytosolic delivery of genes, proteins and most recently, small interfering ribonucleic acids (siRNAs) have been reviewed<sup>106, 107</sup>.

Research<sup>152</sup> has been conducted to develop carrier systems with high efficacy and minimum toxicity to deliver siRNA therapeutics. The cationic polyaspartamide derivatives with a regulated number and spacing of positively charged amino groups in the side chain were prepared from a single platform polymer of poly( $\beta$ -benzyl l-aspartate) to assess their availability as siRNA carriers through polyion complex (PIC) formation<sup>153</sup>. It has been reported<sup>154-155</sup> the evaluation of several polyplex-based gene delivery systems with respect to their effectiveness, toxicity, and cell type dependence in vitro. P123-g-PEI(2K), a cationic graft block copolymer, was demonstrated to successfully deliver genetic material to murine liver following systemic delivery. The introduction of target-specific moieties together with understanding thermodynamics and kinetics of these complexes plays an important role for the design of efficient non-viral polymer-based gene vectors<sup>156</sup>.

Despite global effort over > 20 years trying to design synthetic vectors poor transfection efficiency, complexity<sup>157</sup> of product and toxicity has limited progress towards clinical development. As for example vectors based on cationic polymers such as polyethylenimine (PEI), poly-L-lysine (PLL), and PAMAM dendrimers which were widely studied but apart of being safe and immunogenic showed highly toxics and presented rapid capture by the liver due to their cationic charge. A polyplex system with the adequate clinical risk-benefit ratio is still needed.

#### 1.2.4.4. Polymer conjugates

Polymer conjugates (2-25nm) are polymer-based systems conjugated to a protein or to a drug, **polymer-protein conjugates** and **polymer-drug conjugates**, respectively.

The advantage of conjugating polymer to protein is the improvement of the overall properties and stability of the protein. In fact, the solubility, stability, and half-life of the protein in plasma is improved and additionally conjugation results in a decreased renal clearance, reduced immunogenicity and greater protection against degradative enzymes<sup>158</sup>. Apart from this properties when a small drug is conjugated to a polymer carrier a complete pharmacokinetic change is achieved<sup>81,99</sup>.

It is important to emphasise that polymer-drug and -protein conjugates tested clinically typically are composed of three main parts; (i) the polymer, (ii) a linker, and (iii) the bioactive agent (Figure 1.2. 10), although (iv) an optional component such as cell-specific targeting ligands and imaging agents can also be formed part in the polymer conjugate structure as some that have been already tested clinically.

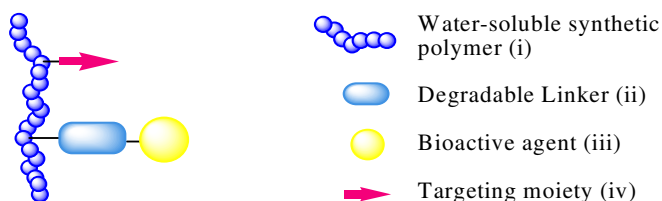


**Figure 1.2. 10** Polymer conjugates structure.

(i) The *polymer backbone*

The polymer carrier is a water-soluble platform capable of solubilising a hydrophobic drug making a more convenient formulation to administer intravenously. Also it should be multifunctional, biocompatible (i.e. non-toxic and non-immunogenic), with a low polydispersity, preferably monodisperse, and ideally biodegradable. If non-degradable, this polymer should have a molecular weight less than 40000Da allowing excretion via the porous glomerular membrane of the kidneys<sup>99</sup> from the body. The presence of functional pendant groups or end groups on the polymer backbone is necessary to allow conjugation of active molecules (e.g. drug, targeting moieties). Finally it should be suitable for large scale manufacture in terms of reproducibility, characterization and cost.

So far, some of the polymers found the most used in clinics (Figure 1.2. 11) are mostly non-biodegradable such as, poly(*N*-(2-hydroxypropyl) methacrylamide) (PHPMA)<sup>114, 159</sup> and poly(ethylene glycol) (PEG)<sup>131, 144</sup>. However, there is a trend towards the use of biodegradable polymers, such as; poly(glutamic acid) (PGA), cyclodextrin (CD), poly (1-hydroxymethylene hydroxymethyl formal) (PHF, Fleximer), hyaluronic acid or sialic acid<sup>160, 161</sup>.

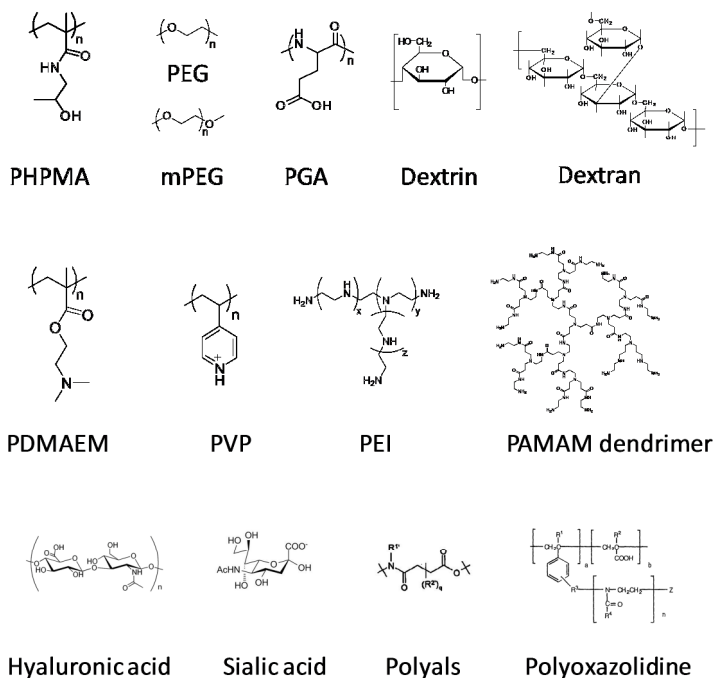


**Figure 1.2. 11** Common polymers and dendrimers used as potential macromolecular carriers in the field of polymer therapeutics.

PEG and HPMA copolymers are non-degradable synthetic polymers which have been extensively studied as polymer conjugates with particular emphasis on the treatment of cancer. HPMA is derived from methacrylamides and was originally obtained by free radical polymerization and later by atom-transfer radical polymerization (ATRP)<sup>162</sup> to control the molecular weight and give narrow molecular weight distributions more suited to biological applications. PHPMA has been shown to be non-toxic up to 30g/kg and biocompatible<sup>163</sup>. Further studies were carried out to ensure a reproducible polymer synthesis with potential drug attachment sites, and further to this oligopeptide side chains were synthesized to promote lysosomal drug release<sup>164</sup>.

PEG is a polyether compound with many applications in the pharmaceutical industry. It is also known as polyethylene oxide (PEO) or polyoxyethylene (POE), depending on its molecular weight. PEG is the reference for the material existing as oligomers and polymers with a molecular mass below

20,000 g/mol, PEO to polymers with a molecular mass above 20,000 g/mol, and POE to a polymer of any molecular mass. PEGs are prepared by polymerization of ethylene oxide and are commercially available over a wide range of molecular weights from 300 g/mol to 10,000,000 g/mol and also commercially produced with various end group functionality.

PEG presents very narrow polydispersities being synthesized commercially with a  $M_w/M_n$  between 1.02 and 1.10, allowing much better characterization of the conjugates. However, the polymer mainchain is not biodegradable and linear PEG conjugates have the disadvantage that drug loading is restricted to conjugation at the terminal end group. PEG has a low toxicity and PEGylation mainly to proteins<sup>103,165</sup> can show several significant pharmacological advantages over the unmodified form due to the increasing in the  $M_w$ , enhancement of stability and reducing of immunogenicity. These good characteristics for PEG have led to a number of compounds PEGylated with drugs<sup>131</sup> that have been approved for clinical use. Examples of marketed polymer conjugates are Neulasta®, PegIntron®, PEGASYS® and Cimzia®.

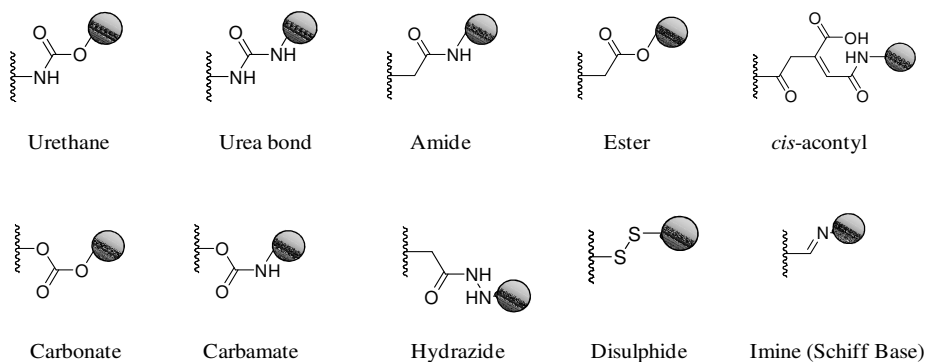
(ii) The *linker*



The linker connects the drug/protein to the polymer backbone. All the components of the conjugate are very important in the design of an effective delivery system but the linker has an especially important role in the system in order to release the drug in the adequate site for optimal therapeutic effect and must be stable during transportation to the site e.g. a tumor<sup>99</sup>. As most drug conjugates prepared to date are designed for lysosomotropic delivery, two broad classes of pendent chain linkers have emerged as the most applicable types of linkers for this delivery pathway: (i) pH labile and (ii) enzyme susceptible linkers, peptidyl linker.

**Peptidyl linkers**, which are designed to be stable in the bloodstream and other biological fluids but are degraded when exposed to specific lysosomal enzymes<sup>125</sup>. Studies *in vitro* using tritosomes (or lysosomal hepatic enzymes) and *in vivo*<sup>125, 166</sup> showed that the rate of release highly depends on the nature and chemical composition of the linker. Both, steric factors (length of the

linker) and structural factors (sequence of the amino acids) affect the cleavage of the drug from the polymer backbone.

**Acid labile linkers** (Figure 1.2 12) are stable during blood circulation at a neutral pH (pH 7.4) but are hydrolyzed under the acidic environment of the endocytic pathway (pH 4-6.5) (e.g. acetal, hydrazone and hydrazine) <sup>167</sup>.



**Figure 1.2. 12** Acid labile linkers used to conjugate drugs to the polymer backbone<sup>125</sup>. Where:  represents the drug and  the polymer backbone.

In case of proteins designed should be different as many time released is not a key issue to achieve therapeutic efficiency, in particular when the molecular target is extracellular, peptidic linkers are the preferred in this situation. In case of the requirement of an intracellular delivery, the endosomotropic route is required in order to avoid arrival to the lysosomes. Disulfide bonds are the most commonly used in this case<sup>81,99,103,170</sup>.

#### 1.2.4.4.1. Polymer-drug conjugates

**Polymer-drug conjugates**<sup>83, 101, 168</sup> are nano-sized hybrid constructs that covalently combine a bioactive agent with a polymer to ensure not only its efficient delivery to the required intracellular compartment but also its availability within a specific/desired period of time. These multicomponent constructs have already been transferred to clinics as anticancer agents, either as single agents or as elements of combinations. The first polymer-drug conjugate to be transferred to the clinics was



designed by Duncan, Kopeček and co-workers<sup>99,169</sup> in the 1980s. Prague-Keele 1, known as PK1 (FCE 28068) (Figure 1.2. 13A), a *N*-(2-hydroxypropyl) methacrylamide (HPMA) copolymer-Doxorubicin (Dox) conjugate. Dox was linked to the polymer through glycine-phenylalanine-leucine-glycine or Gly-Phe-Leu-Gly peptidyl linker and is susceptible degradation by Cathepsin B, a lysosomal thiol protease. Then PK2 (FCE 28069) (Figure 1.2. 13B), HPMA copolymer Gly-Phe-Leu-Gly -doxorubicin (Dox) conjugate containing galactosamine residues as a targeting moiety, was designed and remains the only targeted polymer-anticancer drug conjugate to enter clinical trial to-date<sup>170</sup>.

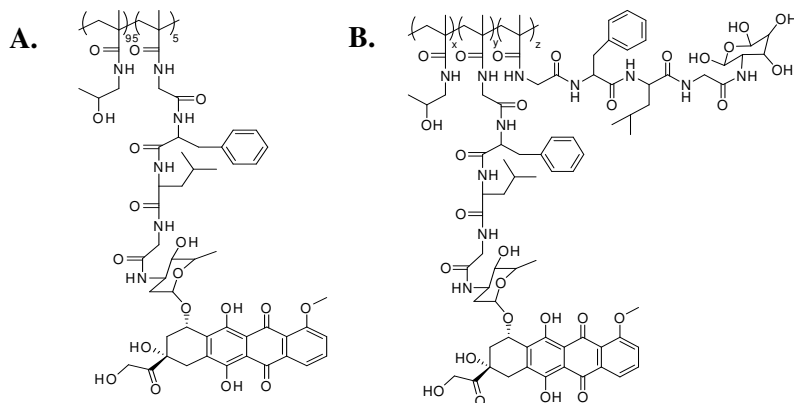


**Figure 1.2. 13** Structures of (A) PK1 and (B) PK2<sup>81</sup>.

Nowadays, after the design and introduction of PK1 and PK2, up to 16 polymer-drug conjugates are in advanced clinical trials<sup>81, 123, 171</sup> see table 1.2 1 in first section.

### 1.2.5. Challenges and future trends for Polymer-Drug Conjugates

Current state of art polymer therapeutics relies on strong foundations coming from 30 years of interdisciplinary research from the bench to the bedside, they can be considered amongst the most successful polymeric nanomedicines. There are a growing number of polymer therapeutics that are products and

also entering clinical development as both novel treatments and imaging agents. They are used as Nano-sized Medicines in the form of individual agents or conjugates or as components of complex, self-assembling nanoparticles and micelles. Consequently, an exponentially growing industrial pipeline is currently available in big pharmaceutical companies as well as in small biotechnologies devoted to specific nanoconjugates. However, in order to move this platform technology further, there are still some challenges to overcome<sup>102,125,171</sup>. It is accepted that future challenges and opportunities to move this platform technology forward are based on: (i) delivery of new anticancer agents focusing on novel molecular targets and (ii) their combination, (iii) development of both new and exciting polymeric materials with well defined architectures and (iv) treatment of diseases other than cancer although cancer treatments are the most exciting and promising treatment disease.

There is a need to improve the control of molecular weight, polydispersity and most importantly architecture of the polymer<sup>83,124, 172, 173</sup>. Biopersistent carriers as polyethylenglycol (PEG) or N-(2-hydroxypropyl)methacrylamide (HPMA) copolymers, can present disadvantages if chronic parenteral administration and/or high doses are required as there is the potential to generate 'lysosomal storage disease' syndrome. Preclinical evidence of intracellular vacuolation with certain PEG-protein conjugates is raising awareness of the potential advantage of biodegradable polymers regarding safety benefit apart from the possibility to use higher molecular weight (Mw) carriers allowing PK optimization, by enhancing the enhanced permeability and retention (EPR)-mediated tumor targeting<sup>120,124</sup>. Biodegradable polymers such as dextrans polypeptides, polyesters or polyacetals could be considered as promising candidates to be used as carriers for targeted drug delivery<sup>102,125</sup>.

Furthermore, there is a need to move towards a better defined polymer structures, avoiding heterogeneous, random-coiled polymeric carriers that can be the cause of future problems and side-effects. New architectures under evaluation include dendrimer (monodisperse structures) or dendronized polymers, hyperbranched polymer, block copolymers and stars polymers (Figure 1.2. 14)<sup>125</sup>.

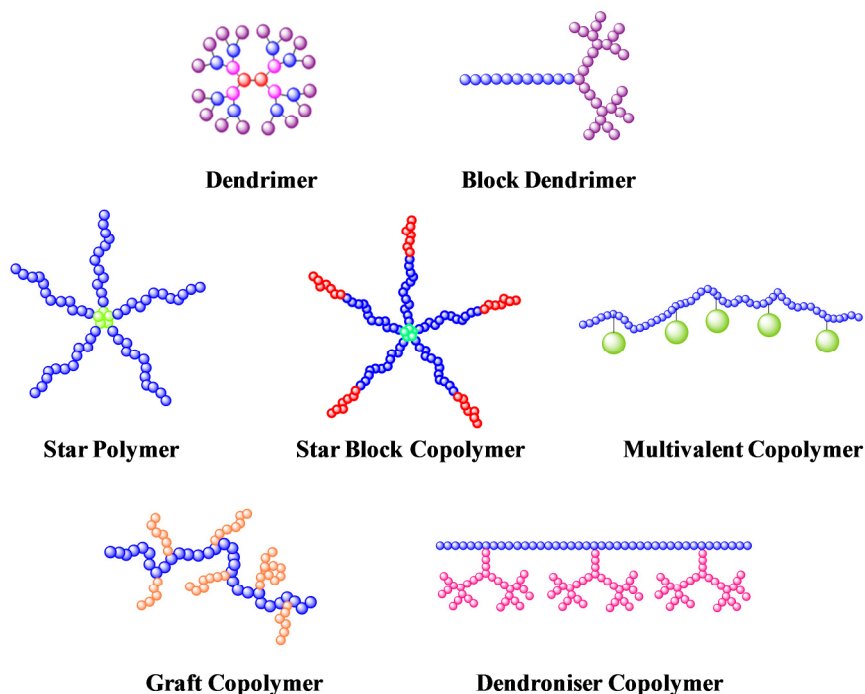
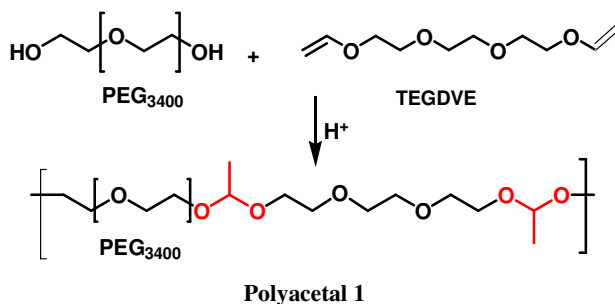


**Figure 1.2. 14** New polymer architecture for the development of better polymeric carrier adapted by Vicent, 2008<sup>123</sup>.

### 1.2.6. Polyacetals as biodegradable drug carriers

Looking for high Mw, biodegradable and pH-responsive polymeric carriers, polyacetals<sup>174</sup> could be defined as one of the most appropriate polymers together with polyesters. Polyacetals have been prepared by the reaction of diols and divinyl ethers using an acid catalyst (Scheme 1.2. 1) which had been previously been used in the development of bioerodible implants intended for contraceptive use<sup>174</sup>.

The polymerization occurs under mild conditions and can be adapted to include monomers with functionalities for the conjugation of therapeutic agents. The first family of hydrolytically labile water-soluble polyacetals was developed at 2002 by Tomlinson *et al.*<sup>175</sup>.



**Scheme 1.2. 1** Synthesis of Polyacetal 1 using the polymerization technique described by Heller and Tomlinson<sup>175</sup>.

Synthesis of high molecular weight polymers containing the acetal moiety as the degradable element affords the possibility of pH-dependent degradation. These hydrolytically labile polymers can be prepared so as to degrade quickly at the lysosomal pH, which results in the release of preferable monomeric components or short polymer chains which can be effectively cleared so avoiding the possibility of deleterious lysosomal accumulation. This would allow the synthesis of anti-cancer polyacetal-drug conjugates at molecular weights above the renal threshold of the polymer to enhance tumor specific uptake via the EPR effect without the subsequent undesirable accumulation at other sites in the body. Furthermore, these biodegradable polyacetals could conceivably be assessed as candidates for the chronic treatment of inflammatory disease which display hyperpermeable vasculature or as a degradable component of polymer-protein systems.

These polyacetals show a clear pH-dependent degradation being relatively stable at pH 7.4 but degrade significantly faster at the acidic pH that is encountered in endosomes and lysosomes, adequate for a lysosomotropic drug delivery (Figure 1.2. 15). In vitro and in vivo studies confirmed that the polyacetals are not toxic (for the polymer itself and its degradation subproducts), they are not taken up extensively by the liver or spleen, and are also long circulating<sup>177,178</sup>. Moreover, the polyacetal-Dox conjugate (Mw 86 KDa) displayed significantly prolonged plasma circulation time and enhanced tumor accumulation compared to the HPMA copolymer-Dox conjugate (CF28068, known as PK1, Mw 30 KDa) in Phase II clinical trials<sup>177</sup>.

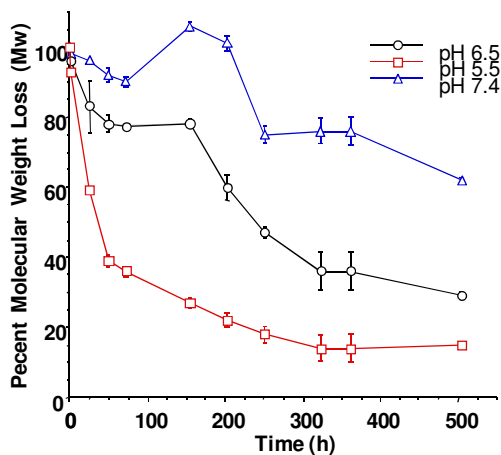


**Figure 1.2. 15** pH-dependent degradation profile of polyacetal 1.

To move a step further on this design in our laboratory we synthesized polyacetals incorporating a drug with bis-hydroxyl functionality into the polymer backbone<sup>179</sup>. Degradation of the polymer backbone in the acidic environment of the lysosome or the extracellular fluid of some tumors would then trigger drug release eliminating the need for a biodegradable linker. For this purpose, we used the *tert*-polymerization process developed for the synthesis of the functionalized polyacetals in combination with the model drug diethylstilbestrol (DES)<sup>176</sup> (Figure 1.2. 16), an anticancer synthetic estrogen which possesses phenolic hydroxyl groups suitable for using the mentioned acetalic technique.

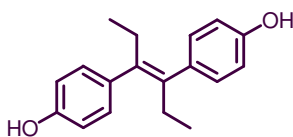


**Figure 1.2. 16** DES molecule.

As described earlier, DES is a synthetic non-steroidal estrogen and its administration was a classic form of androgen deprivation therapy (ADT), standard approach to the treatment of advanced prostate cancer for more than 50 years. Its use, however, has been severely limited by a poor water solubility and wide ranging dose-related toxicities, mainly cardiovascular side effects and in particular thromboembolic events. DES can be considered as an

'old' treatment, however, is taken renewed consideration as very recently has been demonstrated that low-dose DES is safe and effective in castrate-resistant prostate cancer (CRPC) patients when used before the initiation with chemotherapy. Also, a combination of DES to chemotherapeutics such as docetaxel was found to produce a significant level of antitumor activity in patients with metastatic, androgen independent prostate cancer (AIPC). It is hypothesized that, apart from clearly reducing DES toxicity by means of the EPR-mediated tumor targeting, the conjugation of DES to polymeric carriers would more easily allow a low-dose clinical regime as a controlled release of the drug could be achieved for a prolonged period of time. Also, polymer multivalency would allow the synthesis of polymer-based combination conjugates that could better exploit the synergism observed already with, i.e. docetaxel.

Previous research with DES-polyacetals already demonstrated that DES solubility can be greatly enhanced upon polymerization. And more interestingly, the conjugates underwent degradation that was clearly pH-dependent, with greater DES release at acidic pHs. Additionally, the active isomerism of the estrogen was maintained (trans-DES)<sup>179</sup> and the conjugates displayed enhanced in vitro cytotoxicity compared to free DES. These tert-DES polyacetals (Figure 1.2. 17) could therefore be defined as the first water-soluble anticancer polymeric drugs designed for acidic pH-triggered release where the drug is incorporated into the polymer mainchain<sup>179</sup>. Ratifying the utility of this synthetic strategy, another recent example has been reported using curcumin as a diol-functionalized anticancer drug<sup>177</sup>. The polyacetal-based polycurcumins showed a clear antitumor effect in vitro and in vivo in ovarian cancer models

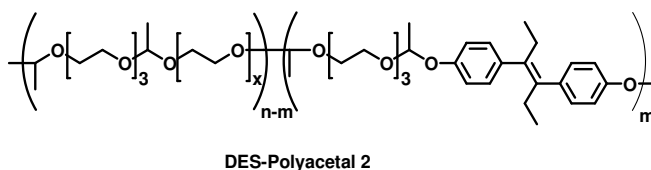


**Figure 1.2. 17** DES-Polyacetal polymer structure.

Taking into account the data described above it is possible to conclude that DES-Polyacetalic structures present then, some advantages such as; (1) EPR-mediated tumour targeting, (2) pH-triggered polymer backbone degradation to release DES locally in the tumour and excreting easily the polymer carrier, (3) tumour-specific uptake decreases toxicity and (4) backbone incorporation eliminates the need for pendent chain conjugation.

### 1.2.7. Physico-chemical characterization

A better understanding of the physicochemical properties and structural characteristics of the conjugates including solution conformation<sup>178</sup>, plays an essential role in the design and tailoring of the therapeutic applications of these macromolecular compounds. This information is crucial for synthetic chemists to understand and therefore solve the most important challenges such as solubility, half-life, tolerability, toxicity, immunogenicity and antigenicity for polymer therapeutics.

A variety of biophysical techniques allow studying many different properties in polymer-drug conjugates. Also, analytical techniques make it possible to study drug release processes *in vitro* and *in vivo*, as for example high performance liquid chromatography, **HPLC**. Liquid chromatography was defined in the early 1900s by the work of the Russian botanist, Mikhail S. Tswett<sup>179</sup>. His pioneering studies focused on separating compounds, extracted from plants using a solvent, in a column packed with particles. Nowadays, liquid chromatography has become one of the most powerful tools in analytical chemistry. Column liquid chromatography and in particular HPLC, is the most powerful and has the highest capacity for sample<sup>180</sup>. HPLC has the ability to separate, identify, and quantitate the compounds that are present in any dissolved sample. HPLC components are shown in a simplified diagram in Figure 1.2. 18. It has a high-pressure pump to generate the flow required, an injector, the column, the detector. The mobile phase exits the detector and can be sent to waste, or collected, as desired. Different types of detectors can be used such as UV or fluorescence, but if the sample does not absorb ultraviolet light or it is not fluorescence, an evaporative-light-scattering detector (ELSD) is used. Also it is possible to combine multiple detectors or to combine with a mass spectrometer (MS), in this second case the system is called LC/MS.

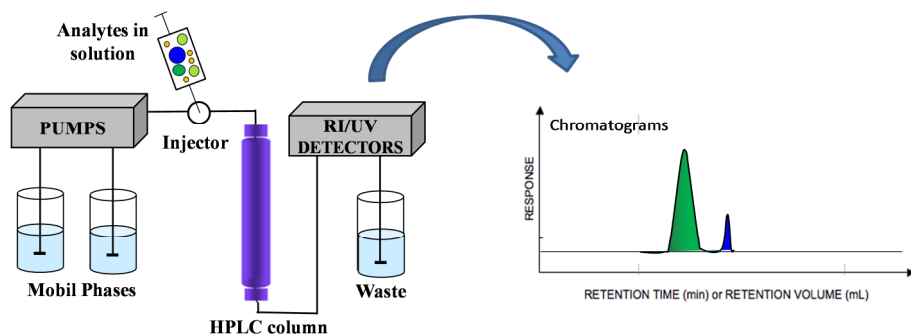


**Figure 1.2. 18** Schematic representation of the HPLC with a gradient elution mode.

Essential information in polymer drug conjugates is the knowledge about their molecular weight ( $M_w$ ) and polydispersity index ( $M_w/M_n$ ), which can be obtained from gel permeation chromatography (GPC). GPC is also known as size exclusion chromatography (SEC) and it involves size separation of the sample through a column packed with beads of a porous gel. Smaller molecules can permeate through the beads of gel; the smaller they are, the greater their retention is<sup>181</sup> (Figure 1.2. 19). The resulting separation reaches its limit and the volume required is known as the total permeation volume,  $V_T$ . The interstitial volume  $V_I$  is defined as followed (Equation 1.2. 1):

$$V_I = V_T - V_V \quad (\text{Eq. 1.2. 1})$$

The most important pieces of information obtained from GPC are the number-average molecular weight ( $M_n$ ), the weight-average molecular weight ( $M_w$ ) and the polydispersity indices ( $M_w/M_n$ ). Equations 1.2. 2 to 1.2. 4 define those numbers.

$$\overline{M}_n = \frac{\sum_i |N_i M_i|}{\sum_i N_i} \quad (\text{Eq. 1.2. 2})$$



$$\overline{M}_w = \frac{\sum_i N_i M_i^2}{\sum_i N_i M_i} \quad (\text{Eq. 1.2. 3})$$

$$PDI = \frac{\overline{M}_w}{\overline{M}_n} \quad (\text{Eq. 1.2. 4})$$

Where  $N_i$  represents the number of polymer of a mass  $M_i$ .

$V_h$  is dependent on the molecular weight of the analytes and on their conformation in solution, which is directly linked to the solvent used as eluant. GPC gives a relative  $M_w$ . For example a protein will have a smaller  $V_h$  than a random coil polymer of the same molecular weight. Thus longer retention times will be observed for a globular-shaped protein, giving a smaller apparent molecular weight than seen for a random-coil polymer of the same molecular weight.

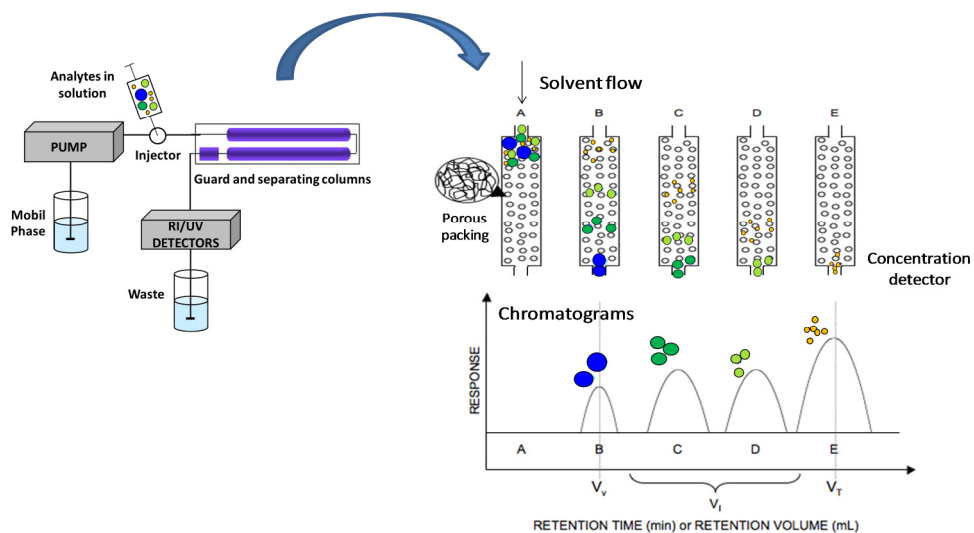


**Figure 1.2. 19** Schematic representation of the GPC system and its separation principle where molecules are separated on the basis of their size in solution ( $V_h$ ) and are detected by a concentration detector such as RI. The smaller  $V_h$ , the longer the molecules will take to permeate and hence the later the signal will appear on the chromatogram.

Properties related to the size can be derived from laser diffraction analysis such as dynamic light scattering (DLS) or electron microscopy studies such as transmission electron microscopy (TEM) (for more detail information see chapter 4 part II). The determination of the attachment of the drug to the polymer is usually obtained by using nuclear magnetic resonance (NMR), UV/Vis or Infrared (IR) techniques and the volume median aerodynamic diameter from time-of-flight (TOF). Matrix assisted laser desorption ionization time-of-flight (MALDI TOF) is a mass spectrometry method to determine polymer Mw distribution and for endgroup analysis in polymers. Each peak in the spectrum represents different degree of polymerization and the peak to peak distance reflects the mass of the repeating unit. Scanning electron microscopy (SEM) shows us the surface of the polymer. Small angle X-ray scattering (SAXS) and small angle neutron scattering (SANS) are used to clarify the conformational properties of polymers in solution<sup>124, 182, 183</sup>. Both techniques tell us the average radius of gyration (Rg) in solution but SANS also gives information about the internal structure of the polymers. In these scattering techniques, solution conditions such as temperature, pH and salt concentration can be adjusted to mimic a physiological environment. The solutions may also be modified to mimic extreme non-physiological conditions, for example in the studies of conjugate degradation (Table 1.2. 2).

**Table 1.2. 2** Examples of techniques used to characterize polymer–drug conjugates<sup>123</sup>.

Property investigated	Techniques employed
Covalent attachment of the drug to the polymer	NMR, FT-IR, MALDI-TOF
Total drug content	HPLC, UV, NMR
Free drug content	HPLC, UV, NMR
Molecular weight/ Polydispersity	GPC, MALDI-TOF, Light Scattering
Size/ Conformation of the conjugate in solution	SANS, SAXS, DLS, TEM, SEM, PGSE-NMR
Formation of supramolecular assemblies	SAXS, NMR, Light Scattering (DLS)

NMR is the most widely used technique to characterize macromolecular structures and their intermolecular interactions with high spatial and temporal

resolution. NMR spectroscopy techniques (more detail information in chapter 4 part II) can provide information such as drug loading, sample heterogeneity and purity, molecular size, aggregation or binding state.  $^1\text{H}$  NMR and  $^{13}\text{C}$  NMR are the most common techniques used for routine analysis to confirm the presence of the desired compound. However, there are other special selective irradiations of particular resonances or the use of more complex pulse sequences e.g. Diffusion-Ordered Spectroscopy (DOSY), COrelation SpectroscopY (COSY), TOtal Correlation Spectroscopy (TOCSY) or pulse-gradient spin echo-NMR (PGSE-NMR). These techniques can provide yet further analysis of polymer conjugates. PGSE-NMR experiments in which compounds in solution diffuse and the degree of diffusion is proportional to the Mw/size of the component. From this, the diffusion coefficients (D) can be determined. The signal of each component decays with different diffusion rates either when varying the gradient strength applied to the sample or when increasing the diffusion time. The signal decay allows the construction of a bilinear NMR data set for the component and it is possible to obtain a two-dimensional chemical shift, whilst yields the range of diffusion coefficients. Combining this information provided by the diffusion experiments with the Stokes-Einstein equation, an estimation of hydrodynamic radii (Rh) can be obtained.

## References

1. Jemal, A.; Bray, F.; Center, M. M.; Ferlay, J.; Ward, E.; Forman, D., Global Cancer Statistics *CA: A Cancer Journal for Clinicians* **2011**, *61* (2), 69-90.
2. Jemal, A.; Bray, F.; Forman, D.; O'Brien, M.; Ferlay, J.; Center, M.; Parkin, D. M., Cancer burden in Africa and opportunities for prevention. *Cancer* **2012**, 1-13.
3. Ferlay, J.; Shin, H. R.; Bray, F.; Forman, D.; Mathers, C.; Parkin, D. M. GLOBOCAN 2008 v1.2, Cancer Incidence and Mortality Worldwide: IARC CancerBase No. 10. Lyon, France: International Agency for Research on Cancer. <http://globocan.iarc.fr>, accessed on day/month/year.
4. Bray, F.; Ren, J. S.; Masuyer, E.; Ferlay, J., Estimates of global cancer prevalence in 2008 for 27 sites in the adult population, submitted.
5. Schröder, F. H.; Hugosson, J.; Roobol, M. J.; Tammela, T. L. J.; Ciatto, S.; Nelen, V.; Kwiatkowski, M.; Lujan, M.; Lilja, H.; Zappa, M.; Denis, L. J.; Recker, F.; Páez, A.; Mänttinen, L.; Bangma, C. H.; Aus, G.; Carlsson, S.; Villers, A.; Rebillard, X.; van der Kwast, T.; Kujala, P. M.; Blijenberg, B. G.; Stenman, U.-H.; Huber, A.; Taari, K.; Hakama, M.; Moss, S. M.; de Koning, H. J.; Auvinen, A., Prostate-Cancer Mortality at 11 Years of Follow-up. *New England Journal of Medicine* **366** (11), 981-990.
6. Sasse, A.; Sasse, E.; Carvalho, A.; Macedo, L., Androgenic suppression combined with radiotherapy for the treatment of prostate adenocarcinoma: a systematic review. *BMC Cancer* **2012**, *12* (1), 54.
7. Hakimi, A. A.; Agalliu, I.; Ho, G. Y.; Ghavamian, R.; Yu, C.; Kattan, M. W.; Rabbani, F., Detection of Prostate Cancer in an Ethnically Diverse, Disadvantaged Population With Multiple Prostate Specific Antigen Measurements Before Biopsy *Journal of Urology* **2012**, *187* (4), 1234-1240.
8. Cornford, F., Evolution of docetaxel-based therapy for metastatic castrate-resistant prostate cancer. *British Journal of Medical and Surgical Urology* **2009**, *3*, 5.
9. Ernsting, M. J.; Foltz, W. D.; Undzys, E.; Tagami, T.; Li, S.-D., Tumor-targeted drug delivery using MR-contrasted docetaxel - Carboxymethylcellulose nanoparticles. *Biomaterials* **2012**, *33* (15), 3931-41.
10. Ernsting, M. J.; Tang, W. L.; MacCallum, N. W.; Li, S.-D., Preclinical pharmacokinetic, biodistribution, and anti-cancer efficacy studies of a docetaxel-carboxymethylcellulose nanoparticle in mouse models. *Biomaterials* **2012**, *33* (5), 1445-1454.

11. Miller, K.; Erez, R.; Segal, E.; Shabat, D.; Satchi-Fainaro, R., Targeting bone metastases with a bispecific anticancer and antiangiogenic polymer-alendronate-taxane conjugate. *Angew Chem Int Ed Engl* **2009**, *48* (16), 2949-54.
12. Marieb, E. N.; Martin, T.; Tonini, C., *Human anatomy & physiology / Elaine Marieb*. 4th ed ed.; Benjamin/Cummings: 1998.
13. Prostate cancer: Early detection. February 21, 2012 ed.; American Cancer Society. Cancer Facts & Figures 2012. Atlanta. Cancer Information Database: **2012**.
14. Bostwick, D. G., High Grade Prostatic Intraepithelial Neoplasia The Most Likely Precursor of Prostate Cancer. **1823**.
15. Rick, F. G.; Szalontay, L.; Schally, A. V.; Block, N. L.; Nadji, M.; Szepeshazi, K.; Vidaurre, I.; Zarandi, M.; Kovacs, M.; Rekasi, Z., Combining Growth Hormone-Releasing Hormone Antagonist With Luteinizing Hormone-Releasing Hormone Antagonist Greatly Augments Benign Prostatic Hyperplasia Shrinkage *Journal of Urology* **2012**, *187* (4), 1498-1504.
16. Brooks, R. V., Androgens. *Clin Endocrinol Metab* **1975**, *4* (3), 503-20.
17. Bassil, N.; Alkaade, S.; Morley, J. E., The benefits and risks of testosterone replacement therapy: a review *Journal of Therapeutics and Clinical Risk Management* **2009**, *5* (3), 427-48.
18. Tuck, S. P.; Francis, R. M., Testosterone, bone and osteoporosis. *Front Horm Res* **2009**, *37*, 123-32.
19. Mooradian, A. D.; Morley, J. E.; Korenman, S. G., Biological actions of androgens *Endocr. Rev.* **1987**, *8* (1), 1-28.
20. Scher, H. I.; Halabi, S.; Tannock, I.; Morris, M.; Sternberg, C. N.; Carducci, M. a.; Eisenberger, M. a.; Higano, C.; Bubley, G. J.; Dreicer, R.; Petrylak, D.; Kantoff, P.; Basch, E.; Kelly, W. K.; Figg, W. D.; Small, E. J.; Beer, T. M.; Wilding, G.; Martin, A.; Hussain, M., Design and end points of clinical trials for patients with progressive prostate cancer and castrate levels of testosterone: recommendations of the Prostate Cancer Clinical Trials Working Group. *Journal of clinical oncology : official journal of the American Society of Clinical Oncology* **2008**, *26*, 1148-59.
21. Thornton, D. Hormone Treatment Basics. Santa Cruz County Prostate Cancer Support Group, <http://www.scprostate.org/index.html>.
22. Kobayashi, Y.; Absher, D. M.; Gulzar, Z. G.; Young, S. R.; McKenney, J. K.; Peehl, D. M.; Brooks, J. D.; Myers, R. M.; Sherlock, G., DNA methylation profiling reveals novel biomarkers and important roles for DNA methyltransferases in prostate cancer. *Genome research* **2011**, *21*, 1017-27.

23. Nelson, W. G.; De Marzo, A. M.; Yegnasubramanian, S., Epigenetic alterations in human prostate cancers. *Endocrinology* **2009**, *150*, 3991-4002.
24. Waterman, M. R.; Keeney, D. S., Genes involved in androgen biosynthesis and the male phenotype. *Horm. Res.* **1992**, *38* (5-6), 217-21.
25. Zuber, M. X.; Simpson, E. R.; Waterman, M. R., Expression of bovine 17 alpha-hydroxylase cytochrome P-450 cDNA in nonsteroidogenic (COS 1) cells. *Science* **1986**, *234* (4781), 1258-61.
26. Boron, W. F.; E.L., B., *Medical Physiology: A Cellular And Molecular Approach*. 2003; p 1300.
27. Payne, A. H.; O'Shaughnessy, P., Structure, function, and regulation of steroidogenic enzymes in the Leydig cell. ". In Payne AH, Hardy MP, Russell LD. *Leydig Cell. Vienna [II]: Cache River Press. pp. 260–285. ISBN 0-9627422-7-9. 1996.*
28. Meinhardt, U.; Mullis, P. E., The essential role of the aromatase/p450arom. *Semin Reprod Med.* **2002**, *Semin Reprod Med.* (3), 277-84.
29. Lopes, R. a. M.; Neves, K. B.; Carneiro, F. S.; Tostes, R. C., Testosterone and vascular function in aging. *Frontiers in physiology* **2012**, *3*, 89.
30. Heinlein , C. A.; Chang, C., The roles of androgen receptors and androgen-binding proteins in nongenomic androgen actions. *Mol. Endocrinol.* **2002**, *16* (10), 2181-7.
31. Roy, A. K.; Lavrovsky, Y.; Song, C. S.; Chen, S.; Jung, M. H.; Velu, N. K.; Bi, B. Y.; Chatterjee, B., Regulation of androgen action. *Vitam. Horm.* **1999**, *55*, 309-52.
32. Bardin, C. W.; Brown, T.; Isomaa, V. V.; Jänne, O. A., Progestins can mimic, inhibit and potentiate the actions of androgens. *Pharmacol. Ther.* **1983**, *23* (3), 443-59.
33. Raudrant, D.; Rabe, T., Progestogens with antiandrogenic properties. *Drugs* **2003**, *63* (5), 463-92.
34. Watson, C. S.; Jeng, Y. J.; Kochukov, M. Y., Nongenomic signaling pathways of estrogen toxicity. *Toxicol Sci.* **2010**, *115* (1), 1-11.
35. Knudsen, K. E.; Cavenee, W. K.; Arden, K. C., D-type cyclins complex with the androgen receptor and inhibit its transcriptional transactivation ability. *Cancer Res.* **1999**, *59* (10), 2297-301.
36. Cardiovascular Physiology of Androgens and Androgen Testosterone. *Endocrine, Metabolic & Immune Disorders - Drug Targets*, **2009**, *9*.
37. Lannigan, D. a., Estrogen receptor phosphorylation. *Steroids* **2003**, *68*, 1-9.

38. Foradori, C. D.; Weiser, M. J.; Handa, R. J., Non-genomic Actions of Androgens. *Front Neuroendocrinol* **2008**, *29* (2), 169-181.
39. Nieto, M.; Finn, S.; Loda, M.; Hahn, W. C., PROSTATE CANCER: Re-focusing on Androgen Receptor Signaling. *Int J Biochem Cell Biol*. **2007**, *39* (9), 15621568.
40. Scher, H. I., Targeting the androgen receptor: improving outcomes for castration-resistant prostate cancer. *Endocrine Related Cancer* **2004**, *11*, 459-476.
41. Osanto, S.; Van Poppel, H., Emerging novel therapies for advanced prostate cancer. *Therapeutic advances in urology* **2012**, *4*, 3-12.
42. Armstrong, A. J.; Carducci, M. A., New drugs in prostate cancer. *Curr Opin Urol*. **2006**, *16* (3), 138-145.
43. Mimeault, M.; Batra, S. K., Recent advances on multiple tumorigenic cascades involved in prostatic cancer progression and targeting therapies. *Carcinogenesis* **2006**, *27* (1), 1-22.
44. Walsh, P. C., Outcomes in Patients With Gleason Score 8–10 Prostate Cancer: Relation to Preoperative PSA Level *Journal of Urology* **2012**, *187* (5), 1641.
45. Pierorazio, P. M.; Ross, A. E.; Lin, B. M.; Epstein, J. I.; Han, M.; Walsh, P. C.; Partin, A. W.; Pavlovich, C. P.; Schaeffer, E. M., Preoperative characteristics of high-Gleason disease predictive of favourable pathological and clinical outcomes at radical prostatectomy. *BJU International* **2012**, no-no.
46. The Veteran's Administration Cooperative Urologic Research Group: histologic grading and clinical staging of prostatic carcinoma. In Tannenbaum M (ed.) *Urologic Pathology: The Prostate*. Lea and Febiger, Philadelphia. 1977; p 171-198.
47. Sanda, M. G., CLINICIAN ' S CORNER A 64-Year-Old Man With Low-Risk Prostate Cancer Review of Prostate Cancer Treatment. **2009**, *301*, 2141-2151.
48. Abdollah, F.; Sun, M.; Schmitges, J.; Thuret, R.; Bianchi, M.; Shariat, S.-F.; Briganti, A.; Jeldres, C.; Perrotte, P.; Montorsi, F.; Karakiewicz, P. I., Survival Benefit of Radical Prostatectomy in Patients with Localized Prostate Cancer: Estimations of the Number Needed to Treat According to Tumor and Patient Characteristics *Journal of Urology, In Press Corrected Proof* **2012**.
49. Mullins, J. K.; Han, M.; Pierorazio, P. M.; Partin, A. W.; Carter, H. B., Radical Prostatectomy Outcome in Men 65 Years Old or Older With Low Risk Prostate Cancer *Journal of Urology* **2012**, *187* (5), 1620-1625.
50. Van Poppel, H.; Joniau, S.; Van Cleynenbreugel, B.; Mottaghy, F. M.; Oyen, R., Diagnostic evaluation of PSA recurrence and review of

- hormonal management after radical prostatectomy *Prostate Cancer Prostatic Dis.* **2009**, *12* (2), 116-23.
51. David Liu, D.; Lehman, H. P.; Frick, K. D.; Carter, H. B., Active Surveillance Versus Surgery for Low Risk Prostate Cancer: A Clinical Decision Analysis. *The Journal of Urology* **2012**, *187* (4), 1241-1246.
  52. Kibel, A. S.; Ciezki, J. P.; Klein, E. A.; Reddy, C. A.; Lubahn, J. D.; Haslag-Minoff, J.; Deasy, J. O.; Michalski, J. M.; Kallogjeri, D.; Piccirillo, J. F.; Rabah, D. M.; Yu, C.; Kattan, M. W.; Stephenson, A. J., Survival Among Men With Clinically Localized Prostate Cancer Treated With Radical Prostatectomy or Radiation Therapy in the Prostate Specific Antigen Era *Journal of Urology* **2012**, *187* (4), 1259-1265.
  53. Ahmed, S.; Lindsey, B.; Davies, J., Salvage cryosurgery for locally recurrent prostate cancer following radiotherapy. *Prostate Cancer Prostatic Dis* **2004**, *8* (1), 31-35.
  54. Uchida, T.; Nakano, M.; Hongo, S.; Shoji, S.; Nagata, Y.; Satoh, T.; Baba, S.; Usui, Y.; Terachi, T., High-intensity focused ultrasound therapy for prostate cancer. *International Journal of Urology* *19* (3), 187-201.
  55. Schubert, M.; Joniau, S.; Gontero, P.; Kneitz, S.; Scholz, C.-J.; Kneitz, B.; Briganti, A.; Karnes, R. J.; Tombal, B.; Walz, J.; Hsu, C.-Y.; Marchioro, G.; Bader, P.; Bangma, C.; Frohneberg, D.; Graefen, M.; Schröder, F.; van Cangh, P.; van Poppel, H.; Spahn, M., The role of adjuvant hormonal treatment after surgery for localized high-risk prostate cancer: results of a matched multiinstitutional analysis. *Advances in urology* **2012**, *2012*, 612707.
  56. Van der Sluis, T. M.; Bui, H. N.; Meuleman, E. J. H.; Heijboer, A. C.; Hartman, J. F.; Van Adrichem, N.; Boevé, E.; De Ronde, W.; Van Moorselaar, R. J. A.; Vis, A. N., Lower Testosterone Levels With Luteinizing Hormone-Releasing Hormone Agonist Therapy Than With Surgical Castration: New Insights Attained by Mass Spectrometry *Journal of Urology* **2012**, *187* (5), 1601-1607.
  57. National Cancer Institute; [www.cancer.gov](http://www.cancer.gov).
  58. Kolvenbag, G. J. C. M.; Blackledge, G. R. P.; Gotting-Smith, K., Bicalutamide (Casodex®) in the treatment of prostate cancer: History of clinical development. *The Prostate* **1998**, *34* (1), 61-72.
  59. Art, K.; Holzbeierlein, J. M., Hormonal and chemotherapeutic options in advanced prostate cancer. *Aging Health* **2008**, *4* (5), 455-462.
  60. Saunders Safety and Efficacy Study of MDV3100 in Patients With Castration-Resistant Prostate Cancer Who Have Been Previously Treated With Docetaxel-based Chemotherapy (AFFIRM).



61. Tran, C.; Ouk, S.; Clegg, N. J.; Chen, Y.; Watson, P. A.; Arora, V.; Wongvipat, J.; Smith-Jones, P. M.; Yoo, D.; Kwon, A.; Wasielewska, T.; Welsbie, D.; Chen, C. D.; Higano, C. S.; Beer, T. M.; Hung, D. T.; Scher, H. I.; Jung, M. E.; Sawyers, C. L., Development of a second-generation antiandrogen for treatment of advanced prostate cancer. *Science* **2009**, *324* (5928), 787-90.
62. Kaisary, A. V.; Tyrrell, C. J.; Peeling, W. B.; Griffiths, K., Comparison of LHRH Analogue (Zoladex) with Orchiectomy in Patients with Metastatic Prostatic Carcinoma. *British Journal of Urology* **1991**, *67* (5), 502-508.
63. Attard, G.; Reid, A. H.; A'Hern, R.; Parker, C.; Oommen, N. B.; Folkerd, E.; Messiou, C.; Molife, L. R.; Maier, G.; Thompson, E.; Olmos, D.; Sinha, R.; Lee, G.; Dowsett, M.; Kaye, S. B.; Dearnaley, D.; Kheoh, T.; Molina, A.; de Bono, J. S., Selective inhibition of CYP17 with abiraterone acetate is highly active in the treatment of castration-resistant prostate cancer. *J Clin Oncol.* **2009**, *27* (23), 3742-8.
64. Witjes, F. J.; Debruyne, F. M.; Fernandez del Moral, P.; Geboers, A. D., Ketoconazole high dose in management of hormonally pretreated patients with progressive metastatic prostate cancer. Dutch South-Eastern Urological Cooperative Group. *Urology* **1989**, *33* (5), 411-5.
65. De Coster, R.; Wouters, W.; Bruynseels, J., P450-dependent enzymes as targets for prostate cancer therapy. *J. Steroid Biochem. Mol. Biol.* **1996**, *56* (1-6), 133-43.
66. Swain, S. M.; Lippman, M. E., *Endocrine therapies of cancer*. Philadelphia, PA: Lippincott, 1990; p 59-109.
67. Deutsch, H. M.; Glinski, J. A.; Hernandez, M.; Haugwitz, R. D.; Narayanan, V. L.; Suffness, M.; Zalkow, L. H., Synthesis of congeners and prodrugs. 3. Water-soluble prodrugs of taxol with potent antitumor activity. *J Med Chem* **1989**, *32* (4), 788-92.
68. Okano, J.; Rustgi, A. K., Paclitaxel induces prolonged activation of the Ras/MEK/ERK pathway independently of activating the programmed cell death machinery. *The Journal of biological chemistry* **2001**, *276*, 19555-64.
69. Speicher, L. A.; Barone, L.; Tew, K. D.; Lines, C. C.; Speicher, L. A.; Barone, L.; Tew, K. D., Combined Antimicrotubule Activity of Estramustine and Taxol in Human Prostatic Carcinoma Cell Lines. **1992**, 4433-4440.
70. Heymach, J. V.; Shackelford, T. J.; Tran, H. T.; Yoo, S.-Y.; Do, K.-A.; Wergin, M.; Saintigny, P.; Vollmer, R. T.; Polascik, T. J.; Snyder, D. C.; Ruffin IV, M. T.; Yan, S.; Dewhirst, M.; Kunnumakkara, A. B.; Aggarwal, B. B.; Wahnefried, W. D., Effect of Low-Fat Diets on Plasma Levels of NF- $\kappa$ B-Regulated Inflammatory Cytokines and

- Angiogenic Factors in Men with Prostate Cancer *Cancer Prev Res October* **2011**, *4*, 1590-1598.
71. Logothetis, C. J., Docetaxel in the Integrated Management of Prostate Cancer. *Oncology* **2002**, *16*.
  72. Izbicka, E.; Campos, D.; Carrizales, G.; Tolcher, A., Biomarkers for Sensitivity to Docetaxel and Paclitaxel in Human Tumor Cell Lines In Vitro. *Cancer Genomics and Proteomics* **2005**, *2*, 219-226.
  73. Chen, M. Y.; Millwood, I. Y.; Wand, H.; Poynten, M.; Law, M.; Kaldor, J. M.; Wesselingh, S.; Price, C. F.; Clark, L. J.; Paull, J. R.; Fairley, C. K., A randomized controlled trial of the safety of candidate microbicide SPL7013 gel when applied to the penis *J. Acquir. Immune Defic. Syndr.* **2009**, *50*, 375-380.
  74. Horoszewicz, J. S.; Leong, S. S.; Kawinski, E.; Horoszewicz, J. S.; Leong, S. S.; Kawinski, E.; Karr, J. P.; Rosenthal, H.; Chu, T. M.; Mirand, E. A.; Murphy, G. P., LNCaP Model of Human Prostatic Carcinoma. **1983**, 1809-1818.
  75. Kampa, M.; Papakonstanti, E. A.; Hatzoglou, A.; Stathopoulos, E. N.; Stournaras, C.; Castanas, E.; Aim, S., The human prostate cancer cell line LNCaP bears functional membrane testosterone receptors that increase PSA secretion and modify actin cytoskeleton 1. 1429-1431.
  76. Kaighn, M. E.; Kirk, D.; Szalay, M.; Lechner, J. F., Growth control of prostatic carcinoma cells in serum-free media: interrelationship of hormone response, cell density, and nutrient media. *Proceedings of the National Academy of Sciences of the United States of America* **1981**, *78*, 5673-6.
  77. Alimirah, F.; Chen, J.; Basrawala, Z.; Xin, H.; Choubey, D., DU-145 and PC-3 human prostate cancer cell lines express androgen receptor: implications for the androgen receptor functions and regulation. *Lett.* **2006**, *580* (9), 2294-300.
  78. Mora, G. R.; Olivier, K. R.; Cheville, J. C.; Mora, G. R.; Olivier, K. R.; Cheville, J. C.; Mitchell, R. F.; Lingle, W. L.; Tindall, D. J., The Cytoskeleton Differentially Localizes the Early Growth Response Gene-1 Protein in Cancer and Benign Cells of the Prostate *Molecular Cance Research* **2004**, *2*, 115-128.
  79. Vicent, M. J.; Duncan, R., Polymer conjugates: nanosized medicines for treating cancer. *Trends in Biotechnology* **2006**, *24* (1), 39-47.
  80. Bross, P. F.; Beitz, J.; Chewn, G.; Chen, X. H.; Duffy, E.; Kieffer, L.; Roy, S.; Sridhara, R.; Rahman, A.; Williams, G.; Pazdur, R., Approval summary: gemtuzumab ozogamicin in relapsed acute myeloid leukemia. *Clinical Cancer Research* **2001**, *7* (6), 1490-1496.
  81. Duncan, R., Polymer conjugates as anticancer nanomedicines. *Nature Reviews Cancer* **2006**, *6* (9), 688-701.

82. Duncan, R.; Gaspar, R., Nanomedicine(s) under the microscope. *Mol Pharm* **2011**, *8* (6), 2101-41.
83. Duncan, R., Polymer therapeutics as nanomedicines: new perspectives. *Current Opinion in Biotechnology* **2011**, *22*, 1-10.
84. Ferrari, M., Cancer nanotechnology: opportunities and challenges. *Nature Rev. Cancer* **2005**, *5*, 161-171.
85. Ringsdorf, H., Hermann Staudinger and the Future of Polymer Research- Jubilees- Beloved Occasions for Cultural Piety *Angewandte Chemie International Edition* **2004**, *43* (9), 1064-1076.
86. Mülhaupt, R., Hermann Staudinger and the Origin of Macromolecular Chemistry. *Angewandte Chemie International Edition* **2004**, *43*, 1054-1063.
87. Tomihata, K.; Suzuki, M.; Oka, T.; Ikada, Y., *A new resorbable monofilament suture*. Elsevier: 1998; Vol. 59, p 13-18.
88. De Santis, R.; Ambrosio, L.; Nicolais, L., Polymer-based composite hip prostheses. *Journal of Inorganic Biochemistry* **2000**, *79* (1-4), 97-102.
89. Boesel, L. F.; Reis, R. L., A review on the polymer properties of Hydrophilic, partially Degradable and Bioactive acrylic Cements (HDBC). *Progress in Polymer Science* **2008**, *2* (33), 180-190.
90. Evans, M. D.; McLean, K. M.; Hughes, T. C.; Sweeney, D. F., A review of the development of a synthetic corneal onlay for refractive correction. *Biomaterials* **2001**, *22* (24), 3319-3328.
91. Nicolson, P. C.; Vogt, J., Soft contact lens polymers: an evolution. *Biomaterials* **2001**, *22* (24), 3273-3283.
92. Barnes, C. P.; Sell, S. A.; Boland, E. D.; Simpson, D. G.; Bowlin, G. L., Nanofiber technology: Designing the next generation of tissue engineering scaffolds *Advanced Drug Delivery Reviews* **2007**, *59* (14), 1413-1433.
93. Baldrick, P., Pharmaceutical excipient development: the need for preclinical guidance. *Regulatory Toxicology and Pharmacology* **2000**, *32* (2), 210-218.
94. Sershen, S.; West, J., Implantable, polymeric systems for modulated drug delivery. *Advanced Drug Delivery Reviews* **2002**, *54* (9), 1225-1235.
95. Lee, K. Y.; Yuk, S. H., Polymeric protein delivery systems. *Progress in Polymer Science* **2007**, *32*, 669-697.
96. Duncan, R.; Connors, T. A.; Meada, H., Drug targeting in cancer therapy: the magic bullet, what next? *Journal of Drug Targeting* **1996**, *3* (5), 317-319.
97. Plan, N. N. C. N. Creating cancer nanotechnology platforms through directed research programs: request for information **2004**.
98. [www.esf.org](http://www.esf.org).

99. Duncan, R., The dawning era of polymer therapeutics. *Nature Reviews Drug Discovery* **2003**, *2* (5), 347-360.
100. Dhal, P. K.; Polomoscank, S. C.; Avila, L. Z.; Holmes-Farley, S. R.; Miller, R. J., Functional polymers as therapeutic agents: concept to marketplace. *Advanced Drug Delivery Review* **2009**, *61*, 1121-1130.
101. Ringsdorf, H., Structure and Properties of Pharmacologically Active Polymers. *Journal of Polymer Science Part C-Polymer Symposium* **1975**, (51), 135-153.
102. Canal, F.; Sanchis, J.; Vicent, M. J., Polymer–drug conjugates as nano-sized medicines. *Current Opinion in Biotechnology* **2011**, *22* (6), 894-900.
103. Veronese, F. M., *PEGylated Protein Drugs: Basic Science and Clinical Applications* 2010; Vol. whole volume.
104. Talelli, M.; Rijcken, C. J. F.; van Nostrum, C. F.; Storm, G.; Hennink, W. E., Micelles based on HPMA copolymers. *Advanced drug delivery reviews* **2010**, *62*, 231-239.
105. Matsumura, Y.; Kataoka, K., Preclinical and clinical studies of anticancer agent-incorporating polymer micelles. *Cancer Sci* **2009**, *100*, 572-579.
106. Wagner, E., Strategies to improve DNA polyplexes for in vivo gene transfer: Will "artificial viruses" be the answer? . *Pharmaceutical Research* **2004**, *21*, 8-14.
107. Vasir, J. K.; Labhasetwar, V., Polymeric nanoparticles for gene delivery. *Expert Opinion Drug Delivery* **2006**, *3*, 325-344.
108. Edinger, D.; Wagner, E., Bioresponsive polymers for the delivery of therapeutic nucleic acids. *Wiley Interdisciplinary Review: Nanomedicine and Nanobiotechnology*, *WIREs* **2011**, *3*, 33-46.
109. Keefe, A. D.; Pai, S.; Ellington, A., Aptamers as therapeutics. *Nature Review Drug Discovery* **2010**, *9*, 537-550.
110. Chipman, S. D.; Oldham, F. B.; Pezzoni, G.; Singer, J. W., Biological and clinical characterization of paclitaxel poliglumex (PPX, CT-2103), a macromolecular polymer-drug conjugate. *International Journal of Nanomedicine* **2006**, *1* (4), 375-383.
111. Li, C.; Wallace, S., Polymer-drug conjugates: Recent development in clinical oncology. *Advanced Drug Delivery Reviews* **2008**, *60* (8), 886-898.
112. Fang, J.; Nakamura, H.; Maeda, H., The EPR effect: Unique features of tumor blood vessels for drug delivery, factors involved, and limitations and augmentation of the effect. *Advanced Drug Delivery Reviews* **2011**, *63* (3), 136-151.
113. Matsumura, Y.; Maeda, H., A New Concept for Macromolecular Therapeutics in Cancer-Chemotherapy - Mechanism of Tumorotropic

- Accumulation of Proteins and the Antitumor Agent Smancs. *Cancer Research* **1986**, *46* (12), 6387-6392.
114. Duncan, R.; Kopečková-Rejmanova, P.; Strohalm, J.; Hume, I.; Cable, H. C.; Pohl, J.; Lloyd, J. B.; Kopeček, J., Anticancer agents coupled to N-(2-hydroxypropyl)methacrylamide copolymers. I. Evaluation of daunomycin and puromycin conjugates in vitro. *British Journal of Cancer* **1987**, *55*, 165-174.
  115. Maeda, H., Polymer conjugated macromolecular drugs for tumor-specific targeting. In *Polymer site-specific Pharmacotherapy*. Domb, A. J.: New York **1994**; p 95-116.
  116. Maeda, H., The Enhanced Permeability and Retention (EPR) Effect in Tumor Vasculature: The Key Role of Tumor-Selective Macromolecular Drug Targeting. *Advances in Enzyme Regulation* **2001**, *41*, 189-207.
  117. Maeda, H., Tumor-selective delivery of macromolecular drugs via the EPR effect: background and future prospects. *Bioconjugate Chemistry* **2010**, *21* (5), 797-802.
  118. Feelisch, M.; Noack, E. A., Correlation between nitric oxide formation during degradation of organic nitrates and activation of guanylate cyclase. *Eur J Pharmacology* **1987**, *139* (1), 19-30.
  119. Seki, T.; Fang, J.; Maeda, H., Enhanced delivery of macromolecular antitumor drugs to tumors by nitroglycerin application. *Cancer Sci* **2009**, *100* (12), 2426-30.
  120. Yasuda, H.; Yamaya, M.; Nakayama, K.; Sasaki, T.; Ebihara, S.; Kanda, A.; Asada, M.; Inoue, D.; Suzuki, T.; Okazaki, T.; Takahashi, H.; Yoshida, M.; Kaneta, T.; Ishizawa, K.; Yamanda, S.; Tomita, N.; Yamasaki, M.; Kikuchi, A.; Kubo, H.; Sasaki, H., Randomized phase II trial comparing nitroglycerin plus vinorelbine and cisplatin with vinorelbine and cisplatin alone in previously untreated stage IIIB/IV non-small-cell lung cancer. *Journal of Clinical Oncology* **2006**, *24* (4), 688-94.
  121. Maeda, H.; Bharate, G. Y.; Daruwalla, J., Polymeric drugs for efficient tumor-targeted drug delivery based on EPR-effect. *European Journal of Pharmaceutics and Biopharmaceutics* **2009**, *71* (3), 409-19.
  122. Daruwalla, J.; Greish, K.; Malcontenti-Wilson, C.; Muralidharan, V.; Lyer, A.; Maeda, H.; Christophi, C., Styrene maleic acid-pirarubicin disrupts tumor microcirculation and enhances the permeability of colorectal liver metastases. *Journal of Vascular Research* **2009**, *46* (3), 218-28.
  123. Vicent, M. J.; Dieudonné, L.; Carbajo, R. J.; Pineda-Lucena, A., Polymer conjugates as therapeutics: future trends, challenges and opportunities. *Expert Opinion Drug Delivery* **2008**, *5* (5), 593-614.

124. Barz, M.; Luxenhofer, R.; Zentel, R.; Vicent, M. J., Overcoming the PEG-addiction: well-defined alternatives to PEG, from structure–property relationships to better defined therapeutics *Polymer Chemistry* **2011**, 2, 1900-1918.
125. Brocchini, S.; Duncan, R., Pendent Drugs, Release from Polymers. In: Encyclopedia of Controlled Drug Delivery. Mathiowitz, E. Ed. New York, Wiley Interscience. pp 786-816. In *Encyclopedia of Controlled Drug Delivery*, Mathiowitz, E., Ed. Wiley Interscience: New York, **1999**; pp 786-816.
126. Jatzkewitz, H., Incorporation of physiologically-active substances into a colloidal blood plasma substitute. I. Incorporation of mescaline peptide into polyvinylpyrrolidone. *Hoppe-Seyler's Zeitschrift fur physiologische Chemie* **1954**, 297 (3-6), 149-156.
127. Trouet, A.; Deprez-de Campeneere, D.; De Duve, C., Chemotherapy through lysosomes with a DNA-daunorubicin complex. *Nature: New biology* **1972**, 239 (91), 110-112.
128. de Duve, C.; de Barse, T.; Poole, B.; Trouet, A.; Tulkens, P.; Van Hoof, F., Commentary. Lysosomotropic agents. *Biochem Pharmacol* **1974**, 23 (18), 2495-531.
129. Canton, I.; Battaglia, G., Endocytosis at the nanoscale. *Chem. Soc. Rev.* **2012**, 41, 2718-2739.
130. Mellman, I., Endocytosis and molecular sorting. *Annual Review of Cell and Developmental Biology* **1996**, 12, 575-625.
131. Greenwald, R. B., PEG drugs: an overview. *Journal of controlled release* **2001**, 74 (1-3), 159-171.
132. Popescu, I.; Suflet, D. M.; Pelin, I. M.; Chitanu, G. C., Biomedical applications of maleic anhydride copolymers. *Review Rev. Roum. Chim.* **2011**, 56 (3), 173-188.
133. Breslow, D. S., Biologically active synthetic polymers. *Pure and Applied Chemistry* **1976**, 46, 103-113.
134. De Stefano, N.; Filippi, M.; Confavreux, C.; Vermersch, P.; Simu, M.; Sindic, C.; Hupperts, R.; Bajenaru, O.; Edan, G.; Grimaldi, L.; Marginean, I.; Medaer, R.; Orefice, G.; Pascu, I.; Pelletier, J.; Sanders, E.; Scarpini, E.; Mancardi, G. L., The results of two multicenter, open-label studies assessing efficacy, tolerability and safety of protiramer, a high molecular weight synthetic copolymeric mixture, in patients with relapsing-remitting multiple sclerosis. *Multiple Sclerosis* **15**, 238-243.
135. Shaunak, S.; Thornton, M.; John, S.; Teo, I.; Peers, E.; Mason, P.; Krausz, T.; Davies, D. S., Reduction of the viral load of HIV-1 after the intraperitoneal administration of dextrin-2-sulphate in patients with AIDS. *AIDS* **1998**, 12, 399-409.

136. Oerlemans, C.; Bult, W.; Bos, M.; Storm, G.; Nijssen, J. F. W.; Hennink, W. E., Polymeric Micelles in Anticancer Therapy: Targeting, Imaging and Triggered Release. *Pharmaceutical research* **2010**, *27*, 2569-2589.
137. Torchilin, V. P., Micellar nanocarriers: Pharmaceutical perspectives. *Pharmaceutical Research* **2007**, *24*, 1-16.
138. Cabral, H.; Matsumoto, Y.; Mizuno, K.; Chen, Q.; Murakami, M.; Kimura, M.; Terada, Y.; Kano, M. R.; Miyazono, K.; Uesaka, M.; Nishiyama, N.; Kataoka, K. Accumulation of sub-100 nm polymeric micelles in poorly permeable tumours depends on size. [www.nature.com/naturenanotechnology](http://www.nature.com/naturenanotechnology).
139. Mikhail, A. S.; Dan, L., Block copolymer micelles for delivery of cancer therapy: transport at the whole body, tissue and cellular levels. *Journal Control Release* **2009**, *138*, 214-23.
140. Chytil, P.; Etrych, T.; Konak, C.; Sirova, M.; Mrkvan, T.; Boucek, J.; Rihova, B.; Ulbrich, K., New HPMA copolymer-based drug carriers with covalently bound hydrophobic substituents for solid tumour targeting. *J Control Release* **2008**, *127* (2), 121-30.
141. Chytil, P.; Etrych, T.; Konak, C.; Sirova, M.; Mrkvan, T.; Rihova, B.; Ulbrich, K., Properties of HPMA copolymer-doxorubicin conjugates with pH-controlled activation: effect of polymer chain modification. *J Control Release* **2006**, *115* (1), 26-36.
142. Jia, Z.; Wong, L.; Davis, T. P.; Bulmus, V., One-pot conversion of RAFT-generated multifunctional block copolymers of HPMA to doxorubicin conjugated acid- and reductant-sensitive crosslinked micelles. *Biomacromolecules* **2008**, *9*, 3106-3113.
143. Andersson, L.; Davies, J.; Duncan, R.; Ferruti, P.; Ford, J.; Kneller, S.; Mendichi, R.; Pasut, G.; Schiavon, O.; Summerford, C.; Tirk, A.; Veronese, F. M.; Vincenzi, V.; Wu, G., Poly(ethylene glycol)-poly(ester-carbonate) block copolymers carrying PEG-peptidyl-doxorubicin pendant side chains: synthesis and evaluation as anticancer conjugates. *Biomacromolecules* **2005**, *6* (2), 914-26.
144. Veronese, F. M.; Schiavon, O.; Pasut, G.; Mendichi, R.; Andersson, L.; Tsirk, A.; Ford, J.; Wu, G.; Kneller, S.; Davies, J.; Duncan, R., PEG-doxorubicin conjugates: influence of polymer structure on drug release, in vitro cytotoxicity, biodistribution, and antitumor activity. *Bioconjug Chem.* **2005**, *16* (4), 775-84.
145. Kataoka, K.; Matsumoto, T.; Yokoyama, M.; Okano, T.; Sakurai, Y.; Fukushima, S.; Okamoto, K.; Kwon, G. S., Doxorubicin-loaded poly(ethylene glycol)-poly( $\beta$ -benzyl-L-aspartate) copolymer micelles: their pharmaceutical characteristics and biological significance. *Journal of Controlled Release* **2000**, *64* (1-3), 143-153.

146. Nakanishi, T.; Fukushima, S.; Okamoto, K.; Suzukia, M.; Matsumura, Y.; Yokoyama, M.; Okano, T.; Sakurai, Y.; Kataoka, K., Development of the polymer micelle carrier system for doxorubicin. *Journal of Controlled Release* **2001**, *74*, 295-302.
147. Soga, O.; van Nostrum, C.; Ramzi, A.; Visser, T.; Soulimani, F.; Frderik, P.; Bomans, P. H. H.; Hennink, W. E., Physicochemical characterization of degradable thermosensitive polymeric micelles. *Langmuir* **2004**, *20*, 9388-9395.
148. Uchino, H.; Matsumura, Y.; Negishi, T.; Koizumi, F.; Hayashi, T.; Honda, T.; Nishiyama, N.; Kataoka, K.; Naito, S.; Kakizoe, T., Cisplatin-incorporating polymeric micelles (NC-6004) can reduce nephrotoxicity and neurotoxicity of cisplatin in rats. *Br J Cancer* **2005**, *93* (6), 678-87.
149. Bae, Y.; Kataoka, K., Intelligent polymers micelles from functional poly(ethylen glycol)-poly(amino acid) block copolymers. *Advanced Drug Delivery Reviews* **2009**, *61*, 768-784.
150. Chandran, S. S.; Nan, A.; Rosen, D.; Ghandehari, H.; Denmeade, S. R., A prostate-specific antigen-activated N-(2-hydroxypropyl)methacrylamide copolymer prodrugs as dual-targeted therapy for prostate cancer. *Molecular Cancer Therapeutics* **2007**, *6*, 2928-2937.
151. Mizumura, Y.; Matsumura, Y.; Hamaguchi, T.; Nishiyama, N.; Kataoka, K.; Kawaguchi, T.; Hrushesky, W. J. M.; Moriyasu, F.; Kakizoe, T., Cisplatin-incorporated Polymeric Micelles Eliminate Nephrotoxicity, While Maintaining Antitumor Activity. *J. Cancer Res.* **2001**, *92*, 328-336.
152. Kumagai, M.; Shimoda, S.; Wakabayashi, R.; Kunisawa, Y.; Ishii, T.; Osada, K.; Itaka, K.; Nishiyama, N.; Kataoka, K.; Nakano, K., Effective transgene expression without toxicity by intraperitoneal administration of PEG-detachable polyplex micelles in mice with peritoneal dissemination. *J Control Release* **2012**.
153. Suma, T.; Miyata, K.; Ishii, T.; Uchida, S.; Uchida, H.; Itaka, K.; Nishiyama, N.; Kataoka, K., Enhanced stability and gene silencing ability of siRNA-loaded polyion complexes formulated from polyaspartamide derivatives with a repetitive array of amino groups in the side chain. *Biomaterials* **2012**, *33* (9), 2770-9.
154. Debus, H.; Beck-Broichsitter, M.; Kissel, T., Optimized preparation of pDNA / poly(ethylene imine) polyplexes using a microfluidic system *Lab on a Chip* **2012**.
155. Gebhart, C. L.; Sriadibhatla, S.; Vinogradov, S.; Lemieux, P.; Alakhov, V.; Kabanov, A., Design and Formulation of Polyplexes Based on



- Pluronic-Polyethyleneimine Conjugates for Gene Transfer. *Bioconjugate Chem.* **2002**, *13* (5), 937–944.
156. Batrakova, E. V.; Kabanov, A. V., Pluronic block copolymers: evolution of drug delivery concept from inert nanocarriers to biological response modifiers. *J Control Release* **2008**, *130* (2), 98-106.
157. Luxenhofer, R.; Schulz, A.; Roques, C.; Li, S.; Bronich, T. K.; Batrakova, E. V.; Jordan, R.; Kabanov, A. V., Doubly amphiphilic poly(2-oxazoline)s as high-capacity delivery systems for hydrophobic drugs *Biomaterials* **2010**, *31* (18), 4972-9.
158. Thanou, M.; Duncan, R., Polymer-protein and polymer-drug conjugates in cancer therapy. *Current Opinion in Investigational Drugs* **2003**, *4* (6), 701-709.
159. Duncan, R.; Seymour, L. W.; Ohare, K. B.; Flanagan, P. A.; Wedge, S.; Hume, I. C.; Ulbrich, K.; Strohalm, J.; Subr, V.; Spreafico, F.; Grandi, M.; Ripamonti, M.; Farao, M.; Suarato, A., Preclinical Evaluation of Polymer-Bound Doxorubicin. *Journal of Controlled Release* **1992**, *19* (1-3), 331-346.
160. Guu, J. A.; Hiuse, G. H.; Juang, T. M., Synthesis and biological properties of antitumor-active conjugates of ADR with dextran. *Journal of Biomaterials Science Polymer Edition* **2002**, *13*, 1135-1151.
161. Mehvar, R., Dextrans for targeted and sustained delivery of therapeutic and imaging agents. *Journal of controlled release* **2000**, *69*, 1-25.
162. Godwin, A.; Hartenstein, M.; Müller, A. H. E.; Brocchini, S., Narrow Molecular Weight Distribution Precursors for Polymer-Drug Conjugates. *Angewandte Chemie* **2001**, *113* (3), 614-617.
163. Říhová, B.; Ulbrich, K.; Kopeček, J.; Mančál, P., Immunogenicity of N-(2-hydroxypropyl)-methacrylamide copolymers—Potential hapten or drug carriers. *Folia Microbiologica* **1983**, *28* (3), 217-227.
164. Duncan, R.; Cable, H. C.; Lloyd, J. B.; Rejmanova, P.; Kopecek, J., Polymers Containing Enzymatically Degradable Bonds .7. Design of Oligopeptide Side-Chains in Poly[N-(2-Hydroxypropyl)Methacrylamide] Co-Polymers to Promote Efficient Degradation by Lysosomal-Enzymes. *Makromolekulare Chemie-Macromolecular Chemistry and Physics* **1983**, *184* (10), 1997-2008.
165. Davis, F., The origin of peganology. *Adv Drug Delivery Rev* **2002**, *54*, 457-458.
166. Duncan, R.; Lloyd, J. B.; Kopecek, J., Degradation of Side-Chains of N-(2-Hydroxypropyl) Methacrylamide Co-Polymers by Lysosomal-Enzymes. *Biochemical and Biophysical Research Communications* **1980**, *94* (1), 284-290.

167. Brocchini, S.; Duncan, R., Pendent Drugs, Release from Polymers. In *Encyclopedia of Controlled Drug Delivery*, Mathiowitz, Ed. Wiley Interscience: New York, 1999; pp 786-816.
168. Sanchis, J.; Canal, F.; Vicent, M. J., Polymer drug conjugates for novel molecular targets. *Nanomedicine* **2010**, *5* (6), 915-935.
169. Vasey, P. A.; Kaye, S. B.; Morrison, R.; Twelves, C.; Wilson, P.; Duncan, R.; Thomson, A. H.; Murray, L. S.; Hilditch, T. E.; Murray, T.; Burtles, S.; Fraier, D.; Frigerio, E.; Cassidy, J., Phase I Clinical and Pharmacokinetics Study of PK1 (*N*-(2-Hydroxypropyl)methacrylamide Copolymer Doxorubicin): First Member of a New Class of Chemotherapeutic Agents-Drug-Polymer Conjugates. *Clinical Cancer Research* **1999**, *5*, 83-94.
170. Seymour, L. W.; Ferry, D. R.; Anderson, D.; Hesslewood, S.; Julyan, P. J.; Poyner, R.; Doran, J.; Young, A. M.; Burtles, S.; Kerr, D. J.; Canc Res Campaign Phase, I. I. I. C., Hepatic drug targeting: Phase I evaluation of polymer-bound doxorubicin. *Journal of Clinical Oncology* **2002**, *20* (6), 1668-1676.
171. Vicent, M. J.; Ringsdorf, H.; Duncan, R., Polymer therapeutics: Clinical applications and challenges for development Preface. *Advanced Drug Delivery Reviews* **2009**, *61* (13), 1117-1120.
172. Samad, A.; Alam, M. I.; Saxena, K., Dendrimers: a class of polymers in the nanotechnology for the delivery of active pharmaceuticals. *Curr Pharm Des* **2009**, *15*, 2958-2969.
173. Montero de Espinosa, L.; Meier, M. A., Synthesis of star- and block-copolymers using ADMET: head-to-tail selectivity during step-growth polymerization. *Chem Commun (Camb)* **2011**, *47*, 1908-1910.
174. Heller, J.; Penhale, D. W. H.; Helwing, R. F., Preparation of polyacetals by the reaction of divinyl ethers and polyols. *Journal of Polymer Science Part C: Polymer Letters* **1980**, *18* (4), 5.
175. Tomlinson, R.; Klee, M.; Garrett, S.; Heller, J.; Duncan, R.; Brocchini, S., Pendent Chain Functionalized Polyacetals That Display pH-Dependent Degradation: A Platform for the Development of Novel Polymer Therapeutics. *Biomacromolecules* **2002**, *35* (2), 473-480.
176. Vicent, M. J.; Tomlinson, R.; Brocchini, S.; Duncan, R., Polyacetal-diethylstilboestrol: a polymeric drug designed for pH-triggered activation. *J Drug Target* **2004**, *12* (8), 491-501.
177. Tang, H. D.; Murphy, C. J.; Zhang, B.; Shen, Y. Q.; Van Kirk, E. A.; Murdoch, W. J.; M., R., Curcumin polymers as anticancer conjugates. *Biomaterials* **2010**, *31* (27), 7139-7149.
178. Paul, A.; Vicent, M. J.; Duncan, R., Using small-angle neutron scattering to study the solution conformation of *N*-(2-

- hydroxypropyl)methacrylamide copolymer-doxorubicin conjugates. *Biomacromolecules* **2007**, 8 (5), 1573-9.
179. Leicester, H. M., Source Book in chemistry 1900-1950 Cambridge, MA: Harvard, 1968; pp. [translation of the original book from Mikhail S. Tswett, *Berichte der Deutschen botanischen Gesellschaft*, 24, 316-23 (1906)].
  180. Ettre, L. S., Nomenclature for Chromatography *Pure Appl. Chem* **1993**, 65, 819-872.
  181. Young, R. J.; Lovell, P. A., *Gel Permeation Chromatography*. London, Chapman & Hall, 1991; p 211-221.
  182. Griffiths, P. C.; Paul, A.; Khayat, Z.; Wan, K. W.; King, S. M.; Grillo, I.; Schweins, R.; Ferruti, P.; Franchini, J.; Duncan, R., Understanding the mechanism of action of poly(amidoamine)s as endosomolytic polymers: correlation of physicochemical and biological properties *Biomacromolecules* **2004**, 5, 1422-1427.
  183. Vicent, M. J.; Greco, F.; Nicholson, R. I.; Paul, A.; Griffiths, P. C.; Duncan, R., Polymer therapeutics designed for a combination therapy of hormone-dependent cancer. *Angew Chem Int Ed Engl* **2005**, 44 (26), 4061-6.

# 2

## Objectives

## AIMS OF THE RESEARCH

This thesis is focused on the design of novel pH-responsive polymer-drug conjugates to be used as single agents or in combination therapy for the treatment of hormone-dependent cancer, in particular prostate cancer. These systems will be based on previously developed polyacetalic systems with the drug incorporated in the polymer mainchain.

In the acidic tumor microenvironment or after the cellular uptake by endocytosis the drop in pH encountered in endosome-lysosomal compartment triggers polymer degradation releasing consequently the drug cargo that diffuses out to the cytosol. In this design, the need to optimized linking chemistry is therefore overpassed. The synthetic estrogen diethylstilbestrol (DES) was used as drug as is clinically relevant in the treatment of prostate cancer and possess an adequate diol functionality to be incorporated in the polymer mainchain. A clear pH-dependent degradation an in vitro proof of concept was achieved with the first generation polyacetals. However this polymer presented some limitations, which include; a non-unique structure, heterogeneity in composition, low drug capability and high polydispersity, which can affect the pharmacological behavior and reproducibility of the therapeutic outcome of this polymer-based nanoconjugate.

The primary focus of this thesis is therefore to move a step further towards a second generation polyacetalic conjugates for the treatment of prostate cancer as single agents, modifying and understanding polymer chemistry/solution conformation (Chapter 4) and as polymer-based combination conjugates (Chapter 5) in order to achieve a possible clinical candidate.

Firstly, a controlled synthesis of DES-based polyacetals with improved properties, such as narrower Mw distributions and higher drug loading will be performed. Main interest will be centered in understanding if slight structural modifications could significantly influence conjugate therapeutic output. These second generation polyacetals will be obtained using a block-co-polymer methodology.

*Tert*-DES and *block*-DES will be then tested in selected prostate cancer cell models. In order to explain the differences encountered once biologically evaluated, an exhaustive characterization of the conformation in solution for

both polyacetalic systems will be carried out by means of different techniques, such as: transmission electron microscopy (TEM), dynamic light scattering (DLS), pulsed-gradient spin-echo NMR (PGSE-NMR) and small-angle neutron scattering (SANS) which have recently been used to good effect for understanding the solution conformation of polymer-conjugates (Chapter 4.II). This will be done in collaboration with Dr. Alison Paul and Dr. Peter Griffiths group at Cardiff University, UK.

Biophysical characterization will be also performed looking at cellular trafficking, molecular mechanism of tert- vs. block- (in collaboration with Dr. Ana Armiñán from our laboratory) and finally *in vivo* proof of concept (in collaboration with CIBBIM-Nanomedicine group at Hospital Vall d'Hebron, Barcelona) will be pursued (Chapter 4.III).

Due to the importance of combination therapy, Chapter 5 will then be focused on improving the polyacetalic constructs by implementing this strategy looking at drug synergism based on the simultaneous administration of endocrine + chemotherapy, wide expertise of the laboratory in this field. To achieve this, an additional monomer will have to be synthesized and incorporated into the polymer to offer the possibility of conjugating a second drug (paclitaxel has been selected here). As with single conjugates exhaustive physicochemical and biophysical characterization, together with preliminary *in vivo* studies including biodistribution, tumor accumulation and antitumor activity of the polyacetals will be performed.

Finally, Chapter 6 and 7 will provide a general discussion and conclusions respectively on the main results achieved in this project.



# 3

## **Materials and General Methods**



### 3. MATERIALS AND METHODS

#### 3.1. Instruments

**Nuclear Magnetic Resonance Spectroscopy: proton and carbon ( $^1\text{H}$  and  $^{13}\text{C}$ , respectively).** Nuclear Magnetic Resonance (NMR) analysis was performed using a BRUKER ADVANCE AC-300 (300 MHz) and NMR data was processed using the program Topspin (Bruker GmbH, Karlsruhe, Germany). The different chemical shifts are reported as s (singlet), d (doublet), t (triplet), q (quartet) or m (multiplet) and expressed by  $\delta$  (ppm) taking as an intern reference the tetramethylsilane signal (TMS) 0.00 ppm, and the intermediate signal in the quintuplet (49.86 ppm) in the carbon spectra. The J-coupling constants are expressed in hertz (Hz). 2D-NMR spectroscopy including Correlation spectroscopy (COSY), total correlation spectroscopy (TOCSY) and Diffusion-ordered spectroscopy (DOSY) to remove spectral overlap, facilitates spectral assignment, and conformational information related to interproton distances available from resonance intensities and the diffusion coefficient of the polymers we obtained. Pulsed Gradient Spin-Echo NMR (PGSE-NMR) was used to determine the diffusion coefficient of the polymers. **Gel Permeation Chromatography (GPC).** Gel permeation chromatograms were obtained either in THF, DMF or in Phosphate buffer solution (0.1%  $\text{NaN}_3$ ) using a Waters 717 plus autosampler with two Waters Styragel 7.8x300mm Columns (HR3 and HR4) for THF or DMF and two TSK-Gel Columns (G2500 and 3000pWXL) for samples in PBS and a Viscotek TDA 302 triple detector Array model 2501, with refractive index (RI), Small Angle Light Scattering, Right Angle Light Scattering, viscosimeter and a UV detector model 2501. OmniSec4.1 software was used to calculate polymer polydispersity and molecular weight. **Reverse Phase-High Performance Liquid Chromatography (RP-HPLC).** Reverse phase (RP) chromatography was performed with a Shimadzu analytical HPLC system using 717plus autosampler and a LICHROCART®, Cat.1.50943 LICHrospher® 100, RP-18 (125 x 4 mm, 5  $\mu\text{m}$ ) column (Lot. L 56118817 No. 721869) purchased from Waters Ltd. (Hertfordshire, UK). **Dynamic Light Scattering (DLS).** DLS measurements were performed using a Malvern Zetasizer NanoZS (Malvern Instruments Ltd, Malvern, UK) in Instituto de Ciencia Molecular (ICMOL) in Paterna, Valencia. **Transmission Electron**

**Microscopy (TEM).** TEM was performed with a Tecnai Spirit G2 FEI and a digital camera Olympus, Soft Image System, model Morada. **Scanning Electron Microscopy (SEM).** SEM technique was carried out using a JEOL JSM 5410 microscope, at an accelerating voltage of 15 KV at different magnifications in the Department of Biomaterials in University of Valencia. **Critical Micelle Concentration (cmc).** Cmc studies were determined in a Jasco FP-6500 spectrofluorometer, using Band width (excitation and emission) of 3nm, Scanning speed of 100nm/nm and data pitch 0.5nm. **Small Angle Neutron Scattering (SANS)** was performed at the Institute Laue-Langevin, ILL in Grenoble (France) and at the ISIS Facility in Oxford (UK) in order to determine the size and shape of the polymers. **Cell studies.** The cell culture work was carried out in a Class II Bio air biological safety cabinet from Telslar. General cell viability assessment was studied using MTT (3-(4,5-dimethyl-2-thiazolyl)-2,5-diphenyl-2H-tetrazolium bromide), the measurements were performed using a Victor<sup>2</sup> Wallac 1420 Multilabel HTS Counter Perkin Elmer plate reader (Northwolk, CT, USA). Live cell confocal fluorescence microscopy studies were carried out at the confocal microscopy service at CIPF (Valencia, Spain) and were performed using a Leica confocal microscope from Leica Microsystems GmbH (Wetzlar, D) equipped with a l-blue 63 oil immersion objective and handled with a TCS SP2 system, equipped with an acoustic optical beam splitter (AOBS). Excitation was with an argon laser (548, 476, 488, 496 and 514 nm) and blue diode (405 nm). Images were captured at an 8-bit gray scale and processed with LCS software Version 2.5.1347 (Leica, Germany) containing multicolor, macro and 3D components. ECL Western blotting detection system (Amersham Pharmacia Biotech, UK) for western blot analysis and the relative protein levels were quantified by densitometry with Scion Image Software.

### 3.2. Materials

Tri(ethylene glycol) divinyl ether (TEGDVE), poly(ethylene glycol) (PEG) Mw 4000Da, p-toluenesulfonic acid monohydrate (p-TSA), diethylstilboestrol (DES), 2-amino-1,3-propanediol (Serinol), 9-Fluorenylmethoxycarbonyl chloride (Fmoc-Cl), succinic anhydride, dioxane, tetrahydrofuran anhydrous (THF) toluene anhydrous, 4-(Dimethylamino)pyridine (DMAP) purum  $\geq 98.0\%$ , N,N-Diisopropylethylamine (DIEA) reagent plus, N-hydroxysuccinimide 98% (NHS) and N-hydroxysulfosuccinimide sodium salt

(sulfo-NHS)  $\geq 98.5\%$  were used as supplied from Sigma-Aldrich (Dorset, UK). Before use, PEG, p-TSA and DES were dried in a vacuum oven 16h at 80 °C and THF was distilled from sodium-benzophenone THF solution. Diisopropylcarbodiimide (DIC), 1-ethyl-3-(3dimethylaminopropyl) carbodiimide hydrochloride (EDAC), 1-hydroxybenzotriazole monohydrate 99.7% (HOBT) were supplied by IRIS Biotech GmbH (Germany). Triethylamine and N,N-dimethylformamide (DMF) were from Fluka Chemika (Masserschmittstr, D). The solvents used to obtain  $^1\text{H}$  NMR and  $^{13}\text{C}$  NMR spectra were deuterated methanol-d 99.8% D (MeOD) from MERCK (U.K.), deuterated chloroform-d 99.8 atom % D ( $\text{CDCl}_3$ ), deuterium oxide 99.8 atom % D ( $\text{D}_2\text{O}$ ) from Carlo Erba Réactifs-SDS (France), and Dimethyl sulfoxide-D6 99.8% ( $\text{DMSO-d}_6$ ) from MERCK (U.K.) which was dried and stored over molecular sieves (4Å). Dichlorometane ( $\text{CH}_2\text{Cl}_2$ ) synthesis grade with approx. 50ppm of amylene, Ethanol (EtOH) absolute GR for analysis, Methanol (MeOH) HPLC grade and acetonitrile (AcCN) HPLC grade were from Scharlau (Spain) and used as supplied. AppliChem (Germany) supplied 2,2'-dihydroxy-(2,2'-bi-indan)-1,1',3,3'-tetrone (Hydrindantin dihydrate). Ninhydrin GR for analysis was from MERCK (Germany). Resins for liquid chromatography Sephadex LH-20 and Sephadex G-10 and pre-packet PD-10 columns were from GE healthcare (U.K.). n-Hexane analytic grade were purchased from VWR (Germany). All other reagents were of general laboratory grade and were purchased from Aldrich or Sigma unless otherwise stated. PC3 and LNCap prostate cancer cell line were ATCC. Tissue culture grade dimethylsulfoxide (DMSO), L-glutamine, 3-(4,5-dimethylthiazol-2-yl)-2,5-diphenyltetrazolium bromide (MTT), Trypan-blue. (St Louis, MO, USA). 0.25% Trypsin-EDTA was from Gibco BRL Life Technologies (Paisley, UK). Heat-inactivated fetal bovine serum and heat-inactivated neonatal bovine serum were from Seromed GmbH (Wien, Austria). F12 and RPMI 1640 medium, Dextran-Texas Red and Oregon green were from Invitrogen (Carlsbad, CA, USA). Fluorescence dye Oregon Green cadaverine (OG-cad) and Oregon green carboxylic acid (succinimidyl ester) (OG-NHS) were from Molecular Probes. Fluorescence dye Cyane 5.5-cadaverine (Cy-cad) was obtained from Shabat and Cyane 5.5-monofunctional succinimidyl ester (Cy-NHS) was from GE Healthcare (Buckinghamshire, UK). Antibodies for western blot analysis: b-Actin (Sigma), p21 (Cell Signaling), caspase 3 (Cell Signalling), Bax (Santa Cruz Biotechnology), and Bcl2(Dako).

### 3.3. Synthesis and Characterisation of PEG-based DES-polyacetalic systems.

#### 3.3.1. Synthesis of Terpolymer (or *Tert*-DES) (1).

##### A) *Strategy 1. Classical methodology.*

**Ter-DES** was synthesised by *tert*-polymerization of vinyl ethers and alcohols in THF by optimisation of a previous reported protocol<sup>1, 2</sup>. Briefly, first all solid reagents were previously dried in a vacuum oven at 80°C for 16 hrs. Then, to a solution of poly(ethylene glycol) (PEG) (Mw=4.000 g/mol, 2 g, 0.5 mmol), *p*-toluene sulfonic acid monohydrate (*p*-TSA) (Mw= 190.22 g/mol , 0.003 g, 0.015 mmol) and diethylstilbestrol (DES) (Mw= 268.34 g/mol ,0.135 g, 0.5 mmol) in distilled THF (6 ml) was slowly added TEGDVE (Mw= 202.25 g/mol, 0.202g, d=0.99, 0.2mL, 1.07 mmol) using a syringe to preserve anhydrous conditions. The reaction was vigorously stirred for 3 hrs. in the dark at RT. Triethylamine (Et<sub>3</sub>N) (0.2ml) was then added to neutralise *p*-TSA catalyst and after rapidly stirred for 30 minutes it was poured into a cold, rapidly stirring mixture of hexane: ether (4:1) (100ml) and then stirred for a further 30 mins to precipitate the polyacetal as a white solid. Then the product was isolated by filtration and the residual solvent was removed by vacuum at RT. An extraction in chloroform with saturated solution of NaHCO<sub>3</sub> (3x20ml) was done to remove any residual *p*TSA. The organic phases were combined, washed with sat. NaCl (20ml), dried over Na<sub>2</sub>SO<sub>4</sub> and filtered. The solvent was removed under vacuum and the residue redissolved in MilliQ water and lyophilised to obtain the desired compound. The polyacetal was again collected and then dried under vacuum for 24h to yield Ter-Des as a white solid (87% yield).

##### B) *Strategy 2. Novel methodology.*

PEG (1000 mg, 0.250 mmol) and DES (100 mg, 0.373 mmol) were added to a 50 ml Schlenk tube equipped with a stirrer bar and a glass stopper. The flask was evacuated under high vacuum (10<sup>-2</sup> bar) for 15 minutes and then refilled with Nitrogen gas. Whilst purging the Schlenk tube with nitrogen, dioxane (anhydrous, sure-seal, 5 ml) was added via syringe and then stirred with gentle heating (~60 °C) until the reagents were fully dissolved. Following this,

*p*-TSA (2 mg, 0.106 mmol, taken from a stock solution of 1 mg/ml in dioxane) was added to the polymer solution and the solution stirred for a further 2 minutes. Whilst purging the flask with nitrogen DEGVE (182  $\mu$ l, 1.12 mmol) was introduced via Gilson pipette and the Schlenk tube was sealed. The reaction mixture was stirred in the dark for 1 hour before sodium hydroxide solution in ethanol (2 ml, 0.1 M) was added directly to quench the catalyst and stirring continued for a further 5 minutes. The sample was purified by precipitation over hexane (100ml) and after make a decantation of much of the solvent it was centrifuged to completely decant the hexane. The residue was dried over nitrogen flux and redissolved in tetrahydrofurane (4mL) and again precipitated over hexane (100mL), centrifuging the solution to decant the solvent and dry the residue over nitrogen flux, repeating this washing manner 3 times to ensure a proper purification. After dried the samples at high vacuum during 4hours the samples were stored in sealed tubes at  $-20^{\circ}\text{C}$  to be stable.

*Tert-DES polyacetal 1*:  $^1\text{H}$  NMR ( $\text{CDCl}_3$ , 300 MHz): 0.77 (t,  $J=7.5$  Hz, DES  $\text{CH}_3$ ), 1.33 (d,  $J=3.9$  Hz, PEG-acetal  $\text{CH}_3$ ), 1.53 (d,  $J=5.4$  Hz, DES-acetal  $\text{CH}_3$ ), 2.13 (dd,  $J=7.5$  Hz,  $J=15.3$ Hz, DES  $\text{CH}_2$ ), 3.59 (m, PEG  $\text{CH}_2$ ), 4.80 (q,  $J=3.9$  Hz, PEG-acetal  $\text{CH}$ ), 5.46 (q,  $J=5.4$  Hz, DES-acetal  $\text{CH}$ ), 7.0-7.2 (m, DES  $\text{ArH}$ ).  $^{13}\text{C}$  NMR ( $\text{CDCl}_3$ , 75 MHz): 13.40, 19.55, 20.16, 64.09, 64.59, 70.55, 99.64, 99.82, 116.82, 129.66, 130.73, 136.20, 138.69, 151.74, 155.24.

### 3.3.2. Synthesis of Block-copolymer (or *Block-DES*) (2).

#### A) *Strategy 1. Procedure A based on the classical methodology.*

Block-DES<sup>2</sup> was synthesised by *co*-polymerisation in THF. In a flask previously dried in a vacuum oven, lyophilised PEG ( $M_w=4000\text{g/mol}$ , 2g, 0.5mmol) and *p*-TSA ( $M_w=190.22\text{g/mol}$ , 0.003g, 0.015mmol) and were dissolved in distilled THF (4ml). Then, TEGDVE ( $M_w=202.23\text{g/mol}$ , 0.5mmol, 0.22ml) was added and the mixture was vigorously stirred for 3h in the dark at RT. Afterwards, DES ( $M_w=268.34\text{g/mol}$ , 0.134g, 0.5mmol) was slowly added to the reaction using a syringe to preserve anhydrous conditions and stirred for 3h more in the dark at RT. Triethylamine (0.2ml) was then added to neutralize *p*-TSA catalyst. After stirring for 30 min. the solution was poured into a cold mixture of hexane: ether (4:1) (100ml) to precipitate the polyacetal **2** under stirring. After additional 30 min. the polymer was collected

and place into a fresh solution of hexane: ether (4:1) and stirred for a further 30 min to achieve an exhaustive wash. The polyacetal was again collected and then dried under vacuum for 24h to obtain Block-Des as a white solid (1,5985g, 0.9562 mmol, 85% yield).

**B) Strategy 2. Procedure B based on the novel methodology.**

PEG (1000 mg, 0.250 mmol) was added to a 50 ml Schlenk tube equipped with a stirrer bar and a glass stopper. The flask was evacuated under high vacuum ( $10^{-2}$  bar) for 15 minutes and then refilled with Nitrogen gas. Whilst purging the Schlenk tube with nitrogen, dioxane (anhydrous, sure-seal, 4 ml) was added via syringe and then stirred with gentle heating ( $\sim 60$  °C) until PEG was fully dissolved. Following this, p-TSA monohydrate (2 mg, 0.106 mmol, taken from a stock solution of 1 mg/ml in dioxane) was added to the solution and stirred for a further 2 minutes. Whilst purging the flask with nitrogen DEGVE (60  $\mu$ l, 0.37 mmol) was introduced via Gilson pipette and the Schlenk tube was sealed. The reaction mixture was stirred in the dark for 45 minutes before more DEGDVE (122  $\mu$ l, 0.75 mmol) was added and after 15min DES (100 mg, 0.373 mmol) was also added and stirred during 1 hour more. Then sodium hydroxide solution (0.5 ml, 0.1 M) was added directly to quench the catalyst and stirring continued for a further 5 minutes. The sample was purified by precipitation over hexane (100ml) and after make a decantation of much of the solvent it was centrifuged to completely decant the hexane. The residue was dried over nitrogen flux and redissolved in tetrahydrofuran (4mL) and again precipitated over hexane (100mL), centrifuging the solution to decant the solvent and dry the residue over nitrogen flux, repeating this washing manner 3 times to ensure a proper purification. After dried the samples at high vacuum during 4hours the samples were stored in sealed tubes at  $-20^{\circ}\text{C}$  to be stable.

*Block-DES Polyacetal 2*: NMR ( $\text{CDCl}_3$ , 300 MHz): 0.7–0.8 (t, DES –CH<sub>3</sub>), 1.2–1.3 (d, PEG–acetal –CH<sub>3</sub>), 1.5–1.6 (d, DES–acetal –CH<sub>3</sub>), 2.1–2.2 (q, DES –CH<sub>2</sub>–), 3.4–3.9 (m, PEG –O–CH<sub>2</sub>–), 4.7–4.8 (q, PEG–acetal –CH–), 5.4–5.5 (q, DES–acetal –CH–), 7.0–7.2 (m, DES Ar–H). <sup>13</sup>C NMR ( $\text{CDCl}_3$ , 75 MHz): 13.44, 19.53, 20.15, 28.51, 64.04, 64.55, 70.52, 99.59, 99.78, 114.42, 114.98, 116.78, 129.64, 130.69, 134.06, 136.35, 138.35, 138.93, 154.97, 155.16, 155.20.

### 3.3.3. Synthesis of N-Fmoc protection of serinol co-monomer (or Fmoc-Serinol) (3).

This is a well known reaction applied to the synthesis of hidroximethylaziridines<sup>3</sup> and it was first reported by Tomlinson, 2002<sup>4</sup>. Serinol-Fmoc was synthesised by condensation between the acyl group in Fmoc and the amine group in Serinol to form an amide bond by elimination of HCl. Serinol (Mw=91,06g/mol, 1.0g, 11mmol) was dissolved in 26.5ml of a solution 10% Na<sub>2</sub>CO<sub>3</sub> (8g Na<sub>2</sub>CO<sub>3</sub> in 80ml distilled water). Then, 15ml of dioxane was added and the mixture was stirred in an ice water bath. Fluorenylmethoxycarbonyl chloride (Fmoc-Cl) (Mw= 260,72mg/mol, 2,86g, 11mmol) was carefully added to the mixture and stirred for 4h at 4°C. After 2h, 15ml of dioxane was added to decrease the viscosity. The mixture was then stirred overnight at RT (ca. 16h). After that time, 100ml of distilled water was added and the product extracted with ethyl acetate (2x100ml). Organic phases were combined and dried over Na<sub>2</sub>SO<sub>4</sub> anhydrous. After filtration the solvent was removed under vacuum to obtain a white solid. Then the solid was redissolved in 40ml dioxane and recrystallized in 150ml hexane. 84% yield.

*Serinol-Fmoc* 3: <sup>1</sup>H NMR (300 MHz, DMSO-d): 3.3-3.4 (m, Serinol-CH<sub>2</sub>), 4.1-4.2 (t, Fmoc ArCH<sub>2</sub>-CH), 4.4-4.5 (t, J=3.2 Hz, Fmoc ArCH<sub>2</sub>-CH), 7.2-7.9 (m, Fmoc ArH). <sup>13</sup>C NMR (75 MHz, DMSO-d): 51.3, 47.34, 64.2, 68.35, 126.7, 127.1, 128.7, 156.2.

### 3.3.4. Synthesis of DES-Serinol-polyacetal, *Tert*-DES-Serinol (or *Tert*-DES-Ser) (4).

*A) Strategy 1. Procedure A based on the classical methodology.*

***Tert*-DES-Ser<sup>2</sup> (4)** was synthesised by *co*-polymerisation in THF. PEG<sub>4000</sub>, p-TSA and Fmoc-Serinol were dried in separate containers at 80°C under high vacuum overnight. The compounds PEG (Mw=4000g/mol, 1g, 0.25mmol), p-TSA (Mw=190.22g/mol, 0.0002g, 0.009mmol), Fmoc-Serinol (Mw=213,13g/mol, 0,053g, 0,25mmol) and DES (Mw=268.34g/mol, 0.062g, 0,25mmol) were added together in a 2-neck round bottomed flask, previously purged with nitrogen and the reagents were dissolved in distilled THF (4ml). The reaction mixture was stirred for 20min. Then, TEGDVE

(Mw=202.23g/mol, 0.75mmol, 0.33ml) was directly added to the reaction and after stirring for 3 hours, triethylamine (0.2 ml) was added until pH 8 and the reaction was stirred for 45min more. Finally, the reaction mixture was poured into a cold hexane: diethyl ether mixture 4:1 for 15 minutes to form a precipitate that was then filtered giving polyacetal **4**. 77% yield.

**B) Strategy 2. Procedure B based on the novel methodology.**

PEG (1 g, 0.250 mmol), DES (100 mg, 0.373 mmol) and Fmoc-Serinol (120 mg, 0.56 mmol) were added to a 50 ml Schlenk tube equipped with a stirrer bar and a glass stopper. The flask was evacuated under high vacuum ( $10^{-2}$  bar) for 15 minutes and then refilled with Nitrogen gas. Whilst purging the Schlenk tube with nitrogen, dioxane (anhydrous, sure-seal, 5 ml) was added via syringe and then stirred with gentle heating ( $\sim 60$  °C) until the reagents were fully dissolved. Following this, *p*-TSA (2 mg, 0.106 mmol, taken from a stock solution of 1 mg/ml in dioxane) was added to the polymer solution and the solution stirred for a further 2 minutes. Whilst purging the flask with nitrogen DEGVE (182  $\mu$ l, 1.12 mmol) was introduced via Gilson pipette and the Schlenk tube was sealed. The reaction mixture was stirred in the dark for 1 hour before sodium hydroxide solution (0.5 ml, 0.1 M) was added directly to quench the catalyst and stirring continued for a further 5 minutes. The sample was purified by precipitation over hexane (100ml) and after make a decantation of much of the solvent it was centrifuged to completely decant the hexane. The residue was dried over nitrogen flux and redissolved in tetrahydrofuran (4mL) and again precipitated over hexane (100mL), centrifuging the solution to decant the solvent and dry the residue over nitrogen flux, repeating this washing manner 3 times to ensure a proper purification. After dried the samples at high vacuum during 4hours the samples were stored in sealed tubes at  $-20^{\circ}\text{C}$  to be stable.

*Tert-DES-Ser 4*:  $^1\text{H}$  NMR ( $\text{CDCl}_3$ , 300 MHz): 0.77 (t,  $J=7.5$  Hz, DES  $\text{CH}_3$ ), 1.33 (d,  $J=3.9$  Hz, PEG-acetal  $\text{CH}_3$ ), 1.50-1.52 (d,  $J=5.4$  Hz, DES-acetal  $\text{CH}_3$ ), 2.13-2.3 (dd,  $J=7.5$  Hz,  $J=15.3$ Hz, DES  $\text{CH}_2$ ), 3.4-3.6 (m, PEG  $\text{CH}_2$ , m, Serinol- $\text{CH}_2$ ), 4.1-4.2 (t, Fmoc Ar  $\text{CH-CH}_2$ -), 4.3-4.4 (t,  $J=3.1$  Hz, Fmoc Ar- $\text{CH-CH}_2$ -) 4.80 (q,  $J=3.9$  Hz, PEG-acetal  $\text{CH}$ ), 5.46 (q,  $J=5.4$  Hz, DES-acetal  $\text{CH}$ ), 7.0-7.2 (m, DES ArH) 7.3-7.8 (m, Fmoc ArH).  $^{13}\text{C}$  NMR ( $\text{CDCl}_3$ , 75 MHz): 13.42, 19.59, 20.43, 63.97, 64.39, 70.45, 100.21, 100.43, 114.82,



116.82, 129.46, 130.70, 136.70, 138.76, 151.93, 155.14, 51.3, 47.34, 64.2, 68.76, 126.7, 127.7, 128.7, 156.5.

### 3.3.5. Synthesis of *Block-DES-Serinol* (or *Block-DES-Ser*)(5).

#### A) *Strategy 1. Procedure A based on the classical methodology.*

***Block-DES-Ser*<sup>2</sup> (5)** was synthesised by a *co*-polymerisation in THF. PEG<sub>4000</sub> (Mw=4000g/mol, 0,61g, 0,15 mmol), p-TSA (Mw=190.22g/mol, 0.0001g, 0.004mmol and Fmoc-Serinol (Mw= 213,13g/mol, 0,064g, 0,3mmol) were dried in separate vessels at 80°C under high vacuum overnight. PEG and p-TSA were weighed together in a double-necked flask and purged with nitrogen. THF was added and the mixture heated gently to improve the solubility of the reactants. After cooling down, TEGDVE (Mw=202.23g/mol, 0.85mmol, 0.375ml) was directly added to the reaction and after 3h stirring, p-TSA dissolved in THF and TEGDVE were also added. After 30min DES (Mw=268.34g/mol, 0.062g, 0,25mmol) (0,3mmol) and Fmoc-Serinol were dissolved together in THF and added to the reaction and left stirring for 3h. Then, triethylamine was added to stop the reaction (pH 8). The reaction mixture was precipitated into a cold hexane: diethyl ether mixture 4:1 for 15min. and after filtration polyacetal **5** obtained in a 34 % yield.

#### B) *Strategy 2: Procedure B based on the novel methodology.*

PEG (1 g, 0.250 mmol) was added to a 50 ml Schlenk tube equipped with a stirrer bar and a glass stopper. The flask was evacuated under high vacuum (10<sup>-2</sup> bar) for 15 minutes and then refilled with Nitrogen gas. Whilst purging the Schlenk tube with nitrogen, dioxane (anhydrous, sure-seal, 4 ml) was added via syringe and then stirred with gentle heating (~60 °C) until PEG was fully dissolved. Following this, p-TSA monohydrate (2 mg, 0.106 mmol, taken from a stock solution of 1 mg/ml in dioxane) was added to the solution and stirred for a further 2 minutes. Whilst purging the flask with nitrogen DEGVE (60 µl, 0.37 mmol) was introduced via Gilson pipette and the Schlenk tube was sealed. The reaction mixture was stirred in the dark for 45 minutes before more DEGVE (122 µl, 0.75 mmol) was added and after 15min DES (100 mg, 0.373 mmol) and Fmoc-Serinol (120 mg, 0.56 mmol) were also added and stirred during 1hour more. Then sodium hydroxide solution (0.5 ml, 0.1 M) was added directly to quench the catalyst and stirring

continued for a further 5 minutes. The sample was purified by precipitation over hexane (100ml) and after make a decantation of much of the solvent it was centrifuged to completely decant the hexane. The residue was dried over nitrogen flux and redissolved in tetrahydrofurane (4mL) and again precipitated over hexane (100mL), centrifuging the solution to decant the solvent and dry the residue over nitrogen flux, repeating this washing manner 3 times to ensure a proper purification. After dried the samples at high vacuum during 4hours the samples were stored in sealed tubes at  $-20^{\circ}\text{C}$  to be stable.

*Block-DES-Ser 5*: NMR ( $\text{CDCl}_3$ , 300 MHz): 0.7–0.8 (t,  $J=7.4$  Hz, DES  $\text{CH}_3$ ), 1.2–1.3 (d,  $J=3.8$  Hz, PEG-acetal  $\text{CH}_3$ ), 1.4–1.5 (d,  $J=5.5$  Hz, DES-acetal  $\text{CH}_3$ ), 2.1–2.2 dd,  $J=7.6$  Hz,  $J=15.4$ Hz, DES  $\text{CH}_2$ ), 3.5-3.9 (m, PEG  $\text{CH}_2$ , m, Serinol- $\text{CH}_2$ ), 4.1-4.2 (t, Fmoc Ar  $\text{CH-CH}_2$ -), 4.3-4.4 (t,  $J=3.1$  Hz, Fmoc Ar- $\text{CH-CH}_2$ -) 4.7-4.8(q,  $J=3.9$  Hz, PEG-acetal  $\text{CH}$ ), 5.4–5.5 (q,  $J=5.4$  Hz, DES-acetal  $\text{CH}$ ), 7.0–7.2 (m,DES ArH) 7.3-7.9 (m, Fmoc ArH).  $^{13}\text{C}$  NMR ( $\text{CDCl}_3$ , 75 MHz): 13.34, 19.54, 20.16, 28.51, 64.04, 64.55, 70.52, 99.61, 99.79, 114.52, 115.12, 116.69, 116.78, 129.74, 130.68, 134.12, 136.25, 138.45, 138.95, 154.68, 155.34, 155.19. 51.32, 47.03, 64.24, 68.3, 126.57, 127.31, 129.3, 156.52.

### 3.3.6.N-Fmoc deprotection of the polyacetals, *Tert-DES-Ser*<sub>NH<sub>2</sub></sub> (**6**) and *Block-DES-Ser*<sub>NH<sub>2</sub></sub><sup>2</sup> (**7**).

The polymers *Tert-DES-Ser 4* and *Block-DES-Ser 5* were dissolved independently in two different reactions in a 20% piperidine/acetonitrile solution (10 ml) and stirred for 1 h. The reaction was monitored by TLC (100% ethyl acetate,  $R_f = 0.7$ ). The reaction mixture was washed with hexane (3 x 15ml) and the acetonitrile removed under vacuum at RT. Then, the residual solid was redissolved in 15ml of hexane and stirred for 2h to yield polyacetals **6** and **7** (90% and 89% respectively).

*Tert-DES-Ser*<sub>NH<sub>2</sub></sub> **6**:  $^1\text{H}$  NMR ( $\text{CDCl}_3$ , 300 MHz): 0.79 (t,  $J=7.3$  Hz, DES  $\text{CH}_3$ ), 1.29 (d,  $J=3.6$  Hz, PEG-acetal  $\text{CH}_3$ ), 1.48-1.51 (d,  $J=4.8$  Hz, DES-acetal  $\text{CH}_3$ ), 2.11-2.2 (dd,  $J=7.6$  Hz,  $J=14.9$  Hz, DES  $\text{CH}_2$ ), 3.58-3.91 (m, PEG  $\text{CH}_2$ ), 4.1-4.2 (t, Fmoc Ar  $\text{CH-CH}_2$ -), 4.3-4.4 (t,  $J=3.1$  Hz, Fmoc Ar- $\text{CH-CH}_2$ -) 4.81 (q,  $J=3.9$  Hz, PEG-acetal  $\text{CH}$ ), 5.45 (q,  $J=5.3$  Hz, DES-acetal  $\text{CH}$ ), 6.9-7.1 (m, DES ArH).  $^{13}\text{C}$  NMR ( $\text{CDCl}_3$ , 75 MHz): 13.43, 19.58, 20.16, 28.62,

47.56, 64.11, 65.01, 67.51, 70.56, 99.66, 99.82, 114.41, 114, 89, 116, 57, 116.82, 128.92, 130.73, 135.60, 138.71, 138, 89, 151.72, 156.24, 155.81.

*Block-DES-Ser<sub>NH2</sub> 7*: <sup>1</sup>H NMR (300MHz, CDCl<sub>3</sub>): 0.7–0.8 (t, J=7.4 Hz DES CH<sub>3</sub>), 1.2–1.3 (d, J=3.7 Hz, PEG-acetal CH<sub>3</sub>), 1.5–1.6 (d, J=5.1 Hz DES-acetal CH<sub>3</sub>), 2.1–2.2 (dd, J=7.5 Hz, DES CH<sub>2</sub>), 3.49–3.9 (m, PEG CH<sub>2</sub>) 4.1–4.2 (t, Fmoc Ar CH-CH<sub>2</sub>-), 4.3–4.4 (t, J=3.1 Hz, Fmoc Ar-CH-CH<sub>2</sub>-), 4.7–4.8 (q, J=4.1 Hz PEG acetal CH), 5.4–5.5 (q, J=5.5 Hz DES-acetal CH), 7.0–7.2 (m, DES ArH). <sup>13</sup>C NMR (CDCl<sub>3</sub>, 75 MHz): 13.45, 19.8, 19.98, 28.58, 47.5, 64.21, 64.56, 67.1, 71.42, 99.69, 99.79, 114.52, 114.88, 116.53, 116.79, 129.74, 130.74, 134.45, 136.66, 138.95, 138.99, 154.77, 155.15, 155.21.

### 3.3.7. Synthesis of Fluorescently-labeled conjugates (Oregon green and Cyane 5.5 conjugation).

The conjugation to these fluorescence dyes is carry out in order to study the cellular uptake and trafficking in prostate cancer cell lines and to develop *in vivo* studies to determine biodistribution and tumour accumulation of the conjugates.

These conjugates were synthesizing using two different strategies. **Strategy 1**; a fluorescence probe, OG or Cy5.5, both as carboxylic acid, was conjugated to Polyacetals *Tert*-DES-Ser<sub>NH2</sub> **6** and *Block*-DES-Ser<sub>NH2</sub> **7** through the reaction between the free amine group in the polyacetal and the carboxylic group in the fluorochromes after removing NHS group. **Strategy 2** is focus first on the succinylation of the polymers *Tert*-DES-Ser<sub>NH2</sub> **6** and *Block*-DES-Ser<sub>NH2</sub> **7** and then to conjugate to OG and Cy5-5, through the carboxylic group in the polyacetals and the free amine groups in the fluorescence dyes.

*A) Strategy 1. Fluorescence-label conjugates through free amine groups in the polyacetals.*

*A.1) Synthesis of OG-carboxylic acid labeled conjugates<sup>2</sup>, Tert-DES-Ser-OG<sub>NHS</sub> (8) and Block-DES-Ser-OG<sub>NHS</sub> (9).*

*Tert*-DES-Ser<sub>NH2</sub> **6** (0,300 g, 0,030mmol) or *Block*-DES-Ser<sub>NH2</sub> **7** (0.300g, 0,022mmol) were dissolved in anhydrous THF in two independent reactions. DIEA was added to adjust the pH until 8-9. Oregon green-carboxylic acid (0.0002 g, 0.0008 mmol) was dissolved in CH<sub>2</sub>Cl<sub>2</sub> and added to the reaction

mixture. The reaction was monitored by TLC (Ethyl acetate: hexane, 1:1 as mobile phase,  $R_f = 0.5$ ). When the reaction was completed (16 hours), the solvent was evaporated under vacuum at RT. The residual product was redissolved in MilliQ H<sub>2</sub>O and purified by two different ways, (i) by PD10 column eluted with water collecting fractions of 1 mL or (ii) by pouring into stirred cold hexane:diethyl ether (4:1) for 1h to precipitate the conjugated polyacetals. In procedure (i), 2  $\mu$ L were taken from each fraction of 1 mL and added to 998  $\mu$ L of MeOH and measured spectrophotometrically using a Victor2Wallac station, in order to identify the fractions containing Polyacetal-OG conjugates and also to quantify the amount of conjugated OG. OG loading was determined to be quantitative.

Then, both polymer OG-carboxylic acid conjugates, *Tert*-DES-Ser-OG<sub>NHS</sub> **8** and *Block*-DES-Ser-OG<sub>NHS</sub> **9** were isolated by water removed in freezer drier.

**A.2) Synthesis of Cy5.5-carboxylic acid labeled conjugates *Tert*-DES-Ser-Cy<sub>NHS</sub> (10) and *Block*-DES-Ser-Cy<sub>NHS</sub> (11).**

*Tert*-DES-Ser<sub>NH<sub>2</sub></sub> **6** (0.100 g, 0.010mmol) or *Block*-DES-Ser<sub>NH<sub>2</sub></sub> **7** (0.100g, 0.0073mmol) were dissolved in anhydrous THF in two independent reactions. DIEA was added to adjust the pH until 8-9. Cyane5.5 carboxylic acid mono dye (0.0002 g, 0.0008 mmol) was dissolved in CH<sub>2</sub>Cl<sub>2</sub> and added to the reaction mixture. When the reaction was completed (around 16 hours), the solvent was evaporated under vacuum at RT. The residue was redissolved in MilliQ water and purified by PD10 column eluted with MilliQ water, collecting fractions of 1 mL. From each fraction, 2  $\mu$ L were taken and added to 998  $\mu$ L of MeOH and measured spectrophotometrically using a Victor2Wallac station, in order to identify the fractions containing the Polyacetal-Cy conjugates and also to quantify the amount of conjugated Cyane. Cy loading was determined to be quantitative. Then, both polymers *Tert*-DES-Ser-Cy<sub>NHS</sub> **10** and *Block*-DES-Ser-Cy<sub>NHS</sub> **11** were isolated by water remove in freezer drier.

**B) Strategy 1. Fluorescence-label conjugates through free carboxylic groups in the polyacetals.**

**B.1) Succinylation of polyacetals *Tert*-DES-Ser<sub>NH<sub>2</sub></sub> **6** and *Block*-DES-Ser<sub>NH<sub>2</sub></sub> **7** to obtain *Tert*-DES-Ser<sub>COOH</sub> **12** and *Block*-DES-Ser<sub>COOH</sub> **13**.**

Deprotected polyacetal **6** (0.60g, 0.058 mmol NH<sub>2</sub> equiv) and **7** (0.60g, 0.058 mmol NH<sub>2</sub> equiv) were dissolved in anhydrous THF (13mL) as two independent reactions, then succinic anhydride (0.0560g, 0.560mmol) and dimethyl amino pyridine (DMAP, 0.102g, 0.835mmol) were added, pH was adjust to 8 with triethylamine (Et<sub>3</sub>N, 100μL). The reaction mixture was stirred 24h at RT, then, the reaction mixture was poured drop by drop over 100 mL of diethyl ether and it was stirred for 30min further in order to precipitate Succinoylated polyacetals Ser<sub>COOH</sub>-Ter-Des **12** and Ser<sub>COOH</sub>-Block-Des **13**. The precipitates were isolated by centrifugation-decantation procedure *Tert-DES-Ser<sub>COOH</sub>* **12** (yield 0.64g, 0.20mmol, 89%, 28.7 % COOH as determined by <sup>1</sup>H NMR) and *Block-DES-Ser<sub>COOH</sub>* **13** (yield 0.55g, 0.17mmol, 76%, 24.6 % COOH as determined by <sup>1</sup>H NMR). M<sub>w</sub> range= 61235-15387 g/mol; M<sub>w</sub>/M<sub>n</sub>=1.2-1.4 as determined by aqueous GPC.

*Tert/Block-DES-Ser<sub>COOH</sub>* **12** and **13**, respectively: <sup>1</sup>H NMR (300MHz, CDCl<sub>3</sub>): 1.244-1.148ppm (18H, d, J=5.4Hz acetal-CH<sub>3</sub>); 2.542ppm (4H, m, Succ NCO-CH<sub>2</sub>-CH<sub>2</sub>-COOH); 3.575ppm (924H, m, PEG-CH<sub>2</sub>-O), 4.754 – 4.700ppm (6H, q, J=5.4Hz, acetal-CH-).

Three different methods were used to purify this product:

a) Size Exclusion Liquid Chromatography (SEC) using a PD10 column (G25 Sephadex resine). A PD10 column (1x5cm) was previously washed and equilibrated with ddH<sub>2</sub>O as eluent, then, the crude (0.06g,) was dissolved in a maximum of 2mL of ddH<sub>2</sub>O. 25 fractions of 1mL each were collected and freeze dried to analyze by <sup>1</sup>H NMR. Products were confirmed and recollected, SerSucc-Ter-Des 12 (0.021g, 37%) and SerSucc-Block-Des 13 (0.028g, 51%).

b) SEC by sephadex LH20 column. LH20 column (17.5x3cm) was equilibrated with HPLC grade MeOH, previously filtered and sonicated, also used as eluent. In this case , the crude (0.016g) was dissolved in MeOH (3ml). 15 fractions were collected (10mL each) and concentrated with a stream of N<sub>2</sub> until dryness. All of them were analyzed by <sup>1</sup>H NMR. Product 12 (0.04g, 72%) and 13 (0.034g, 61%).

c) Dialysis through a Spectra Por membrane. A membrane with a Mw cutoff of 3500g/mol was used. The crude (0.12g) was dissolved in 15ml ddH<sub>2</sub>O

introduce in the membrane (previously hydrated) and dialyzed at 4°C against ddH<sub>2</sub>O (4X5L) for 24 h. The solution was lyophilized to yield the purified conjugates, **12** (0.032g, 58%) and **13** (0.03g, 54%). Products identities were confirmed by <sup>1</sup>H NMR.

All products were characterized by <sup>1</sup>H NMR before and after purification to compare results, and stored under N<sub>2</sub> at -20°C.

***B.2) Synthesis of OG-cadaverine labeled conjugates Tert-DES-Ser-OG<sub>cad</sub> (14) and Block-DES-Ser-OG<sub>cad</sub> (15).***

Succinoylated polyacetal *Tert*-DES-Ser<sub>COOH</sub> **12** or *Block*-DES-Ser<sub>COOH</sub> **13** (0.1g, 0.008 mmol COOH equiv) was dissolved in 0.5mL of anhydrous THF, under N<sub>2</sub> atmosphere. Diisopropylcarboimide (DIC, 6.2μL, 0.040mmol) was added and after 5 min 1-hydroxybenzotriazole hydrate (HOBT, 0.0103g, 0.076mmol) was also added as solid, followed 10min later of the OG-cadaverine (0.0002g, 0.0008mmol, dissolved in 0.01mL anhydrous DMF). The pH was adjusted to 8-9 with DIEA and when the reaction was completed after 24hours, the solvent was evaporated under vacuum at RT. The product was isolated by removing the solvent under vacuum and in order to remove completely any trace of un-reacted compounds or reaction subproduct, the residue was redissolved in MilliQ H<sub>2</sub>O and purified by PD10 column eluted with MilliQ water, collecting fractions of 1 mL. From each fraction, 2 μL were taken and added to 998 μL of MeOH and measured spectrophotometrically using a Victor2Wallac station, in order to identify the fractions containing the Polyacetal-OG conjugates and also to quantify the amount of conjugated OG. Then, both polymers OG-cad conjugates, *Tert*-DES-Ser-OG<sub>cad</sub> **14** and *Block*-DES-Ser-OG<sub>cad</sub> **15** were isolated by removal of water in a freezer dryer and by confirmed by H NMR the presence of the polyacetal-OG conjugates.

***B.3) Synthesis of Cy5.5-cadaverine labeled conjugates Tert-DES-Ser-Cy<sub>cad</sub> (16) and Block-DES-Ser-Cy<sub>cad</sub> (17).***

Succinoylated polyacetals **12** or **13** were conjugated with Cyane 5.5-cadaverine using the same procedure as that described for **14** and **15**. The polymers **16** and **17** (0.050g, 0,030mmol) were dissolved independently as 2 reactions, in anhydrous THF (10ml). Diisopropylcarboimide (DIC, 6.2μL,

0.040mmol) was added and after 5 min 1-hydroxybenzotriazole hydrate (HOBT, 0.0103g, 0.076mmol) was also added as solid, followed 10min later of the Cy-cadaverine (0.0002g, 0.0008mmol, dissolved in 0.01mL anhydrous DMF). The pH was adjusted to 8-9 with DIEA and when the reaction was completed after 24hours, the solvent was evaporated under vacuum at RT. The product was isolated by removing the solvent under vacuum and in order to remove completely any trace of un-reacted compounds or reaction subproducts, the residue was redissolved in MilliQ water and purified by PD10 column eluted with MilliQ water, collecting fractions of 1 mL. From each fraction, 2  $\mu$ L were taken and added to 998  $\mu$ L of MeOH and measured spectrophotometrically using a Victor2Wallac station, in order to identify the fractions containing the Polyacetal-Cy conjugates and also to quantify the amount of conjugated Cyane. Cy loading was determined to be quantitative. Then, both polymers Cy-cadaverine conjugates, *Tert*-DES-Ser-Cy<sub>cad</sub> **16** and Block-DES-Ser-Cy<sub>cad</sub> **17** were isolated by removal of water in a freezer dryer.

### 3.3.8.Synthesis of Paclitaxel-DES conjugates , novel conjugates used for Combination Therapy.

In **Strategy 1**, a second drug, paclitaxel (PTX) was conjugated<sup>5</sup> to the succinoylated polyacetals, *Tert*-DES-Ser<sub>COOH</sub> **12** and Block-DES-Ser<sub>COOH</sub> **13**. In the other hand, using the **strategy 2**, the succinoylated form of Paclitaxel (PTX<sub>COOH</sub>) was conjugated to the polyacetals *Tert*-DES-Ser<sub>NH2</sub> **6** and Block-DES-Ser<sub>NH2</sub> **7**.

*A) Strategy 1. Synthesis of Tert-DES-Ser-PTX (18) and Block-DES-Ser-PTX (19).*

Succinoylated polyacetal *Tert*-DES-Ser<sub>COOH</sub> **12** or Block-DES-Ser<sub>COOH</sub> **13** (0.1g, 0.008 mmol COOH equiv) were dissolved in 0.5mL of anhydrous THF, under N<sub>2</sub> atmosphere as two different reactions.

Diisopropylcarboimide (DIC, 6.2 $\mu$ L, 0.040mmol) was added and after 5 min 1-hydroxybenzotriazole hydrate (HOBT, 0.0103g, 0.076mmol) was also added as solid, followed 10 min later of the Paclitaxel (PTX, 0.022g, 0.026 mmol, dissolved in 0.5mL of anhydrous THF). The pH was adjusted to 8-9 with DIEA and when the reactions were completed after 24 hours, the solvent was evaporated under vacuum at RT. The product was isolated by removing

the solvent under vacuum and the residue was washed with hexane (30min stirring) and centrifuged. The supernatant was evaporated by N<sub>2</sub> stream and the crude was purified by SEC using an LH20 column eluted by methanol (HPLC grade) in order to remove completely any trace of un-reacted compounds or reaction subproducts. The solvent of all the fractions was evaporated and the product was analyzed by <sup>1</sup>H-NMR confirming the presence of the PTX-conjugates, *Tert*-DES-Ser-PTX **18** and *Block*-DES-Ser-PTX **19** in some of the fractions. The paclitaxel conjugates were stored at -20°C. M<sub>w</sub> 47682g/mol, and M<sub>w</sub>/M<sub>n</sub>=1.4 as determined by aqueous GPC.

*Tert*-DES-Ser-PTX **18** and *Block*-DES-Ser-PTX **19**: <sup>1</sup>H-NMR (300MHz, CDCl<sub>3</sub>): 6.27 (s, C<sub>10</sub>-H), 6.20 (t, C<sub>13</sub>-H), 5.79 (dd, C<sub>3'</sub>-H), 5.66 (d, C<sub>2</sub>-H), 5.51 (d, C<sub>2'</sub>-H), 4.95 (d, C<sub>5</sub>-H), 4.42 (broad, C<sub>7</sub>-H), 3.61 (OCH<sub>2</sub>CH<sub>2</sub>O), 2.77 (m, COCH<sub>2</sub>CH<sub>2</sub>CO<sub>2</sub>), 1.66 (s, C<sub>19</sub>-H), 1.21 and 1.12 (s, C<sub>16,17</sub>-H).

**B) Strategy 2. Paclitaxel-DES conjugates using 2'-succinyl-paclitaxel.**

### **B.1) Synthesis of 2'-succinyl-paclitaxel<sup>5</sup> (PTX<sub>COOH</sub>) (20).**

2'-succinyl-paclitaxel **20** was prepared dissolving 50 mg paclitaxel (M<sub>w</sub> = 853.906g/mol, 0.06 mmol) and 73 mg succinic anhydride (0.56 mmol) react in 3 mL anhydrous pyridine at room temperature for 3 h. The pyridine was then evaporated and the residue was treated with 5 mL water, stirred for 20 min and filtered. The precipitate was recrystallized from acetone and water to yield 2'-succinyl-paclitaxel (PTX<sub>COOH</sub>) (20 mg). Yield: 46%. The structure was confirmed by <sup>1</sup>H-NMR. The δ for C<sub>2</sub>-H shifted from 4.79 to 5.51 indicating esterification at C<sub>2'</sub> position.

### **B.2) Synthesis of *Tert*-DES-Ser-PTX<sub>COOH</sub> (21) and *Block*-DES-Ser-PTX<sub>COOH</sub> (22).**

2'-succinyl-paclitaxel **20** (M<sub>w</sub>= 925.93 g/mol, 14 mg, 0.0015 mmol) was dissolved in 1.5 ml of anhydrous DMSO or THF. 1-Ethyl-3-(3-dimethylaminopropyl) carbodiimide, 3.14 mg EDC (M<sub>w</sub> = 155.24 g/mol, 0.02 mmol) was then added and the mixture was stirred at room temperature for 10min. *N*-hydroxysulfosuccinimide, 4.93 mg Sulfo-NHS (M<sub>w</sub> = 217,1g/mol, 0.02 mmol) was carefully added and stirred for 45 min at RT. Finally, *Tert*-DES-Ser<sub>NH<sub>2</sub></sub> **6** or *Block*-DES-Ser<sub>NH<sub>2</sub></sub> **7** was added (to obtain **21** or **22**, respectively) to the reaction mixture and the pH adjusted to 8 with DIEA.



Then the mixture was stirred during 16 h more a RT. Reactions were monitored by TLC (ethyl acetate as mobile phase) which showed complete conversion of 2'-succinyl-paclitaxel ( $R_f = 0.28$ ) to its corresponding polymer conjugate ( $R_f = 0$ ). Conjugates were extracted from the reaction mixture by precipitation into hexane and purified by dialysis against distilled water during 16 h. The conjugates with paclitaxel were obtained and confirmed by  $^1\text{H-NMR}$ .

*Tert-DES-Ser-PTX<sub>COOH</sub>* **21** and *Block-DES-Ser-PTX<sub>COOH</sub>* **22**:  $^1\text{H-NMR}$  (300MHz,  $\text{CDCl}_3$ ): 6.27 (s,  $\text{C}_{10}\text{-H}$ ), 6.20 (t,  $\text{C}_{13}\text{-H}$ ), 5.79 (dd,  $\text{C}_{3'}\text{-H}$ ), 5.66 (d,  $\text{C}_2\text{-H}$ ), 5.51 (d,  $\text{C}_{2'}\text{-H}$ ), 4.95 (d,  $\text{C}_5\text{-H}$ ), 4.42 (broad,  $\text{C}_7\text{-H}$ ), 3.61 ( $\text{OCH}_2\text{CH}_2\text{O}$ ), 2.77 (m,  $\text{COCH}_2\text{CH}_2\text{CO}_2$ ), 1.66 (s,  $\text{C}_{19}\text{-H}$ ), 1.21 and 1.12 (s,  $\text{C}_{16,17}\text{-H}$ ).

### 3.3.9. Synthesis of Fluorescence-labeled PTX-conjugates.

Following the **strategy 1**, paclitaxel (PTX) or 2'-succinyl-paclitaxel ( $\text{PTX}_{\text{COOH}}$ ) was conjugated to OG or Cy-polyacetals. In the other hand the **strategy 2** is based on the conjugation of the fluorescence dye, OG or Cyane5.5 (both as carboxylic acid form) to polyacetals *Tert-DES-Ser-PTX<sub>COOH</sub>* **21** and *Block-DES-Ser-PTX<sub>COOH</sub>* **22**.

#### A) *Strategy 1. Synthesis of fluorescence-labeled-PTX conjugates I.*

##### A.1) **Synthesis of *Tert-DES-Ser-PTX<sub>COOH</sub>-OG<sub>NHS</sub>* (23), *Block-DES-Ser-PTX<sub>COOH</sub>-OG<sub>NHS</sub>* (24), *Tert-DES-Ser-PTX<sub>COOH</sub>-Cy<sub>NHS</sub>* (25) and *Block-DES-Ser-PTX<sub>COOH</sub>-Cy<sub>NHS</sub>* (26).**

As starting compound can be any of the fluorescence-labeled polyacetals synthesised as: *Tert-DES-Ser-OG<sub>NHS</sub>* **8**, *Block-DES-Ser-OG<sub>NHS</sub>* **9**, *Tert-DES-Ser-Cy<sub>NHS</sub>* **10** and *Block-DES-Ser-Cy<sub>NHS</sub>* **11**. To these polyacetals 2'-succinyl-paclitaxel ( $\text{PTX}_{\text{COOH}}$ ) was conjugated through the free amine groups in the polyacetal.

The procedure used is the same described above to obtain these polyacetals **8**, **9**, **10** and **11**, were the polyacetals are dissolved in anhydrous THF and DIEA was added to adjust the pH until 9. Then  $\text{PTX}_{\text{COOH}}$  (0.0002 g, 0.0008 mmol) was dissolved in 0.01mL anhydrous DMF and added to the reaction mixture. When the reaction was completed (24hours), the solvent was evaporated under vacuum at RT and the residue was redissolved in MilliQ water to purify

by PD10 column. It was eluted with MilliQ water, collecting fractions of 1mL. The fractions were dried with the freezer drier and analyzed by HNMR. The fractions with the conjugate were recollected to obtain: *Tert*-DES-Ser-PTX<sub>COOH</sub>-OG<sub>NHS</sub> **23**, *Block*-DES-Ser-PTX<sub>COOH</sub>-OG<sub>NHS</sub> **24**, *Tert*-DES-Ser-PTX<sub>COOH</sub>-Cy<sub>NHS</sub> **25** and *Block*-DES-Ser-PTX<sub>COOH</sub>-Cy<sub>NHS</sub> **26**.

**A.2) Synthesis of *Tert*-DES-Ser-PTX-OG<sub>cad</sub> (27), *Block*-DES-Ser-PTX-OG<sub>cad</sub> (28), *Tert*-DES-Ser-PTX-Cy<sub>cad</sub> (29) and *Block*-DES-Ser-PTX-Cy<sub>cad</sub> (30).**

The fluorescence-labeled polyacetals synthesised as: *Tert*-DES-Ser-OG<sub>cad</sub> **14**, *Block*-DES-Ser-OG<sub>cad</sub> **15**, *Tert*-DES-Ser-Cy<sub>cad</sub> **16** and *Block*-DES-Ser-Cy<sub>cad</sub> **17** were employed to conjugate paclitaxel (PTX) through the carboxylic group in the polyacetal.

Fluorescence-labelled polyacetals **14**, **15**, **16** or **17** (0.1g, 0.008 mmol COOH equiv) were dissolved in 0.5mL of anhydrous THF, under N<sub>2</sub> atmosphere as four different reactions. Diisopropylcarbodiimide (DIC, 6.2μL, 0.040mmol) was added and after 5 min 1-hydroxybenzotriazole hydrate (HOBT, 0.0103g, 0.076mmol) was also added as solid, followed 10 min later of the Paclitaxel (PTX, 0.022g, 0.026 mmol, dissolved in 0.5mL of anhydrous THF). The pH was adjusted to 8-9 with DIEA and when the reactions were completed after 24 hours, the solvent was evaporated under vacuum at RT. The residue was washed with hexane (30min stirring), centrifuged and the supernatant was evaporated by N<sub>2</sub> stream. In order to remove completely any trace of unreacted compounds or reaction subproducts, the crude was purified by SEC using an LH20 column eluted by methanol (HPLC grade) and recollecting fractions of 1mL. Then the solvent of the fractions was evaporated under vacuum at RT and analyzed by <sup>1</sup>HNMR confirming the presence of the desired compound in some of them isolating, *Tert*-DES-Ser-PTX-OG<sub>cad</sub> **27**, *Block*-DES-Ser-PTX-OG<sub>cad</sub> **28**, *Tert*-DES-Ser-PTX-Cy<sub>cad</sub> **29** and *Block*-DES-Ser-PTX-Cy<sub>cad</sub> **30**.

**B) Strategy 2. Synthesis of fluorescence-labeled-PTX conjugates II.**

**B.1) Synthesis of OG<sub>NHS</sub>/Cy<sub>NHS</sub>-labeled PTX<sub>COOH</sub> conjugates, *Tert*-DES-Ser-PTX<sub>COOH</sub>-OG<sub>NHS</sub> (31), *Block*-DES-Ser-PTX<sub>COOH</sub>-OG<sub>NHS</sub>**

**(32), *Tert*-DES-Ser-PTX<sub>COOH</sub>-Cy<sub>NHS</sub> (33) and *Block*-DES-Ser-PTX<sub>COOH</sub>-Cy<sub>NHS</sub> (34).**

The conjugation of *Tert*-DES-Ser-PTX<sub>COOH</sub> **21** and *Block*-DES-Ser-PTX<sub>COOH</sub> **22** with OG<sub>NHS</sub> or Cy<sub>NHS</sub> were done using same procedure described for **8**, **9**, **10** and **11**. Conjugates **21** (0.300 g, 0.030 mmol) or **22** (0.300 g, 0.022 mmol) were dissolved in anhydrous THF and DIEA added until pH 9. OG<sub>NHS</sub> (0.0002 g, 0.0008 mmol) or Cy<sub>NHS</sub> (0.002 g, 0.002 mmol) dissolved in 0.01mL anhydrous DMF was added and the reaction mixture was stirred during 16 h. The reaction was monitor by TLC (Ethyl acetate: hexane, 1:1 as mobile phase, R<sub>f</sub> = 0.5). After solvent removal under vacuum at RT, the residue was redissolved in MilliQ water and purified by PD10 column eluted with MilliQ water, collecting fractions of 1 mL. From each fraction, 2 μL were taken and added to 998 μL of MeOH, in order to measure the fluorescence and to identify the fractions containing the Polyacetal-Cy or OG PTX-conjugates and also to quantify the amount of conjugated Cyane or Oregon green. Then, polymers Cy or OG PTX-conjugates, *Tert*-DES-Ser-PTX<sub>COOH</sub>-OG<sub>NHS</sub> **31**, *Block*-DES-Ser-PTX<sub>COOH</sub>-OG<sub>NHS</sub> **32**, *Tert*-DES-Ser-PTX<sub>COOH</sub>-Cy<sub>NHS</sub> **33** and *Block*-DES-Ser-PTX<sub>COOH</sub>-Cy<sub>NHS</sub> **34** were isolated by removal of water in a freezer dryer.

### 3.4. NMR Spectroscopy

For samples with low molecular weight such as monomers only 5mg of compound was needed to performance <sup>1</sup>H and <sup>13</sup>C NMR analysis. The NMR tube to use must be clean and dry to obtain the appropriate results for each sample. For samples with high molecular weight (polymers conjugates), around 30 mg of each compound was needed to analyse them. All the samples were dissolved in 0.6ml of the appropriate deuterated solvent (the most used was CDCl<sub>3</sub>). COSY, DOSY and PGSE-NMR were the other experiments used in this thesis. COSY is the most simple bidimensional experiment consisting in two pulses separate by time t<sub>1</sub>. Two-dimensional diffusion-ordered NMR spectroscopy (DOSY) was performed with a stimulated echo sequence using bipolar gradient pulses. The lengths of pulses and delays were held constant and 16 spectra of 24 scans each were acquired with the strength of the diffusion gradient varying between 5% and 100%. The lengths of the diffusion gradient and the stimulated echo were optimized for each sample. Typical values were δ = 6–7 ms, Δ = 160–170 ms. PGSE-NMR technique was

employed to determine the diffusion coefficient of the polyacetals, which were dissolved in MeOD and D<sub>2</sub>O with a concentration of 1mg drug/mL. The experiments were done at 25 °C and at 37 °C.

NMR analysis was operating in frequencies of 300 MHz and processed and analysed using the TopSpin® 2.0 software.

### **3.5. Determination of the Molecular Weight (Mw) and Polydispersity (Pdi) of the polyacetals using Gel Permeation Chromatography (GPC), also known as Size Exclusion Chromatography (SEC).**

GPC, also known as Size Exclusion Chromatography (SEC), is an important analytical tool used to evaluate polydispersity (Pdi) and molecular weight (Mw) characteristics of natural or synthetic polymers and proteins. Unlike HPLC, GPC relies, under ideal conditions, on a pure physical separation, where theoretically no chemical interactions of the sample with the GPC column (stationary phase) should be observed<sup>6, 7</sup>. To be more precise, GPC separates molecules upon their size in solution, which is directly proportional to their hydrodynamic volume (Vh).

In this thesis, GPC measurements were taken in two different solvents, PBS and THF used as mobile phase. The mobile phase preparation, column calibration, sample preparation and methods used for both systems are described more in detail below.

PEG standards were chosen as GPC calibrating kit, commercially available. They allow a relative comparison of the molecular weight and polydispersity of the polymers.

The SEC equipment consists on a Waters 717 plus autosampler with two Waters Styragel 7.8x300mm columns in series (HR3 and HR4) for THF or DMF and two TSK-Gel Columns (G2500 and 3000 PWXL) for samples in PBS and a Viscotek TDA 302 triple detector Array with refractive index (RI), Small Angle Light Scattering, Right Angle Light Scattering, viscosimeter and a UV detector model 2501. Polydispersity and molecular weight of the polyacetals were determined using the mentioned above software OmniSec 4.1. Calibration was achieved with well defined poly(ethylene glycol)

standards in THF as provided by Polymer Standards Service (PSS)/Mainz, Germany.

### **Preparation of the mobile phase used**

*Aqueous mobil phase.* For 1 L of PBS eluent, 5 PBS tablets were dissolved up to 1 L with double distilled water. 1 mg of sodium azide was added to the solution to prevent bacterial growth in the buffer. The solution was then filtered through a nylon membrane filter (0.2  $\mu\text{m}$ ) and sonicated for 0.5 h before use.

*Organic mobil phase.* To a new HPLC grade THF bottle (2.5 L), 625 mg of BHT (250 ppm) was added as a solid to stabilise the mobile phase. The organic solution was then used without further preparation as the organic GPC system was equipped with a degasser.

### **Sample preparations and running conditions**

For the GPC measurements, all the polymer samples were prepared in a concentration of 3mg/ml dissolved in the previous prepared and stabilised mobile phase (THF or PBS). In the case of organic GPC, toluene (20  $\mu\text{L}$ ) was added and was used as an internal flow marker. Prior injection, the samples were filtered through single-use syringe filters (0.2  $\mu\text{m}$  nylon membrane) and sonicated for 30 min. Then they were injected (110  $\mu\text{L}$ ) into the GPC loop (100  $\mu\text{L}$ ). The samples were running for 35min. at 25 °C with a GPC flow rate of 1 mL/min. The detection of the samples was done by differential refractive index and the data were analysed using the OmniSec 4.1 software.

## **3.6. Determination of total and free DES content in DES-polyacetal conjugates.**

### **3.6.1. Total drug loading**

- *Indirect quantification*

Total drug loading can be determined by a total hydrolysis of the acetal bound heating the sample in an acid pH. The samples were

dissolved in 100 $\mu$ L of HCl (pH 2) and then heated in a thermo-block at 80°C and 400RPM for 30min. After cooling down to RT, samples were neutralized and analyzed by RP-HPLC. Flow 1mL/min, gradient 90:10 ddH<sub>2</sub>O: AcCN (both solvents had 0.1% TFA), run time 35min, column C18RP, UV detector 280 nm. The calibration curve was done using free drug from 0.01 to 1mg/mL concentration range using the method described in table 3.1. DES possesses an absorbance of 280 nm very easy to detect by UV-vis and the calibration curve was performance. Oestradiol was used as internal standard.

Once the polymer was washed, for example by precipitation over hexane, the solvent was evaporated and re-dissolved in acetonitrile to be injected in the RP-HPLC and determine the DES which was not conjugated to the polymer.

**Table 3. 1** Method employed to make the calibration curve of DES in the RP-HPLC.

t (min)	Flow (mL/min)	% H <sub>2</sub> O	% ACN
0	1	70	30
25	1	10	90
28	1	10	90
31	1	70	30
35	1	70	30

- *Direct quantification*

Another method to determine the total drug loading is doing a direct quantification using UV.

Free DES was indirectly calculated by knowing the absorbance of the conjugated. Here, a calibration curve of DES in ddH<sub>2</sub>O at 280nm was carried out using a concentration range from 0.001 to 1mg/ml. Then, the absorbance of the conjugates (5mg/ml in ddH<sub>2</sub>O) was measured in the UV-spectrophotometer.

### 3.6.2. Free drug content

In order to determine free drug content, polyacetal-DES conjugate solutions (1mg/mL and 3 mg/mL) were directly injected and analyzed by RP-HPLC using the same HPLC conditions describe above for the determination of total drug content. Oestradiol was added as internal standard.

The same procedures described above to determine free and total DES were used to determine total and free paclitaxel content in polyacetal-PTX conjugates.

### 3.7. Free amino group quantification by Ninhydrin assay<sup>8</sup>.

Ninhydrin reagent was prepared according to a reported methodology by Dr. Shih-Wen Sun, adjusting amount of reagents to actual needs. In general, Ninhydrin (0.500g, 2.58mmol) and Hydrindantin (0.075g, 0.23mmol) were weighted in a 100ml flask and covered with aluminum paper, because these compounds are light sensitive. Solids were dissolved in 18.75ml DMSO anhydrous under a stream of nitrogen gas. After adding 6.25ml sodium acetate buffer (pH=7, 4N) previously prepared (46 ml Acetic acid concentrated (99.7% v/v + 16.06g NaOH + dd water up to  $V_T=100$ ml), the mixture was bubbled with nitrogen for at least 2 min, sealed and stored (at -20°C). This reagent only works for three days, after that it is not reliable.

Free serinol was used as standard. Calibration curve was calculated with serinol like standard and a calibration curve was performed. A serinol stock solution of 10.8mg/mL and a polyacetal stock solution of 102.8mg/mL were prepared. Aliquots were taken to prepared standards at different concentration and the same was done with polymer sample, taking two aliquots with different volume. For all analysis final volume was 1.500 $\mu$ L, sample M1 was 50 $\mu$ L and M2 was 100 $\mu$ L.

Calibration curve was made mixing 750 $\mu$ l serinol solution of different concentrations (between 0.004-0.04mg/mL) and 750 $\mu$ l ninhydrin solution, in brown eppendorfs and heated in a boiling water bath for 30 min. After heating, tubes were immediately cooled down in an ice-bath. Then, 5ml of an

EtOH solution 50% in ddH<sub>2</sub>O was added into each tube and thoroughly mixed with a vortex for 15sec. The absorbance output was measured at 570nm with a UV-Visible spectrophotometer.

### **3.8. Determination of Critical Micelle Concentration (CMC) of the polyacetals synthesised**

In order to determine the CMC of the systems synthesised, two different fluorochromes, diphenylhexatriene (DPH) and Pyrene were used. 0.5mg of Pyrene was dissolved in 40ml acetone to obtain a 0.0125mg/ml (62.5  $\mu$ M) stock solution. Then, 0.002 $\mu$ l of this solution was added to an aqueous polymer solution in (5mg/ml). Pyrene was sonicated until the acetone solution was removed and to induce the formation of the micelles and after 24h incubation, the samples were analysed. Alternatively, 4mg DPH was dissolved in 1ml THF (6mM). To generate a stock solution the desired final concentration was 2mM, therefore, 33.3 $\mu$ l was taken from the 6mM solution and then added to 66.6 $\mu$ l THF. 2.5 $\mu$ l of a 0.2mM stock solution was added to the polymer solution in phosphate buffer solution (5mg/ml) to analyse the samples.

### **3.9. Dynamic Light Scattering (DLS) studies**

DLS measurements were performed at 25 °C using a Malvern Zetasizer NanoZS instrument, equipped with a 532-nm laser at a fixed scattering angle of 90°. Polymer conjugate solutions (1 mg/ml and 3 mg/ml) were prepared using MilliQ H<sub>2</sub>O and phosphate buffer solution (PBS) at pH 7.4. The solutions were sonicated for 10 min and filtered through a 0.22 $\mu$ m cellulose membrane filter before analysis. Micelle size distribution by volume (%) was measured (diameter, nm) for each conjugate ( $n \geq 3$ ).

### **3.10. Transmission and Scanning electron microscopy (TEM) and (SEM) techniques**

Polymer conjugate solutions, from 0.5 mg/ml to 3 mg/ml, were prepared using MilliQ H<sub>2</sub>O and PBS at pH 7.4. The solutions were sonicated for 10 min and filtered through a 0.45 $\mu$ m cellulose membrane filter before analysis. For TEM, the sample can be quickly prepared by the deposition of 1 $\mu$ l of a dilute sample containing the polymer onto support films. In SEM, also 1 $\mu$ l of a



dilute sample is applied on a gold-coated metal disk obtained either by low vacuum sputter coating or by high vacuum evaporation.

### 3.11. Small Angle Neutron Scattering (SANS) studies

SANS experiments were doing in collaboration with Dr. Alison Paul in Cardiff University, UK. The experiments were carried out in the Institut Laue-Langevin (ILL)<sup>9</sup> in Grenoble (France) the most powerful of the reactor neutron sources, 57 MW HFR (High-Flux Reactor)) (Figure 3. 1A) with the help of Ralf Schweins and at ISIS<sup>10-12</sup> Facility, Rutherford Appleton Laboratory in Harwell Science & Innovation Campus, Didcot, OX11 0QX U.K, one of the most known spallation neutron source in the world, which is based around a 200 mA, 800 MeV, proton synchrotron (Figure 3. 1B) operating at 50 Hz, and a tantalum target which releases approximately 12 neutrons for every incident proton.

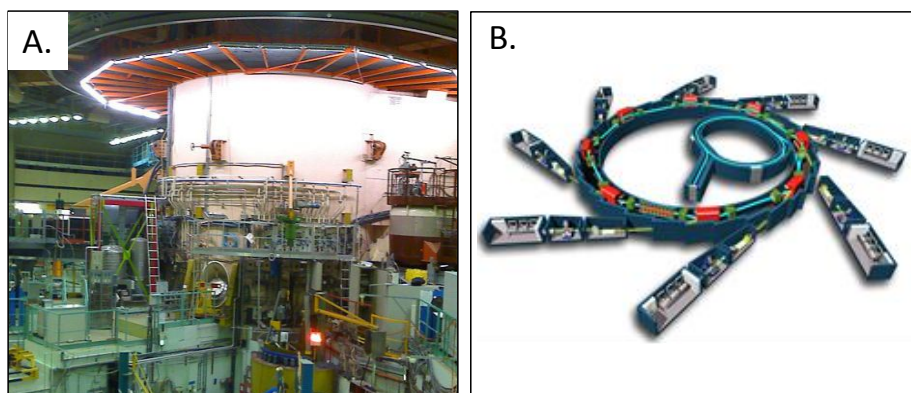


**Figure 3. 1** (A) Reactor at ILL, Grenoble (France) (image taken from [www.ill.eu](http://www.ill.eu)) and (B) Scheme of a synchrotron such as it could be found at ISIS, Oxford (UK) (image taken from ©EPSIM 3D/JF Santarelli).

SANS experiments were carried out for all the conjugates in two different deuterated solvents, D<sub>2</sub>O and MeOD, to confirm the polymer aggregations formed in water but not in organic solvents. The conjugates were dissolved in a concentration of 1mg/mL equivalents of drug and at 10mg/mL of polymer and the solutions were added to a round small cell of 1mL of capacity which was inserted in the rack for SANS measurements. For this study was necessary to measure also an empty cell (as a control for all the samples), a

cell filled with deuterated methanol (as a control for the samples with MeOD) and another cell filled with deuterated water (as a control for the samples with D<sub>2</sub>O).

### 3.12. pH-dependent degradation in buffer solution

Polyacetals (8 mg/mL) were incubated at 37°C in phosphate buffer solution (PBS) at pH 5.5, 6.5 and 7.4 for 20 days. 100 µL for HPLC and 50 µL for GPC analysis of the sample solutions were taken at various time points 0, 15, 30 min and 2, 8 and 24 h and every 24 h up to achieve complete degradation. Samples were frozen with liquid nitrogen and stored at -80°C until analyzed.

Prior to analysis, the pH of acidic samples was neutralized with ammonium formate buffer (0.1M, 100 µL for pH 5.5 and 50 µL for 6.5), in order to stop any further degradation, to normalized concentrations 100 µL PBS was added to the samples of pH 7.4 and 50 µL to the sample of pH 6.5. Next, the samples were directly analyzed either by GPC (%Mw Loss, PBS as mobile Phase, flow 0.8 mL/min) and by RP-HPLC, using a C18 LiChroSpher 100 column (5 µm), with the UV detector settled at  $\lambda = 280$  nm with a flow rate of 1 mL/min. The eluent A was H<sub>2</sub>O and eluent B was MeCN. Oestradiol was used as HPLC internal reference standard; 100 µL of a 10 µg/mL stock solution was added to each sample. The elution was performed by the following gradient: from 30% B to 90% B over 25 min, 3 min isocratic, then from 90% B to 30% B over 3 min and keeping these conditions for 4 min. (trans-DES retention time (tr) 11min, cis-isomer tr 13 min, oestradiol tr 10 min). A calibration curve of DES was used to quantify the total DES release from the conjugates by HPLC.

### 3.13. Plasma Stability

Conjugates (8 mg/mL) were incubated at 37°C in freshly extracted serum from Wistar rats for up to 24 h. At scheduled times, samples of 100 µL were collected; 10 µL of 100 µg/mL solution of oestradiol in MeOH, as internal standard, and 135 µL of MeCN were added to each sample in order to precipitate serum proteins. Following centrifugation (14000 rpm, 5 min), supernatants were analyzed by HPLC as reported above.

### **3.14. Techniques and methods in cell culture**

Cell culture was performed according to the guidelines given by The United Kingdom Co-ordinating Committee on Cancer Research<sup>13</sup>. All cell work was carried out in a Class II laminar flow hood, pre-sterilised by Klericide® and 70 % v/v ethanol in double distilled water spray to avoid contaminant environments and keep the cells in the best conditions.

The protocol to follow for working in a culture cell starts in having sterile all the material which will be in direct contact with cultures. Some flasks, pipets, etc., can be sterile directly from manufacturers but the reusable glassware must be washed, rinsed thoroughly, and then sterilized by autoclaving or by dry heat before reusing. Everything which goes inside the cabinet, place of cellular work, must be sterilized by flushing them with the ethanol solution mentioned above.

In this project two different human prostate cancer cells lines were employed to carry out the *in vitro* experiments, PC3 and LNCaP described in Chapter 1 (section 1.1.6). Both cell lines were kept under aseptic conditions, without the addition of penicillin or streptomycin.

#### **3.14.1. Thawing and recovering cells**

When cryopreserved cells are needed for study, they should be thawed rapidly and plated at high density to optimize recovery.

Cryogenic vials of frozen cells (1million cells/ml per vial) were kept at -196 °C in liquid nitrogen until required. Upon use, the frozen vials were defrosted in a 37 °C water bath and immediately added to a universal sterile container with 9 mL of media. Then, cells were pelleted by centrifugation for 5 min at 400g and the supernatant was removed. Then, they were re-suspended in 5 mL of fresh media before being placed into P100plate. Cells were grown for 24 h in a 37 °C incubator and their growth was checked under the light microscope, the culture medium was changed and allowed for growing. Cells were passaged when confluence was reached.

### 3.14.2. Cell maintenance and passaging

PC3 cells were grown in F12 with 5.0mM L-glutamine and 10% (v/v) of fetal bovine serum (FCS) and LNCAP cells grown in RPMI with 10% (v/v) FCS. The incubator must be at 37°C with 5% of CO<sub>2</sub> (Table 3.2). The medium was changed each two days to induce the growth. Once 70-90% cell confluence was reached the medium was removed and the cells were washed with 10mL PBS. 1mL of trypsin was then added and after 5 min at 37°C (until detached), 9 mL of free medium was added and cells were collected in a corning to centrifuge 5 min at 400 rcf at RT. The medium was carefully removed and the cells resuspended in fresh medium.

**Table 3. 2** Conditions for the cell line growth.

Cell line	Medium	% SBF Treatment	Incubator conditions
PC3	F12	10%	37°C with 5% CO <sub>2</sub>
LNCaP	RPMI	10%	37°C with 5% CO <sub>2</sub>

Then, the cells were counted to determine standard culture conditions to performance accurate experiments.

To count cells, aliquots of suspended cells (100 µL) were mixed at a 1:1 v/v ratio with trypan blue (0.2 % trypan blue in PBS) in a sterile tube. Trypan blue is a blue dye able to penetrate dead cell membranes. Blue-stained cells are not viable, thus this method gives an indication of the number of viable cells in suspension after being placed in a haemocytometer slide (Neubauer Zählkammer). Cells from ten × 0.1 mm<sup>3</sup> squares (five from the top and five from the bottom chamber of the haemocytometer) (Figure 3. 2) were counted using a light microscope.

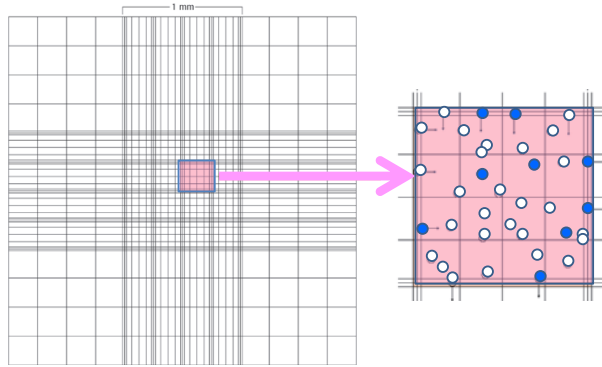


**Figure 3. 2** Haemocytometer thick glass slide used for counting cells. The addition of trypan blue helps to distinguish viable, unstained cells (white circles) from non-viable, blue-stained cells (blue circles).

The average number of cells per mL of cell suspension was calculated as below (Equation 3.1):

$$\text{Cells / mL} = \text{mean} \times 2 \times 10^4 \quad (\text{Eq 3.1})$$

Where the mean is the arithmetic mean of the ten values, 2 takes into account the trypan blue dilution and  $10^4$  accounts for the conversion from  $0.1 \text{ mm}^3$  to mL.

After cells counting, the cell suspension was diluted with the medium in order to obtain the appropriate seeding density required for the experiment.

### 3.14.3. Freezing cells

Cell lines may be frozen for long-term storage to preserve cells, avoid senescence, reduce the risk of contamination, and minimize effects of genetic drift.

First, cells were trypsinized, centrifuged into pellets and re-suspended in fresh medium. After counting, cells were again centrifuged and re-dissolved in the appropriate solution for freezing, 900  $\mu\text{l}$  FBS (90 %) and 100  $\mu\text{l}$  sterile DMSO (10 %) to give a final concentration of  $10^6$  cells/mL suspension. Aliquots (1 mL) of this suspension were placed into 1 mL sterile and cryogenic vials, placed at  $-20 \text{ }^\circ\text{C}$  for 1-2 h, at  $-80 \text{ }^\circ\text{C}$  overnight and finally storage at  $-196 \text{ }^\circ\text{C}$  in liquid nitrogen until use.

Without the use of a cryoprotective agent, freezing would be lethal to the cells in most cases. Generally, a cryoprotective agent such as dimethylsulfoxide (DMSO) is used in conjunction with complete medium for preserving cells at  $-70^{\circ}\text{C}$  or lower. DMSO acts to reduce the freezing point and allows a slower cooling rate. Gradual freezing reduces the risk of ice crystal formation and cell damage.

### **3.14.4. MTT or MTS assays to assess cell viability: Growth curve**

#### *MTT assay conditions*

20 $\mu\text{L}$  MTT of a 5 mg/mL solution in PBS was added to each well of the plate. Then, the cells were incubated for a further 4h. After removal of the medium, the precipitated formazan crystals were dissolved in optical grade DMSO (100  $\mu\text{L}$ ), and after 30min the optical density of the solution was determined spectrophotometrically (in a Perkin Elmer precisely 1420 Victor3<sup>TM</sup> Multilabel Counter) at 570 nm using a microtitre plate reader.

#### *MTS assay conditions*

10 $\mu\text{L}$  MTS was added to each well, and the incubation was continued for 2h more. Mitochondrial dehydrogenase enzymes of viable cells converted MTS tetrazolium into a colored formazan product. The optical density of samples was measured at 490 nm.

Those assays allow measuring the viability (cell counting), the proliferation of the cells (cell culture assays) and also determine and compare the cytotoxicity of drugs alone or conjugated to polymers.

#### Determination of cell growth

On day 0, cells were seeded into sterile, flat-bottomed, 96-well plates (100  $\mu\text{L}$ /well, seeding densities of  $4 \cdot 10^4$  or  $10^4$  cells/mL) using a multi-channel pipette, and they were then allowed to settle for 24 h. The external well rows of the plate were filled with culture media to prevent surrounding wells from dehydrating (Figure 3. 3).

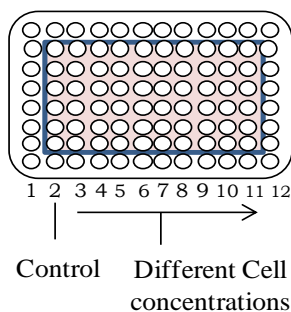


**Figure 3. 3** Sterile 96-well microtitre plate for carry on a cellular Growth study by MTT or MTS assay. From left to right it was increasing the concentration of cells. Column 2 was the control data. All the surrounding wells were filled with PBS for the best maintenance conditions of the cells.

Normally a cell growth study could be follow during approx. 7 days. Each day, 20  $\mu\text{L}$  MTT of a 5 mg/mL solution in autoclaved PBS was added to each well of the plate and the cells were incubated for 5h. Then, the medium from the wells in this row ( $n = 6$ ) was aspirated and replaced with optical-grade DMSO (100  $\mu\text{L}$ /well) to solubilize the purple formazan crystals. The plates were then incubated for a further 30 min to allow the crystals to dissolve. Absorbance of the optical density of the solution was determined spectrophotometrically (in a Perkin Elmer precisely 1420 Victor3<sup>TM</sup> Multilabel Counter) using a microtitre UV plate reader with an emission wavelength of  $\lambda = 550$  nm.

The formazan-DMSO mixture was then removed from the wells under local exhaust, and replaced with PBS (100  $\mu\text{L}$ /well). Plates were returned to the incubator and this process was continued daily over a period of 7 days.

### 3.14.5. Evaluation of polymer cytotoxicity using the MTT assay

The MTT assay, described in Section 3.12.4, was also used to establish the cytotoxicity of free drugs and drugs conjugated to polymers. Cells were used in their exponential phase of growth.

MTT assay was the most used cell viability assay although MTS assay was used as well for some experiments. The studies were carried out after 72h incubation against two different prostate cancer cell lines, PC3 and LNCaP.

They were seeded on day 0 into a sterile 96-well microtitre plate (Figure 3. 4) at a seeding density of  $3.2 \times 10^4$  PC3 cell/mL and  $5 \times 10^4$  LNCaP cell/mL which allow adhering for 24h. Plates were incubated in a humidified atmosphere containing 5% CO<sub>2</sub> at 37°C.

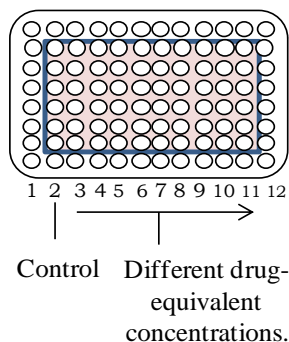


**Figure 3. 4** Sterile 96-well microtitre plate for carry on a cell viability study by MTT or MTS assay. The effect of the compounds in causing death or changing the metabolism of the cells can be deduced comparing cells treated with drug compounds (which produce purple formazan) with the formazan produced by untreated control cells.

On day 1, the medium was replaced by different concentrations of drug (alone or conjugated to a polymer dissolved in medium) from 0.01 to 1mg/ml drug-equivalent (from left (column 3) to right (column 12) the concentration of drug equivalents was increasing). Column 2 was fresh medium alone used as a control. All the surrounding wells were filled with phosphate buffer solution (PBS) for the best maintenance conditions of the treated cells.

On day 4 (after a 72 h incubation), MTT solution (20  $\mu$ L; 5 mg/mL in PBS) was added and the plates were incubated for a further 5 h. The media was then removed, and the formazan crystals dissolved in optical grade DMSO (100  $\mu$ L). After incubation at 37 °C for 30 min, the plates were analysed by UV absorbance at  $\lambda = 550$  nm.

#### 3.14.6. Haemolytic Activity of Free DES and DES-polyacetals

Freshly prepared DES-Na, DES-polyacetals, dextran Mw = 74.000 g/mol and poly(ethyleneimine) (PEI; Mw = 750. 000 g/mol) solutions in phosphate buffered saline (PBS) at pH 7.4 and DES 1 (3% DMSO in PBS) (range of



concentrations 0–2mg/ml), were plated (100ml) into non-sterile 96-well microtitre plates. Blood was taken from an adult male Wistar rat (250 g), by cardiac puncture immediately after death (by 4% CO<sub>2</sub> asphyxiation) and placed in a lithium/heparinised tube (10.0 ml) on ice. Erythrocytes (RBC) were isolated by centrifugation at 1500g for 10min at 4°C (repeated 3 times). Using the final pellet, a 2% w/v RBC solution was prepared with pre-chilled PBS and it was added (100 ml) to the previously prepared microtitre plates containing the test compounds. The plate was then incubated for 24 h at 37°C before centrifugation at 1500g for 10min at room temperature. The supernatant was then placed in another 96-well microtitre plate and haemoglobin (Hb) release measured spectrophotometrically (OD550) using a Victor2Wallac station using PBS as the blank.

Hb release for each sample was expressed as a percentage of the release produced by 0.5% w/v Triton X-100, used as a reference control to produce 100% lysis. PEI and dextran were also used as reference polymers.

#### **3.14.7. Confocal fluorescence microscopy: live cell imaging**

PC3 and LNCaP cells were seeded at a density of  $3.2 \times 10^4$  cell/mL and  $5 \times 10^4$  cell/mL, respectively, on glass bottom culture dishes (10 cm<sup>2</sup> Petri plate) and allowed to seed for 24h. Then, OG-labeled conjugates were added. Pulse and chase experiments were performed after 5 min, 15 min and 1 h incubations at 37°C, the medium was removed, the cells washed twice with PBS supplemented with 10% (v/v) of fetal bovine serum (FBS, 3 mL, 37°C) and the glass removed and fixed on the microscope chamber. In order to capture the images, in some samples the lysosomal marker Dextran-Texas red was also used to identify possible co-localization and therefore establish an endocytic pathway. A volume of 5µl of a Dextran-Texas Red solution (1mg/mL) was added and after 1h incubation, the medium was replaced with fresh one and the cells incubated for further 5h.

#### **3.14.8. Flow cytometry analysis**

Cellular uptake was studied by the flow cytometry technique. The experiments were carried out at 37°C and at 4°C to evaluate if the internalization followed an endocytosis or a diffusion mechanism. PC3( $3.2 \times 10^4$  cell/mL) and LNCAP ( $5 \times 10^4$  cell/mL) cells were plated and

following 24 hours exposed to OG-labeled polyacetals, Ser-OG-Ter-Des and Ser-OG-Block-Des diluted in F12 medium (for PC3 cells) and RPMI medium (for LNCAP cells) for 0, 5, 15 and 30 minutes and 1, 2 and 5 hours. Cells were then washed twice with cold PBS, sorted and analyzed by flow cytometry.

#### **3.14.9. Flow cytometry: Annexin-PI**

In order to study apoptotic processes after treatment with DES-polyacetals, PC3 cells were seeded in P35 plates (8 cm<sup>2</sup>) at density 11000 cell/cm<sup>2</sup> and after 24 hours, the medium was removed and the cells were treated with the polymers. The concentration used was the IC50 previously obtained in cytotoxicity studies. After 24 hours, the medium was reserved and the cells were lifted with Acummax. Cell suspension was centrifuged and the pellet was resuspended in 100 µl of 1X binding buffer (BD Pharmigen). 5µl of Annexin antibody and/or 5 µl of PI were added in the corresponding tube, the cell suspension was vortexed and incubated for 15 min at room temperature in the dark. Then, 400µl of binding buffer was added to each tube and analyzed by flow cytometry. The same protocol was used in androgen-sensitive human prostate adenocarcinoma cells, LNCAP, derived from the left supraclavicular lymph node metastasis.

#### **3.14.10. Western Blot**

To determine protein levels, cells with and without compounds ( 72 hours) were rinsed twice with ice-cold PBS and then lysed with ice-cold lysis buffer (50mM TrisHCl pH=8, 150mM NaCl, 0.02% NaN<sub>3</sub> azide, 0.1% SDS, 1% NP40, 0.5% DOC, Protease inhibitor cocktail tablets 1X). Cell lysates were centrifuged at 10000g for 10 minutes at 4°C; the supernatant was then mixed with 5xSDS sample buffer, boiled for five minutes, and separated through 8% to 15% SDS-PAGE gels. After electrophoresis, the proteins were transferred to PVDF membranes by electrophoretic transfer. The membranes were blocked in 5% skim milk for 2 hours, rinsed, and incubated overnight at 4°C with primary antibodies such as b-Actin, p21, caspase 3, Bax and Bcl2. The excess antibody was removed washing the membrane in PBS/0.1% Tween 20. The relative protein levels were quantified by densitometry with Scion Image programme. Results were standardized using b-Actin as the reference.

### **3.14.11. Cell cycle assay**

With the aim to study changes in the cell cycle after treatment with the free drug, DES-polyacetals were seeded in P38 plates (8 cm<sup>2</sup>) at density 11000 cell/cm<sup>2</sup> and after 24 hours, the medium was removed and the cells were treated with the polymers. The concentration used was the IC<sub>50</sub> obtained in previous studies of cytotoxicity. After 72 hours of incubation, the cell cycle was measured by flow cytometry. The protocol followed is detailed below. At first the medium culture was analyze as a control because in the medium there are dead cells that must be taken into account. Later, the cells were washed twice with PBS 1x and lifted with trypsin 1x. The cell suspension was centrifuged and the pellet was fixed adding 1 ml of ethanol 70%. While the ethanol was added, it was very important to vortex the sample to prevent the formation of cellular aggregates.

Cells were incubated for 1hour at -20°C with ethanol. Later the cell suspension was centrifuged at 400G for 10 minutes, resuspended in PBS and incubated for 30 minutes at 37°C and again the cell suspension centrifuged at 400G for 10 minutes more and the pellet was resuspended with Propidium Iodade Solution (50 µg/ml Propidium Iodade and 1 mg/ml RNase in PBS). The solution was incubated at room temperature for 1 hour. Finally, the sample was analysed by flow cytometry. The same protocol was used in androgen-sensitive human prostate adenocarcinoma cells, LNCAP, derived from the left supraclavicular lymph node metastasis.

### **3.14.12. Statistical Analysis**

All results are given as means ± SD (n≥3). When only two groups were compared, the Student's t test for small sample size was used to estimate statistical significance. If more than two groups were compared evaluation of significance was performed using one way-Analysis Of Variance (ANOVA) followed by Bonferroni post hoc test. Graph pad Instant software (Graph Pad Software Inc. CA, USA) was used. In all cases, statistical significance was set at p <0.05.

### **3.15. Biodistribution and tumor accumulation of the conjugates with Cy5.5 in a Xenograft mice model**

Polyacetal in vivo biodistribution in selected tumor models was measured by means of tissue fluorescence (FRI) using the IVIS® Spectrum in The Molecular Biology and Biochemistry Research Center for *Nanomedicine (CIBBIM-Nanomedicine)* (Vall d'Hebron Hospital Barcelona, Spain) Simó Schwartz Jr. group). Hsd:Athymic Nude-Foxn1nu mice and HT29 luciferasa C4 human cell line were used in this experiment t, currently, PC3 and LNCaP Xenograph models are being developed in Barcelona. The antitumoral effect of the test substance is indirectly measured by means of the tumor volume records measured using a caliper and means of the tumor bioluminescence (BLI) using the IVIS® Spectrum. Mice receive subcutaneous (s.c.) tumor cell injection ( $0.25 \times 10^6$  cells/100  $\mu$ l DPBS) in the rear right flank and thereafter are treated with the test substance. Tumor volume is measured twice a week by caliper measurements and bioluminescence imaging. The volume was calculated according to the formula  $D \times d^2$ , and the bioluminescence signal was quantified in photons per second. Polyacetal-cy5.5 conjugates were used in this study.

## References

1. Vicent, M. J.; Tomlinson, R.; Brocchini, S.; Duncan, R., Polyacetal-diethylstilboestrol: a polymeric drug designed for pH-triggered activation. *J Drug Target* **2004**, *12* (8), 491-501.
2. Giménez, V.; James, C.; Armiñan, A.; Schweinsc, R.; Paul, A.; Vicent, M. J., Demonstrating the importance of Polymer-Conjugate Conformation in Solution on its Therapeutic Output: Diethylstilbestrol (DES)-Polyacetals as prostate cancer treatment. *Journal of Controlled Release* **2012**, *159* (2), 290-301.
3. Jun Young, C., Highly Efficient Synthesis of enantiomerically enriched 2-hydroximethylaziridines by Enzymatic Desymmetrization. . *Organic Letters* **2007**, *9* (2), 215-218.
4. Tomlinson, R.; Klee, M.; Garrett, S.; Heller, J.; Duncan, R.; Brocchini, S., Pendent Chain Functionalized Polyacetals That Display pH-Dependent Degradation: A Platform for the Development of Novel Polymer Therapeutics. *Biomacromolecules* **2002**, *35* (2), 473-480.
5. Li, C.; Yu, D.; Inoue, T.; Yang, D. J.; Milas, L.; Hunter, N. R.; Edmund, E. K.; Wallace, S., Synthesis and evaluation of water-soluble polyethylene glycol-paclitaxel conjugate as a paclitaxel prodrug. *Anticancer Drugs* **1996**, *7*, 642-648.
6. Billingham, N. C.; Jenkins, A. D., *The Chemical Structure of Polymers*. American Elsevier Publishing Company, New York: Amsterdam and London, **1972**; Vol. 1, p 121-191.
7. Painter, P. C.; Coleman, M. M., *Molecular Weight and Branching*. Boca Raton, CRC Press LLC: **1997**; p 339-394.
8. Sun, S.-W., Efficiency improvements on nynthridin method for amino acid quantification. *Journal of Food Composition and Analysis* **2006**, *19*, 112-117.
9. Ibel, K., *Guide to Neutron Research Facilities at the ILL, Scientific Coordination Office, ILL*. 1994.
10. King, S. M., *Small Angle Neutron Scattering*. Wiley: **1999**; Vol. Ch 7, p 171.
11. Finney, J. L., ISIS - A Resource for Neutron Studies of Condensed Matter. *Europhys. News* **1989**, *20*, 1.
12. Boland, B. C.; Whapham, S., *User Guide to Experimental Facilities at ISIS*. 1992.
13. UKCCCR, UKCCCR guidelines for the use of cell lines in cancer research. *British Journal of Cancer* **2000**, *82* (9), 1495-1509.

# 4

***Tert-DES vs. Block-DES***  
**polyacetalic conjugates**

## 4. *Tert*-DES vs. *Block*-DES polyacetals

### 4.1. SYNTHESIS, CHARACTERIZATION AND *IN VITRO* STUDIES

#### 4.1.1. Introduction

The development of better polymeric carriers is an ongoing challenge to achieve second generation polymer therapeutics. There is an urgent need to develop biodegradable polymers that can better exploit EPR-mediated tumor targeting<sup>1</sup> and to move away from heterogeneous towards better defined polymer structures. Biodegradable polymers such as dextrans<sup>2</sup>, polyesters<sup>3</sup> or polyacetals<sup>4, 5</sup> could be considered as promising candidates to be used as carriers for targeted drug delivery. To allow the use of polymers of higher molecular weight, a family of hydrolytically labile, water-soluble polyacetals were developed<sup>5</sup>. These polymers can contain functional groups that allow side-chain conjugation, and a doxorubicin conjugate has been already reported<sup>4</sup>. These polyacetals are relatively stable at pH 7.4 (10% loss of molecular weight over 72 h), but degrade faster at the acidic pH that is encountered in endosomes and lysosomes (40% of the molecular weight is lost over 24 h at pH 5.5). *In vitro* and *in vivo* studies confirmed that the polyacetals are not toxic and also long circulating, i.e. they are not taken up extensively by the liver or spleen<sup>5</sup>. Moreover, the polyacetal–doxorubicin conjugate (Mw 86KDa) displayed significantly prolonged plasma circulation time and enhanced tumor accumulation compared to the HPMA copolymer doxorubicin conjugate PK1 (Mw 30KDa)<sup>4</sup>.

Polyacetals can be prepared by a mild polymerization method involving the reaction of diols with divinyl ethers<sup>7</sup>. To move a step further on this design Vicent et al. synthesized polyacetals incorporating a drug with bis-hydroxyl functionality into the polymer backbone<sup>6</sup>. Degradation of the polymer backbone in the acidic environment of the lysosome or the extracellular fluid of some tumors would then trigger drug release eliminating the need for a biodegradable linker. For this purpose, the *tert*-polymerization process developed for the synthesis of the functionalized polyacetals was used<sup>4,5</sup> in combination with the model drug diethylstilbestrol (DES). . The previous research with DES-polyacetals already demonstrated that DES solubility can be greatly enhanced upon polymerization. And more interestingly, the

conjugates underwent degradation that was clearly pH-dependent, with greater DES release at acidic pHs. Additionally, the active isomerism of the estrogen was maintained (*trans*-DES)<sup>6</sup> and the conjugates displayed enhanced *in vitro* cytotoxicity compared to free DES. These *tert*-DES polyacetals could therefore be defined as the first water-soluble anticancer polymeric drugs designed for acidic pH-triggered release where the drug is incorporated into the polymer mainchain<sup>6</sup>. Ratifying the utility of this synthetic strategy, another recent example has been reported using curcumin as a diol-functionalized anticancer drug. The polyacetal-based polycurcumins showed a clear antitumor effect *in vitro* and *in vivo* in ovarian cancer models<sup>8</sup>.

The first synthesized *tert*-polymer had a drug content of ~4 wt% and a polydispersity (Mw/Mn) around 1.8. The initial aim of the current study was to synthesize a second generation of DES-based polyacetals with improved properties, such as narrower Mw distributions and higher drug loading, and more importantly to study with these model systems, if slight structural modifications could significantly influence conjugate therapeutic output. These second generation polyacetals were obtained using a block-*co*-polymer methodology. *Tert*-DES and *block*-DES were then tested in selected prostate cancer cell models<sup>9</sup>.

#### 4.1.2. Synthesis and Characterization of DES-polyacetals

In this chapter the design of novel DES-polyacetals as block-*co*-polymers systems (*block*-DES) with amphiphilic character will be described. The original *Tert*-DES will be used as reference conjugate and their biological output will be compared.

##### *Optimization of DES-polyacetals synthetic approach*

The original synthetic polymerization approach presented some limitations such as poor batch to batch reproducibility and poor product stability due to the presence of unreacted traces of weak acid that could trigger polyacetal degradation. Therefore, different conditions were tried in order to optimize the synthesis and to control the obtaining of the desired product e.g. different reaction times, temperature, monomer equivalents, the way reactants were added and different reaction solvents. The different conditions used are shown in Table 4.1. 1.



The improvements here were made by synthesizing using Schlenk line conditions, which provide advantages on the polymerization as the reagents could be dried quickly and the anhydrous environment kept during the whole process. Also checking the progress of the reaction by  $^1\text{H}$ NMR the reaction times were reduced from between 3-16 hours to just 1 hour at room temperature<sup>10</sup>. The monomers employed were PEG of different including 2000, 4000 and 6000g/mol. It was determining that the best results obtaining were with 4000g/mol, as the one with 6000g/mol resulted in highly heterogeneous polymer and when PEG 2000 g/mol was used, a much lower DES payload was achieved. Therefore, PEG 4000g/mol was selected for all further studies.

**Table 4.1. 1** Conditions tested during polyacetal synthesis optimization.

T <sup>a</sup> (°C)	Reaction time	Co- monomers Mw(g/mol)	DVE	Catalyst	Base	Reaction solvent	Solvent Conditions	Reactants conditions	Method to add reactants
25 4 36	3, 4, 24 and 36 h	PEG 2000	TEGDVE	p-TSA	Et <sub>3</sub> N	THF	Distilled with Na	Dried 16h (v.o., 37,80 ,100°C)	In solution (same reactant solvent)
	5, 7, 9 days	PEG 4000	DEGDVE	La-sulph	Py	Dioxane	Anh. Bottle		
		PEG 6000 DES 268 Serinol-F 315			Triflic ac	DIEA NaOH	DCM Toluene DMF	HPLC grade HPLC grade with molecular sieves	No dried (rt)

Where; F: Fmoc group, sulph.: sulphonate, Py: pyridine, Na: sodium, rt: room temperature, anh: anhydrous and v.o.: vacuum oven.

Different solvents were tested and dioxane was the best option as a clear product with almost no presence of impurities or subproducts from polymer degradation was achieved before purification (Figure 4.1. 1).

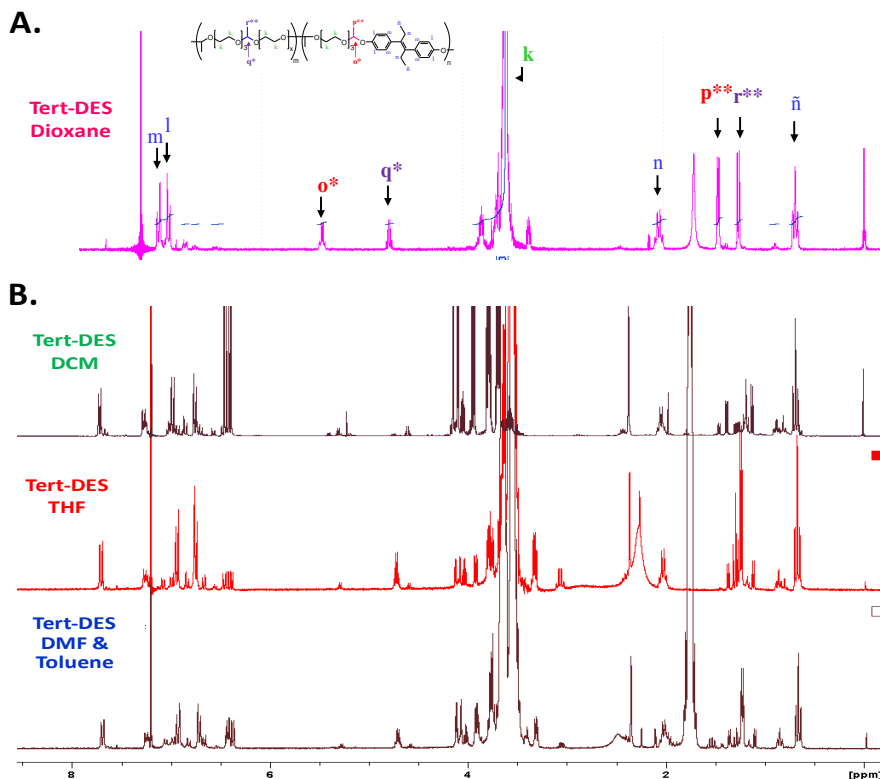


**Figure 4.1.**  $^1\text{H}$  NMR of Tert-DES synthesized in different solvents; (A) THF, Toluene, Dichloromethane (DCM), Dimethylformamide (DMF); (B) Dioxane.

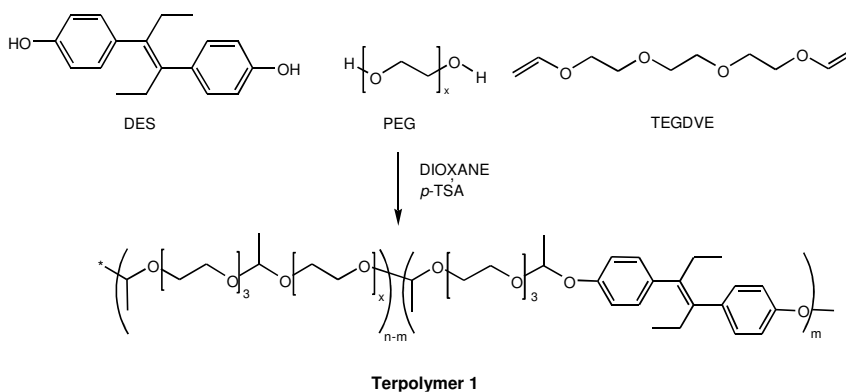
The acid catalyst (p-TSA) was quenched more easily using a small quantity of sodium hydroxide in place of the previously used triethylamine, which was subsequently easily removed during the purification step. Different purification approaches were taken, mostly based on precipitation over hexane or different mixtures of hexane and diethyl ether (4:1, 3:1, 2:1, 1:1), but also ultrafiltration was studied, where poor water soluble polymers were dissolved in a mixture water/acetone. It was found that precipitation worked better than ultrafiltration for DES-polyacetals. The purification, which takes approximately 2 hours therefore yields the resulting materials (after freeze-drying) in good quantity after just 24 hours. Then, the polyacetals were

purged under nitrogen and different storage conditions were evaluated (4°C (fridge), -20°C (freezer) and at RT (desiccator) being -20°C the best found.

Summarizing, the final selected conditions for all reactions were: PEG 4000, DES and Serinol-Fmoc as co-monomers, pTSA as catalyst, the reaction solvent was anhydrous dioxane and the base used to quench the reaction was NaOH. The reaction was carried out in schlenk conditions at 25°C during 1h. The precipitation of the polyacetals over hexane was employed as purification method. It is important to note that, in the case of *Block*-DES, these changes clearly impact the efficiency of the reaction; in particular reaction time was reduced from 6h with the original conditions to 1.5h with the optimized method.

### ***Tert*-DES-polyacetal 1 (*Tert*-DES)**

A family of *Tert*-DES-polyacetals **1** (*tert*-DES) was synthesized following the *tert*-polymerization technique previously described (Scheme 4.1. 1) and using <sup>1</sup>H-NMR in order to confirm the presence of the drug in the polymer mainchain. <sup>1</sup>H-NMR allowed quantification of DES loading as for the presence of two distinct sets of acetal peaks, which correspond to the two possible mainchain acetals; from PEG at 1.25–1.3(d) and 4.7–4.8(q)ppm and from DES at 1.5–1.6(d) and 5.4–5.5(q)ppm (Figure 4.1. 2).



**Scheme 4.1. 1** Synthesis of DES-polyacetal **1** (*Tert*-DES).

Water-soluble *tert*-DES polyacetals obtained had Mw range from 34000 g/mol to 38000 g/mol and with Mw/Mn from 1.5 to 1.7 as determined by size exclusion chromatography (GPC) (THF, 0.8 ml/min). DES total loading in the different water-soluble *tert*-polyacetals varied from 3 to 6 wt% with a free drug content always < 0.5 wt% of total drug (Table 4.1. 2). A DES loading greater than 6 wt% yielded non-water soluble materials.

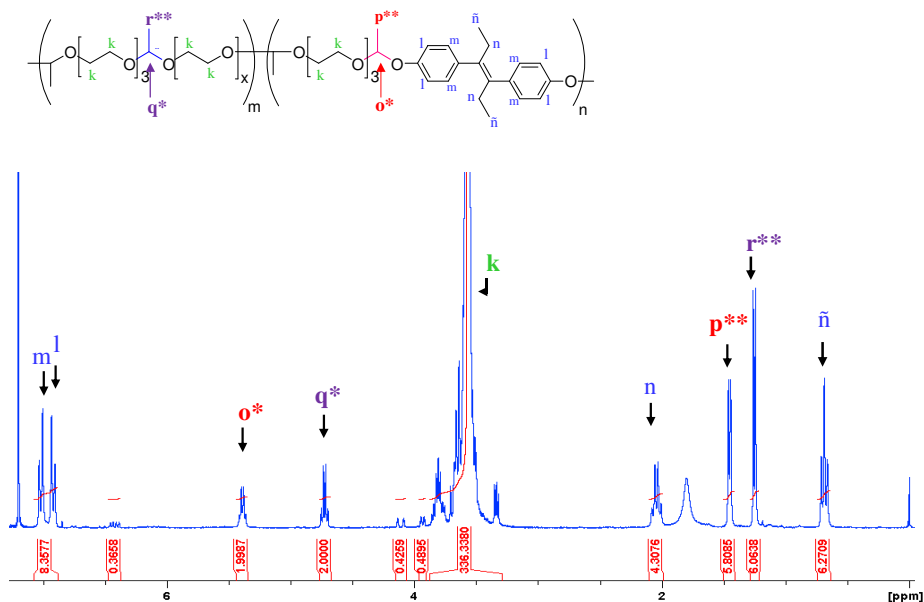


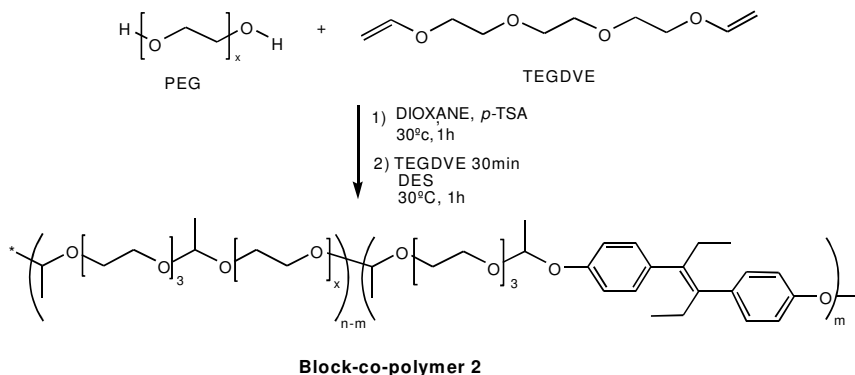
**Figure 4.1.** <sup>1</sup>H-NMR spectra of DES-polyacetal **1** (*Tert*-DES).

### Block-co-polymers **2** (*Block*-DES)

In parallel, a family of amphiphilic *block-co*-polymers, *Block*-DES-polyacetal **2** (*block*-DES), was also synthesized. The synthetic strategy was based on the same polymerization technique described above but using a sequential approach.

The main synthetic differences for the *tert*- and *block*- polymers were based on the DES addition time point. When DES was added at the beginning of the reaction together with poly(ethyleneglycol) (PEG) and tri(ethylene glycol) divinyl ether (TEGDVE) (in a one-pot polymerization

approach) a *tert*-polymer was formed. In contrast, if DES incorporation was performed in a second step after PEG block formation an amphiphilic *block-co*-polymer could be achieved (Scheme 4.1. 2). The DES loading was confirmed by  $^1\text{H-NMR}$  in all cases (Figure 4.1. 3 ; integration  $o^*$  vs  $q^*$  and  $p^{**}$  vs  $r^{**}$ ).



**Scheme 4.1. 2** Synthetic approach followed to obtain *Block*-DES 2.

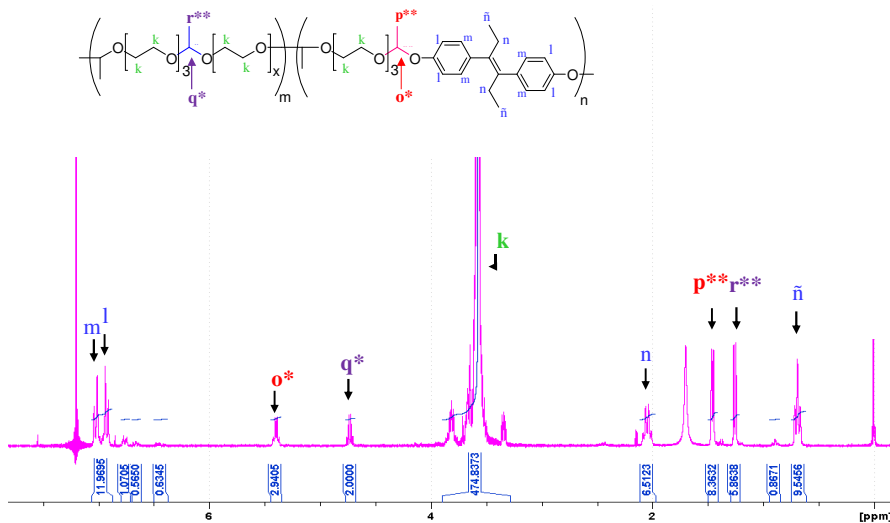


**Figure 4.1. 3** Example of  $^1\text{H-NMR}$  spectrum of *Block*-DES 2 with assigned signals.

*Block*-DES polyacetals with an adequate water solubility were able to be obtained with a drug payload greater than that obtained for the *tert*-DES (from 2 to 9 wt%) with a free drug content always < 0.5 wt% of total drug, a Mw ranging from 26.000 g/mol to 35.000 g/mol and a moderate Mw/Mn from 1.3 to 1.6 as determined by GPC in THF (Table 4.1. 2).

**Table 4.1. 2** Physico-chemical characteristics of the polyacetals synthesized.

Conjugate	DES Loading <sup>a</sup> (wt%)	Free DES content <sup>b</sup> (wt% of total drug)	Mw <sup>c</sup> (g/mol)	Mw/Mn <sup>c</sup>
<i>Tert</i> -DES 1a	2.8 ± 0.2	0.2 ± 0.1	35.280	1.70
<i>Tert</i> -DES 1b	4.0 ± 0.2	0.3 ± 0.1	34.400	1.63
<i>Tert</i> -DES 1c	5.7 ± 0.3	0.2 ± 0.2	37.607	1.54
<b><i>Block</i>-DES 2a</b>	<b>2.0 ± 0.1</b>	<b>0.2 ± 0.1</b>	<b>28.081</b>	<b>1.40</b>
<b><i>Block</i>-DES 2b</b>	<b>4.3 ± 0.3</b>	<b>0.1 ± 0.2</b>	<b>28.780</b>	<b>1.27</b>
<b><i>Block</i>-DES 2c</b>	<b>7.3 ± 0.3</b>	<b>0.2 ± 0.1</b>	<b>34.300</b>	<b>1.42</b>
<b><i>Block</i>-DES 2d</b>	<b>9.5 ± 0.2</b>	<b>0.3 ± 0.2</b>	<b>26.700</b>	<b>1.60</b>

(a) Determined by <sup>1</sup>H NMR; (b) Determined by HPLC analysis; (c) Determined by size exclusion chromatography (GPC, Viscotek TDA<sup>TM</sup>); DES: Diethylstilbestrol, Mw: Molecular weight, Mw/Mn: polydispersity index.

### 4.1.3. Kinetics of Drug Release

#### pH-dependent Degradation of DES-Polyacetals 1 and 2.

Essential characteristics for polymer–drug conjugates are stability during blood circulation and the capability for drug release from the carrier under selected physiological triggers. Therefore, in order to show the applicability of

this approach, it was essential to determine pH-responsiveness of the conjugates under conditions encountered in a biological environment.

The pH-dependent degradation profile for DES-polyacetals was hypothesized to be similar to that previously described for APEG<sup>4,5</sup>, however it was already demonstrated for *tert*-DES **1** that the presence of the aromatic groups adjacent to the acetal moiety affects polymer degradation rate at acidic pH, being much faster when DES was present in comparison to the parent APEG systems<sup>6</sup>.

HPLC (at 280 nm) was used as quantitative method to determine the amount of DES released from *block*-DES **2** in comparison to *tert*-DES **1**. As expected, a strongly pH dependence on polyacetal degradation was observed for both polymers, with % DES released decreasing pH 5.5 >> pH 6.5 > pH 7.4, which is an ideal profile for a lysosomotropic drug delivery route (Figure 4.1. 4 A,B).

At acidic pH, *block*-DES presented a slightly faster drug release rate in comparison to its *tert*-DES counterpart (as example see **1b** vs. **2b** in Figure 4.1. 4)..

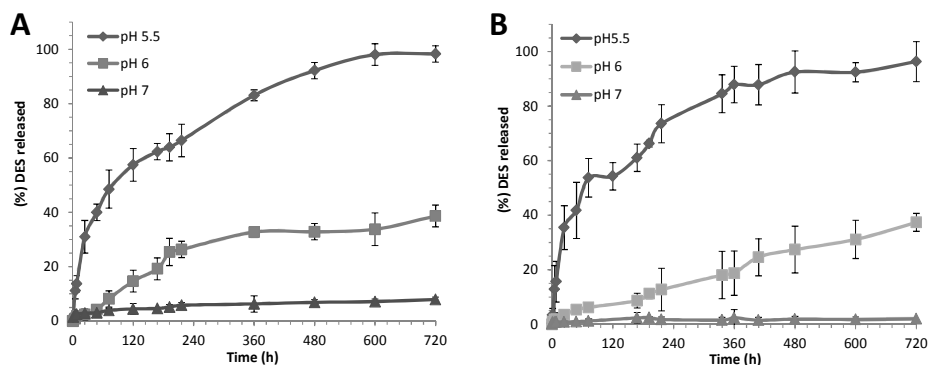


**Figure 4.1. 4** pH-Dependent DES release: (A) *tert*-DES **1b** at pH 7.4, 6.5 and 5.5; (B) *block*-DES **2b** at pH 7.4, 6.5 and 5.5. The results show the percentage of DES release from total at each time point. Mean values  $\pm$  SD ( $n = 3$ ).

Importantly, for both polymers the DES was released predominantly as the active isomer of *trans*-DES (>80%) (Figure 4.1. 5).

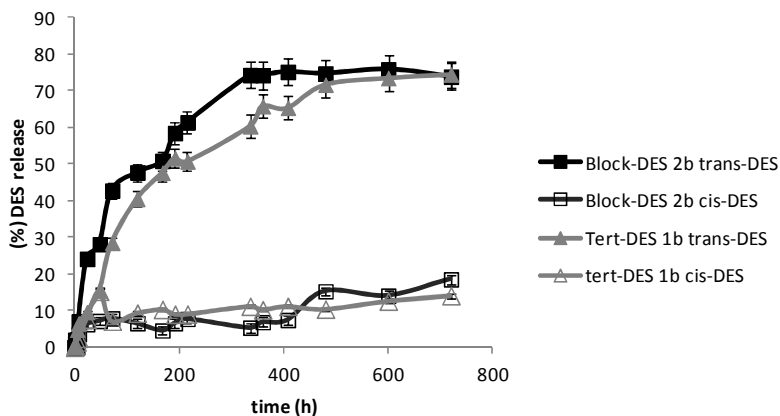


**Figure 4.1. 5** pH-Dependent DES release as *cis*- and *trans*-DES forms from *tert*-DES **1b** and *block*-DES **2b** at pH 5.5. The results show the percentage of DES release from total at each time point. Mean values  $\pm$  SD ( $n = 3$ ).

Due to the relative hydrophobic/ hydrophilic ratio depending on polyacetal DES loading, it is clear that the different DES content could affect conjugate conformation and consequently also influence drug release kinetics. In fact, as it can be seen in Figure 4.1. 6 A.B., a greater DES loading yielded to a slower drug release rate in both designs, being more important for *block*-DES family.

*Block*-DES showed what could be considered a ‘biphasic release profile’ typically observed in biodegradable nanoparticulate systems. This biphasic pattern in *block*-DES can more clearly be seen in those polyacetals with greater drug loading ( $2c > 2b > 2a$ ) (Figure 4.1. 6 B).

As these systems are designed for intravenous (i.v.) administration it is important to explore conjugate stability in plasma trying to mimic physiological conditions. Both, *tert*-DES and *block*-DES showed non-significant drug release up to 24 h incubation (See next section 4.1.4).



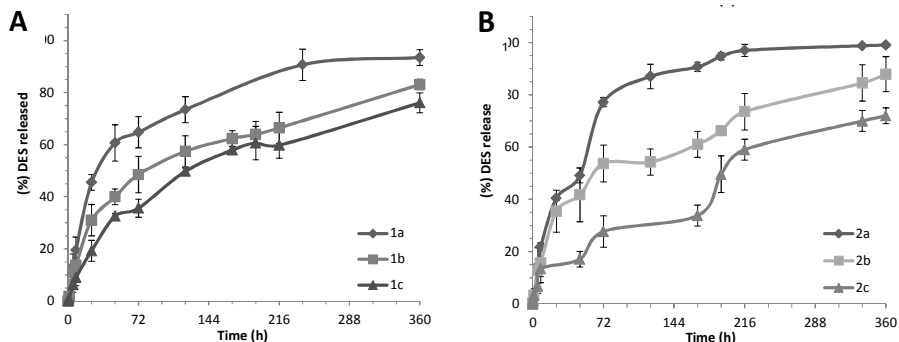


**Figure 4.1.6** pH-Dependent DES release from: (A) *tert*-DES **1a-c** at pH 5.5, (B) *block*-DES **2a-c** at pH 5.5. The results show the percentage of DES release from total at each time point. Mean values  $\pm$  SD (n = 3).

#### 4.1.4. Plasma Stability of DES-polyacetals

The polymers were dissolved and incubated for up to 24 h in plasma at 37°C. Plasma was obtained from the fresh blood of adult male Wistar rats and to allow analysis protein precipitation was carried out with acetonitrile (see experimental methods chapter 3, for detailed information). DES released was then measured as above-described by HPLC.

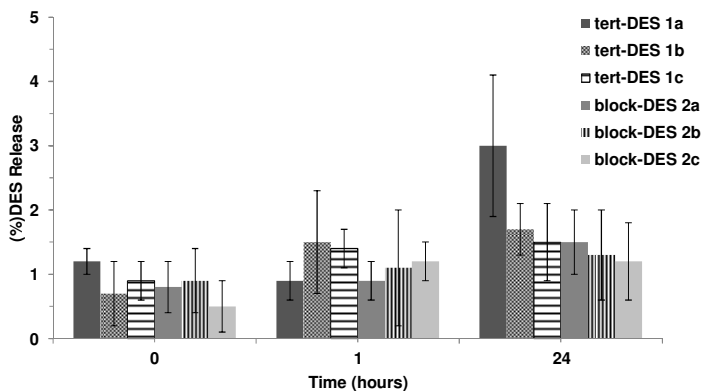


**Figure 4.1.7** Stability in plasma of DES-polyacetal derivatives (mean  $\pm$  SD, n=3).

Both, *tert*-DES and *block*-DES showed non-significant drug release up to 24 h incubation in presence of plasma at 37°C confirming polyacetal plasma stability(see Figure 4.1. 7).

#### 4.1.5. Preliminary biological evaluation in cell models.

Once the polyacetalic systems were synthesized and characterized, their evaluation as anticancer agents were carried out in selected prostate cancer cell lines. *In vitro* antitumor activity of DES should preferably be assessed using an estrogen responsive cell line, however, DES also inhibits Bcl-2 protein<sup>12,13</sup>, the assembly of microtubular proteins<sup>14,15</sup> and even the telomerase activity<sup>16</sup> and therefore, has been shown to be also cytotoxic in non-estrogen responsive cell lines, such as 3T3 fibroblast<sup>17</sup>, MOP<sup>18</sup> or B16F10 melanoma cells<sup>19</sup>. Therefore, the biological evaluation of DES-polyacetals (**1**) and (**2**) was carried out in two different human prostate cancer cell lines, namely PC3 (Hormone Independent) and LNCaP (Hormone Dependent). For comparison, in cell viability studies, free DES as sodium salt (NaDES) was used.

Techniques such as cell-live confocal fluorescence microscopy (to avoid artefacts with fixation) and flow cytometry techniques were employed with fluorescence labelled derivative polymers. The fluorescent marker chosen for labelling purposes was Oregon green (OG) as has been reported to be stable against changes in pH. The fluorescent analogue conjugates were employed to carry out biophysical studies such as cell binding (at 4°C and 37°C) and cell internalization (at 37°C). Using these techniques gives scope to evaluate the endocytic route the conjugates follow by the incubation of them along with fluorescent markers of specific organelles. In this study a lysosomal marker was used, Texas Dextran red. Normally, polymer–drug conjugates are internalized by endocytosis, circulating to the appropriate cellular compartment and free drug is released enzymatically or chemically, which causes a significant delay in the onset of action compared to the free drug.

Specific experiments were also designed to elucidate the mechanism of action of the different systems including drug release mechanisms<sup>20</sup>, their ability to trigger and block specific cell process (e.g. apoptosis<sup>21</sup>, or angiogenesis<sup>22</sup>) (See Chapter 4.2).

Finally, it is important to note that the influence of the polymer architecture on biological properties is not well described in the literature. Therefore, one of the most important goals in this chapter was to understand the effect of architecture on conjugate biological output, normally anticancer activity and cell trafficking.

#### **4.1.5.1. Amino-pendant polyacetals (APEG).**

It was planned to study the differences between *tert*- and *block*-DES on cell trafficking and *in vivo* biodistribution. In order to carry out these experiments, fluorescently labeled polyacetal derivatives were required. The original structure do not allow any post-polymerization modification, therefore, additional co-monomer with side-chain functionality had to be employed.

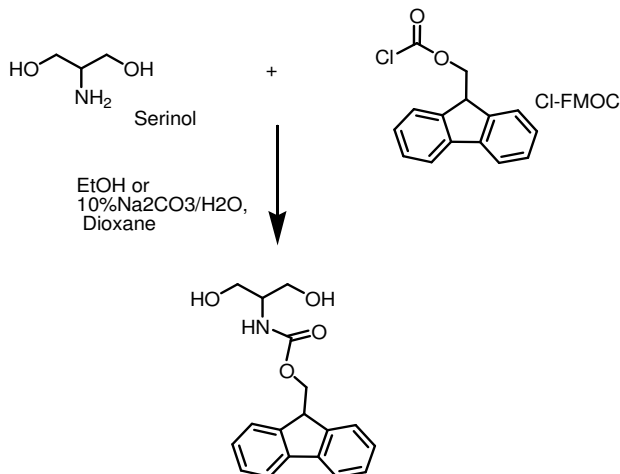
Based on a previously described synthesis<sup>5</sup>, an Fmoc-N-protected serinol was selected as the amino-functionalised monomer chosen. These molecules contains the diol functionality required for polymerization and incorporation into the polymer backbone, and, at the same time contains an amino group that allows side-chain post-polymerization modifications. NH<sub>2</sub> group should be protected to avoid the formation of undesired side-reactions. The Fmoc protecting group was found to have an advantage as it can be easily removed in basic media, preventing the degradation of the acetal bonds previously formed<sup>5</sup>.

The introduction of the new monomer allowed the introduction of fluorescence probes for cell studies (OG), NIR dyes for *in vivo* analysis (Cy5.5) and also offered the opportunity for second drug incorporation yielding polyacetals designed for combination therapy combining endocrine therapy plus chemotherapy<sup>20</sup> (further details in Chapter 5).

#### **Synthesis of Fmoc-protected serinol 3**

First, serinol protected with fmoc group was synthesized to have the new co-monomer ready to incorporate in the polyacetalic systems, *tert* and *block*-DES. Fmoc-protected serinol **3** was synthesized (Scheme 4.1. 3) as

reported by Tomlinson et al<sup>5</sup>. The structure was confirmed by <sup>1</sup>H-NMR (Figure 4.1. 8).



**Scheme 4.1. 3** Synthesis of Serinol-Fmoc monomer **3**.

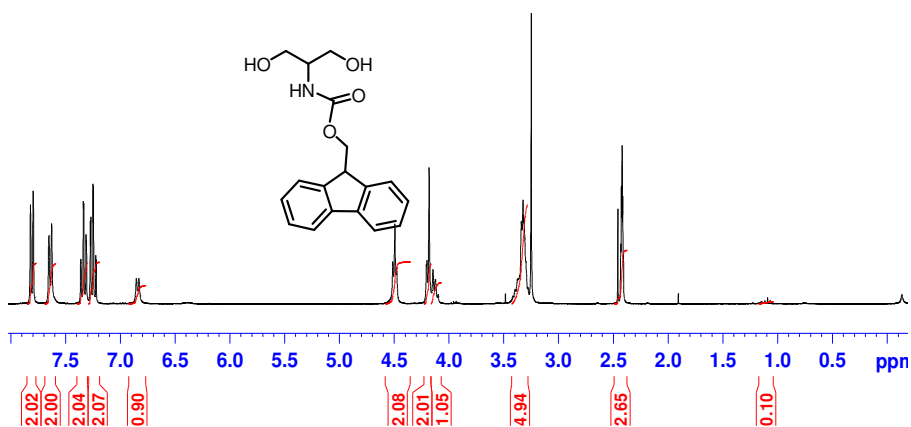
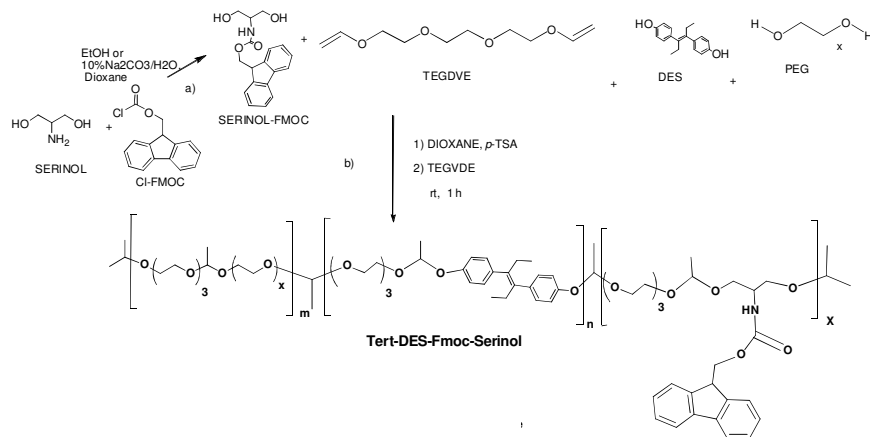


**Figure 4.1. 8** <sup>1</sup>H-NMR spectrum of Serinol-Fmoc monomer **3**.

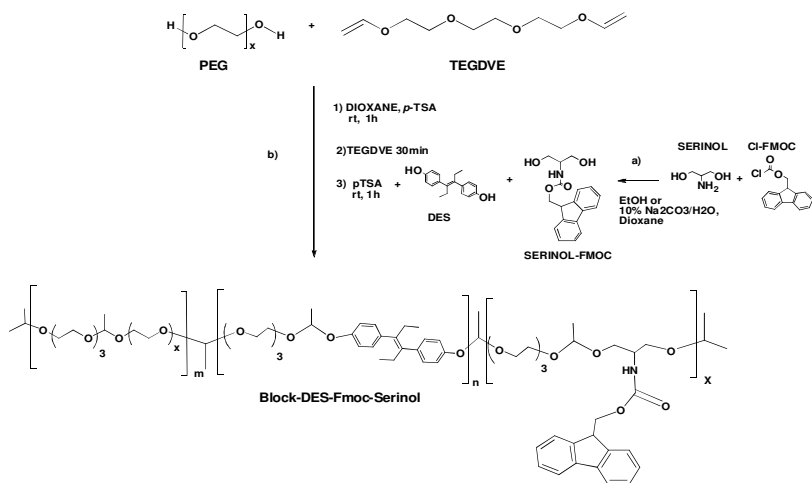
### Synthesis of APEG-DES-polyacetals derivatives.

Subsequently, a family of APEG-DES-polyacetals were synthesized using the same procedure described for *Tert*-DES **1** and *Block*-DES **2** but adding Serinol-Fmoc **3** as a co-monomer with DES yielding *Tert*-DES-Ser **4** (Scheme 4.1. 4) and *Block*-DES-Ser **5** (Scheme 4.1. 5). <sup>1</sup>H NMR

confirmed the presence of the Fmoc-Serinol **3** with a new set of polyacetal signals at 4.3ppm and the aromatic signals from Fmoc group 7.3, 7.4, 7.6 and 7.8 ppm (Figure 4.1. 9 and 4.1. 10) for **4** and **5** respectively), which allowed for the calculation of the drug loading.



**Scheme 4.1. 4** Synthesis of *Tert*-DES-Ser **4**.



**Scheme 4.1. 5** Synthesis of *Block*-DES-Ser **5**.

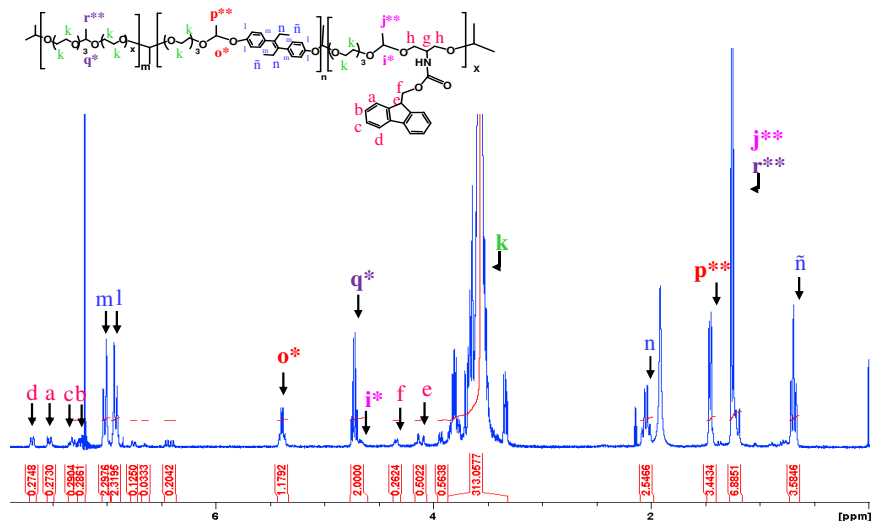


Figure 4.1.9  $^1\text{H}$  NMR spectra of *Tert*-DES-Ser 4.

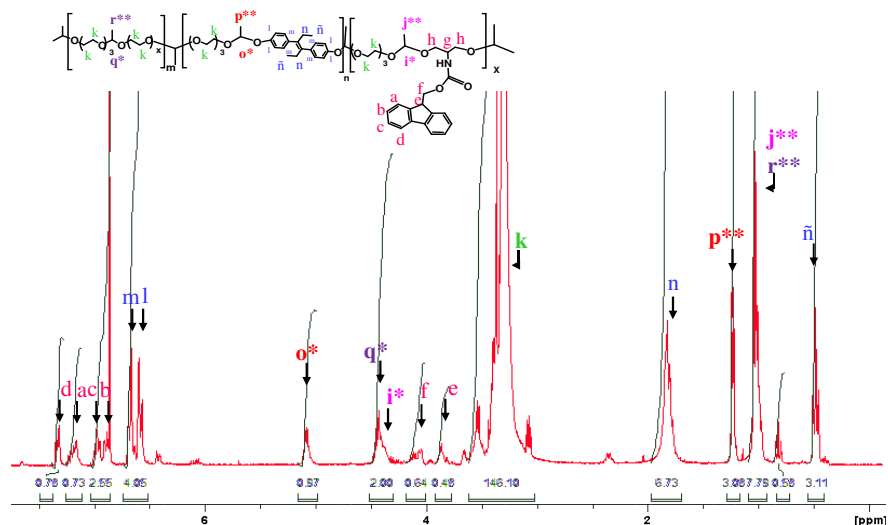
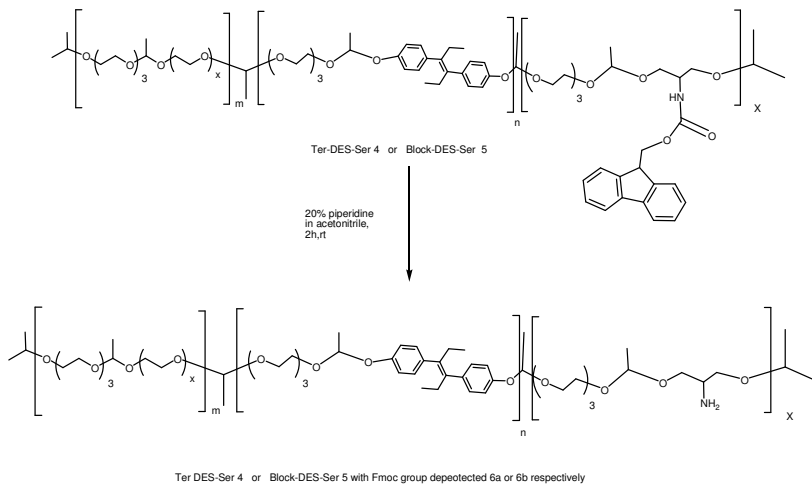


Figure 4.1.10  $^1\text{H}$  NMR spectra of *Block*-DES-Ser 5.

Afterwards, *Tert*-DES-Ser 4 and *Block*-DES-Ser 5 were deprotected using piperidine in order to obtain *Tert*-DES-Ser 6 and *Block*-DES-Ser 7, ready for further side-chain compound conjugation. The absence of the aromatic peaks from the Fmoc group and the maintenance of the two distinct sets of

acetal peaks in the  $^1\text{H-NMR}$  spectra (Figure 4.1. 11) confirmed that the deprotection had been successful and that serinol was present in the polyacetal.



**Scheme 4.1. 6** Synthesis of *Tert*-DES-Ser 4 or *Block*-DES-Ser 5 with Fmoc group deprotected, yielding 6 or 7 respectively.

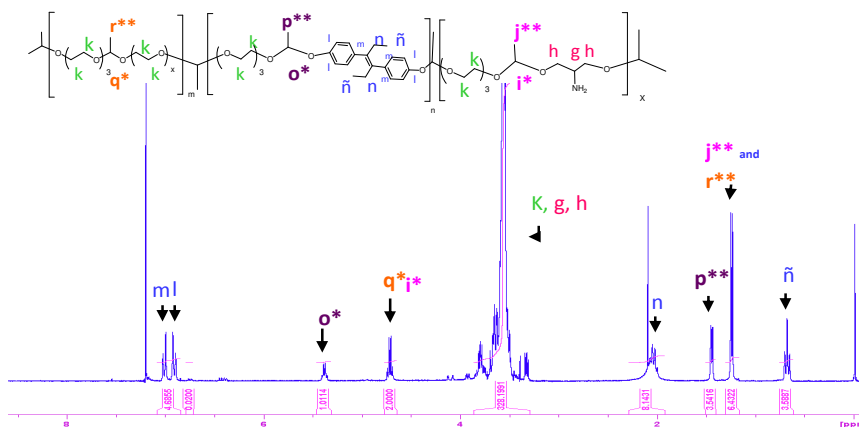


**Figure 4.1. 11** An example  $^1\text{H-NMR}$  spectra showing successful Fmoc-deprotection and preservation of DES and serinol in the APEG conjugate polymers.

### Determination of amine groups

In order to determine the total quantity of amino groups present in the deprotected polyacetals, a quantitative method using ninhydrin (mentioned in chapter 3) was carried out. According to literature, this method offered a linear relationship ( $R^2 > 0.98$ ) of absorbance versus the amino acid concentration up to  $50 \mu\text{g/mL}$  for all amino acid tested<sup>23</sup> (Figure 4.1. 12).

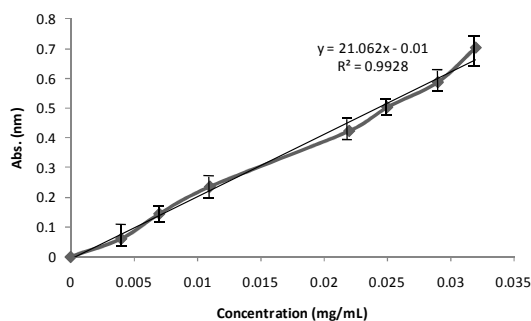


**Figure 4.1. 12** Calibration curve use to quantify the pendant amino groups in the polyacetals.

Using this calibration curve, polymers were measured to quantify the existing amine group from serinol ( $-\text{NH}_2$ ) (Table 4.1. 3).

**Table 4.1. 3** Physico-chemical characteristics of DES-Serinol polyacetals.

Conjugate	DES Loading <sup>a</sup> (wt%)	Free DES content <sup>a,b,c</sup> (wt% of total drug)	Serinol <sup>a,c</sup> Loading (wt%)	Mw <sup>d</sup> (g/mol)	Mw/Mn <sup>d</sup>
<i>Tert</i> -DES-Ser 4a	4.5 ± 0.3	0.2 ± 0.1	3.0 ± 0.3	37.801	1.63
<i>Tert</i> -DES-Ser 4b	4.9 ± 0.2	0.4 ± 0.1	7.0 ± 0.1	41.451	1.69
<b><i>Block</i>-DES-Ser 5a</b>	<b>4.7 ± 0.4</b>	<b>0.4 ± 0.2</b>	<b>3.0 ± 0.2</b>	<b>30.768</b>	<b>1.50</b>
<b><i>Block</i> -DES-Ser 5b</b>	<b>4.8 ± 0.2</b>	<b>0.1 ± 0.2</b>	<b>6.1 ± 0.2</b>	<b>31.373</b>	<b>1.55</b>

<sup>a</sup>Determined by <sup>1</sup>H NMR; <sup>b</sup>Determined by HPLC analysis; <sup>c</sup>Determined by ninydrine assay; <sup>d</sup>Determined by size exclusion chromatography



(GPC, Viscotek TDA<sup>TM</sup>); DES: Diethylstilbestrol, Ser: Serinol, Mw: Molecular weight, Mw/Mn: polydispersity index.

### Conjugation of APEG-DES polyacetals with different fluorochromes.

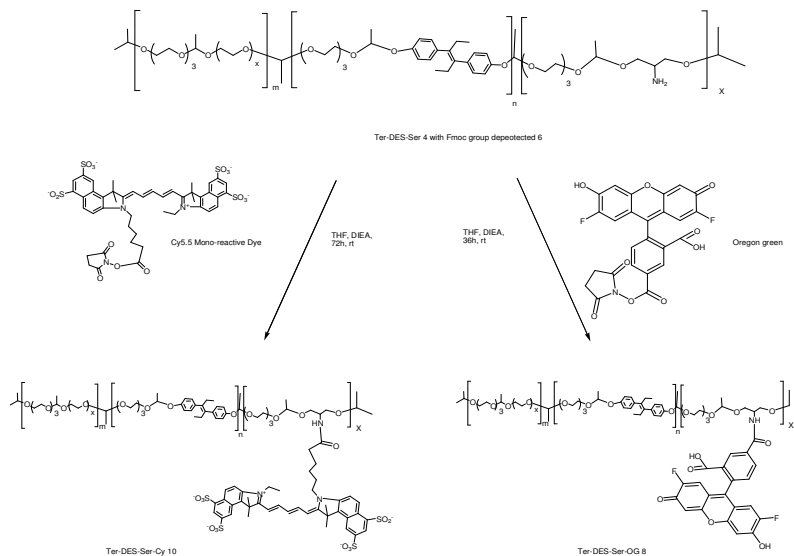
Using a carbodiimide-mediated coupling, the conjugation of *Tert*-DES-Ser **4** and *Block*-DES-Ser **5** with Oregon Green yielded *Tert*-DES-Ser-OG **8**, *Block*-DES-Ser-OG **9** and with Cy 5.5 *Tert*-DES-Ser-Cy **10** (scheme 4.1 7) and *Block*-DES-Ser-Cy **11** (scheme 4.1 8) were achieved. All DES-polyacetals conjugated with Cy5.5 or OG are compiled in table 4.1.4.

**Table 4.1. 4** Physico-chemical characteristics of the polyacetals with serinol synthesized.

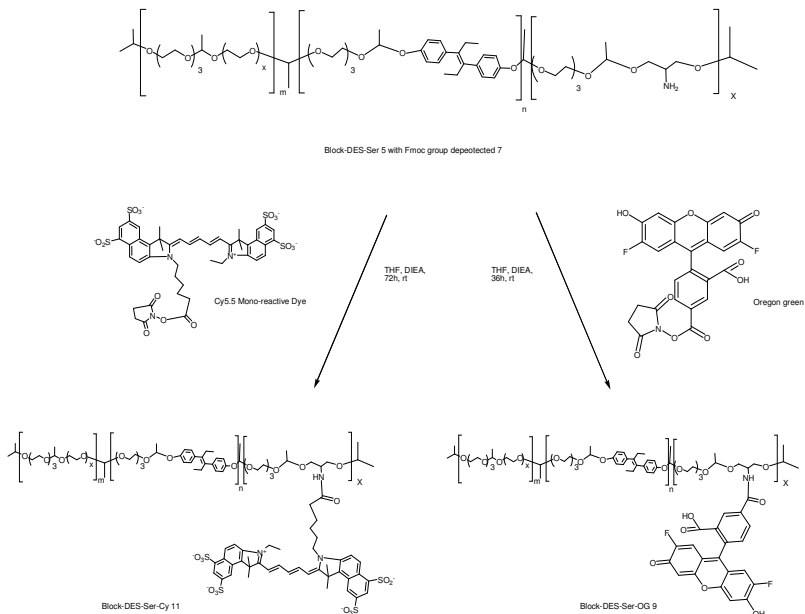
Conjugate	OregonGreen <sup>a,b</sup> content (wt%)	Cyane 5.5 <sup>a,b</sup> content (wt%)
<i>Tert</i> -DES-Ser-OG 8a (*)	0.8 ± 0.2	-
<i>Tert</i> -DES-Ser-Cy 10a (*)	-	0.6 ± 0.1
<b><i>Block</i> -DES-Ser-OG 9a (*)</b>	<b>0.8 ± 0.2</b>	-
<b><i>Block</i> -DES-Ser-Cy 11a (*)</b>	-	<b>0.6 ± 0.1</b>

<sup>a</sup>. Determined by Fluorimetry (Victor2 Wallac Station); <sup>b</sup>. Determined by HPLC analysis; \*synthesized from *Tert* -DES-Ser 4a and \* from *Block*-DES-Ser 5a. Serinol and DES loading are described in Table 4.1. 3.

To synthesize OG- or Cy5- labeled- *tert*- and *block*-DES-Ser, another procedure was tested (as it was described in chapter 3). After deprotection, the Polyacetals were succinoylated to obtain *tert*- and *block*- DES-Ser<sub>COOH</sub> (**12** and **13**, respectively) and amino-fluorochromes ( cadaverine in the case of OG) attached yielding *tert*-DES-Ser-OG<sub>cad</sub> **14**, *block*- DES-Ser-OG<sub>cad</sub> **15**, *block*-DES-Ser-Cy<sub>cad</sub> **16** and *block*-DES-Ser-Cy<sub>cad</sub> **17**. However, with this second procedure polymer degradation was observed along each step diminishing conjugate stability. For this reason the first procedure (Scheme 4.1. 7 and 4.1. 8) was selected for polyacetal labeling.



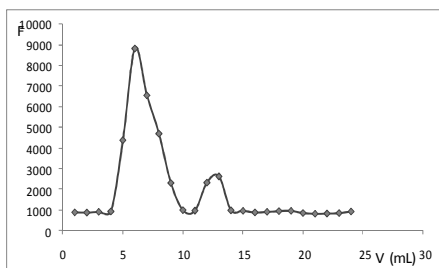
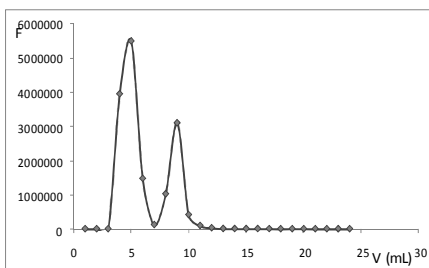
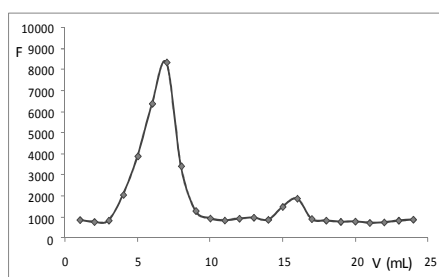
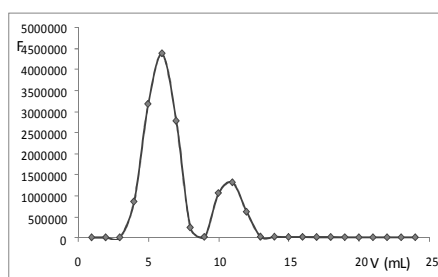
**Scheme 4.1. 7** Scheme to synthesize OG- or Cy5.5- *Tert*-DES-Ser.



**Scheme 4.1. 8** Scheme to synthesize OG- or Cyane5.5-*Block*-DES-Ser.

In order to purify and determine the total fluorescent loading, the OG ( $\lambda_{em}$ : 535,  $\lambda_{exc}$ : 485) and Cy5.5 ( $\lambda_{em}$ : 694,  $\lambda_{exc}$ : 675) labeled conjugates

were purified by SEC (Sephadex G25, PD10 column) and the total fluorescence of each aliquot (1 ml) quantified by a fluorimetry. An adequate filter in the NIR area was required for Cy5.5. In both cases conjugation efficiency was >80% (Figure 4.1. 13).

**A. *Tert*-DES-Ser-Cy 10****B. *Tert*-DES-Ser-OG 8****C. *Block*-DES-Ser-Cy 11****D. *Block*-DES-Ser-OG 9**

**Figure 4.1. 13** Representative images of the elution profile of labeled conjugates used to quantify Cy5 (A, C) and OG- (B, D) polymer loading

The compounds labeled with OG were used in cell experiments in order to study cell trafficking mechanisms in prostate cancer cell lines. Polyacetals labeled with Cy5.5 were used for the *in vivo* studies described chapter 5 (IVIS Spectrum<sup>®</sup>).

**4.1.5.2. *In vitro* studies in prostate cancer cell lines.**

Ethical and economical considerations are essential to develop new therapies, for this reason *in vitro* pre-screening is favorable for making the first studies and determine if continue the study to *in vivo* models.

In most cases, cells must be grown in culture for days to obtain sufficient cell density to carry out the different studies. Maintenance of cells in long-term culture requires strict adherence to aseptic technique to avoid contamination and potential loss of valuable cell lines. Cell biology studies require several special skills in order to be able to preserve the structure, function, behavior, and biology of the cells in culture. Techniques such as cell passaging (trypsinization), freezing and storing were carried out. An important factor influencing the growth of cells in culture is the use of the appropriate media for covering all the necessities of the cells to get a proper growth. The media provides all the nutrients for growing cells but sometimes is complemented with antibiotics, fungicides, or both to inhibit contamination. In the case of LNCaP (lymph node cancer of the prostate) androgen-sensitive and PC-3 (bone cancer of the prostate cancer) androgen independent human prostate adenocarcinoma cells, any of those supplements were added in order to avoid any possible interaction in the internalization or uptake studies with our conjugates.

One of the media used was the Roswell Park Memorial Institute medium, commonly referred to as RPMI which it was traditionally been used for growth of Human lymphoid cells. This medium contains a great deal of phosphate and is formulated for use in a 5% carbon dioxide atmosphere. Other of the media used was a nutrient mixture designed to cultivate a wide variety of mammalian and hybridoma cells, called F12. PC3 cells were grown in F12 supplemented by addition of 5.0mM L-glutamine and 10% (v/v) of fetal bovine serum (FCS). LNCaP cells were grown in RPMI with 10% (v/v) FCS.

#### 4.1.5.2.1. **Cell model characterization: Cell Growth Curve**

To generate a growth curve is very useful in order to understand the behavior of the cell line and therefore, to be able to design experiments in the adequate cell growth phase. Generally, cell growth can be modeled with four different phases: lag phase, exponential (or log phase), stationary phase (or plateau), and death phase (Figure 4.1. 14).

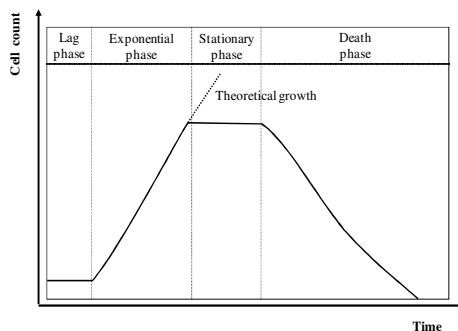


**Figure 4.1. 14** Schematic representation of the four different phases in a growth curve.

In lag phase, the cells are adapted to growth conditions and the individual cells are maturing. During the exponential phase (also called the logarithmic phase) the cell is divided (cell doubling). This type of exponential growth based on plotting the natural logarithm of cell number against time produces a straight line. The growth rate depends upon the growth conditions, which affect the frequency of cell division events and the probability of both daughter cells surviving. The stationary phase has a constant value as the rate of cell growth is equal to the rate of cell death. At death phase, cells probably die as a result of accumulation of toxic products, contaminations and contact inhibition. However, cancerous cells typically lose this property of contact inhibition and thus grow in an uncontrolled manner even when in contact with neighboring cells.

It is important to remark that MTT or MTS assays ( $n > 4$ ) were the techniques employed (see chapter 3 methodologies on cell culture) to carry out the growth studies. And all cells were used in their exponential growth phase.

#### *MTT assay and MTS assays*

The MTT assay was initially introduced by Mosmann in 1983<sup>24</sup> as a method to assess cell viability. The yellow tetrazole MTT (3-(4,5-dimethylthiazol-2-yl)-2,5-diphenyl tetrazolium bromide) or MTS (3-(4,5-dimethylthiazol-2-yl)-5-(3-carboxy methoxyphenyl)-2-(4-sulfopheyyl) 2H-tetrazolium) colorimetric assay are used for measuring the activity of enzymes<sup>24</sup>. That is to say, viable cells can reduce the yellow solution of the substrate into purple insoluble formazan crystals by a redox reaction

mediated by the mitochondrial respiration products NADH and NADPH<sup>24-29</sup> (Figure 4.1. 15).

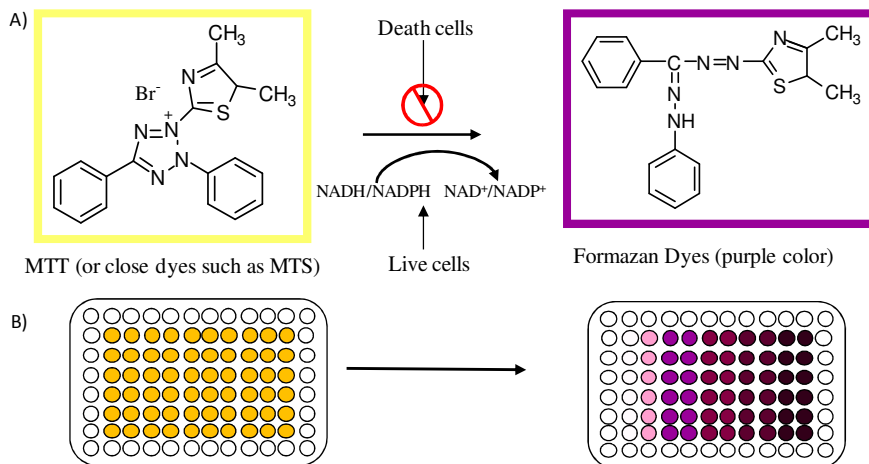


**Figure 4.1. 15** A) Mitochondrial reductase reduces MTT or MTS (in the presence of phenazine methosulfate (PMS)) to purple formazan dyes. This conversion is used to measure viable (living) cells. B) Microtitre plate before (yellow) and after (different tones of purple) an MTT assay. Increasing the amounts of cells the purple coloring is proportionally increased.

MTS needs the presence of phenazine methosulfate (PMS) to produce formazan products. The MTS assay could be described as a 'one-step' MTT assay, avoiding the intermittent steps of the MTT assay. However this convenience makes the MTS assay susceptible to colormetric interference as the intermittent steps in the MTT assay remove traces of colored compounds, whilst these remain in the microtitre plate in the one-step MTS assay. Precautions are needed to ensure the results obtained by this method which can be complemented using qualitative observations under a microscope.

The growth curves obtained for both selected cell lines, LNCaP and PC3 at different seeding densities are shown in the following figures (Figure 4.1. 16 and 4.1. 17, respectively).

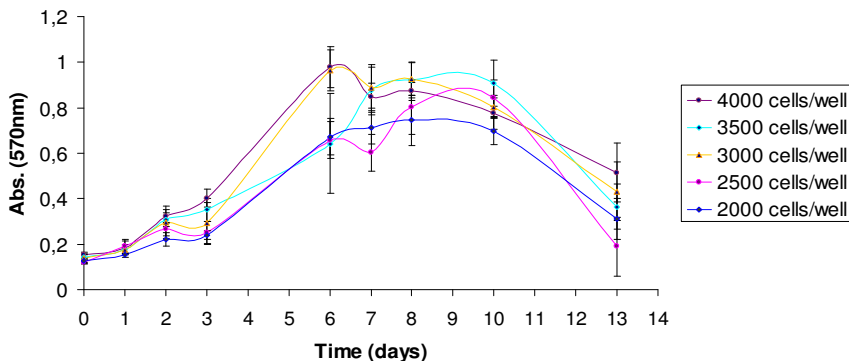


**Figure 4.1. 16** Growth curve for optimizing the LNCaP cell seeding density.

Each profile shape obtained from the different concentrations of LNCaP cells is showing clearly the four phases (lag, exponential, stationary and death phase). But the most consistent shape is that obtained with the seeding density of 4000cells/well in the case of LNCaP.

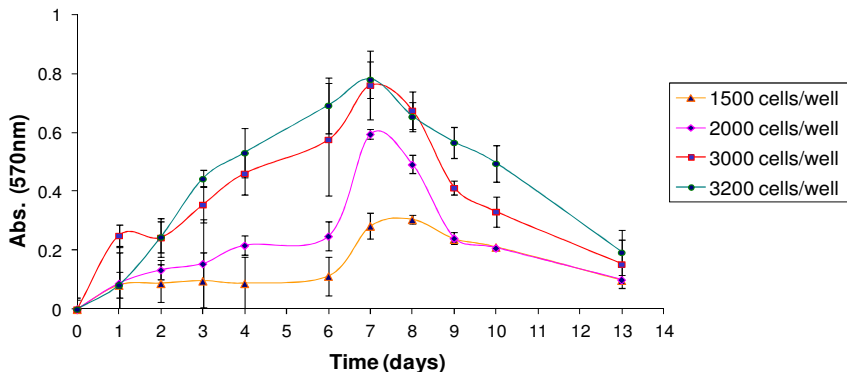


**Figure 4.1. 17** Growth curve to optimize PC3 cell seeding density.

In the case of PC3 cells, only the shape profile from the density of 3200 cells/well shows the four phases related to the optimum growth curve, and therefore this seeding density was selected for the experiments. In both selected seeding values, the exponential growth phase occurs between day 1 and 4, the best conditions for in vitro experiments.

#### 4.1.5.2.2. Cell Viability Studies

The IC50 value is defined as the polymer concentration at which cell growth is inhibited by 50 % and computer generated IC50 values were compared with the values directly read on the graphs at 50 % of cell viability. Cell viability is usually expressed as a percentage of the viable cells (equation 4.1. 1) and as mean  $\pm$  standard error of the mean.

$$\text{Cell Viability (\%)} = \frac{Abs_{550x} \times 100}{Abs_{550Control}} \quad (\text{Eq 4.1. 1})$$

Where,  $Abs_{550x}$  is the absorbance measured for the compound at a polymer concentration x and  $Abs_{550Control}$  is the absorbance measured for control cells.

The concentration-response curves generated from this data were then fit to the logarithmic function derived from the Hill Equation (Equation 4.1. 2).

$$y = R_{\min} + (R_{\max} - R_{\min}) / (1 + (x / IC_{50})^p) \quad (\text{Eq 4.1. 2})$$

Where  $R_{\max}$  was fixed at 100 and  $R_{\min}$  was fixed at 0<sup>30</sup>.

Different concentrations of drug alone (DES or its salt Na-DES) or conjugated to a polymer (*Tert*-DES and *Block*-DES with different drug equivalents), were evaluated by MTT assays after 72h in both cell lines PC3 and LNCaP cell lines. The IC50 obtained are shown in Table 4.1. 5.

The free drug DES was also evaluated as a salt, DES-Na, because the poor water solubility of the DES.

**Table 4.1. 5** IC50 of the drug and polyacetals evaluated by MTT after 72h in PC3 and LNCaP prostate cancer cell lines.

IC <sub>50</sub> (mg/mL DES eq)	PC3	LNCaP
NaDES	0.060	0.044
Tert-DES 1b	0.172	0.070
Block-DES 2b	0.052	0.049



Probably due to the androgen-dependent character, DES derivatives displayed greater cytotoxicity against LNCaP than against PC3 cell line (Figure 4.1. 18). *Block*-DES displayed greater cytotoxicity than the *tert*-polymer and the free drug in both cell lines. This could be explained by the difference in conformation adopted in solution. As seen in the degradation studies, the faster kinetics of DES release from *Block*-DES compared with *Tert*-DES could be one of the reasons for the observed cytotoxicity increase. Also, the amphiphilic character of the block-copolymer could result in a polymeric micelle formation with consequently different cell internalization mechanism.

Encouragingly, *Block*-DES IC<sub>50</sub> values were non-significantly different from those obtained with NaDES (IC<sub>50</sub> value for **2b** = 0.052 and 0.049 mg/mL, DES-equiv. IC<sub>50</sub> value for NaDES = 0.060 and 0.044 mg/mL, DES-equiv. against PC3 and LNCaP, respectively), even following a different cell pharmacokinetics (endocytosis for *Block*-DES vs. diffusion for free DES) (Figure 4.1. 18).

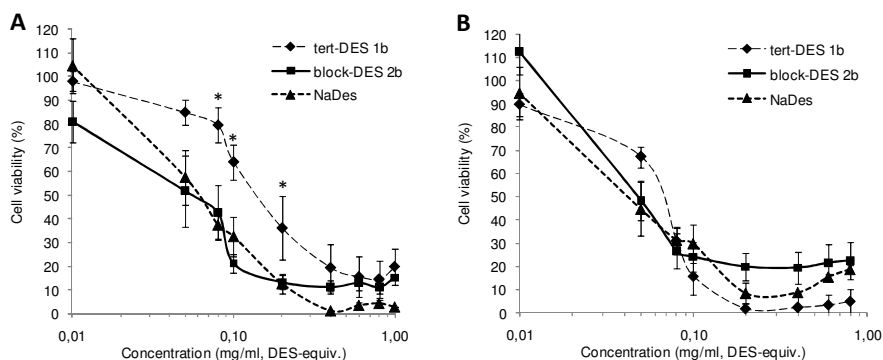


**Figure 4.1. 18** Cytotoxicity of DES derivatives measured by MTT assay after 72 h incubation. *Tert*-DES vs *block*-DES in (A) PC3 cells and (B) LNCaP cells. Data are expressed as mean  $\pm$  SD ( $n \geq 3$ ). \*  $p < 0.05$ .

This could be due to the enhancement of DES water solubility prior to its intracellular release following endocytic uptake. More importantly, *block*-DES **2** showed greater cytotoxicity than *tert*-DES **1** in both cell lines (IC<sub>50</sub> value for **2b** = 0.052 and 0.049 mg/mL, IC<sub>50</sub> value for **1b** = 0.172 and 0.070 mg/mL, DES-equiv. against PC3 and LNCaP,

respectively). The combination of the two key features already described, a slightly faster and biphasic drug release profile at acidic pH from *block*-DES (Figure 4.1. 4B).

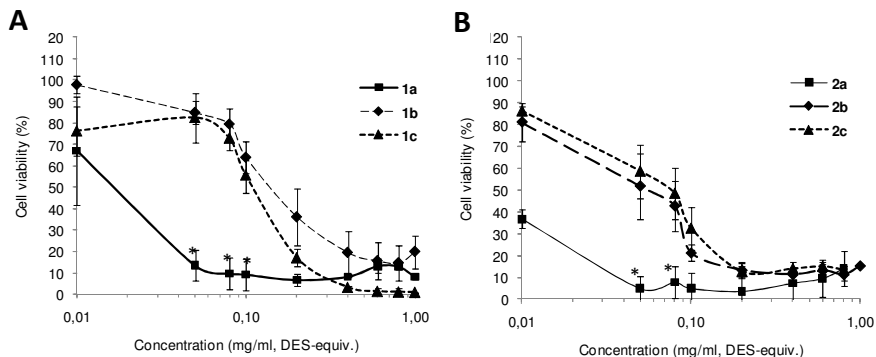


**Figure 4.1. 19** Cytotoxicity of DES derivatives measured by MTT assay after 72 h incubation. DES content influence on cytotoxicity against PC3 cells (A) *tert*-DES 1a-c vs (B) *block*-DES 2a-c. Data are expressed as mean  $\pm$  SD ( $n \geq 3$ ). \*  $p < 0.05$ .

The inherent cytotoxicity of the DES-polyacetals not only depend on monomer arrangement, but also on total DES content, being significantly different when loadings below 3 wt% are compared with those above. This effect seems to be more important in the androgen-independent PC3 cells (Figure 4.1. 19) than in the hormone-dependent LNCaP cells, indicating the complexity of DES molecular mechanisms of action.

#### 4.1.5.2.3. Haemocompatibility studies

The primary purpose of giving intravenous (i.v.) medications<sup>31</sup> is to initiate a rapid systemic response to medication. The i.v. route for medication administration is one of the fastest ways to deliver the drug which once is injected is immediately available to the body. Other advantage of using i.v. is the control of amount of drug deliver in the body and it is able to maintain drug levels in the blood for therapeutic response. The i.v. administration should be used if the drug to be delivered would be destroyed by digestive enzymes, is poorly absorbed

by the tissue, or is painful or irritating when given by intra-muscular (im) or subcutaneous (sc) injection. The drugs which are i.v. administered should not be compatible with i.v. fluids or other drugs but the mean of being incompatible is a risk to cause drug crystallization which can clog the i.v. line or to cause an embolus effect on the patient<sup>31</sup>.

The drug delivery rate is an important factor when medication is i.v. administered. Some drugs are delivered rapidly over several minutes to obtain therapeutic effect. However drugs are most effective when delivered slowly and intermittently throughout the day. Each drug acts different and it is needed to find its best conditions to be administrated (amount per day) to achieve the therapeutic effect desired.

It is important to note that, as already described for *tert*-DES<sup>6</sup>, *block*-DES-polyacetals also displayed much lower hemolytic activity than their free counterpart (3%, 4% and 90% Hb released in 1 h; 5%, 4% and 100% Hb released in 24 h for **1**, **2** and NaDES, respectively, at 2 mg/ml DES-equiv.) (Figure 4.1. 20). This proves the suitability of these nanoconjugates for *i.v.* injection in subsequent *in vivo* studies.

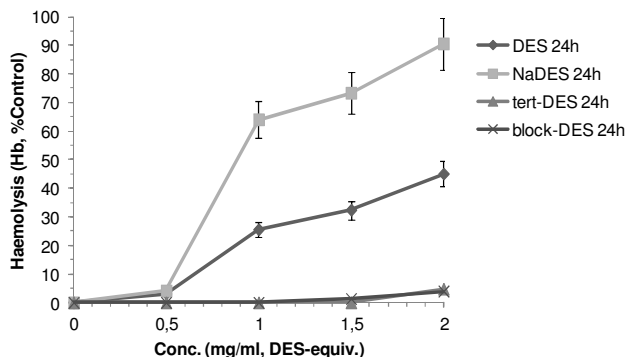


**Figure 4.1. 20** Haemolytic activity of DES, NaDES and DES-polyacetals at 24h. Data expressed as mean  $\pm$  SEM (n=3).

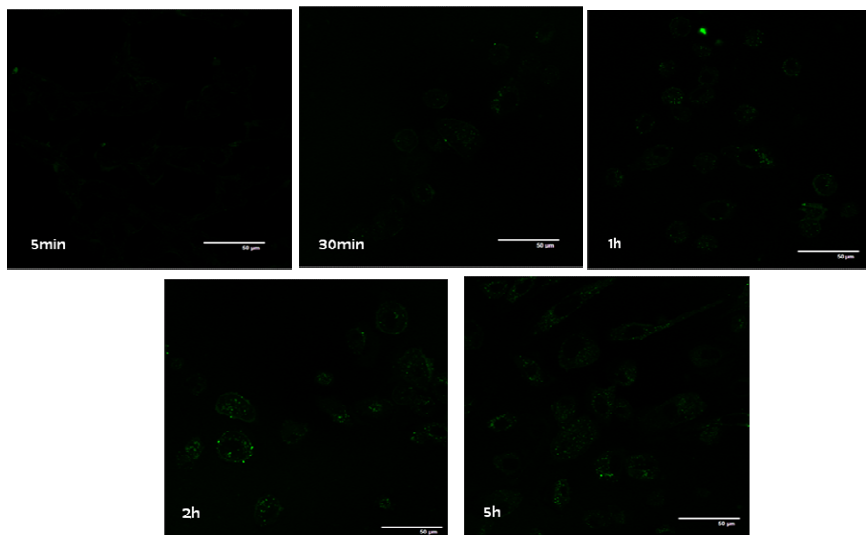
#### 4.1.5.2.4. Confocal fluorescence microscopy: live-cell imaging

As complementary studies to the previous described above, confocal fluorescence microscopy experiments were carried out to permit better observation of the cell trafficking for the conjugates. Live cell imaging

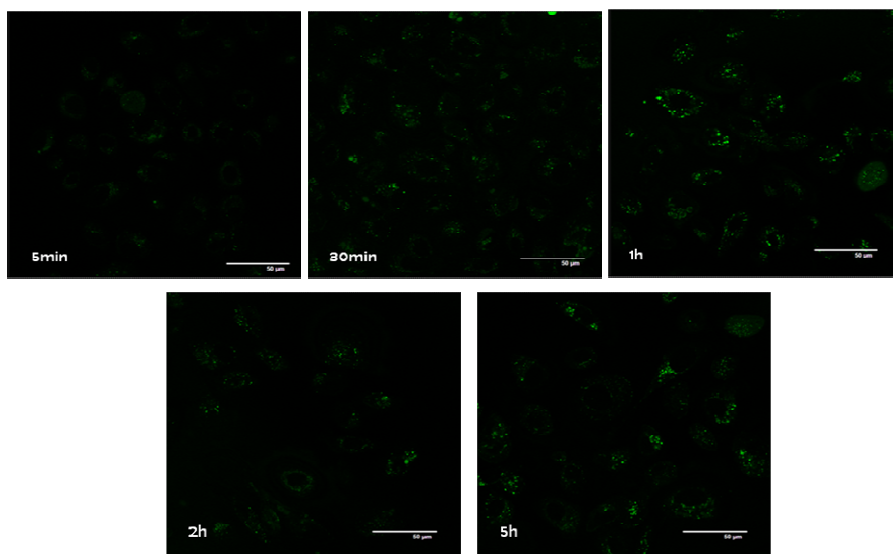
was used to avoid any fluorescence artifact induced by fixation protocols<sup>32-35</sup>.

### **A. LNCaP cell line**

#### 1. *Tert*-DES-Ser-OG **8a**

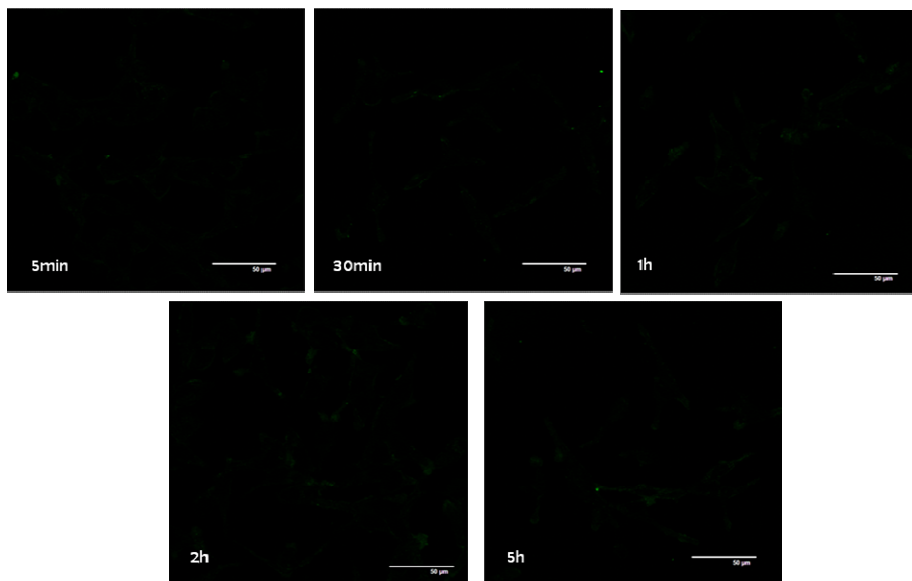


#### 2. *Block*-DES-Ser-OG **9a**



## **B. PC3 cell line**

### 1. *Tert*-DES-Ser-OG **8a**



### 2. *Block*-DES-Ser-OG **9a**

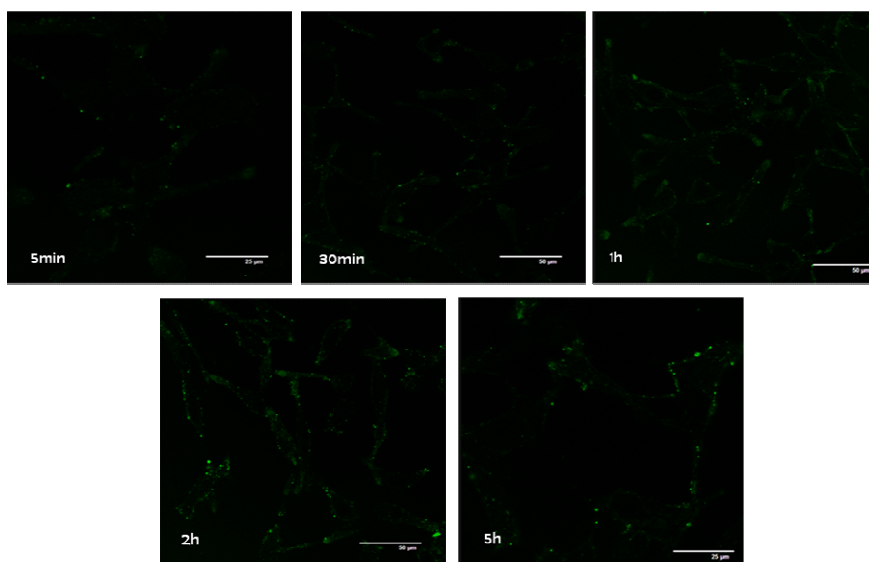
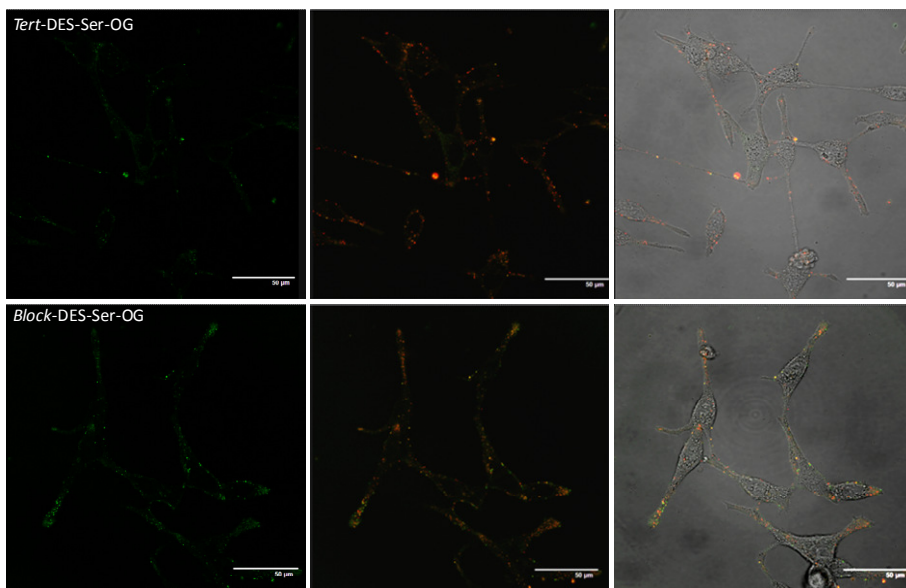


**Figure 4.1. 21** Kinetics of cell trafficking with polyacetals **8a** and **9a** in prostate cancer cell lines (A) LNCaP and (B) PC3.

A.



B.

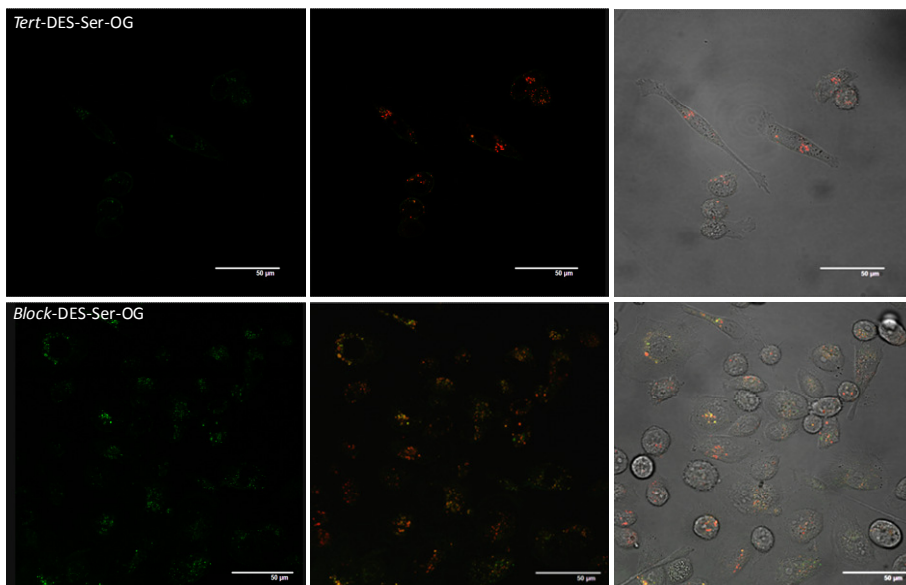


**Figure 4.1. 22** Confocal microscopy images were taken from live: (A) PC3 cells, (B) LNCaP cells after 2 h incubation with tert-DES-Ser-OG 8a and block-DES-Ser-OG 9a. Dextran-Texas Red was employed as lysosomal

marker (in red) and polymers were labeled with OG (in green, left panel). Co-localization is seen in yellow (central panel).

Cell trafficking studies were done for the polyacetals with 4wt% DES, *Tert*-DES-Ser-OG (**8a**) and *Block*-DES-Ser-OG (**9a**), in LNCaP and PC3 cell lines. (Figure 4.1. 21 and Figure 4.1. 22)).

Low membrane-associated fluorescence was observed in all cases studied at the different incubation times. Both conjugates enter the cell by the endocytic route as demonstrated by the observed co-localization with the lysosomal marker dextran-texas red (Figure 4.4. 22). In general, LNCaP cells seems to have slightly higher uptake rate compared with PC3 cells; and even more interestingly, the percentage of block-DES inside the cells is greater than that observed for tert-DES in both cell lines (Figure 4.4. 22).

## 4.2. INVESTIGATING CONFORMATION IN SOLUTION OF DES-POLYACETALS

### 4.2.1. Introduction

In order to better explain the results obtained in the cell models used it was hypothesized that the conformation adopted by the polyacetals in solution could be responsible for the differences observed in drug-release kinetics, cell uptake and therefore cell viability. The size and shape of nanoconjugates in solution are critical aspects for cellular internalization and on drug release kinetics from the polymer carrier<sup>36,37</sup>. Amphiphilic block copolymers in aqueous solution are known to form aggregates or self-assemble into nanosized particles (e.g., micelles or polymersomes). This is an important feature to take into account for biomedical applications as subtle differences in size and/or shape could significantly alter conjugate therapeutic value. Therefore, aside from obtaining polyacetal information solely from NMR and GPC, further exhaustive characterization of polyacetal solution conformation in physiological environment was considered crucial to understand the therapeutic potential of these novel nanopharmaceuticals.

To allow better comparison, only polyacetals containing ~4 wt% DES loading (namely, *tert*-DES **1b** and *block*-DES **2b**) were selected to carry out the experiments described in this section.

Due to presence of hydrophobic moieties within the structures, systems, characterization of any concentration dependent aggregation behavior was first carried out.

### 4.2.2. Determination of Critical micelle concentration (cmc) of the conjugates.

Different methods have been employed in order to determine the critical aggregation concentrations (CAC), (akin to the critical micelle concentration (CMC) of conventional small-molecule surfactants), of these nanoconstructs, such as dye solubilization and surface tension studies. These methods are tedious and time-consuming and require large volume of surfactant solution. CMC is defined as the concentration of polymer above which micelles are spontaneously formed.



**Surface tension.** Different concentrations of the polymers in distilled water (from  $10^{-4}$  to 10mg/mL) were necessary to determine the polyacetal CMC using a tensiometer taking into account the bubble pressure (Figure 4.2. 1). In this method a capillary tube is immersed in the liquid sample. A constant flow of gas is passing through the tube forming small bubbles into the liquid. The pressure needed to form a bubble is measured and the surface tension of the sample is calculated from the pressure difference between inside and outside the bubble and the radius of the bubble.

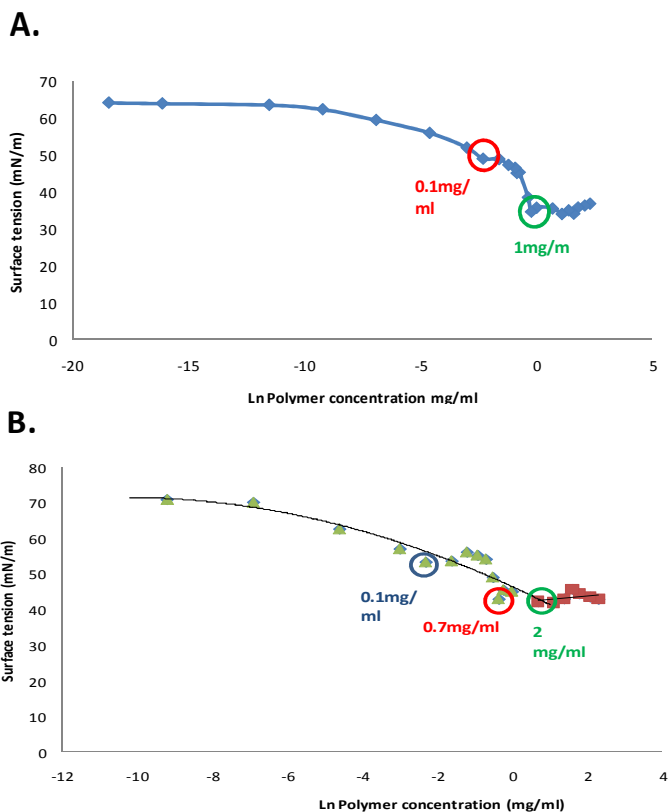


**Figure 4.2. 1** CMC determination for (A) *Tert*-DES and (B) *Block*-DES.

In *Tert*-DES two different critical micelle concentrations were determined at 0.1 and 1mg/ml and cmc for *Block*-DES were found as 0.1, 0.7 and 2 mg/ml.

Other manner to identify the cmc of a compound is by dye solubilization procedures.

**Dye solubilization procedures.** The measurements were done in a spectrofluorometer using two different fluorochromes, diphenylhexatriene (DPH) and pyrene. Upon the introduction of diphenylhexatriene (DPH) or pyrene (surface active materials) into the systems they will initially partition into the interface, reducing the system free energy by i) lowering the energy of the interface (calculated as area x surface tension) and ii) by removing the hydrophobic parts of the surfactant from contact with water. Subsequently, when the surface coverage by the polymer increases and the surface free energy (surface tension) has decreased, the polymer chains start aggregating into micelles, thus again decreasing the system free energy by decreasing the contact area of hydrophobic parts of the surfactant with water. Upon reaching CMC, any further addition of polymers will just increase the number of micelles (in an ideal case).

There are several theoretical definitions of CMC. One well-known definition is that the CMC is the total concentration of surfactants (equation 4.2.1). If  $C = \text{CMC}$ ,

$$(d3F/dCt^3) = 0 \quad (\text{eq. 4.2.1})$$

where  $C_t$  is the total concentration and  $F$  is the function of surfactant solution;  $F = a[\text{micelle}] + b[\text{monomer}]$  ( $a$  and  $b$  are proportional constants).

Therefore, the CMC depends on the method of measuring the samples, since  $a$  and  $b$  depend on the properties of the solution such as conductance and photochemical characteristics.

When the degree of aggregation is monodisperse, the CMC is not related to the method of measurement. On the other hand, when the degree of aggregation is multidisperse, the CMC is related to both the method of measurement and the dispersion.

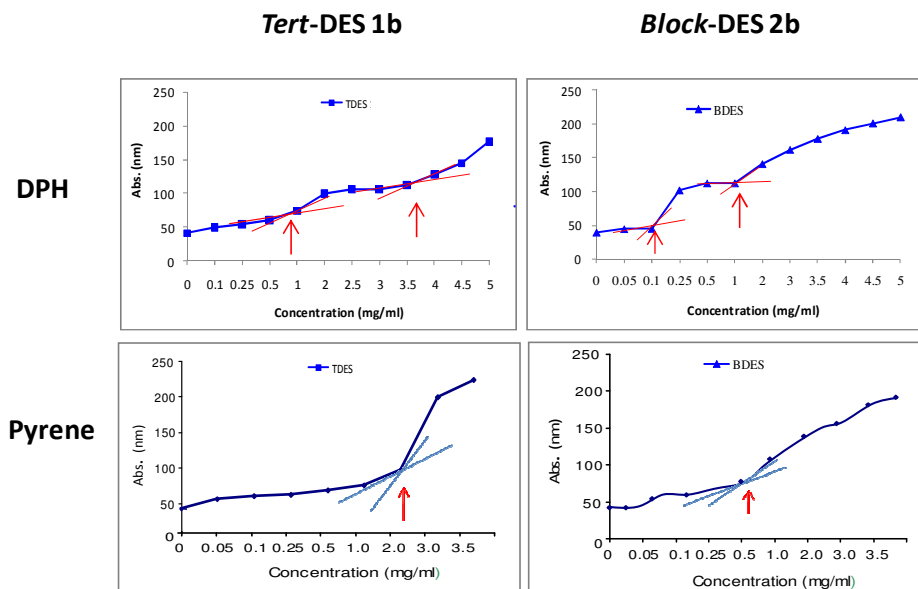
The CMC is an important characteristic of an amphiphilic polymer. Before reaching the CMC, the surface tension changes strongly with the concentration of the polymer. After reaching the CMC, the surface tension stays more constant.

*Tert*-DES and *Block*-DES dissolved in Pyrene and DPH solutions were analyzed by fluorimetry (Table 4.2. 1) in order to obtain their CMC.

**Table 4.2. 1** Parameters used in the fluorimeter to measure the cmc of the polyacetals.

Spectrofluorimeter	Jasco FP-6500
Emission	400-500nm DPH & 380-410 Pyrene
Excitation	340nm DPH & 394nm Pyrene
Band width (Ex)	3nm
Band width (Em)	3nm
Scanning speed	100nm/nm
Data pitch	0.5nm
Sensitivity	Manual
PMT Voltage	300v DPH & 200v Pyrene

In Figure 4.2. 2 is shown the cmc for *Tert*-DES and for *Block*-DES in both solutions. As it can be seen, in both cases multiple CACs were found, with that obtained for *block*-DES CAC much lower than for *tert*-DES in all cases (i.e. first *tert*-DES **1b** CAC= 0.7 mg/mL; first *block*-DES **2b** CAC= 0.1, mg/mL).

**Figure 4.2. 2** CMC determination for *Tert*-DES **1b** and *Block*-DES **2b** in DPH and Pyrene solution.

All subsequent studies were carried out at solution concentrations above the previously determined CAC value, and under conditions designed to mimic physiological environment (salt buffer, pH and temperature).

#### 4.2.3. Transmission and Scanning Electron Microscopy, TEM and SEM.

Electron microscopy (EM) allows the visualization of objects that are as small as 1 nm. Here the specimen is not illuminated with light but bombarded by electrons to produce an image. Globally, a distinction is made between transmission electron microscopy (TEM) to study the inner structure of objects (tissues, cells, viruses) and (scanning electron microscopy SEM) to visualize the surface of tissues, macromolecular aggregates and materials.

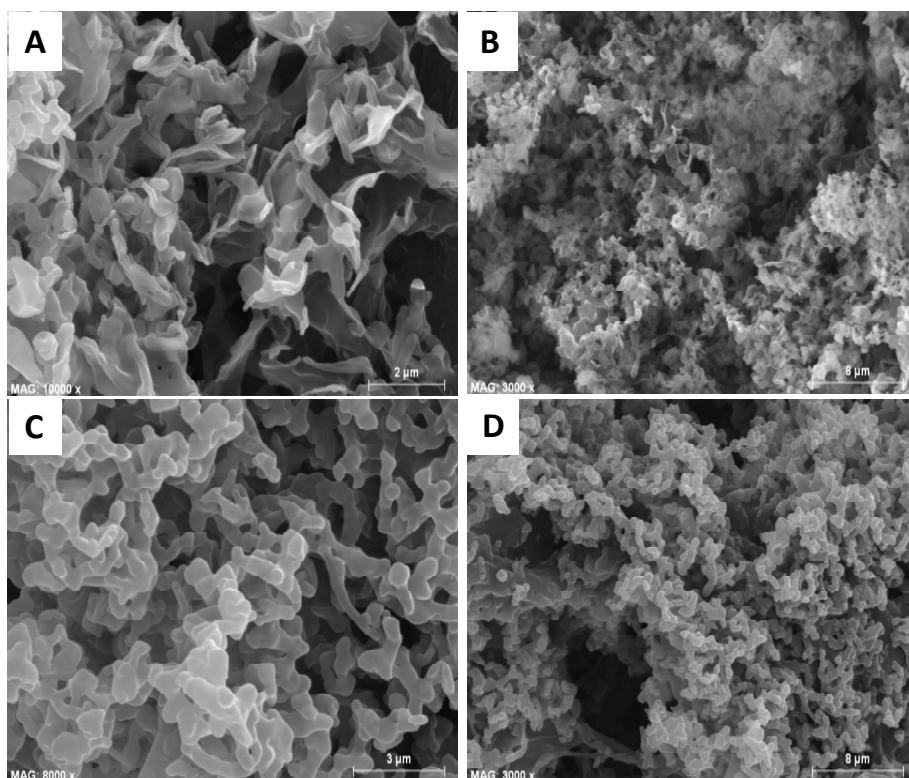


**Figure 4.2. 3** Scanning electron microscopy images for *Tert*-DES **1b** (A and B) and for *Block*-DES **2b** (C and D) at concentration above CAC.

In **SEM**, 1 $\mu$ l of a dilute sample is applied on a gold-coated metal disk obtained either by low vacuum sputter coating or by high vacuum evaporation. The image is produced where primary electrons from the source bombard the sample according to a scanning pattern and cause emission of secondary electrons. Therefore, in SEM an image of the surface of the object is made (examples shown in Figure 4.2.3).

Using SEM, there was a clear difference in the materials, *Block*-DES appeared to have a more particulated surface (Figure 4.2. 3C-D) when compared with *Tert*-DES (Figure 4.2. 3A-B). This could indicate a more homogeneous structural composition for *Block*-DES that could be beneficial for cellular internalization kinetics .

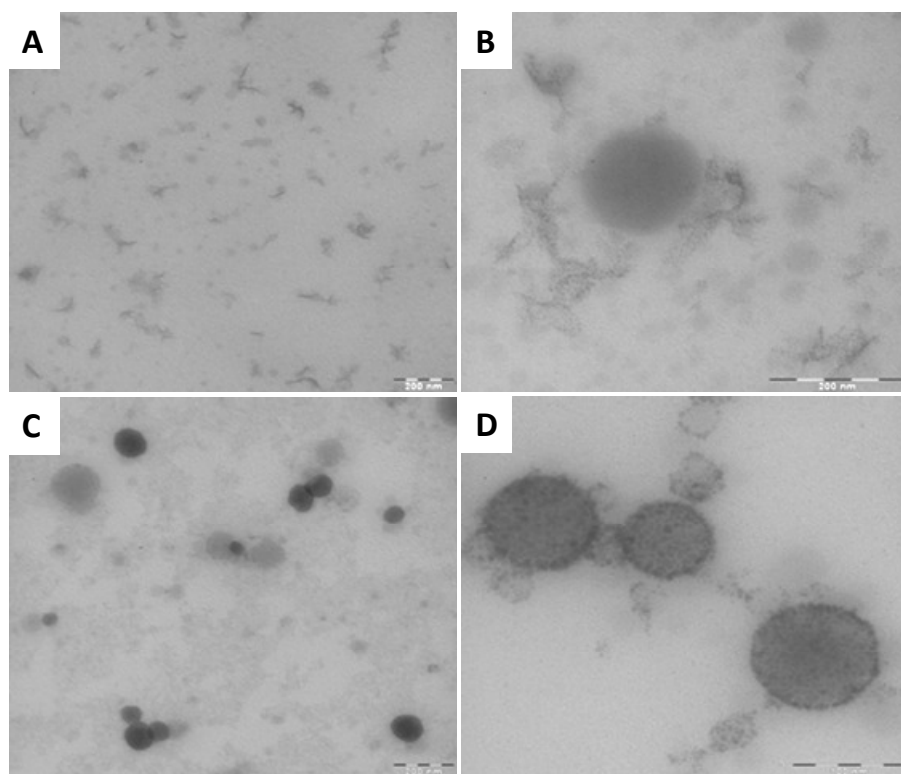


**Figure 4.2. 4** Transmission electron microscopy for *Tert*-DES 1b (A and B) and for *Block*-DES 2b (C and D).

**TEM** was used in order to achieve more detailed information on polyacetal conformation and size. For TEM, the sample can be quickly prepared by the deposition of 1 $\mu$ l of a dilute sample containing the polymer onto support films. TEM is usually applied on materials of <1  $\mu$ m of size to visualize also aggregates of macromolecules (Figure 4.2. 4).

By **TEM** it was possible to observe well-defined particles of approximately 120 nm diameter and in high abundance for the *Block*-DES polyacetal (Figure 4.2. 4 D). This was more noticeable when a solution of 1 mg/ml of *Block*-DES was studied (Figure 4.2. 4 C). However, the same nanoparticles were difficult to find with the *Tert*-DES system even at the same concentration. In fact the *Tert*-DES system seemed to present a different conformation (Figure 4.2. 4 B).

#### 4.2.4. Dynamic Light Scattering, DLS technique.

This technique is also known as Photon Correlation Spectroscopy or Quasi-Elastic Light Scattering. This technique determines the size distribution profile of small particles in solution. Particles, emulsions and molecules in suspension undergo Brownian motion, induced by the bombardment of solvent molecules that themselves are moving due to their thermal energy. If particles or molecules are illuminated with a laser, the intensity of the scattered light fluctuates at a rate that is dependent upon the size of the particles (Figure 4.2.5).

Smaller particles are “kicked” further by the solvent molecules and therefore move more rapidly than larger particles. Analysis of these intensity fluctuations yields the velocity of the Brownian motion and hence the particle size by using the Stokes-Einstein relationship (see equation 4.2. 2). This equation is used for calculating diffusion of spherical particles through liquid with low Reynolds number.

$$D = \frac{k_B T}{6\pi \eta r} \quad (\text{eq. 4.2. 2})$$

Where  $D$  is the diffusion constant,  $k_B$  is Boltzmann’ constant,  $T$  is the absolute temperature,  $\eta$  is viscosity and  $r$  is the radius of the spherical particle.  $D$  is often used to calculate the hydrodynamic radius of a sphere using this equation. It is important to note that the size determined by dynamic

light scattering is the size of a sphere that moves in the same manner as the scatterer. So, if the scatterer is a random coil polymer, the radius of gyration is not the same if static light scattering is used. Size determination includes other molecules or solvent molecules that move with the particle.

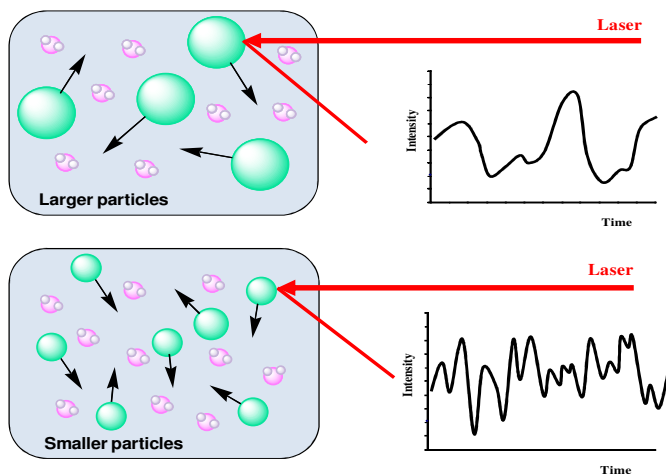


**Figure 4.2. 5** Hypothetical Dynamic light scattering of large particles (on the top) and small particles (on the bottom).

Dynamic Light Scattering analysis corroborates a narrow size distribution of approx. 120 nm for *Block*-DES ( $128\pm 20$  nm in MilliQ water and  $139\pm 31$  nm in PBS). However, a lack of reproducibility on *Tert*-DES distribution reflects the poor stability of this polyacetal in solution. Therefore, both polymers clearly have a different conformational structure in solution that could influence their therapeutic output when evaluated in biological conditions (Figure 4.2.6).

The results obtained by DLS for the *Block*-DES are in good agreement with the data obtained from TEM images.

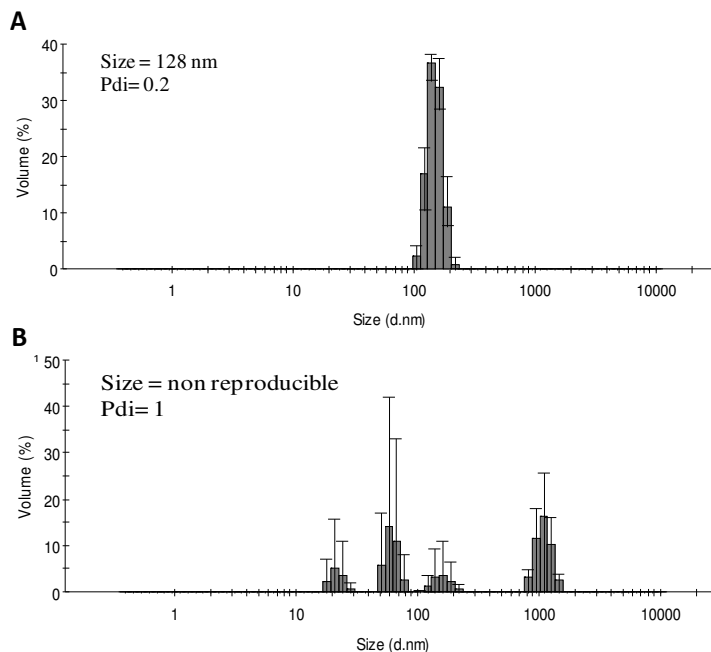


**Figure 4.2. 6** DLS profiles for (A) *Block*-DES and (B) *Tert*-DES in PBS.

#### 4.2.5. Pulsed-Gradient Spin-Echo NMR (PGSE-NMR) experiments to determine solution behavior of DES-polyacetals 1b and 2b.

##### 4.2.5.1. Introduction

The thermal motion, or diffusion, of a molecule is its most basic form of transport and is characterized by the self-diffusion coefficient,  $D_s$ . The Diffusion coefficient can be related to molecular size by using the Stokes-Einstein equation, as was mentioned in section 4.4.4,  $D_s = K_B T / f$  where  $f$  is the friction factor, which for a particle of hydrodynamic radius  $R_h$  in a solvent of viscosity  $\eta$  is given by  $f = 6\pi\eta R_h$ . This relationship introduces the possibility of indirectly calculating particle size via direct measurements of  $D_s$  which can be done through the technique of pulsed gradient spin echo NMR.



### ***Pulsed Spin Echo- NMR***

In 1950, Pulsed spin echo NMR was first described by E Hahn who, after refocusing the decaying magnetic spins of a sample using a  $180^\circ$  *rf* pulse, observed a secondary NMR signal which he called a spin echo. A sample is placed in a magnetic field which produces a net magnetization in the *z* direction,  $M_z$ . This net magnetization is then rotated from the *z* plane into the *xy*-plane by a  $90^\circ$  ( $\pi/2$ ) *rf* pulse. When this pulse has finished the net *xy*-magnetization created will undergo exponential free induction decay as the spins de-phase via  $T_2^*$  relaxation (a combination of true  $T_2$  spin-spin relaxation but also relaxation from any non-uniformity in the magnetic field) (Figure 4.2. 7). A second *rf* pulse of  $180^\circ$  ( $\pi$ ) after time  $\tau$  completely reverses the phases of the decaying spins and any non-uniformities in the magnetic field act to rephrase the spins and net magnetization is then regained, producing a signal called spin echo. With this the problem of non-homogeneous magnetic fields is eliminated. The spin echo has a slightly smaller maximum signal than the original free induction decay (FID) as  $T_2$  relaxation has occurred.  $T_2$  can be calculated after measuring the attenuation of the spin echo.

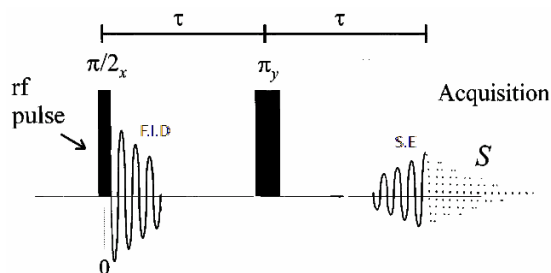


**Figure 4.2. 7** Diagram showing the process occurred in a standard pulsed spin echo-NMR experiment where the free induction decay (F.I.D) signal is refocused using a  $\pi$  *rf* pulse, producing a spin echo, S.E. (Figure taken from<sup>38</sup>).

### ***Pulsed Gradient Spin Echo- NMR***

In PGSE-NMR, the diffusion coefficient is measured instead of measuring  $T_2$ . For this two gradient pulses, with a duration of  $\delta$  and a magnitude of  $g$ , are introduced (Figure 4.2. 8). The gradient pulse tries to label the spins

with phase angles dependent on their position in space<sup>39,40</sup>. The first of these gradients occurs shortly after the first  $90^\circ$  rf pulse cause the spins to experience the phase shift, which is reversed upon the application of the second gradient at  $t_1 + \Delta$ . If no diffusion occurs, the reversing of the phase shift by the second gradient will restore the signal. However if diffusion has occurred the amplitude of the returned signal will be decreasing causing further attenuation of the spin echo which can be measured. The sequence has some disadvantages; the long period of time of magnetization is in the transverse, xy-plane where if  $T_2$  is large there can be a severe loss of signal<sup>40</sup>. This problem is overcome by using a stimulated echo sequence (STE). STE PGSE-NMR experiments have replaced the  $180^\circ$  pulse with two of  $90^\circ$  (Figure 4.2. 9).

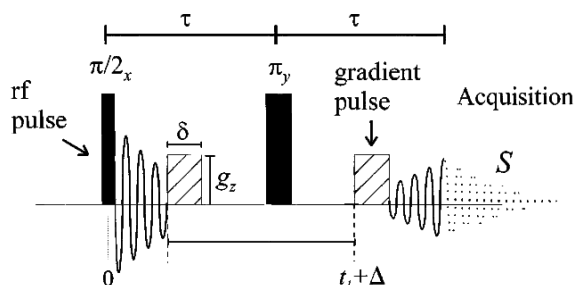


**Figure 4.2. 8** Diagram showing the pulse sequence for a PGSE-NMR experiment. Taken from Price, W.S.<sup>38</sup>.

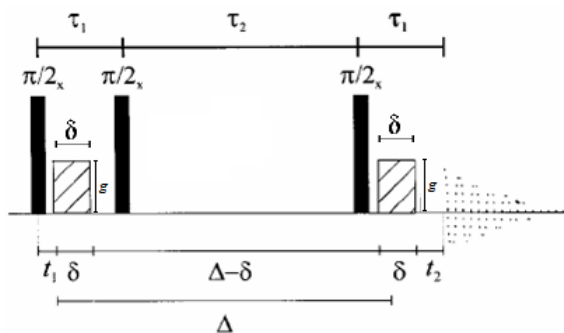


**Figure 4.2. 9** Diagram showing the pulse sequence for a stimulated echo PGSE-NMR experiment. Modified from Price, W.S.<sup>387</sup>.

The first pulse moves the magnetization into the  $xy$ -plane where it experiences the first gradient as it was before. This magnetization is then stored by the second  $90^0$  pulse which moves the  $y$ -components into the  $z$  direction. After time,  $\tau_2$ , the third pulse will bring the magnetization back into the  $yz$ -plane where it produces the STE signal. The advantage of this sequence is that while stored in the  $z$  direction the magnetization only experiences  $T_1$  relaxation. This means that, as  $T_1$  is generally longer than  $T_2$ , the time between the two gradient pulses,  $\Delta$ , can be longer, allowing any eddy currents (currents produced when a conductor go through a magnetic field) that may have been produced by the heat of the gradient coils to dissipate.

Pulsed magnetic gradients of length  $\delta$  and magnitude  $g$  first encode and then decode the positions of spin active nuclei within the sample. In the presence of diffusion, the decoding process will not perfectly mirror the encoding process and an attenuation of the spin echo occurs. Thirty-two 1D spectra are run where  $\delta$  is progressively increased and the self-diffusion coefficient,  $D_s$  obtained from fitting the attenuation of the signal over the 32 spectra (see Figure 4.2.10  $D_s$ ) allows the size of the particles to be calculated as well as their chemical environment (i.e. aggregated or not).

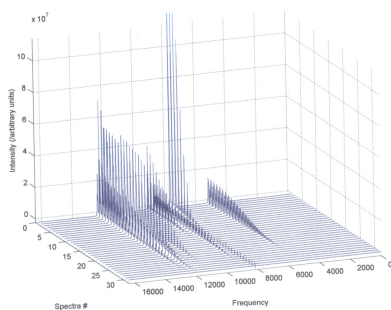


**Figure 4.2. 10** Diagram showing the thirty-two 1D spectra on a 2D plot showing the signal attenuation.(Modified from Price, W.S.<sup>38</sup>.)

### *Extracting the self-diffusion coefficient*

The self-diffusion coefficient is calculated by fitting the attenuated integrals obtained from the spectrometer to equation 4.2.3:

$$A(\delta, g, \Delta) = KD_s$$

where ;

$$K = A(0) \exp \left[ -\gamma^2 G^2 \left( \frac{30\Delta(\delta + \sigma)^2 - (10\delta^3 + 30\sigma\delta^2 + 35\delta^2\sigma + 14\sigma^3)}{30} \right) \right] \quad (\text{eq. 4.2.3})$$

Where  $A_0$  is the signal amplitude in the absence of the field gradient,  $A(\delta, G, \Delta)$  the signal amplitude in the presence of the field gradient,  $\gamma$  is the magnetogyric ratio,  $\Delta$  the diffusion time,  $\sigma$  the gradient ramp time,  $\delta$  the gradient pulse length and  $G$  the gradient field strength.

Equation 4.2.4 shows that the gradient field strength,  $G$ , is dependent on the power that the gradient is set to,  $I$ , multiplied by the maximum percentage of  $I$  that the gradient can actually reach,  $DAC_{\max}$ , multiplied by a constant giving the rate of change of  $G$  with  $I$  called the coil constant,

$$\frac{dG}{dI} \cdot G = \frac{dG}{dI} \cdot I \cdot DAC_{\max} \quad (\text{eq. 4.2. 4})$$

### Results of PGSE-NMR obtained for DES-Polyacetals

An indication of the relative particle sizes was obtained by PGSE-NMR measurements, which have the benefit of being non-perturbative, ensuring any structures formed by the *Tert*-DES conjugate are not disrupted by the measurement. Figure 4.2. 12 shows PGSE-NMR data for 10 mg/mL solutions of *Tert*-DES and *Block*-DES, plotted according to equation 4.2.3 (see materials and methods section), using the normalized signal intensity. Presented in this manner, the difference in slopes indicates a clear difference in the obtained self-diffusion rates between the two conjugates, with the *Tert*-DES conjugate ( $D_s = 2.72 \times 10^{-11} \text{ m}^2 \text{ s}^{-1}$ ) moving more slowly than the *Block*-DES counterpart ( $D_s = 5.87 \times 10^{-11} \text{ m}^2 \text{ s}^{-1}$ ) indicating clearly that different solution structures are formed in each case.

In order to further elucidate the structure of the aggregates or nanoparticles that are formed, *tert*- **1b** and *block*-copolymer **2b** conjugates containing a fixed DES content of 4 wt% were also studied by Small-Angle Neutron Scattering (SANS).

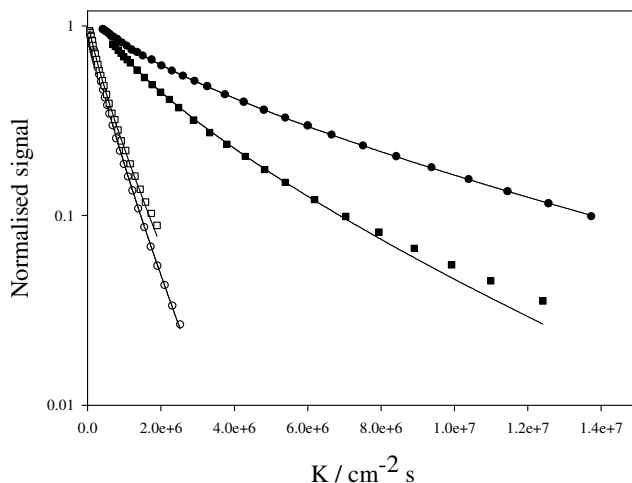


**Figure 4.2. 11** Normalized PGSE-NMR data from 1wt% conjugate solutions at 25°C; *Tert*-DES in D2O (filled circles) and methanol (open circles); *Block*-DES in D2O (filled squares) and methanol (open squares).

#### 4.2.6. Determination of solution behavior of DES-polyacetals by SANS.

Small angle neutron scattering is a neutron technique able to analyze structures at length scales from 1 nm to more than 100 nm. It has a wide range of applications from studies of polymers and biomolecules to nanoparticles to microemulsions and liposomes used for cosmetics and drug delivery.

##### Introduction to neutron radiation

Small angle scattering (SAS) is the name given to techniques using small angle neutron (SANS), X-ray (SAXS) and light (SALS, or LS) scattering. In these techniques radiation is scattered by a sample and the resulting scattering pattern is analyzed to provide information about the size, shape and orientation of some component of the sample.

##### *Neutron Sources*<sup>41</sup>

There are two different sources for the production of neutrons in sufficient quantities for worthwhile experiments. The most obvious is to use a nuclear reactor where neutrons are released by the fission of uranium-235. Each

fission releases 2 - 3 neutrons, although one of these is needed to sustain the chain reaction. Nowadays, the most powerful reactor (also called "steady-state" or "continuous") neutron sources in the world is the 57 MW HFR (High-Flux Reactor) at the Institute Max von Laue - Paul Langevin (ILL) in Grenoble, France<sup>42</sup>. The ILL is jointly operated by Austria, France, Germany, Spain, Switzerland and the United Kingdom. The facility commenced operation in 1972.

The second approach to neutron production is when an accelerator or synchrotron source uses high energy proton beams to chip away neutrons from high molecular weight elements. This is called spallation. The most powerful spallation neutron source in the world is the ISIS Facility<sup>41,43,44</sup> in Oxfordshire (UK). It is based around a 200 m A, 800 MeV and the proton synchrotron operate at 50 Hz. ISIS is operated by the United Kingdom but also receives funding from Australia, France, Germany, India, Italy, Japan, the Netherlands and Sweden. The facility commenced operation in late 1984.

Today there are some 37 neutron sources in 21 countries<sup>45</sup>; of these, 23 are in continental Europe, including Russia and Scandinavia, 10 are in North America (including Canada), 2 are in Japan with 1 in each of Australia and India. Five of the sources are spallation sources, the remainder are generally aging reactors, although some, such as the ILL, have undergone recent refurbishment to extend their useful lifetimes. The total number of SANS instruments at these sources is 32; of which 18 are to be found at the European facilities<sup>42</sup>. Despite this apparent glut of facilities and instruments, the demand for SANS beam time typically outstrips the time actually available by a factor of 2 or 3.

***Small angle neutron Scattering. Theoretical basis used in this work.***

In small angle neutron scattering, the scattering intensity of a particle,  $I(Q)$  is dependent upon the number of scattering bodies within the sample solution,  $N_p$ , the volume of those scattering bodies,  $V_p$ , is the difference in scattering length density between the scattering body and the solvent it is in ( $\Delta\rho$ ). The form factor describes the particle size and shape,  $P(Q)$ , the structure factor describes interactions between different scattering bodies,  $S(Q)$  and the background incoherent scattering,  $B_{inc}$  (equation 4.2.5).

$$I(Q) = N_p V_p^2 (\Delta\rho)^2 P(Q, R) S(Q) + B_{inc} \quad (\text{eq. 4.2.5})$$

The radius of gyration of all the polyacetals was calculated using the Guinier approximation where for dilute systems, at low  $Q$  values the scattering intensity is dependant only upon the overall particle size (equation 4.2.6).

$$\frac{I(Q) - B_{inc}}{n_p V} = V_p (\Delta\rho)^2 e\left(-\frac{Q^2 R_g^2}{3}\right) \quad (\text{eq. 4.2.6})$$

Scattering data was also analyzed using the modeling program FISH<sup>8</sup> which contains numerous models for  $P(Q)$ ,  $S(Q)$  and contrast steps which can be combined to create suitable models to fit scattering data. FISH uses a least-squares iterative fitting process in which the parameters of a fitting model may be turned on or off, *i.e.* the program is either allowed to change the value of a parameter to achieve a better fit, or not. This means that known values such as scattering length densities can be entered and turned off, and unknown values such as ellipticity or length parameters can be turned on.

### The Scattering Vector

In neutron scattering experiments, instruments count the number of scattered neutrons as a function of wave vector  $Q$ , which depends on the scattering angle  $\theta$  and wavelength  $\lambda$ . The quantity referred to the scattering vector ( $Q$ ) is the modulus of the substract between the incident,  $k_i$ , and the scattered,  $k_s$ , wavevectors, (Figure 4.2. 12), and is given by equation 4.2.7.  $Q$  has dimensions of  $(\text{length})^{-1}$  ( $\text{nm}^{-1}$  or  $\text{\AA}^{-1}$ ).

$$Q = |Q| = |K_s - K_i| = \frac{4\pi}{\lambda} \sin \frac{\theta}{2} \quad (\text{eq. 4.2.7})$$

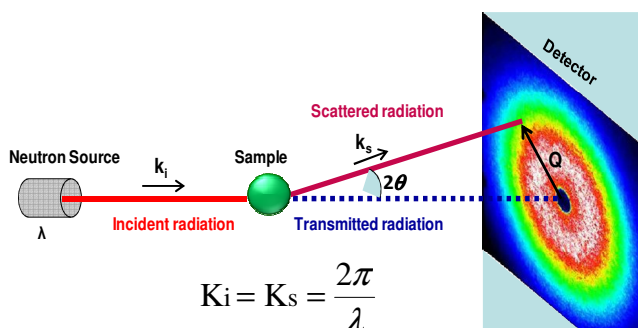


**Figure 4.2. 12** Schematic representation of a SANS experiment. The distance between the sample to the detector is usually 1 – 20 m and the scattering angle  $\theta < 10^\circ$ .

### The Contrast Term

The contrast is the square of the difference in neutron scattering length densities  $\rho$  values between the scattering interested part of the sample,  $d_p$ , and the surrounding medium or matrix,  $d_m$  (equation 4.2. 8).

$$(\Delta\rho)^2 = (\rho_p - \rho_m)^2 \quad (\text{eq. 4.2. 8})$$

If  $(\Delta\rho)^2$  is zero then Equation 1 is also zero and there is no SANS and it is said that the scattering bodies are at contrast match. This technique of contrast matching can be used to dramatically simplify the scattering pattern of a multi-component sample where the contrast-weighted summation of SANS from each individual component are measured. Solvents, polymers and substrates present different neutron scattering length densities, the most common solvents and polymers are shown in Table 4.2. 2 and some common substrates in Table 4.2. 3.

**Table 4.2. 2** Scattering length densities of some common solvents and polymers.

Solvent	d (h form) ( $10^{10}\text{cm}^{-2}$ )	d (d form) ( $10^{10}\text{cm}^{-2}$ )	Polymer	d (h form) ( $10^{10}\text{cm}^{-2}$ )	d (h form) ( $10^{10}\text{cm}^{-2}$ )
Water	-0.56	+6.38	PB	-0.47	+6.82
Octane	-0.53	+6.43	PE	-0.33	+8.24
Cyclohexane	-0.28	+6.70	PS	+1.42	+6.42
Toluene	+0.94	+5.66	PEO	+0.64	+6.46
Chloroform	+2.39	+3.16	PDMS	+0.06	+4.66
Carbon Tet.	+2.81	+2.81	PMMA	+1.10	+7.22

**Table 4.2. 3** Scattering length densities of some common substrates.

Substrate	d ( $10^{10}\text{cm}^{-2}$ )	Substrate	d ( $10^{10}\text{cm}^{-2}$ )
Silicon	+2.07	SiO <sub>2</sub>	+3.15
Quartz	+3.47	TiO <sub>2</sub>	+2.57

The scattering length density of a molecule is very sensitive to the value of the density used in its calculation and so a reliable knowledge of the latter is a pre-requisite for a successful contrast matching experiment.



### The Form Factor

The form factor describes how  $(ds / dW)(Q)$  is modulated by interference effects between radiation scattered by different parts of the same scattering body. Consequently it is very dependent on the shape of the scattering body. The general form of  $P(Q)$  is given by Van de Hulst's equation 4.2.9<sup>47</sup>.

$$P(Q) = \frac{1}{V_P^2} \left| \int_0^V \exp[if(Q\alpha)] dV_P \right| \quad (\text{eq. 4.2.9})$$

This factor represents a shape parameter, which gives information about length or a radius of gyration. Analytic expressions exist for some common shapes (Table 4.2. 4) from which other topologies more complex<sup>48</sup> can be deduced.

**Table 4.2. 4** Analytic expressions for the most common shapes.

Sphere of radius $R_p$	$P(Q) = \left[ \frac{3 (\text{Sin}(QR_p) - QR_p \text{Cos}(QR_p))}{(QR_p)^3} \right]^2$
Disc of negligible thickness and radius $R_p$ ( $J_1$ is a first-order Bessel function)	$P(Q) = \frac{2}{(QR_p)^2} \left[ 1 - \frac{J_1(2QR_p)}{QR_p} \right]$
Rod of negligible cross-section and length $L$ ( $S_i$ is the Sine integral function)	$P(Q) = \frac{2S_i(QL)}{QL} - \frac{\text{Sin}^2(QL/2)}{(QL/2)}$
Gaussian random coil with z-average radius of gyration $R_g$ , polydispersity $(Y+1)$ and $U = \frac{(QR_g)^2}{(1+2Y)}$	$P(Q) = \frac{2 \left[ (1+UY)^{-1/2} + U - 1 \right]}{(1+Y) U^2}$
Concentrated polymer solution with screening length $\xi$ where $\xi = R_g \left( \frac{\phi}{\phi^*} \right)^{-1/(2+1/\nu)}$	$P(Q) = P(0) \left[ \frac{1}{1 + (Q\xi)^2} \right]$

### *The Structure Factor*

The structure factor describes how  $(ds/dW)(Q)$  is modulated by interference effects between radiation scattered by different scattering bodies.

$$S(Q) = 1 + \frac{4\pi N_p}{QV} \int_0^{\infty} [g(r) - 1] r \sin(Qr) dr \quad (\text{eq. 4.2.10})$$

As this is dependent on the ordering of structures in the solution, it can be investigated to give information about relative positions of the scattering bodies. The position of scattering bodies is usually obtained from the radial distribution function term,  $G(r)$ :

$$G(r) = \frac{4\pi N_p r^2}{V} g(r) \quad (\text{eq. 4.2.11})$$

where  $r$  is the radial distance.

An alternative procedure involves one of the many approximate forms of  $S(Q)$  that have been developed (to describe particular types of systems) to calculate the expected shape of  $(ds/dW)(Q)$ . This may then be model-fitted to the observed scattering data. Unfortunately, as  $N_p$  is 0, the concentration of scattering bodies becomes more dilute, so  $S(Q)$  is 1, meaning that this type of insight into the microscopic structure can only be obtained in concentrated and/or strongly interacting samples<sup>49</sup>.

## **Results from SANS obtained for DES-Polyacetals**

### *a) Tert-DES and Block-DES with similar DES loading.*

SANS measurements were performed at the ISIS spallation neutron source, mentioned above, using the time-of-flight diffractometer, LOQ. ISIS offers a pulsed neutron source, where neutrons are produced by bombarding a tantalum target with synchrotron-accelerated protons. Approximately 12 neutrons are released per incident proton and there are approximately 50 proton-tantalum collisions per second. In these pulsed sources the neutron detector is in a fixed geometry and the  $Q$  value is varied by using the variety of neutron wavelengths produced (wavelengths which can be sorted from their

time-of-flight). The ISIS LOQ site can produce Q values ranging from, approximately 0.008- 0.34 Å<sup>-1</sup>.

The conjugates *tert*-DES **1b** and *block*-DES **2b** (4wt%DES) were dissolved at 1 wt% concentration of polymer in D<sub>2</sub>O (Figure 4.2. 13A) and MeOD (Figure 4.2. 13B) at 37 °C, conditions mimicking those experienced during cellular uptake. The solvents used must be deuterated in order to provide contrast due that the scattering from hydrogen is distinct from that of deuterium. Hydrogen is one of the few elements that has a negative scatter, which means that neutrons deflected from hydrogen are 180° out of phase relative to those deflected by the other elements. These features are important for the technique of contrast variation. All experiments were performed in 2mm quartz cells with typical measuring times of 1 hour per sample.

The scattering data for polyacetals was fitted to form factors for polydisperse Gaussian coils, spherical and rods; the fits are shown in appendix 1 and the values obtained are presented in Table 4.2.5 The scattering data was corrected for the scattering and transmission of the solvent and quartz cell and normalized by placing on an absolute intensity scale with a well characterized standard.

**Table 4.2. 5** Data obtained from analysis of scattering data using Guinier and Zimm approximations and FISH computer modeling (where Rg = radius of gyration, dnf = did not fit, R = rod spherical radius, L = rod length).

Polyacetal	wt% DES/ Serinol	Gaussian coil			Rod model		Spherical model	
		Guinier Rg / Å	Zimm Rg / Å	Rg / Å	L / Å	R / Å	R / Å	R / Å
<b>1b</b>	4.3/ -	80	75	0	20	0	0	50
<b>2b</b>	5.5/ -	60	60	dnf	-	2	60	80
<b>4</b>	4.6/ 3.4	10	20	05	10	0	65	70
<b>5</b>	5.3/3.7	20	10	-			70	75

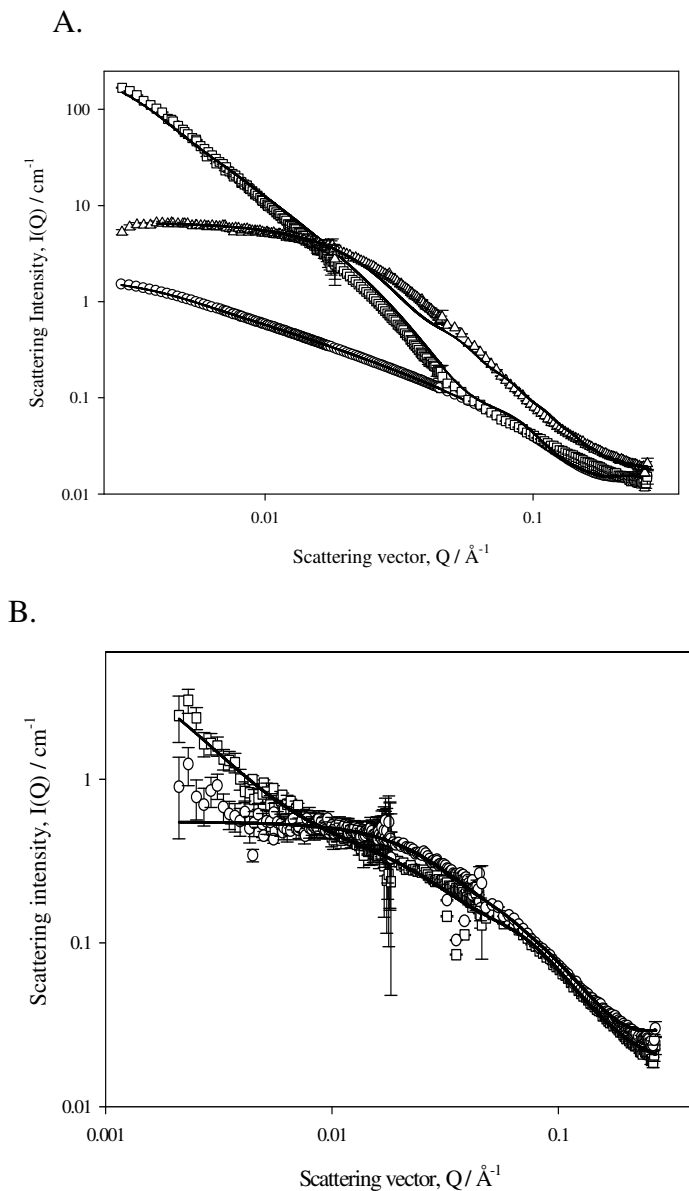


**Figure 4.2. 13** SANS from 1wt% conjugates solutions in (A) D2O. Lines are best-fits to the data as described in the text. (B) MeOD. Solid lines are best-fits to a rod model. *Tert*-DES (triangles), *Block*-DES (squares), dilute block-DES solution (circles).

In aqueous solution a significant difference between scattering profiles from the two conjugates is evident, suggesting a difference in particle morphology between the two conjugates in this solvent. For the *tert*-polymer, the modeling analysis indicates the presence of a single species in solution, which was best fitted by a model for a solid disk (diameter 20 nm, thickness 2.5 nm). This indicates that there is some aggregation of the *tert*-DES, as indicated by the fluorescence studies. By comparison it was not possible to model the *block*-copolymer data for the PBS solution using a single species, rather the analysis suggests that two sets of co-existing rods are present in solution, one comparatively long and thin (approximately 100 nm in length, 2 nm in diameter), the other more disk-like (80 nm diameter, 10 nm thick) being the second one more abundant and consistent with the size of the structures observed by TEM and DLS, and significantly larger than the structures indicated by SANS for the *tert*-DES. A second solution of the *block*-DES in PBS was studied at a concentration below the CAC (0.008 wt%), and this was accurately described by a single rod model, with the same dimensions as those present in the sample at  $C > CAC$  (100nm length, 2nm diameter).

These characterization data indicate that the molecular structure of the conjugate has a significant effect on the solution behaviour; even at the same overall acetal and DES contents i.e. the segregated arrangement of the DES units can induce sufficient amphiphilic nature in the molecule to induce the formation of large aggregate structures. This is further indicated by a parallel study in methanol rather than PBS as shown in figure 4.2. 11 (PGSE-NMR) and 4.2. 13B (SANS). The SANS data for the two conjugates in methanol were fitted to the same model of a single short rod (1.5nm diameter, 18.5 nm in length) with an attractive structure factor required to account for the scattering at low  $Q$  for *block*-DES. Both polyacetal and DES are methanol soluble, hence the solvent has a similar affinity for both components of the conjugate. From the similarity between data obtained for the two conjugates by both PGSE-NMR and SANS data (Fig. 4.2. 11 and 4.2. 13), it is evident that the loss of the solvophobicity of the *block*-DES on switching from PBS to methanol is sufficient to remove the driving force for aggregation of the DES-rich region of the molecule observed in D<sub>2</sub>O/PBS, and with it the large difference in solution structures observed between the *block*-DES and *tert*-

DES conjugates. Hence the solution behavior in aqueous media is driven by the hydrophobicity of the DES.

It was thus determined that, compared to the *tert*-DES polymer, *block*-DES presents a more stable and better defined particulate conformation in the nanosized range, that could explain its different biological behavior in prostate cancer cell models.

**Table 4.2. 6** Size and shape of the polyacetals after analysis of scattering SANS data.

<b>Polymer</b>	<b>SANS characterization (shape, size)</b>
<i>Tert</i> -DES <b>1b</b>	Solid disk: thick 2.5nm, diameter 20nm
<i>Block</i> -DES <b>2b</b>	Rod: length 100nm, diameter 2nm Disk: thick 10nm, diameter 80nm

*b) Drug influence in solution conformation.*

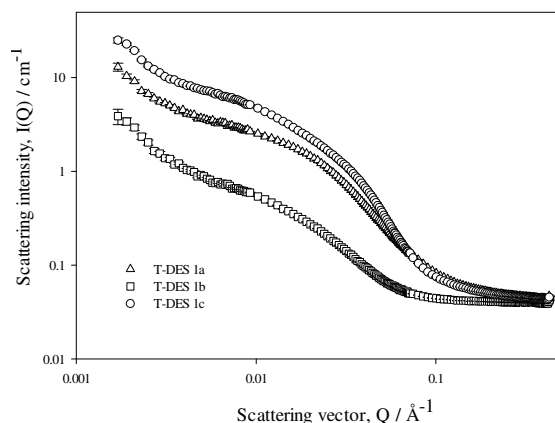
In order to identify any effect of polyacetal drug loading on polymer solution conformation; *Block*-DES and *Tert*-DES of different DES loadings were also compared.

*b.1) Tert-DES with different DES loading*

Significant changes in the scattering profile were observed in d-water (Figure 4.2 14 A) when DES loading was varied. The *tert*-polymer with a drug loading of 2 and 6wt%DES are more similar than the one with 4wt%DES, which the curve indicates a shape similar to a rod conformation contrary for *Block*-DES with 4wt%DES which has a more flat curve indicating a more spherical morphology. In d-methanol (Figure 4.2. 14 B) an increase in drug loading from 2 to 6 wt% had a little effect on the scattering profiles and therefore little effect on the polymer size and shape.

In any case, the scattering curves do not fit to random coil or spheres, so we can clearly state that there are defined structures present in solution, and that they are non-spherical.

A.



B.

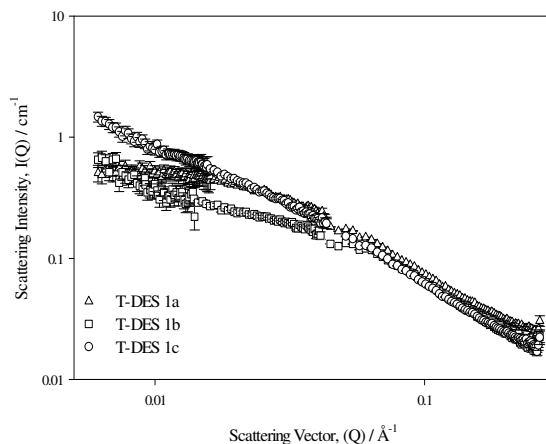


**Figure 4.2. 14** SANS from 1wt% conjugates solutions of *Tert*-DES at different drug concentrations (T-DES 1a, 1b and 1c with 2,4 and 6wt%DES respectively) in (A) D2O and (B) MeOD. T-DES 1a (triangles), T-DES 1b (squares), T-DES 1c (circles).

### b.2) *Block*-DES with different DES loading

As expected in d-methanol (Figure 4.2. 16 B) an increasing in the drug capacity from 2 to 4wt%DES had a little effect on the scattering profiles and therefore little effect on the size and shape. However at 6 wt% DES loading

there was a change in the scatter profile indicating a possible change polymer conformation.

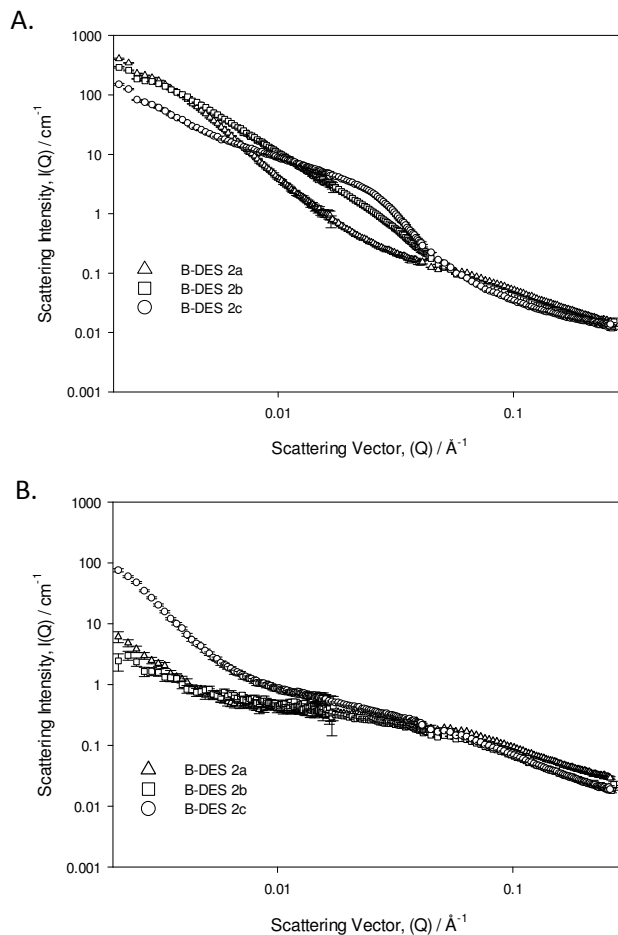


**Figure 4.2. 15** SANS from 1wt% conjugates solutions of *Block-DES* at different drug concentrations (*Block-DES 2a*, *2b* and *2c* with 2,4 and 6wt%DES respectively) in (A) D<sub>2</sub>O and (B) MeOD. *Block-DES 2a* (triangles), *Block-DES 2b* (squares), *Block-DES 2c* (circles).

In d-water (Figure 4.2. 15 A) drug loading effect is even more significant, already from 2 to 4 wt% DES a significant change in the scattering was observed. This change in scattering was even more visible at 6 wt% loading.



From the scattering curves there is clearly a more significant effect of drug loading as *block*-copolymer than as *tert*-DES.

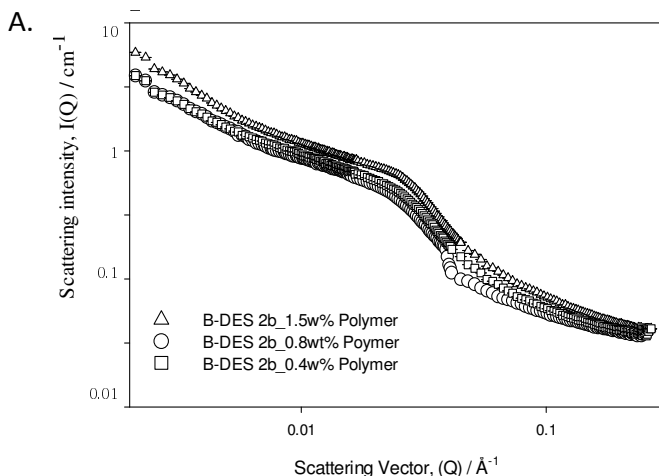
Comparing to the fitted parameters for the *Block*-DES **2b** data, it was observed that *Block*-DES **2c** sample is fitted only by a two rod model, indicating a disk-like structure which is smaller than the *Block*-DES **2b**, co-existing with a small approximately spherical structure (65/55).

SANS data indicate a change in solution behavior as drug loading changes, and from the fits we used a constant  $Q^{-n}$  background to fit the low  $Q$  data, and the mid-high  $Q$  range data reflects a consistent rod-like structure of radius 40-45 Å with an increasing rod length  $2 < 4 < 6$  wt% DES:  $300 < 550 < 820$  Å.

c) *Polymer concentration influence on solution conformation.*

Different polymer concentrations (1.5, 0.8 and 0.4 wt%) of *Block*-DES and *Tert*-DES were also studied in order to understand the influence of polymer concentration on solution conformation (Figure 4.2. 16).

From the fitting, *Block*-DES **2b** at 1.5wt% of polymer clearly contains some large structures that are at the limit of accurate description by SANS.



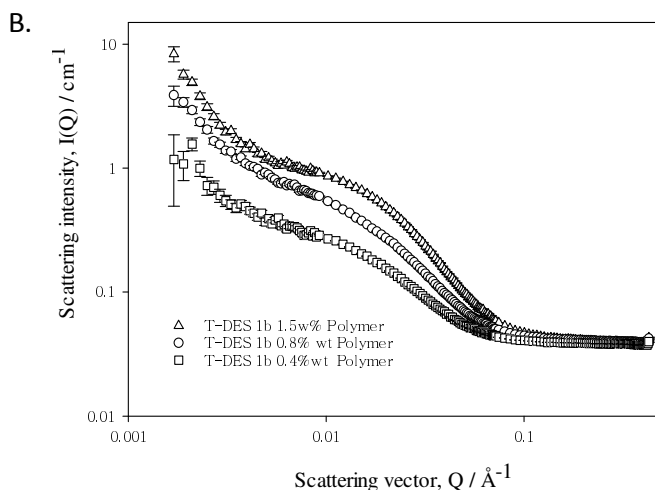


**Figure 4.2. 16** SANS from conjugates solutions of *Block-DES 2b* (A) and *Tert-DES 1b* (B) at different polymer concentrations (1.5 triangles), 0.8 (circles) and 0.4 (squares) wt% Polymer in D<sub>2</sub>O.

**Table 4.2. 7** Size and shape of the polyacetals after analysis of scattering SANS data.

Polymer <i>Block-DES 2b</i>	SANS characterization radius/length or thickness ( $\text{\AA}$ )
1.5wt%polymer	Rod: 2/100 Disk: 80/10
0.8wt%polymer	Rod: 250/320 Thin Disk: 1000/85
0.4wt%polymer	Rod: 30/120 Disk: 880/220 $\text{\AA}$ Disk: 500/260
Polymer <i>Tert-DES 1b</i>	SANS characterization radius/length or thickness ( $\text{\AA}$ )
1.5wt%polymer	Long Rods: 800/100 and 20/1000
0.8wt%polymer	Small Rod: 125/320 Disk: 880/220
0.4wt%polymer	Thin Disk: 1000/ 85

The data can only be fitted with the two rod model, and the fitted parameters imply there are large disk-like structures present in solution. At 0.8 wt% the solution structure seems to be a single thin disk-like structure with a very large radius of 1000Å and thickness 85Å. This data also fitted well to a single rod of smaller dimensions 125Å radius, 320Å length in the presence of a Q-n term where n=2. At 0.4wt% the solution structure was difficult to pin-down as there were comparable fits for different models: (i) A disk of 880Å radius and 220Å thickness coexisting with a short rod of 30Å, 120Å length; (ii) the best fit is from a disk radius 500Å thickness 260Å with a Q<sup>n</sup> term at n=3. Table 4.2. 7 summarized all these data.

Clearly, the solution structure for *Block*-DES **2b** is concentration dependent, with evidence for rod and disk-like structures present in solution.

### 4.3. MECHANISM OF ACTION AND *IN VIVO* STUDIES WITH DES-POLYACETALS

#### 4.3.1. Introduction

The synthetic estrogen Diethylstilbestrol was first administered to woman as natural supplement estrogen production. But in 1971, the Food and Drug Administration (FDA) issued a drug bulletin advising physicians to stop prescribing DES to pregnant women due to its involvement in a rare vaginal cancer in female offspring. However, the use of DES in prostate cancer patients was maintained. As seen, DES is a very old drug, but its mechanism of action is still not completely elucidated. A mode of action via a hormonal imbalance or uncontrolled stimulation of target cell proliferation is the most commonly considered, but a mechanism of metabolic activation of estrogens and subsequent alteration of DNA or other important cellular targets may also apply due to its impaired side effects.

To understand the molecular basis of prostate cancer or any prostate cancer treatment it is important to face a number of issues concerning the heterogeneity of the disease or the resistance to prevailing therapies. Estrogens such as DES, diffuse into their target cells and interact with the estrogen receptor. Target cells include the female reproductive tract, the mammary gland, the hypothalamus, and the pituitary. Estrogen binding triggers the hepatic synthesis of sex hormone binding globulin (SHBG), thyroid-binding globulin (TBG), and other serum proteins and suppress follicle-stimulating hormone (FSH) from the anterior pituitary. The combination of an estrogen with a progestin suppresses the hypothalamic-pituitary system, decreasing the secretion of gonadotropin-releasing hormone (GnRH).

Several oncogenic activations, through genomic or non-genomic pathways, to neoplastic progression of prostate cancer cells have been studied. These oncogenes confer metabolic and growth promoting advantages to tumor cells.

Molecularly, prostate cancer cells are capable to survive with an uncontrolled growth able to cause invasion-metastasis to other organs. These alterations can be triggered by the activation of growth factors, signaling proteins (kinase

transcription factors and co-regulators) and multiple proteases required for the disease progression (Figure 4.3.1).

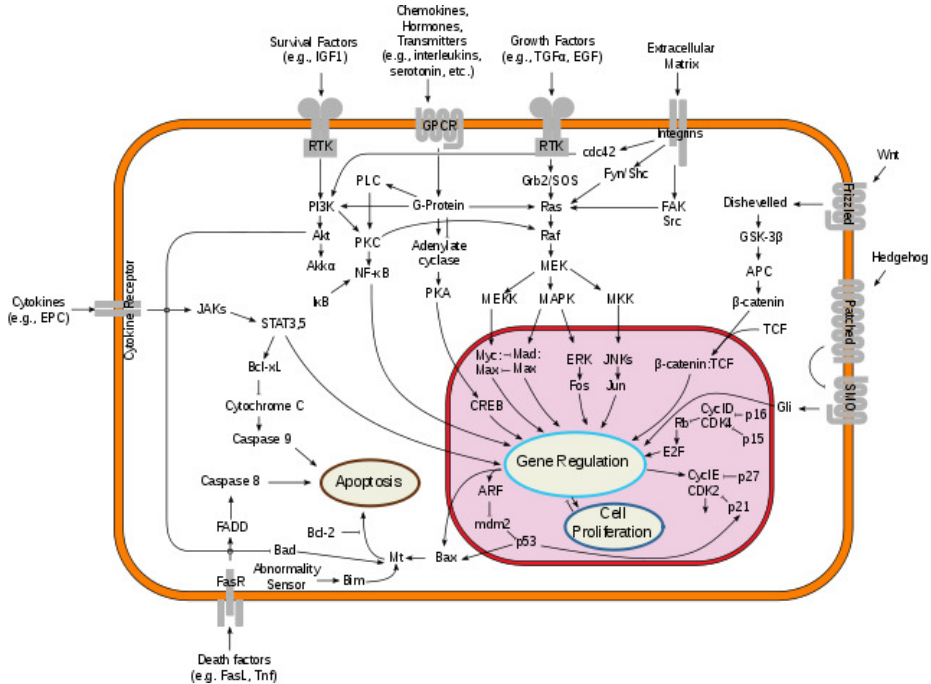


**Figure 4.3. 1** An overview of major signal transduction pathways. The figure shows examples of pathways for proliferation (Ras/MAPK), STAT signaling (STAT's) and survival/metabolism (PI3K/Akt). (Picture taken from Reece, J., 2002<sup>50</sup>).

**Growth factor receptors**

Insulin growth factors (IGF), (ii) the Wnt signaling pathway, (iii) the epithelium growth factor receptor (EGFR), (iv) the human epidermal growth factor receptor 2, Her-2/neu (ERBB2) and (v) the critical mediator of multiple oncogenic signaling pathway, phosphoinositide-3 kinase (PI3K/AKT) have been shown to be implicated in prostate cancer development and progression.

*(i) Insulin growth factor*

Insulin-like growth factor (IGF) is mainly secreted by the liver as a result of stimulation by the growth hormone (GH) and it is important for the regulation

of normal and cancer physiology. The IGF has been shown to be involved in the promotion of cell proliferation and the inhibition of cell death (apoptosis). IGF-1 expression is required to achieve maximal growth.

Insulin-like growth factor 1 (IGF-1)<sup>51</sup> binds the receptor tyrosine kinase (IGF1R) which has been shown to be very important in prostate adenocarcinogenesis, where there is a significant correlation between high IGF1R activity and prostate cancer. At the same time there is a decreased of tumor growth when the pathway is inhibited<sup>51</sup>. When IGF is decreased subsequent to the down-regulation of IGF-1 receptor expression there is an association with advanced, metastatic disease. This decrease in IGF-1 receptor may confer a survival advantage to prostate cancer cells that have entered the circulation by making them resistant to the differentiative effects of IGF-1 at metastatic sites such as bone. The molecular mechanisms that affect IGF-1 receptor down-regulation seem to be involved with novel actions of the androgen receptor<sup>52</sup>. It has been also shown that both IGF1R protein and mRNA are upregulated in primary prostate adenocarcinoma, as opposed to benign prostatic hyperplasia<sup>53</sup>. Reducing the expression of IGF1R via antisense RNA retards tumor growth of prostate cancer cells<sup>53</sup>.

On the other hand, Insulin-like growth factor 2 (IGF-2) is thought to be a primary growth factor required for early development and also essential for the function of organs such as the brain, liver and kidney.

IGF availability in the serum is regulated *in vivo* by IGF binding protein 3 (IGFBP3)<sup>55</sup>. The prostate cancer cell line, PC3 decrease in growth after treatment with 5-FU, attributable to a decreased bioavailability of IGF1, although IGFBP3 may play an important role later in prostate adenocarcinoma migration and cell-matrix adhesion in an IGF1 independent mechanism<sup>56</sup>. It can also promote apoptosis in a poorly understood mechanism independent of IGF<sup>57</sup>..

Both IGFs, IGF1 and IGF2, bind the receptor tyrosine kinase, IGF1R (Figure 4.3. 2). Through the receptor's tyrosine kinase activity<sup>58</sup> several downstream signaling pathways are activated, including the phosphatidylinositol 3-kinase (PI3K), AKT, TOR, S6 kinase, and mitogen-activated protein kinase (MAPK) pathways, by which the antiapoptotic and proneoplastic effects of IGF-1 work.

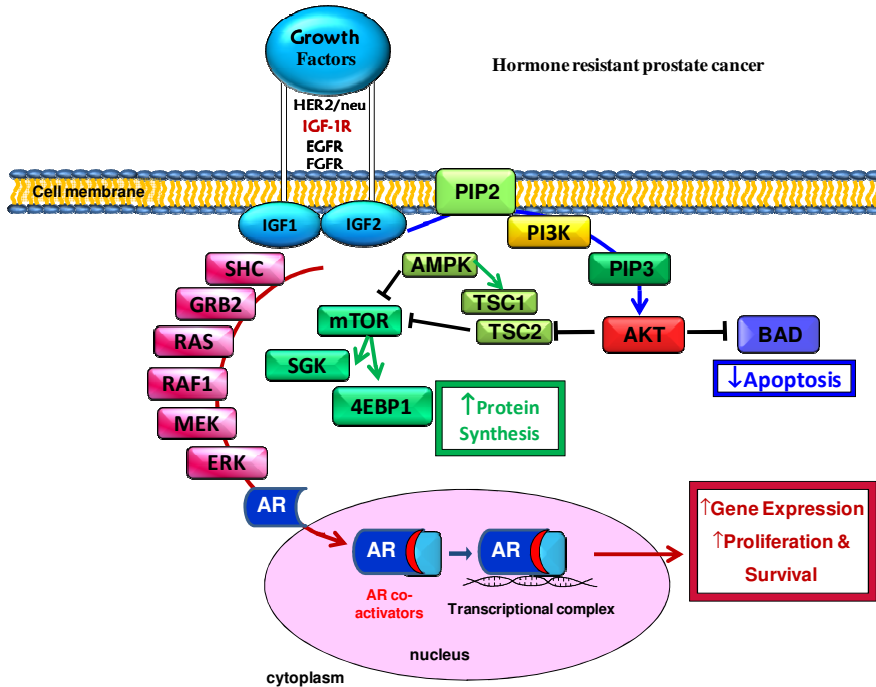


**Figure 4.3. 2** IGF1 and IGF2 signaling pathway involved in prostate cancer. (Figure adapted from Fürstenberger, G. *et al.* 2002<sup>59</sup>).

IGF pathway is capable of inducing activation of the androgen receptor in the absence of androgens<sup>60</sup>. The IGF pathway via its action on the PI3K/AKT pathway phosphorylates the androgen receptor inhibitor Foxo1<sup>61</sup>.

Finally it is important to mention that, IGF1 signaling pathway can also be modulated by the stimulation of the metalloprotease MT1-MMP<sup>62</sup> triggering actin rearrangements in the cytoskeleton that may activate integrins and lead to the promigratory cell behaviour<sup>63</sup>.

(ii) The protooncogenic protein, Wnt.

The molecular name Wnt is derived from *Wingless*, the *Drosophila melanogaster* segment-polarity gene, and *Integrase-1*, the vertebrate homologue. Wnt signaling has been shown to regulate T cell development and activation, and dendritic cell maturation.

As Wnt pathway is important in the natural development of the prostate<sup>64</sup>, the Wnt signalling pathway is considered one of the major oncogenic signaling pathways involved in the carcinogenesis of prostate cancer. The inhibition of the pathway with WIF1 reduce the tumor size in addition to reducing MMP2 and 9 in PC3 cells<sup>65</sup>. Wnt family protein, Wnt11, increase invasiveness for both LNCaP and PC3 cell lines<sup>66</sup>.

The central molecule of the pathway<sup>67</sup> is  $\beta$ -catenin (Figure 4.3. 3), which acts as a coactivator of the androgen receptor. Catenin exists in three cellular pools—at the membrane (associated with E-cadherin,  $\beta$ -catenin and other molecules, involved in cell adhesion), cytoplasm and nucleus.

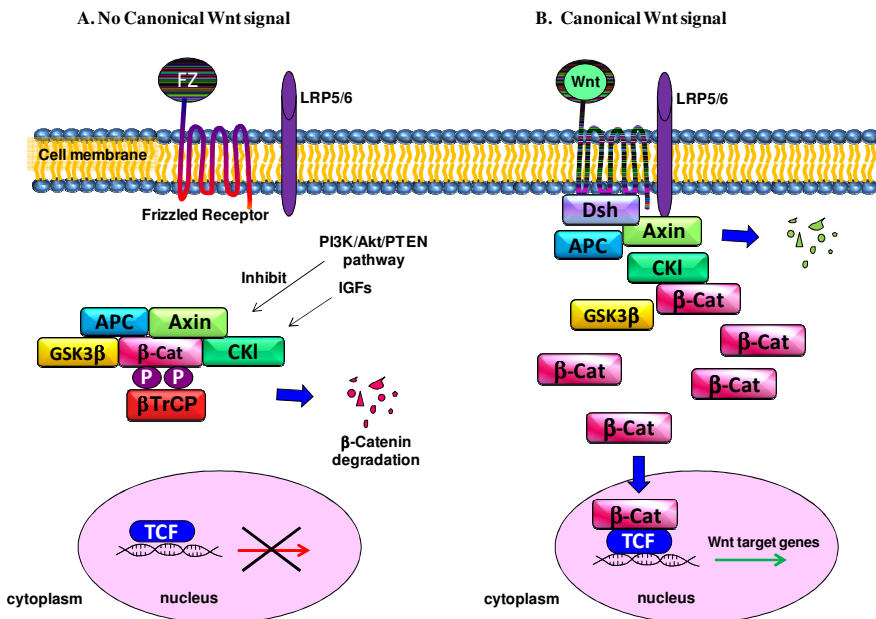


**Figure 4.3. 3** The Wnt signaling pathway showing some influences of other signaling pathways and factors (picture adapted from He *et al.* 2003<sup>68</sup>).

It is possible to observe the molecular differences in the absence or presence of a Wnt ligand (Figure 4.3. 3). In the absence of a Wnt signal,  $\beta$ -catenin is sequestered in a multiprotein degradation complex containing the scaffold protein Axin, the tumor suppressor gene product adenomatosis polyposis coli complex (APC), kinases CKI and GSK3b, among others. When Wnt signaling is inactive, the APC phosphorylates  $\beta$ -catenin, which is ubiquitinated by the



$\beta$ -TrCP–E3-ligase complex and subsequently degraded by the proteasome machinery. There is no transcription of Wnt target genes. In Figure 4.3. 3B, Wnt ligand associates with Fz and LRP5/6 co-receptors. This in turn can lead to translocation of Axin to the plasma membrane through interaction with LRP5/6 and Dsh/Fz. Translocation results in Axin degradation and/or dissociation of the multiprotein complex. GSK3 $\beta$  also might be displaced from this complex through Dsh action.  $\beta$ -catenin is then released from the multiprotein complex, accumulates in the cytoplasm in a non-phosphorylated form, and subsequently translocates into the nucleus where by association with TCF/LEF factors it promotes transcription of Wnt target genes.

It is important to note that, intracellular signaling pathways<sup>69</sup> are frequently interconnected. For instance, IGF-1 receptor stimulation facilitates dissociation of  $\beta$ -catenin at the cell membrane into the cytoplasmic pool in colorectal cells and potentiates  $\beta$ -catenin –TCF/LEF transcription in hepatoma cells. The expression of  $\beta$ -catenin and GSK3 is diminished in prostate cancer cell lines of greater invasive potential<sup>70</sup> and in bone metastases appears downregulated, compared with that seen in corresponding primary tumors in patients with untreated prostate cancer<sup>71</sup>.

### (iii) Epidermal growth factor receptor

Epidermal growth factor receptor (EGFR) is a transmembrane tyrosine kinase receptor that plays a central role in regulating cell division and death. EGFR belongs to the HER family of receptors which comprise four related proteins (EGFR(HER1/ErbB1), ERBB2(HER2), ERBB3(HER3) and ERBB4(HER4)).

EGFR participates in several signaling cascades (Figure 4.3. 4) including Akt, MAPK and STAT and others that affect gene transcription, which in turn results in cancer cell proliferation, reduced apoptosis, invasion and metastasis and also stimulates tumor-induced angiogenesis. Higher association of EGFR was correlated with higher serum PSA.

EGFR involves three important signaling pathways.

- The RAS-RAF-MAPK pathway, where phosphorylated EGFR recruits the guanine-nucleotide exchange factor via the GRB2 and Shc adapter proteins, activating RAS and subsequently stimulating

RAF and the MAP kinase pathway to affect cell proliferation, tumor invasion, and metastasis.

- The PI3K/AKT pathway, which activates the major cellular survival and anti-apoptosis signals via activating nuclear transcription factors such as NFKB, described below.
- The JAK/STAT pathway which is also implicated in activating transcription of genes associated with cell survival. EGFR activation may also lead to phosphorylation of PLCG and subsequent hydrolysis of phosphatidylinositol 4,5 biphosphate (PIP<sub>2</sub>) into inositol 1,4,5-triphosphate (IP<sub>3</sub>) and diacylglycerol (DAG), resulting in activation of protein kinase C (PRKC) and CAMK.

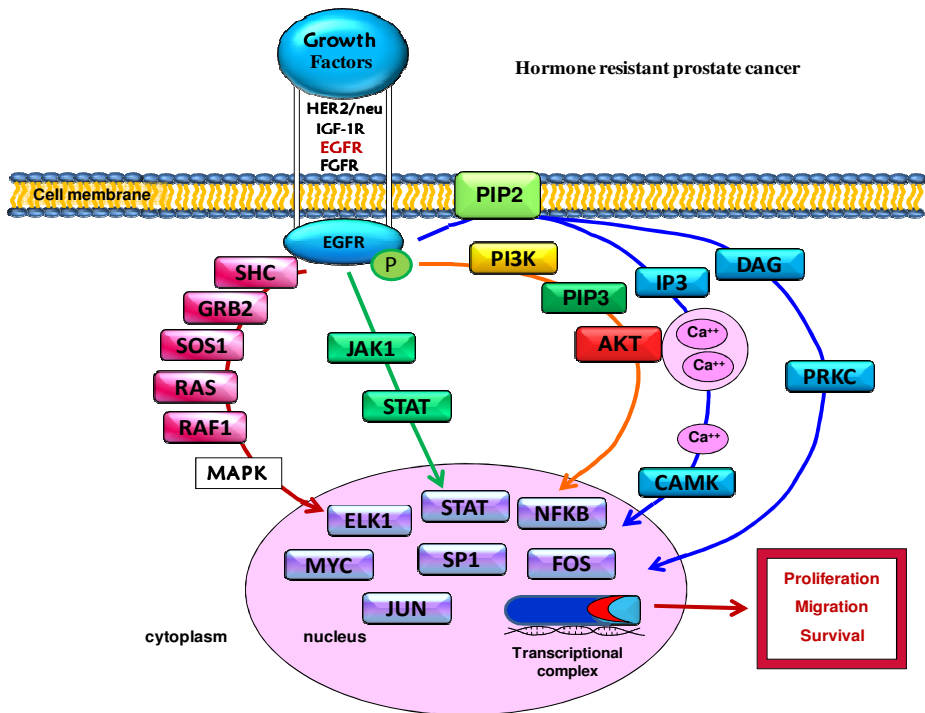


**Figure 4.3. 4** The EGFR signaling pathway encountered in the treatment of prostate cancer (picture adapted from McDonagh, E.M. *et al.* 2007<sup>72</sup>).

(iv) *Her-2/neu* (*ERBB2*)

*Her2/neu* is a transmembrane tyrosine kinase important in differentiation and cell growth. This proto-oncogene, has been implicated particularly in breast cancer but plays as well an important role in understanding prostate adenocarcinoma oncogenesis. It has been shown a correlation between higher levels of serum *Her/Neu* in patients with advanced and also metastatic prostate cancer but not with non-metastatic or localized disease patients.

*Her/Neu* is capable of activating the androgen receptor in the androgen independent stage<sup>51</sup>. It can promote survival of LNCaP cells through the Akt pathway even in the absence of androgens. The interaction between *Her-Neu* and the androgen receptor is regulated by a miRNA, miR-331-3p<sup>73</sup>, which can inhibit the PI3K/Akt signalling (Figure 4.3. 5), in addition to reduce the AR-regulated PSA expression. However, the relation between *Her/neu* and AR does not occurred in LNCaP cells, where a decreased AR mRNA in addition to decreased AR and AR regulated PSA could be found<sup>74</sup>.

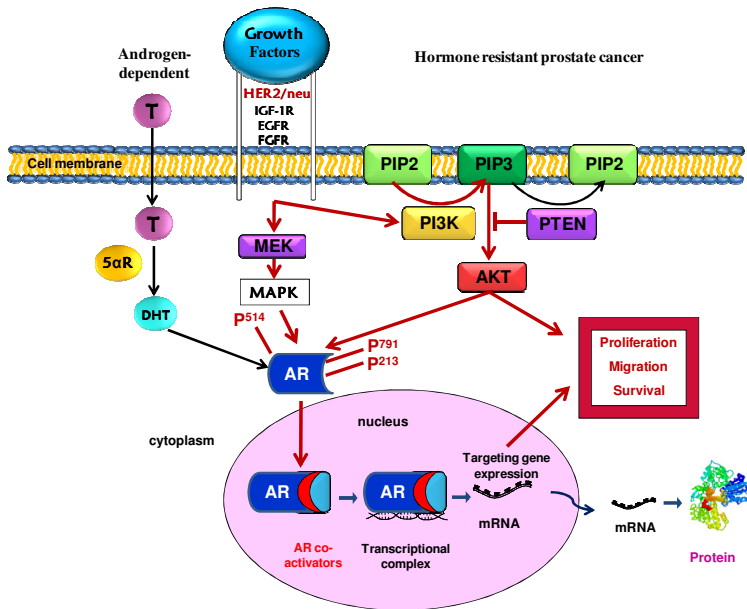


**Figure 4.3. 5** A model of *HER-2/neu* activation of the Akt-AR pathway that promotes survival and proliferation of androgen-dependent prostate cancer cells upon androgen deprivation (Figure adapted from Feldman, B.J. *et al*, 2001<sup>79</sup>).

Her/neu has been found to be important in bone metastasis of prostate cancer and the over-expression of this protein has a direct correlation with a poor prognosis<sup>75</sup>. Orthotopic transfection of Her2/Neu facilitates metastasis, and as demonstrated with PC3 cell line transfected with Her2/neu. After inoculation, these cells trigger metastasis all over the abdomen, in the retroperitoneum and in the kidneys<sup>76</sup>. Molecularly, the Her2/Neu receptor is part of a signaling cascade that involves the downstream enhancement of Akt and MMP-9, whereby the cancer cell is allowed to penetrate the matrix and facilitate angiogenesis<sup>77,78</sup>.

*(v) Phosphoinositide-3/AKT*

Phosphoinositide-3 Kinase (PI3K) is a critical mediator of multiple oncogenic signaling pathways. PI3K is activated by the receptor tyrosine kinases generating PI(3,4)P(2) and PI(3,4,5)P(3) (PIP3).

Most important PI3K downstream targets include Akt family of serine-threonine kinases, recruited by PIP3 to the plasma membrane and phosphorylated by PDK1 kinase.

Akt interacts with these phospholipids, causing its translocation to the inner membrane, where it is phosphorylated and activated by PDK1 and PDK2. Activated Akt modulates the function of numerous substrates involved in the regulation of cell survival, cell cycle progression and cellular growth.

In recent years, it has been shown that PI3K/Akt signaling pathway components are frequently altered in human cancers. Cancer treatment by chemotherapy and  $\gamma$ -irradiation kills target cells primarily by the induction of apoptosis.

The negative regulator of PI3K-Akt pathway (Figure 4.3. 6) includes a phosphatase PTEN that presents a high specificity for lipid substrates<sup>80</sup>. In prostate cancer, PTEN is usually lost resulting in hyperactive PI3K/akt pathway promoting prostate cancer progression. PTEN alterations are more common in metastatic cancers and studies have identified biallelic loss of PTEN in ~50% of metastatic hormone-refractory prostate cancer<sup>81</sup>.

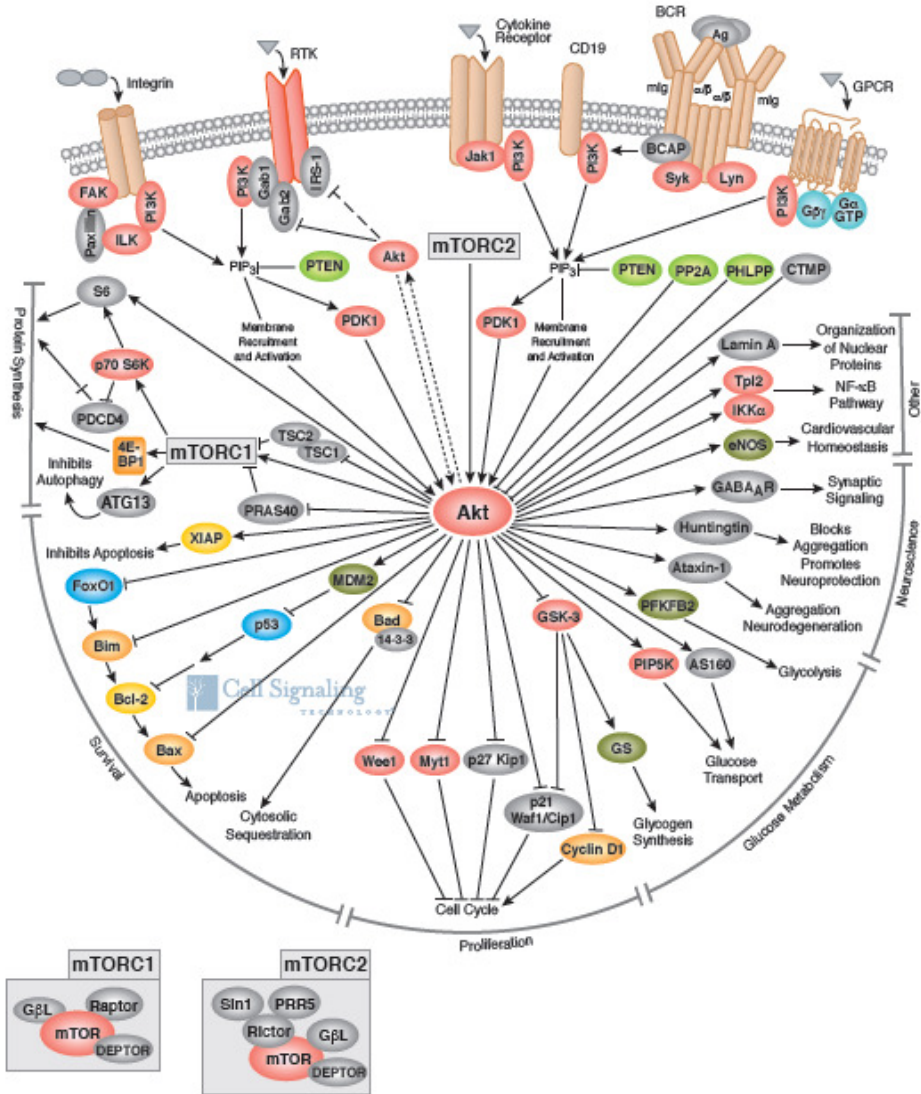


**Figure 4.3.** 6 PI3K/Akt signaling pathway involved in prostate cancer. (Photo: Cell Signaling Technology(R)).

Targeting PI3K-Akt pathway to treat prostate cancer patients is a very promising area of research. Currently, some small inhibitors<sup>82</sup> are undergoing clinical trials for prostate cancer therapy, as for example mTOR inhibitor RAD001 (everolimus) alone or in combination with gefitinib<sup>83</sup>. PI3K and Akt

are also attractive drug targets for prostate cancer therapy, but despite serious efforts inhibitors targeting the kinase activity lack specificity<sup>84</sup>.

All the molecular targets described are involved in key prostate cancer mechanisms of survival, proliferation (cell cycle) or autophagy. Therefore, in this chapter we described DES-polyacetals molecular mechanism based on such pathways and targets.

### **Mechanism of action of Diethylstilbestrol**

The mechanism of action of this important human carcinogen is still unknown; however, the most widely discussed mechanisms for DES, looking at the most recent contemporary clinical trials, are related to the hormonal action to treat advanced prostate cancer. There is an evidence to support the ability of DES to achieve complete testosterone blockade by blocking LH leaving FSH unaffected. DES also inhibits dihydroepiandrosterone sulfate serum levels<sup>85</sup>.

The Veterans Administration Cooperative Urological Research Group (VACURG) I study<sup>86</sup> showed that the endocrine treatment delays progression and also the time to progression increased in non-metastatic disease. Because of the switch of the majority of patients from the placebo arm to the endocrine treatment arm at the time of progression, the findings do not exclude the possibility of an effect of endocrine treatment on survival<sup>87</sup>. However, it has been found that DES also presents anti-tumor properties and clinical effectiveness in prostate cancer resistant to first-line hormonal therapy<sup>88</sup>. The side-effects at high DES dose (e.g. 5 mg dose) were associated with increased mortality from cardiovascular causes compared with castration<sup>86,89</sup>. However, low-dose DES has shown anti-tumor efficacy with limited cardiovascular side effects and it should be considered for secondary hormone manoeuvres.

Relevant clinical studies indicate that 1 mg of DES in castrate-resistant prostate cancer (CRPC) produced a biological response (change in PSA level) and improved the median survival of patients when used as a second-line hormone therapy after standard androgen deprivation with bicalutamide and LHRH analogues<sup>88</sup>. These findings were for low doses of DES. The 1 mg dose is associated with a reduced toxicity, including fewer thromboembolic and cardiovascular events. It produces a decrease cancer-related death per

year in high risk patients. Low-dose DES appears to be safe and effective for CRPC before initiating chemotherapy. The cost/efficiency ratio may encourage physicians to consider DES as a therapy option before chemotherapy in non-symptomatic CRPC<sup>88</sup>. To avoid the cardiovascular complication, a combination of prophylactic aspirin (100mg once daily) with 1mg oral DES (three times daily or 2 mg twice daily) was administered to the patients<sup>90</sup>. Of 18 patients, 66% had PSA levels reduced to, 0.6 or at least up to a 50% reduction. Gynaecomastia was noted in 2 of 18 patients. No thromboembolic complications were noted.

Estrogenic therapies induce secondary responses in patients with an androgen-independent state of prostate cancer, which suggests an additional mechanism of action besides that of suppression of the pituitary–gonadal axis. Several studies<sup>91</sup> suggest that DES can produce PSA responses in a significant proportion of patients in an androgen-independent state of prostate cancer. The mechanism is yet unclear but may represent a direct cytotoxic effect on the cells, probably by apoptotic mechanisms as it was mentioned above<sup>92</sup>.

#### **4.3.2. Useful *in vitro* techniques to determine the mechanism of action of DES-polyacetals.**

### **Apoptosis or Programmed Cell Death**

Apoptosis is defined as a highly regulated cellular pathway responsible for the elimination of cells in the organism that are no longer needed or extensively damaged (Figure 4.3. 7). This process is characterized by the loss of plasma membrane, asymmetry and attachment, condensation of the cytoplasm and nucleus, and internucleosomal cleavage of DNA. Apoptosis can be initiated by different stimuli, including infectious, anticancer or toxic agents, but also by growth factor withdrawal, heat shock, ischemia or degenerative processes.

There are several pathways resulting in apoptosis, all of which involve cysteine aspartyl-specific proteases (caspases). Depending on the nature of these stimuli, two different apoptotic pathways can be activated: the extrinsic and the intrinsic pathways, although they are connected in different steps of the process.

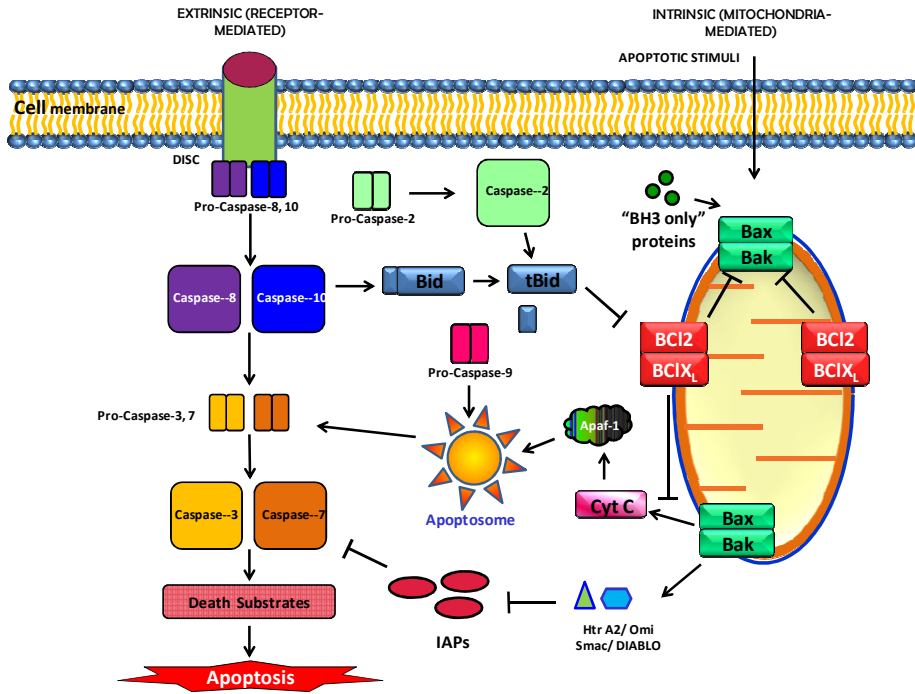


**Figure 4.3. 7** Extrinsic and intrinsic apoptosis pathways (Figure adapted from G.S. Salvesen and C.S. Duckett, 2002<sup>93</sup>).

The extrinsic apoptotic pathway<sup>94</sup> is triggered by ligand binding to cell-surface receptors, resulting in the recruitment of various proteins to form the death-inducing signaling complex (DISC). This complex promotes activation of caspase-8, which in turn activates caspase-3. Caspase-3 then induces the cellular changes that characterize apoptosis. The intrinsic pathway<sup>94,95</sup>, in contrast, is triggered by cytotoxic stress, which induces the translocation of pro-apoptotic Bcl-2 family members, such as Bax, to the mitochondria. This leads to the release of mitochondrial cytochrome c into the cytosol, where it promotes the oligomerization of the pro-apoptotic factor Apaf-1 into a complex called the "apoptosome". The apoptosome recruits and activates caspase-9, which in turn promotes the activation of caspase-3. This process is



further regulated by X-linked inhibitor of apoptosis (XIAP) protein, which inhibits the activity of both caspase-9 and caspase-3. Both extrinsic and intrinsic pathways are shown in figure 4.3. 7.

In normal cells (Figure 4.3. 8, left diagram), the distribution of phospholipids is asymmetric, with the inner membrane containing anionic phospholipids (such as phosphatidylserine) and the outer membrane having mostly neutral phospholipids. In apoptotic cells (Figure 4.3. 8, right diagram), the amount of phosphatidylserine (PS) on the outer surface of the membrane increases, exposing PS to the surrounding liquid. Annexin-V, a calcium-dependent phospholipid-binding protein, has a high affinity for PS. Although it will not bind to normal living cells, Annexin-V will bind to the PS exposed on the surface of apoptotic cells. Thus, Annexin-V has proved suitable for detecting apoptotic cells. Roche Applied Science supplies a number of products for the detection of PS translocation by Annexin-V, which is typically used in conjunction with a vital dye such as propidium iodide (PI) to identify early apoptotic cells.

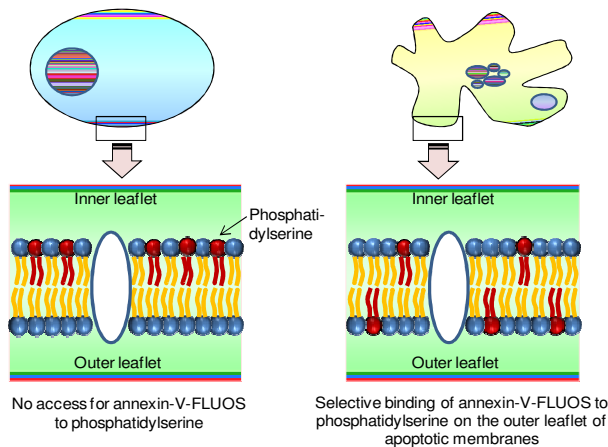


**Figure 4.3. 8** Detection of surface morphology changes during apoptosis. During apoptosis, the distribution of neutral phospholipids (black symbols) and anionic phospholipids such as phosphatidylserine (red symbols) in the cell membrane changes (picture adapted from<sup>96</sup>).

## Cell Cycle Analysis

In an organism, the rate of cell division is a tightly regulated process that is intimately associated with growth, differentiation and tissue turnover. Generally, cells do not undergo division unless they receive signals that instruct them to enter the active segments of the cell cycle. Resting cells are said to be in the G<sub>0</sub> phase (quiescence) (Figure 4.3. 9). The signals that induce cells to divide are diverse and trigger a large number of signal transduction cascades. A thorough discussion of the types of signals and the variety of responses they can elicit are beyond the scope of this chapter. Generally, signals that direct cells to enter the cell cycle are called growth factors, cytokines, or mitogens.

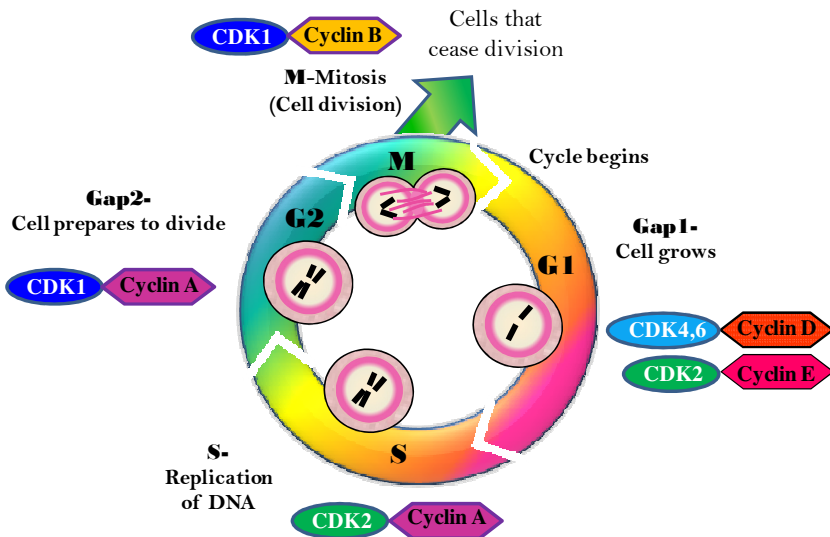


**Figure 4.3. 9** Cell cycle: A schematic overview. Mammalian cell cycle regulation by CDK/cyclin holoenzymes and CKIs. The cell cycle consists of four distinct phases: G<sub>1</sub>, S (DNA replication), G<sub>2</sub>, and M (mitosis). Activation of specific CDK/cyclin complexes drives progression through these cell cycle phases. CKIs of the Cip/kip and the INK4 families interact with and inactivate CDK/cyclin holoenzymes, thereby blocking cell cycle progression and cell proliferation.

### ***Control on the Cell Cycle***<sup>96</sup>

Once the cell is instructed to divide, it enters the active phase of the cell cycle, which can be broken down into four segments:

- During G1 (G = gap), the cell prepares to synthesize DNA. In the latter stages of G1, the cell passes through a restriction point (R) and is then committed to complete the cycle.
- In S phase the cell undergoes DNA synthesis and replicates its genome.
- During G2 the cell prepares to undergo division and checks its replication using DNA repair enzymes.
- In M phase, the cell undergoes division by mitosis or meiosis and then re-enters G1 or G0.

In most instances, the decision for a cell to undergo division is regulated by the passage of a cell from G1 to S phase. Progression through the cell cycle is controlled by a group of kinases called cyclin-dependent kinases (CDKs), (Figure 4.3. 8). CDKs are activated by associating with proteins, called cyclins, whose levels of expression change during different phases of the cell cycle. Once associated with cyclins, CDKs are activated by phosphorylation via CDK-activating kinase (CAKs) or by dephosphorylation via a phosphatase called CDC25. D-types cyclins are the primary cyclins that respond to external cellular factors. Their levels are low in G1, but increase towards the G1/S. Cyclin D regulates CDK4 and CDK6. Cyclin E is expressed during the G1/S transition and is degraded in S. Cyclin E regulates CDK2 and perhaps CDK3. When S phase begins, cyclin A increase and activate CDK2. The cyclin A/CDK2 complex is thought to have a direct role in DNA replication. The progression through mitosis is regulated by the presence of cyclin B. association of Cyclin B with CDC2 forms the primary kinase present during mitosis (MPF=M-phase/maturation promoting factor). Cyclin B is degraded during anaphase and regulates the cell's progression out of mitosis and into G1.

## Key protein expression analyzed by Western Blot

The western blot also named the protein immunoblot is an analytical technique used to detect specific proteins. It uses gel electrophoresis to separate native proteins by 3-D structure or denatured proteins by the length of the polypeptide. The proteins are then transferred to a membrane (typically nitrocellulose or PVDF), where they are detected using antibodies specific to the target protein<sup>97,98</sup>. Figure 4.3. 10 shows an example of western blotting of apoptosis-related proteins.

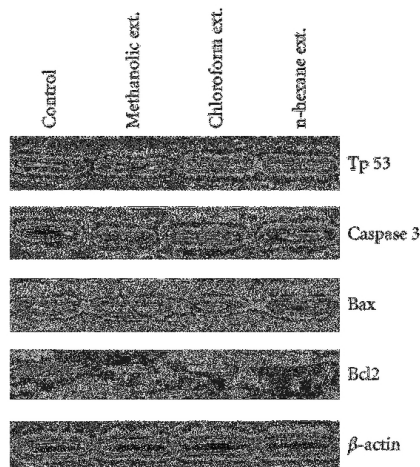


**Figure 4.3. 10** Example of protein immunoblotting/western blotting of apoptosis-related proteins. In this example, the protein-expression study show upregulation of Tp53, Caspase-3, and Bax but downregulation of Bcl-2.

### 4.3.3. Results

#### 4.3.3.1. Cell death studies by Flow Cytometry: Annexin V-PI

The apoptotic processes after cell treatment with *Block-DES* and *Tert-DES* was studied by Flow cytometry using Annexin V and PI (Figure 4.3. 8).

When Annexin is used combined to propidium iodide (PI) it is possible to differentiate early apoptotic from late apoptotic or necrotic cells (Table 4.3. 1).

**Table 4.3. 1** Distinguishing apoptosis from necrosis using Annexin-V and propidium iodide (PI).

	Normal cells	Early Apoptotic cells	Late Apoptotic cells	Necrotic cells
<b>Annexin-V</b>	-	+	+	-
<b>Propidium Iodide</b>	-	-	+	+

Typical histograms from FACS analysis are shown below (Figure 4.3. 11, Figure 4.3. 12 and Figure 4.3.13) after AnnexinV-PI test using DES-polyacetalic systems in PC3 and LNCaP cell lines. Data from these histograms were analyzed and represented in Figure 4.3. 14.

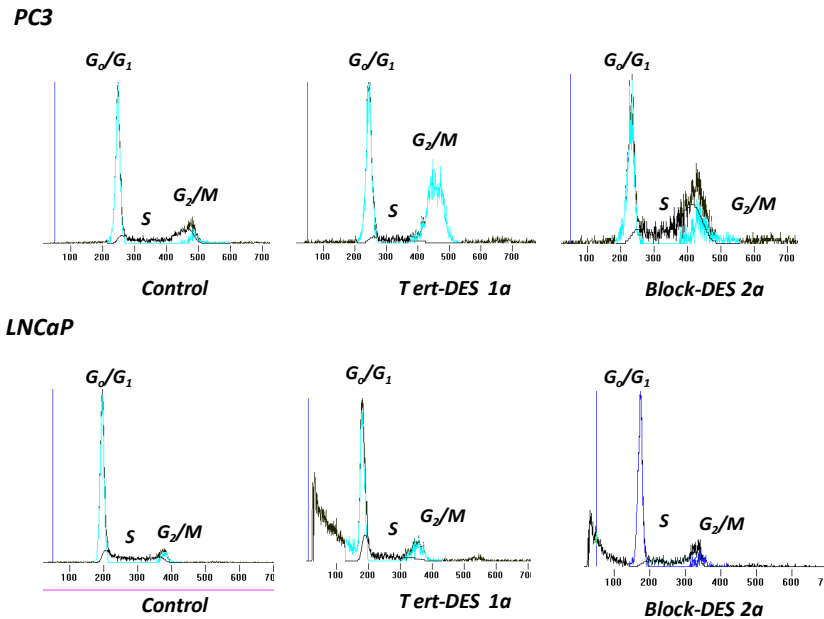


**Figure 4.3. 11** Typical flow cytometric profile of the DNA content in PC3 and LNCaP cell lines stained with AnnexinV and PI. A prominent subG<sub>1</sub> peak (between 100 and 200) should appear in apoptotic cells but not in normal cells.

Looking at Figure 4.3. 12 is possible to observe that flow cytometric analysis clearly differentiates normal cells (quadrant E3) with low Annexin and low PI staining, apoptotic cells (quadrant E4) with high Annexin and low PI staining,

late apoptotic (quadrant E2) with high Annexin and high PI staining and necrotic (quadrant E1).

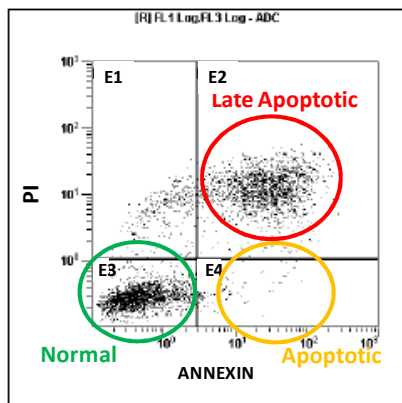
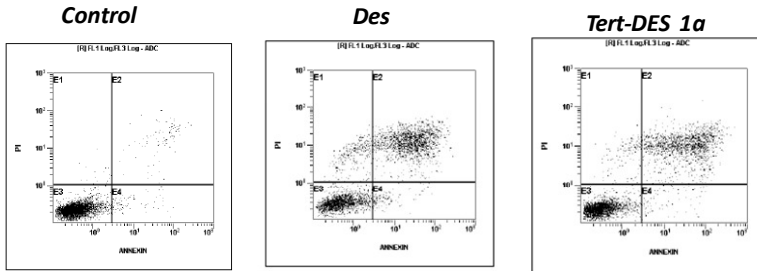


**Figure 4.3. 12** Typical histogram from FACS analysis after AnnexinV-PI test. Single parameter histograms are shown at the top (Annexin) and on the right side (PI) of the diagram. Two parameter histograms are shown in quadrants E1-E4.

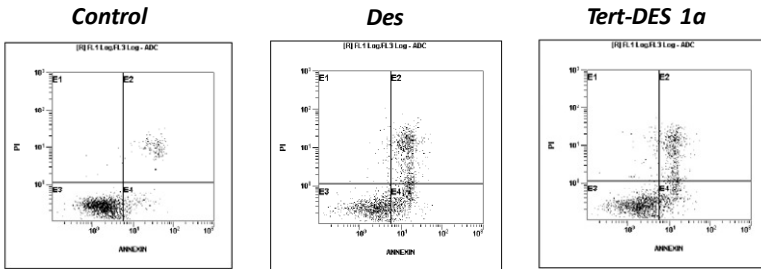
Herein, cell death analysis for *Block-DES* and *Tert-DES* in PC3 and in LNCaP cells was carried out Figure 4.3. 13 shows an example of the histograms obtained for the control, free DES and the *Tert-DES 1a* in both prostate cancer cell lines.

All molecular mechanism studies were performed using the corresponding  $IC_{50}$  concentration determined for all DES derivatives ( $IC_{50}$ , 0.060 mg/ml for Na DES, 0.052 mg/ml for *Block-DES* and 0.172 mg/ml for *Tert-DES* against PC3 cells; 0.044 mg/ml for NaDES, 0.049 mg/ml for *Block-DES* and 0.070 mg/ml for *Tert-DES* against LNCaP cells).

**PC3**

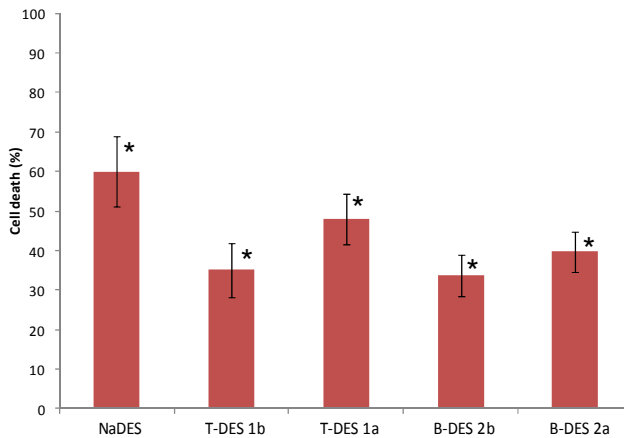


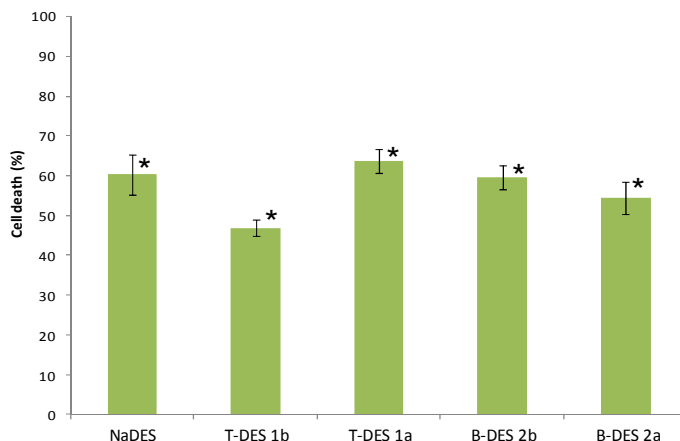
**LNCaP**



**Figure 4.3. 13** Example of obtained histogram from FACS analysis after AnnexinV-PI test. PC3 and LNCaP Cell lines were cultivated with the drug alone and DES-polyacetals. Cells were stained with Annexin-V and PI, then incubated and analyzed.

**A.**



**B.**

**Figure 4.3. 14** Annexin-PI test with *Tert*-DES and *Block*-DES polyacetals in PC3 (A) and LNCaP (B) cell lines. Data are expressed as mean  $\pm$  SD ( $n \geq 3$ ). \*  $p < 0.05$ . Cell death (%) expressed as Annexin V-positive cells (quadrants E2+E4)

DES-Polyacetals induced slightly more cell death in LNCaP (Figure 4.3.14B) than in PC3 (Figure 4.3.14A) cells, probably due to the hormone-dependent property presented in the LNCaP line vs. the androgen independence in PC3. These differences were not observed for free DES.

**Table 4.3. 2** Annexin V-PI studies at 24h for *Tert*-DES and *Block*-DES. Data are expressed as mean  $\pm$  SEM ( $n \geq 3$ ).

Annexin/PI (% <sup>cd</sup> )	Control	NaDES	Tert-DES		Block-DES	
			<i>1a</i>	<i>1b</i>	<i>2a</i>	<i>2b</i>
<b>PC3</b>	7.76 $\pm$ 0.4	60 $\pm$ 8.8	48 $\pm$ 6.5	35 $\pm$ 6.9	40 $\pm$ 5.1	33 $\pm$ 5.2
<b>LNCaP</b>	4.27 $\pm$ 0.8	60 $\pm$ 4.1	62 $\pm$ 5	46 $\pm$ 3.3	55 $\pm$ 6.9	60 $\pm$ 5.8

Where %<sup>cd</sup> is the percentage of Annexin V positive cells (*1a* 2.8wt%DES, *1b*; 4wt%DES, *2a*; 2wt%DES and *2b*; 4.3wt%DES).

Regarding drug loading influence, whereas *Tert*-DES behavior was clearly dependent on loading independently on the cell line used with greater percentage of cell death with the lowest DES loaded conjugate (*1a*), Block-DES pattern was influenced by the cell line tested as no significant differences



in activity with polyacetal **2a** (2 wt%DES) vs. **2b** (4.3 wt% DES) were observed in LNCaP cells (Figure 4.3.14B and Table 4.3.1)

#### 4.3.3.2 Cell cycle analysis

Cell cycle analysis after 24h treatment with the DES derivatives showed to be highly dependent on the cell line used and in the polyacetal conformation.

In the PC3 cell line, *Block*-DES (**2a** and **2b**) seemed to modulate proteins involve in the regulation of the S phase. However, *Tert*-DES (**1a** and **1b**) arrested cells at the G2/M phase (Table 4.3.3 and Figure 4.3. 15). On the hand, in LNCaP cells (Table 4.3.4 and Figure 4.3. 16) no significant differences were observed within the polyacetals as in all cases cells were arrested in G0/G1 phase. In any case no significant differences were encountered if different DES loadings were compared.

This data clearly reflected the importance of cell line selection together with the treatment to be analyzed, the major differences could be triggered due to the endocrine character of DES and the different androgen dependence of the two cell lines studied.

**Table 4.3. 3** Cell cycle in PC3 cell line for Ter-DES (*1a* and *1b*) and Block-DES (*2a* and *2b*). Data are expressed as mean  $\pm$  SEM (n  $\geq$  3).

	<b>G0/G1</b>	<b>S</b>	<b>G2/M</b>
<b>DES</b>	41.4 $\pm$ 10.0	43.7 $\pm$ 14.8	14.7 $\pm$ 4.8
<b><i>Tert</i>-DES 1b</b>	22.5 $\pm$ 0.1	18.2 $\pm$ 12.2	55.8 $\pm$ 12.3
<b><i>Tert</i>-DES 1a</b>	21.4 $\pm$ 8.7	27.8 $\pm$ 7.8	50.7 $\pm$ 4.5
<b><i>Block</i>-DES 2b</b>	33.9 $\pm$ 6.1	39.9 $\pm$ 5.5	26.1 $\pm$ 2.9
<b><i>Block</i>-DES 2a</b>	32.7 $\pm$ 7.4	43.4 $\pm$ 8.7	23.8 $\pm$ 10.5

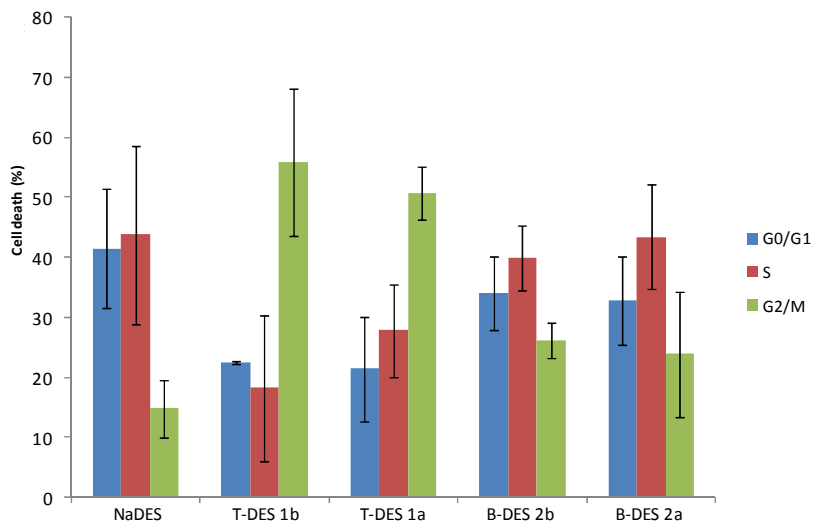


**Figure 4.3. 15** Cell cycle study for *Tert*-DES and *Block*-DES polyacetals in PC3 cell line. Data are expressed as mean  $\pm$  SD ( $n \geq 3$ ). \*  $p < 0.05$ .

**Table 4.3. 4** Cell cycle in LNCaP cell line for *Ter*-DES (*1a* and *1b*) and *Block*-DES (*2a* and *2b*). Data are expressed as mean  $\pm$  SEM ( $n \geq 3$ ).

	<b>G0/G1</b>	<b>S</b>	<b>G2/M</b>
<b>DES</b>	66.8 $\pm$ 1.8	15.1 $\pm$ 0.9	18.1 $\pm$ 0.9
<b><i>Tert</i>-DES 1b</b>	71.7 $\pm$ 4.2	14.5 $\pm$ 3.1	13.7 $\pm$ 1.1
<b><i>Tert</i>-DES 1a</b>	61.9 $\pm$ 10.3	28.4 $\pm$ 11	9.7 $\pm$ 1.2
<b><i>Block</i>-DES 2b</b>	65.9 $\pm$ 1.9	9.5 $\pm$ 4.2	24.6 $\pm$ 2.2
<b><i>Block</i>-DES 2a</b>	71.2 $\pm$ 6.2	14.5 $\pm$ 6.9	12.4 $\pm$ 4.0

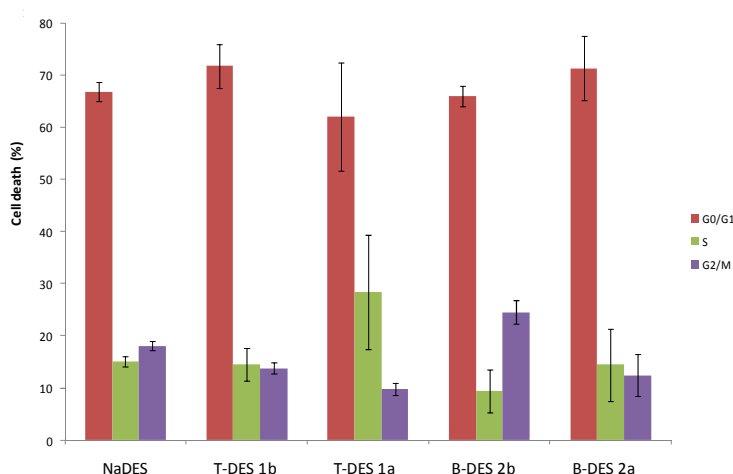


**Figure 4.3. 16** Cell cycle in LNCaP cell line for Tert-DES and Block-DES.

Complementary studies focused on the Akt route were carried out in order to fully understand the differences encountered so far by trying to evaluate the relation of this pathway with autophagy, apoptosis and cellular cycle. Western Blot was used to analyze the level of expression of key proteins in these three molecular machineries.

#### **4.3.3.3. Determination of Akt, Autophagy and Apoptosis-Related Proteins by Protein Immunoblotting.**

Protein immunoblotting of apoptosis-related proteins was studied using four specific markers, namely: caspase-3, Bcl2, p53 and Bax. To determine the possible involvement of an autophagy signaling pathway the protein LC3B was also studied (Figure 4.3.17). In all cases, 40 $\mu$ g extracted protein was upload and  $\beta$ -actine was used as loading control.

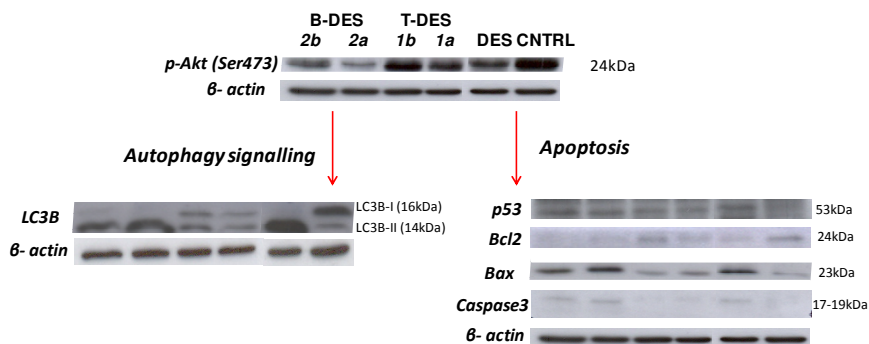


**Figure 4.3. 17** Protein immunoblotting/western blotting of Akt pathway, autophagy and apoptosis-related proteins in PC3 prostate adenocarcinoma cell line. The treatment was done with *Tert*-DES (*1a, 1b*) and *Block*-DES (*2b, 2b*).

*Akt pathway.* Akt will be activated after phosphorylation (p-Akt). The control sample showed that p-Akt was highly expressed while in those cells treated with DES derivatives the p-Akt expression was downregulated, being this effect more important with the *Block*-DES. *Block*-DES *2a*, with less than 3wt%DES showed less p-Akt protein expression than *Block*-DES *2b* with more than 3wt%DES showing the influence of drug loading on Akt pathway. Probably due to the different DES release kinetics and therefore a different DES dose present after 24 h in each case. It is clear that protein expression is time- and concentration-dependent.

*Autophagy.* Looking the protein-expression study for autophagy, *Block*-DES showed upregulation of LC3B. Contrary to *Block*-DES, *Tert*-DES showed downregulation of LC3B, which can be observed for both LC3B component proteins, LC3B-I and LC3B-II. The fact of observing both proteins could be explained by a slower process for *Tert*-DES in the conversion from LC3B-I into LC3B-II (Figure 4.3. 17).

*Apoptosis.* Protein immunoblotting results indicated that compared with controls, the expression of p53, Caspase-3 and Bax proteins was higher in PC3 cells treated with *Block*-DES than with *Tert*-DES. However, Bcl-2 was downregulated in the treatment of PC-3 cells with *Block*-DES, this could indicate the proapoptotic character of this nanoconjugate. *Tert*-DES showed upregulation of Bcl2 and p53 together with a downregulation for Bax and Caspase-3 protein. Bcl2 and Bax are part of the mitochondrial apoptotic cell

death pathway, thus when Bcl2 is expressed, Bax should be downregulated, this is in good agreement with our results.

*Cell cycle*. P21 is a protein highly involved in cell cycle and clearly correlated with p53 that could show correlation with apoptosis. Therefore the expression of these two proteins were studied in presence of our DES derivatives (Figure 4.3. 18)

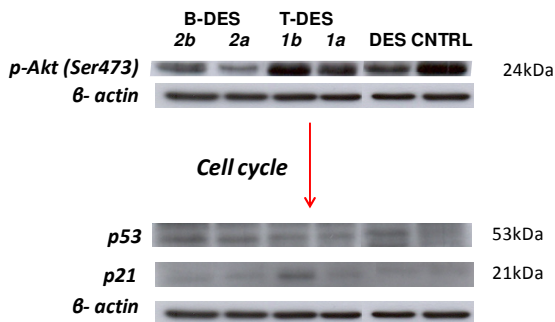


**Figure 4.3. 18** Protein immunoblotting of cell cycle-related proteins in PC3 cell line upon incubation in presence of free DES, *Tert-DES I* and *Block-DES 2*.

The western blotting results compared with controls showed that the expression of p21 was higher in PC3 cells treated with *Tert-DES* than with *Block-DES*, being even greater for *1b* with more than 3wt% of DES than with *Tert-DES 1a*. P21 is a protein involved in G2 and Mitosis phases in cell cycle. It indicated that the cell cycle stopped between G2/M by inhibition of cycline B and Cdk1 production, taking place an accumulation in G2 phase (Figure 4.3. 19). This data was in good agreement with the previous data obtained in the cell cycle studies by FACS (Figure 4.3. 15).

P53 was up-regulated with both *Block-* and *Tert-DES* treatment indicating cell death induction.

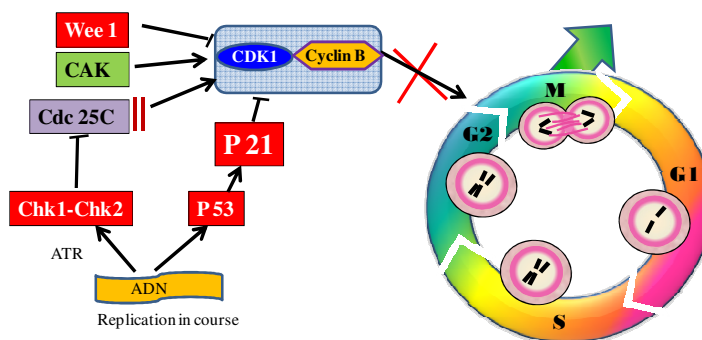


**Figure 4.3. 19** Schematic representation of the relationship of the protein p21 involved in cell cycle.

Protein immunoblotting of apoptosis-related proteins was also performed in the androgen sensitive LNCaP prostate adenocarcinoma cell line. The proteins used involved in apoptosis were p53, Bax and caspase-3 (Figure 4.3. 20).

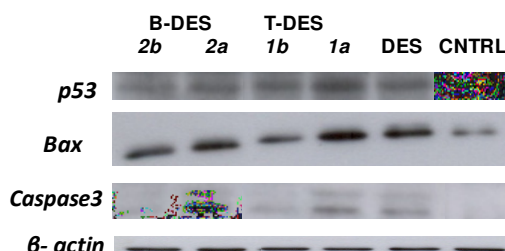


**Figure 4.3. 20** Western blotting of proteins related with apoptosis in LNCaP cell line. Cells were incubated in absence and presence of DES, *Tert*-DES and *Block*-DES polyacetals for 24 h.

Protein immunoblotting study showed that the expression of p53, Caspase-3 and Bax proteins was higher in LNCaP cells treated with *Block*-DES and *Tert*-DES with DES loading lower than 3wt% probably due to a faster DES released and therefore greater free DES content after 24 hours incubation.

Summarizing, cell studies based in cytometry and western blotting assays demonstrated that both polymer behave similarly following akt pathway in both prostate cancer cell lines although the property of being hormono sensitive for LNCaP makes slightly different results which better results for the block-DES and with higher drug loading. Further experiments will be take place in order to elucidate if DES provokes autophagy in the cells.

#### 4.3.4. *In vivo* studies in xenograft mice models.

It is important to note here that all the *in vivo* studies were performed by our collaborators at CIBBIM-Nanomedicine Vall d'Hebron Hospital, Barcelona, Dr. Ibane Abasolo, Dr. Yolanda Fernández and Dr. Simó Schwartz Jr.

##### 4.3.4.1. Body weight studies

Preliminary *in vivo* studies were carried out using *Tert*-DES **1b** and *Block*-DES **2b** to determine in a first stage polymer toxicity after their i.v. administration (Figure 4.3. 21).

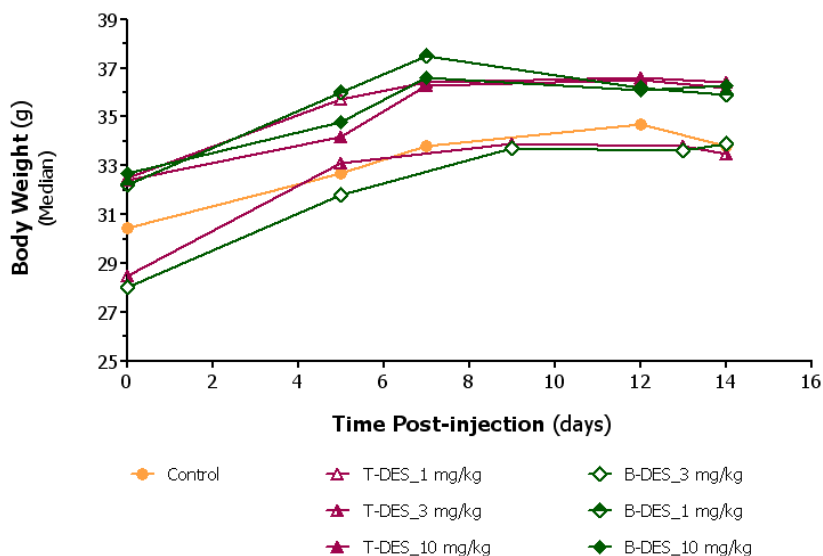


**Figure 4.3. 21** Body weight control for CD1 mice after polyacetal i.v. administration.

It was found that a single i.v. dose of 10 mg/kg of DES polymers did not induce any significant loss of weight in CD1 mice and they did not alter the blood levels of 10 different biological parameters regarding kidney, liver and muscle functionality (BILT, total proteins, AST, ALT, CK, LDH, Alb, creatinin and urea) (Table 4.3. 4).

**Table 4.3. 4** Biochemical parameters for CD1 mice after polyacetal i.v. administration.

	BILT (mg/dL)	Proteínas Totales (g/dL)	AST (U/L)	ALT (U/L)	CK (U/L)	LDH (U/L)	Albumina (g/dL)	Creatinina (mg/dL)	Urea (mg/dL)	
<b>CONTROL</b>	0,17 ± 0,04	4,12 ± 0,27	66 ± 38	24 ± 4,8	429,2 ± 484,3	375,6 ± 148,4	2,263 ± 0,184	0,306 ± 0,012	36,4 ± 6,8	
<b>DES</b>	1mg/kg	0,19 ± 0,01	4,10 ± 0,37	41 ± 10	18 ± 2,8	187,4 ± 111,0	288,7 ± 73,8	2,262 ± 0,128	0,280 ± 0,010	43,1 ± 6,0
	3mg/kg	0,18 ± 0,01	4,40 ± 0,11	68 ± 18	23 ± 6,2	182,5 ± 145,0	383,4 ± 124,6	2,480 ± 0,086	0,293 ± 0,031	42,8 ± 6,1
	10 mg/kg	0,15 ± 0,02	4,30 ± 0,30	52 ± 6	24 ± 11,8	293,0 ± 128,2	483,8 ± 87,7	2,436 ± 0,128	0,290 ± 0,016	42,8 ± 2,7
<b>DES</b>	1mg/kg	0,18 ± 0,05	4,18 ± 0,21	64 ± 24	22 ± 0,8	224,6 ± 298,5	339,0 ± 186,9	2,302 ± 0,110	0,302 ± 0,012	47,3 ± 6,0
	3mg/kg	0,18 ± 0,07	4,31 ± 0,40	77 ± 47	26 ± 4,8	648,4 ± 726,4	451,0 ± 226,7	2,480 ± 0,180	0,287 ± 0,038	46,8 ± 4,6
	10 mg/kg	0,16 ± 0,02	4,21 ± 0,28	63 ± 32	21 ± 4,8	237,5 ± 408,2	391,4 ± 143,8	2,338 ± 0,128	0,274 ± 0,028	42,8 ± 8,7

#### 4.3.4.2. *In vivo* biodistribution and tumor accumulation in a xenograft mouse model.

Biodistribution studies allow following the compound of interest into the body once it is i.v. administrated through the vein tail. To carry out the biodistribution experiment optical image was used and therefore Cy5 labeled conjugates were synthesized see detailed information in chapter 4.2). NIR properties of Cy5.5. dye allow better tissue penetration than a normal fluorescence probe, such as OG. At different intervals of time, the animals were euthanized and dissected to take the organs of interest (usually blood, liver, spleen, kidney, pancreas, brain, bone, stomach, and upper and lower large intestine). Quantification of Cy5.5. in each organ was also performed and expresses as  $\mu\text{gdye/g}$  tissue. NIR scanner was used to quantitatively assess Cy5.5 signal at 21 micrometer resolution. Each tissue was imaged using the IVIS-100 (Xenogen Co., Alameda, CA).

To carry out preliminary information on *in vivo* polymer fate, HT-29 Firefly luciferase (Fluc)-C4 human colon cancer cells ( $0.25 \times 10^6$  cells/100 $\mu\text{l}$  DPBS) were injected s.c. in the rear right flank in female athymic nu/nu mice to gain a well-vascularized xenograft model.

*Tert*-DES-Ser-Cy5.5 **10a** (4.3 wt% DES loading) was administered to 3 mice intravenously (i.v.) once a week at different doses: 3.5, 5 and 7 mg/Kg in order to determine the effective dose to be used in exhaustive biodistribution and activity experiments (Figure 4.3. 22). Tumor volume was measured twice a week by caliper measurements and bioluminescence imaging. The volume was calculated according to the formula  $D \times d^2/2$  and the bioluminescence signal was quantified in photons per second.



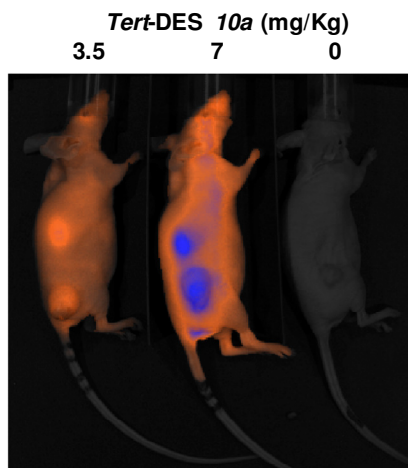


**Figure 4.3. 22** Tumor accumulation; *In vivo* fluorescence imaging of subcutaneous Xenograft models after 3 days of intravenous injection of 3.5, 5 and 7 mg/kg *Tert*-DES-Ser-Cy5.5 polyacetal **10a**.

As expected, the conjugate was accumulated into the tumor in a dose- and time-dependent manner, being the highest dose used (7 mg/kg) much more efficient in inducing compound tumor accumulation. Then, bolus injection of high doses of the compounds may be favoring tumor accumulation in good agreement with previously reported preclinical studies with polymer-drug conjugates<sup>98</sup>. Therefore, 7 mg/kg was selected for further studies.

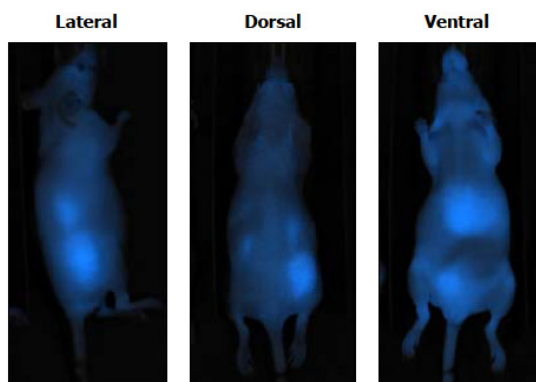


**Figure 4.3. 23** Tissue accumulation; Cyane fluorescence detected into tumor, kidneys, liver and urine by *in vivo* fluorescence imaging after 3 days of i.v. injection of 7 mg/kg **10a**.

It was also observed that *Tert*-DES-Ser-Cy5.5 **10a** was accumulated mainly in the kidneys and in the liver, apart from the tumor. Thus, the polymer small fragments might be being eliminated by renal excretion, and the large fragments (aggregates as determined by SANS) through the hepatic excretory system, however this hypothesis should be still fully demonstrated (Figure 4.3. 23).

To corroborate the above observations, a longer study was carried out up to two weeks with the selected 7 mg/kg dose (Figure 4.3. 24).

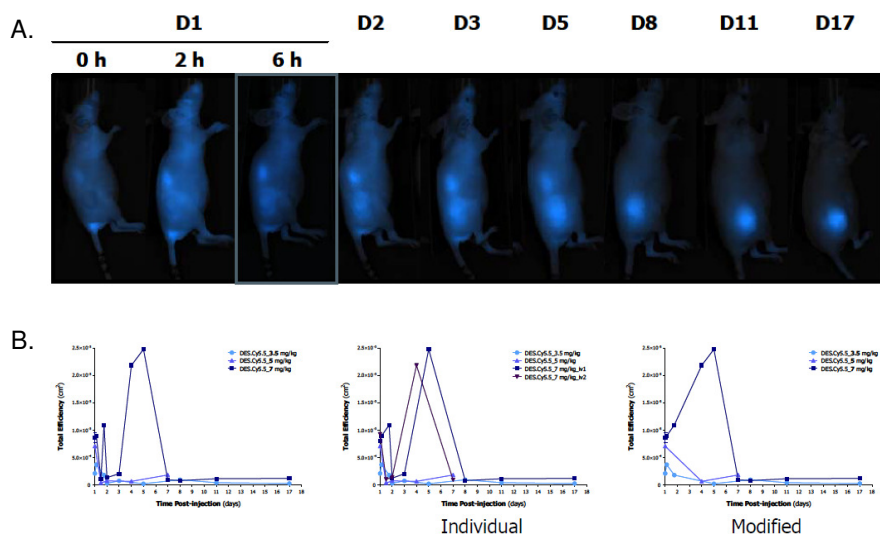


**Figure 4.3. 24** *Tert*-DES-Ser-Cy5.5 tumor accumulation results. **A.** *In vivo* fluorescence imaging of subcutaneous HT-29 colon bearing mice after i.v. injection of 7 mg/kg of Cy5.5-labelled-*Tert*-DES **10a** polyacetal. The tumor accumulation can be easily visualized at 6h-17days (D=day) postinjection. **B.** The fluorescence intensity was recorded and quantified as Efficiency over time.

The *Tert*-DES-Ser-Cy5.5 (7 mg/kg) tumor accumulation started at 6 h, being maximum after 4 or 5 days, and was maintained for up to 17 days post-injection. *Tert*-DES-Ser-Cy5.5 was again detected mainly in the tumor, kidneys and in the liver.

Once demonstrated an efficient tumor accumulation also a preliminary antitumor activity with *Tert*-DES and *Block*-DES was performed in a PC3 xenograft model established at CIBBIMM\_Nanomedicine. It was proposed to carry out the dose-dependent *Tert*- and *Block*-DES-Ser-Cy5.5 biodistribution assay using prostate cancer cells (PC3) trying to increase the dose from 7mg/Kg to 10 and 30mg/Kg, once at week using Cy5.5 and PBS as controls and taking time-course at 1, 4, 5, 6, 7 and 8 days. FRI quantification and BLI quantification were the selected techniques to quantify the compound accumulation and the tumor growth inhibition respectively.

#### ***4.3.4.3. Antitumoral effect on subcutaneous PC-3 tumors in Athymic nu/nu mice.***

In this case the mice were male Hsd:Athymic Nude-Foxn1nu and the cell line to be injected subcutaneously was the PC-3 Fluc human prostate cancer. As the previous experiment, mice received a subcutaneous (s.c.) tumor cell injection (in this case  $5 \times 10^6$  cells/100 $\mu$ l DPBS) in the rear right flank and thereafter were treated with the test substance.

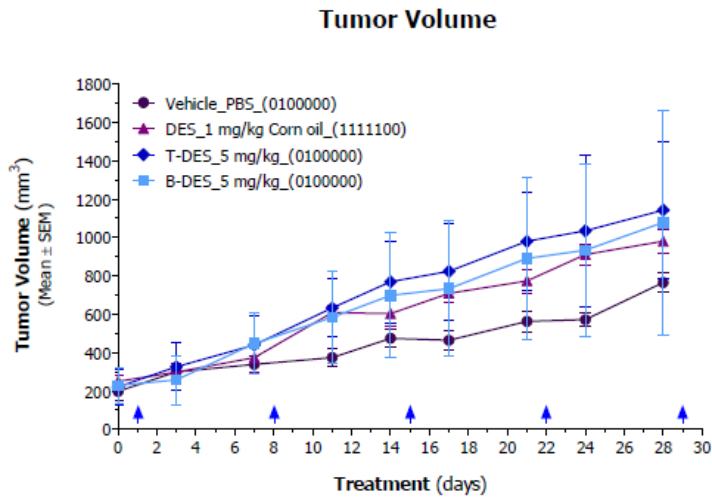
For tumor growth inhibition studies *Tert*-DES **1b** and *Block*-DES **2b**, (drug loading of 4wt%DES) were used.

- **Tumor volume and tumor growth studies**

The treatment consisted in the oral gavage administration in mice of 1mg/kg of DES once at day during 5days (binary representation; 1111100) and i.v. administration of 5mg/kg of the DES-polyacetals once at week (binary representation; 01000000) (Figure 4.3. 25).

The volume (Figure 4.3. 25A) and growth (Figure 4.3. 25B) of the tumor were measured during 32 days.. Unfortunately, the results showed that DES-polyacetalic systems do not show a tumor growth delay. It could be due to the need of a greater dose. However, the water solubility of these polyacetals, at this point, was limited and thus, other alternatives were sought, from the synthetic protocols (Chapter 3) to the use of combination therapy (Chapter 5).

A.



B.

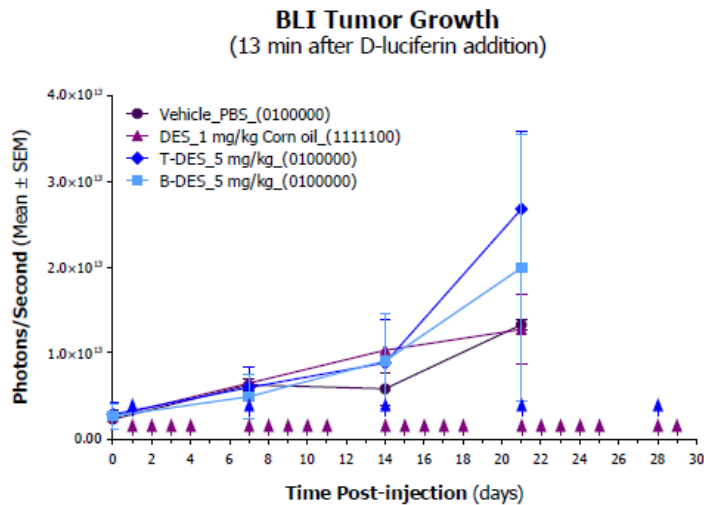
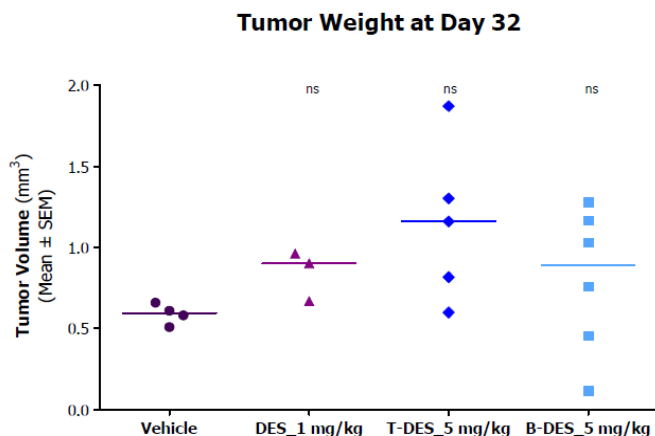


**Figure 4.3. 25** Tumor growth inhibition. Comparative analysis of the localized subcutaneous growth of PC3-Fluc prostate cancer cells treated with the DES, *Tert*-DES and *Block*-DES in athymic nude mice by external measurements of tumor volume (A), and by tumor bioluminescent signals (B).

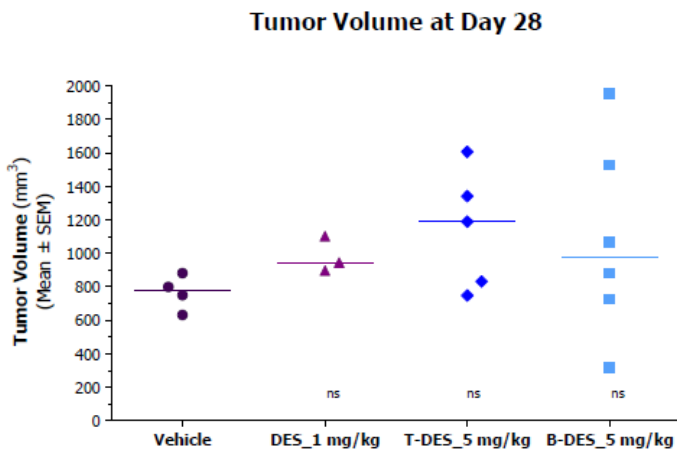
It is important to note that DES-polyacetals did not show any sign of toxicity and were very well tolerated by mice. To get a closer look to tumor progression last day of the experiment (day 32) tumors were extracted and

weighted (Figure 4.3. 26). Non-significant differences between *Tert*-DES and the *Block*-DES were observed.

A.

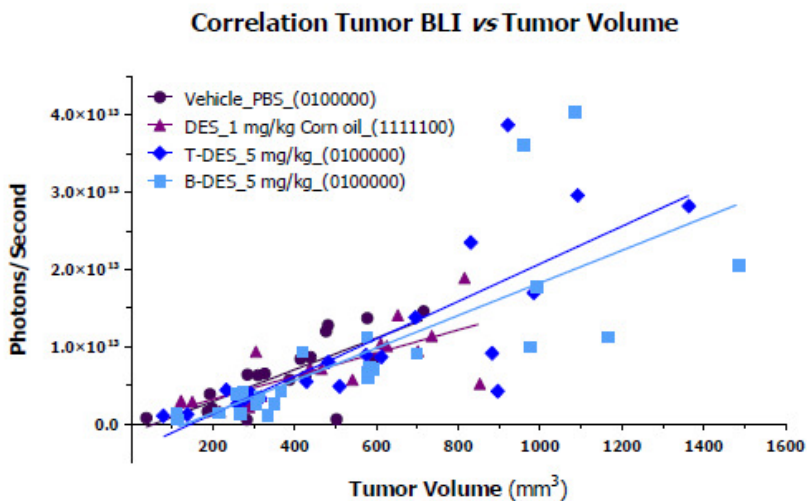


B.



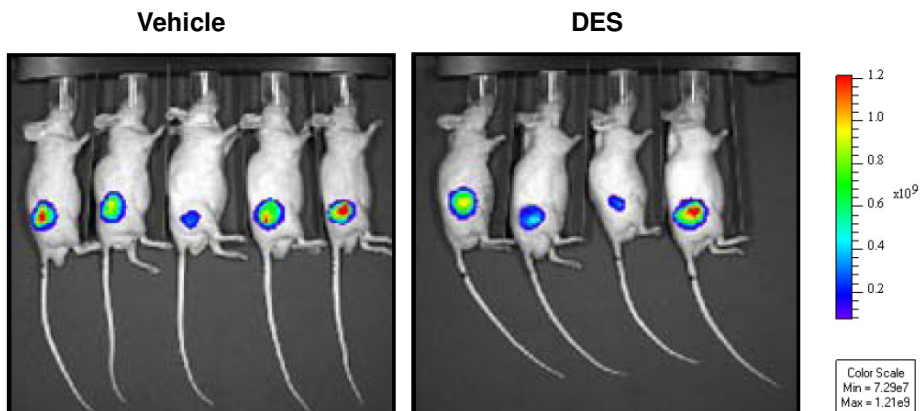
**Figure 4.3. 26** Effect of the DES-polyacetals (*tert*-DES **1b** and *block*-DES **2b**) on Tumor Weight (A) and Tumor Volume (B) at the end of the experiment. Scatter plots show all values with the median values represented by a bar. Statistical analysis was done using a Dunn's Multiple Comparison test.

A correlation study between tumor volume and bioluminescence (Figure 4.3 27) corroborated the conclusions previously obtained.



**Figure 4.3. 27** Correlation between tumor volume and bioluminescence. The correlation  $r^2$  value was 0.5793 ( $p=0.0002$ ), 0.5436 ( $p=0.0007$ ), 0.6384 ( $p<0.0001$ ) and 0.5610 ( $p<0.0001$ ) for vehicle, DES, *Tert*-DES-Ser-Cy **10a** and *Block*-DES-Ser-Cy **11a**, respectively.

Figure 4.3. 28 shows the images of *in vivo* monitoring of subcutaneous PC3.Fluc tumor growth after 29 days DES-polyacetals treatment.



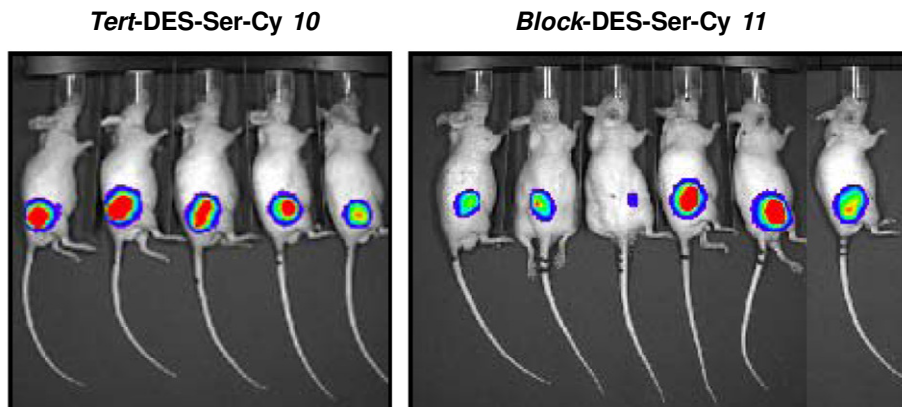


**Figure 4.3. 28** Representative images of the mice at day 21 after treatment with DES 1mg/kg or *Tert*- or *Block*-DES (*1b* and *2b* resp.) at 5mg/kg for 29days. Images were set at the same pseudocolor scale to show relative bioluminescent changes over time.

Body weight was also taken (Figure 4.3. 29) to ensure the DES-polyacetals does not make any variance in mice weight and to rule out any possibility of damage from DES-polyacetals to mice.

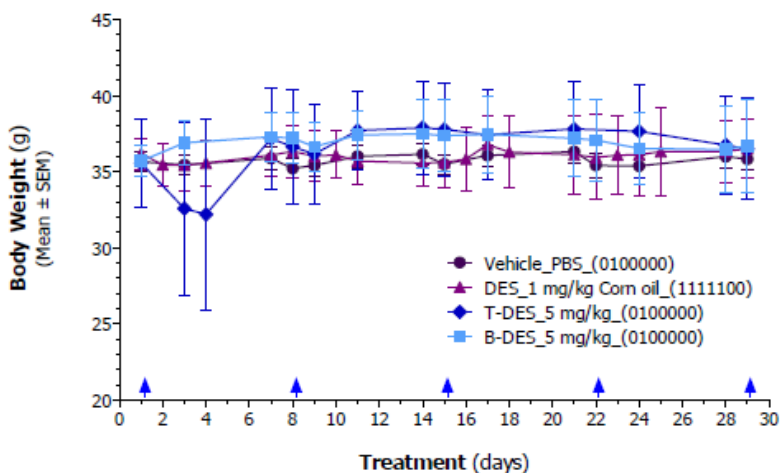


**Figure 4.3. 29** Body weight profiles of treated mice.

The body weight gain of DES and both DES-polyacetals were monitored at administration day along the experiment and was not observed any change in the mice's weight<sup>1</sup>.

Summarizing, the dose of 1mg/kg of DES during five days a week, and the 5mg/kg of the DES-polyacetals, *Tert*-DES **1b** and *Block*-DES **2b**, once at week did not induce tumor growth delay. Importantly, it was shown that either DES or DES-polyacetals induced animal body weight loss.

Due to the results obtained it was proposed to move a step further in order to improve the system and develop advanced conjugates by means of combination therapy approach to treat prostate cancer. The design, synthesis, characterization and biological evaluation in vitro and in vivo of DES-based combination polyacetals is described in Chapter 5.

---

<sup>1</sup> During the experiment some events, including deaths at different days occurred. In the control group, 1 animal was put down at day 7 of treatment due to penis prolapsed, in DES group at day 14, 1 animal was found death and other was put down due also to penis prolapsed and in the *Tert*-DES group, 1 animal was put down due to lesions produced by a fight between the animals. However in the group of *Block*-DES was not found any animal death.



## References

1. Vicent, M. J.; Dieudonné, L.; Carbajo, R. J.; Pineda-Lucena, A., Polymer conjugates as therapeutics: future trends, challenges and opportunities. *Expert Opinion Drug Delivery* **2008**, *5* (5), 593-614.
2. Hardwicke, J.; Ferguson, E. L.; Moseley, R.; Stephens, P.; Thomas, D. W.; Duncan, R., Dextrin-rhEGF conjugates as bioresponsive nanomedicines for wound repair. *J Control Release* **2008**, *130* (3), 275-83.
3. Erdmann, L.; Macedo, B.; Urich, K. E., Degradable poly(anhydride ester) implants: effects of localized salicylic acid release on bone. *Biomaterials* **2000**, *21* (24), 6-10.
4. Tomlinson, R.; Heller, J.; Brocchini, S.; Duncan, R., Polyacetal-doxorubicin conjugates designed for pH-dependent degradation. *Bioconjugate Chemistry* **2003**, *14* (6), 1096-1106.
5. Tomlinson, R.; Klee, M.; Garrett, S.; Heller, J.; Duncan, R.; Brocchini, S., Pendant Chain Functionalized Polyacetals That Display pH-Dependent Degradation: A Platform for the Development of Novel Polymer Therapeutics. *Biomacromolecules* **2002**, *35* (2), 473-480.
6. Vicent, M. J.; Tomlinson, R.; Brocchini, S.; Duncan, R., Polyacetal-diethylstilboestrol: a polymeric drug designed for pH-triggered activation. *J Drug Target* **2004**, *12* (8), 491-501.
7. Heller, J.; Penhale, D. W. H.; Helwing, R. F., Preparation of polyacetals by the reaction of divinyl ethers and polyols. *Journal of Polymer Science Part C: Polymer Letters* **1980**, *18* (4), 5.
8. Tang, H.D.; Murphy, C.J.; Zhang, B.; Shen, Y.Q.; Van Kirk, E.A.; Murdoch, W.J.; Radosz, M. Curcumin polymers as anticancer conjugates. *Biomaterials* **2010**, *31*(27), 7139-7149.
9. Giménez, V.; Craig, J.; Armiñán, A.; Schweins, R.; Paul, A.; Vicent, M.J. Demonstrating the importance of Polymer-Conjugate Conformation in Solution on its Therapeutic Output: Diethylstilbestrol (DES)-Polyacetals as Model Systems. *J. Control. Rel.* **2012**, *159*(2), 290-301

10. England, R.M.; Masiá, E.; Giménez, V.; Lucas, R.; Vicent, M.J. Polyacetal-Stilbene conjugates- the first examples of polymer therapeutics for the inhibition of HIF-1 in the treatment of solid tumours. *J. Control. Rel.* **2012**, *Accepted*
11. Cheow, W. S.; Hadinoto, K., Enhancing encapsulation efficiency of highly water-soluble antibiotic in poly(lactic-co-glycolic acid) nanoparticles: Modifications of standard nanoparticle preparation methods. *Colloid Surf. A-Physicochem. Eng. Asp.* **2011**, *370* (1-3), 79-86.
12. Laia, Z.-W.; Fiorea, N. C.; Hahn, P. J.; Gasiewicz, T. A.; Silverstone, A. E., Differential Effects of Diethylstilbestrol and 2,3,7,8-Tetrachlorodibenzo-p-dioxin on Thymocyte Differentiation, Proliferation, and Apoptosis in bcl-2 Transgenic Mouse Fetal Thymus Organ Culture. *Toxicol. Appl. Pharmacol* **2000**, *168* (1), 15-23.
13. Malkowicz, S. B., The Role of Diethylstilbestrol in the treatment of Prostate Cancer. *Urology* **2001**, *58* (Suppl 2A), 108-113.
14. Hartley-Asp, B.; Deinum, J.; Wallin, M., Diethylstilbestrol induces metaphase arrest and inhibits microtubule assembly. *Mut. Res. Lett.* **1985**, *143* (4), 231-235.
15. Metzler, M.; Pfeiffer, E., Effects of estrogens on microtubule polymerization in vitro: correlation with estrogenicity. *Environ. Health Perspect* **1995**, *103*, 21-23.
16. Geier, R.; Adler, S.; Rashid, G.; Klein, A., The Synthetic Estrogen Diethylstilbestrol (DES) Inhibits the Telomerase Activity and Gene Expression of Prostate Cancer Cells. *Prostate* **2010**, *70* (12), 1307-1312.
17. Sharp, D. C.; Parry, J. M., Diethylstilbestrol-The binding and effects of DES upon the polymerization and depolymerization of purified microtubule protein in vitro. *Carcinogenesis* **1985**, *6* (6), 865-871.
18. Kalach, J. J.; Joly-Pharaboz, M. O.; Chantepie, J.; Nicolas, B.; Descotes, F.; Mauduit, C.; Benahmed, M.; André, J., Divergent biological effects of estradiol and diethylstilbestrol in the prostate cancer cell line MOP. *J. Ster. Biochem. Mol. Biol.* **2005**, *96*, 119-128.

19. Frigault, M. M.; Lacoste, J.; Swift, J. L.; Brown, C. M., Live-cell microscopy: Tips and tools. *J. Cell Sci.* **2009**, *122*, 753-763.
20. Vicent, M. J.; Greco, F.; Nicholson, R. I.; Paul, A.; Griffiths, P. C.; Duncan, R., Polymer therapeutics designed for a combination therapy of hormone-dependent cancer. *Angew Chem Int Ed Engl* **2005**, *44* (26), 4061-6.
21. Vicent, M. J., Polymer-drug conjugates as modulators of cellular apoptosis. *AAPS J* **2007**, *9* (2), E200-7.
22. Satchi-Fainaro, R.; Puder, M.; Davies, J. W.; Tran, H. T.; Sampson, D. A.; Greene, A. K.; Corfas, G.; Folkman, J., Targeting angiogenesis with a conjugate of HPMA copolymer and TNP-470. *Nat. Med.* **2004**, *10*, 255-261.
23. Sun, S.-W., Efficiency improvements on nynhidrin method for amino acid quantification. *Journal of Food Composition and Analysis* **2006**, *19*, 112-117.
24. Mosmann, T., Rapid colorimetric assay for cellular growth and survival: application to proliferation and cytotoxicity assays. *Journal of Immunological Methods* **1983**, *65* (1-2), 55-63.
25. Vistica, D. T.; Skehan, P.; Scudiero, D.; Monks, A.; Pittman, A.; Boyd, M. R., Tetrazolium-based assays for cellular viability: a critical examination of selected parameters affecting formazan production. *Cancer Research* **1991**, *51* (10), 2515-2520.
26. Slater, T. F.; Sawyer, B.; Strauli, U., Studies on Succinate-Tetrazolium Reductase Systems. Iii. Points of Coupling of Four Different Tetrazolium Salts. *Biochimica et Biophysica Acta* **1963**, *77*, 383-393.
27. Denizot, F.; Lang, R., Rapid colorimetric assay for cell growth and survival. Modifications to the tetrazolium dye procedure giving improved sensitivity and reliability. *Journal of Immunological Methods* **1986**, *89* (2), 271-277.
28. Twentyman, P. R.; Luscombe, M., A study of some variables in a tetrazolium dye (MTT) based assay for cell growth and chemosensitivity. *British Journal of Cancer* **1987**, *56* (3), 279-285.

29. Sgouras, D.; Duncan, R., Methods for the evaluation of biocompatibility of soluble synthetic polymers which have potential for biomedical use: 1- Use of the tetrazolium- based colorimetric assay (MTT) as a preliminary screen for evaluation in vitro cytotoxicity. *Journal of Materials Science: Materials in Medicine* **1990**, *1* (2), 61-68.
30. Kean, T.; Roth, S.; Thanou, M., Trimethylated chitosans as non-viral gene delivery vectors: Cytotoxicity and transfection efficiency. *Journal of Controlled Release* **2005**, *103* (3), 643-653.
31. *Intravenous Administration*. Springhouse Corporation: Springhouse, PA, 2000t.
32. Richardson, S. C. W.; Wallom, K.-L.; Ferguson, E. L.; Deacon, S. P. E.; Davies, M. W.; Powell, A. J.; Piper, R. C.; Duncan, R., The use of fluorescence microscopy to define polymer localisation to the late endocytic compartments in cells that are targets for drug delivery. *J. Control. Release* **2008**, *127*, 1-11.
33. Day, R. N.; Schaufele, F., Imaging molecular interactions in living cells. *Mol. Endocrinol.* **2005**, *19*, 1675-1685.
34. Stephens, D. J.; Allan, V. J., Light microscopy techniques for live cell imaging. *Science* **2003**, *300*, 82-86.
35. Watson, P., Live cell imaging for target and drug discovery. *Drug News Perspect.* **2009**, *22*, 69-78.
36. Paul, A.; Vicent, M. J.; Duncan, R., Using small-angle neutron scattering to study the solution conformation of N-(2-hydroxypropyl)methacrylamide copolymer-doxorubicin conjugates. *Biomacromolecules* **2007**, *8* (5), 1573-9.
37. Barz, M.; Luxenhofer, R.; Zentel, R.; Kabanov, A. V., The uptake of N-(2-hydroxypropyl)-methacrylamide based homo, random and block copolymers by human multi-drug resistant breast adenocarcinoma cells. *Biomaterials* **2009**, *30* (29), 5682-5690.
38. Price, W. S., *Pulsed-field gradient nuclear magnetic resonance as a tool for studying translational diffusion: Part 1. Basic theory*. 1997; Vol. 9, p 299-336.

39. Price, W. S., Experiment and Application .Diffusion Fundamentals 2.Applications of Pulsed Gradient Spin-Echo NMR. Diffusion Measurements to Solution Dynamics and Organization. *The Open-Access Journal for the Basic Principles of Diffusion Theory* **2005**, 112.1-112.9.
40. Johnson, C. S., Diffusion ordered nuclear magnetic resonance spectroscopy: principles and applications. *Progress in Nuclear Magnetic Resonance Spectroscopy* **1999**, 34 (3-4), 203-256.
41. Finney, J. L., ISIS - A Resource for Neutron Studies of Condensed Matter. *Europhys. News* **1989**, 20, 1.
42. Ibel, K., *Guide to Neutron Research Facilities at the ILL, Scientific Coordination Office, ILL*. 1994.
43. Boland, B. C.; Whapham, S., *User Guide to Experimental Facilities at ISIS*. 1992.
44. Wilson, C. C., ISIS, the UK Spallation Neutron Source - a Guided Tour. *Neutron News* **1990**, 1, 14.
45. Riste, T., Neutron Beam Sources in OECD Countries. *Neutron News* **1995**, 6, 32.
46. Heenan, R. K.; King, S. M.; Turner, D. S.; Treadgold, J. R., SANS2d at the ISIS Second Target Station. In *ICANS-XVIII17th Meeting of the International Collaboration on Advanced Neutron Sources*, Santa Fe, New Mexico, April 25-29, 2005.
47. van de Hulst, H. C., *Light Scattering by Small Particles*. New York, 1957.
48. Livsey, I., Neutron scattering from concentric cylinders. Intraparticle interference function and radius of gyration. *J. Chem. Soc., Faraday Trans. 2* **1987**, 83 (8), 1445-1452.
49. Ottewill, R. H., *Small Angle Neutron Scattering* Special Publication No. 43 ed.; Royal Society of Chemistry: **1982**.
50. Reece, J.; Campbell, N. *Biology*, San Francisco: Benjamin Cummings. **2002**.

51. Dasgupta, S.; Srinidhi, S.; Vishwanatha, J. K., Oncogenic activation in prostate cancer progression and metastasis: Molecular insights and future challenges. *Journal of Carcinogenesis* **2012**, *11* (4), 39-50.
52. Roberts Jr., C. T., IGF-1 and prostate cancer. *Novartis Found Symp* **2004**, *262*, 193-9.
53. Hellowell, G. O.; Turner, G. D.; Davies, D. R.; Poulosom, R.; Brewster, S. F.; Macaulay, V. M., Expression of the type I insulin-like growth factor receptor is up-regulated in primary prostate cancer and commonly persists in metastatic disease. *Cancer Res* **2002**, *62*, 2942-50.
54. Burfeind, P.; Chernicky, C. L.; Rininsland, F.; Ilan, J., Antisense RNA to the type I insulin-like growth factor receptor suppresses tumor growth and prevents invasion by rat prostate cancer cells in vivo. *Proceedings of the National Academy of Sciences of the United States of America* **1996**, *93*, 7263-8.
55. Safarinejad, M. R.; Shafiei, N.; Safarinejad, S., Relationship of insulin-like growth factor (IGF) binding protein-3 (IGFBP-3) gene polymorphism with the susceptibility to development of prostate cancer and influence of serum of IGF-1, and IGFBP-3. *Growth Horm IGF Res* **2011**, *21*, 146-54.
56. Massoner, P.; Colleselli, D.; Matscheski, A.; Pircher, H.; Geley, S.; Jansen Dürr, P.; al., e., Novel mechanism of IGF-binding protein-3 action on prostate cancer cells; inhibition of proliferation, adhesion, and motility. *Endocr. Relat. Cancer* **2009**, *16*, 795-808.
57. Shahjee, H.; Bhattacharyya, N.; Zappala, G.; Wiench, M.; Prakash, S.; Rechler, M. M., An N-terminal fragment of insulin-like growth factor binding protein-3 (IGFBP-3) induces apoptosis in human prostate cancer cells in an IGF-independent manner. *Growth Horm IGF Res* **2007**, *18*, 188-97.
58. Aggarwal, R. R.; Ryan, C. J.; Chan, J. M., Insulin-like growth factor pathway: A link between androgen deprivation therapy (ADT), insulin resistance, and disease progression in patients with prostate cancer? *Urol Oncol* **2011**, [In Press].

59. Fürstenberger, G.; Senn, H.-J., Insulin-like growth factors and cancer. *The Lancet Oncology* **2002**, *3* (5), 298-302.
60. Culig, Z.; Hobisch, A.; Cronauer, M. V.; Radmayr, C.; Trapman, J.; Hittmair, A.; Bartsch, G.; Klocker, H., Androgen receptor activation in prostatic tumor cell lines by insulin-like growth factor-I, keratinocyte growth factor, and epidermal growth factor. *Cancer Res* **1994**, *54* (20), 5474-8.
61. Fan, W.; Yanase, T.; Morinaga, H.; Okabe, T.; Nomura, M.; Daitoku, H.; Fukamizu, A.; Kato, S.; Takayanagi, R.; Nawata, H., Insulin-like growth factor 1/insulin signaling activates androgen signaling through direct interactions of Foxo1 with androgen receptor. *J Biol Chem.* **2007**, *282* (10), 7329-38.
62. Sroka, I. C.; McDaniel, K.; Nagle, R. B.; Bowden, G. T., Differential localization of MT1-MMP in human prostate cancer tissue: role of IGF-1R in MT1-MMP expression. *Prostate* **2008**, *68* (5), 463-76.
63. Marelli, M. M.; Moretti, R. M.; Procacci, P.; Motta, M.; Limonta, P., Insulin-like growth factor-I promotes migration in human androgen-independent prostate cancer cells via the alphavbeta3 integrin and PI3-K/Akt signaling. *Int J Oncol.* **2006**, *28* (3), 723-30.
64. Kharaihvili, G.; Simkova, D.; Makharoblidze, E.; Trtkova, K.; Kolar, Z.; Bouchal, J., Wnt signaling in prostate development and carcinogenesis. *Biomed Pap Med Fac Univ Palacky Olomouc Czech Repub* **2011**, *155* (1), 11-8.
65. Yee, D. S.; Tang, Y.; Li, X.; Liu, Z.; Guo, Y.; Ghaffar, S.; McQueen, P.; Atreya, D.; Xie, J.; Simoneau, A. R.; Hoang, B. H.; Zi, X., The Wnt inhibitory factor 1 restoration in prostate cancer cells was associated with reduced tumor growth, decreased capacity of cell migration and invasion and a reversal of epithelial to mesenchymal transition. *Mol Cancer* **2010**, *9*, 162.
66. Uysal-Onganer, P.; Kawano, Y.; Caro, M.; Walker, M. M.; Diez, S.; Darrington, R. S.; Waxman, J.; Kypta, R. M., Wnt-11 promotes neuroendocrine-like differentiation, survival and migration of prostate cancer cells. *Mol Cancer* **2010**, *10* (9), 55.

67. Surh, Y.-J., Cancer chemoprevention with dietary phytochemicals. *Nature Reviews Cancer* **2003**, *3*, 768-780.
68. Zhou, L.; An, N.; Haydon, R. C.; Zhou, Q.; Cheng, H.; Peng, Y.; Jiang, W.; Vanichakarn, P.; Szatkowski, J. P.; Park, J. Y.; Breyer, B.; He, T. C., Tyrosine kinase inhibitor STI-571/Gleevec down-regulates the b-catenin signaling activity *Cancer Letters* **2003**, *193* (2), 161-170.
69. Yardy, G. W.; Brewster, S. F., Wnt signalling and prostate cancer. *Prostate Cancer Prostatic Dis* **2005**, *8* (2), 119-126.
70. Davies, G.; Jiang, W. G.; Mason, M. D., Cell-cell adhesion molecules and signaling intermediates and their role in the invasive potential of prostate cancer cells. *J Urol* **2000**, *163*, 985-992.
71. Bryden, A. A.; Hoyland, J. A.; Freemont, A. J.; Clarke, N. W.; Schembri Wismayer, D.; George, N. J., E-cadherin and beta-catenin are down-regulated in prostatic bone metastases. *Br J Urol Int* **2002**, *89* (4), 400-403.
72. McDonagh, E. M.; Whirl-Carrillo, M.; Garten, Y.; Altman, R. B.; Klein, T. E., From pharmacogenomic knowledge acquisition to clinical applications: the PharmGKB as a clinical pharmacogenomic biomarker resource. *Biomarkers in Medicine* **2011**, *5* (6), 795-806.
73. Epis, M. R.; Giles, K. M.; Barker, A.; Kendrick, T. S.; Leedman, P. J., miR-331-3p regulates ERBB-2 expression and androgen receptor signaling in prostate cancer. *J Biol Chem* **2009**, *284*, 24696-704.
74. Cai, C.; Portnoy, D. C.; Wang, H.; Jiang, X.; Chen, S.; Balk, S. P., Androgen receptor expression in prostate cancer cells is suppressed by activation of epidermal growth factor receptor and ErbB2 *Cancer Res* **2009**, *69*, 5202-9.
75. Nishio, Y.; Yamada, Y.; Kokubo, H.; Nakamura, K.; Aoki, S.; Taki, T.; al., e., Prognostic significance of immunohistochemical expression of the HER-2/neu oncoprotein in bone metastatic prostate cancer. *Urology* **2006**, *68*, 110-5.
76. Zhau, H. Y.; Zhou, J.; Symmans, W. F.; Chen, B. Q.; Chang, S. M.; Sikes, R. A. e. a., Transfected neu oncogene induces human prostate cancer metastasis *Prostate* **1996**, *28*, 73-83.



77. Di Lorenzo, G.; Autorino, R.; De Laurentiis, M.; Cindolo, L.; D'Armiento, M.; Bianco, A. R.; De Placido, S., HER-2/NEU receptor in prostate cancer development and progression to androgen independence. *Tumori* **2004**, *90*, 163-170.
78. Chinni, S. R.; Yamamoto, H.; Dong, Z.; Sabbota, A.; Bonfil, R. D.; Cher, M. L., CXCL12/CXCR4 transactivates HER2 in lipid rafts of prostate cancer cells and promotes growth of metastatic deposits in bone. *Mol Cancer Res* **2008**, *6*, 446-57.
79. Feldman, B. J.; Feldman, D., The development of androgen-independent prostate cancer. *Nature Reviews Cancer* **2001**, *1*, 34-45.
80. Myers, M. P.; Stolarov, J. P.; Eng, C.; Li, J.; Wang, S. I.; Wigler, M. H. e. a., P-TEN, the tumor suppressor from human chromosome 10q23, is a dual-specificity phosphatase. *Proc Natl Acad Sci U S A* **1997**, *94*, 9052-7.
81. Garraway, L. A.; Widlund, H. R.; Rubin, M. A.; Getz, G.; Berger, A. J.; Ramaswamy, S.; Beroukhi, R.; Milner, D. A.; Granter, S. R.; Du, J.; Lee, C.; Wagner, S. N.; Li, C.; Golub, T. R.; Rimm, D. L.; Meyerson, M. L.; Fisher, D. E.; Sellers, W. R., Integrative genomic analyses identify MTF1 as a lineage survival oncogene amplified in malignant melanoma. *Nature* **2005**, *436*, 117-22.
82. Morgan, T. M.; Koreckij, T. D.; Corey, E., Targeted Therapy for Advanced Prostate Cancer: Inhibition of the PI3K/Akt/mTOR Pathway. *Curr Cancer Drug Targets* **2009**, *9* (2), 237-249.
83. Bianco, R.; Garofalo, S.; Rosa, R.; Damiano, V.; Gelardi, T.; Daniele, G.; Marciano, R.; Ciardiello, F.; Tortora, G., Inhibition of mTOR pathway by everolimus cooperates with EGFR inhibitors in human tumours sensitive and resistant to anti-EGFR drugs. *Br J Cancer* **2008**, *98* (5), 923-930.
84. Antonarakis, E. S.; Carducci, M. A.; Eisenberger, M. A., Novel targeted therapeutics for metastatic castration-resistant prostate cancer. *Cancer Lett* **2010**, *291*, 1-13.

85. Byar, D. P.; Corle, D. K., Hormone therapy for prostate cancer: Results of the Veterans Administration Cooperative Urological Research Group studies. *J Natl Cancer Inst Monogr (NCI Monogr)* **1988**, *7*, 165-170.
86. d'Ancona, F. C. H.; Debruyn, F. M. J., Endocrine approaches in the therapy of prostate carcinoma. *Human Reproduction Update* **2005**, *11*, 309-317.
87. Bosset, P.-O.; Albiges, L.; Seisen, T.; de la Motte Rouge, T.; Phé, V.; Bitker, M.-O.; Rouprêt, M., Current role of diethylstilbestrol in the management of advanced prostate cancer. *BJU International* **2012**.
88. Blackard, C. E., The Veterans' Administration Cooperative Urological Research Group studies of carcinoma of the prostate: a review. *Cancer Chemother Rep* **1975**, *59*, 225-227.
89. Rosenbaum, E.; Wygoda, M.; Gips, M., Diethylstilbestrol is an active agent in prostate cancer patients after failure to complete androgen blockade. *J Clin Oncol, suppl.* **2000**, *19*, 1372, 349a.
90. Shadidi, M.; Norman, A. R.; Gadd, J.; Simpson, J.; Huddart, R. A.; Horwich, A.; Dearnaley, D. P., Prospective review of diethylstilbestrol in advanced prostate cancer no longer responding to androgen suppression. *Proc Am Soc Clin Oncol* **2001**, *20*.
91. Robertson, C. N.; Roberson, K. M.; Padilla, G. M.; O'Brien, E. T.; Cook, J. M.; Kim, C. S.; Fine, R. L., Induction of apoptosis by diethylstilbestrol in hormone-insensitive prostate cancer cells. *J Natl Cancer Inst* **1996**, *88*, 908-917.
92. Salvesen, G. S.; Duckett, C. S., IAP proteins: blocking the road to death's door. *Nat Rev Mol Cell Biol* **2002**, *3* (6), 401-410.
93. Kufe, D. W.; Pollock, R. E.; Weichselbaum, R. R.; Bast Jr., R. C.; Gansler, T. S.; Holland, J. F.; Frei, E., Cancer Medicine. In [Online] ed., C. M. t., Ed. BC Decker Inc.: Hamilton, Ontario, 2003.
94. Legewie, S.; Blüthgen, N.; Herzel, H., Mathematical modeling identifies inhibitors of apoptosis as mediators of positive feedback and bistability. *PLoS Comput. Biol. PLoS computational biology* **2006**, *2* (9), 120.

95. Roche Diagnostics GmbH, E. D. E. Apoptosis, Cytotoxicity and Cell Proliferation Manual. [http://www.roche-applied-science.com/sis/apoptosis/docs/Apoptosis\\_Cytotox\\_CelProl\\_4th\\_edition.pdf](http://www.roche-applied-science.com/sis/apoptosis/docs/Apoptosis_Cytotox_CelProl_4th_edition.pdf).
96. Towbin, H.; Staehelin, T.; Gordon, J., Electrophoretic transfer of proteins from polyacrylamide gels to nitrocellulose sheets: procedure and some applications. *Proceedings of the National Academy of Sciences of the United States of America* **1979**, 79 (9), 4350-4354.
97. Renart, J.; Reiser, J.; Stark, G. R., Transfer of proteins from gels to diazobenzoyloxymethyl-paper and detection with antisera: a method for studying antibody specificity and antigen structure *Proceedings of the National Academy of Sciences USA* **1979**, 76 (7), 3116-3120.
98. Duncan, R.; Seymour, L. W.; Ohare, K. B.; Flanagan, P. A.; Wedge, S.; Hume, I. C.; Ulbrich, K.; Strohal, J.; Subr, V.; Spreafico, F.; Grandi, M.; Ripamonti, M.; Farao, M.; Suarato, A., Preclinical Evaluation of Polymer-Bound Doxorubicin. *Journal of Controlled Release* **1992**, 19 (1-3), 331-346.

# 5

## **Polyacetal-based Combination Therapy for the Treatment of Hormono-Dependent Diseases**

## 5.1 Introduction

### 5.1.1 Combination Therapy

Combination therapy is referred when more than one drug or type of therapy (i.e. Chemotherapy, radiotherapy, etc.) is simultaneous administrated to treat a disease. One of the advantages of using combination therapy is the capability to modulate different signaling pathways in diseased cells, maximizing the therapeutic effect and possibly overcoming mechanisms of resistance<sup>1</sup>. It is believed that the future of cancer therapy will mainly rely on specific targets and in most cases in their combination, in order to obtain more selectivity, efficacy and lower toxicity.

In last decades combination therapy has been more used and in particular further advances have been obtained for cancer treatment. Sometimes combination chemotherapy is used not to cure but to reduce symptoms and prolong life, useful for people with advanced cancers not suitable for radiotherapy or surgical treatment. To determine which of the treatments, a single or a combination therapy is best, it is important to know the stage and size of the tumor and the risk of recurrence.

For some cancers, the combination therapy includes surgery, radiation therapy and chemotherapy. Surgery or radiation therapy kills cancer cells locally in a specific site however chemotherapy also destroys cancer cells that have spread to different sites. Sometimes radiation therapy or chemotherapy is given before surgery in order to shrink a tumor to achieve a complete removal of the tumor and is given after to help to kill any remaining cancer cells.

The design of combination therapy involves the knowledge of several issues such as the tumor cell kinetics, biochemical synergy, tumor cell kinetics, fractional cell kill; dose scheduling, intensity and total dose, non-overlapping toxicity; active agents, tumor cell resistance, non-cross resistant agents and host rescue. In addition, these principles are considered the bases for adjuvant and neoadjuvant approaches<sup>2</sup>.

Four main types of combination therapy are routinely used in clinic:

*1) Combination of different types of therapy.*

Combination of surgery, radiotherapy and chemotherapy<sup>3</sup> are routinely used in the clinics as different cycle phases. More recently, a new therapy which combines radiation with a prostate specific antigen (PSA)-based vaccine has been transfer to phase II for patients with prostate cancer<sup>4</sup>. Based on preclinical observations, it was demonstrated that the radiation therapy increased the stimulation of immune system altering tumor cells and making them more susceptible<sup>3</sup>. Hormone therapies are sometimes also used in combination with radiation therapy or surgery to improve survival time for men with aggressive tumors. In fact, combination therapy improves survival time for men with aggressive cancers as it was demonstrated in 2009 in a study realized at the Mount Sinai Medical Center in New York. Combination therapy involving radioactive seed implants, external beam radiation, and hormonal therapy were given to 181 men with a Gleason score of 8 or higher (see annex 1). And after eight years, the prostate cancer survival rates were 87% with this combined therapy.

*2) Chemotherapy combinations.*

Since the 1940s, the combination of different chemotherapeutic agents has been developed allowing for remarkable survival improvement, particularly in childhood leukaemia and Hodgkin's disease<sup>2</sup>. This progression was based on biochemical synergy, tumor cell kinetics, non-overlapping toxicity, an increase of fractional cell kill, non-cross-resistant agent and tumor cell resistance<sup>2</sup>. The action mechanism of the drugs consists on causing DNA damage, acting as topoisomerase I including camptothecins: irinotecan and topotecan, or topoisomerase II such as amsarine, etoposide and etoposide phosphate. For example, in colorectal cancer before to administer 5-fluorouracil (5-FU), is given leucovorin (LV) which enhance the fixation of 5-FU and consequently its therapeutic effect. Several traditional treatments based on anthracycline combination<sup>2,5</sup> have been reported for cancer therapy such as AC (anthracycline and cyclophosphamide) and CAF

(cyclophosphamide, adriamycin and 5-FU) and also, methotrexate containing combinations are CMF (cyclophosphamide, methotrexate and 5-FU), and CMFVP (cyclophosphamide, methotrexate, 5-FU, vincristine and prednisone<sup>6</sup>). Currently, new possibilities are being explored in order to increase response, reduce side effects, and maximize therapeutic benefit. Combinations based on paclitaxel (PTX) are<sup>7, 8</sup> also studied to achieve an increase on the therapeutic index of the drug alone. For example research on PTX in combination with carboplatin for ovary<sup>9</sup> and lung cancer or with vinorelbine for non-small lung cancer<sup>10</sup> have been reported and a novel combination of PTX, 5-FU, folinic acid and cisplatin in Phase II have showed promising results in patients with advanced gastric cancer. This combination therapy improves also the single PTX administration's time, changing from three times per week to once a week getting the same therapeutic effect and a reduction of side effects<sup>11</sup>. On the other hand, small molecule chemotherapy combinations can also be used as palliative treatment by decreasing the symptoms and prolonging the life expectancy<sup>12</sup>; as well as adjuvant therapy pre- or post surgery, in order to decrease the tumor mass in advanced and metastatic cancer previously at the operation or eradicating the undetectable micro-metastasis in a post surgical treatment<sup>13</sup>.

Recent studies have evaluated the efficacy and tolerance of PTX and carboplatin combination in patients with castration-resistant prostate cancer. It was demonstrated that this combination shown an active and well-tolerated regimen, which merits to be further evaluated in the context of salvage treatment. Genistein-topotecan combination is another example which has been studied to demonstrate their potential anticancer efficacy in prostate models. Genistein is very similar to 17 $\beta$ -estradiol (estrogen) which can compete with it and bind to estrogen receptors and topotecan is a water-soluble chemotherapeutic agent that is a topoisomerase inhibitor derived of camptothecin. The combination of both agents were tested in LNCaP prostate cancer cells showing that this cocktail could be a very attractive phytotherapeutic alternative or adjuvant therapy for prostate cancer<sup>14</sup>.

Genistein has been also combined with selenium as in 2006<sup>15</sup> selenite was reported as a novel chemotherapeutic agent for prostate cancer. Then, the combination genistein-selenium was found to have chemopreventive value

and/or may be adjuvant to standard therapy for prostate tumors independent of hormonal status<sup>16</sup>.

### 3) *Combinations based on endocrine therapy*

Hormone-dependent cancers such as prostate and breast carcinoma<sup>6</sup> can be treated with surgery, radiotherapy, chemotherapy or any of their combinations in order to enhance treatment efficiency. Indeed, clinical studies combining endocrine and chemotherapy have been reported already since the 1980s<sup>17</sup>.

The endocrine therapy is focus in the inhibition of estrogen production (using estrogen receptor modulator agents, SERM<sup>6</sup>, which block the estrogen receptor), but the use of another therapy (for example aromatase inhibitors<sup>18</sup>) can improve the survival rate of a patient.

Recently, to treat breast cancer, the combination of endocrine therapy with adjuvant bisphosphate therapy (zoledronic acid) has been described for bone protection. The estrogen suppression induced by aromatase inhibitors is related with the bone loss and consequently prevent future chronic disease and fracture<sup>19</sup>. Clinical trials were carried out to confirm the anti-tumor activity of zoledronic acid<sup>20</sup>. Then, a study with 1805 pre menopausal woman with hormone-responsive breast cancer who were treated with endocrine therapy was performance, and some of them were combining the therapy with zoledronic acid. Data shows that after 5 years of endocrine therapy with zoledronic, patients displayed significant prolonged disease free survival and relapse free survival. These positive results were attributing to the antimetastatic properties of zoledronic acid and highlight the importance of such combination<sup>20, 21</sup>. Similar results were also obtained in the CALGB 79809 trial<sup>21</sup>.

In prostate cancer, different type of hormone therapy have been studied to block testosterone and therefore, tumor growth<sup>22</sup>. The agent acting on the luteinizing-hormone-releasing-hormone (LH-RH) pro- or anti-LHRH (analogues or antagonist)<sup>23</sup> and anti-androgens (AAs)<sup>24</sup> are the main endocrine therapeutics reported.



In contrast with breast cancer, hormonal therapy in prostate cancer is mainly used for an application pre- and post radiotherapy in order to decrease the tumor weight and to ensure the tumor overcome after the radiation<sup>25</sup>. A particular study with androgen ablation, LHRH analogues, prescribed with external irradiation described an increase in clinical and biochemical relapse-free survival in patients with advanced prostate cancer<sup>25</sup>.

#### *4) Combinations based on monoclonal antibodies.*

In recent years, antibody therapies have played important roles in cancer treatment either alone or in combination with other therapeutic agents. The monoclonal antibody trastuzumab (Herceptin®) is routinely used in combination with a chemotherapeutic agent in the treatment of HER2 breast cancer<sup>26</sup>. Other monoclonal antibodies such as rituximab (Rituxan®)<sup>10</sup> or bevacizumab (Avastin®)<sup>27</sup>, are used for metastatic treatment in colorectal cancer or non small cell lung and esophageal cancer (NSCLC) and they in combination of chemotherapy are used for the treatment of advanced breast cancer<sup>28, 29</sup>. Currently, bevacizumab, the first antiangiogenic drug to be granted US FDA approval to market in February 2004, is combined with 5-FU based chemotherapy, carboplatin or PTX for the treatment of metastatic colorectal cancer, NSCLC and metastatic breast<sup>28</sup> cancer respectively. More multi-agent therapies are currently in clinical trials using the same rationale, targeting different molecular pathways to maximize the efficacy. Several antiangiogenic drugs in combination with chemotherapy and with inhibitors of specific molecular pathways, such as erlotinib (Tarceva), had arrived to Phase III. However they did not improve the patient survival<sup>30</sup> being the lack of a deep understanding of the molecular pathways in cancer disease the main problem for these bad results.

In summary, combination therapy plays an important role in cancer treatment and an improvement in the knowledge and understanding of the molecular pathways will allow to better solve any problem when designing combination therapy, reducing side effects and enhancing the anticancer agent's penetration and therefore their efficacy.

### 5.1.2 Rationale to develop Polymer-based combination Therapies

The application of drug delivery systems (DDS) has been mainly restricted to the delivery of single agents; however, their use to deliver “cocktails” of therapeutics is still largely unexplored.<sup>31</sup> This might seem unusual since combination therapy is routinely used in cancer treatment and indeed the combination of different therapeutic agents often improves therapeutic profile. In the last ten years, a number of pioneering studies have been carried out that highlight the suitability of different DDS to deliver drug combinations. In fact, Celator Technologies Inc. has developed CombiPlex® technology, a novel approach that identifies a synergistic ratio of two or more drugs and locks the ratio in a drug delivery vehicle, to deliver and maintain the synergistic ratio through pharmacokinetic control in patients<sup>32</sup>. CombiPlex® has already led to two liposome-based products in Phase II clinical development, namely CPX-1 (irinotecan : floxuridine) for the treatment of colorectal cancer<sup>32</sup> and CPX-351 (cytarabine : daunorubicin)<sup>32</sup> for patients diagnosed with acute myeloid leukemia (AML). Although at much earlier stages, the promising approaches offered by combination therapy has been also identified in the case of polymer-drug conjugates. This chapter is focused on combination therapy using polymer drug conjugates.

As it was explained before in Chapter 1, section 1.2, polymer drug conjugates are nanosized drug delivery systems in which the drug is covalently bound to a polymer carrier and the main benefits compared to the parent free drug are: (a) passive tumour targeting by the enhanced permeability and retention (EPR) effect<sup>33</sup>, (b) decreased toxicity<sup>34</sup>, (c) increased solubility in biological fluids<sup>35</sup> (d) ability to overpass some mechanisms of drug resistance<sup>36</sup> and (e) ability to elicit immunostimulatory effects<sup>37, 38</sup>. After, the success of the first generation of polymer-drug conjugate are having in market and clinical trials, a second generation appeared based on combination therapy<sup>39</sup>. The term “polymer-drug conjugates for combination therapy” involved at least four types of systems (Figure 5. 1).

Type I is already in clinical trials, and families II to IV are mainly in preclinical status and few of them are under *in vivo* evaluation.

1. Type I: polymer-drug conjugate plus free drugs. This concept is developed based on the combination of a polymer-drug conjugate carrying a single drug administered with a low molecular weight drug or different types of therapy (e.g. radiotherapy).
2. Type II: polymer-drug conjugate plus polymer-drug conjugate. In this second family, two different polymer-drug conjugates, each carrying a single therapeutic agent.
3. Type III: single polymeric carrier carrying a combination of drugs. The third type involves two or more drugs attached to a single polymer carrier.
4. Type IV: polymer-directed enzyme prodrug therapy (PDEPT) and polymer enzyme liposome therapy (PELT). PDEPT relies on the combination of polymer-drug conjugate with a polymer-enzyme conjugate responsible of the selective release of the drug at the tumor site. PELT is a comparable strategy where a polymer enzyme conjugate is administered in combination with the liposome to induce its degradation allowing the drug release encapsulated inside.

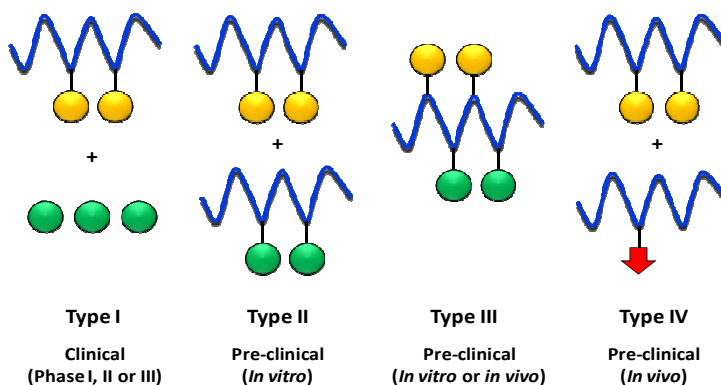


**Figure 5. 1** Schematic representation of the four different types of polymer-based combination therapy for targeted **drug delivery by the EPR effect**<sup>12</sup>.

Examples of each system are described below and all of the examples are classified in Table 5. 1.

## 1. Type I: Polymer drug conjugate + low molecular weight drugs.

The use of drug combinations for cancer treatment is well established<sup>40</sup>. Therefore, the use of polymer-drug conjugates in combination with free drugs can be considered as a reasonable idea.

### Clinical Trials

**-PGA-paclitaxel + cisplatin (Phase I)/ PGA-paclitaxel + carboplatin (Phase III):** Clinical studies were developed with PGA-PTX conjugate, Opaxio<sup>®</sup>, in combination with platinates. Phase I studies have been performed in order to determine the toxicity, maximum tolerated dose (MTD) and pharmacokinetics of PGA-PTX. For instance a phase I study was assessed on 43 patients with advanced solid tumors combining a fixed dose of cisplatin (75mg/m<sup>2</sup>) with increasing doses of PGA-PTX, demonstrating that this combination showed good activity in refractory patients<sup>41</sup>. A second phase I study carried out on 22 patients with advanced solid tumors, the combination of Opaxio with carboplatin<sup>42</sup> was tested and the previous three partial responses were observed being the MTD 225mg/ml. Besides, partial responses were observed in patients who had previously failed paclitaxel therapy. After those promising results with phase I trials, a Phase III clinical trial named STELLAR 3 was developed on 400 patients with NSCLC cancer and poor performance status to assess and compare PGA-PTX plus carboplatin against PTX plus carboplatin. However no improvement in patient's survival was observed, although the combination containing the conjugate was less toxic<sup>42</sup>.

Furthermore, based on previous results suggesting that the anticancer activity of Opaxio<sup>®</sup> might be affected by estrogen levels, a new clinical trial developed by Cell Therapeutics Inc., is currently being developed in female patients with advanced NSCLC and baseline estradiol greater than 25pg/ml, again comparing carboplatin plus PGA-paclitaxel or plus paclitaxel<sup>43</sup>. Nevertheless, since no comparisons were done against the conjugates alone, the added therapeutic value of such combination compared to mono-therapy became complicate to quantify.

**Table 5. 1** Examples of the four different types of polymer-based combination therapy for targeted drug delivery

Status	Name	Family	Carrier	Drugs	Drug types
<b>In Vitro</b>	CPT-PEG-LHRH + CPT-PEG-BH3	II	PEG	CPT LHRH	Chemotherapeutic Targeting residue
	HPMA-Dox-DEX	III	HPMA copolymer	BH3 Dox DEX	Proapoptotic protein Chemotherapeutic Antiinflammatory
	PEG-poly(aspartate hydrazide) block Copolymer-Dox-WOR	III	PEG-poly(aspartate hydrazide)	Dox WOR	Chemotherapeutic Phosphatidylinositol-3kinase inhibitor
	<b>Preclinical (In vivo)</b>	HPMA-AGM-Dox	III	HPMA copolymer	AGM Dox
	HPMA copolymer-Dox + HPMA copolymer mesochlorin e6	II	HPMA copolymer	Dox Mscle6	Chemotherapeutic Phototherapy
	PEG-(ZnPP) + PEG-(DAO)	II	PEG	ZnPP DAO	Hemoxygenase inhibitor enzyme oxidative chemotherapeutic type
	PEG-NO-EPI	III	PEG	NO EPI	signalling molecule Chemotherapeutic
	CPT-PEG-LHRH-BH3	III	PEG branched	CPT LHRH BH3	Chemotherapeutic Targeting residue Proapoptotic protein
	HPMA-TNP-470-ALN	III	HPAM copolymer	ALN TNP 470	Bone targeting and antiangiogenic agent Anti angiogenic agent
	HPMA-PTX-ALN	III	HPMA copolymer	PTX ALN	Chemotherapeutic Bone targeting and antiangiogenic agent
	HPMA-Gem-Dox	III	HPMA copolymer	Gem Dox	Chemotherapeutic Chemotherapeutic
	HPMA copolymer-Dox + HPMA copolymer- cathepsin B	IV	HPMA copolymer	Dox Cathepsin B	Chemotherapeutic Proteolytic enzyme
	HPMA copolymer-Dox + HPMA copolymer- $\beta$ - lactamase	IV	HPMA copolymer	Dox B-lactamase	Chemotherapeutic Proteolytic enzyme
<b>Clinical</b>					
Phase I	PGA-PTX + cisplatin	I	PGA	PTX Cisplatin	Chemotherapeutic Chemotherapeutic
Phase II	PGA-PTX + radiotherapy	I	PGA	PTX Radiotherapy	Chemotherapeutic Radiotherapy
Phase III	PGA-PTX + carboplatin	I	PGA	PTX Carboplatin	Chemotherapeutic Chemotherapeutic

**-PGA-paclitaxel + radiotherapy (Phase II):** .Chemotherapy plus radiotherapy are a common combination of therapies in clinical practice and particularly in cancer therapy the use of polymer-drug conjugates combined with radiotherapy are been a promising approach. Polymer-drug conjugates are known to passively accumulate in the tumor tissue as a result of the leaky tumor vasculature (EPR effect) <sup>33</sup>. As radiotherapy impacts on tumor vasculature magnifying the EPR effect, the combination of polymer-drug conjugate and radiotherapy combination is extremely interesting. An example of this combination in Phase II is PGA-paclitaxel and radiotherapy. First, the study was assessed on 21 patients with esophageal and gastric cancer and it was established the safety and the MTD in 80mg/m<sup>2</sup>. Besides, additional analysis included a complete clinical response in 33% of patients with loco-regional disease <sup>44</sup>. And recently, phase II studies in glioblastoma ratified the higher efficiency of PGA-PTX after radiotherapy<sup>45</sup>.

Recently, Lammers et al. has demonstrated the synergistic interaction between radiotherapy and chemotherapy<sup>46</sup>. The study involved two polymer-drug conjugate, HPMA copolymer-Dox and HPMA copolymer-Gem and it was proved that radiotherapy could enhance the tumor accumulation of both anticancer agents and that selective drug delivery increased the therapeutic index of the active agent.

## **2. Type II: Polymer drug conjugates + polymer-drug conjugate.**

### **Pre-clinical *in vitro***

**-CPT-PEG-LHRH + CPT-PEG-BH3:** Minko et al. developed a system based on the combination of the proapoptotic chemotherapeutic drug camptothecin (CPT), the hormone therapy with LHRH and the target BH3 (proapoptotic peptide) domain peptide<sup>47</sup>. In order to evaluate the best combination, the author tested free CPT, CPT-PEG, CPT-PEG-BH3 or CPT-PEG-LHRH conjugate and mixture of CPT-PEG-LHRH and CPT-PEG-BH3 in human ovarian carcinoma cells. The result of this study lead to an increase of the proapoptotic activity when the combination CPT-PEG-LHRH plus CPT-PEG-BH3 was employed <sup>48</sup>.

**Pre-clinical *in vivo***

**-HPMA copolymer-DOX + HPMA copolymer-mesochlorine 6:** The combination of HPMA copolymer-Dox with HPMA copolymer-mesochlorine 6 showed more activity than either conjugate alone with an enhancement of the activity when the antibody OV-TL16 was added for active targeting<sup>49</sup>. It was demonstrated that in mice N2A neuroblastoma tumors, this combination led to a total regression of the tumor. On the contrary, each single conjugate or free drugs were not able to achieve any effect.<sup>50</sup> Furthermore, in a very recent study, the same authors demonstrated the efficacy of this strategy by exposing an ovarian carcinoma cell line to sequential administration of two polymer conjugates, namely HPMA copolymer-SOS (i.e. 2,5-bis(5-hydroxymethyl-2-thienyl)furan), followed by HPMA copolymer-mesochlorine 6 monoethylenediamine and observed a synergistic effect<sup>51</sup>.

**-PEG-(ZnPP) + PEG-(DAO):** Treatment PEG-zinc protoporphyrin (ZnPP, a heme oxygenase inhibitor) followed by PEG-D-amino acid oxidase (DAO)/D-proline induced a significantly inhibited tumour growth in animal models, contrary of each single conjugate<sup>52</sup>.

**3. Type III: Single polymeric carrier carrying a combination of drugs.**

This family has not to be confused to polymer-drug conjugate with a targeting residue<sup>53</sup>. Two or more drugs covalently linked to the same polymer have a specific therapeutic action whereas when a targeting moiety is conjugated, it is only used to address the conjugate to a target site, described as a first polymer drug conjugate generation.

**Pre-clinical *in vitro***

**-HPMA-Dox-DEX:** In 2008, a combination copolymer based on HPMA was selected to carry the anticancer agent Dox and a well-known corticosteroid with anti-inflammatory properties, dexamethasone (DEX)<sup>54</sup>. Using a library of conjugates containing the single agents, Dox and DEX or the combination of both, the authors studied the physicochemical properties of the newly generated two-drug containing copolymer, its stability in aqueous solutions of pH, and its release rates upon activation with carboxiesterases. No differences were observed between the copolymers containing only one, and the

copolymer containing both pharmacologically active agents, indicating that Dox and DEX can be co-conjugated to the same HPMA copolymer without affecting their release profiles<sup>54</sup>.

**-PEG-poly(aspartate hydrazide) block copolymers-Dox-WOR:** In another example, Kwon and collaborators developed an interesting system based on polymer-drug conjugates and polymeric micelles. An amphiphilic polymer constituted by poly(ethylene glycol)-poly(aspartate hydrazide) (PEG-PAH) block copolymers was prepared, and Dox and the phosphatidylinositol-3 kinase inhibitor wortmannin (WOR) were attached alone or in combination, at different drug ratios. Physicochemical studies confirmed that the conjugates assembled to form micellar structures. It was observed that the delivery of both agents via the micellar system reduced the amount of drug necessary to elicit biological activity<sup>55</sup>.

### **Pre-clinical *in vivo***

**- HPMA copolymer-AGM-Dox:** Vicent *et al.* developed HPMA copolymer-AGM-Dox, combination conjugate in which the aromatase inhibitor aminoglutethimide (AGM) and the chemotherapeutic agent Dox were simultaneously conjugated to the same polymeric backbone. AGM's mechanism of action is the inhibition of aromatase enzyme, responsible for estrogen production, in consequence blocking estrogen activity. This conjugate carrying both drugs was more active than the combination of two polymer conjugates each carrying a single drug<sup>56-58</sup>. Preliminary mechanistic studies suggested that such increased activity could be due to a variety of factors, including drug release rate, conjugate conformation in solution and activation of certain molecular pathways, in particular, induction of apoptosis by downregulation of Bcl-2 protein<sup>58</sup>. Recently, studies *in vivo* has been shown for this combination conjugate and it was demonstrated higher activity for HPMA-AGM-Dox than for HPMA-Dox in 4T1 breast cancer model<sup>59</sup>.

**- HPMA-Gem-Dox:** As in the case of HPMA-AGM-Dox, when tested *in vivo* in a tumor rat model, the combination conjugate HPMA-Gemcitabine (Gem)-Dox was more active than the combination of two polymer conjugates each carrying a single drug, and even more than the combination of the free drugs. This activity enhancement was due to a more strongly apoptosis induction than in the controls and a marked angiogenesis inhibition<sup>60</sup>.



- **PEG-NO-EPI**: In cancer cells, anthracyclines such as epirubicin (EPI) and the diffusible messenger nitric oxide (NO) can act synergistically<sup>61</sup>. By modulating the presence of reactive oxygen species (ROS), NO can controlled the pro- and anti-apoptotic properties of chemotherapeutic agents. It has been already demonstrated with PEG-EPI-NO conjugates that, in cardiomyocytes as well as in an *in vivo* mouse model, NO counterbalances EPI induced cardio-toxicity<sup>61, 62</sup>. *In vivo* studies in a model for colon adenocarcinoma confirmed that the PEG-NO-EPI conjugate displayed anticancer activity but was less cardio-toxic<sup>62</sup>. Conjugation of both agents onto a single chain ensures that they undergo the same body distribution, thus maximizing the benefits of this combination.

- **HPMA-TNP470-ALN/ HPMA-PTX-ALN**: Taking advantage of the concept of combination therapy<sup>12</sup>, caplostatin has been recently combined with the aminobisphosphonate alendronate (ALN) (HPMA copolymer-ALN-TNP-470 conjugate) for the treatment of calcified neoplasm and osteosarcoma. TNP-470, a synthetic analog of fumagillin, is known to be an anti-angiogenic agent and an inhibitor of tumor growth<sup>63</sup>. In this combination, ALN has the double function of targeting moiety (to promote bone targeting) and of pharmacologically active agent. *In vitro* evaluation confirmed its antiangiogenic and antitumor properties and the *in vivo* assessment further strengthened these positive results with almost complete tumor regression observed in a human osteosarcoma model<sup>64</sup>. In the same line, and considering that the efficacy of ‘metronomic chemotherapy’ (chemotherapy administered at low and frequent doses) can be significantly increased when administered in combination with anti-angiogenic drugs<sup>65</sup>, Satchi-Fainaro *et al.* developed the successful idea of combining PTX and alendronate on the same HPMA polymeric carrier (HPMA-PTX-ALN conjugate). In this study, ALN showed clear anti-angiogenic properties in addition to its well-known bone targeting. This conjugate seemed to be a good candidate for the treatment of osteosarcomas and bone metastasis<sup>66</sup>.

- **CPT-PEG-LHRH-BH3**: Minko *et al* performed a branched PEG polymer building on the proapoptotic BH3 based PEG conjugate previously described and the promising data from the combination of different conjugates<sup>47</sup>. They synthesized a six-branched conjugate containing equimolecular amounts of CPT, BH3 and LHRH. *In vitro* studies showed that such multicomponent

conjugate was almost 100 times more cytotoxic than the single conjugates and displayed enhanced antitumor activity *in vivo* when compared with monotherapy<sup>48</sup>.

#### **4. Type IV: Polymer-directed enzyme prodrug therapy (PDEPT) and polymer enzyme liposome therapy (PELT).**

Polymer-directed enzyme prodrug therapy is a two components strategy based on polymer conjugates. In this approach, a polymer-drug conjugate is combined with a polymer-enzyme conjugate with the aim of achieving selective release of the drug at the tumor site. Indeed, the linker binding the drug to the polymer in the first conjugate has to be designed to be degraded by the enzyme of the second conjugate.

##### **Pre-clinical *in vivo***

**-HPMA copolymer-Dox + HPMA copolymer-Cathepsin B:** This novel design is commonly named polymer enzyme prodrug therapy (PDEPT) and it is based on the combination of one polymer drug-conjugate (e.g. HPMA copolymer-Dox) which needs a polymer enzyme-conjugate (e.g. HPMA copolymer-Cathepsin B) to reach a drug control release in the tumor site. The HPMA copolymer-Dox has shown anticancer activity reaching phase II clinical trial. In this polymer drug-conjugate, Dox is linked to the polymer via an enzyme (cathepsin B) labile linker and its efficacy depended of its exposure to the lysosome enzyme cathepsin B, its cellular uptake rate and obviously to the enzyme amount. The idea of this combination is to assure the rate of cathepsin B and when both conjugates are present in the tumor lysosome, the *in situ* cathepsin B enhanced by the HPMA copolymer-cathepsin B achieved the degradation of the linker and the drug release. Preclinical study confirmed that the HPMA-cathepsin B was able to trigger Dox release in animal models, with an area under the curve (AUC) almost 4 fold higher than that obtained with HPMA copolymer-Dox alone.<sup>67</sup>

**-HPMA copolymer-Dox + HPMA copolymer- $\beta$ -lactamase:** With the combination of HPMA copolymer-Dox with HPMA copolymer- $\beta$ -lactamase, the same principle of PDEPT is developed. Here Dox is linked to HPMA via a GlyGly-cephalosporin linker sensitive to the non-mammalian  $\beta$ -lactamase but not to the cathepsin B<sup>68</sup>. In this study, mice treated with the combination

increased survival and decreased tumor growth compared to the control. While non toxicity was determinate, immune response could be an issue due to the use of non-human protein. Polymer-protein conjugate is a well known strategy to prolonging circulation time of protein in blood stream and decreasing their immunogenicity<sup>69</sup>, which suggests that after optimization, PDEPT has a great therapeutic potential and further studies with catalytic antibodies have demonstrated its value.

### **5.1.3 Challenges to develop the most efficient conjugated systems for combination therapy.**

The presence of two or more therapeutic agents on a single polymeric chain opens new therapeutic possibilities. In order to design a proper and efficient polymer-drug conjugates for combination therapy it is important to take into account some basic parameters:

(i) One of the first aims is to identify the appropriate drug combinations and drug ratios. Most drug combinations are based on the assumption that by targeting different cellular pathways there is an enhancement in the therapeutic benefit and a decrease in the toxicity. However no all the studies have reach this statement <sup>70</sup>. It is important to understand that two combined drugs in the same system will release together, so it is important then the selection of the drugs, if they will follow the same internalization pathway and the optimal ratio of drug between each of them. In this context, as mentioned before, the Canadian company, Celator Technologies Inc. has developed a methodical approach to asses different drug ratios within their liposomal technology<sup>32</sup>, which has lead to different liposomal formulation already in Phase II clinical trials. It will be very interesting to have further studies with the similar approach applied to the development of combination polymer-drug conjugate.

(ii) The kinetics of drug(s) release. In a polymer-drug conjugate the drug release rate is essential to reach its activity then the linker by which the drug is linked should be enzymatic or chemically labile at the target site, furthermore stable in blood. In the 80s, HPMA-GFLG-Dox <sup>71</sup> was developed based on the study of release kinetics of different peptidyl linkers for selective

cleavage in the lysosomal compartment. It was observed that different linkers displayed different release rate and that the biodegradability of the linker depend on the drug carried on. Indeed, the linker –GlyGly- is non biodegradable when it is designed in the conjugate HPMA-GlyGly-Dox however when it is used in the conjugate HPMA-GlyGly-melphalan, the drug released is achieved<sup>72</sup>. In addition when more than one drug is linked to the carrier, the drug release could be affected by the presence of the second agent even when both drugs were linked by the same linker.<sup>57</sup>

(iii) The loading capacity. This is a limited parameter in the design of a system, so first it is necessary to well known the polymer capacity for having the higher drug loading to lead a higher therapeutic effect always keeping the water solubility<sup>71, 73, 74</sup>.

(iv) The correlation of *in vitro* studies with behavior *in vivo*. Before *in vivo* studies are performed, preliminary *in vitro* screening is carried out against cells using standard cell viability assays. However, such *in vitro* studies are usefulness due to the accumulation of the conjugates in the tumor tissue is via the EPR effect, which can be only observed *in vivo* models. Normally the free drug is more active *in vitro* than the conjugate but *in vivo* studies show opposite trends. However ethical considerations and cost are reasonable issues in favor of *in vitro* pre-screening. In the case of polymer based combination therapy *in vitro* assays are very convenient because it allows a comparison of the relative activity of different polymer-drug conjugates, as well as testing different drug ratios and gives the possibility to carry out experiments to determine the mechanism of action of the systems including their ability to trigger the drug or the blockade of specific cell process.

And, (v) finally, last issue to consider is the physico-chemical characterization<sup>39</sup>. Compared to small molecules, polymer-drug conjugates are relatively complex systems to fully characterize. Then, the attachment of a second drug to the same carrier complicates the matter even further. For all the compounds to be developed into medicines an exhaustive characterization is needed to understand perfectly their biological behavior. A variety of techniques to characterize polymer-drug conjugates include NMR, HPLC, GPC, DLS, SANS, etc. as it has been already mentioned in Chapter 1.

### 5.1.4 Combination Index<sup>75,76</sup>

The Combination Index (CI) allows calculation of  $n$  chemical interactions (synergism, additive effect, antagonism) at all effect levels simultaneously. Knowledge of mechanisms of action is not needed. The toxicity of a mixture depends on the toxicity of the components and how the components interact with each other in a dose-dependent way.

Chemicals in a mixture may show zero interaction or may interact in two ways:

- Synergistically: The effect of the combination is greater than that expected from the sum of their individual effects (more than an additive effect)
- Antagonistically: The effect of the combination is less than that expected from the sum of their individual effects (less than an additive effect)

Synergism and antagonism may be defined as departures (deviations) from zero interaction additive effect) between chemicals in a mixture (Equation 5.1).

$$[D_1 / (D_m)_1] + [D_2 / (D_m)_2] = 1 \quad (\text{Eq. 5. 1})$$

Where  $D_1$  and  $D_2$  are the doses of drugs 1 and 2 that in combination produce some specific effect (i. e. 50% inhibition of luminescence) and  $(D_m)_1$  and  $(D_m)_2$  are the doses of the drugs that when applied singly also have the same effect (50% inhibition of luminescence). An isobologram can graphically display chemical interactions (Figure 5. 2), the  $x$  and  $y$  axes representing the doses of drugs 1 and 2. The lines of the isobologram show dose combinations of the two chemicals, 1 and 2, that yielded the same effect (Figure 5. 2):

- A straight line connecting dose of chemical 1 ( $D_1$ ) and dose of chemical 2 ( $D_2$ ) on the respective  $x$  and  $y$  axes that yield 50% effect ( $D_m$ ,  $EC_{50}$ ,  $ED_{50}$ ) represents ZERO INTERACTION OR ADDITIVE EFFECT (Isobologram equation = 1).

- When the line connecting both doses lie below and to the left of the line of additivity (concave-up line) gives a SYNERGISM EFFECT (Isobologram equation  $< 1$ ).
- When the line connecting both doses lie above and to the right of the line of additivity (concave-down) represents an ANTAGONISM EFFECT (Isobologram equation  $> 1$ ).

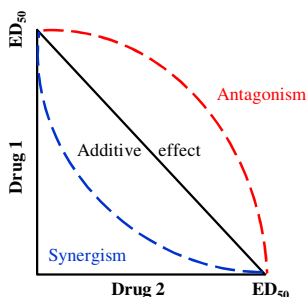


**Figure 5. 2** Isobologram graph representing synergism and antagonism effect combining two different drugs<sup>76</sup>.

The isobologram is a dose-oriented graphic that can give information on the interaction of two drugs at any effect level ( $EC_{10}$ ,  $EC_{20}$ ,  $EC_{50}$ ...) but has some practical limitations as it is designed for two-three drugs<sup>76</sup>. Chou<sup>77</sup> generalizes the isobologram equation for  $n$  drugs, is independent of the mechanism of action but takes into account both the potency of each drug and combinations of these drugs and the shapes of their dose-effect curves.

### 5.1.5 Paclitaxel as second chemotherapeutic drug in the polyacetalic system.

Paclitaxel (Figure 5. 3) is a costly compound to develop as a drug because its lack of aqueous solubility and its very difficult isolation from a limited biological source. However and fortunately for cancer patients it was continued a research with paclitaxel in animal models for various tumors showing excellent activity against B16 Melanoma, P1534 leukemia and MX-1 mammary xenograft<sup>78, 79</sup>. Based on this, the National Cancer Institute in 1977 took the decision to proceed with full-scale preclinical development and

clinical trials of paclitaxel. In 1979 an important discovery from Dr. Susan Horwitz created a great interest on this drug, she discovered that paclitaxel promoted the assembly of tubulin into stable microtubules<sup>80</sup> operating as antimetabolic drug. Paclitaxel is still the only naturally occurring drug that acts by promoting the assembly of tubulin.

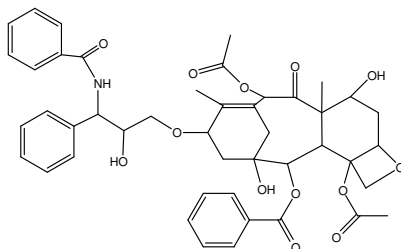


**Figure 5. 3** Molecule of Paclitaxel (already mentioned at chapter 1).

There is an interest of using PTX as anticancer agent for the treatment of prostate cancer<sup>81</sup> because it was demonstrated by *in vitro* studies an enhancement in the therapeutic effect. This effect can be improved using more anticancer drugs as for example DES. Currently in the clinics for prostate cancer docetaxel (DCX), drug from the same family as PTX, is used as Montgomery et al<sup>82</sup> reported using a combination of those both drugs, DES and DCM or by Rubenstein and collaborators reporting an study with DES and PTX<sup>83</sup>.

The present project aims to improve the therapeutic effect of the already reported DES-polyacetals by combining in the same carrier a second drug in combination, paclitaxel (endocrine + chemotherapy). and also looking at drug synergism.

The design of a successful prodrug requires a reasonably quickly conversion after injection or infusion but chemical stability prior to administration. When PTX is orally administered it is poorly absorbed for its low solubility, this drug is mainly used iv. In PTX, chemical derivatization at either the C 2' or the C 7' position appeared to offer the best prospects for achieving the best prodrug. The majority of the strategies to improve the parenteral delivery properties of poorly soluble drugs, involve the esterification of the alcohol

groups at these positions of the parent compound. 2'ester derivatives of PTX were synthesized to increase aqueous solubility and permit paclitaxel release under physiological conditions.

Paclitaxel is involved in numerous anticancer conjugates which are currently in advanced phase of clinical trials<sup>84</sup>. The most advanced PTX-conjugated system is Opaxio<sup>®</sup> (poly-L-glutamic acid (PGA)-paclitaxel conjugate (formerly Xyotax<sup>®</sup>) as potential treatment for ovarian, non-small cell lung, esophageal cancer and glioblastoma<sup>85, 86</sup>. And for the treatment of prostate cancer have been studied micellar-based drugs containing paclitaxel<sup>87</sup> or used as a combination of several anticancer agents, such as estramustine plus paclitaxel<sup>88</sup> or docetaxel plus paclitaxel<sup>89</sup>, all of them were already mentioned in Chapter 1.

## 5.2 Synthesis and Characterization of novel Paclitaxel-DES conjugates used for Combination Therapy.

To synthesize the novel combination therapy systems the same polyacetal-based synthesis explained in previous chapters were employed. Then, both drugs, PTX and DES were incorporated as a random distribution, to form *tert*-polymers, or as a sequential approach to form *block-co*-polymers.

Both drugs were linked into the polymer but in a different manner, DES forming part of the main chain of the polymer and PTX attached in the polymer side chain through serinol moieties.

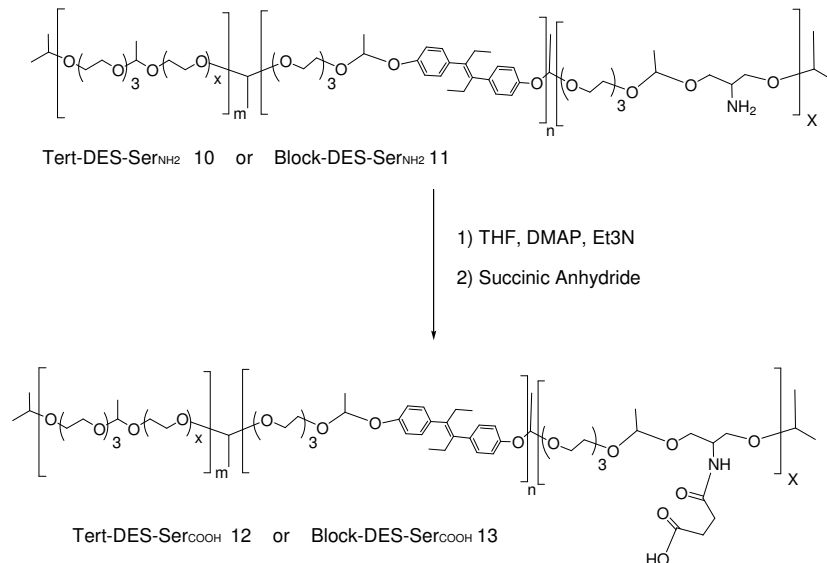
### 5.2.1. Strategy 1: Synthesis of *Tert*-DES-Ser-PTX (18) and *Block*-DES-Ser-PTX (19).

*Succinoylated polyacetals, Tert-DES-Ser<sub>COOH</sub> 12 and Block-DES-Ser<sub>COOH</sub> 13 (see scheme 5. 1) were conjugated with a second drug, Paclitaxel.*

Paclitaxel was conjugated to succinoylated polyacetals *Tert*-DES-Ser<sub>COOH</sub> **12** or *Block*-DES-Ser<sub>COOH</sub> **13** in basic conditions to obtain *Tert*-DES-Ser-PTX **18** and *Block*-DES-Ser-PTX **19** (see scheme 5. 2); their identities were confirmed by <sup>1</sup>HNMR (Figure 5. 4). Paclitaxel conjugates were stored at -20°C. *Tert*-



DES-Ser-PTX **18**  $M_w$  49.618 g/mol,  $M_w/M_n=1.5$  and *Block*-DES-Ser-PTX **19**  $M_w$  47.682 g/mol,  $M_w/M_n=1.4$  as determined by aqueous GPC.



**Scheme 5. 1** Synthesis of *Tert*-DES-Ser<sub>COOH</sub> **12** or *Block*-DES-Ser-<sub>COOH</sub> **13**.

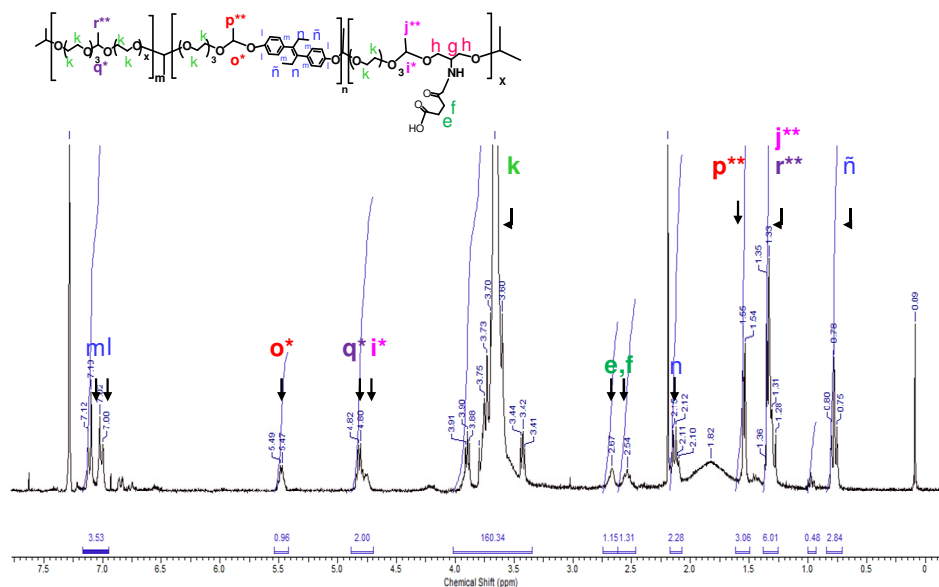
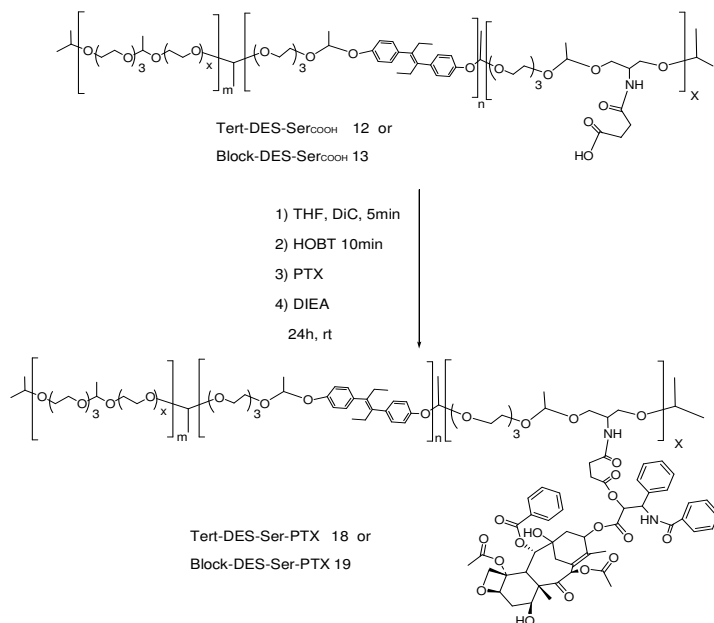


**Figure 5. 4** <sup>1</sup>H NMR spectrum of *Tert*-DES-Ser<sub>COOH</sub> **12** or *Block*-DES-Ser-<sub>COOH</sub> **13**



**Scheme 5. 2** Synthesis of *Tert*-DES-Ser-PTX 18 or *Block*-DES-Ser-PTX 19.

The <sup>1</sup>HNMR spectrum of *Tert*-DES-Ser-PTX 18 or *Block*-DES-Ser-PTX 19 (Figure 5. 5) confirmed the formation of the ester bond between the DES-SerinolNH<sub>2</sub>-polyacetal and the paclitaxel.

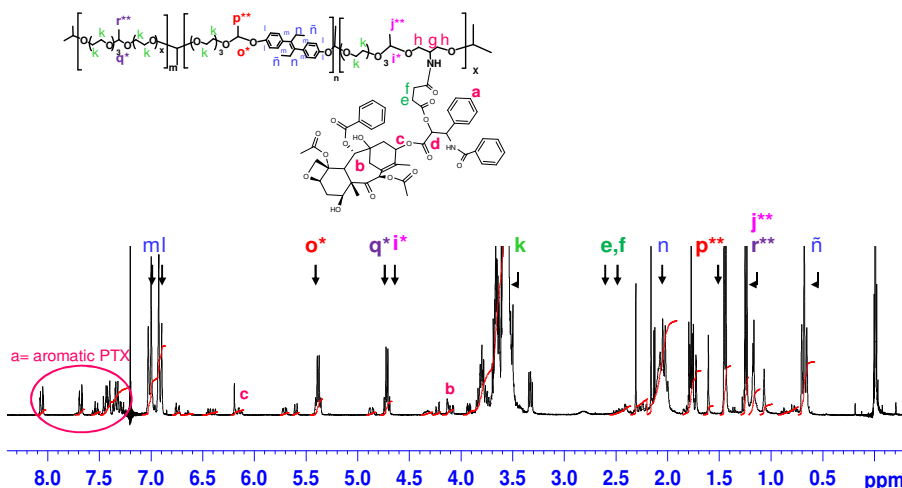
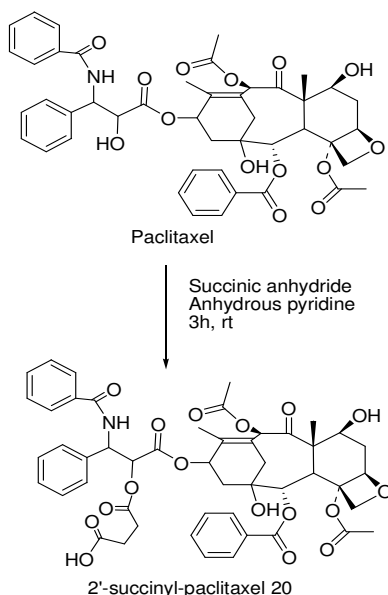


**Figure 5. 5** <sup>1</sup>HNMR spectrum of *Tert*-DES-Ser-PTX 18 or *Block*-DES-Ser-PTX 19.

### 5.2.2. Strategy 2: Synthesis of *Tert*-DES-Ser-PTX<sub>COOH</sub> (21) and *Block*-DES-Ser-PTX<sub>COOH</sub> (22).

*Polyacetals Tert*-DES-Ser<sub>NH<sub>2</sub></sub> **6** and *Block*-DES-Ser<sub>NH<sub>2</sub></sub> **7** were conjugated with the succinoylated form of Paclitaxel (PTX<sub>COOH</sub>).

First, 2'-succinyl-paclitaxel (PTX<sub>COOH</sub>) **20** (Scheme 5. 3) confirmed by <sup>1</sup>HNMR (Figure 5. 6) was prepared according to Deutsch *et al*<sup>90</sup>. PTX was chemically modified by succinylation to introduce carboxylic acid functional groups to which the primary amines present in *Tert*-DES-Ser<sub>NH<sub>2</sub></sub> **6** and *Block*-DES-Ser<sub>NH<sub>2</sub></sub> **7** could be bound to, using a simple carbodiimide coupling reaction with EDC and Sulfo-NHS to form *Tert*-DES-Ser-PTX **21** and *Block*-DES-Ser-PTX **22**, respectively (Scheme 5. 4). The conjugates with PTX were obtained and their identity also confirmed by <sup>1</sup>H-NMR (Figure 5. 5) and signals schematically represented in Figure 5. 7.



**Scheme 5. 3** Synthesis of 2'-succinyl-paclitaxel 20.

Evidence for the site of esterification for 2'-succinyl-paclitaxel (PTX<sub>COOH</sub>) **20** was obtained from <sup>1</sup>HNMR (Figure 5. 6), where the C2' proton of the non-succinylated paclitaxel at 4.8 ppm appeared as a doublet at 5.54 ppm. And

also it was possible to observe the new sets of peaks of 4 protons that corresponded to the succinyl molecule at 2.64 and 2.76ppm.

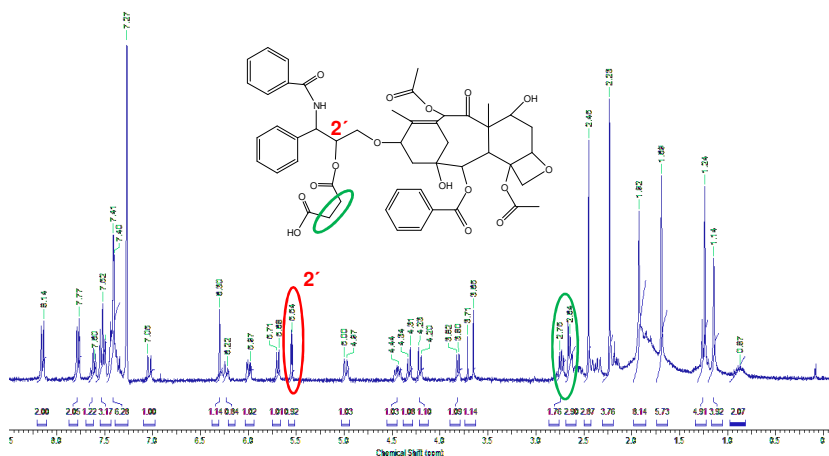
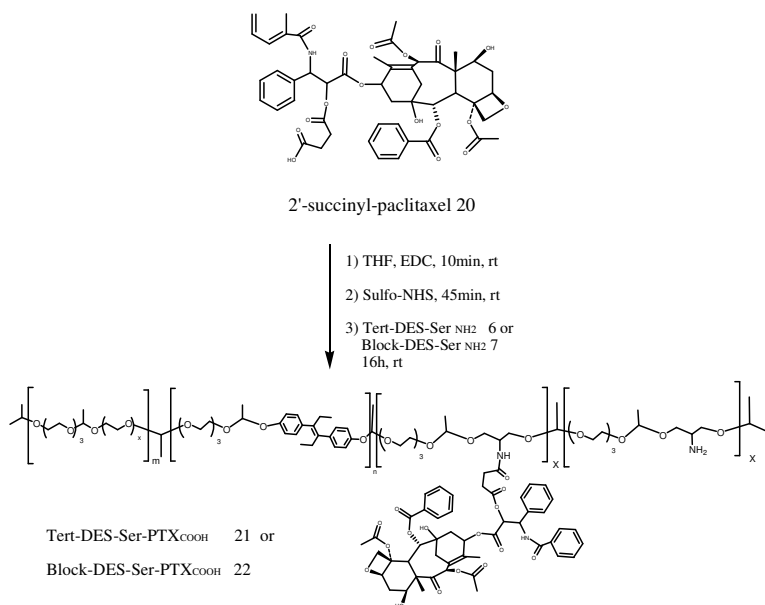


**Figure 5.6**  $^1\text{H}$ NMR spectrum of 2'-succinyl-paclitaxel 20.



**Scheme 5.4** Synthesis of *Tert*-DES-Ser-PTX **21** or *Block*-DES-Ser-PTX **22**.

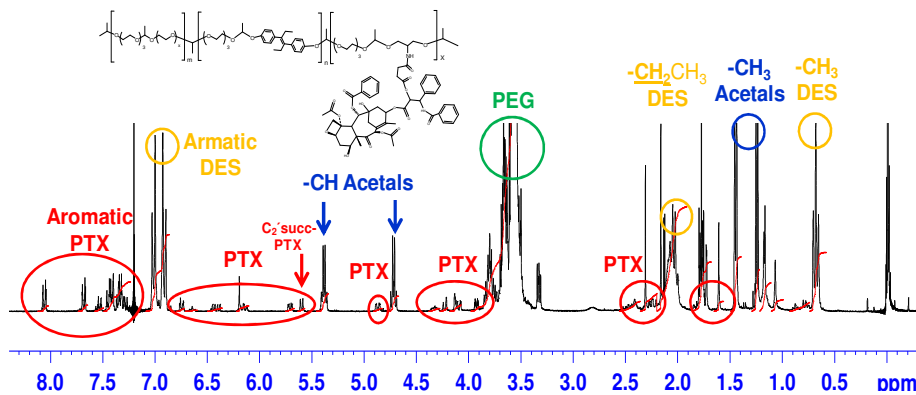


**Figure 5. 7**  $^1\text{H}$ NMR spectrum with assigned signals fobtaned from *Tert*-DES-Ser-PTX **21** or *Block*-DES-Ser-PTX **22**.

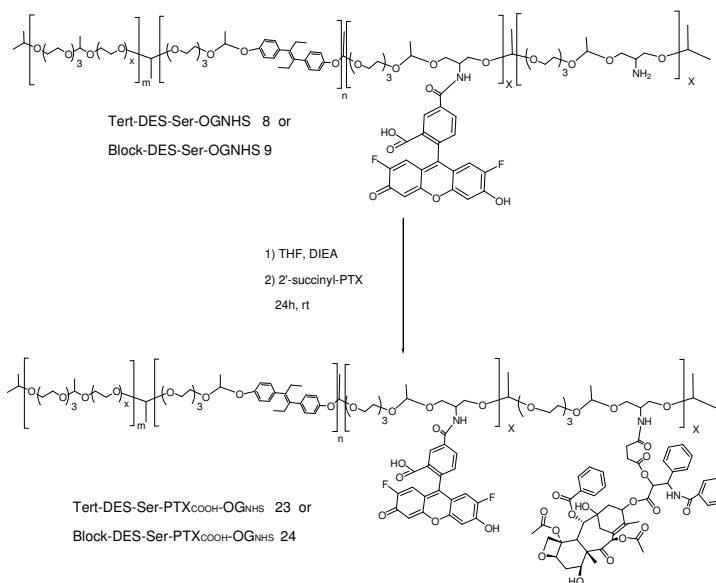
The  $^1\text{H}$ NMR spectrum of *Tert*-DES-Ser-PTX **21** or *Block*-DES-Ser-PTX **22** (Figure 5. 7) also confirmed the formation of an ester bond between the DES-SerinolNH<sub>2</sub>-polyacetal and the 2'-succinyl-paclitaxel **20**.

### 5.2.3 Synthesis and Characterization of Fluorescence-labeled paclitaxel conjugates, *Tert*-DES-Ser-PTX-OG and *Block*-DES-Ser-PTX-OG and *Tert*-DES-Ser-PTX-Cy and *Block*-DES-Ser-PTX-Cy.

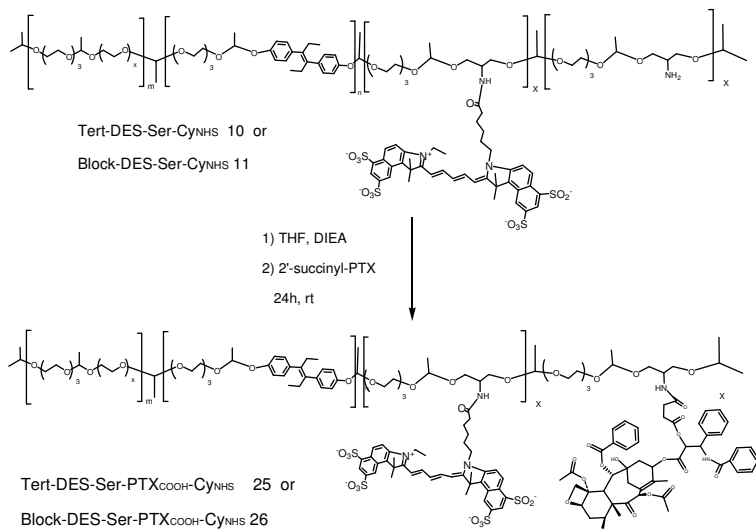
#### 5.2.3.1 Strategy 1. Synthesis of fluorescence-labeled-PTX conjugates I.

a) Synthesis of *Tert*-DES-Ser-PTX<sub>COOH</sub>-OG<sub>NHS</sub> (**23**), *Block*-DES-Ser-PTX<sub>COOH</sub>-OG<sub>NHS</sub> (**24**), *Tert*-DES-Ser-PTX<sub>COOH</sub>-Cy<sub>NHS</sub> (**25**) and *Block*-DES-Ser-PTX<sub>COOH</sub>-Cy<sub>NHS</sub> (**26**).

As starting compound can be any of the fluorescence-labeled polyacetals synthesized: *Tert*-DES-Ser-OG<sub>NHS</sub> **8**, *Block*-DES-Ser-OG<sub>NHS</sub> **9**, *Tert*-DES-Ser-Cy<sub>NHS</sub> **10** or *Block*-DES-Ser-Cy<sub>NHS</sub> **11**. To these polyacetals 2'-succinyl-paclitaxel (PTX<sub>COOH</sub>) was conjugated through the free amine groups from the serinol moiety. The residue was purified by PD10 column and analyzed by  $^1\text{H}$ NMR. The fractions with the conjugate were recollected to obtain: *Tert*-DES-Ser-PTX<sub>COOH</sub>-OG<sub>NHS</sub> **23**, *Block*-DES-Ser-PTX<sub>COOH</sub>-OG<sub>NHS</sub> **24** (see Scheme 5. 5), *Tert*-DES-Ser-PTX<sub>COOH</sub>-Cy<sub>NHS</sub> **25** and *Block*-DES-Ser-PTX<sub>COOH</sub>-Cy<sub>NHS</sub> **26** (see Scheme 5. 6).



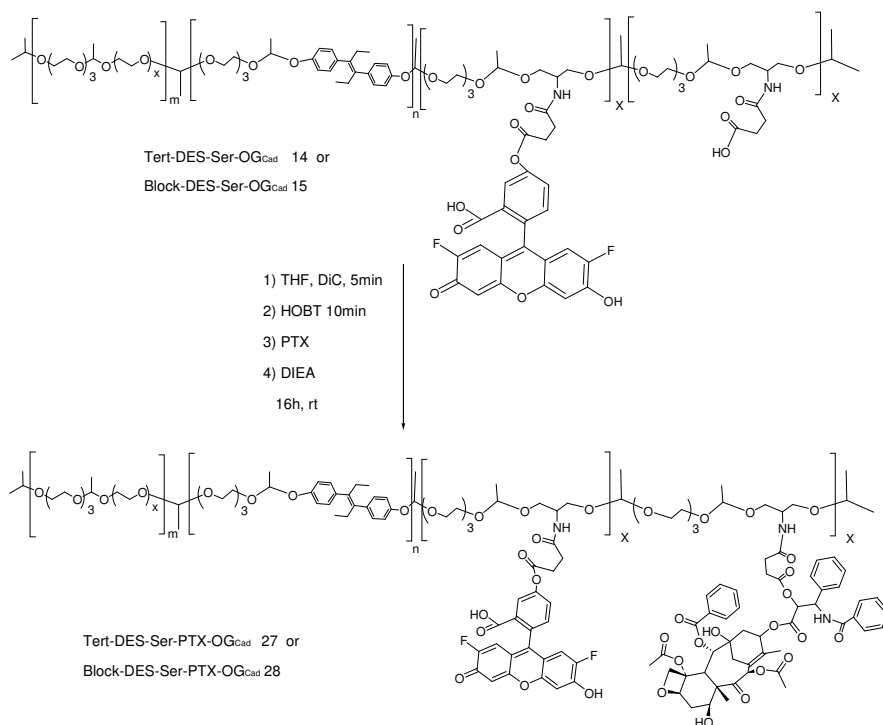
**Scheme 5. 5** Synthesis of *Tert*-DES-Ser-PTX<sub>COOH</sub>-OG<sub>NHS</sub> **23** or *Block*-DES-Ser-PTX<sub>COOH</sub>-OG<sub>NHS</sub> **24**.



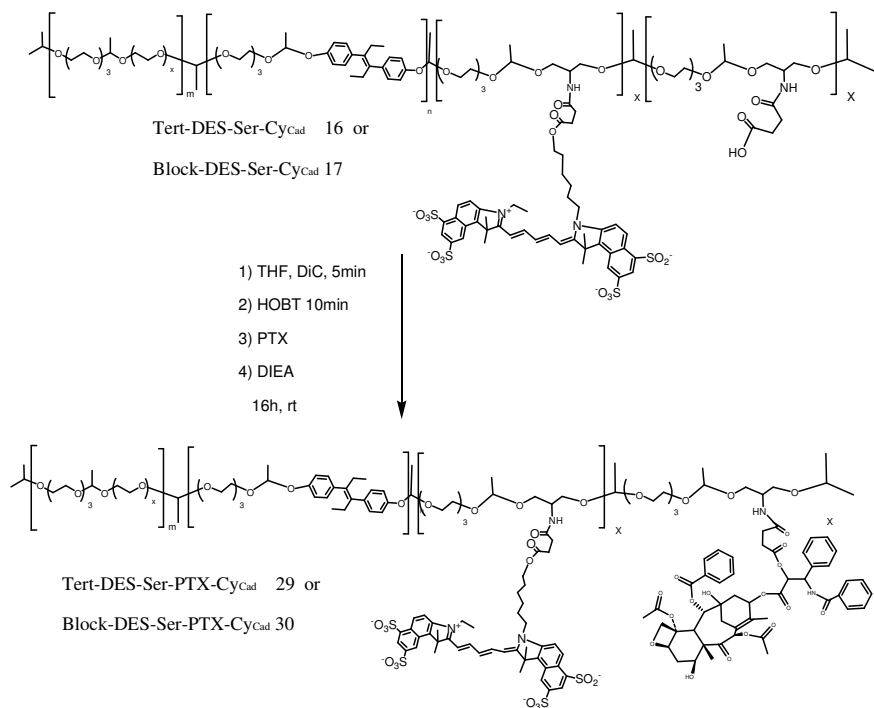
**Scheme 5. 6** Synthesis of *Tert*-DES-Ser-PTX<sub>COOH</sub>-Cy<sub>NHS</sub> **25** or *Block*-DES-Ser-PTX<sub>COOH</sub>-Cy<sub>NHS</sub> **26**.

**b) Synthesis of *Tert*-DES-Ser-PTX-OG<sub>cad</sub> (27), *Block*-DES-Ser-PTX-OG<sub>cad</sub> (28), *Tert*-DES-Ser-PTX-Cy<sub>cad</sub> (29) and *Block*-DES-Ser-PTX-Cy<sub>cad</sub> (30).**

As starting compound any of the already fluorescently-labeled polyacetal synthesized could be used, such as: *Tert*-DES-Ser-OG<sub>cad</sub> **14**, *Block*-DES-Ser-OG<sub>cad</sub> **15**, *Tert*-DES-Ser-Cy<sub>NH<sub>2</sub></sub> **16** or *Block*-DES-Ser-Cy<sub>NH<sub>2</sub></sub> **17**. To these polyacetals PTX was conjugated through the free carboxylic group in the polyacetal succinoylated serinol-side chain. The residue was washed with hexane and the crude was purified by LH20 column the fractions were analyzed by <sup>1</sup>HNMR confirming the presence of the desired compounds, *Tert*-DES-Ser-PTX-OG<sub>cad</sub> **27**, *Block*-DES-Ser-PTX-OG<sub>cad</sub> **28** (see Scheme 5. 7), *Tert*-DES-Ser-PTX-Cy<sub>NH<sub>2</sub></sub> **29** and *Block*-DES-Ser-PTX-Cy<sub>NH<sub>2</sub></sub> **30** (see Scheme 5. 8).



**Scheme 5. 7** Synthesis of *Tert*-DES-Ser-PTX-OG<sub>cad</sub> **27** or *Block*-DES-Ser-PTX-OG<sub>cad</sub> **28**.



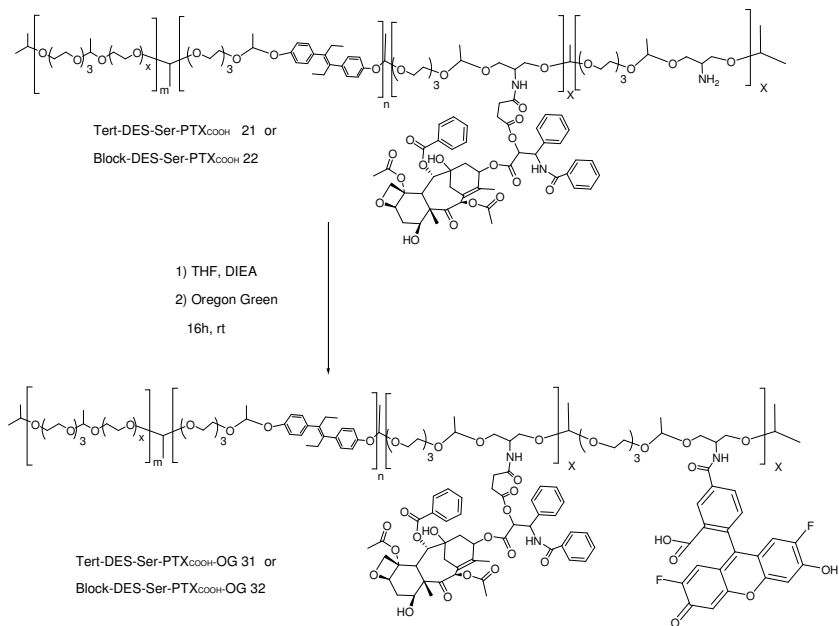
**Scheme 5. 8** Synthesis of *Tert*-DES-Ser-PTX-Cy<sub>cad</sub> 29 or *Block*-DES-Ser-PTX-Cy<sub>cad</sub> 30.

### 5.2.3.2 Strategy 2. Synthesis of fluorescently-labelled-PTX conjugates II.

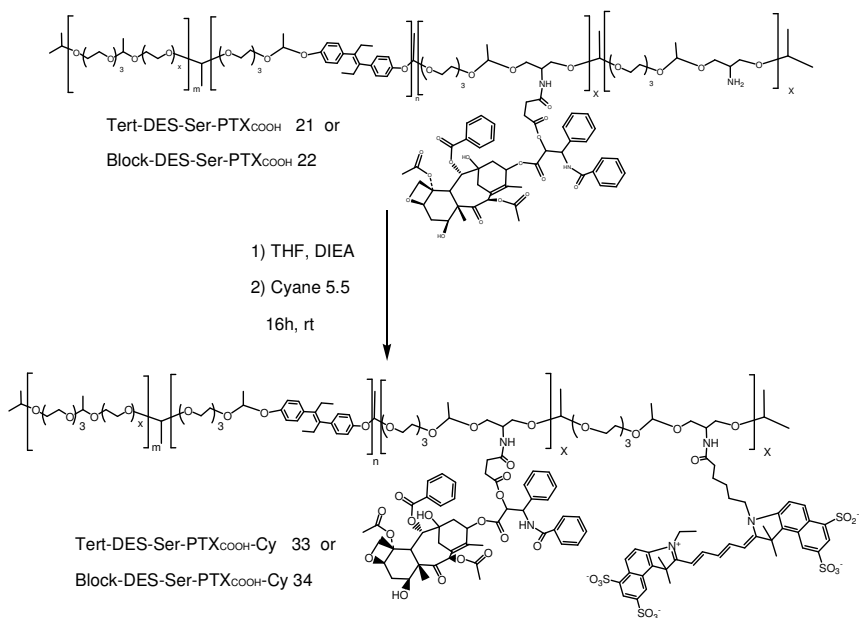
**a) Synthesis of OG<sub>NHS</sub>/Cy<sub>NHS</sub>-labeled PTX<sub>COOH</sub> conjugates, *Tert*-DES-Ser-PTX<sub>COOH</sub>-OG<sub>NHS</sub> (31), *Block*-DES-Ser-PTX<sub>COOH</sub>-OG<sub>NHS</sub> (32), *Tert*-DES-Ser-PTX<sub>COOH</sub>-Cy<sub>NHS</sub> (33) and *Block*-DES-Ser-PTX<sub>COOH</sub>-Cy<sub>NHS</sub> (34).**

The conjugation of *Tert*-DES-Ser-PTX<sub>COOH</sub> 21 and *Block*-DES-Ser-PTX<sub>COOH</sub> 22 with OG<sub>NHS</sub> or Cy<sub>NHS</sub> were done using same procedure described for 8, 9, 10 and 11. Then Cy5.5 or OG PTX-conjugates were obtained, *Tert*-DES-Ser-PTX<sub>COOH</sub>-OG<sub>NHS</sub> 31, *Block*-DES-Ser-PTX<sub>COOH</sub>-OG<sub>NHS</sub> 32 (Scheme 5. 9), *Tert*-DES-Ser-PTX<sub>COOH</sub>-Cy<sub>NHS</sub> 33 and *Block*-DES-Ser-PTX<sub>COOH</sub>-Cy<sub>NHS</sub> 34, (Scheme 5. 10).





**Scheme 5. 9** Synthesis of *Tert*-DES-Ser-PTX<sub>COOH</sub>-OG<sub>NHS</sub> **31** or *Block*-DES-Ser-PTX<sub>COOH</sub>-OG<sub>NHS</sub> **32**.



**Scheme 5. 10** Synthesis of *Tert*-DES-Ser-PTX<sub>COOH</sub>-Cy<sub>NHS</sub> **33** or *Block*-DES-Ser-PTX<sub>COOH</sub>-Cy<sub>NHS</sub> **34**.

The second strategy resulted to be the most efficient, thus all the compounds were finally obtained using this procedure. The quantification of the fluorescent dyes were done by fluorescent measurements using a Fluorimetry Victor 2 Wallac station as it was reported in Chapter 4.1 (section 4.1.5. 1 (4)). The physicochemical characteristic of all combination conjugates synthesized are summarized in Table 5. 2.

**Table 5. 2** Physico-chemical characteristics of the synthesized polyacetals for combination therapy.

Conjugate	DES Loading <sup>a</sup> (wt%)	Free DES content <sup>a,b,c</sup> (wt% of total drug)	PTX Loading <sup>a</sup> (wt%)	Free PTX content <sup>b</sup> (wt% of total drug)	Mw <sup>d</sup> (g/mol)	Mw/Mn <sup>d</sup>
T-DES-Ser-PTX 21 a	<b>0.3 ± 0.3</b>	0.1 ± 0.1	<b>0.7 ± 0.1</b>	0.2 ± 0.1	27.546	1.60
T-DES-Ser-PTX 21b	<b>1.5 ± 0.3</b>	0.2 ± 0.1	<b>0.8 ± 0.1</b>	0.2 ± 0.1	29.331	1.60
T-DES-Ser-PTX 21c	<b>2.0 ± 0.2</b>	0.2 ± 0.1	<b>1.7 ± 0.1</b>	0.4 ± 0.1	30.124	1.62
B-DES-Ser-PTX 22a	<b>0.5 ± 0.2</b>	0.1 ± 0.1	<b>0.7 ± 0.1</b>	0.2 ± 0.1	27.210	1.54
B-DES-Ser-PTX 22b	<b>2.0 ± 0.2</b>	0.2 ± 0.1	<b>1.8 ± 0.1</b>	0.3 ± 0.1	28.200	1.55
B-DES-Ser-PTX 22c	<b>2.1 ± 0.2</b>	0.1 ± 0.1	<b>2.6 ± 0.1</b>	0.4 ± 0.1	28.230	1.55

<sup>a</sup>Determined by <sup>1</sup>H NMR; <sup>b</sup>Determined by HPLC analysis; <sup>c</sup>Determined by ninhydrine assay; <sup>d</sup>Determined by size exclusion chromatography (GPC, Viscotek TDA<sup>TM</sup>; DES: Diethylstilbestrol, Ser: Serinol, PTX: paclitaxel, Mw: Molecular weight, Mw/Mn: polydispersity index).

### 5.3 Physicochemical characterization: SANS and PGSE-NMR studies.

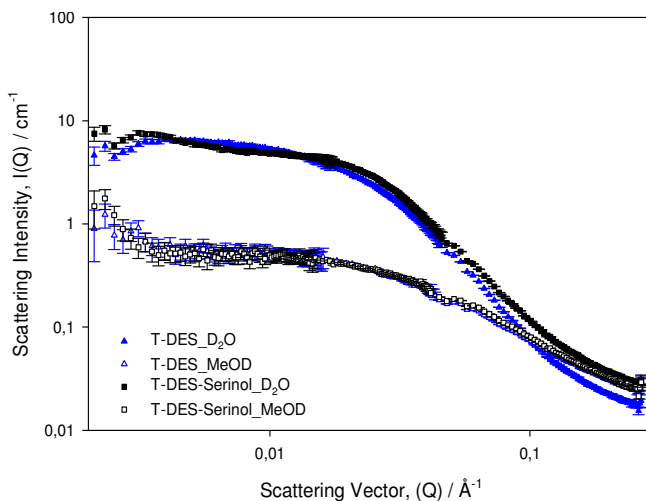
As it was explained already in Chapter 4.2, the size and shape of a nanoconjugate in solution is critical for understanding cellular internalization and ultimately therapeutic output. For this reason, PFG-NMR and SANS experiments were also performed with the polyacetal-based combination conjugates prior to any biological studies.

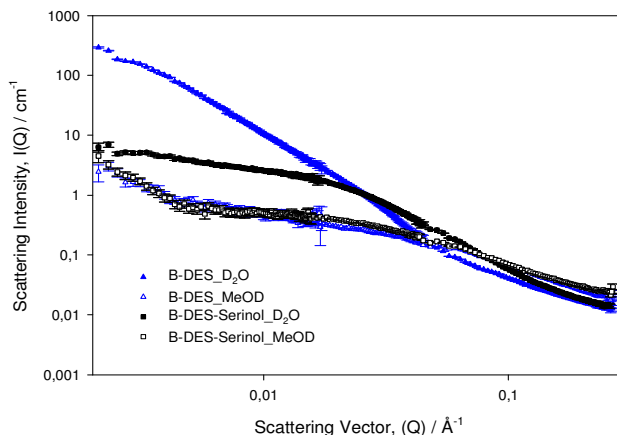
As already reported above, in order to incorporate PTX or a fluorescent dye in the polyacetalic system the monomer serinol had to be incorporated in the polymer main chain. Therefore, the precursors with serinol bearing Fmoc-protected amine group were analyzed by SANS in order to determine if the presence of serinol could influence *Tert*- or *Block*-polyacetal solution conformation.

#### a) Influence of Serinol in polyacetal conformation.

Polyacetals bearing Fmoc-protected serinol, *Tert*-DES-Ser and *Block*-DES-Ser with similar DES loading were studied. The comparison between *Tert*- and *Block* with and without serinol was performed to facilitate any possible conformational influence due to the presence of the serinol monomer (Figure 5 8.)

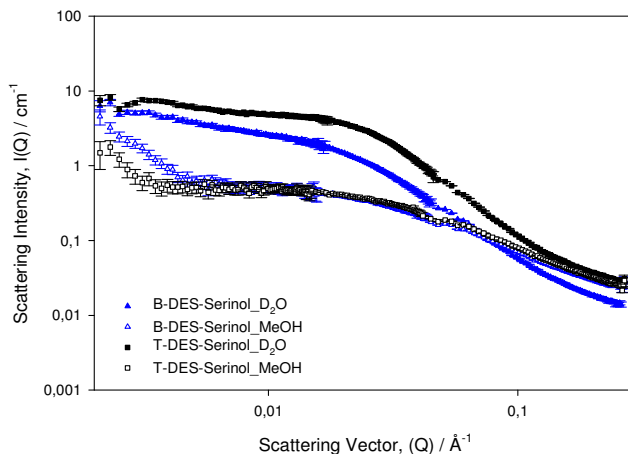
A.



**B.**

**Figure 5. 8** SANS data from (A) *Tert*-polymers and (B) *Block*-polymers in D<sub>2</sub>O and MeOD solutions at fixed DES content (4wt%) concentrations. (A) *Tert*-DES (blue triangles, D<sub>2</sub>O (filled), MeOD (open)); *Tert*-DES-Ser (black squares, D<sub>2</sub>O (filled), MeOD (open)); (B) *Block*-DES (blue triangles, D<sub>2</sub>O (filled), MeOD (open)); *Block*-DES-Ser (black square, D<sub>2</sub>O (filled), MeOD (open)). Error bars are shown. Where shown, lines are best model fits to the data as described in the text.

Figure 5.8 A shows *Tert*-DES **1b** vs. *Tert*-DES-Ser **4b** and Figure 5.8B *Block*-DES **2b** vs. *Block*-DES-Ser **5b**. In both graphs the scatter obtained from the conjugates in two different solvents, *d*-water and *d*-methanol, has been represented.

**A.**

B.

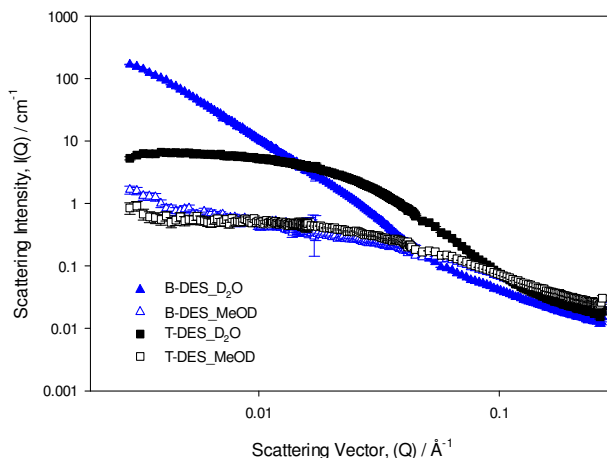


**Figure 5. 9 (A)** SANS data from *Tert*-DES-Ser, 3.7wt%DES and 3.1wt%Serinol, (black squares) and block-DES-Serinol, 3.6wt%DES and 3.2wt%Serinol, (blue triangles) polymer solutions in D<sub>2</sub>O (filled figures) and MeOD (open figures). **(B)** SANS data from *Tert*-DES (black squares) and Block-DES-Serinol (blue triangles) polymer solutions in D<sub>2</sub>O (filled figures) and MeOD (open figures) both at same DES concentration 4wt%. Error bars are shown.

After serinol incorporation, when analyzed in *d*-methanol, the scattering profiles at high and low  $Q$  seemed to be identical for *tert* and *block* systems. However, when the polyacetals were studied in *d*-water, whereas the scattering profiles for the *tert*-polymers looked similar, the profiles for the *block*-polyacetals were very different. This fact confirmed that serinol induced a more dominant effect on solution conformation with the *block* distribution.

In Figure 5. 9 A. the comparison between both polymers with serinol, *Tert*-DES-Ser (black squares) and *Block*-DES-Ser (blue triangles) in *d*-water and *d*-methanol is shown. To allow better comparison with the original polyacetals those are again represented in Figure 5. 9 B (previously reported in chapter 4.2).

Looking the scattering profiles in Figure 5. 9 A, in *d*-methanol, at high  $Q$  the profiles were very similar. On the other hand, at low  $Q$  differences were encountered which could indicate a different polymer conformation. However, these differences in *d*-water were much less pronounced if

compared with the polyacetals **1b** and **2b** (Fig 5. 9B), without serinol moieties. The scattering profiles were of similar shape but just a change in intensity was observed. These results could indicate that the serinol triggered a more dominant effect on the conjugate solution conformation than the fact of being *block*-or *tert*-.

Summarizing, the addition of serinol dramatically changed the scattering shape and the differences seen between *Tert*-DES and *Block*-DES polymers were significantly diminished.

**b) Solution conformation of polyacetal-based combination conjugates. Influence of the presence of paclitaxel in DES-polyacetals.**

In Figure 5. 10, *Tert*-DES-Ser-PTX and both parent single conjugates, one without PTX (*Tert*-DES-Ser) and the other without DES (*Tert*-Ser-PTX) have been represented in order to detect and compare any effect on solution conformation due to the incorporation of each component.

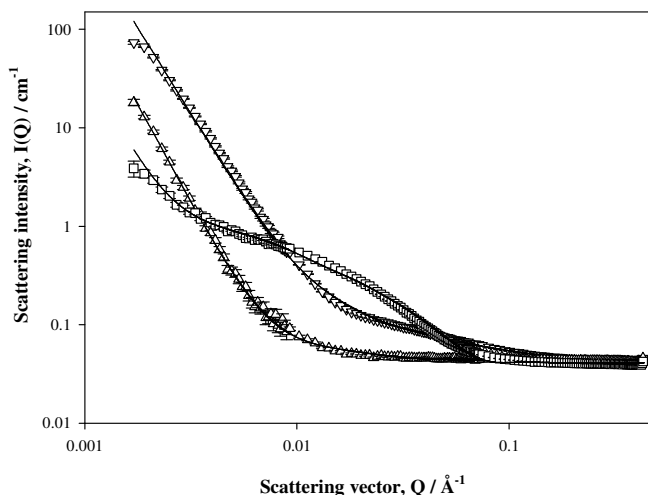


**Figure 5. 10** SANS data from 1wt% *Tert*-polymer solutions in D2O. *Tert*-DES **1b** (squares); *Tert*-DES-Ser-PTX **21a** (inverted triangles); *Tert*-Ser-PTX Ia (triangles). Error bars are shown. Where shown, lines are best model fits to the data as described in the text.

Significant scattering profile differences could be observed when compare *Tert*-DES-Ser with the synthesized polyacetals containing PTX, *Tert*-DES-Ser-PTX **21b** and *Tert*-Ser-PTX **1a**, both with profiles similar in shape but not in intensity. This fact clearly demonstrated that the incorporation of PTX is one of the major driven forces regarding solution conformation.

Finally, after the analysis of scattering data coming from Guinier and Zimm approximations, the FISH computer modeling was used in order to get the conformation of the conjugates. All modeling was done in collaboration with Dr. Alison Paul at Cardiff University.

Summarizing the main results of this approach it could be said that, the *Tert*-Ser-PTX sample was best fitted to a thin rod of radius 10Å, length 300Å, with a  $Q^{-n}$  term with  $n=3.5$ . It was also shown that the scattering was dominated by a  $Q^{-4}$  term with the addition of PTX to *Tert*-DES-Ser yielding *Tert*-DES-Ser-PTX; this could indicate the presence of extremely large structures that are out of the resolution for a SANS experiment. The same was true for the *Block*-DES-Ser-PTX. This experiment clearly confirmed that PTX is the one driven solution conformation of the polyacetals probably due for its high hydrophobicity that could induce significant differences in aggregation parameters.

### PGSE-NMR studies with DES-Serinol Polyacetals

Again, as it was done for *Tert*-DES and *Block*-DES in chapter 4, the relative particle sizes of the conjugates were obtained by PGSE-NMR measurements. Figure 5. 11 shows PGSE-NMR data for 10 mg/mL solutions of *Tert*-DES-Ser and *Block*-DES-Ser, plotted according to equation 4.2.3 (see chapter 4.II section), using the normalized signal intensity. Presented in this manner, the difference in slopes indicated a clear difference in the obtained self-diffusion rates between the two conjugates, with the *Tert*-DES-Ser conjugate,  $D_s=4.50 \times 10^{-11} \text{ m}^2 \text{ s}^{-1}$  (for *tert*-DES,  $D_s=2.72 \times 10^{-11} \text{ m}^2 \text{ s}^{-1}$ ) moving more slowly than the *Block*-DES-Ser counterpart  $D_s=5.17 \times 10^{-11} \text{ m}^2 \text{ s}^{-1}$  (for *block*-DES,  $D_s=5.87 \times 10^{-11} \text{ m}^2 \text{ s}^{-1}$ ) similar to that found for the polyacetals without serinol (**1b** and **2b**). The diffusion coefficient values obtained clearly indicated that different solution structures were formed in each case.

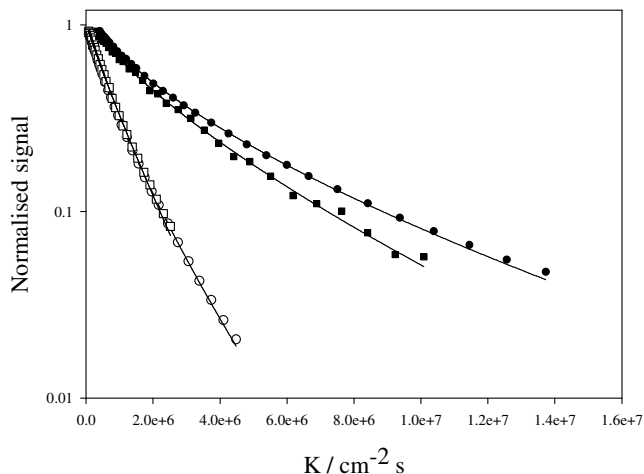


**Figure 5. 11** Normalized PGSE-NMR data from 1wt% conjugate solutions at 25°C; *Tert-DES-Ser* in D2O (filled circles) and methanol (open circles); *Block-DES-Ser* in D2O (filled squares) and methanol (open squares). All of them are fitted to stretch diffusion coefficients.

#### 5.4 Biological evaluation of *Polyacetal-DES-Ser-PTX* combination conjugates<sup>1</sup>.

##### 5.4.1 Evaluation of DES-PTX derivatives in Breast and prostate human cell models

##### 5.4.1. 1 *In vitro* Efficacy of DES-Polyacetals conjugates in breast cancer cell models.

Single (*Tert-DES 1b* and *Block-DES 2b*) and combination polyacetals (*Tert-DES-Ser-PTX 21a* and *Block-DES-Ser-PTX 22a*) were tested against MDA-MB-4355.eGFP breast cancer cells to evaluate their cytotoxic effect in this hormone-independent cell line (Figure 5. 12A and B).

<sup>1</sup> To Note all these experiments have been performed at Dr- Schwartz Jr. Lab. at CIBBIMM-Nanomedicine, Hospital Vall d'Hebron, Barcelona.



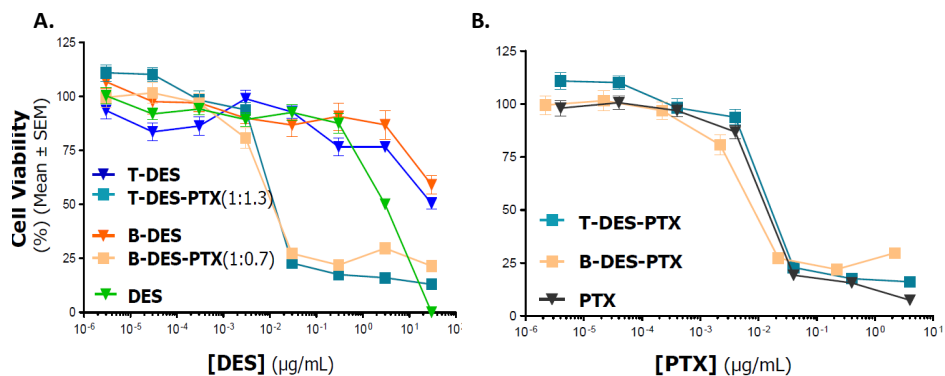


**Figure 5. 12** *In vitro* MTT cell viability assays after 72 h incubation of DES derivatives against MDA-MB-4355.eGFP breast cancer cell line; (A) at concentrations of DES equivalents; (B) at concentrations of PTX equivalents used. T-DES= *Tert*-DES **1b**; B-DES= *Block*-DES **2b**; T-DES-PTX=*Tert*-DES-Ser-PTX **21a** ; B-DES-PTX=*Block*-DES-Ser-PTX **22a**.

In MDA-MB-4355.eGFP cells the  $IC_{50}$  (Table 5. 3) value encountered for the combination conjugate *Tert*-DES-PTX was twice as lower as its *Block*-DES-PTX analogue (0.006  $\mu\text{g/ml}$  vs. 0.012  $\mu\text{g/ml}$  PTX-equiv., respectively) and more importantly, even lower than the parent free drug (0.006 vs. 0.009  $\mu\text{g/ml}$ , PTX-equiv.).

**Table 5. 3**  $IC_{50}$  values for DES-PTX polymers compared with free PTX (n=3).

$IC_{50}$ ( $\mu\text{g PTX/ml}$ )		
T-DES-PTX	B-DES-PTX	PTX
0.006 $\pm$ 0.001	0.012 $\pm$ 0.001	0.009 $\pm$ 0.001

#### 5.4.1. 2 *In vitro* Efficacy of DES-Polyacetals conjugates in prostate cancer cell models.

*In vitro* cell viability assays (72h MTT assay) were carried out in the two prostate cancer cell lines already mentioned in Chapter 4, PC-3 cells (androgen independent) and LNCaP cells (androgen sensitive).

### a) *In vitro* efficacy of DES-PTX-polyacetals conjugates

DES derivatives were tested in PC-3 cell line (Figure 5. 13 A,B) and LNCaP cells (Figure 5. 13 C,D) to obtain the *in vitro* efficacy of the polymers.

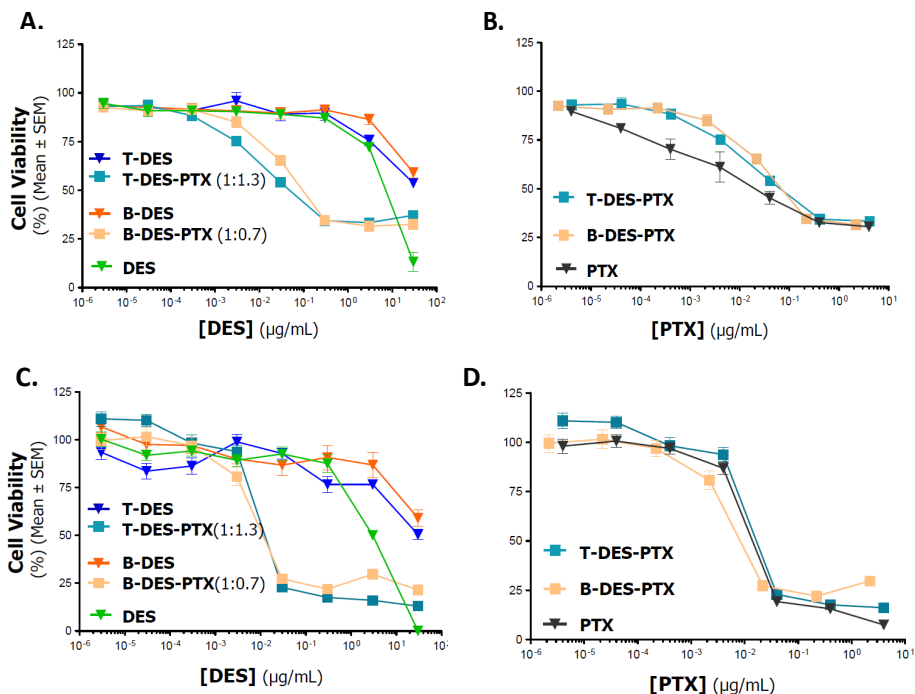


**Figure 5. 13** *In vitro* MTT cell viability assays of the polyacetals and of the single drugs, at concentrations of DES-equivalents (A, C) and at concentrations of PTX-equivalents (B, D), in PC3 (A, B) and in LNCaP (C, D) prostate cancer cells.

Looking at the Figure 5. 13 and Table 5. 4 it was clearly observed that in PC3 cell line, DES was active only at high concentrations and the DES-PTX combination polymers were not more active than the single PTX. In LNCaP was possible to observe that DES was as well active at high concentrations and the polyacetal *Block-DES-PTX* was more active than PTX alone.

**Table 5. 4** IC<sub>50</sub> values of the single drugs and the polyacetals at concentrations of DES (A, C) and at concentrations of PTX (B, D), in PC3 (A, B) and LNCaP (C, D) prostate cancer cells.

A. IC <sub>50</sub> (µg DES/mL)			B. IC <sub>50</sub> (µg PTX/mL)		
T-DES-PTX	B-DES-PTX	DES	T-DES-PTX	B-DES-PTX	PTX
0.019 ± 0.079	0.280 ± 0.154	7.250 ± 2.681	0.258 ± 0.107	0.204 ± 0.113	0.010 ± 0.005

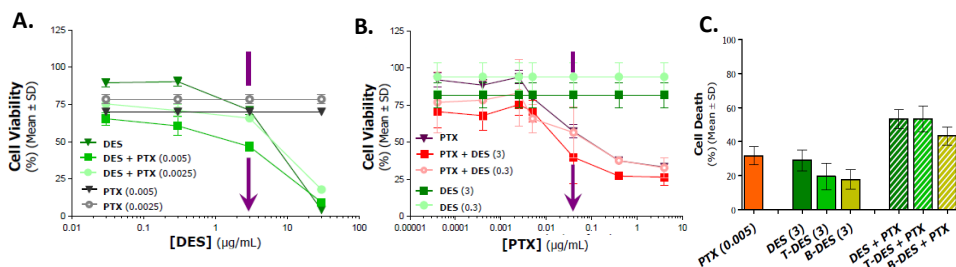
  

C. IC <sub>50</sub> (µg DES/mL)			D. IC <sub>50</sub> (µg PTX/mL)		
T-DES-PTX	B-DES-PTX	DES	T-DES-PTX	B-DES-PTX	PTX
0.015 ± 0.001	0.017 ± 0.001	2.240 ± 0.920	0.020 ± 0.002	0.012 ± 0.001	0.015 ± 0.003

**b) *In vitro* free drug combination efficacy with DES-Polyacetals.**

To optimize drug ratio for combination conjugates, MTT assays were performed to compare drug combinations (single drugs DES+PTX, PTX+ *Tert*-DES and PTX+ *Block*-DES polymers) in PC-3 and LNCaP prostate cancer cell lines (Figure 5. 14).

**PC3 cell line**



**LNCaP cell line**

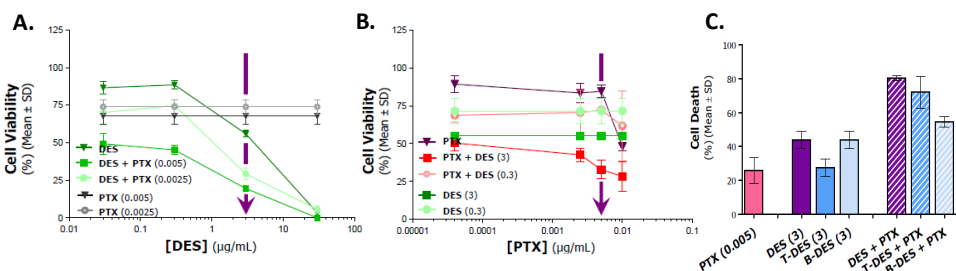


**Figure 5. 14** *In vitro* MTT cell viability assays after 72 h of the single drugs, the combination of single drugs and the combination of PTX with DES-

polymers, at fixed concentration of PTX in a concentrations range of DES (**A**) and at fixed concentrations of DES in a concentrations range of PTX (**B**) and cell death percentage at concentrations indicated with an arrow in cell viability graphs (**C**).

The experiments were carried out fixing the concentration of one of the drugs but trying a concentration range of the other drug. For example if PTX was fixed, a test with a range of DES concentrations was performed. And also fixing the concentration of DES and trying a test with a concentration range of PTX. The fixed PTX concentrations were 0.0025 and 0.005  $\mu\text{g/mL}$  and the fixed DES concentrations were 0.3 and 3  $\mu\text{g/mL}$ .

It was showed that the best results were obtained with high DES doses in both prostate cancer cell lines. DES and PTX may have clear synergism in LNCaP cells at 3 $\mu\text{g/mL}$  of DES and 0.005  $\mu\text{g/mL}$  of PTX.

### c) *In Vitro* Efficacy of PTX-polyacetal conjugates, single vs. combination.

The compound *Tert*-DES-PTX was compared with PTX alone and with PTX conjugated only to the polymer *Tert*-PTX (or T-PTX), in both prostate cancer cell lines as Figure 5.15 shows below.

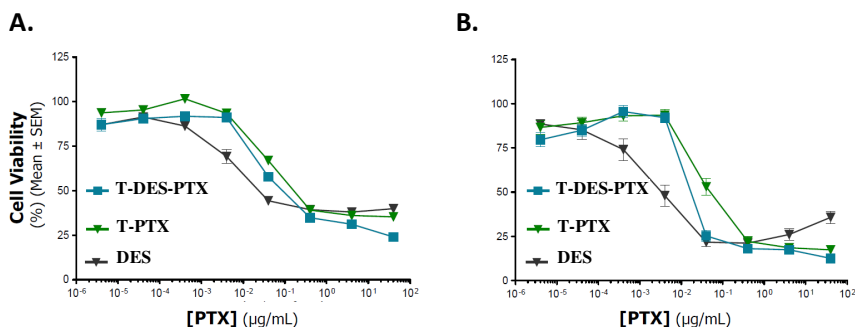


**Figure 5. 15** *In vitro* MTT cell viability assays of PTX, T-PTX (*Tert*-PTX) and T-DES-PTX (*Tert*-DES-Ser-PTX) compounds. PC-3 (**A**) and LNCaP (**B**) cells. Assays were performed in triplicates and mean and SEM are represented for each concentration point tested.

As already described in chapter 4, the polymers and the single drug were more active in LNCaP cell lines, due to DES is a estrogen and this cell line presents

androgen-sensitivity (Table 5. 5). And more importantly, the combination conjugate showed a significantly greater activity than the single PTX conjugate in both cell lines.

**Table 5. 5** IC<sub>50</sub> values for PTX, *Tert*-PTX (*Tert*-Ser-PTX or T-PTX) and *Tert*-DES-PTX compounds in PC-3 (A) and LNCaP cell lines (B).

A.	IC <sub>50</sub> (µg PTX/mL)			B.	IC <sub>50</sub> (µg PTX/mL)		
	PTX	T-PTX	T-DES-PTX		PTX	T-PTX	T-DES-PTX
	0.067 ± 0.027	0.764 ± 0.381	0.234 ± 0.093		0.007 ± 0.003	0.152 ± 0.141	0.036 ± 0.036

**d) Evaluation of the combined DES-PTX polyacetals to determine synergistic, additive or antagonistic effect.**

As it was mentioned in the introduction the combination index, CI indicates if the combination of several drugs, in this case PTX and DES, presents an additive, synergistic or an antagonistic effect after administration of both drugs using the same carrier system. CI is obtained by using the equation 5.1;  $[D_1/(D_m)_1] + [D_2/(D_m)_2] = 1$  (1 and 2 are the different drugs; D<sub>1</sub> and D<sub>2</sub>= doses of the drugs that in combination produce 50% inhibition of luminescence; (D<sub>m</sub>)<sub>1</sub> and (D<sub>m</sub>)<sub>2</sub> correspond to the doses of the drugs when applied singly causing as well 50% inhibition of luminescence).

In this case is represented; 1=DES and 2=PTX:

- For *Tert*-polyacetals (*Tert*- represented as well as T-) conjugates:  
D<sub>1</sub>=IC50 T-DES-Ser-PTX and D<sub>2</sub>= IC50 T-DES-Ser-PTX  
(D<sub>m</sub>)<sub>1</sub>=IC50 T-DES and (D<sub>m</sub>)<sub>2</sub>= IC50 T-PTX
- For *Block*-polyacetals (*Block*- represented as well as B-) conjugates:  
D<sub>1</sub>=IC50 B-DES-Ser-PTX and D<sub>2</sub>= IC50 B-DES-Ser-PTX  
(D<sub>m</sub>)<sub>1</sub>=IC50 B-DES and (D<sub>m</sub>)<sub>2</sub>= IC50 B-PTX

The IC<sub>50</sub> of T-DES and B-DES were already reported in the Table 4.1.6 (Chapter 4.1) for PC3 and LNCaP cell lines. However, we summarize all data here to allow better understanding (Table 5. 6).

**Table 5. 6** IC<sub>50</sub> for *Tert*-DES, *Block*-DES and their analogues in combination with PTX (DES-PTX-poyacetalic-based) systems.

IC50	PC-3(µg/mL DES eq)	PC-3(µg/mL PTX eq)	LNCaP(µg/mL DES eq)	LNCaP(µg/mL PTX eq)
T-DES <i>1b</i>	172	-	70	-
B-DES <i>2b</i>	52	-	49	-
T-PTX	-	0.764	-	0,152
B-PTX	-	-	-	-
T-DES-Ser-PTX <i>21b</i>	0.019	0.258	0.015	0.020
B-DES-Ser-PTX <i>22b</i>	0.280	0.204	0.017	0.012

Combined polyacetals:  $[IC_{50}((Tert \text{ or } Block)\text{-DES-Ser-PTX})/ IC_{50}((Tert \text{ or } Block)\text{-DES})]+[IC_{50}((Tert \text{ or } Block)\text{-DES-Ser-PTX})/ IC_{50}((Tert \text{ or } Block)\text{-PTX})]$ . *Tert*-DES-Ser-PTX conjugate presents a CI=0.2 µg/mL in LNCaP and CI=0.4 µg/mL in PC3. *Block*-DES-Ser-PTX system has the same CI=0.3 µg/mL in both cell lines.

All the data are below one, then as it was mentioned above when the isobologram equation  $<1$ , the effect of combining DES and PTX in the same polymeric carrier yielded a clear synergistic effect against prostate cancer cell lines PC3 and LNCaP.

Looking at all those experiments performed in PCa cell lines, it was possible to conclude that:

- The single therapy with the *Tert*- and *Block* -DES and the free DES were active at concentrations higher than 3µg/mL.
- The combination therapy with *Tert*- and *Block-Ser*-DES-PTX polyacetals showed similar activity than free PTX.
- Both drugs, DES and PTX, demonstrated a synergistic effect in PCa cells, being the androgen-dependent LNCaP slightly more sensitive. In addition, *Tert*-DES-PTX conjugates presented slightly better results than the *Block*-DES-PTX polyacetals.
- *Tert*-DES-PTX polyacetals showed higher *in vitro* efficacy than the *Tert*-PTX, in particular in LNCaP cells.

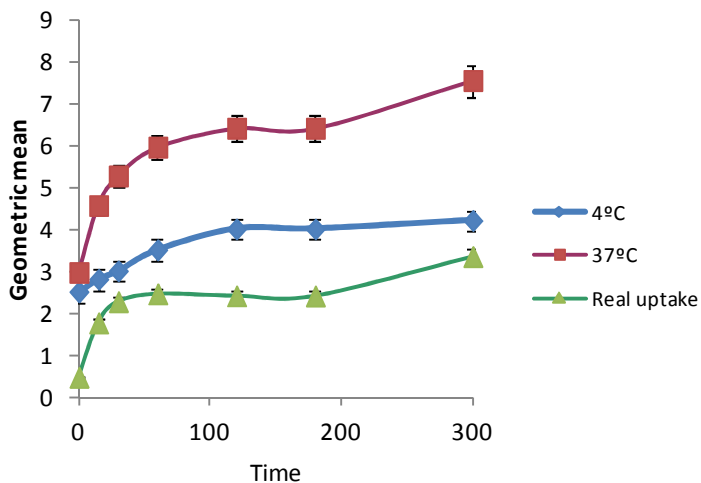
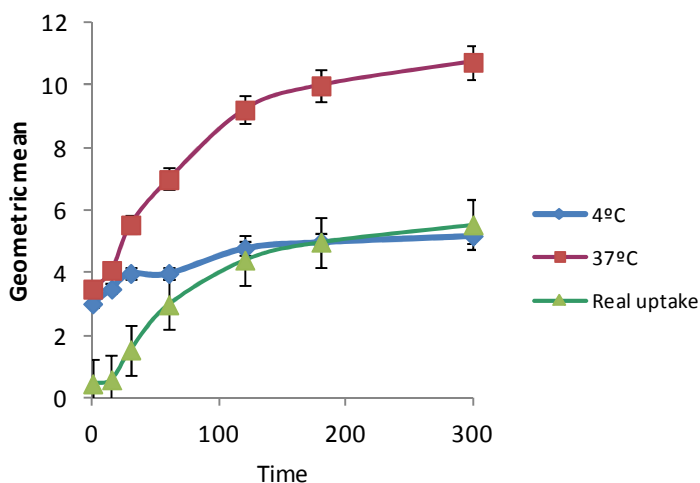
### 5.4.1. 3 Evaluation of cellular internalization of DES-Polyacetals by flow cytometry in prostate cancer cell models.

In order to elucidate possible differences in the cell internalization mechanism between *Tert*-DES-Ser-PTX and *Block*-DES-Ser-PTX, flow cytometry studies were carried out in both prostate cancer cell models.

The combination polymers labeled with OG were used for these studies (*Tert*-DES-Ser-PTX-OG and *Block*-DES-Ser-PTX-OG) and their cellular uptake analyzed by flow cytometry at 37°C (total uptake) and at 4°C (cell binding) in order to determine whether the main cell internalization mechanism was energy-dependent. Figure 5. 16 shows a representative example of the internalization profiles of conjugates at 37°C and at 4°C in PC3 (Figure 5.16 A and B) and LNCaP (Figure 5. 18 A and B) cell lines. The time-dependent profiles indicated an energy-dependent uptake mechanism and significant differences between 37°C and 4°C.

In order to observe better the different behavior of these two conjugates have, both conjugates, *Tert*-DES-Ser-PTX-OG and its *Block* analogue, were represented in the same graph at 37°C (Figure 5. 17). Both systems were rapidly internalized by the PC3 cells in a time dependent manner and through an energy-dependent mechanism as could be observed by the cell associated fluorescence differences at 4°C and 37°C (Figure 5. 16 B and 5. 17 B). However, *Tert*-polyacetal was much faster internalized by PC3 cells comparing with its *Block*- analog but the total uptake after 5 hours was much greater for the *Block*-DES-PTX combination conjugate.

The same studies were carried out in LNCaP prostate cancer cells (Figure 5.18A,B). Figure 5.19 compare uptake of both combination conjugates at 37°C in order to easily observe the differences between them.

**A.****B.**

**Figure 5. 16** Flow cytometry internalization studies for the combined polyacetals, (A) *Tert*-DES-Ser-PTX and (B) *Block*-DES-Ser-PTX. Both conjugates done at 4°C and at 37°C in PC3 cell line. Graphical view of the geometric mean.



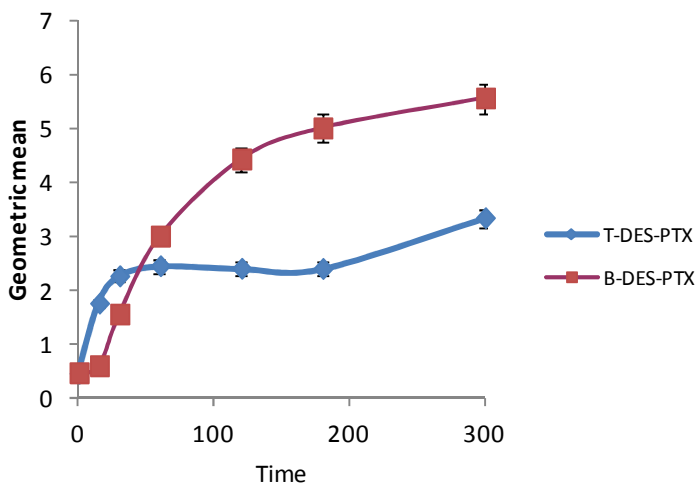
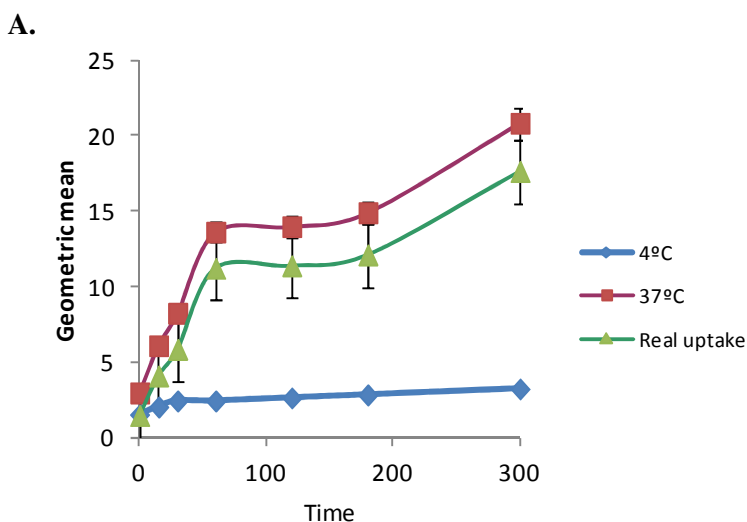


**Figure 5. 17** Flow cytometry studies for *Tert*-DES-Ser-PTX (blue) and *Block*-DES-Ser-PTX (red) at 37°C in PC3 cell line.

In LNCaP cell line, the greatest uptake was registered with *Tert*-DES-PTX-OG. But both polyacetalic systems internalize rapidly by the cells in a time dependent manner and also through an energy-dependent mechanism as could be observed by the cell associated fluorescence differences at 4°C and 37°C (Figure 5.18A and B). Contrarily to PC3 cells, The uptake of *Tert*-DES-PTX was greater than that observed for *Block*-DES-PTX in LNCaP cell line.



B.

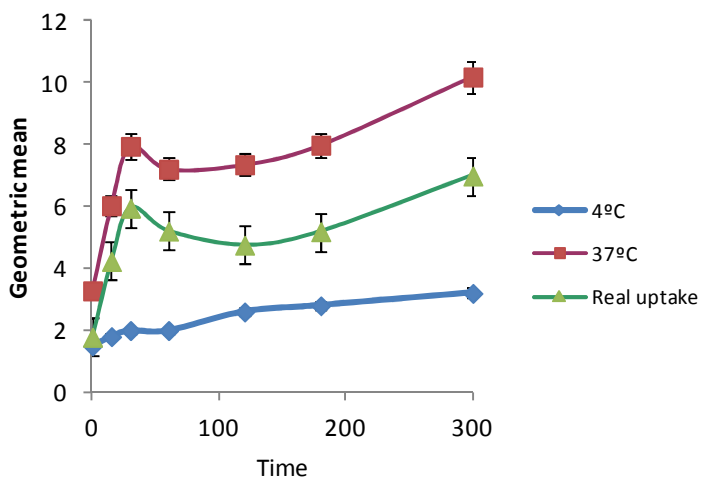


**Figure 5. 18** Flow cytometry studies for the combined polyacetals, (A) tert-DES-Ser-PTX and (B) Block-DES-Ser-PTX. Both conjugates done at 4°C and at 37°C in LNCaP cell line.

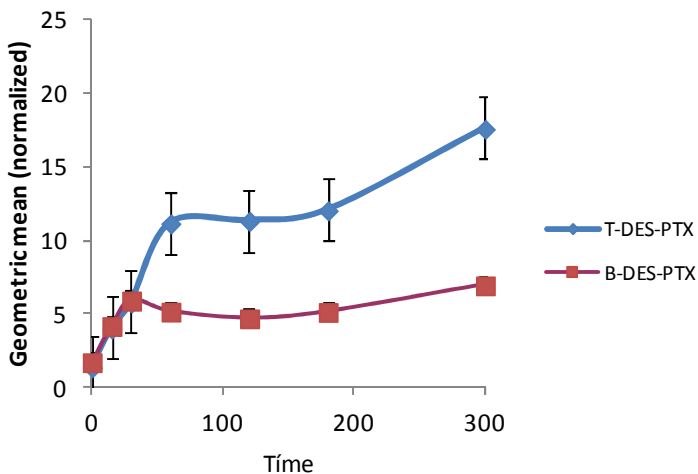


**Figure 5. 19** Flow cytometry studies for the combined polyacetals, tert-DES-Ser-PTX (blue) and Block-DES-Ser-PTX (red) at 37°C in LNCaP cell line.

## 5.4.2 Evaluation of DES-polyacetals *in vivo* breast model

### 5.4.2. 1 *In vivo* & *ex vivo* biodistribution of *Tert*- and *Block-Ser*-DES-PTX polymer-Cy5.5 in mice MDA-MB-435S xenografts.

The compound tumor accumulation and whole-body biodistribution study was carried out in 8 week-old female (Hsd:Athymic Nude-Foxn1nu/nu) Athymic nude mice carrying a subcutaneous tumor in the right dorsal flank. As in chapter 4.3, the compounds tissue-accumulations were measured non-invasively by means of *in vivo* and *ex vivo* fluorescence reflectance imaging (FLI) from the lateral, ventral and dorsal views using the IVIS<sup>®</sup> Spectrum. The fluorescence signal was quantified in Radiant Efficiency. In addition, at different end time-points, compound tissue-accumulations were determined by *ex vivo* FLI. The polyacetals loaded with both drugs, DES and PTX, and labeled with Cy5.5 NIR dye, were chosen to carry out the *in vivo* tumor-accumulation and whole-body biodistribution assays.

#### ***In vivo* studies. *Tert*- and *Block-Ser*-DES-PTX-polymer Cy5.5 tumor-accumulation.**

*In vivo* Cy5.5 tumor accumulation of *Tert*- and *Block-Ser*-DES-PTX-Cy5.5 (**25a** and **26a**, resp.) conjugates were analyzed at 0, 3, 6 and 24 h (Figure 5.20 and 5.21).

Mice were scanned from the dorsal side to monitor renal excretion (**A**), lateral view for tumor accumulation (**B**) and ventral view for hepatic excretion (**C**). However, due to the auto fluorescence from some parts of the mouse, the entire animal except the subcutaneous tumor was shielded to facilitate the tumor-accumulation detection and quantification.

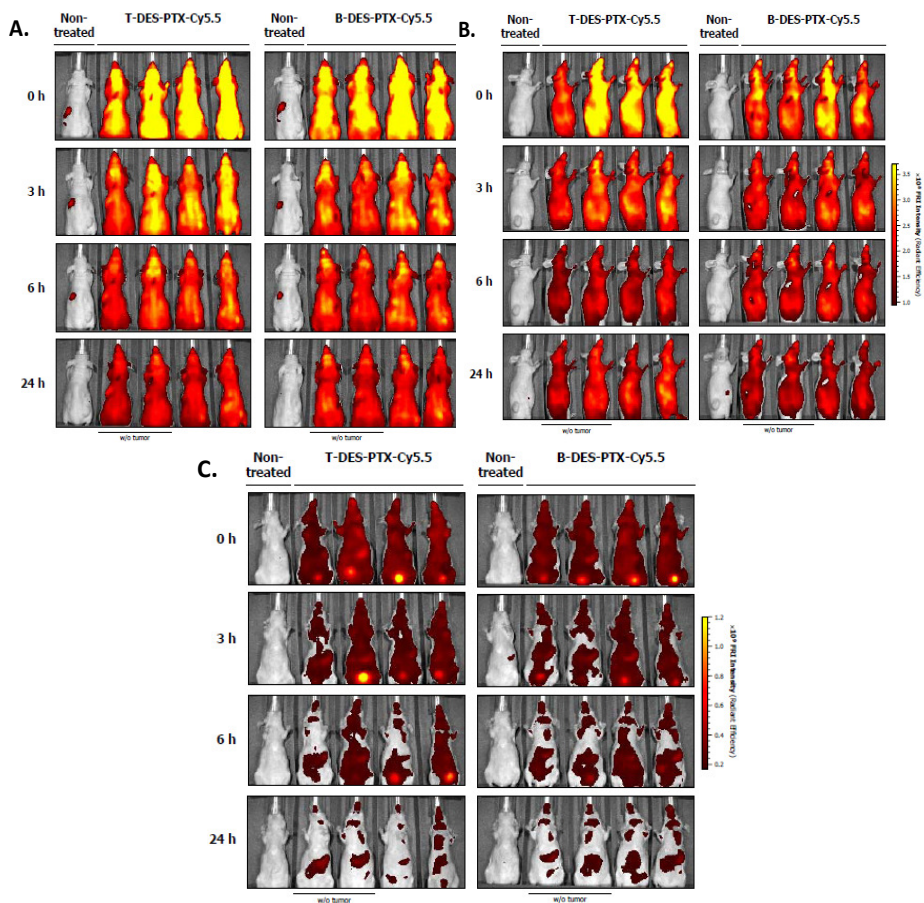


**Figure 5. 20** Whole-body biodistribution of *Tert*- and *Block-Ser*-DES-PTX-Cy5.5 polyacetals measured by the means of *in vivo* FLI from the dorsal (A), lateral (B) and ventral (C) views using the IVIS<sup>®</sup> Spectrum.

In Figure 5. 21 the tumor-accumulation of the Cy5.5-labelled polyacetals at different times post-treatment is represented. As control, untreated mice with tumor, and treated mice without tumor were used as control. It was possible to determine after this *in vivo* study that, *Tert*- and *Block-Ser*-DES-PTX-Cy5.5 present the maximum tumor-accumulation after 3 h of polyacetals administration. From 3 h up to 24 h post-administration the tumor accumulation of the combination polymers was decreased indicating mostly renal excretion.

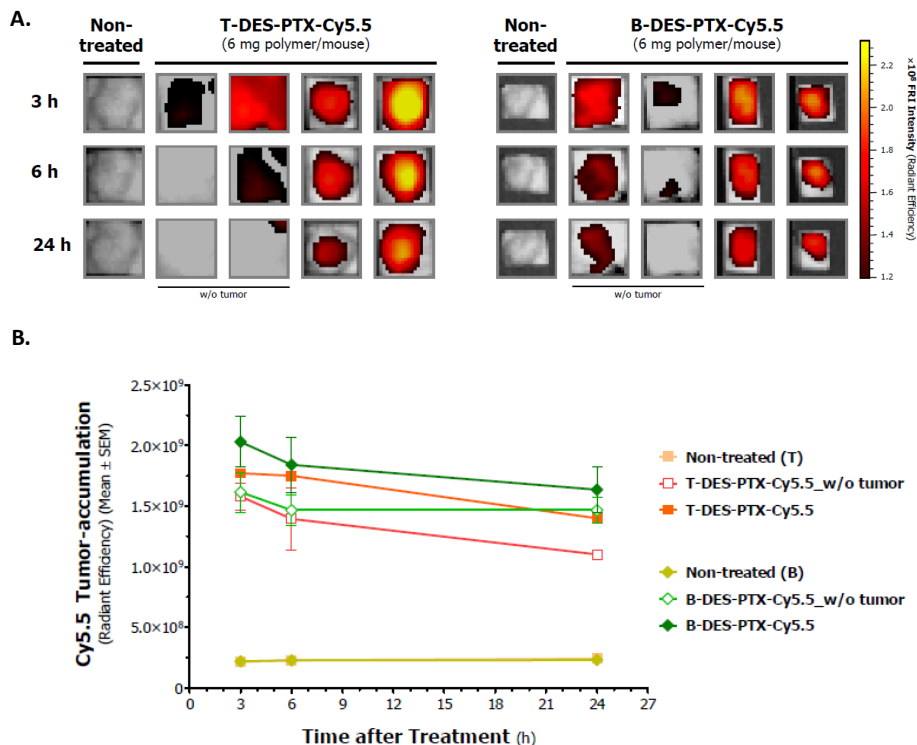


**Figure 5. 21** *In vivo* MDA-MB-435S subcutaneous tumor-accumulation after a single administration of 6 mg polymer/mouse of *Tert-Ser-DES-PTX-Cy5.5* **25a** (A, right panel) and *Block-Ser-DES-PTX-Cy5.5* **26a** (A, left panel). (B) Cy5.5 tumor-accumulation quantified by Radiant Efficiency.

***Ex vivo* studies: *Tert-* and *Block-Ser-DES-PTX-Cy5.5* polymer tumor-accumulation and excretion.**

Compound tissue-accumulation was determined by *ex vivo* FLI using the IVIS<sup>®</sup> Spectrum at 24 h after administration (Figure 5. 22).

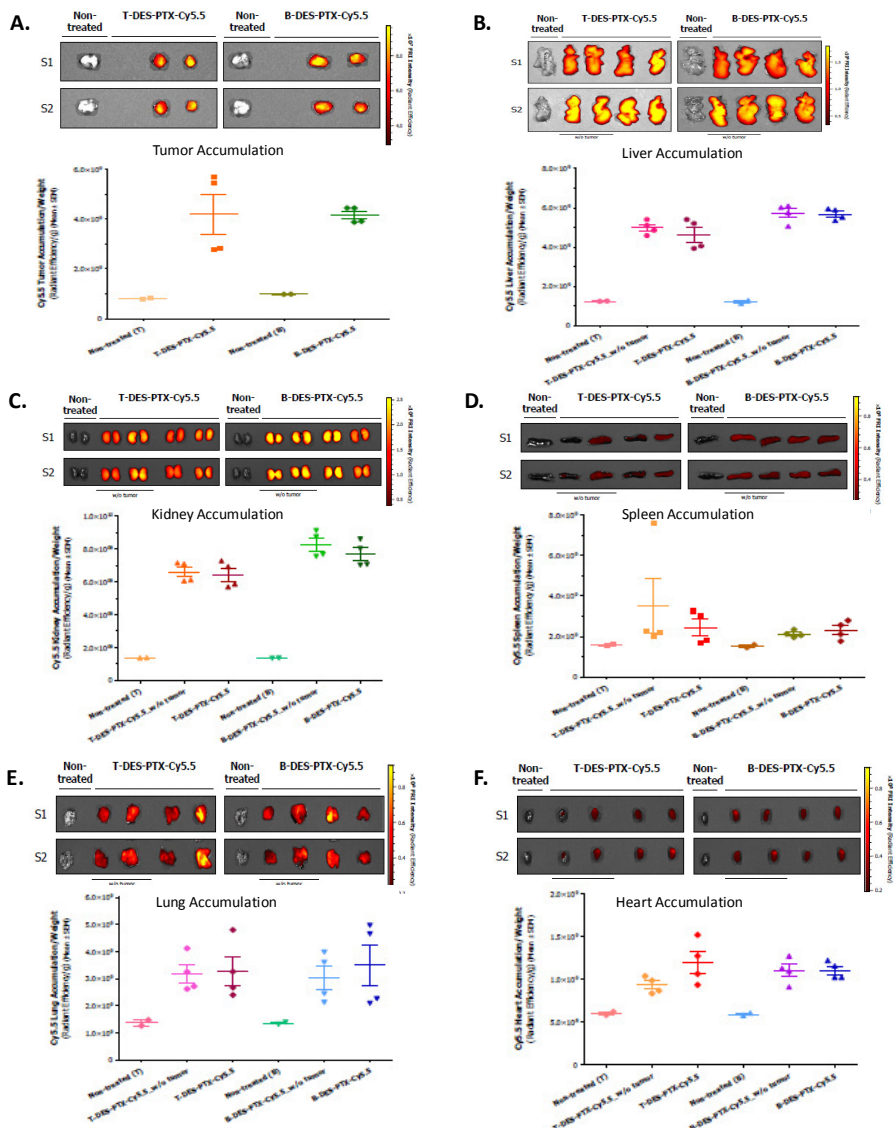


**Figure 5. 22** Tissue accumulation of T-DES-PTX-Cy5.5 and B-DES-PTX-Cy5.5 in different organs: tumor (A), liver (B), kidneys (C), spleen (D), lungs (E) and heart (F). The compounds are measured non-invasively by FLI and the fluorescence signal is quantified in Radiant Efficiency.

*Tert-* and *Block-*DES-PTX-Cy5.5 polyacetals reached and accumulated in MDA-MB-453S subcutaneous tumors, being tumor-accumulation maximum at 3h post-administration. The accumulations were also detected in the liver

and kidneys which indicated the polyacetals excretion is throughout the hepatic and renal excretion routes without any sign of organ toxicity.

*Ex vivo Tert-* and *Block-Ser-DES-PTX-Cy5.5* tissue-accumulations had been detected mainly in tumor, liver and kidneys as it observed in Figure 5.22 A-C.

Lung-accumulation was also observed for both DES-PTX polyacetals as it observed in Figure 5.22 E. The presence of Cy5.5 in lungs could be related with aggregates formed in the injection solution. The non bearing-tumor mice that received the DES-PTX-Cy5.5 polyacetals showed similar Cy5.5 tissue-accumulations than the bearing-tumor mice (Figure 5. 23).

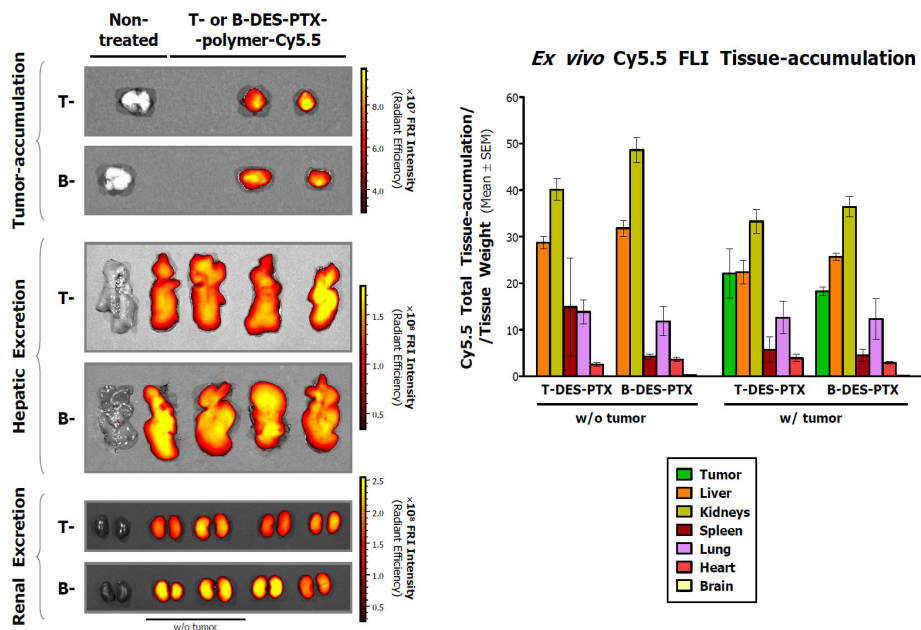


**Figure 5. 23** Tissue distribution and excretion of polyacetals with DES and PTX labeled with Cy5.5. The compounds are measured non-invasively by FLI and the fluorescence signal is quantified in Radiant Efficiency.

### Future and Ongoing Perspectives in Biological studies

After analyzing the reported preliminary results, ongoing experiments not able to be concluded due to time constrains are being devoted to study the *in vivo* tolerability and therapeutic efficacy of *Tert-PTX* vs *Tert-DES-PTX* in the breast cancer xenograft model and in a non-invasive NOD-SCID LNCaP

orthotopic prostate tumor with spontaneous metastases mouse model LNCaP (Figure 5. 24) in order to achieve in vivo proof of concept for drug synergism (DES + PTX).

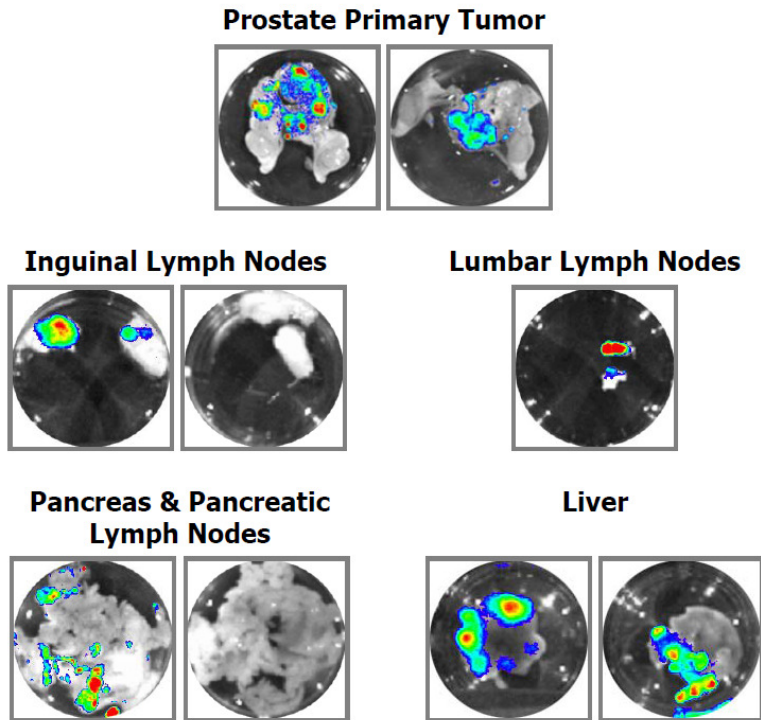


**Figure 5. 24** Illustration of *ex vivo* BLI images of prostatic tumor and spontaneous metastasis.



## References

1. Broxterman, H. J.; Georgopapadakou, N. H., Anticancer therapeutics: "Addictive" targets, multi-targeted drugs, new drug combinations. *Drug Resist Updat* **2005**, *8* (4), 183-97.
2. Rampino, M.; Ricardi, U.; Munoz, F.; Reali, A.; Barone, C.; Musu, A. R.; Balcet, V.; Franco, P.; Grillo, R.; Bustreo, S.; Pecorari, G.; Cavalot, A.; Garzino Demo, P.; Ciuffreda, L.; Ragona, R.; Schena, M., Concomitant Adjuvant Chemoradiotherapy with Weekly Low-dose Cisplatin for High-risk Squamous Cell Carcinoma of the Head and Neck: a Phase II Prospective Trial. *Clin Oncol (R Coll Radiol)*. **2011**, *23* (2), 134-140.
3. Perry, M. e., *The chemotherapy source book*. Williams & wilkins: maryland USA, **1992**.
4. Gulley, J. L.; Arlen, P. M.; Bastian, A.; Morin, S.; Marte, J.; Beetham, P.; Tsang, K. Y.; Yokokawa, J.; Hodge, J. W.; Ménard, C.; Camphausen, K.; Coleman, C. N.; Sullivan, F.; Steinberg, S. M.; Schlom, J.; Dahut, W., Combining a recombinant cancer vaccine with standard definitive radiotherapy in patients with localized prostate cancer. *Clin Cancer Res* **2005**, *11* (9), 3353-62.
5. Tanabe, M.; Ito, Y.; Tokudome, N.; Sugihara, T.; Miura, H.; Takahashi, S.; Seto, Y.; Iwase, T.; Hatake, K., Possible use of combination chemotherapy with mitomycin C and methotrexate for metastatic breast cancer pretreated with anthracycline and taxanes. *Breast Cancer* **2009**, *16* (4), 301-306.
6. Jordan, V. C., Tamoxifen (ICI46,474) as a targeted therapy to treat and prevent breast cancer. *Br J Pharmacol* **2006**, *147* (S1), S269-S276.
7. Dipetrillo, T.; Suntharalingam, M.; Ng, T.; Fontaine, J.; Horiba, N.; Oldenburg, N.; Perez, K.; Birnbaum, A.; Battafarano, R.; Burrows, W.; Safran, H., Neoadjuvant paclitaxel poliglumex, cisplatin, and radiation for esophageal cancer: a phase 2 trial. *Am J Clin Oncol* **2012**, *35* (1), 64-7.
8. Langer, C. J.; O'Byrne, K. J.; Socinski, M. A.; Mikhailov, S. M.; Leśniewski-Kmak, K.; Smakal, M.; Ciuleanu, T. E.; Orlov, S. V.; Dediu, M.; Heigener, D.; Eisenfeld, A. J.; Sandalic, L.; Oldham, F. B.; Singer, J. W.; Ross, H. J., Phase III trial comparing paclitaxel poliglumex (CT-2103, PPX) in combination with carboplatin versus standard paclitaxel and carboplatin in the treatment of PS 2 patients with chemotherapy-naïve advanced non-small cell lung cancer. *J Thorac Oncol* **2008**, *3* (6), 623-30.

9. Muggia, F., Platinum compounds 30 years after the introduction of cisplatin: implications for the treatment of ovarian cancer. *Gynecol Oncol* **2009**, *112* (1), 275-81.
10. Berhoun, M.; Banu, E.; Scotte, F.; Prognon, P.; Oudard, S.; Bonan, B., Therapeutic Strategy for Treatment of Metastatic Non-Small Cell Lung Cancer. *The Annals of Pharmacotherapy* **2008**, *42* (11), 1640-1652.
11. Honecker, F.; Kollmannsberger, C.; Quietzsch, D.; Haag, C.; Schroeder, M.; Spott, C.; Hartmann, J. T.; Baronius, W.; Hempel, V.; Kanz, L.; Bokemeyer, C., Phase II study of weekly paclitaxel plus 24-h continuous infusion 5-fluorouracil, folinic acid and 3-weekly cisplatin for the treatment of patients with advanced gastric cancer. *Anticancer Drugs* **2002**, *13* (5), 497-503.
12. Greco, F.; Vicent, M. J., Combination therapy: Opportunities and challenges for polymer-drug conjugates as anticancer nanomedicines. *Advanced Drug Delivery Reviews* **2009**, *61* (13), 1203-1213.
13. ÅKeson, M.; Zetterqvist, B.-M.; DahlÖF, K.; BrÄNnstrÖM, M.; Horvath, G., Effect of adjuvant paclitaxel and carboplatin for advanced stage epithelial ovarian cancer: A population-based cohort study of all patients in western Sweden with long-term follow-up. *Acta Obstetricia et Gynecologica Scandinavica* **2008**, *87* (12), 1343-1352.
14. Hörmann, V.; Kumi-Diaka, J.; Durity, M.; Rathinavelu, A., Anticancer activities of genistein- topotecan combination in prostate cancer cells. *Journal of Cellular and Molecular Medicine*, n/a-n/a.
15. Knox, S. J. *Selenium is a Chemotherapeutic Agent for the Treatment of Prostate Cancer*; Stanford University, Stanford, CA 94305: **2006**; p 13.
16. Kumi-Diaka, J.; Merchant, K.; Haces, A.; Hormann, V.; Johnson, M., Genistein-Selenium Combination Induces Growth Arrest in Prostate Cancer Cells. *Journal of Medicinal Food* **2010**, *13* (4), 840-850.
17. Pearson, O. H.; Hubay, C. A.; Gordon, N. H.; Marshall, J. S.; Crowe, J. P.; Arafah, B. M.; McGuire, W., Endocrine versus endocrine plus five-drug chemotherapy in postmenopausal women with stage II estrogen receptor-positive breast cancer. *Cancer* **1989**, *64* (9), 1819-23.
18. Jordan, V. C.; Brodie, A. M., Development and evolution of therapies targeted to the estrogen receptor for the treatment and prevention of breast cancer. *Steroids* **2007**, *72* (1), 7-25
19. Logman, J. F.; Heeg, B. M.; Botteman, M. F.; Kaura, S.; van Hout, B. A., Economic evaluation of zoledronic acid for the prevention of osteoporotic fractures in postmenopausal women with early-stage breast cancer receiving aromatase inhibitors in the UK. *Ann Oncol* **2010**, *21* (7), 1529-36.
20. Gnant, M.; Mlineritsch, B.; Schippinger, W., On behalf of the ABCSG, Adjuvant ovarian suppression combined with tamoxifen or anastrozole,

- alone or in combination with zoledronic acid, in premenopausal women with hormone-responsive, stage I and II breast cancer: first efficacy results from ABCSG-12. *Journal of Clinical Oncology* **2008**, *26* (15S).
21. Shapiro, C. L.; Halabi, S.; Gibson, G.; Weckstein, D. J.; Kirshner, J.; Sikov, W. M.; Winer, E. P.; Hudis, C. A.; Isaacs, C.; Weckstein, D.; Schilsky, R. L.; Paskett, E., Effect of zoledronic acid (ZA) on bone mineral density (BMD) in premenopausal women who develop ovarian failure (OF) due to adjuvant chemotherapy (AdC): First results from CALGB trial. *Journal of Clinical Oncology* **2008**, *26* (15S (May 20 Supplement)), 512.
  22. Nielson, J. B., *Hormone Therapy for prostate cancer*. WB Saunders Elsevier: Philadelphia, 2009; p 3082-3100.
  23. Moul, J. W.; Chodak, G., Combination hormonal therapy: a reassessment within advanced prostate cancer. *Prostate Cancer Prostatic Dis* **7** (S1), S2-S7.
  24. Hsieh, A. C.; Ryan, C. J., Novel Concepts in Androgen Receptor Blockade. *The Cancer Journal* **2008**, *14* (1), 11-14 10.1097/PPO.0b013e318161d13e.
  25. Bolla, M.; Fournier, P.; Beneyton, V.; Tessier, A.; Jover, F.; Verry, C., Combination of external irradiation and androgen suppression for prostate cancer: facts and questions. *Cancer Radiother* **2010**, *14* (6-7), 510-514.
  26. Metro, G.; Mottolese, M.; Fabi, A., HER-2-positive metastatic breast cancer: trastuzumab and beyond. *Expert Opinion on Pharmacotherapy* **2008**, *9* (15), 2583-2601.
  27. Van Poppel, H., Treatment of Advanced and Metastatic Renal Cancer: A Revolution? *European Urology Supplements* **2009**, *8* (5), 483-488.
  28. Heinemann, V., Review of bevacizumab in the treatment of metastatic breast cancer. *European Journal of Cancer Supplements* **2008**, *6* (8), 13-18.
  29. Adler, M. J.; Dimitrov, D. S., Therapeutic Antibodies Against Cancer. *Hematology/Oncology Clinics of North America* **26** (3), 447-481.
  30. Jones, D., Avastin-Tarceva combination fails in lung cancer. *Nat Biotech* **2009**, *27* (2), 108-109.
  31. Greco, F.; Vicent, M. J., Polymer-drug conjugates: current status and future trends. *Front Biosci* **2008**, *13*, 2744-56.
  32. <http://www.celatorpharma.com>
  33. Maeda, H., Polymer conjugated macromolecular drugs for tumour-specific targeting. In *Polymeric site-specific Pharmacotherapy*, Ltd, J. W. a. S., Ed. USA, 1994; pp 96-116.
  34. Vasey, P. A.; Kaye, S. B.; Morrison, R.; Twelves, C.; Wilson, P.; Duncan, R.; Thomson, A. H.; Murray, L. S.; Hilditch, T. E.; Murray,

- T.; Burtles, S.; Fraier, D.; Frigerio, E.; Cassidy, J., Phase I clinical and pharmacokinetic study of PK1 [N-(2-hydroxypropyl)methacrylamide copolymer doxorubicin]: first member of a new class of chemotherapeutic agents-drug-polymer conjugates. Cancer Research Campaign Phase I/II Committee. *Clin Cancer Res* **1999**, *5* (1), 83-94.
35. Meerum Terwogt, J. M.; Ten Bokkel Huinink, W. W.; Schellens, J. H. M.; Schot, M.; Mandjes, I.; Zurlo, M.; Rocchetti, M.; Rosing, H.; Beijnen, K. J. H., Phase I clinical and pharmacokinetic study of PNU166945, a novel water soluble polymer conjugated prodrug of paclitaxel. *Anticancer Drugs Des* **2001**, *12*, 8.
36. Minko, T.; Kopeckova, P.; Pozharov, V.; Kopecek, J., HPMa copolymer bound adriamycin overcomes MDR1 gene encoded resistance in a human ovarian carcinoma cell line. *J Control Release* **1998**, *54* (2), 223-33.
37. Rihova, B.; Strohalm, J.; Prausova, J.; Kubackova, K.; Jelinkova, M.; Rozprimova, L.; Sirova, M.; Plocova, D.; Etrych, T.; Subr, V.; Mrkvan, T.; Kovar, M.; Ulbrich, K., Cytostatic and immunomobilizing activities of polymer-bound drugs: experimental and first clinical data. *J Control Release* **2003**, *91* (1-2), 1-16.
38. Sirova, M.; Strohalm, J.; Subr, V.; Plocova, D.; Rossmann, P.; Mrkvan, T.; Ulbrich, K.; Rihova, B., Treatment with HPMa copolymer-based doxorubicin conjugate containing human immunoglobulin induces long-lasting systemic anti-tumour immunity in mice. *Cancer Immunol Immunother* **2007**, *56* (1), 35-47.
39. Greco, F.; Vicent, M. J., Combination therapy: opportunities and challenges for polymer-drug conjugates as anticancer nanomedicines. *Adv Drug Deliv Rev* **2009**, *61* (13), 1203-13.
40. Gee, J. M.; Howell, A.; Gullick, W. J.; Benz, C. C.; Sutherland, R. L.; Santen, R. J.; Martin, L. A.; Ciardiello, F.; Miller, W. R.; Dowsett, M.; Barrett-Lee, P.; Robertson, J. F.; Johnston, S. R.; Jones, H. E.; Wakeling, A. E.; Duncan, R.; Nicholson, R. I., Consensus statement. Workshop on therapeutic resistance in breast cancer: impact of growth factor signalling pathways and implications for future treatment. *Endocr Relat Cancer* **2005**, *12 Suppl 1*, S1-7.
41. Verschraegen, C. F.; Skubitz, K.; Daud, A.; Kudelka, A. P.; Rabinowitz, I.; Allievi, C.; Eisenfeld, A.; Singer, J. W.; Oldham, F. B., A phase I and pharmacokinetic study of paclitaxel poliglumex and cisplatin in patients with advanced solid tumors. *Cancer Chemother Pharmacol* **2009**, *63* (5), 903-10.
42. Langer, C. J.; O'Byrne, K. J.; Socinski, M. A.; Mikhailov, S. M.; Lesniewski-Kmak, K.; Smakal, M.; Ciuleanu, T. E.; Orlov, S. V.; Dediu, M.; Heigener, D.; Eisenfeld, A. J.; Sandalic, L.; Oldham, F. B.;

- Singer, J. W.; Ross, H. J., Phase III trial comparing paclitaxel poliglumex (CT-2103, PPX) in combination with carboplatin versus standard paclitaxel and carboplatin in the treatment of PS 2 patients with chemotherapy-naïve advanced non-small cell lung cancer. *J Thorac Oncol* **2008**, *3* (6), 623-30.
43. [www.ctiseattle.com](http://www.ctiseattle.com).
  44. Dipetrillo, T.; Milas, L.; Evans, D.; Akerman, P.; Ng, T.; Miner, T.; Cruft, D.; Chauhan, B.; Iannitti, D.; Harrington, D.; Safran, H., Paclitaxel poliglumex (PPX-Xyotax) and concurrent radiation for esophageal and gastric cancer: a phase I study. *Am J Clin Oncol* **2006**, *29* (4), 376-9.
  45. Jeyapalan, S.; Goldman, M.; Boxerman, J.; Donahue, J.; Elinzano, H.; Evans, M. D.; O'Connor, B.; Puthawala, M. Y.; Oyelese, A.; Cielo, D.; Blitstein, M.; Dargush, M.; Santaniello, A.; Constantinou, M.; Dipetrillo, T.; Safran, H. In *Paclitaxel poliglumex (PPX), temozolamide (TMZ) and radiation (RT) for newly diagnosed high-grade gliomas: a Brown University Oncology Group (BRUOG) phase II study*, 9th International Symposium on Polymer Therapeutics: From Laboratory to Clinical Practice. Centro de Investigación Príncipe Felipe, Valencia, Spain., **2012**.
  46. Lammers, T.; Peschke, P.; Kuhnlein, R.; Subr, V.; Ulbrich, K.; Debus, J.; Huber, P.; Hennink, W.; Storm, G., Effect of radiotherapy and hyperthermia on the tumor accumulation of HPMA copolymer-based drug delivery systems. *J Control Release* **2007**, *117* (3), 333-41.
  47. Khandare, J. J.; Chandna, P.; Wang, Y.; Pozharov, V. P.; Minko, T., Novel polymeric prodrug with multivalent components for cancer therapy. *J Pharmacol Exp Ther* **2006**, *317* (3), 929-37.
  48. Khandare, J. J.; minko, T., Polymer-drug conjugates: progress in polymeric prodrugs. *prog. polym. Sci.* **2006**, *31*, 38.
  49. Shiah, J. G.; Sun, Y.; Kopeckova, P.; Peterson, C. M.; Straight, R. C.; Kopecek, J., Combination chemotherapy and photodynamic therapy of targetable N-(2-hydroxypropyl)methacrylamide copolymer-doxorubicin/mesochlorin e(6)-OV-TL 16 antibody immunoconjugates. *J Control Release* **2001**, *74* (1-3), 249-53.
  50. Krinick, N. L.; Sun, Y.; Joyner, D.; Spikes, J. D.; Straight, R. C.; Kopecek, J., A polymeric drug delivery system for the simultaneous delivery of drugs activatable by enzymes and/or light. *J Biomater Sci Polym Ed* **1994**, *5* (4), 303-24.
  51. Hongrapipat, J.; Kopeckova, P.; Liu, J.; Prakongpan, S.; Kopecek, J., Combination chemotherapy and photodynamic therapy with fab' fragment targeted HPMA copolymer conjugates in human ovarian carcinoma cells. *Mol Pharm* **2008**, *5* (5), 696-709.

52. Fang, J.; Sawa, T.; Akaike, T.; Greish, K.; Maeda, H., Enhancement of chemotherapeutic response of tumor cells by a heme oxygenase inhibitor, pegylated zinc protoporphyrin. *Int J Cancer* **2004**, *109* (1), 1-8.
53. Seymour, L. W.; Ferry, D. R.; Anderson, D.; Hesslewood, S.; Julyan, P. J.; Poyner, R.; Doran, J.; Young, A. M.; Burtles, S.; Kerr, D. J., Hepatic drug targeting: phase I evaluation of polymer-bound doxorubicin. *J Clin Oncol* **2002**, *20* (6), 1668-76.
54. Krakovicova, H.; Etrych, T.; Ulbrich, K., HPMA-based polymer conjugates with drug combination. *Eur J Pharm Sci* **2009**, *37* (3-4), 405-12.
55. Bae, Y.; Diezi, T. A.; Zhao, A.; Kwon, G. S., Mixed polymeric micelles for combination cancer chemotherapy through the concurrent delivery of multiple chemotherapeutic agents. *J Control Release* **2007**, *122* (3), 324-30.
56. Greco, F.; Vicent, M. J.; Penning, N. A.; Nicholson, R. I.; Duncan, R., HPMA copolymer-aminoglutethimide conjugates inhibit aromatase in MCF-7 cell lines. *J Drug Target* **2005**, *13* (8-9), 459-70.
57. Vicent, M. J.; Greco, F.; Nicholson, R. I.; Paul, A.; Griffiths, P. C.; Duncan, R., Polymer therapeutics designed for a combination therapy of hormone-dependent cancer. *Angew Chem Int Ed Engl* **2005**, *44* (26), 4061-6.
58. Greco, F.; Vicent, M. J.; Gee, S.; Jones, A. T.; Gee, J.; Nicholson, R. I.; Duncan, R., Investigating the mechanism of enhanced cytotoxicity of HPMA copolymer-Dox-AGM in breast cancer cells. *J Control Release* **2007**, *117* (1), 28-39.
59. Deladriere, C.; Masia, E.; Lucas, R.; Vicent, M. J. In *Evaluation of polymer conjugates based on combination in breast cancer mouse models*, 9th International Symposium on Polymer Therapeutics: From Laboratory to Clinical Practice. Centro de Investigación Principe Felipe, Valencia, Spain, **2012**.
60. Lammers, T.; Subr, V.; Ulbrich, K.; Peschke, P.; Huber, P. E.; Hennink, W. E.; Storm, G., Simultaneous delivery of doxorubicin and gemcitabine to tumors in vivo using prototypic polymeric drug carriers. *Biomaterials* **2009**, *30* (20), 3466-75.
61. Santucci, L.; Mencarelli, A.; Renga, B.; Pasut, G.; Veronese, F.; Zacheo, A.; Germani, A.; Fiorucci, S., Nitric oxide modulates proapoptotic and antiapoptotic properties of chemotherapy agents: the case of NO-pegylated epirubicin. *Faseb Journal* **2006**, *20* (2), 765-+.
62. Santucci, L.; Mencarelli, A.; Renga, B.; Ceccobelli, D.; Pasut, G.; Veronese, F. M.; Distrutti, E.; Fiorucci, S., Cardiac safety and

- antitumoral activity of a new nitric oxide derivative of pegylated epirubicin in mice. *Anti-Cancer Drugs* **2007**, *18* (9), 1081-1091.
63. Kragh, M.; Spang-Thomsen, M.; Kristjansen, P. E., Time until initiation of tumor growth is an effective measure of the anti-angiogenic effect of TNP-470 on human glioblastoma in nude mice. *Oncol Rep* **1999**, *6* (4), 759-62.
  64. Segal, E.; Pan, H.; Ofek, P.; Udagawa, T.; Kopeckova, P.; Kopecek, J.; Satchi-Fainaro, R., Targeting angiogenesis-dependent calcified neoplasms using combined polymer therapeutics. *PLoS ONE* **2009**, *4* (4), e5233.
  65. Browder, T.; Butterfield, C. E.; Kraling, B. M.; Shi, B.; Marshall, B.; O'Reilly, M. S.; Folkman, J., Antiangiogenic scheduling of chemotherapy improves efficacy against experimental drug-resistant cancer. *Cancer Res* **2000**, *60*, 1878-1886.
  66. Miller, K.; Erez, R.; Segal, E.; Shabat, D.; Satchi-Fainaro, R., Targeting bone metastases with a bispecific anticancer and antiangiogenic polymer-alendronate-taxane conjugate. *Angew Chem Int Ed Engl* **2009**, *48* (16), 2949-54.
  67. Satchi-Fainaro, R.; Hailu, H.; Davies, J. W.; Summerford, C.; Duncan, R., PDEPT: polymer-directed enzyme prodrug therapy. 2. HPMA copolymer-beta-lactamase and HPMA copolymer-C-Dox as a model combination. *Bioconjug Chem* **2003**, *14* (4), 797-804.
  68. Satchi-Fainaro, R.; Wrasidlo, W.; Lode, H. N.; Shabat, D., Synthesis and characterization of a catalytic antibody-HPMA copolymer-Conjugate as a tool for tumor selective prodrug activation. *Bioorg Med Chem* **2002**, *10* (9), 3023-9.
  69. veronese, F. M.; Harris, J. M. E., Peptide Protein PEGylation III: advances in chemistry and clinical applications. *Adv Drug Deliv Rev* **2008**, *60*, 88.
  70. Jones, D., Avastin-Tarceva combination fails in lung cancer. *Nat Biotechnol* **2009**, *27* (2), 108-9.
  71. Duncan, R., N-(2-hydroxypropyl) methacrylamide copolymer conjugate. In *Polymeric Drug Delivery System*, Kwon, G. S., Ed. New York, 2005; pp 1-92.
  72. Duncan, R.; Hume, I. C.; Yardley, H. J.; Flanagan, P. A.; Ulbrich, K.; Subr, V.; Strohalm, J., Macromolecular prodrugs for use in targeted cancer chemotherapy: melphalan covalently coupled to N-(2-hydroxypropyl) methacrylamide copolymers. *J. Control. Release* **1991**, *16*, 15.
  73. Singer, J. W.; Shaffer, S.; Baker, B.; Bernareggi, A.; Stromatt, S.; Nienstedt, D.; Besman, M., Paclitaxel poliglumex (XYOTAX; CT-

- 2103): an intracellularly targeted taxane. *Anticancer Drugs* **2005**, *16* (3), 243-54.
74. Bhatt, R.; de Vries, P.; Tulinsky, J.; Bellamy, G.; Baker, B.; Singer, J. W.; Klein, P., Synthesis and in vivo antitumor activity of poly(l-glutamic acid) conjugates of 20S-camptothecin. *J Med Chem* **2003**, *46* (1), 190-3.
75. Peer, D.; Karp, J. M.; Hong, S.; Farokhzad, O. C.; Margalit, R.; Langer, R., Nanocarriers as an emerging platform for cancer therapy. *Nat Nanotechnol* **2007**, *2* (12), 751-60.
76. Rodea-Palomares, I.; Petre, A. L.; Boltes, K.; Leganés, F.; Perdigón-Melón, J. A.; Rosal, R.; Fernández-Piñas, F., Application of the combination index (CI)-isobologram equation to study the toxicological interactions of lipid regulators in two aquatic bioluminescent organisms. *Water Research* *44* (2), 427-438.
77. Chou, T.C., Drug Combination Studies and Their Synergy Quantification Using the Chou-Talalay Method. *Cancer Research* *70* (2), 440-446.
78. Suffness, M.; Cordell, G. A., *Antitumor alkaloids*. Academic Press: New York, **1985**; Vol. 25, p 1-369.
79. Kingston David, G. I., Taxol, an Exciting Anticancer Drug from *Taxus brevifolia*. In *Human Medicinal Agents from Plants*, American Chemical Society: **1993**; Vol. 534, pp 138-148.
80. Schiff, P. B.; Fant, J.; Horwitz, S. B., Promotion of microtubule assembly in vitro by taxol. *Nature* **1979**, *277* (5698), 665-667.
81. Petrylak, D. P., Docetaxel for the treatment of hormone-refractory prostate cancer. *Rev Urol* **2003**, *5* (Suppl 2), S14-21.
82. Montgomery, R. B.; Nelson, P. S.; Lin, D.; Ryan, C. W.; Garzotto, M.; Beer, T. M., Diethylstilbestrol and docetaxel. *Cancer* **2007**, *110* (5), 996-1002.
83. Rubenstein, M.; Tsui, P.; Guinan, P., Bispecific antisense oligonucleotides with multiple binding sites for the treatment of prostate tumors and their applicability to combination therapy. *Methods Find Exp Clin Pharmacol* **2006**, *28* (8), 515.
84. Luo, C.; Wang, Y.; Chen, Q.; Han, X.; Liu, X.; Sun, J.; He, Z., Advances of Paclitaxel Formulations Based on Nanosystem Delivery Technology. *Mini Rev Med Chem* **2012**, *12* (5), 434-444.
85. Chipman, S. D.; Oldham, F. B.; Pezzoni, G.; Singer, J. W., Biological and clinical characterization of paclitaxel poliglumex (PPX, CT-2103), a macromolecular polymer-drug conjugate. *International Journal of Nanomedicine* **2006**, *1* (4), 375-383.



86. Li, C.; Wallace, S., Polymer-drug conjugates: Recent development in clinical oncology. *Advanced Drug Delivery Reviews* **2008**, *60* (8), 886-898.
87. Soga, O.; van Nostrum, C.; Ramzi, A.; Visser, T.; Soulimani, F.; Frderik, P.; Bomans, P. H. H.; Hennink, W. E., Physicochemical characterization of degradable thermosensitive polymeric micelles. *Langmuir* **2004**, *20*, 9388-9395.
88. Speicher, L. A.; Barone, L.; Tew, K. D.; Lines, C. C.; Speicher, L. A.; Barone, L.; Tew, K. D., Combined Antimicrotubule Activity of Estramustine and Taxol in Human Prostatic Carcinoma Cell Lines. **1992**, 4433-4440.
89. Izbicka, E.; Campos, D.; Carrizales, G.; Tolcher, A., Biomarkers for Sensitivity to Docetaxel and Paclitaxel in Human Tumor Cell Lines In Vitro. *Cancer Genomics and Proteomics* **2005**, *2*, 219-226.
90. Deutsch, H. M.; Glinski, J. A.; Hernandez, M.; al., e., Water-soluble prodrugs of paclitaxel with potent antitumor activity. *Journal Med Chem* **1989**, *32*, 788-92.

# 6

## General Discussion

Prostate Cancer is the second worldwide leading cause of death in men over fifty years old<sup>1</sup>. Nowadays, there is no effective treatment against advanced or metastatic prostate cancer stages. Thus, there is a need to enhance the therapeutic armory in order to increase survival rates and improve prostate cancer patient life-style. For this reason, one of our objectives in the Polymer Therapeutics laboratory and in this thesis in particular, has been devoted to achieve an effective therapeutic platform capable to diminish prostate cancer. Rationally designed polymer conjugates<sup>2-4</sup>, as single conjugates and in combination therapy, have been developed for this purpose.

During the past decade, the importance of polymeric anticancer drug delivery systems has exponentially grown<sup>2-5</sup>. The fast evolution of polymer chemistry and bioconjugation techniques, and a deeper understanding of cell biology have opened up exciting new challenges and opportunities within polymer therapeutics field<sup>7</sup>. Four main directions have to be considered to develop polymer conjugate 'platform technology' further: the control of the synthetic process, the exhaustive characterization of the conjugate architectures, the conquest of combination therapy and the disclosure of new therapeutic targets<sup>4,6,8</sup>.

Following the Ringsdorf model<sup>6</sup>, polymer–drug conjugates are constituted by three components: i) the hydrophilic polymer backbone that acts as a carrier, ii) the linker to attach the polymer to the bioactive agent and iii) the low-molecular weight biologically active molecule which are covalently bound to the polymer through a bioresponsive linker to be delivered. The main objective of these conjugates is not only to enhance the solubility of the hydrophobic drug but also to improve drug pharmacokinetic profile at systemic and at cellular level; polymer conjugation increases drug plasma half-life and volume of distribution and it reduces clearance<sup>7</sup> by the kidneys or liver. The polymer could also enhance drug stability in plasma if necessary. The ideal spacer should be stable in the blood stream but able to release the drug payload at an optimum rate upon arrival to the specific cellular target<sup>7</sup>. The linker becomes active by triggering drug release under certain conditions, such as a change in pH<sup>8</sup> or in the presence of enzymes<sup>9</sup>, such as esterases, lipases or proteases. Clinical proof of concept for polymer drug conjugates has been already achieved mainly as efficient anticancer therapy, as single agents or as elements of combinations. They have the potential to improve pharmacological therapy of a variety of solid tumours mainly due to two mechanism: (i) Polymer-drug conjugation promotes passive tumour targeting

by the enhanced permeability and retention (EPR) effect<sup>10</sup> and (ii) allows for lysosomotropic drug delivery<sup>11</sup> following endocytic<sup>12</sup> capture<sup>3,13</sup>.

Biopersistent carriers as polyethylenglycol (PEG) or N-(2-hydroxypropyl)methacrylamide (HPMA) copolymers, can present disadvantages if chronic parenteral administration and/or high doses are required as there is the potential to generate 'lysosomal storage disease' syndrome. Preclinical evidence of intracellular vacuolation with certain PEG-protein conjugates is raising awareness of the potential advantage of biodegradable polymers regarding safety benefit apart from the possibility to use higher molecular weight (Mw) carriers allowing PK optimization, by enhancing the enhanced permeability and retention (EPR)-mediated tumor targeting<sup>13</sup>. Biodegradable polymers such as polyacetals, firstly described by Heller et al.<sup>17</sup>, could be considered as promising candidates to be used as carriers for targeted drug delivery. To allow use of polymers of higher molecular weight (Mw), a family of hydrolytically labile water-soluble polyacetals was developed<sup>14</sup>. These can be functionalized to allow side-chain conjugation to a drug payload such as doxorubicin (Dox)<sup>15</sup>. These polyacetals show a clear pH-dependent degradation being relatively stable at pH 7.4 but degrade significantly faster at the acidic pH that is encountered in endosomes and lysosomes. *In vitro* and *in vivo* studies confirmed that the polyacetals are not toxic, they are not taken up extensively by the liver or spleen, and are also long circulating<sup>15</sup>. Polyacetals can be prepared by a mild polymerization method involving the reaction of diols with divinyl ethers<sup>17</sup>. To move a step further Vicent et al.<sup>18</sup> synthesized polyacetals incorporating a drug with bis-hydroxyl functionality into the polymer backbone. Degradation of the polymer backbone in the acidic environment of the lysosome or the extracellular fluid of some tumors would then trigger drug release eliminating the need for a biodegradable linker. For this purpose, the *tert*-polymerization process developed for the synthesis of the functionalized polyacetals<sup>15</sup> in combination with the drug diethylstilbestrol (DES) was used<sup>18</sup>. DES is a synthetic non-steroidal estrogen and its administration was a classic form of androgen deprivation therapy (ADT), standard approach to the treatment of advanced prostate cancer for more than 50 years. Its use, however, has been severely limited by a poor water solubility and wide ranging dose-related toxicities, mainly cardiovascular side effects and in particular thromboembolic events. DES can be considered as an 'old' treatment, however, is taken renewed consideration as very recently has been

demonstrated that low-dose DES is safe and effective in castrate-resistant prostate cancer (CRPC) patients when used before the initiation with chemotherapy<sup>16</sup>. Also, a combination of DES to chemotherapeutics such as docetaxel<sup>17</sup> was found to produce a significant level of antitumor activity in patients with metastatic, androgen independent prostate cancer (AIPC). It was hypothesized that, apart from clearly reducing DES toxicity by means of the EPR-mediated tumor targeting, the conjugation of DES to polymeric carriers would more easily allow a low-dose clinical regime as a controlled release of the drug could be achieved for a prolonged period of time. Also, polymer multivalency would allow the synthesis of polymer-based combination conjugates that could better exploit the synergism observed already with taxols<sup>17</sup>.

The group previous research with DES-polyacetals already demonstrated that DES solubility could be greatly enhanced upon polymerization. And more interestingly, the conjugates underwent degradation that was clearly pH-dependent, with greater DES release at acidic pHs. Additionally, the active isomerism of the estrogen was maintained (*trans*-DES)<sup>18</sup> and the conjugates displayed enhanced in vitro cytotoxicity compared to free DES. These tert-DES polyacetals could therefore be defined as the first water-soluble anticancer polymeric drugs designed for acidic pH-triggered release where the drug is incorporated into the polymer mainchain<sup>18</sup>. However, the first synthesized tert-polymers had a drug content of ~4 wt% and a polydispersity (Mw/Mn) around 1.8.

Therefore, the initial aim of this thesis was to synthesize a second generation of DES-based polyacetals with improved properties, such as narrower Mw distributions and higher drug loading, and more importantly to study with these model systems, if slight structural modifications could significantly influence conjugate therapeutic output. These second generation polyacetals were obtained using a block-co-polymer methodology (Chapter 4) and implementing the concept of polymer-based combination therapy (Chapter 5).

Different factors have been carefully considered during the rational design of such polymer-drug conjugates 1) the selection of the drug carrier polymer; which will continue being PEG-polyacetals, 2) the bioresponsiveness of the linking chemistry within the polymer mainchain (pH responsive polyacetals) and in the polymer side chains (ester bonds), and 3) the necessity to design a system with more controlled architecture to allow higher drug capacity maintaining aqueous solubility.

The results show in chapter 4 indicate that the conformation of both polymers, *tert*- and *block-co*-polymers, adopted in solution was different due to the amphiphilic character of the *block-co*-polymer, indicated by a different CAC in both systems. Both, *tert*- and *block*-DES, showed clear pH-dependent drug release kinetics, however drug release profile was significantly different with a slightly greater DES release and a 'biphasic' mode for *block*-DES, indicative of the presence of particulate assemblies<sup>18</sup>.

It has become clear that the Mw and physicochemical properties of the polymer is the most important driver governing biodistribution, elimination and metabolism of a suitable conjugate. In order to determine the Mw of the biodegradable or biostable conjugates the GPC technique was used. The conformations adopted by the conjugates in solution (size and shape) were studied by transmission and scanning electron microscopy (TEM and SEM, resp.), dynamic light scattering (DLS), pulsed-gradient spin echo NMR (PGSE-NMR) and small-angle neutron scattering (SANS). Using these techniques, marked differences were found between *tert*-DES and *block*-DES. TEM allowed the observation of well-defined particles of approximately 100 nm diameter for *block*-DES in high abundance at a solution concentration of 3 mg/ml and shows a more glomerular surface by using SEM. The particle size and the stability of the aggregates formed were confirmed by DLS measurements at different conjugate concentrations (1 mg/mL and 3 mg/mL, always above the CAC). In contrast to the *block*- copolymer, it was not possible to obtain an indication of particle size for *tert*-DES, by either TEM or DLS.

After exhaustive conformational studies by several techniques including SANS and PGSE-NMR (performed in collaboration with Dr Paul at Cardiff Univ.), it was demonstrated that the molecular structure of the conjugate has a significant effect on the solution behavior; even at the same overall acetal and DES contents. Clear evidence has been obtained of significantly different conformation in solution for both polymers. In aqueous solution *tert*-DES is present as single system with an approximate diameter of 20 nm with 2 nm thickness. On the other hand, for *block*-DES two sets of coexisting species are present, one with similar shape but greater length than *tert*-DES (100 nm length, 2 nm thickness) and a second and more abundant system with a disk-like conformation (80 nm diameter, 10 nm thickness). being the second one

more abundant and consistent with the size of the structures observed by TEM and DLS, and significantly larger than the structures indicated by SANS for the *tert*-DES. It was thus determined that, compared to the *tert*-DES polymer, *block*-DES presents a more stable and better defined particulate conformation in the nanosized range, that could present better biological behavior than the *tert*-DES in prostate cancer cell models.

Next step was to explore differences in cell uptake of those conjugates in the most common human prostatic adenocarcinoma, LNCaP and PC3 cell lines. LNCaP<sup>19</sup> takes its name of being isolated from a Lymph Node metastasis and is an androgen-dependent cell line (androgen receptor positive, AR+). PC3 cell line<sup>20</sup> was isolated from bone metastasis and it is androgen-independent (androgen negative, AR-). However, the original *tert*- or *block*-DES structures do not provide with any extra anchoring positions. Therefore, a functional pendent chain suitable for drug or dye conjugation was incorporated following the already described approach by Tomlinson et al.<sup>14</sup>. Then, through the novel serinol moieties as co-monomers, the conjugates were able to label with Oregon Green (OG), a fluorescent marker which allow following the compounds into the cells. The polyacetals now named as *tert*-DES-Ser-OG and *block*-DES-Ser-OG were then tested by confocal fluorescence live-cell imaging for better characterization of conjugates cell trafficking by avoiding any fluorescence artifact induced by fixation protocols. Low membrane-associated fluorescence was observed in all cases studied at the different incubation times. Both conjugates enter the cell by the endocytic route as demonstrated by the observed co-localization with the lysosomal marker dextran-texas red. In general, LNCaP cells seems to have slightly higher uptake rate compared with PC3 cells; and even more interestingly, the percentage of *block*-DES inside the cells is greater than that observed for *tert* DES in both cell lines.

The different release kinetics together with a greater cell uptake probably induced by a more spherical shape<sup>21-24</sup>, yielded to an enhancement in cytotoxicity for *block*-DES in LNCaP and PC3 cell lines. Not only monomer arrangement but also DES loading showed a significant effect on polyacetal cytotoxicity.

DES-polyacetal molecular mechanism of action was also evaluated trying to understand if the differences in polymer solution conformation that induced differences in conjugate cytotoxic activity could be also explained by a

change in cell signaling pathway (cell death and cell cycle mechanisms). These experiments were carried out in collaboration with a postdoctoral researcher in our lab, Dr Ana Armiñán.

Cell studies based in cytometry and western blotting assays demonstrated that both polymer behave similarly following akt pathway in both prostate cancer cell lines although the property of being hormono sensitive for LNCaP makes slightly different results which better results for the block-DES and with higher drug loading because of the hormonal agent DES. Nowadays further experiments are taking place in order to elucidate if DES provokes autophagy in the cells.

In order to achieve *in vivo* proof of concept of our promising *in vitro* results, whole body biodistribution on a tumor xenograft mice model (looking at tumor accumulation by the EPR effect) and preliminary toxicological studies in balb/c mice were also performed.

The *in vivo* experiments were carried out by our collaborators from the CIBBIMM Nanomedicine lab. at Vall d'Hebron Hospital in Barcelona. In a first stage, after *i.v.* administration through mouse tail vein, polymer toxicity was studied. The results showed that a single *i.v.* dose of 10 mg/kg of DES polymers did not induce any significant loss of weight in mice and they did not alter the blood levels of 10 different biological parameters regarding kidney, liver and muscle functionality (BILT, total proteins, AST, ALT, CK, LDH, Alb, creatinin and urea). DES-polyacetals were then labeled through the serinol moieties with the NIR dye Cy5.5 allowing *in vivo* monitoring by non-invasive optical imaging techniques, by means of IVIS<sup>®</sup> Spectrum equipment.

In order to determine the required dose for the biodistribution experiments, *Tert*-DES-Ser-Cy was *i.v.* administered once weekly at different doses in a HT-29 colon tumor xenograft mouse model. As expected, *Tert*-DES-Ser-Cy was accumulated into tumor in a dose-dependent manner, accumulation in tumor was directly correlated with the dose given, observing better tumor accumulation with greater doses<sup>25</sup>. A polyacetal concentration of 7 mg/kg was the selected dose to proceed with the animal biodistribution and anticancer activity experiments. At 7mg/Kg, tumor accumulation started after 6 h post-treatment, being maximum after 4-5 days and maintained for up to 17 days post-injection. Apart from compound accumulation in tumors, *tert*-DES was also mainly detected in kidney and liver. Thus, the polymer small fragments might be being eliminated by the renal excretory system and the large fragments/aggregates through hepatic excretion,



Our collaborators in Barcelona also established a PC3 prostate cancer xenograft mouse model in order to evaluate the anticancer activity of the DES-polyacetal synthesized. However, non-significant activity was observed in any case study. DES-polyacetals as single agents would need greater dose or more frequent dose scheduled than that given (not clinically relevant), or more interestingly an advanced designed using the concept of polymer-based combination therapy.

Therefore, in a second part of the thesis (Chapter 5) the efforts were devoted to identify synergistic drug combinations and design combination polyacetals that would allow a potential clinical candidate for prostate cancer treatment. Due to previously reported data<sup>17</sup> DES-Taxol combinations showed clinical relevance in advanced prostate cancer patients. Therefore, paclitaxel was selected as chemotherapeutic drug to be combined with our DES endocrine therapy.

One of the advantages of using combination therapy<sup>26</sup> is on one side synergism as both drugs when are conjugated within the same polymer carrier will arrive simultaneously to the same damaged cell modulating key signaling pathways at the same time. Also, drug combination could diminish the development of drug resistance<sup>27</sup> as a pathogen or tumor has less resistance to multiple drugs simultaneously. Other advantage is the possibility of increase drug loading to lead higher therapeutic effect, although it is necessary to know well the polymer capacity and keeping the water solubility<sup>28-30</sup> of the system. Other parameters to be taken into account in combination design are: drug ratio, drug release kinetics as the presence of a second drug in the same carriers could dramatically change drug release kinetics and therefore therapeutic output<sup>31</sup>

To synthesize DES-PTX-polyacetal combination conjugates, serinol moieties were used again as co-monomer in order to offer the required new anchoring positions to incorporate PTX, as in the case of Cy5.5 or OG dyes. Thus, the structures of these novel systems consisted on a drug, DES, incorporated in the polymer main-chain and a second drug, PTX, conjugated to the polymer side-chains, yielding *tert*-DES-Ser-PTX and *block*-DES-Ser-PTX combination conjugates.

The conjugates were synthesized and fully characterized before any biological evaluation. As for the single conjugates, solution conformation for the combination conjugates were also studied by SANS, in collaboration with Dr. Alison Paul at Cardiff University. In a first stage model Fmoc-protected

serinol conjugates were compared showing that the differences encountered for the single *Tert*- vs. *Block*- polyacetals were then diminished. This effect was even more dramatic when PTX was introduced. The results showed that the single *Tert*-PTX conjugate solution conformation corresponded to a thin rod of radius 10Å, length 300Å, with a Q-n term with n= 3.5. When PTX was added to *Tert*-DES the scattering was dominated by a Q-4 term, indicating the presence of extremely large structures that were outside of the resolution of the SANS experiment. This experiment clearly showed that the PTX dominated the structures formed in solution and in that case monomer arrangement was not a major event.

*In vitro* efficacy assays of these synthesized combined conjugates are tested in breast cancer and in hormone-dependent and -independent prostate cancer cell lines looking at cell viability to determine the half maximal inhibitory concentration (IC<sub>50</sub>) values. It was demonstrated that the combination conjugates present lower IC<sub>50</sub> than the conjugate with only one drug (DES) in the breast and both prostate human cells.

In MDA-MB-4355.eGFP cells the IC<sub>50</sub> value for the combination conjugate *Tert*-DES-PTX was twice as lower as its *Block*-DES-PTX analogue (0.006 µg/ml vs. 0.012 µg/ml PTX-equiv., respectively) and more importantly, even lower than the parent free drug (0.006 vs. 0.009 µg/ml, PTX-equiv.).

In PC3, the polyacetal *Tert*-DES-PTX seemed to be more active than PTX alone and slightly more than the *Block*-analogue conjugated. Contrary, in the LNCaP cell line, the polyacetal *Block*-DES-PTX was more active than PTX alone and that its analogue *tert*-DES.

The expected synergism was obtained when both drugs, DES and PTX, are combined in the same system and it was found the same effect in both prostate cancer cell lines. *Tert*-DES-PTX presents a CI=0.24µg/mL in LNCaP and CI=0.45µg/mL in PC3. *Block*-DES-PTX has the same CI=0.37µg/mL in both cell lines.

In order to elucidate possible differences in the cell internalization mechanism between both combination conjugates, *Tert*-DES-Ser-PTX and *Block*-DES-Ser-PTX, flow cytometry studies were carried out in both prostate cancer cell lines. It was found that in PC3 cell line, *Block*-polyacetal showed greater uptake after 5 hours incubation, on the contrary in LNCaP cell lines, the greatest uptake was registered with *Tert*-DES-PTX-OG. Therefore, co

significant differences could be directly associated to the conjugate itself ratifying the solution conformation results obtained by SANS.

Whole body *in vivo* preliminary biodistribution studies with cy5.5. labeled combination conjugates were performed in a MDA-MB-435Luc human breast cancer athymic nude mouse model by means of non-invasive optical imaging techniques. These experiments were also performance in Dr. Schwartz group in Barcelona. *In vivo* and *ex vivo* tumour-accumulation and whole-body tissue biodistribution were carried out based on the acquisition of fluorescence emission of the fluorophore Cy5.5 conjugated to the DES-PTX-polyacetals, as well as by HPLC quantification of tissue Cy5.5 levels. These studies showed that tumor-accumulation was greater at 3h, decreasing for up to 24 h post-administration. The accumulations were also detected in the liver and kidneys, which indicated the polyacetals excretion is throughout the hepatic and renal excretion routes without any sign of organ toxicity. The small amount of lung-accumulation observed could be related with aggregates formed in the injection solution. It was observed that both combined conjugates, *Tert*-polymer and *Block-polymer* present similar results in tumor and accumulation assays, thus and a bit faster synthesis, *Tert*-DES-PTX-polyacetal combination conjugate was selected to be further evaluated in orthotopic prostate cancer animal models.

*In vivo* tolerability and therapeutic efficacy studies of *Tert*-DES-PTX-polyacetal combination conjugate are currently being performed at CIBBIMM-Nanomedicine in an LNCaP orthotopic prostate tumor mouse model. The combination conjugate will be compared regarding anticancer activity with *Tert*-PTX-polyacetal single conjugate. If the results are successful, the conjugates will be also evaluated in a non-invasive intraprostatic PC3 Tumor and Metastasis Growth Studies *In Vivo* and *Ex Vivo* looking at the prostate Primary Tumor, liver, pancreas and lymph nodes is being also studying in Schwartz group at Vall d'Hebron Hospital, Barcelona by Dr. Ibane Abasolo, Dr. Yolanda Fernández.

Our results and others already reported<sup>18,21, 22, 32-34</sup> ratify the impact of conjugate solution properties and combination therapy on biological behavior and therefore nanomedicine therapeutic output.

## References

1. Ferlay, J.; Shin, H. R.; Bray, F.; Forman, D.; Mathers, C.; Parkin, D. M. GLOBOCAN 2008 v1.2, Cancer Incidence and Mortality Worldwide: IARC CancerBase No. 10. Lyon, France: International Agency for Research on Cancer. <http://globocan.iarc.fr>, accessed on day/month/year.
2. Duncan, R.; Gaspar, R., Nanomedicine(s) under the microscope. *Mol Pharm* **2011**, *8* (6), 2101-41.
3. Duncan, R., Polymer conjugates as anticancer nanomedicines. *Nature Reviews Cancer* **2006**, *6* (9), 688-701.
4. Duncan, R., Polymer therapeutics as nanomedicines: new perspectives. *Current Opinion in Biotechnology* **2011**, *22*, 1-10.
5. Ferrari, M., Cancer nanotechnology: opportunities and challenges. *Nature Rev. Cancer* **2005**, *5*, 161-171.
6. Ringsdorf, H., Structure and Properties of Pharmacologically Active Polymers. *Journal of Polymer Science Part C-Polymer Symposium* **1975**, (51), 135-153.
7. Duncan, R., The dawning era of polymer therapeutics. *Nature Reviews Drug Discovery* **2003**, *2* (5), 347-360.
8. Brocchini, S.; Duncan, R., Pendent Drugs, Release from Polymers. In *Encyclopedia of Controlled Drug Delivery*, Mathiowitz, Ed. Wiley Interscience: New York, 1999; pp 786-816.
9. Brocchini, S.; Duncan, R., Pendent Drugs, Release from Polymers. In: *Encyclopedia of Controlled Drug Delivery*. Mathiowitz, E. Ed. New York, Wiley Interscience. pp 786-816. In *Encyclopedia of Controlled Drug Delivery*, Mathiowitz, E., Ed. Wiley Interscience: New York, 1999; pp 786-816.
10. Matsumura, Y.; Maeda, H., A New Concept for Macromolecular Therapeutics in Cancer-Chemotherapy - Mechanism of Tumoritropic Accumulation of Proteins and the Antitumor Agent Smancs. *Cancer Research* **1986**, *46* (12), 6387-6392.
11. de Duve, C.; de Barse, T.; Poole, B.; Trouet, A.; Tulkens, P.; Van Hoof, F., Commentary. Lysosomotropic agents. *Biochem Pharmacol* **1974**, *23* (18), 2495-531.
12. Canton, I.; Battaglia, G., Endocytosis at the nanoscale. *Chem. Soc. Rev.* **2012**, *41*, 2718-2739.
13. Vicent, M. J.; Duncan, R., Polymer conjugates: nanosized medicines for treating cancer. *Trends in Biotechnology* **2006**, *24* (1), 39-47.
14. Tomlinson, R.; Klee, M.; Garrett, S.; Heller, J.; Duncan, R.; Brocchini, S., Pendent Chain Functionalized Polyacetals That Display pH-Dependent Degradation: A Platform for the Development of Novel Polymer Therapeutics. *Biomacromolecules* **2002**, *35* (2), 473-480.

15. Tomlinson, R.; Heller, J.; Brocchini, S.; Duncan, R., Polyacetal-doxorubicin conjugates designed for pH-dependent degradation. *Bioconjugate Chemistry* **2003**, *14* (6), 1096-1106.
16. Bosset, P.-O.; Albiges, L.; Seisen, T.; de la Motte Rouge, T.; Phé, V.; Bitker, M.-O.; Rouprêt, M., Current role of diethylstilbestrol in the management of advanced prostate cancer. *BJU International* **2012**.
17. Montgomery, R. B.; Nelson, P. S.; Lin, D.; Ryan, C. W.; Garzotto, M.; Beer, T. M., Diethylstilbestrol and docetaxel. *Cancer* **2007**, *110* (5), 996-1002.
18. Giménez, V.; James, C.; Armiñan, A.; Schweinsc, R.; Paul, A.; Vicent, M. J., Demonstrating the importance of Polymer-Conjugate Conformation in Solution on its Therapeutic Output: Diethylstilbestrol (DES)-Polyacetals as prostate cancer treatment. *Journal of Controlled Release* **2012**, *159* (2), 290-301.
19. Horoszewicz, J. S.; Leong, S. S.; Kawinski, E.; Horoszewicz, J. S.; Leong, S. S.; Kawinski, E.; Karr, J. P.; Rosenthal, H.; Chu, T. M.; Mirand, E. A.; Murphy, G. P., LNCaP Model of Human Prostatic Carcinoma. **1983**, 1809-1818.
20. Alimirah, F.; Chen, J.; Basrawala, Z.; Xin, H.; Choubey, D., DU-145 and PC-3 human prostate cancer cell lines express androgen receptor: implications for the androgen receptor functions and regulation. *Lett.* **2006**, *580* (9), 2294-300.
21. Barz, M.; Luxenhofer, R.; Zentel, R.; Kabanov, A. V., The uptake of N-(2-hydroxypropyl)-methacrylamide based homo, random and block copolymers by human multi-drug resistant breast adenocarcinoma cells. *Biomaterials* **2009**, *30* (29), 5682-5690.
22. Kabanov, A. V.; Alakhov, V. Y., Pluronic block copolymers in drug delivery: from micellar nanocontainers to biological response modifiers. *Crit Rev Ther Drug Carrier Syst* **2002**, *19* (1), 1-72.
23. Saad, M.; Garbuzenko, O. B.; Ber, E.; Chandna, P.; Khandare, J. J.; Pozharov, V. P.; Minko, T., Receptor targeted polymers, dendrimers, liposomes: Which nanocarrier is the most efficient for tumor-specific treatment and imaging? *Journal of Controlled Release* **2008**, *130* (2), 107-114.
24. Vicent, M. J.; Dieudonne, L.; Carbajo, R. J.; Pineda-Lucena, A., Polymer conjugates as therapeutics: future trends, challenges and opportunities. *Expert Opin Drug Deliv.* **2008**, *5* (5), 593-614.
25. Duncan, R.; Seymour, L. W.; Ohare, K. B.; Flanagan, P. A.; Wedge, S.; Hume, I. C.; Ulbrich, K.; Strohalm, J.; Subr, V.; Spreafico, F.; Grandi, M.; Ripamonti, M.; Farao, M.; Suarato, A., Preclinical Evaluation of Polymer-Bound Doxorubicin. *Journal of Controlled Release* **1992**, *19* (1-3), 331-346.

26. Greco, F.; Vicent, M. J., Combination therapy: Opportunities and challenges for polymer-drug conjugates as anticancer nanomedicines. *Advanced Drug Delivery Reviews* **2009**, *61* (13), 1203-1213.
27. Broxterman, H. J.; Georgopapadakou, N. H., Anticancer therapeutics: "Addictive" targets, multi-targeted drugs, new drug combinations. *Drug Resist Updat* **2005**, *8* (4), 183-97.
28. Duncan, R., N-(2-hydroxypropyl) methacrylamide copolymer conjugate. In *Polymeric Drug Delivery System*, Kwon, G. S., Ed. New York, 2005; pp 1-92.
29. Singer, J. W.; Shaffer, S.; Baker, B.; Bernareggi, A.; Stromatt, S.; Nienstedt, D.; Besman, M., Paclitaxel poliglumex (XYOTAX; CT-2103): an intracellularly targeted taxane. *Anticancer Drugs* **2005**, *16* (3), 243-54.
30. Bhatt, R.; de Vries, P.; Tulinsky, J.; Bellamy, G.; Baker, B.; Singer, J. W.; Klein, P., Synthesis and in vivo antitumor activity of poly(L-glutamic acid) conjugates of 20S-camptothecin. *J Med Chem* **2003**, *46* (1), 190-3.
31. Vicent, M. J.; Greco, F.; Nicholson, R. I.; Paul, A.; Griffiths, P. C.; Duncan, R., Polymer therapeutics designed for a combination therapy of hormone-dependent cancer. *Angew Chem Int Ed Engl* **2005**, *44* (26), 4061-6.
32. Barz, M.; Luxenhofer, R.; Zentel, R.; Vicent, M. J., Overcoming the PEG-addiction: well-defined alternatives to PEG, from structure-property relationships to better defined therapeutics. *Polymer Chemistry* **2011**, *2*, 1900-1918.
33. Grayson, S. M.; Godbey, W. T., The role of macromolecular architecture in passively targeted polymeric carriers for drug and gene delivery. *J. Drug Target.* **2008**, *16* (5), 329-356.
34. Griffiths, P. C.; Paul, A.; Apostolovic, B.; Klok, H. A.; de Luca, E.; King, S. M.; Heenan, R. K., Conformational consequences of cooperative binding of a coiled-coil peptide motif to poly(N-(2-hydroxypropyl) methacrylamide) HPMA copolymers. *Journal of Controlled Release* **2011**, *153* (2), 173-179.



# 7

## Conclusions



### 1. DES-polyacetal systems as single conjugates.

- A novel family of DES-polyacetals, *Block-DES*, with greater drug loading and lower polydispersity than the parent first generation (*Tert-DES*) was developed. Both polymers were exhaustively characterized and evaluated not only from a physic-chemical point of view but also looking at biophysical characterization parameters. *Block-DES* has an amphiphilic character and therefore different conformation in solution.
- DES-polyacetals showed a clear pH-dependent degradation, with faster DES release under acidic environment. *Block-DES* showed faster rate of DES release at acidic pH than the *Tert-DES* and more importantly a bimodal drug release kinetics, indicating a different solution conformation. Both systems presented plasma stability.
- Multiple CACs were found for both polymers, being much lower for *Block-DES* than for *Tert-DES* (i.e first *Tert-DES* **1b** CAC= 0.7 mg/mL; first *Block-DES* **2b** CAC= 0.1 mg/mL). PGSE-NMR studies indicated a clear difference in the obtained self-diffusion rates between the two conjugates, with the *Tert-DES* conjugate ( $D_s=2.72 \times 10^{-11} \text{ m}^2 \text{ s}^{-1}$ ) moving more slowly than the *Block-DES* counterpart ( $D_s=5.87 \times 10^{-11} \text{ m}^2 \text{ s}^{-1}$ ) indicating clearly that different solution structures were formed in each case. Other physicochemical techniques such as DLS, TEM, SEM and SANS were performed in aqueous solution for both polyacetals. SANS experiments demonstrated that *Tert-DES* was present as single system with an approximate diameter of 20 nm with 2 nm thickness. *Block-DES* is characterized by two sets of coexisting species; one system is 100 nm length, 2 nm thickness (similar shape but greater length than *Tert-DES*) and a second and more abundant system of 80 nm diameter, 10 nm thickness, a disk-like conformation. The second one more abundant and consistent with the size of the structures observed by TEM and DLS, and significantly larger than the structures indicated by SANS for the *Tert-DES*.
- *Block-DES* displayed greater cytotoxicity in PC3 and LNCaP human prostate cancer cells than the *Tert-DES*.

- An additional monomer, serinol, was incorporated into the main chain of the polyacetal carrier (described first by Tomlinson et al) in order to allow a functional pendent chain suitable for drug or dye conjugation. The DES-polyacetals were conjugated to Oregon Green for Cell Trafficking (*Tert*-DES-Ser-OG vs. *Block*-DES-Ser-OG), to Cyane 5.5 for *in vivo* assays (yielding *Tert*-DES-Ser-Cy5.5 vs. *Block*-DES-Ser-Cy5.5) and finally conjugated to Paclitaxel as second anticancer drug chosen to form systems for Combination Therapy (yielding *Tert*-DES-Ser-PTX vs. *Block*-DES-Ser-PTX).
- Both conjugates, *Tert*-DES-Ser-OG vs. *Block*-DES-Ser-OG, enter the cell by the endocytic route as demonstrated the confocal studies, although the percentage of *Block*-DES inside the cells is greater than that observed for *tert*-DES in both cell lines.
- Molecular mechanism studies in prostate cancer cell lines reflected a clear dependence on the cell line studied. DES derivatives clearly modulates AKT signaling pathway triggering cell death through apoptotis (Bcl-2, Bax) and autophagy (LC3 mainly with *Block*-DES in PC3 cells), and also they could influenced cell cycle (p21 modulation) arresting cells in different stages depending on the cell line used.
- Preliminary *in vivo studies* were carried out in a xenograft model with human colon cancer cells, which showed no toxicity *in vivo* for DES-polyacetals up to 10 mg/kg and a clear tumour accumulation up to 17 days for *Tert*-DES. *Non-significant* antitumor activity was observed in a PC3 prostate cancer xenograft model with the single conjugates, therefore the combination therapy approach was followed.

## 2. Design of polyacetal-based combination therapy

- **Polyacetal-based combination conjugates** were developed based of the single DES-polyacetals already synthesized and adding the chemotherapeutic Paclitaxel.
- Those combination conjugates were also fluorescent labelled with OG (*Tert*- and *Block*- DES-Ser-PTX-OG) and with Cy5.5 (*Tert*- and

*Block-DES-Ser-PTX-Cy5.5*) to carried out the different *in vitro* (cell trafficking) and *in vivo* (biodistribution, tumour accumulation) assays respectively.

- In order to study polymer conformation, PGSE-NMR and SANS studies were carried out in those conjugates when serinol and then paclitaxel were added. Polymers with serinol modified its structure, obtaining self-diffusion rates between the two conjugates, with the *Tert-DES-Serinol* conjugate,  $D_s=4.50 \times 10^{-11} \text{ m}^2 \text{ s}^{-1}$  (without serinol,  $D_s$  for *Tert-DES* was  $2.72 \times 10^{-11} \text{ m}^2 \text{ s}^{-1}$ ) moving more slowly than the *Block-DES-Serinol* counterpart  $D_s=5.17 \times 10^{-11} \text{ m}^2 \text{ s}^{-1}$  (for *Block-DES*,  $D_s$  was  $5.87 \times 10^{-11} \text{ m}^2 \text{ s}^{-1}$ ) similar data observed for the parent polyacetals. Those values in the diffusion coefficient clearly indicate that different solution structures occurred in each case.
- SANS studies confirmed that when serinol was incorporated into the system, and as well the drug Paclitaxel, a dominant effect on the polymer structure was triggered. *Tert-Ser-PTX* sample was best fitted to a thin rod of radius  $10 \text{ \AA}$ , length  $300 \text{ \AA}$ , with a  $Q^{-n}$  term with  $n=3.5$ . When PTX was added to *Tert-DES-Ser* forming *Tert-DES-Ser-PTX*, the scattering was dominated by a  $Q^{-4}$  term, indicating the presence of extremely large structures that were outside of the resolution of the SANS experiment. This experiment clearly showed that the PTX drove solution conformation.
- The combination polyacetals were tested *in vitro* and preliminary *in vivo* in breast and prostate cancer models.
- *In vitro* efficacy assays were performed in breast and prostate cancer cell lines and showed clear synergism ( $CI > 1$ ) when both drugs, DES and PTX, were combined in the same system as *Tert-* or *Block-*architectures. *In vitro* breast cancer cells MDA-MB-453S were used and a greater cytotoxicity was found for the DES-PTX polyacetals when compared to free PTX. In PC3 androgen-independent prostate cancer cells, the polyacetal *Tert-DES-Ser-PTX* polyacetal seemed to be more active than PTX alone. On the contrary, in the LNCaP androgen-dependent cell line, *Block-DES-Ser-PTX* showed greater cytotoxicity than free PTX alone or PTX-polyacetal conjugate.

- Non-significant differences regarding cell internalization were observed with the *Tert-* vs. *Block-* combination conjugates; however the uptake kinetics was greatly influenced by the cell line used.
- When the combination polymers were conjugated to Cy5.5, *in vivo* biodistribution studies showed tumor accumulation being maximum at 3h post-administration. Accumulation in the liver and kidneys were as well detected indicating that the polyacetals excretion is throughout the hepatic and renal excretion routes without any sign of organ toxicity.
- *In vivo* tolerability and therapeutic efficacy of all the systems are on ongoing studies using orthotopic prostate cancer (LNCaP androgen-dependent PCa cells). And as well, studies on non-invasive intraprostatic PC3 Tumor and Metastasis Growth Studies *in vivo* and *ex vivo* are being carrying out to corroborate the preliminary data already obtained.

## Collaborations

- PGSE-NMR studies have been performances in collaboration with Alison Paul, PhD and Peter Griffiths, PhD at Cardiff University.
- SANS studies have been performances in collaboration with Alison Paul, PhD from Cardiff University at ILL in Grenoble (France) and at ISIS in Oxford (UK).
- *In vivo* studies have been carried out by our collaborators Ibane Abasolo, PhD and Yolanda Fenandez, PhD from Dr Schwartz Jr. group at Vall d'Hebron Hospital in Barcelona.
- Molecular mechanisms in our lab at CIPF in collaboration with Dr Ana Armiñán.



# Appendix **1**

**TNM staging**

## Appendix 1

### **DEFINITION AND CLASSIFICATION OF TNM STAGING**

-Supporting information of Chapter 1. Introduction: Prostate Cancer

**Stage** is a term used to define the size and scope of a cancer. The goal is to diagnose the cancer as early as possible, before it has spread beyond the prostate region. Different tests are carried out in order to establish tumor progression stage by Digital Rectal Exam (DRE), radiological studies (X-rays, CT scans, bone scans, MRI scan or other imaging tests (See Glossary) and pathology (inspection of tumor specimens under a microscope after surgery).

#### *1) Evaluation of the Tumor (T)*

**Stage TX:** No available information on primary tumor.

**Stage T0:** No evidence of primary tumor.

**Stage Tis:** Carcinoma in situ.

**Stage T1:** The tumor is less than 2cm in diameter, cannot be felt. Stage T1a and T1b tumors are diagnosed after surgery to improve urine flow. The part of the prostate removed is found to contain cancer. T1c tumors are usually diagnosed because the PSA is elevated, prompting a biopsy.

**Stage T2:** T2 tumors can be felt, it measures between 2-4cm of diameter, but are confined to the prostate gland. T2a tumors involve less than one half of one lobe of the prostate. T2b tumors involve more than one half of one lobe. T2c tumors involve both lobes.

**Stage T3:** The tumor is greater than 4cm in diameter. T3 tumors extend beyond the prostate gland. T3a tumors extend beyond the prostate capsule. T3b tumors extend into the seminal vesicle. Patients who are found to have disease beyond the prostate after surgery are said to have “surgical T3 disease” or “pathologic T3 disease”.

Stage is what the doctor feels (DRE), or sees (scans). It tells us how far along the growth pathway the cancer has progressed.

**Stage T4:** The tumor has spread or invaded tissues next to the prostate (other than the seminal vesicles). T4 is classified as T4a and T4b depending on structures involved and resectable (T4a) versus unresectable (T4b) nature lesion. T4a tumor has spread to the neck of the bladder, the external sphincter (muscles that help control urination), or the rectum. T4b tumor has spread to the floor or/and the wall of the pelvis.

### **2) Evaluation of the regional lymph nodes (N)**

**NX:** cannot evaluate the regional lymph nodes.

**N0:** cancer has not spread to any lymph nodes.

**N1:** cancer has spread to a single regional lymph node (inside the pelvis), no larger than 2 cm of diameter.

**N2:** cancer has spread to one or more regional lymph nodes and it is between 2-6 cm in diameter.

**N3:** Cancer has spread to a lymph node and is larger than 6 cm.

### **3) Evaluation of distant metastasis (M)**

**MX:** cannot evaluate distant metastasis.

**M0:** The cancer has not metastasized beyond the regional lymph nodes.

**M1:** The cancer has metastasized to distant lymph nodes, outside of the pelvis, bones or other distant organs such as lung, liver or brain. M1a cancer has spread to lymph nodes beyond the regional ones. M1b cancer has spread to bone. M1c cancer has spread to other sites (regardless of bone involvement).





# Appendix **2**

**OBJECTIVES, METHODOLOGY AND  
CONCLUSIONS OF THE PROJECT IN  
SPANISH**

## INDICE

1. Objetivos.....	329
2. Metodología.....	332
2.1 Instrumentos .....	332
2.2 Materiales .....	333
2.3 Síntesis de los poliacetales con DES y poliacetales para terapia de combinación con DES y PTX.....	335
2.3.1 Síntesis del Terpolímero (o <i>Ter-DES</i> ) (1). .....	335
2.3.2 Síntesis del Bloque-co-polimero (o <i>Block-DES</i> ) (2). .....	336
2.3.3 Síntesis de protección del Serinol con el grupo Fmoc (Fmoc-Serinol) (3).....	338
2.3.4 Síntesis de poliacetales con DES y Serinol, <i>Tert-DES-Serinol</i> (o <i>Tert-DES-Ser</i> ) (4) y Bloque-DES-serinol (o Bloque-DES-Ser).....	338
2.3.5 Desprotección del grupo -Fmoc de los poliacetales, <i>Ter-DES-Ser<sub>NH<sub>2</sub></sub></i> (6) y <i>Block-DES-Ser<sub>NH<sub>2</sub></sub></i> <sup>2</sup> (7).....	338
2.3.6 Síntesis de conjugados marcados fluorescentemente con Oregon green (OG) o con Cyane 5.5.....	339
2.3.7 Síntesis de <i>Ter-DES-Ser-PTX<sub>COOH</sub></i> (21) y <i>Bloque-DES-Ser-PTX<sub>COOH</sub></i> (22). .....	340
2.3.8 Síntesis de conjugados con PTX marcados con OG ó Cyane5.5.	340
2.4 Estudios de <sup>1</sup> H-RMN.....	341
2.5 Técnica de GPC.....	341
2.6 Determinación del contenido de fármaco libre y total en los conjugados con DES.....	341
2.7 Determinación de la Concentración Micelar Crítica (CMC) de los polímeros conjugados.....	342
2.8 Estudios de dispersión dinámica de luz (Dynamic Light Scattering (DLS)). .....	343
2.9 Técnicas de microscopía de transmisión y muestreo electrónicas (Transmission and Scanning electron microscopy (TEM) and (SEM))... ..	343
2.10 Estudios de dispersion de neutrones de ángulo pequeño (Small Angle Neutron Scattering (SANS)).....	343
2.11 Estudios de degradación dependientes de pH en disolución tampón. ....	344
2.12 Estabilidad en Plasma.....	344
2.13 Viabilidad celular en células de cáncer de próstata, LNCaP y PC3.	344
2.14 Biodistribución y acumulación en el tumor y distintos órganos de los conjugados poliacetálicos marcados con Cyane5.5 en modelos xenografos de ratón. ....	346
3. Conclusiones.....	347

## **1. OBJETIVOS DE LA INVESTIGACIÓN**

Ésta tesis se centra en el diseño de nuevos conjugados polímero-fármaco sensibles a pH para usarse como agentes únicos o en terapia de combinación para el tratamiento del cáncer hormono-dependiente, en particular cáncer de próstata. Éstos conjugados se basan en sistemas poliacetálicos previamente desarrollados en los que el fármaco forma parte de la cadena principal del polímero.

En el microambiente tumoral o después de la absorción celular por endocitosis, el descenso del pH encontrado en el compartimiento ácido del endosoma lisosomal, desencadena la degradación del polímero y como consecuencia la liberación del fármaco que se difunde fuera en el citosol.

En el diseño de nuestros sistemas, la necesidad de optimizar la química de enlace para unir el fármaco al polímero está por lo tanto superada, ya que en éstos sistemas poliacetálicos el fármaco forma parte de la cadena principal. El dietilestilbestrol (DES), estrógeno sintético que fue utilizado como fármaco y es clínicamente relevante en el tratamiento del cáncer de próstata, posee una funcionalidad adecuada (grupos dioles) para llevar a cabo dicha incorporación a la cadena polimérica base. Una clara degradación dependiente del pH y ensayos de prueba de concepto *in vitro* se obtuvieron con la primera generación de poliacetálicos. Sin embargo presentaron algunas limitaciones, que incluyen; una estructura no única, heterogeneidad en la composición, carga de fármaco bajo y una alta polidispersidad, afectando el comportamiento farmacológico y reproducibilidad de los resultados terapéuticos de este nanoconjugado basado en polímero.

Por lo tanto, el objetivo principal de esta tesis es avanzar un paso más hacia una segunda generación de conjugados poliacetálicos para el tratamiento del cáncer de próstata como agentes únicos, modificando y entendiendo la química del polímero/ conformación en disolución (capítulo 4) y como conjugados de combinación a base de polímero (capítulo 5) con el fin de lograr un posible candidato clínico.

En primer lugar, se realizará la síntesis controlada de Poliacetálicos basada en DES con propiedades mejoradas, como distribuciones de Mw más estrechas y mayor capacidad de carga de fármaco. El principal interés se centrará en la

comprensión de si ligeras modificaciones estructurales podrían influir significativamente en el rendimiento del conjugado terapéutico. Ésta segunda generación de poliacetales se obtendrá utilizando una metodología de bloque-co-polímero.

*Ter*-DES (primera generación) y *bloque*-DES (segunda generación) serán entonces probados en modelos celulares de cáncer de próstata seleccionados. Una vez evaluados biológicamente y con el fin de explicar las diferencias encontradas, se llevará a cabo una caracterización exhaustiva de ambos sistemas poliacetalicos mediante diferentes técnicas, tales como: microscopía electrónica de transmisión (TEM), dispersión de la luz dinámica (DLS), estudios de difusión de resonancia magnética nuclear (PGSE-RMN) y dispersión de neutrones de pequeño ángulo (SANS), utilizadas para la comprensión de la conformación en disolución de los polímeros conjugados a buen efecto (capítulo 4.II). Esto se hará en colaboración con el grupo de la Dr. Alison Paul y el Dr. Peter Griffiths en la Universidad de Cardiff, Reino Unido.

También se realizará una caracterización biofísica observando internalización celular, el mecanismo molecular del *ter* - vs *bloque*- (en colaboración con Dr. Ana Armiñán de nuestro laboratorio) y finalmente se desarrollarán estudios de prueba de concepto *in vivo* (en colaboración con el grupo del Dr Schwartz Jr., Dr. Ibane Abasolo y Dr. Yolanda Fernández, del departamento de Nanomedicina CIBBIM en el Hospital Vall d ' Hebron, Barcelona) (capítulo 4.III).

Debido a la importancia de la terapia de combinación, el capítulo 5 se centrará en mejorar las construcciones poliacetalicas mediante la aplicación de esta estrategia analizando el posible sinergismo de fármacos basado en la administración simultánea de endocrino + quimioterapia. Para lograrlo, un monómero adicional tendrá que ser sintetizado e incorporado en el polímero ofreciendo la posibilidad de un nuevo punto de anclaje y así conjugar un segundo fármaco (paclitaxel es el que se seleccionó para ser combinado con DES). Como se hizo para los conjugados individuales, los sistemas de combinación también serán caracterizados de manera exhaustiva, fisicoquímica y biofísicamente, junto con estudios preliminares *in vivo* que incluirán ensayos de biodistribución, acumulación de tumor y actividad antitumoral de los poliacetales.

Por último, los capítulos 6 y 7 proporcionarán una discusión general y las conclusiones respectivamente sobre los principales resultados obtenidos en este proyecto.

## **2. METODOLOGÍA**

### **2.1 Instrumentos**

Los análisis monodimensionales por **resonancia magnética nuclear (RMN)**  $^1\text{H}$ -RMN,  $^{13}\text{C}$ -RMN y los experimentos de dos dimensiones DOSY (Diffusion Ordered Spectroscopy) y COSY (Correlated Spectroscopy) han sido realizados con un espectrómetro Bruker Advance AC-300 (300MHz). Los datos obtenidos han sido procesados utilizando el programa Topspin (Bruker GmbH, Karlsruhe, Alemania).

Se utilizó **cromatografía líquida de alta eficacia en fase reversa (RP-HPLC**, reverse phase-high performance liquid chromatography) con un cromatógrafo para el análisis de muestras Shimadzu con auto-muestreador 717plus. La columna cromatográfica utilizada fue una RP-18 (125 x 4 mm, 5  $\mu\text{m}$ ), LICHroCART®, Cat.1.50943 LiChrospher® 100, obtenida en Waters Ltd (Hertfordshire, Reino Unido). Las fases móviles utilizados fueron filtradas previamente a través de membranas de 0.45 $\mu\text{m}$  y desgasificadas en un baño de ultrasonidos durante 30 min.

Con el fin de obtener los pesos moleculares (Mw) y la polidispersidad (Mw/Mn) de los conjugados y los portadores poliméricos, se utilizó la metodología de **cromatografía de exclusión molecular o de filtración en gel (SEC, GPC)**. Los análisis se realizaron en un Triple Detector Array (TDA<sup>TM</sup>) de Viskotek (TDA3 302) y un detector UV modelo 2501. Las columnas empleadas fueron dos columnas TSK-Gel (G2500 y 3000). OmniSec 4.1 fue el software utilizado para calcular Mw/Mn y Mw de los polímeros y conjugados poliméricos sintetizados. Como fase móvil se utilizó THF, DMF o tampón fosfato salino (PBS, Phosphate Buffer Saline) (0.1%  $\text{NaN}_3$ ) filtrado previamente a través de membranas de 0.22 $\mu\text{m}$  y desgasificado en un baño de ultrasonidos durante 30min.

Para las medidas del tamaño de partícula se empleó la técnica de dispersión de luz **DLS (Dynamic Light Scattering)**. Estas medidas se realizaron en un equipo Zetasizer NanoZS (Malvern Instruments Ltd, Marlvern, Reino Unido) en el Instituto de Ciencia Molecular (ICMOL) en Paterna, Valencia. Estudios con **Microscopia de Trasmisión Electrónica (TEM)** fueron llevados a cabo con un sistema Tecnai Spirit G2 FEI y una cámara digital Olympus, Soft Image System, model Morada en el CIPF y la **Microscopia de Escaneo**

**Electrónica (SEM)** se realizó en un microscopio JEOL JSM 5410 en el Departamento de Biomateriales en la Universidad de Valencia. Para estudiar las **Concentraciones Críticas Micelares (cmc)** se empleó un espectrofotómetro Jasco FP-6500 usando un ancho de banda (excitación y emisión) de 3nm y la velocidad de escaneo era de 100nm. Los experimentos con **Dispersión de Neutrones de Pequeño Ángulo (SANS)** se realizaron en el Institute Laue-Langevin, ILL en Grenoble (Francia) y en el ISIS Facility en Oxford (Reino Unido) para determinar el tamaño y forma de los conjugados. Todos los procesos relacionados con el cultivo celular se llevaron a cabo en una cabina de flujo laminar recirculante vertical con seguridad biológica clase II (Telstar). Las medidas de viabilidad celular y fluorescencia de los compuestos se llevaron a cabo en Victor<sup>2</sup> Wallac 1420 Multilabel HTS Counter Perkin Elmer (Northwolk, CT, EEUU). Los estudios de internalización celular mediante **microscopía confocal** de fluorescencia fueron hechos a través del Servicio de Microscopía Confocal del CIPF (Valencia). Las imágenes fueron adquiridas con un microscopio (invertido) láser confocal Leica, modelo TCS SP2 AOBS (Leyca Microsystems Heidelberg GMBH, Mannheim, Germany) usando un objetivo de inmersión de 63X Plan-Apochromat-Lambda Blue 1.4 N.A. La longitud de onda ( $\lambda$ ) usada para excitar el fluorocromo fue: 488nm para el Oregon Green (OG), utilizando para ello un láser de argón. Las aperturas de los canales para la detección de la emisión del OG fueron: de 503 a 604nm. Las imágenes fueron tomadas bidimensionalmente y en pseudo color (255 niveles de color), con una resolución de 1024x1024 pixels. Todas las imágenes fueron adquiridas bajo las mismas condiciones y los análisis de distribución de fluorescencia fueron hechos mediante el software de Leica “Leica Lite” versión 2.61.

Los estudios de biodistribución en modelos tumorales *in vivo* fueron medidos por tejido fluorescente (FRI) usando el espectro de IVIS® fueron llevados en el CIBBIM-Nanomedicina, en el Hospital Vall d’Hebron de Barcelona.

## 2.2 Materiales

Tri(etilene glicol) divinil éter (TEGDVE), polietilenglicol (PEG) Mw 4000Da, ácido p-toluenesulfónico monohidratado (p-TSA), dietilestilbestrol (DES), 2-amino-1,3-propanodiol (Serinol), 9-Fluorenilmetiloxicarbonil de cloro (Fmoc-Cl), anhídrido succínico, dioxano, tetrahidrofurano anhídrido



(THF) tolueno anhídrido, 4-(Dimetilamino)piridina (DMAP) pureza  $\geq 98.0\%$ , N,N-Diisopropiletilamine (DIEA), N-hidroxisuccinimida 98% (NHS) y la sal de sodio de N-hidroxisulfosuccinimida (sulfo-NHS)  $\geq 98.5\%$  fueron suministradas por Sigma-Aldrich (Dorset, UK). Antes de utilizarse, el THF fue destilado con benzofenona de sodio. Diisopropilcarbodiimida (DIC), 1-etil-3-(3dimetilaminopropil) carbodiimida hidrociorada (EDAC), 1-hidroxibenzotriazolole monohidratado 99.7% (HOBT) fueron administradas por IRIS Biotech GmbH (Alemania). Triethylamine y N,N-dimethylformamide (DMF) se obtuvieron de Fluka Chemika (Masserschmittstr, D). Respecto a los disolventes deuterados utilizados en Resonancia Magnética Nuclear (RMN): N,N-dimetilformamida- $d_6$  (DMF- $d_6$ ), cloroformo- $d_1$  ( $CDCl_3-d_1$ ), agua deuterada- $d_2$  ( $D_2O$ ), dimetilsulfoxido- $d_6$  (DMSO- $d_6$ ), metanol- $d_1$  (MeOH- $d_1$ ). Diclorometano ( $CH_2Cl_2$ ) con grado síntesis, Etanol (EtOH) absoluto, Metanol (MeOH) con grado de HPLC y acetonitrilo (AcCN) también de grado HPLC fueron suministrados por Scharlau (España). AppliChem (Alemania) suministró el 2,2'-dihidroxi-(2,2'-bi-indan)-1,1',3,3'-tetrona (Hidrintantino dihidratado). Ninhidrina GR para análisis se obtuvo de MERCK (Alemania). Las resinas para cromatografía líquida tales como Sephadex LH-20 y Sephadex G-10 y las columnas pre-empaquetadas PD-10 se obtuvieron de GE healthcare (Reino Unido). n-Hexano de grado analítico se obtuvieron de VWR (Alemania). El resto de disolventes de uso habitual en el laboratorio como acetona se obtuvieron de Aldrich or Sigma. Las líneas celulares de cáncer de próstata PC3 y LNCaP se obtuvieron de American Type Culture Collection (ATCC) (Rockville, MD, EEUU). Dimetilsulfóxido de grado biotecnológico (DMSO), bromuro de 4-(4,5-dimetil tiazol-2-il)-2,5-difenil tetrazolio (MTT), hidrocioruro de leupeptina y Trypan-blue se obtuvieron de Sigma-Adrich Co. (St Louis, MO, EEUU). El suplemento de crecimiento endotelial (ECGS) fue suministrado por BD<sup>TM</sup> Biosciences (San Jose, CA, USA). 0.25% tripsina-EDTA se obtuvo de Gibco BRL Life Technologies (Paisley, Reino Unido). El suero fetal bovino inactivado (FBS), los medios F12 y RPMI 1640 y el marcador lisosomal Dextran-Texas Red fueron suministrado por Invitrogen (Carlsbad, CA, EEUU). El marcador fluorescente Oregon Green cadaverine (OG-cad) y Oregon green acido carboxílico (OG-NHS) fueron de Molecular Probes. El fluorescente Cy 5.5-cadaverina se obtuvo de Shabat y el Cyane 5.5-monofuncional succinimidil éster (Cy-NHS) de GE Healthcare (Buckinghamshire, UK). Los anticuerpos para la realización

de los análisis de western blot: b-Actin (Sigma), p21 (Cell Signaling), caspasa 3 (Cell Signalling), Bax (Santa Cruz Biotechnology), y Bcl2(Dako).

### **2.3 Síntesis de los poliacetales con DES (*Ter*-DES, *Bloque*-DES, Serinol-Fmoc, *Ter*-DES-Ser, *Bloque*-DES-Ser y sus derivados marcados con OG y Cyane5.5) y poliacetales para terapia de combinación con DES y PTX (*Ter*-DES-Ser-PTX, *Bloque*-DES-Ser-PTX y sus derivados con OG y Cyane5.5).**

#### **2.3.1 Síntesis del Terpolímero (o *Ter*-DES) (1).**

##### *A) Estrategia 1. Metodología clásica.*

**Ter-DES** se sintetizó mediante *tert*-polimerización entre vinil éteres y alcoholes en THF optimizando el protocolo ya publicado<sup>1, 2</sup>. Todos los reactivos se secaron previamente en un horno a vacío a 80°C durante 16 hrs. A una disolución con polietilenglicol (PEG) (Mw=4.000 g/mol, 2 g, 0.5 mmol), ácido para-toluen sulfónico monohidratado (Mw= 190.22 g/mol , 0.003 g, 0.015 mmol) y dietilestilbestrol (DES) (Mw= 268.34 g/mol ,0.135 g, 0.5 mmol) en THF destilado (6 ml), se añadió TEGDVE lentamente (Mw= 202.25 g/mol, 0.202g, d=0.99, 0.2mL, 1.07 mmol) usando una jeringa que conserve las condiciones anhidridas. La reacción fue vigorosamente agitada durante 3h a temperatura ambiente y cubierta con papel de aluminio para proteger de la luz. Entonces, se añadió trietilamina (Et<sub>3</sub>N) (0.2ml) para neutralizar el catalizador p-TSA y tras 30 minutos de agitación la mezcla de reacción se añadió gota a gota sobre una mezcla fría de hexano:éter (4:1) (100ml) que se dejó agitando 30 minutos más para que el poliactal precipite como un sólido blanco. Entonces, el producto fue aislado mediante filtración y el disolvente se evaporó a vacío y temperatura ambiente. Para eliminar posibles trazas de catalizador se realizó una extracción en cloroformo en una solución saturada de NaHCO<sub>3</sub> (3x20ml). Las fases orgánicas se combinaron, lavaron con una disolución saturada de NaCl (20ml) y se secaron con Na<sub>2</sub>SO<sub>4</sub>. Una vez filtrado el sulfato sódico, los restos de disolvente se evaporaron a vacío. El producto se re-disolvió en agua MilliQ y se liofilizó para obtener el compuesto deseado. El poliactal fue de nuevo recolectado y secado bajo vacío durante 24h para obtener Ter-DES como un sólido blanco.

##### *B) Estrategia 2. Nueva metodología.*

PEG (1000 mg, 0.250 mmol) y DES (100 mg, 0.373 mmol) se añadieron a un tubo Schlenk de 50 ml, equipado con un imán magnético y un tapón de vidrio. Se evacuó el tubo bajo condiciones de alto vacío ( $10^{-2}$  bar) durante 15 minutos y se rellenó con gas Nitrógeno. Mientras el tubo Schlenk se purgaba, se añadió dioxano anhídrido (5 ml) mediante una jeringa y se agitó y calentó la reacción ( $\sim 60$  °C) hasta la completa disolución de los reactivos. A continuación, *p*-TSA (2 mg, 0.106 mmol, tomado de una disolución madre de 1 mg/ml en dioxano) fue añadido a la disolución del polímero y dejándolo agitar durante 2 minutos más. Mientras seguía purgándose con nitrógeno, DEGDVE (182  $\mu$ l, 1.12 mmol) fue añadido con una pipeta Gilson y el tubo Schlenk se selló para conservar las condiciones anhidras. La mezcla de reacción fue agitada en la oscuridad durante 1 hora antes de añadir una disolución de hidróxido sódico en etanol (2 ml, 0.1 M) para quenchar la reacción. A continuación la mezcla se añadió gota a gota sobre hexano (100ml) para precipitar el polímero conjugado y tras 5 minutos de agitación, el disolvente se decantó. Para una completa eliminación del hexano, el residuo se centrifugó y una vez aislado el producto, se secó con flujo de nitrógeno y se re-disolvió en THF (4ml) para volverlo a precipitar sobre hexano (100ml), siguiendo los mismos pasos que anteriormente, decantando el hexano y secando el residuo con nitrógeno. Dicha operación se repitió 3 veces para asegurarnos una correcta purificación. Después de secar el producto a alto vacío durante 4 horas las muestras fueron almacenadas en tubos sellados a  $-20^{\circ}\text{C}$  para su estabilidad.

### 2.3.2 Síntesis del Bloque-co-polímero (o *Bloque-DES*) (2).

#### A) *Estrategía 1. Procedimiento A basado en la metodología clásica.*

Bloque-DES<sup>2</sup> fue sintetizado mediante co-polimerización en THF. En un matraz Redondo secado previamente en estufa de vacío, se añadió PEG liofilizado ( $M_w=4000\text{g/mol}$ , 2g, 0.5mmol) y *p*-TSA ( $M_w=190.22\text{g/mol}$ , 0.003g, 0.015mmol) y fueron disueltos en THF destilado (4ml). A continuación, TEGDVE ( $M_w=202.23\text{g/mol}$ , 0.5mmol, 0.22ml) fue añadido y la mezcla fue vigorosamente agitada durante 3h en la oscuridad y a temperatura ambiente. Entonces, DES ( $M_w=268.34\text{g/mol}$ , 0.134g, 0.5mmol) fue añadido lentamente a la reacción usando una jeringa para preservar la reacción en condiciones anhidras y agitadas durante 3h más. Transcurrido ese tiempo, trietilamina (0.2ml) fue entonces añadido para neutralizar el

catalizador *p*-TSA dejándolo agitar durante 30 minutos para entonces añadir la disolución gota a gota sobre una mezcla fría de hexano: éter (4:1) (100ml) y así precipitar el poliactal **2**. Después de 30 minutos adicionales de agitación, el polímero fue recolectado y de nuevo precipitado sobre otra mezcla fresca de hexano: éter (4:1) y agitado por 30 min más para lograr un lavado más eficiente. El Poliactal otra vez se recolectó y se secó a vacío durante 24h para obtener el bloque-DES como un sólido blanco.

**B) Estrategia2. Procedimiento B basado en la nueva metodología.**

Se añadió PEG (1000 mg, 0.250 mmol) a un tubo Schlenk de 50 ml equipado con un imán magnético y un tapón de vidrio. Se evacuó el tubo bajo condiciones de alto vacío ( $10^{-2}$  bar) durante 15 minutos y se rellenó con gas Nitrógeno. Mientras el tubo Schlenk se purgaba, se añadió dioxano anhídrido (5 ml) mediante una jeringa y se agitó y calentó la reacción ( $\sim 60$  °C) hasta que el PEG se disolvió completamente. A continuación, *p*-TSA (2 mg, 0.106 mmol, tomado de una disolución madre de 1 mg/ml en dioxano) fue añadido a la disolución del polímero y dejándolo agitar durante 2 minutos más. Mientras seguía purgándose con nitrógeno, DEGVE (60  $\mu$ l, 0.37 mmol) fue añadido con una pipeta Gilson y el tubo Schlenk se selló para conservar las condiciones anhidras. La mezcla de reacción se agitó durante 45 min antes de añadir más DEGDVE (122  $\mu$ l, 0.75 mmol) y 15 min después el DES (100 mg, 0.373 mmol) también se añadió y se agitó durante 1h más. Entonces una disolución de hidróxido sódico en etanol (2 ml, 0.1 M) fue añadida para quenchar la reacción dejándolo agitando 5 minutos. A continuación la mezcla se añadió gota a gota sobre hexano (100ml) para precipitar el polímero conjugado y tras 5 minutos de agitación, el disolvente se decantó. Para una completa eliminación del hexano, el residuo se centrifugó y una vez aislado el producto, se secó con flujo de nitrógeno y se re-disolvió en THF (4ml) para volverlo a precipitar sobre hexano (100ml), siguiendo los mismos pasos que anteriormente, decantando el hexano y secando el residuo con nitrógeno. Dicha operación se repitió 3 veces para asegurarnos una correcta purificación. Después de secar el producto a alto vacío durante 4 horas las muestras fueron almacenadas en tubos sellados a  $-20^{\circ}\text{C}$  para su estabilidad.

### 2.3.3 Síntesis de protección del Serinol con el grupo Fmoc (Fmoc-Serinol) (3).

Reacción publicada previamente por Tomlinson, 2002<sup>4</sup>. Serinol-Fmoc fue sintetizado por condensación entre el grupo acil del grupo Fmoc y el grupo amino del serinol para la formación del enlace amida con consecuente eliminación de HCl. Serinol ( $M_w=91,06\text{g/mol}$ , 1.0g, 11mmol) se disolvió en 26.5ml de una disolución 10%  $\text{Na}_2\text{CO}_3$  (8g  $\text{Na}_2\text{CO}_3$  en 80ml de agua destilada). Entonces, se añadieron 15ml de dioxano y la mezcla se agitó sobre un baño de hielo. Fluorenilmetiloxicarbonil clorado (Fmoc-Cl) ( $M_w=260,72\text{mg/mol}$ , 2,86g, 11mmol) fue cuidadosamente añadido y la mezcla de reacción se agitó durante 4h a 4°C. Transcurridas 2h, se añadió 15ml de dioxano para disminuir su viscosidad. Tras 16 h de agitación, se añadieron 100ml de agua destilada para poder extraer el compuesto con etil acetato (2x100ml). Las fases orgánicas se combinaron y se secaron sobre  $\text{Na}_2\text{SO}_4$  anhidro. Después de filtrar, el disolvente se evaporó a vacío para obtener un sólido blanco, el cual se redisolvió en 40ml de dioxano y se recristalizó en 150ml de hexano.

### 2.3.4 Síntesis de poliacetales con DES y Serinol, *Tert*-DES-Serinol (o *Tert*-DES-Ser) (4) y Bloque-DES-serinol (o Bloque-DES-Ser)

Las síntesis de ambos poliacetales, *Ter*-DES-Serinol y *Bloque*-DES-Serinol, se llevaron a cabo utilizando los mismos procedimientos descritos en las estrategias 2 de i y ii respectivamente con la novedad de incorporar el nuevo monómero (0.58mmol) a la reacción. Para obtener el *ter*-DES-Serinol, el monómero se añadió junto con el PEG y el DES y para sintetizar el bloque-DES-Serinol, el serinol se añadió 5 minutos después del DES, para tener así controlada la formación de los bloques, primero se forma el bloque de polímero y a continuación el bloque con DES y serinol.

### 2.3.5 Desprotección del grupo -Fmoc de los poliacetales, *Ter*-DES-Ser<sub>NH2</sub> (6) y *Block*-DES-Ser<sub>NH2</sub><sup>2</sup> (7).

Los polímeros *Ter*-DES-Ser 4 y *Bloque*-DES-Ser 5 fueron disueltos independientemente en dos reacciones diferentes en 10ml de una mezcla piperidine/acetonitrile (20%) y se agitaron durante 1 h. La reacción se

monitorizó mediante TLC (100% etil acetato,  $R_f = 0.7$ ). La mezcla de reacción se lavó con hexano (3 x 15ml) y el acetonitrilo se eliminó a vacío a temperatura ambiente. El residuo se redisolvió en 15ml de hexano y se agitó durante 2h para obtener los poliacetales **6** y **7**.

### 2.3.6 Síntesis de conjugados marcados fluorescentemente con Oregon green (OG) o con Cyane 5.5.

Los conjugados marcados fluorescentemente con OG se utilizaron para llevar a cabo estudios *in vitro* como internalización celular y marcados con Cy5.5 para realizar estudios *in vivo* y determinar la biodistribución y acumulación en tumor de los conjugados.

Estos conjugados se sintetizaron mediante dos estrategias diferentes. **Estrategia 1**; el marcador fluorescente, OG o Cy5.5, ambos en forma de ácido carboxílico, fue conjugado a los poliacetales *Ter*-DES-Ser<sub>NH<sub>2</sub></sub> **6** y *Block*-DES-Ser<sub>NH<sub>2</sub></sub> **7** a través de la reacción entre el grupo amino libre del Poliacetal y el grupo carboxilo del fluorocromo una vez se ha eliminado el grupo NHS. **Estrategia 2** se centra en la succinilación de los polímeros *Tert*-DES-Ser<sub>NH<sub>2</sub></sub> **6** y *Block*-DES-Ser<sub>NH<sub>2</sub></sub> **7** y entonces se conjugó el OG y Cy5-5, a través del grupo carboxilo en los poliacetales y el grupo amino del marcador.

Ambas estrategias se obtuvieron con resultados parecidos pero en nuestro proyecto escogemos la opción 1 por motivos posteriores, ya que para incorporar el segundo fármaco, como estará como paclitaxel succinilado, se conjugará a través del grupo amino del polímero.

#### *Procedimiento de la estrategia 2:*

*Tert*-DES-Ser<sub>NH<sub>2</sub></sub> **6** (0,300 g, 0,030mmol) o *Block*-DES-Ser<sub>NH<sub>2</sub></sub> **7** (0.300g, 0,022mmol) fueron disueltos en THF anhidro. Se añadió DIEA hasta ajustar el pH a 9 y a continuación se disolvió Oregon Green (OG<sub>COOH</sub> con ácido carboxílico) o Cyane 5.5 (Cy5.5<sub>COOH</sub> con ácido carboxílico) (0.0002 g, 0.0008 mmol) en CH<sub>2</sub>Cl<sub>2</sub> y se añadió a la reacción. La reacción se monitorizó mediante TLC (Etil acetato: hexano 1:1,  $R_f = 0.5$ ). Tras 16 h de agitación el disolvente se evaporó, el residuo se redisolvió en agua MilliQ y se purificó mediante columnas PD10 eluyendo con agua MilliQ y recolectando fracciones de 1ml. Para identificar qué fracciones estaban conjugadas con el marcador, OG o Cy, y posteriormente determinar el porcentaje total

conjugado, se tomaron 2  $\mu\text{L}$  de cada fracción y se añadieron a 998  $\mu\text{L}$  de MeOH y las disoluciones se midieron en un espectrofotómetro Victor2Wallac. Los polímeros conjugados con Oregon Green y Cyane, *Ter-DES-Ser-OG<sub>NHS</sub>* **8**, *Bloque-DES-Ser-OG<sub>NHS</sub>* **9**, *Ter-DES-Ser-Cy<sub>NHS</sub>* **10** y *Bloque-DES-Ser-Cy<sub>NHS</sub>* **11** se liofilizaron para aislar los compuestos.

### 2.3.7 Síntesis de *Ter-DES-Ser-PTX<sub>COOH</sub>* (**21**) y *Bloque-DES-Ser-PTX<sub>COOH</sub>* (**22**).

Paclitaxel succiniloado **20** (Mw= 925.93 g/mol, 14 mg, 0.0015 mmol) se disolvió en 1.5 ml de THF anhidro y se añadió 3.14 mg de 1-Etil-3-(3-dimetilaminopropil) carbodiimida EDC (Mw = 155.24 g/mol, 0.02 mmol) agitando la reacción a temperatura ambiente durante 10min. Transcurrido ese tiempo, se añadió cuidadosamente *N*-hidroxisulfosuccinimida, 4.93 mg Sulfo-NHS (Mw = 217,1g/mol, 0.02 mmol) y se agitó durante 45 min a RT. Finalmente, *Ter-DES-Ser<sub>NH2</sub>* **6** o *Bloque-DES-Ser<sub>NH2</sub>* **7** fue añadido (para obtener respectivamente, **21** o **22**) y se ajustó el pH con DIEA. La mezcla de reacción fue agitada durante 16 h a temperatura ambiente y los conjugados fueron extraídos mediante precipitación sobre hexano y purificado por dialisis en agua durante 16 h.

### 2.3.8 Síntesis de conjugados con PTX marcados con OG ó Cyane5.5.

2'-Paclitaxel-succiniloado (PTX<sub>COOH</sub>) se conjugó a polímeros poliactalicos marcados previamente con OG o Cyane.

Los polímeros marcados con fluorocromos, sintetizados previamente, tales como: *Ter-DES-Ser-OG<sub>NHS</sub>* **8**, *Bloque-DES-Ser-OG<sub>NHS</sub>* **9**, *Ter-DES-Ser-Cy<sub>NHS</sub>* **10** y *Bloque-DES-Ser-Cy<sub>NHS</sub>* **11** se disolvieron en THF anhidro y se añadió DIEA para ajustar el pH hasta 9. A continuación se añadió paclitaxel succiniloado (PTX<sub>COOH</sub>) (0.0002 g, 0.0008 mmol) **20** disuelto en 0.01mL DMF. Tras 24 h de agitación el disolvente se evaporó a vacío, el residuo se re-disolvió en agua MilliQ y se purificó mediante columnas PD10 recolectando fracciones de 1ml y posteriormente deshidratándolas mediante liofilización obteniendo: *Ter-DES-Ser-PTX<sub>COOH</sub>-OG<sub>NHS</sub>* **23**, *Bloque-DES-Ser-PTX<sub>COOH</sub>-OG<sub>NHS</sub>* **24**, *Ter-DES-Ser-PTX<sub>COOH</sub>-Cy<sub>NHS</sub>* **25** y *Bloque-DES-Ser-PTX<sub>COOH</sub>-Cy<sub>NHS</sub>* **26**.

**2.4 Estudios de  $^1\text{H}$ -RMN.** Se realizaron espectros de  $^1\text{H}$ -RMN de cada uno de los productos obtenidos utilizando disolventes como  $\text{D}_2\text{O}$ , MeOD, DMSO, DMF, todos deuterados. Todos los experimentos se llevaron a cabo a temperatura ambiente.

**2.5 Técnica de GPC.** Los polímeros fueron preparados a una concentración de 3mg/ml disueltos en la fase móvil previamente preparada y estabilizada (THF o PBS). En el caso del disolvente orgánico, se añadió tolueno (20  $\mu\text{L}$ ) como marcador de flujo interno. Las muestras fueron filtradas mediante filtros individuales de nylon (membrana de 0.2  $\mu\text{m}$ ) y sonicadas durante 3 minutos. A continuación las muestras fueron inyectadas (110  $\mu\text{L}$ ) con un método de 35min de duración, 1 mL/min de flujo y una temperatura de 25  $^\circ\text{C}$ . La detección de las muestras se hicieron con el índice refractivo y los datos analizados el software de OmniSec 4.1.

**2.6 Determinación del contenido de fármaco libre y total en los conjugados con DES.**

#### Determinación de la carga de fármaco total

- **Cuantificación indirecta**

El dietilestilbestrol (DES) posee un máximo de absorbancia de 280nm por lo cual es fácil detectarla por UV-vis. Previamente se realizó una curva de calibrado de 0.01 a 1mg/mL utilizando como disolvente MeOH en HPLC, empleando el método descrito en la tabla 2.6.1.

**Tabla 2.6.1** Método empleado para la calibración de DES en HPLC.

t (min)	Flow (mL/min)	% H <sub>2</sub> O	% ACN
0	1	70	30
25	1	10	90
28	1	10	90
31	1	70	30
35	1	70	30

La carga de fármaco total se determina al analizar las muestras una vez hidrolizado el enlace acetálico mediante una fuente de calor en un ambiente de pH ácido. Las muestras se disolvieron en 100 $\mu\text{L}$  de HCl 1M (pH 2) y se



calentaron a 80°C durante 30min. A continuación se analizaron las muestras mediante HPLC con el mismo método empleado para realizar la calibración de DES. Oestradiol se utilizó como patrón interno.

Se determinó la cantidad de DES que no se unió a la cadena poliactética mediante análisis por HPLC del residuo obtenido tras lavar la muestra con hexano y disolverlo en acetonitrilo para inyectarlo en el HPL.

- **Cuantificación directa**

La carga de fármaco se calcula directamente por la absorbancia en UV-vis del conjugado obtenido. Al igual que en el método indirecto, previamente se realizó una curva de calibrado de DES en MeOH a 280nm empleando concentraciones de 0.001 a 1mg/mL. Los productos se disolvieron en ddH<sub>2</sub>O a una concentración conocida (1-2 mg/mL) y se midió su absorbancia a 280nm en cubetas de cuarzo con ayuda de un espectrofotómetro.

### **Determinación de fármaco libre**

De 1 a 3mg de cada Poliacetal con DES disueltos en metanol se inyectaron en el HPLC utilizando las mismas condiciones anteriormente descritas en la tabla 4.3.1.

Los mismos procedimientos descritos previamente para determinar la carga total (de forma directa e indirecta) y libre de un fármaco fue empleado para la determinar de paclitaxel en los conjugados poliactéticos.

### **2.7 Determinación de la Concentración Micelar Crítica (CMC) de los polímeros conjugados.**

Dos fluorocromos, difenilhexatrieno (DPH) y Pireno fueron usados para determinar la CMC de los compuestos.

0.5mg de pireno fueron disueltos en 40ml de acetona para obtener 0.0125mg/ml (62.5  $\mu$ M) de disolución stock. Entonces, 0.002 $\mu$ l de la disolución fueron añadidas a una disolución acuosa del polímero (5mg/ml). A continuación, la disolución se sonicó para conseguir la evaporación de la

acetona e inducir a la formación de micelas. A las 24h de incubación las muestras fueron analizadas.

Alternativamente, 2.5µl de una disolución stock de 0.2mM de DPH en THF fueron añadidos a una disolución polimérica en solución tampón de fosfato (5mg/ml) para analizar las muestras.

## **2.8 Estudios de dispersión dinámica de luz (Dynamic Light Scattering (DLS)).**

Las disoluciones de los conjugados (1 mg/ml y 3 mg/ml) en agua MilliQ y solución tampón fosfatada (PBS) a pH 7.4 fueron medidas en un sistema de medida de DLS a 25 °C . Las disoluciones fueron sonicadas durante 10min y filtradas mediante un filtro de membrana de celulosa de 0.22µm antes de analizar. La distribución micelar celular fue medida por volumen en unidades nm de diámetro para cada conjugado ( $n \geq 3$ ).

## **2.9 Técnicas de microscopía de transmisión y muestreo electrónicas (Transmission and Scanning electron microscopy (TEM) and (SEM)).**

Disoluciones de conjugados desde 0.5 mg/ml a 3 mg/ml, fueron preparadas usando agua MilliQ y PBS a pH 7.4. Las disoluciones fueron sonicadas durante 10 minutos y filtradas mediante un filtro de membrana de celulosa de 0.45µm antes de su análisis. Para analizar por TEM, la muestra se prepara rápidamente por deposición de 1µl de la disolución de la muestra en un soporte destinado a las medidas de TEM. Para los análisis con SEM 1µl de la muestra diluida se aplicó a un disco metálico que se cubrió con carbono mediante evaporación a alto vacío.

## **2.10 Estudios de dispersión de neutrones de ángulo pequeño (Small Angle Neutron Scattering (SANS)).**

Los experimentos con SANS fueron llevados a cabo con la colaboración de la Dr. Alison Paul de la Universidad de Cardiff (Reino Unido) y realizados en el Instituto Laue-Langevin (ILL)<sup>9</sup> en Grenoble (Francia) por neutrones provenientes de un reactor (57 MW HFR (High-Flux Reactor)) y en el laboratorio Appleton Rutherford, en el ISIS<sup>10-12</sup> Facility, en Osford (Reino Unido) mediante una fuente de neutrones provenientes de un sincrotrón.

Los conjugados se disolvieron en dos diferentes disolventes ambos deuterados, D<sub>2</sub>O and MeOD a una concentración de 1 mg/mL equivalentes de fármaco y 10mg/mL de polímero. Las disoluciones se añadieron en una celda redonda de 1mL de capacidad destinadas para las medidas de SANS, las cuales se analizaron también vacías y con los disolventes deuterados utilizados para disolver las muestras para tener así los controles positivos.

### **2.11 Estudios de degradación dependientes de pH en disolución tampón**

Los poliacetales (8 mg/mL) fueron incubados a 37°C en disolución tampón de fosfato (PBS) a pH 5.5, 6.5 ay 7.4 durante 30días. 100 µL destinados para analizar en el HPLC y 50 µL para estudios de GPC fueron tomados de cada muestra a diferentes tiempos, a tiempo cero, 15, 30 min, 2, 8 y 24 h y cada 24h hasta completar el 100% de liberación del fármaco. Las alícuotas se recogieron y congelaron en nitrógeno líquido y almacenadas a -80°C hasta su análisis en HPLC con el método previamente descrito (Tabla 4.3.1).

### **2.12 Estabilidad en Plasma**

Los conjugados (8 mg/mL) se incubaron 24h a 37°C en fresco suero extraído de ratas Wistar y se recolectaron 100 µL de las disoluciones a distintos tiempos, 0min, 1h y 24 h. A éstos 100 µL se añadió 10 µL de una disolución de 100 µg/mL de oestradiol en MeOH utilizado como patrón interno y 135 µL de MeCN para precipitar las proteínas del suero. La mezcla se centrifuge (14000 rpm, 5 min), analizados los supernadantes mediante HPLC con el método previamente descrito (Tabla 4.3.1).

### **2.13 Viabilidad celular en células de cáncer de próstata, LNCaP y PC3**

En primer lugar, se optimizó la densidad celular para llevar a cabo los posteriores ensayos de MTT mediante curvas de crecimiento a distintas densidades. 3200cél/pocillo fue la proporción elegida en la línea celular de PC3, en cambio para la línea celular LNCaP se eligió 4000cél/pocillo.

La citotoxicidad de los poliacetales fue evaluada mediante MTT. Las células fueron sembradas en placas estériles de 96 pocillos (2.5x10<sup>3</sup>cél/pocillo) utilizando como medio de cultivo F-12 suplementado

con 10%(v/v) de suero bobino fetal (FBS) para las PC3 y RPMI también con un 10%(v/v) de FBS para las LNCaP. Las células se incubaron 72h antes de la adición de los compuestos citados, con el fin de alcanzar una absorbancia final de 0.3-0.5. Se prepararon distintas concentraciones del producto a testar (0-5mg/mL), filtrando previamente antes de disolver el compuesto. Tras las 72h, se añadió en cada pocillo 20µL del reactivo MTT (5mg/mL en PBS), y se incubaron a 37°C durante 24 y 72h. Finalizado el tiempo, se eliminó el medio y los cristales de formazan se redisolvieron en 100µL de DMSO. Las placas se midieron en un lector Victor Wallac a 570nm. Como control positivo se empleó dietilestilbestrol (DES).

La viabilidad celular se calculó como porcentaje de viabilidad de las células control no tratadas.

### ***Mecanismo de internalización celular***

La técnica de microscopía confocal de fluorescencia en célula viva se empleó principalmente para detectar de forma cualitativa la forma de internalización del polímero y evitar los posibles artefactos que puede ocasionar la fijación de las células. Para estos estudios, se emplearon los compuestos poliacetalicos marcados con OG en las dos líneas celulares PC3 y LNCaP.

Para poder determinar la posible vía endocítica y si los poliacetales internalizaron en la célula en el compartimento lisosomal, el marcador Dextran-Texas red (5µl) fue añadido después de 1h de incubación, el medio se reemplazó con medio fresco y las células se incubaron durante 5h más.

Las células fueron sembradas en placas Petri (10cm<sup>2</sup>) a la densidad celular determinada para cada línea celular, entonces fueron cultivadas durante un periodo de 48horas anteriores al experimento. A continuación, se añadieron 10µL de una disolución 0.5mg/mL del compuesto (0.8%mol/mol OG). Los experimentos se realizaron tras periodos de incubación de 5',30',1h, 2h y 5h a 37°C. Después, el medio celular se eliminó y las células se lavaron por triplicado con PBS 10%(v/v) FBS. El cristal se retiró de la placa Petri y fue colocado en la cámara confocal. La planificación horaria de cada experimento se realizó siguiendo las instrucciones detalladas a continuación:

- t=5 min: el conjugado se incubó durante 5 minutos (tiempo *pulse*), a continuación se eliminó el medio y se reemplazó por medio nuevo. Las imágenes se tomaron tras 5 min de incubación (tiempo *chase*).
- t=30 min: 15min de tratamiento seguido de 30min de *chase*.
- t=1 h: 1h de tratamiento y 1h de *chase*.
- t= 5 h: 1h de tratamiento seguida de 5h de *chase*.

## **2.14 Biodistribution y acumulación en el tumor y distintos órganos de los conjugados poliacetalicos marcados con Cyane5.5 en modelos xenografos de ratón.**

Células tumorales de colon humanas HT-29 Firefly luciferasa (Fluc)-C4( $0.25 \times 10^6$  cells/100 $\mu$ l DPBS) fueron tripsinizadas y resuspendidas en matrigel (1:1). Las células fueron inyectadas de forma subcutánea en el flanco derecho de ratones atimicos femeninos nu/un (Hsd:Atimicos Nu-Foxn1nu) para ganar una buena vascularización del modelo xenográfico.

El tamaño de los tumores se medirá con un calibrador y con una frecuencia que dependerá del grado de crecimiento de bioluminiscencia (BLI) del tumor usando el IVIS® Spectrum (asegurándonos previamente que los tumores no exceden del tamaño máximo permitido (1,5 cm de diámetro)). El volumen de los tumores se calcula de acuerdo a la siguiente fórmula:  $(4/3)\pi r_1^2 r_2$  ( $r_1 < r_2$ ) (1/2 anchura x longitud<sup>2</sup>). La biodistribución de los poliacetales se determinó midiendo la fluorescencia (FRI) usando el sistema IVIS-100 (IVIS® Spectrum) con escáner IR cercano en el que la señal de Cy5.5 a 21 $\mu$ m de resolución estaba expresado en  $\mu$ g marcador/g tejido.

Estos ensayos fueron llevados a cabo en el grupo del Dr. Simó Schwartz Jr., en el centro de nanomedicina-CIBBIM en el Hospital de la Vall d'Hebron de Barcelona, dónde actualmente, modelos xenográficos de células tumorales de prostata humana PC3 y LNCaP están siendo desarrollados.

Los poliacetales conjugados con el marcador cyane5.5 fueron usados en este estudio.

### **3. CONCLUSIONES DEL PROYECTO**

#### ***1. Sistemas DES-poliacetálicos como conjugados individuales.***

- Se sintetizó una nueva familia de poliacetálicos con DES llamados, *Bloque-DES*, con mayor carga de fármaco y menor polidispersidad que los de primera generación (*Ter-DES*). Ambos polímeros fueron caracterizados exhaustivamente y evaluados no sólo desde un punto fisicoquímico sino también analizando los parámetros de caracterización biofísicos. *Bloque-DES* presenta un carácter anfífilo por lo que en disolución adopta diferente conformación.
- Los poliacetálicos con DES mostraron claramente una degradación dependiente de pH, con una liberación del fármaco DES más rápida en condiciones ácidas. *Bloque-DES* demostró tener una liberación de DES más rápida que el *Ter-DES* y una cinética de liberación de fármaco bimodal indicando así una conformación diferente en disolución. Ambos sistemas presentaron estabilidad en plasma.
- Se encontraron múltiples CACs en ambos polímeros, siendo los valores para el *Bloque-DES* mucho más bajos que para el *Ter-DES* (p.ej. el primer CAC para el *Ter-DES 1b* fue CAC= 0.7 mg/mL; el primero para el *Bloque-DES 2b* fue CAC= 0.1 mg/mL). Los estudios de PGSE-NMR indicaron una clara diferencia en los valores de difusión entre ambos conjugados, obteniendo con el conjugado de *Ter-DES* ( $D_s=2.72 \times 10^{-11} \text{ m}^2 \text{ s}^{-1}$ ) un movimiento mucho más lento que con el *Bloque-DES* ( $D_s=5.87 \times 10^{-11} \text{ m}^2 \text{ s}^{-1}$ ), éste resultado demostró claramente las diferentes estructuras formadas en disolución de ambos conjugados. Otras técnicas fisicoquímicas que se llevaron a cabo fueron DLS, TEM, SEM y SANS y en las que ambos poliacetálicos con DES se analizaron en disolución acuosa. Los experimentos con SANS demostraron que *Ter-DES* se trataba de un único sistema de un diámetro aproximado de 20nm y un espesor de 2 nm. En cambio *Bloque-DES* se caracterizó como una mezcla en la que coexistían dos especies, una de 100 nm de longitud y 2 nm de espesor (presentando una forma similar pero más grande en longitud que el *Tert-DES*) y la segunda especie consistía en una conformación tipo disco de 80 nm de diámetro y 10 nm de espesor. Se encontró que ésta segunda

especie era mucho más abundante que la primera y además mucho más consistente con los resultados obtenidos por TEM y DLS. Mediante SANS también se demostró la presencia de una especie mayor que las estructuras obtenidas para el *Tert*-DES.

- *Bloque-DES* resultó tener mayor citotoxicidad que el *Ter*-DES en células humanas de cáncer de próstata en las líneas celulares PC3 y LNCaP.
- Un monómero adicional, serinol, se incorporó en la cadena principal del sistema poliactalico (descrito por primera vez por Tomlinson et al) de manera que permitía disponer de una cadena funcional lateral accesible para la conjugación de otro fármaco o de un marcador fluorescente. Los poliactales con DES fueron conjugados con Oregon Green para posteriores estudios de internalización celular (*Ter*-DES-Ser-OG vs. *Bloque*-DES-Ser-OG), con Cyane 5.5 para los correspondientes ensayos *in vivo* (obteniendo *Ter*-DES-Ser-Cy5.5 vs. *Bloque*-DES-Ser-Cy5.5) y también conjugados a un segundo fármaco, Paclitaxel (PTX) para formar sistemas para Terapia de Combinación (obteniendo *Ter*-DES-Ser-PTX vs. *Bloque*-DES-Ser-PTX).
- Ambos conjugados, *Ter*-DES-Ser-OG vs. *Bloque*-DES-Ser-OG, entran en la célula mediante ruta endocítica como demostraron los estudios de microscopia confocal, aunque el porcentaje de *Bloque*-DES en el interior de las células es mayor que el que se observa para *ter*-DES en ambas líneas celulares.
- Estudios de mecanismos moleculares se llevaron a cabo en ambas líneas celulares de cáncer de próstata (PC3 y LNCaP) demostrando una clara dependencia en las líneas celulares utilizadas. Derivados de DES claramente modulan la vía de señalización Akt resultando muerte celular a través de apoptosis ((Bcl-2, Bax) y autofagia (principalmente LC3 con el *Bloque*-DES en células PC3), y también podrían influenciar en el ciclo celular (modulación de p21) bloqueando las células en diferentes estados del ciclo celular dependiendo la línea celular tratada.

Se llevaron a cabo estudios preliminares *in vivo* en modelos xenográficos con células humanas de cáncer de colon, obteniendo una

toxicidad negativa para los poliacetales con DES hasta 10 mg/kg y una clara acumulación en tumor hasta el día 17 para el *Tert*-DES. No se encontró una significativa actividad antitumoral en modelos xenográficos de células de cáncer de próstata PC3 con los conjugados individuales, por lo que se empezó a estudiar los sistemas de Terapia de Combinación.

## 2. Diseño de nuevos sistemas basados en poliacetales para terapia de combinación.

- **Los conjugados de combinación basados en poliacetales** fueron desarrollados a partir de los sistemas **individuales poliactalicos de DES** ya sintetizados y con la novedad de incorporar Paclitaxel como segundo fármaco quimioterapéutico.
- Éstos conjugados de combinación fueron marcados fluorescentemente con OG (*Tert*-and *Block*- DES-Ser-PTX-OG) y con Cy5.5 (*Tert*- and *Block*- DES-Ser-PTX-Cy5.5) para llevar a cabo los diferentes estudios *in vitro* (internalización celular) e *in vivo* (biodistribución, acumulación en tejido y tumor) respectivamente.
- Para poder estudiar la conformación de los polímeros, se llevaron a cabo estudios con PGSE-NMR y SANS con los conjugados cuando serinol y paclitaxel fueron incorporados en los sistemas. Cuando a los polímeros se les incorporaba el serinol se podía observar un cambio en la estructura debido a los diferentes coeficientes de difusión, con presencia de serinol, el conjugado tiene un coeficiente de  $D_s$  *Tert*-DES-Serinol =  $4.50 \times 10^{-11} \text{ m}^2 \text{ s}^{-1}$  (sin serinol,  $D_s$  *Tert*-DES =  $2.72 \times 10^{-11} \text{ m}^2 \text{ s}^{-1}$ ), el cual se mueve más lentamente que su análogo *Block*-DES-Serinol con un coeficiente de difusión de  $D_s = 5.17 \times 10^{-11} \text{ m}^2 \text{ s}^{-1}$  (para el *Block*-DES,  $D_s$  era  $5.87 \times 10^{-11} \text{ m}^2 \text{ s}^{-1}$ ) resultados muy parecidos para los poliacetales iniciales *tert*- y *block*-DES. Los valores obtenidos indican claramente que diferentes estructuras en disolución ocurren en cada caso.
- Experimentos con SANS confirmaron que cuando serinol fue incorporado al sistema poliactalico, al igual que al añadir el Paclitaxel, provocaba un efecto dominante sobre la estructura del



polímero. La muestra de *Tert-Ser-PTX* encajaba adecuadamente como un cilindro delgado de radio 10Å, longitud de 300Å y con el término  $Q^{-n}$  como  $n= 3.5$ . Cuando PTX se añadió a *Tert-DES-Ser* formando *Tert-DES-Ser-PTX*, el término  $Q^{-4}$  fue dominante indicando la presencia de estructuras más grandes localizadas fuera del alcance de resolución del experimento de SANS. Éste experimento demostró claramente que el PTX conducía a una diferente conformación en disolución.

- Los poliacetales para combinación fueron probados *in vitro* y se hicieron ensayos preliminares *in vivo* en modelos cancerígenos de mama y próstata.
- Los ensayos de eficacia *in vitro* se realizaron en líneas celulares de cáncer de mama y próstata y mostraron un claro sinergismo cuando ambos fármacos, DES y PTX, fueron combinados en el mismo sistema y con diferentes arquitecturas *Tert-* o *Block-*. Los ensayos *in vitro* en células de cáncer de mama MDA-MB-453S dieron una mayor toxicidad para los poliacetales con ambos fármacos poliacetales-DES-PTX comparandolos con los resultados de PTX a solas. En células de cáncer de próstata independientes de andrógenos como son las células PC3, el poliacetal *Tert-DES-Ser-PTX* pareció ser más activo que el PTX a solas. Por el contrario en células dependientes de andrógeno como la línea celular LNCaP *Block-DES-Ser-PTX* mostró mayor citotoxicidad que el PTX solo o el conjugado poliacetalico *Tert-PTX* (sin el fármaco DES).
- No se observaron diferencias significativas con lo que respecta a los estudios de internalización celular con los conjugados de combinación. Sin embargo las cinéticas de captación fueron muy influenciadas dependiendo la línea celular empleada.
- Cuando los polímeros de combinación fueron conjugados a Cy5.5, los estudios de biodistribución *in vivo* mostraron acumulación en el tumor siendo máximo a las 3 horas de administración del conjugado. También se detectó acumulación en los riñones y en el hígado indicando que la excreción de los poliacetales se producía a través de las rutas hepáticas y renales sin observar ninguna señal de toxicidad en los órganos. Actualmente se están llevando a cabo estudios de

tolerabilidad *in vivo* y eficacia terapéutica de todos los sistemas usando ortotópicos de cáncer de próstata (células de cáncer de próstata dependientes de andrógeno LNCaP). También se están realizando estudios no invasivos intraprostáticos con tumores de PC3 de crecimiento de tumor y metástasis *in vivo* y *ex vivo* para confirmar los resultados.

### **Colaboraciones**

- Los estudios de PGSE-NMR se realizaron con la colaboración de la Dr. Alison Paul y el Dr. Peter Griffiths en la Universidad de Cardiff (Reino Unido).
- Los experimentos de SANS se llevaron a cabo en el ILL de Grenoble (Francia) y en el ISIS de Oxford (Reino Unido) con la colaboración de la Dr. Alison Paul de la Universidad de Cardiff (Reino Unido).
- Los ensayos *in vivo* se llevaron a cabo por nuestros colaboradores Dr. Ibane Abasolo y Dr. Yolanda Fernández del grupo del Dr. Schwartz Jr. en el Hospital Vall d'Hebron de Barcelona (España).
- Finalmente, los ensayos sobre mecanismos moleculares se realizaron en nuestro laboratorio Polímeros Terapéuticos en el CIPF con la colaboración de la Dr Ana Armiñán.



## **Acknowledgements**

I would like to thank all the people that have supported me and have formed part in somehow in this thesis during these 6 years.

First, I would like to thank my supervisor Dr. María Jesús Vicent and Centro de Investigación Príncipe Felipe (CIPF) in Valencia for giving me the Predoctoral CIPF fellowship and have the financial support to carry out this thesis.

I want to express my gratitude to María Jesús for her guidance and advice through these years. Your dedication to science and all your knowledge to create from zero the Polymer therapeutics group is very admirable. I am sure all this effort will bring you lot of satisfactions and high achievements. I was the first person who started in this group and I never will forget that. Thank you very much Maria Jesús for your support, help and time!

Thanks to CIPF for providing the necessary infrastructure to develop this project.

Thanks to all the people that have formed or are forming part of the Polymer therapeutics group during these years. Thanks Puri for the good moments we had in the lab, Lucile for sharing your polymer knowledge in the beginning of my thesis, Maria Helena for the useful work you do in the lab, Jezabel for your help with the cells, Rut for your advices for Boston, Aroa for providing your fresh energy and radiance that the group needed. Many thanks Ana and Richard for your collaboration in this thesis, Ana for your great work with the cells and amiable talks and Richard for having always time for helping and particularly for the comfortable conversations and efficient advices. Thanks Fabiana for sharing with me great moments from the first year and for taking care and support me during my stay at USA, very important for me, Ximo for the interesting conversations, your extensive knowledge and your particular way of explain science make it much enjoyable, thanks to you and Fabiana for your support, fun talks, coffee moments and for having always time for me. Thanks Esther for your friendship and for your sincere and affective conversations. I would like to thanks particularly to Coralie, Gabriela and Inma for sharing and walking together all of us in the thesis' experience. Thanks Coralie for the nice time, the several delicious French breakfasts and for your help with the polymer synthesis when I was in USA. And highly regarded and special thanks to Inma for your support and confidence, you always will be my "pequeña Inma" and to Gabriela for being next to me in the good and bad moments, you are the personification of goodness. Thanks a lot girls, for making these years much more pleasant, for your support

and for sharing your time and your shoulders and accept me with all my stress and discouragements!

I was so lucky to have very good students, Tere, Claudia, Mary, Lolin, Carmen and Ariane, thanks all of you and the rest of students who came to the lab, Tibolt, Gianni, Helena, Chiara, Hemda, Conxin, Catalina, thanks to Marta for being so nice, Gemma for the happy time at Sant Feliu and markedly many thanks to David, a great friend, thanks for give me the funniest moments of the last years and for your kind talks and messages.

Thanks also all the postdocs that have joined the group in some period, Edgar for the good moments we had with you and Matthias for the polymer knowledge you share with all of us and to the new girls in the group, Amaya, Ant and Marina.

I should also show my gratitude to Ruth Duncan for her time and visits to our lab and sharing and teaching her amazing work of polymers therapeutics from her extensive scientific career. Thanks Rut for improving our polymer knowledge.

I would like to thanks all my CIPF colleagues, Lucía, Maria Grazia, Edu, Cristina, Imelda, Bea, Susana, Vanessa, Pilar and all the people from the organic lab, Gemma, Salva, Toni, Nacho, Oscar, Amador, Raúl, Silvia, in particular to Natalia for her support and amicable talks. Thanks to the I12 group especially to Laura for her friendship and support from the beginning and for the positive talks, one of the first at Cardiff. Also I would like to thanks the confocal team, Eva y Alberto, the TEM group, mainly to Mario for his help and laughs in the images analysis and the IT team from CIPF. And thanks to David and Pablo from the ICMOL of University of Valencia for helping with the DLS experiments.

Some parts of this thesis would not be possible without the collaboration of Dr. Simó Schwartz group in Vall d'Hebron Hospital in Barcelona, mainly to Dr. Ibane Abasolo and Dr. Yolanda Fernández for their hard work in the biological studies, their advices and their very useful help and time during last months.

From the four months I spent at Cardiff I would like to thanks Dr. Alison Paul, I was so lucky to have the opportunity to learn from her. Thanks a lot Alison for allowing me to stay in your lab, your discussions and advices in science especially with sans experiments were and have been very valuable and profitable to improve my scientific knowledge. I am also very grateful to Dr. Peter Griffiths for the useful discussions in the group meetings and I would like to thank you, together with the EPSRC Platform (EP/CO13220/1) for the travel support I had to stay at Cardiff. I would also like to say thanks to the group, Filiz, Abdul, Gemma, Lucia for helping me to find a nice apartment and particularly to Craig for the

agreeable conversations and for all his help with the SANS and PGSE-NMR experiments. Also I would like to thank both ISIS (Oxford, UK) and Institut Laue-Langevin (Grenoble, France) for beam time allocation and consumables funding.

I should show my gratitude to the people from Novartis for making a great and warm experience in the USA. Thanks Cameron for being such an amazing person and impressive scientist, for your hospitality, your patience, for being my supervisor and teaching me so many techniques and science. Thanks Nika for highly contributing to my comfort, Christine for taking care of me, for the great moments and trips and thanks again to bring me to the hospital that weekend. Tanzina I never will forget such a familiar and warm Thanksgiving Day and neither the fantastic time I had with you and Aleem in my birthday, thanks my Bangladeshi sister. And thanks the entire group who make me feel like in a big family, Junping, Janetta, Laura, Dyuti, John, and Robert.

To my friends outside the lab, for understanding my “no time” but always being next to me supporting me, Vero, Ampa, Nerina, Kitzia, Gloria, Bea, Kristof, Tine, Wouter and Raquel.

A big thank goes to a very special person, Ruben, who has been next to me during last years and has supported me while working in my writing phase. Thanks to let me use your computer for finishing writing it when mine was broken and specially thanks a lot for your patience, comprehension and love during all this period.

And finally the biggest thank you of all naturally goes to my parents, for their love and support every day, my loving mum and my comprehensive father, you are the most important for me in life. Also thanks to the rest of my family, my beautiful and clever sisters and brother, their partners and my adorable niece and sweet nephew. They have always backed me up in my choice of life, listened and encouraged and never doubted that I was able to put a final dot to this project.

**THANK YOU VERY MUCH TO ALL OF YOU!**

